EUROPEAN SEISMOLOGICAL COMMISSION
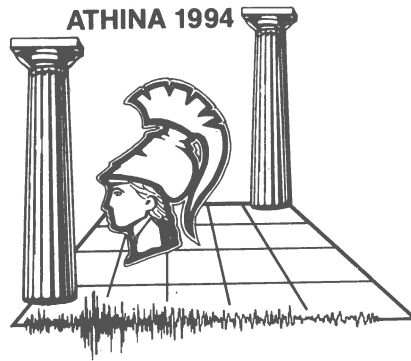
ATHINA 1994

**XXIV General Assembly
1994 September 19-24
Athens, Greece**

Proceedings
and Activity Report 1992-1994
Volume II

University of Athens
Faculty of Sciences
Subfaculty of Geosciences
Department of Geophysics & Geothermy

EUROPEAN SEISMOLOGICAL COMMISSION

ATHINA 1994

XXIV General Assembly
1994 September 19-24
Athens, Greece

Proceedings
and Activity Report 1992-1994
Volume II

University of Athens
Faculty of Sciences
Subfaculty of Geosciences
Department of Geophysics & Geothermy

National Library of Greece

European Seismological Commission
General
Assembly (24: 1994 :Athens)
  Proceedings and Activity Report 1992-1994
  INDEX
  ISBN 960-85242-2-9
  Volume I
  ISBN 960-85242-3-7
  University of Athens
  Faculty of Sciences
  Subfaculty of Geosciences
  Department of Geophysics & Geothermy

Edited by: Kostas Makropoulos
           Peter Suhadolc

I.U.G.G.
International Asssociation of Seismology and Physics of the Earth's Interior
European Seismological Commission

Volume II

INDEX

Volume II

Sub-comission E   Earthquake Prediction
Chairperson: H. Berckhemer

NEW MAGNITUDE ASSESSMENT FOR EARTHQUAKES IN THE NE PART OF THE IBERIAN PENINSULA. PRELIMINARY RESULTS

J. Batlló[1,3], J. Vila[2,3] and A. M. Correig[2,3]

[1] *Observatori de l'Ebre. CSIC.* E-43520 Roquetes (Tarragona), Spain.
[2] *Dept. Astronomia i Meteorologia. U. de Barcelona.* Martí Franques 1, E-08028 Barcelona, Spain.
[3] *Laboratori d'Estudis Geofísics "Eduard Fontserè".* IEC, Martí Franques 1, E-08028 Barcelona, Spain.

Abstract

Magnitude estimates of earthquakes ocurred in the NE part of the Iberian peninsula have been investigated. A new magnitude equation for local and regional earthquakes recorded at station EBR has been developed. Also, an azimuthal dependence of the station correction term has been found, this introduces uncertainty on the available magnitude estimates and on the available values of the regional seismic wave attenuation.

Introduction and goals

A local magnitude equation has been developed for the short period (1 Hz) seismograph (operated in the same way since June 1974) at "Observatori de l'Ebre" (EBR-SP, Lat. 40° 49' N, Lon. 0° 30' E, alt. 40 m.). The main goals are:

- To give a magnitude estimate to small earthquakes produced in the surrounding zones.

- To extent the instrumental magnitude estimates to older regional earthquakes for which instrumental magnitude was not available up to now.

Methodology

We proceed as follows:

- We used Båth (1981) aproach to develope an independent local magnitude M_L equation.It may be defined in the following way

$$M_L = \log A + \kappa(T)\log(\Delta/100) + \log I(T) + \varphi. \qquad (1)$$

Where A is the zero to peak ground displacement (in millimeters), $\kappa(T)$ is the seismic wave attenuation, $I(T)$ is the amplitude response of the standard Wood-Anderson seismograph and φ is the station correction.

- As seismic wave attenuation values we used those calculated by Vives and Canas (1992) for the L_g waves with seismograms of the same instruments we are using. They found the anelastic attenuation γ of the L_g waves for the region of our interest to be (fig. 1):

$$\gamma = (0.0042 \pm 0.0007)\, f^{(0.5792\pm0.0591)}\, km^{-1} \qquad (2)$$

and using this result, it is easy to show that

$$\kappa(T) = \gamma(T)\,\log e \frac{\Delta}{\log \Delta} + \frac{1}{2} \qquad (3)$$

- We assume $T = 0.5\ Hz$ for convenience (this is the maximum magnification frequency for our system).

The resulting Magnitude equation is

$$M_L = \log A + 0.5\log \Delta + 2.7\ 10^{-3}\,\Delta - 5.4\ 10^{-3}\frac{\Delta}{\log \Delta} + \varphi. \qquad (4)$$

Equation test and Station correction

To test the developed equation we proceed as follow:

- We selected 340 earthquakes recorded at EBR station between 1984 and 1993, which epicenters lie at distances shorter than 400 km from EBR and which magnitudes are given in the IGN (Instituto Geográfico Nacional) catalogues (fig.2). Also, There is a LDG (Laboratoire de Detection et Geophysique) magnitude estimation for a lot of them.
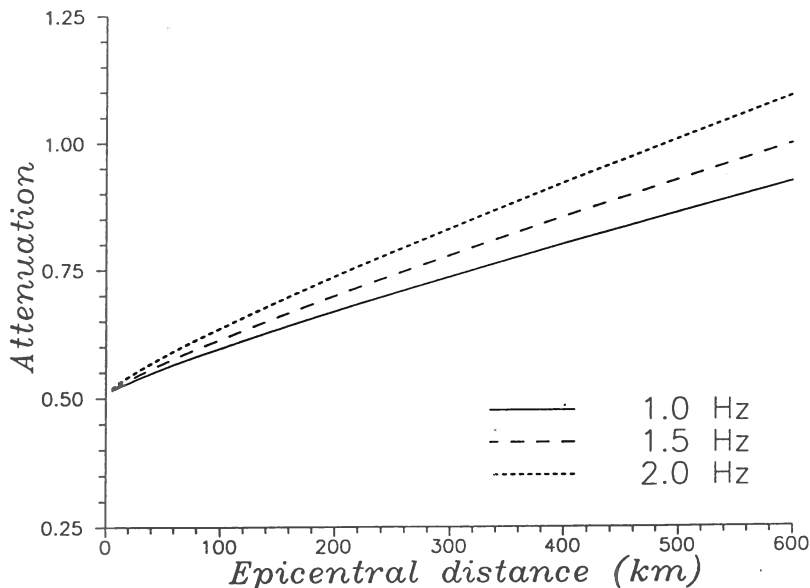
Figure 1: L_g seismic wave attenuation for the eastern part of the Iberian peninsula as calculated by Vives and Canas (1992).

- We read the maximum peak to peak amplitude A_{P-P} and its corresponding frequency. We realiced that this frequency value lies around $2Hz$ (also, this is the maximum magnification frequency) and we use $A_{P-P}/2$ as zero to peak amplitude.

- We calculate a M_L magnitude estimate for every earthquake using our developed equation and amplitude data for the vertical component.

- We compare this estimate with those calculated using the M_{Lg} defined by Nuttli (1973) and M_L as defined by Richter (1935).

The results of this process show that the developed equation is esentially correct. The linear correlation among our calculated magnitude and those calculated using Richter's and Nuttli's formulae are good (fig. 3). They agree extremely well in the case $M_L - M_{Lg}$. This fact shows that the maximum amplitude recorded on these seismograms corresponds to the L_g wave as espected (also, that the use of Nuttli equation is a good approximation).

To calculate the station correction we plot our obtained magnitude estimations vs. the IGN M_{Lg} and LDG M_L ones and we fit a straight line

by minimum squares linear regression to the obtained points (fig. 4). The results are:

$$M_L = -0.95(\pm 0.16) + 0.96(\pm 0.05)M_{IGN} \qquad (5)$$

$$M_L = -0.97(\pm 0.19) + 0.96(\pm 0.06)M_{LDG} \qquad (6)$$

and the resulting station correction is ≈ 1.0

Finally, we obtain a formula for the calculation of the local magnitude at EBR seismic station in the form

$$M_L = \log A + 0.5 \log \Delta + 2.7\,10^{-3}\,\Delta - 5.4\,10^{-3}\,\frac{\Delta}{\log \Delta} + 1.0. \qquad (7)$$

Application and discussion

It is known that EBR records of some earthquakes originated to the south show amplitudes quite smaller than those of similar earthquakes originated to the north. This has been observed also in other near stations (VAN). To analize this observation we fit IGN magnitudes vs. our magnitude estimations independently for earthquakes located to the north (250 events) and those located to the south (84 events). The results are:

- To the north (fig. 5, left)

$$M_L = -1.26(\pm 0.18) + 1.05(\pm 0.06)M_{IGN} \qquad (8)$$

- To the south (fig. 5, right)

$$M_L = -0.86(\pm 0.40) + 0.96(\pm 0.13)M_{IGN} \qquad (9)$$

As it is shown, there is a station correction offset on depending on the back-azimuth of the recorded earthquakes. We cannot offer any conclusive explanation for this fact. We may postulate several causes:

- Attenuation shows a great azimuthal dependence. Studies on seismic wave attenuation for this zone do not show, up to the present, great evidence on this sense.

- Geological geometry of this zone tends to destroy (or inhibits the generation) of L_g waves. No studies in this sense have been undertaken up to the present.
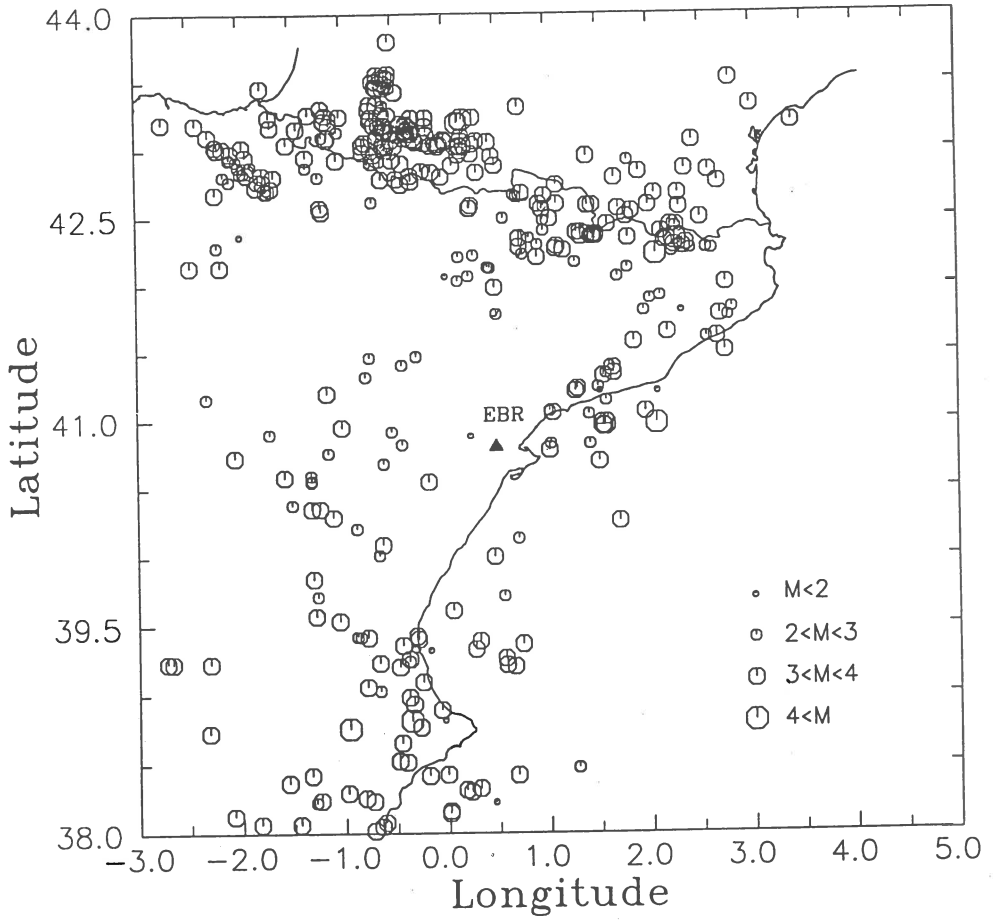
Figure 2: Epicentral location of earthquakes used to fit our M_L local magnitude equation
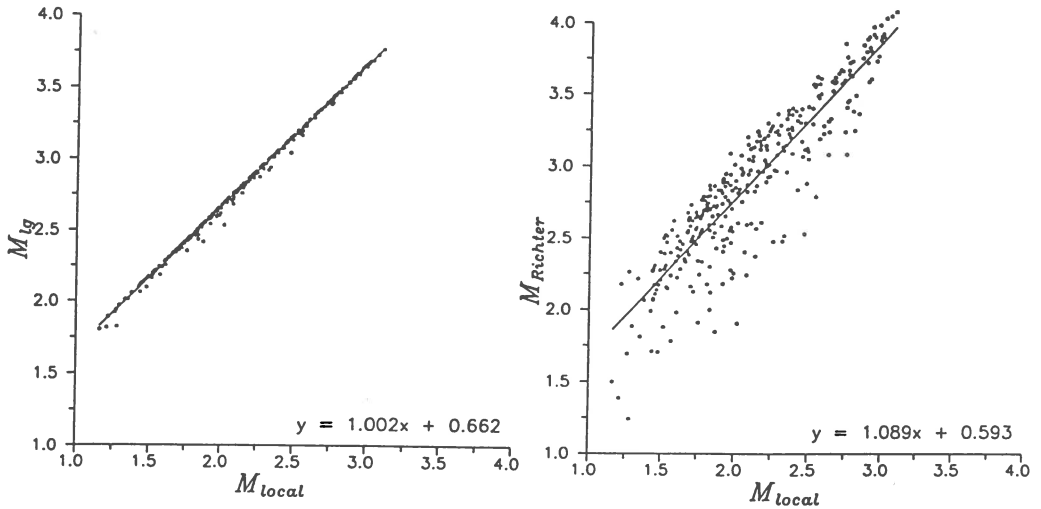
Figure 3: Fitting of calculated M_L vs. Nuttli's M_{Lg} (left) and M_L vs. Richter's M_L (right) magnitude estimates.

- Magnitude estimates for earthquakes located to the south of EBR should be quite lower. This means that some problem (or artifact) is present on the process of calculation of magnitude estimates by IGN, at least in the studied range. It is not likely because they have been tested against NEIC and LDG estimates and show very good correlation.

Conclusions

Main conclusions of the carried analysis may be stated as follows:

- A local magnitude M_L equation have been developed for the short period seismograph at EBR station. Its validity extends for eartquakes ranging on $2.0 < M_L < 4.$ and distances up to 400 km.

- It has been shown that maximum recorded amplitude corresponds to the L_g wave.
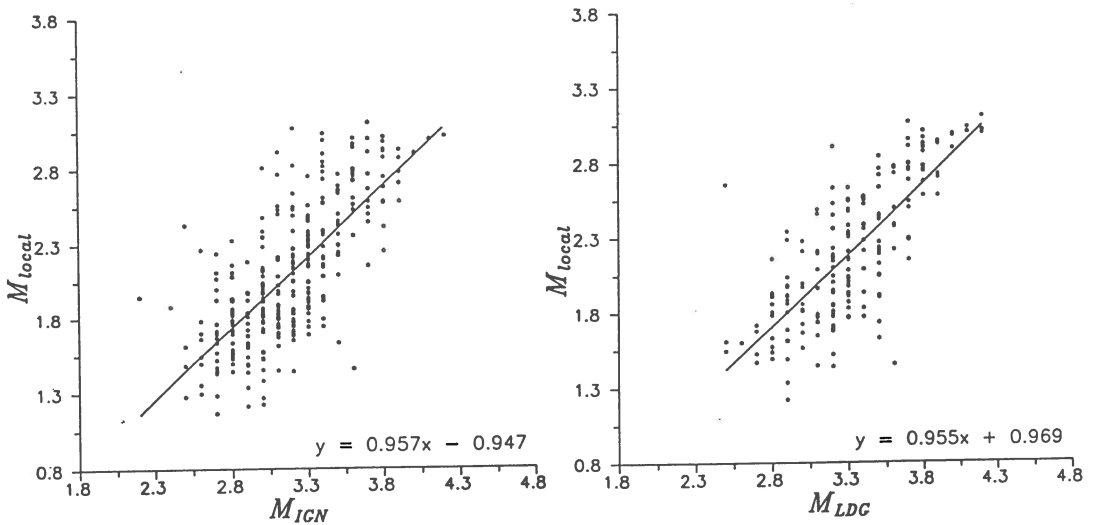
Figure 4: Fitting of calculated M_L vs. IGN's M_{Lg} (left) and M_L vs. LDG's M_L (right) magnitude estimates.

- Azimuthal dependence of the station correction has been shown. This introduces questions in magnitude estimation and seismic waves attenuation that should be further studied.

Bibliography

Båth, M., 1981. Earthquake Magnitude - Recent Research and Current Trends. *Earth-Sci. Rev.*, **17**, 315-398.

Nuttli, O. W., 1973. Seismic wave attenuation and magnitude relations for eastern North America. *J. Geophys. Res.*, **78**, 876-885.

Richter, C. F., 1935. An instrumental earthquake magnitude scale. *Bull. Seismol. Soc. Am.*, **25**, 1-32.

Vives, V. and J. A. Canas, 1992. Anelastic attenuation and pseudoacceleration relations in eastern Iberia. In: *Proceedings of the tenth world conference on Earthquake Engineering.* Balkema, Rotterdam. ISBN:90 5410 060 5, p. 299-304.
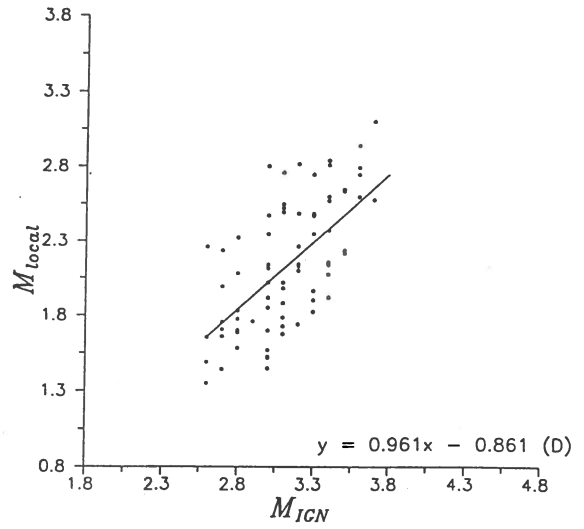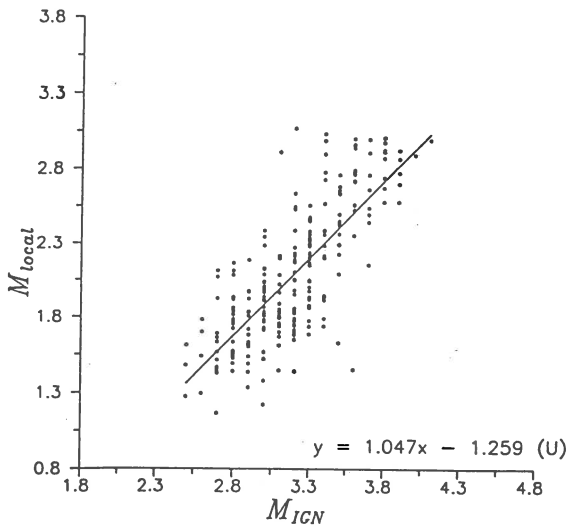
Figure 5: Fitting of calculated M_L vs. IGN's M_{Lg} magnitude estimates for earthquakes which epicenter lie to the north of EBR (left) and M_L vs. LDG's M_L fitting for earthquakes to the south of EBR (right).

REFRACTION OF SEA WAVES APPROACHING THE BRITISH ISLES AND ITS EFFECT ON THE GENERATION OF MICROSEISMS.

Jack Darbyshire
Unit for Coastal and Estuarine Studies, Marine Science Laboratories
Menai Bridge, U.K.

Abstract

Previous work has shown that microseisms as recorded in North Wales are related to the sea wave climate in two regions, the Bristol Channel area and an area to the south-west of Scotland, called for convenience the North Channel area. It was decided to investigate the refraction of approaching sea waves in these regions. In the case of the Bristol Channel, the direction of approach of the waves was varied from 75° to 95° and for the North Channel from 95° to 145°.

In the Bristol Channel area, there was a strong focussing point off the north-coast of Cornwall where the coastal outline was relatively smooth and could give rise to considerable reflection.

In the North Channel case, the topography is much more complicated but there was a focussing point off the Isle of Islay and the coast of Kintyre for directions 95° to 145°.

It is therefore possible that these focussing areas could give rise to microseism generation and could be checked with two storms which occurred recently, one very severe one which was acting for most of the time to the south of the British Isles and a less severe one which moved from the south to the north of the British Isles and so could be expected affect both the regions considered. A wave prediction program was prepared which allowed for the effect of refraction in determining the wave direction and amplitude.The history of sets of waves arriving at intervals of 4.5° from 0° to 180° and travel distance units of 1 hour was used for the Bristol Channel case while for the northern case, the distance interval was one half hour's travel and the angular increment was taken to be 1.5°.

The results showed that large waves of large amplitude could arrive at many points on the Cornish coast with normal incidence. The position was not so clear in the northern case but there was appreciable wave energy propagating normal to the coast of the Isle of Islay but very little appeared to arrive off the coast of Kintyre. The depth grid system use for calculating the refraction was 23 km. and it is possible that with a smaller grid, some activity could be shown to arrive at Kintyre.

Introduction

Although it has been accepted for some time (e.g. Longuet-Higgins,1950) that secondary microseisms are caused by the onset of two sets of waves of half the microseism frequency meeting in opposite directions. It was initially suggested that this could happen in mid-ocean with sets of waves coming from different storms or sets generated in different areas of the same storm. THis turned out, however, to be a relatively rare occurrence and the wave sets must in the majority of cases be caused by coastal reflection. An investigation of microseisms recorded at Menai Bridge, Wales, for the past eight years,(Darbyshire, 1990,1991), has shown that the microseisms are closely related to the wave conditions at two sea areas, one in the Bristol Channel and another in an area to the south-west of Scotland which was called for convenience, the North Channel area. Waves were hindcasted for these two areas and the variation of energies predicted

for sea waves of over 14 seconds period, agreed very well with variation of microseism energy of over 7 seconds period at Menai Bridge. These investigations did not go into the effect of refraction on the waves incident in these areas and the hindcast program was extended to allow for this and its effect on both amplitude and direction. Such a program was suggested by Elliott (1983).

Refraction diagrams for waves approaching the British Isles.
A 23 km. depth grid system extending westward from the coast of the British Isles to the 2000 metre contour was used.. The wave orthogonals (rays) were taken from various locations near the western edge. For the south-west coast of Scotland for 15 second period waves a series of initial directions of approach from 95° to 145° as shown in Figures 1a and 1b were taken. One set is given for 12 sec. waves with an angle of 95°.In all the cases shown, there is considerable refraction and the lines cross, indicating focussing, near the coasts of the Isle of Islay and the Kintyre peninsula. Both these coasts are relatively smooth and unindented. The lines approach these coasts at nearly normal incidence and so some straight reflection could be expected.

Figure 2 shows similar diagrams for the south-west coast of England for initial directions of 85° to 95° for 15 sec. waves and 95° for 12 sec. waves. Here the focussing is much more marked particularly in the area near Lands End. Again the waves appear to be approaching normal to the coast in several places and reflection could be expected.

Using wave refraction diagrams for wave hindcasting.
It is possible to use refraction diagrams for hindcasting wave parameters near the coast. Now, however, the lines are started near the coast and extended towards the west. A series of six hourly charts are used in conjunction with the depth chart and the refraction lines prolonged off the depth grid on towards the western edge of the weather chart, as the speed does not then depend on the depth. Initial directions at 1.5° intervals from 0° to 180° were taken from various points along the Scottish coast at steps of a travel distance of one half hour for the wave period concerned. For the English coast the corresponding numbers were 4.5° and one hour's travel. When the lines had been completed, they were traced back from the edge towards the recording point and at every three hours the position was noted and the relevant wind chart for that time was used to obtain the wind speed and direction for that point. These values are introduced into the wave prediction process and continued until the end of the line is reached. Three hourly values are obtained by interpolating the six hourly values.

During December 1994, there were two storms of particular interest. One for 27-30th. was very intense and gave rise to the highest microseisms ever recorded at Menai Bridge. The storm was acting most of the time to the south of the British Isles.. The other storm was from 17-19th. and was not so intense but moved from the south to the north of the British Isles. A curve showing the variation of the microseism energy with frequency less than 0.14 Hz. is shown in Figure 3.

The hindcasting program was applied and the results for various points near the coast are shown in Figures 4 and 5. The directions are indicated by arrows and the (wave energy)² values for frequencies lower than 0.07 Hz by the numbers. Figure 4 shows the effect of the two storms at the south-

west coast of England. As would be expected from Figure 2, with the later storm,shown at the top of the diagram, there is intense activity near Lands End with values of 49.2 and 38.4 $m^4 \times 10^{-1}$, with directions approaching the coast. There is also some activity between 3 and 18 $m^4 \times 10^{-1}$ off other parts of the Cornish coast. The effect is much smaller with the earlier storm, shown at the bottom,the only appreciable value being 4.10 $m^4 \times 10^{-1}$ off Lands End.

The effect of the two storms is about the same with the Scottish coast, there being values of 3.2 and 1.46 $m^4 \times 10^{-1}$ off and normal to the coast of the Isle of Islay for 29.12.94 1200 and 2.85 $m^4 \times 10^{-1}$ for 19.12.94 0000. The effect on both the northern and southern cases are comparable for the first storm but clearly the effect in the south is much larger for the second storm. It was not possible to detect any activity off the coast of Kintyre for both storms and it may be necessary to use a finer grid with such a complicated topography as the south-west coast of Scotland.

Conclusions.

It has been shown that the reflection of waves coming from the Atlantic Ocean is quite possible off the coast of Cornwall and it can give rise to microseisms. There is also some reflection off the Isle of Islay off the Scottish coast which at times is as large as the effect off Cornwall.It is possible that the use of a finer depth grid would lead be advantageous in dealing with refraction off the coast of Scotland.

References.

Darbyshire,J. 1990. Analysis of twenty storms during the winter of 1987-8.
     Ph. Earth Planet. Inter., 63:181-195.
Darbyshire,J. 1991. A further investigation of microseisms in North Wales.
     Phys Earth Planet.Inter.,67:330-347.
Elliott,A., 1987.Wave prediction by an empirical tracing model. Appendix by
     by J.Darbyshire. In:Advances in Underwater Technology, Ocean Science
     and Engineering.Vol 12, Modelling the Offshore Environment,
     Graham and Trotman, London, p.117.
Longuet-Higgins,M.S. 1950. A theory of the origin of microseisms.
     Philos.Trans. London.,Ser. AA,243:1-35.
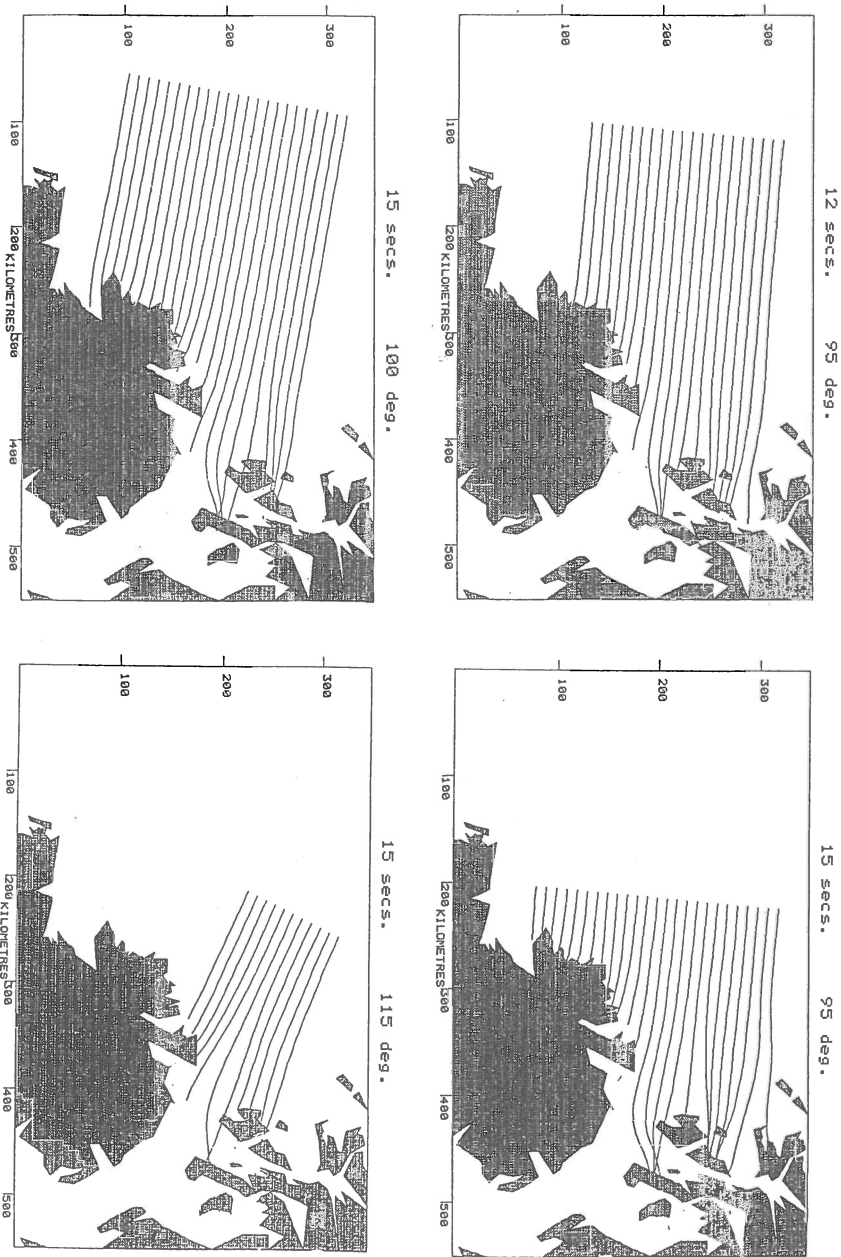
Figure 1a. Wave ray paths with initial direction of approach of 95° to 115° with 15 secs. period and 95° with 12 secs. period arriving at the south-west coast of Scotland.
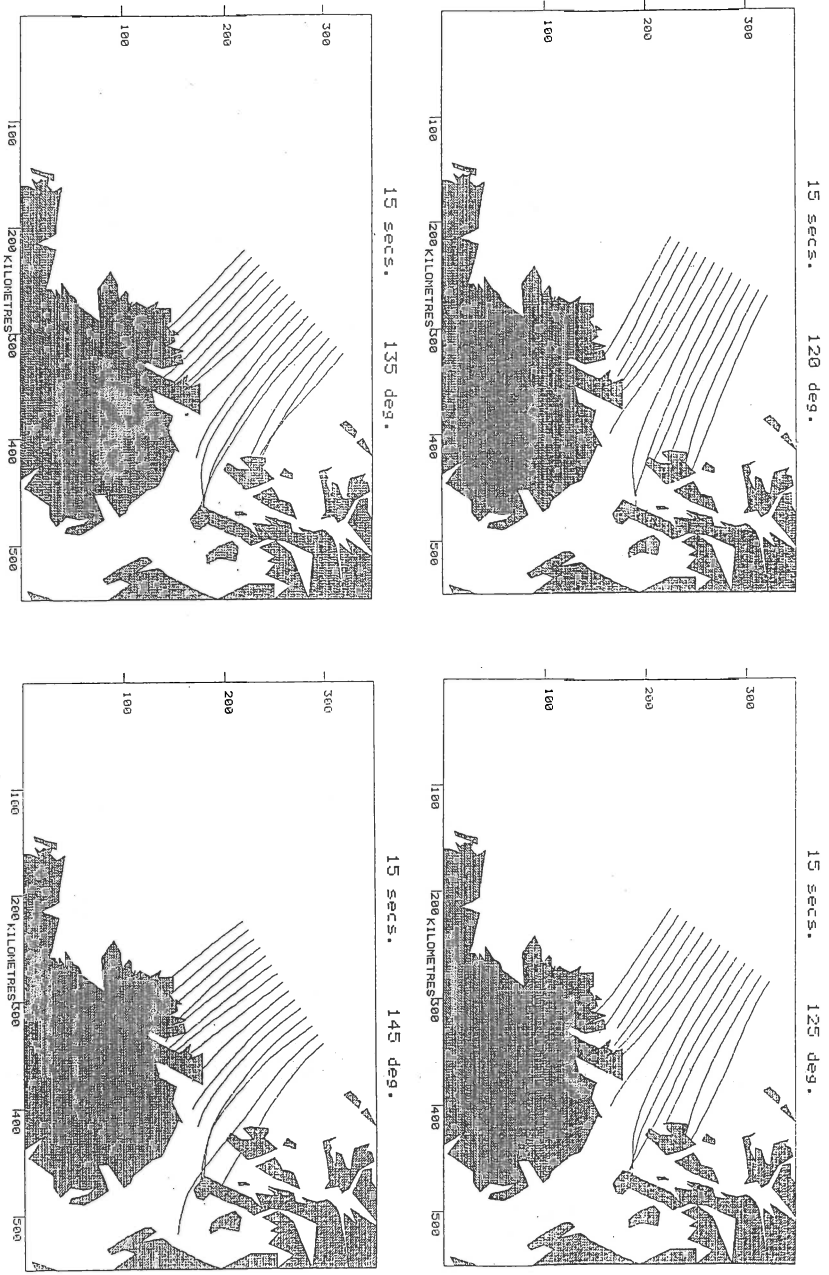
Figure 1b. Wave ray paths with initial direction of approach
of 120° to 145° with 15 secs. period arriving at the
south-west coast of Scotland.
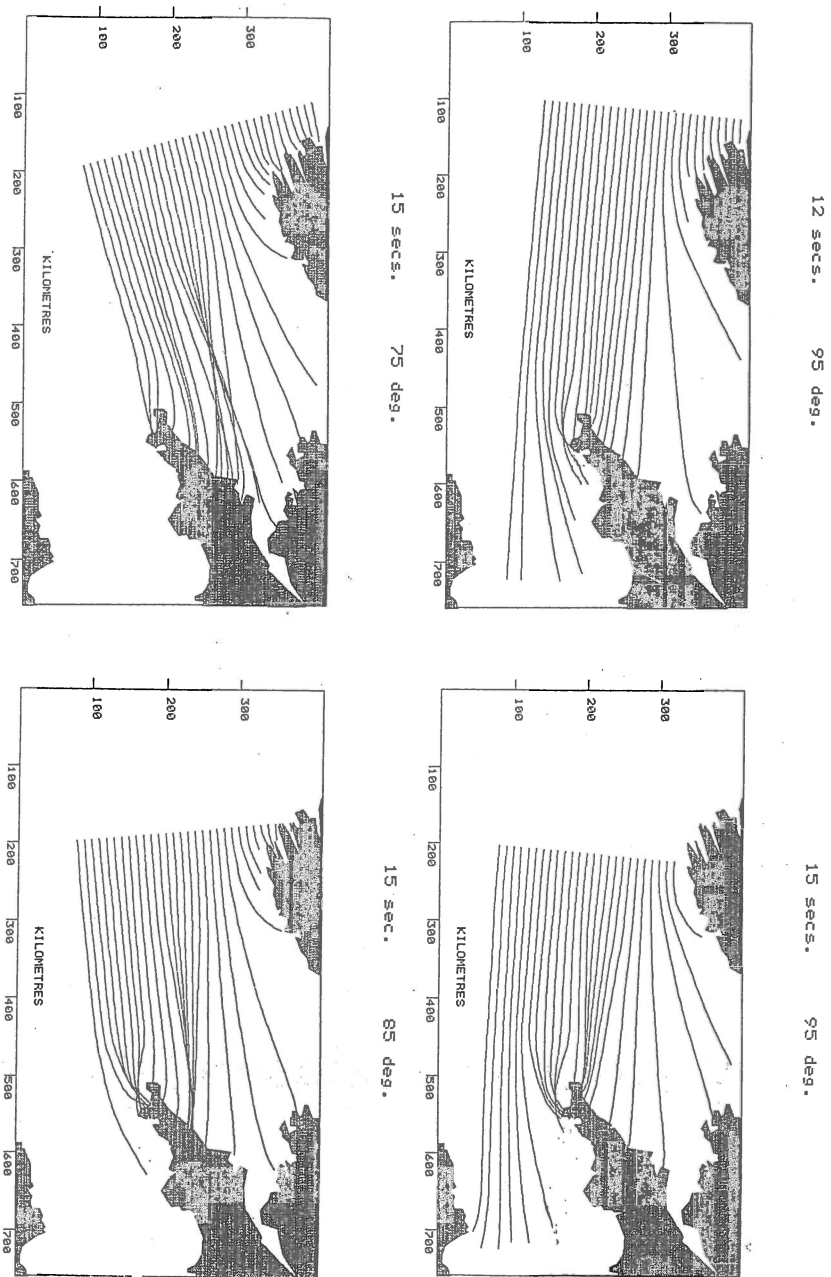
Figure 2. Wave ray paths with initial direction of approach of 75° to 95° with 15 secs. period and 95° with 12 secs. period arriving at the south-west coast of England.

654

MICROSEISM ENERGY

$m^2 s^{-2} \times 3.12 \times 10^{14}$
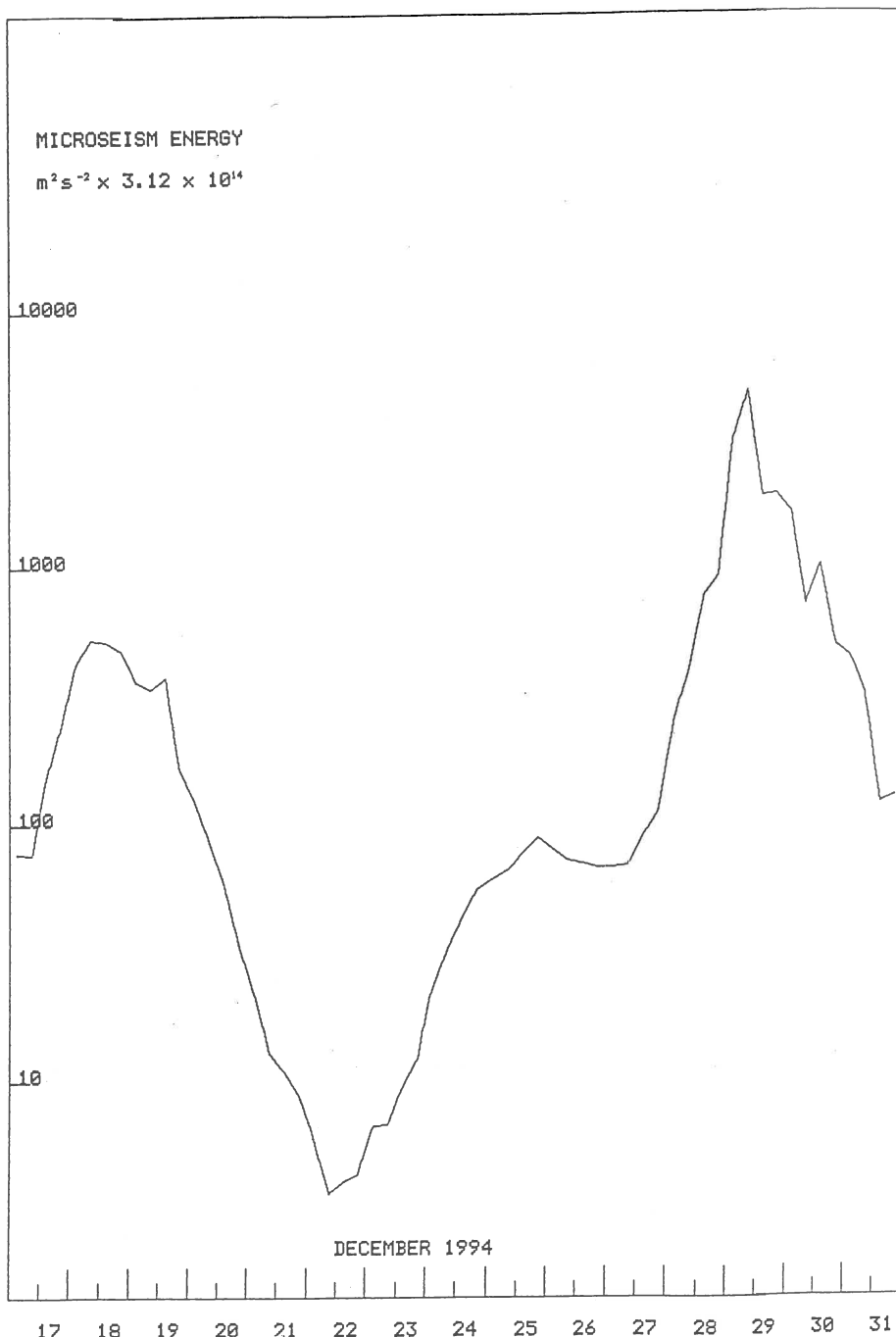
Figura 3   Variation of microseism energy with lower frequency than
0.14 Hz (7 secs.) at Menai Bridge for 17-31 December 1994.
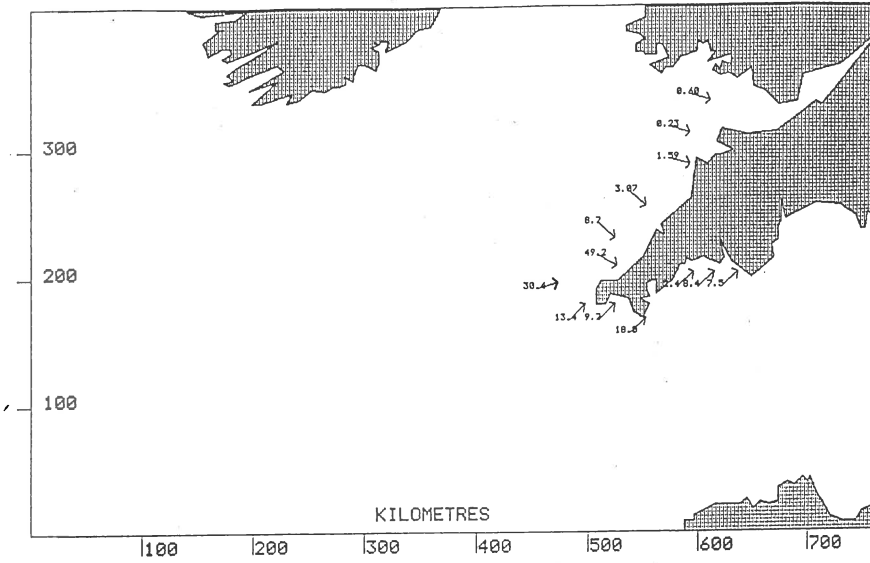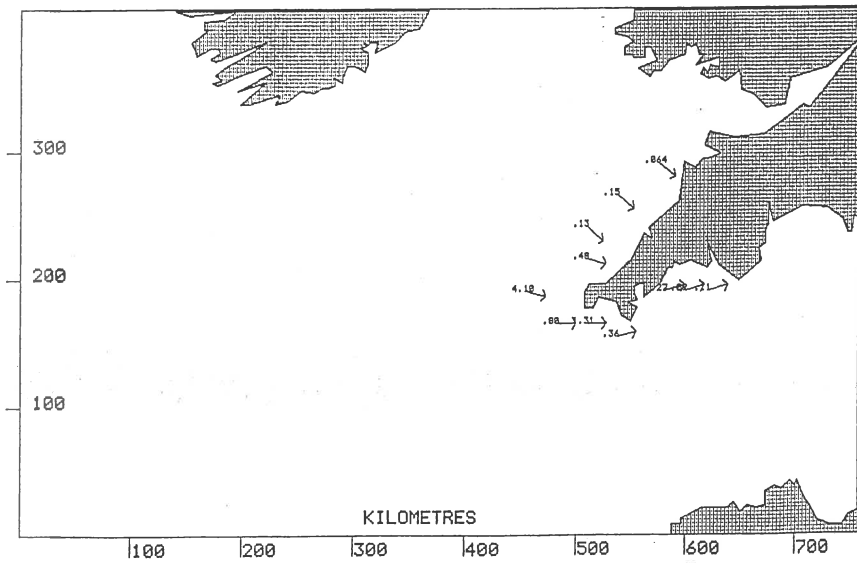
Figure 4. Arrows indicating the direction, and numbers the square of
the energy of waves of frequency less than 0.07 Hz. (14 secs.)
in units of $m^4 \times 10^{-1}$, arriving at the south-west coast of
England for 29.12.94 1200 (top) and 19.12.94 0000 (bottom).
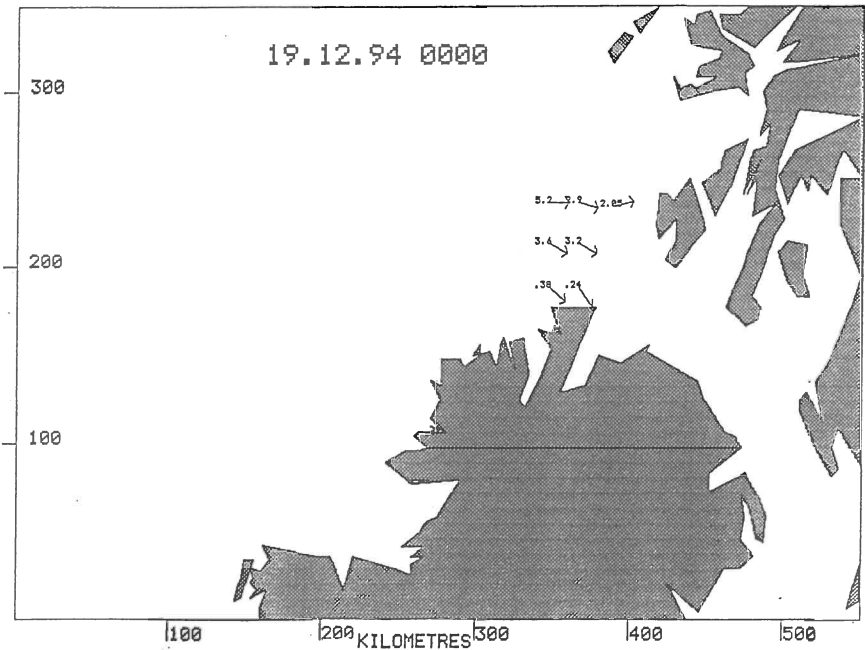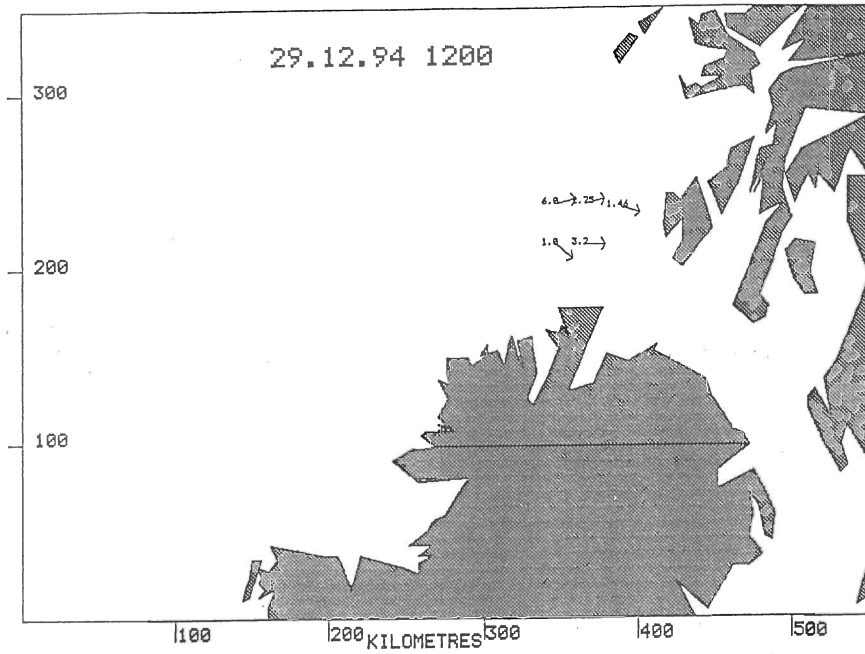
Figure 5.   Arrows indicating the direction, and numbers the square of
the energy of waves of frequency less than 0.07 Hz. (14 sec.)
in units of $m^4 x 10^{-1}$, arriving at the south-west coast of
Scotland for 29.12.94 1200 (top) and 19.12.94 0000 (bottom).

SPATIAL AND DIURNAL NOISE CHARACTERISTICS OF THE FINESS ARRAY

T. Tiira, M. Tarvainen, A. Tuppurainen[1]

Institute of Seismology, P.O. Box 19 (Et. Hesperiankatu 4),
FIN-00014 University of Helsinki, Finland

Abstract

The technical upgrade of FINESS array in 1993 has improved the quality of data. Different aspects of noise characteristics of the array have been studied. The diurnal variation of noise is much higher during working days compared with weekends. The cultural noise above 2Hz dominates the diurnal variation of noise. The importance of spatial noise characteristics in tuning the beamforming processes is displayed. Different array configurations give extra suppression of incoherent noise compared to theoretical values at some frequency ranges. So, it is possible to improve the capabilities of the detector system by selecting optimum array configurations for beams according to nature of phases that are searched for. The short term alterations of the noise level were studied by examining the output of the detector system. Two directions, 272° and 335°, were found to dominate the azimuth distribution of low velocity detections.

1. Introduction

The FINESS array in southern Finland has been designed for detecting and locating local and regional events (Korhonen *et al.* 1987), but it has proved to be very efficient also in detecting teleseismic events (Uski 1990). The deployment of the array resembles those of NORESS array in Norway (Mykkeltveit 1985) and GERESS array in Germany (Harjes 1990). The array consists of 16 vertical short period instruments assembled in 3 rings with a 3-component station at the center. The diameter of the array is about 2km.

The array has gone through technical upgrade in 1993. New vaults were built for all substations. New telephone lines were built from substations to central station. All electronic equipment were changed. At the old array the instrumental noise was higher due to the old amplifiers and long analogous line transfer. Previously the data was digitized at the center station now at vault of each station. The instrumental noise is now over 20dB lower than seismic noise. Previously the instrumental noise was significant compared to the seismic noise. To illustrate the improvement in quality of the data average of spectra of noise samples taken every hour from each of the stations during one day are plotted in Fig. 1. The noise samples were collected on the second Monday of two consecutive years. The data of FINESS is much more uniform

---

1. Also: Center for Seismic Studies, 1300 N. 17th Street, Suite 1450, Arlington, VA 22209, United States

than data of the old array (FINESA). Only one of the substations of FINESS has slightly different behaviour in low frequencies due to older A/D converter that will be replaced in the future. It was not possible to test the possible change of average noise levels due to arbitrary alterations in local noise conditions. When noise spectra of FINESS were compared to those of 5 nearest seismic stations it was found that at most of the area between 1Hz and 10Hz FINESS had the lowest noise level.
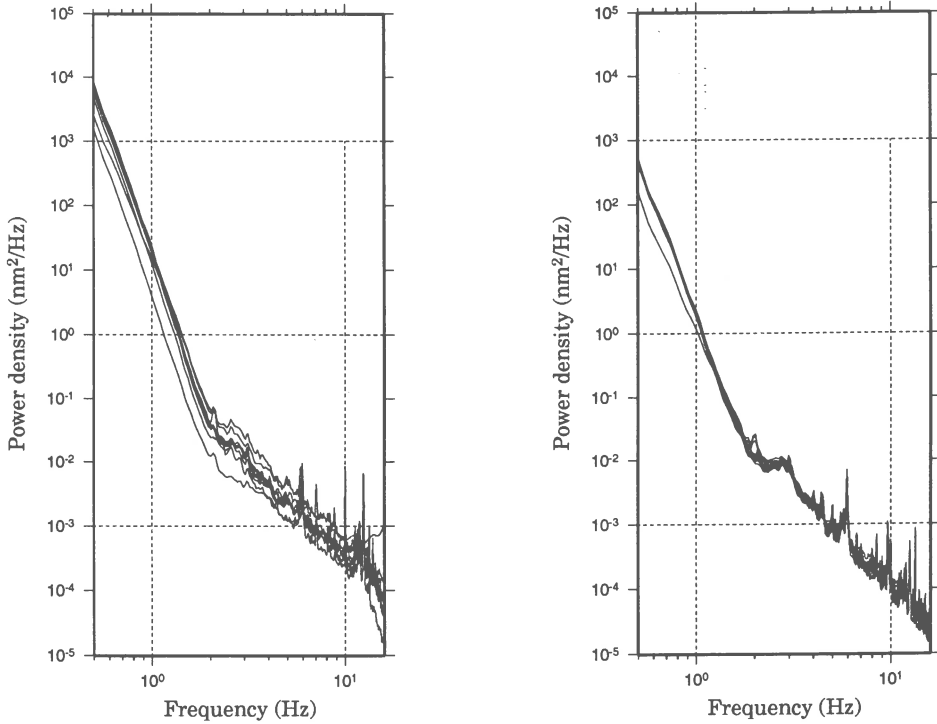
Figure 1. a) Average noise power spectra of one day from each of the substations of the old FINESA array. b) Similar picture from the upgraded FINESS array. The noise samples were 8192 samples long. The noise samples were collected every hour.

2. Temporal variation of FINESS noise

The weekly variation of noise was studied by computing spectra of 204.8s noise samples from every hour of the week. Each spectrum was compared to the average of the whole week. The diurnal variation in the ground motion power

spectra was clear in working days above 2Hz. At lower frequencies this pattern breaks, showing that below 1 Hz most of the noise is not of cultural origin. Local weather conditions have influence on the noise level between 0.5Hz and 2.0Hz (Luosto 1976). Above 2Hz the noise levels during night at working days were comparable with daytime noise levels at the weekend. The difference in diurnal variation of noise between working days and weekends is displayed in Fig. 2.

The percential variation of noise compared to average ground motion power spectrum of the corresponding time period shows that during weekends the diurnal variation is weak. Only a few hours during night have lower average noise level. During working days there is a period of high noise level between 7am and 7pm local time.
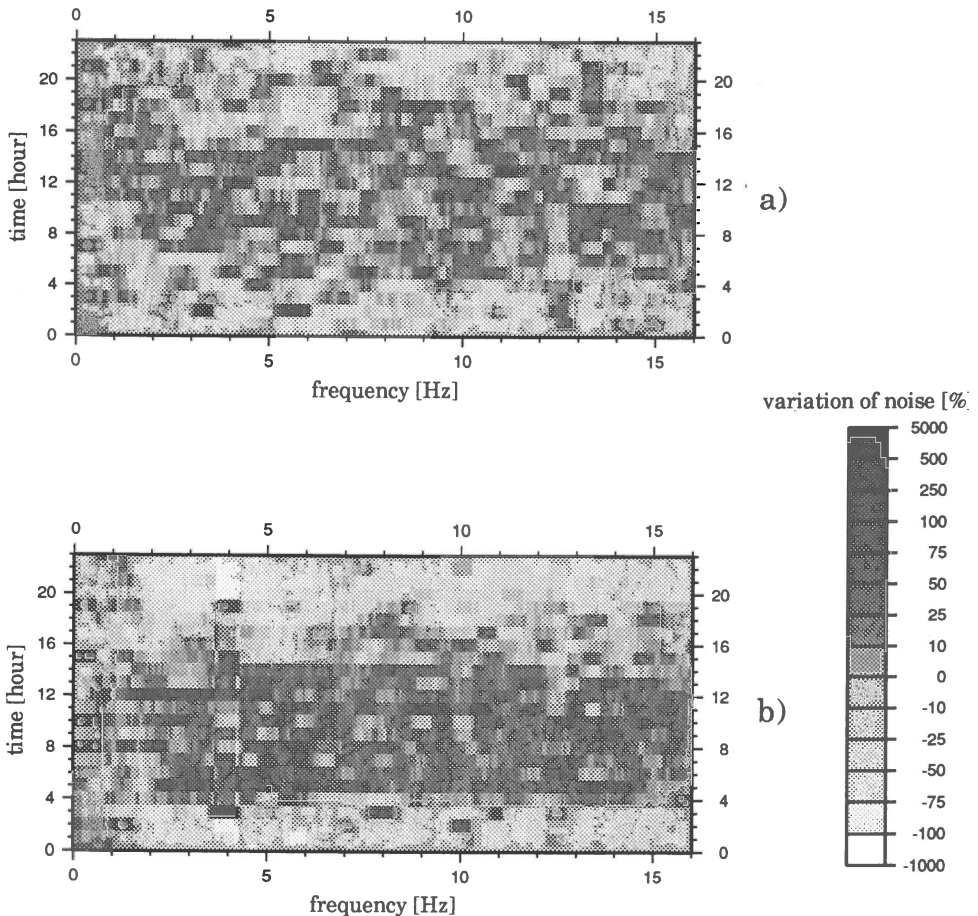
Figure 2. a) Diurnal variation of noise at 2 weekends, 28.-29. May 1994 and 18.- 19. June 1994. b) Diurnal variation of noise during working days of one week,

23.-27. May 1994. The gray shades imply percential variation of noise. The time is GMT (local time = GMT+3).
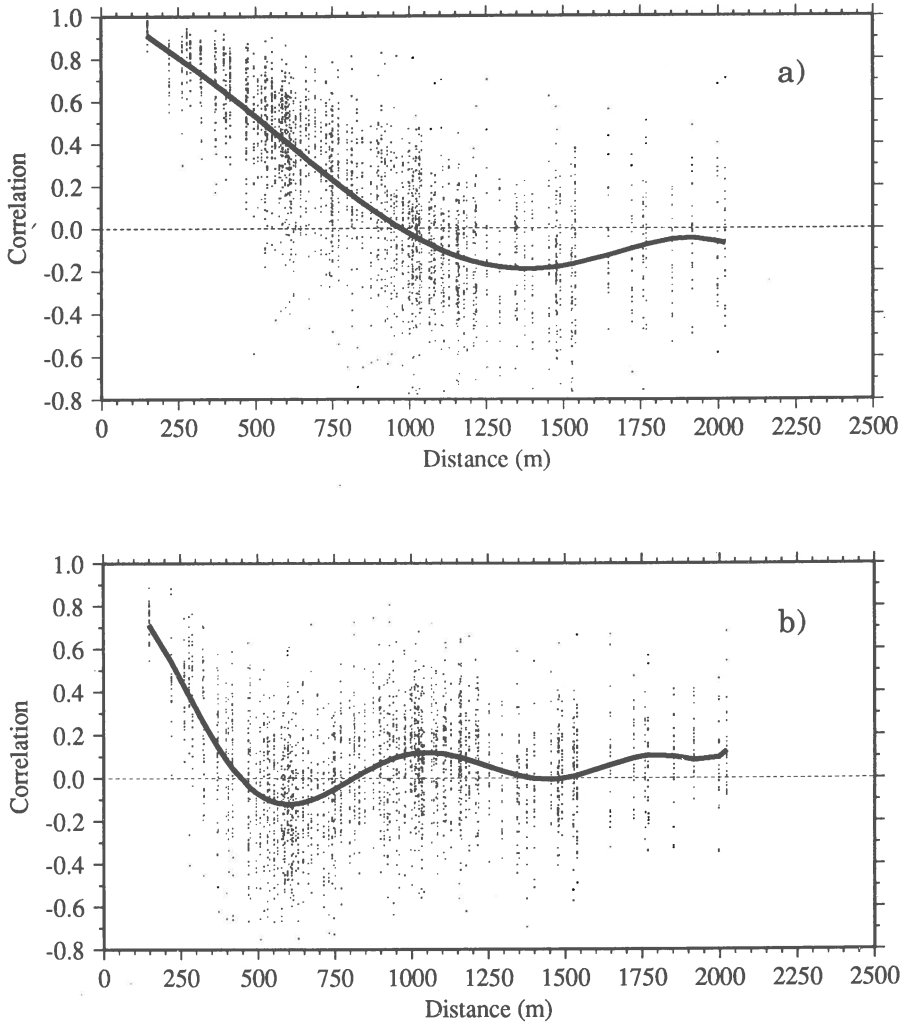
Figure 3. FINESS noise correlations versus interstation separation in meters for frequency bands 1.5Hz-2.0Hz (a) and 3.0Hz-4.0Hz (b). The frequency bands were obtained by filtering the data with very sharp finite impulse response low- and highpass filters with 255 coefficients.

3. Spatial characteristics of FINESS noise

The spatial noise characteristics have an important role in tuning the beamforming processes of an array. In theory the beamforming suppresses the incoherent noise by factor $N^{1/2}$, where N is number of substations, but different array configurations may give extra suppression in some frequency ranges. To show this cross-correlations of noise samples as function of intersensor distance were computed. The correlations have been computed with zero lag between all substations.The results show that different frequencies have minimum at different intersensor distances (Fig. 3). At frequency band from 1.5 to 2.0 Hz the minimum is at 1380m. At band from 3 to 4 Hz it is at 600m. The higher the frequency is, the shorter is the optimum distance of sensors.
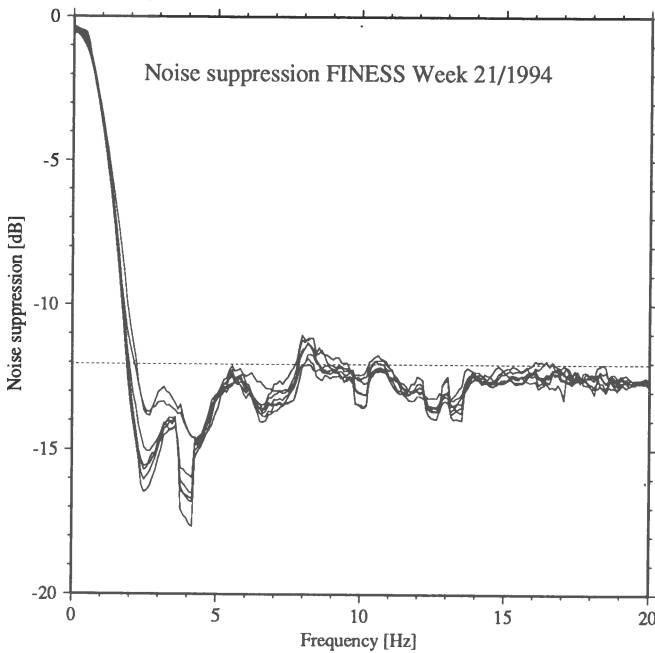
Figure 4. The noise suppression spectra computed every hour on week 21 this year for the whole array. The theoretical line 12.04 of noise suppression for 16 sensors is marked on the pictures.

Further, the noise suppression spectra were computed for different sensor configurations to reveal optimum arrangements for different frequency bands.

The noise suppression was computed as ratio of the beam power spectrum B(f) and the average of the spectra of all sensors M(f) (Mykkeltveit *et al.* 1990).

$$SUPP(f) = 10\log S(f) = 10\log B(f) - 10\log M(f)$$

In Fig. 4 there is an example of noise suppression spectra. The noise suppression goes clearly below the theoretical line between 2Hz to 5Hz, which is important area in detecting local and regional phases. Extra suppression can be gained by selecting subsets of sensors which have different average intersensor distances, though smaller number of sensors weakens the noise suppression at most of the frequency range.

Similar noise suppression spectra were computed with different array subconfigurations. Part of the sensors were omitted to produce subarrays with different average intersensor distances. The 6 instruments of C-ring with A0 at the center give strongest noise suppression below 1.8Hz. From this point to 2.7Hz the sensors of A- and C-rings give best results. At higher frequencies the whole array has strongest noise suppression. These results can be used for selecting more efficient array configurations for beamforming in the detector system of the array.
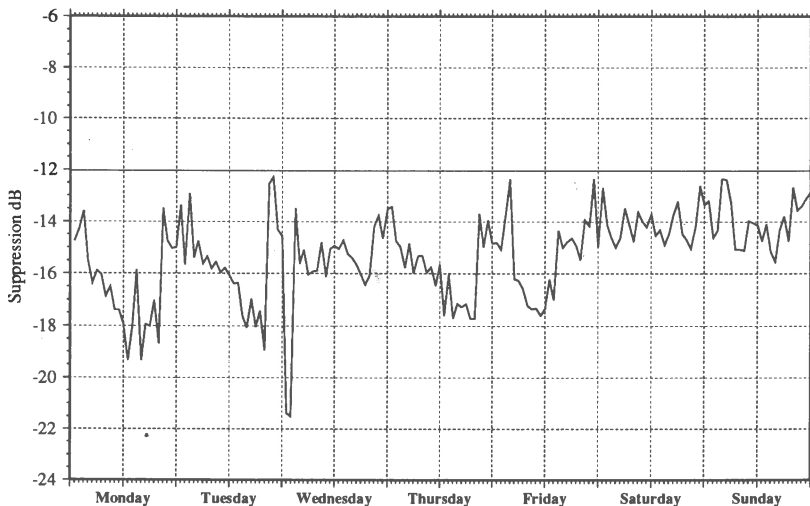
Figure 5. Maximum noise suppression for each hour of the week 21/1994. Theoretical level of noise suppression with 16 substations is marked in the picture.
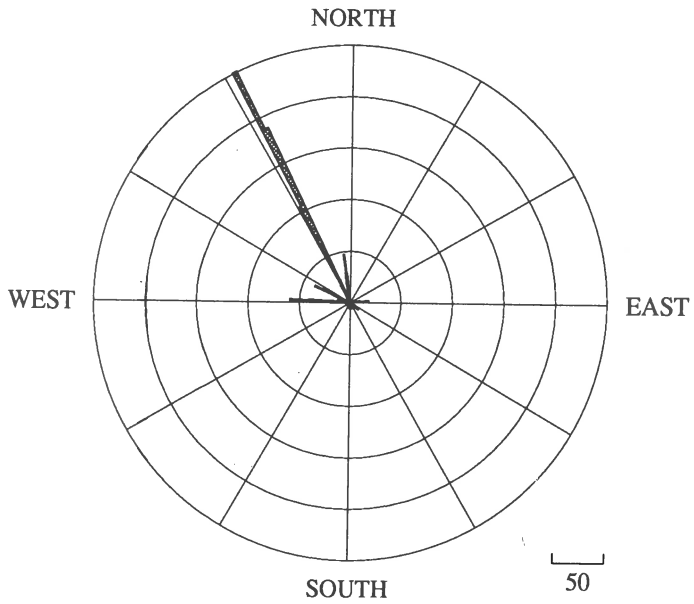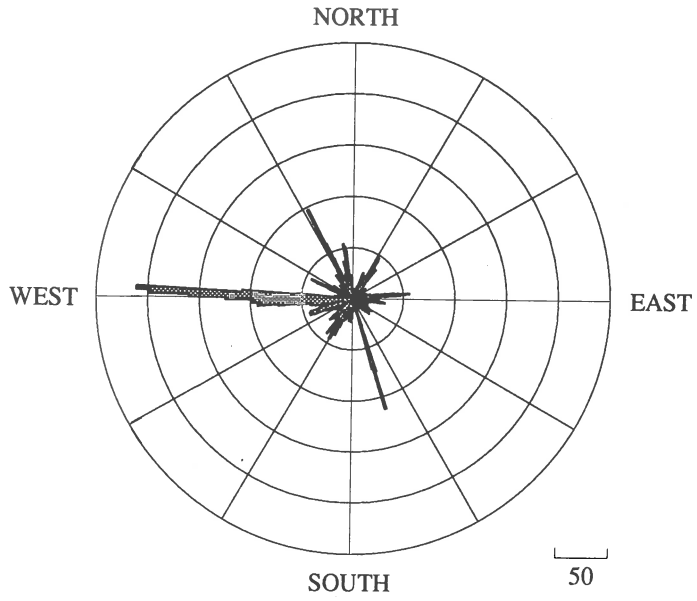
Figure 6. Azimuthal distribution of low velocity (<3.0km/h) detections from Jan-

uary to August 1994. a) Detections with coherency<0.5. b) Detections with coherency>0.5.

Some diurnal variation was observed in noise suppression levels, when maximum noise suppression from the whole frequency range was computed for one week (Fig 5.) At weekend the diurnal variation is weak. At working days both the noise suppression and the variation are much stronger. The noise suppression is stronger during working hours and it has sudden drop at midnight local time.

4. Noise detections

Human activity in the vicinity of the array has a significant role in temporal noise variations. The sources of short-term alterations in the seismic noise levels were examined by analysing the output of detector system. The noise bursts were separated from S-phases by using velocity. All detections with velocity below 3.0 km/h were collected from January to August 1994.

Two directions seemed to dominate the azimuth distribution of the detections. When the detections were divided into 2 groups according to coherency, it was found that, most of the detections from west had coherency below 0.5. (Fig. 6a) And most of the low velocity detections from northeast had coherency below 0.5. (Fig.6b)

When temporal distributions of detections from these directions were studied, it was found that most of the detections from West came during winter. It is possible that frost has amplified these bursts of noise during winter. The detections from northeasterly direction were made in February and during spring and summer. It seems that activity causing detections from this direction is not continuous. The diurnal variation showed that most of the detection were made at night. The STA/LTA ratio of the detections was relatively low so it is possible that during daytime these noise sources are embedded by cultural noise.

5. Discussion and conclusions.

The technical upgrade has strongly improved the quality of data. In the previous instalment older amplifiers and analogous line transfer caused instrumental noise, which varied from substation to substation. Now the data is uniform and average level of instrumental noise is lower.

The diurnal variation is strong during working days as expected. The difference between weekends and working days is significant. During weekends only a period of few hours after midnight local time has significantly lower noise level. The peak in noise level is in the afternoon. These characteristics suggest that most of the diurnal variation is caused by traffic during weekends. During working days there is a clear period of high noise level between 7am and 7pm local time. It is attributed both to industrial activity and heavy traffic during working hours. These diurnal alterations in noise levels are seen mostly above

2Hz. Below 1Hz diurnal variation is not observable.

In processing of array data beamforming is used for suppressing incoherent noise. Therefore, the FINESS array has superior detecting and locating capability compared to single three-component substation (Tarvainen 1994). The study of spatial noise characteristics by computing cross-correlations as a function of intersensor distance showed that some extra noise suppression compared to theoretical level can be gained. Subconfigurations of array with different average intersensor distances gave extra noise suppression in some frequency ranges though smaller number of substations reduced the suppression of incoherent noise in beamforming at most frequencies. The forming of noise suppression spectra with different array configurations confirmed these results. The capabilities of the detector system can be improved by selecting optimum array configurations for beams according to nature of phases that are sought after.

The noise detection were identified using velocity. When detections with velocity below 3.0km/h were studied, it was found that two narrow sectors dominated the azimuth distribution of these detections. The centres of these sectors were at 272° and 332°. In northerly directions there are 3 seismic stations from 70 to 120km from FINESS, but none of them have detected these bursts of noise. We think these detections are caused by some small scale industrial activity relatively close to the array. Also traffic has been considered as a possible source of these bursts of noise but the narrow azimuth distributions and temporal distribution of the detections do not support this theory. Excessive sources of low velocity noise bursts are not uncommon in vicinity of seismic stations in populated areas see e.g. Kværna (1990). Since these detections are weak, have low velocity and very sharp azimuthal distribution they are not harmful in the location process.

References

Harjes, H.-P., 1990. Design and siting of a new regional array in Central Europe. *Bull. Seism. Soc. Am.*, **80**, Part B, 1801-1817.

Korhonen H., S. Pirhonen, F. Ringdal, S. Mykkeltveit, T. Kværna, P. W. Larsen and R. Paulsen, 1987. The FINESA array and the preliminary results of data analysis, Institute of Seismology, University of Helsinki Report S-16, 70pp.

Kværna, T, 1990. Sources of short-term fluctuations in the seismic noise level at NORESS. *Phys. Earth Planet. Inter.*, **63**, 277-283.

Luosto, U., 1976. Short-period noise variations in southern Finland. *Geophysica*, **14**, 111-120.

Mykkeltveit, S., 1985. A new regional array in Norway: design work and results from analysis of data from a provisional installation, in *The VELA Program: A Twenty-Five Year Review of Basic Research, A. U. Kerr, Editor, Defence Advanced Research Projects Agency.*

Mykkeltveit, S., J. Fyen, F. Ringdal and T. Kværna, 1990. Spatial characteristics of the NORESS noise field and implications for array processing. *Phys. Earth Planet. Inter., 63, 277-283.*

Tarvainen, M., 1994. The capability of three-component substation FIA1 at local and regional distances. Comparisons with FINESA and Helsinki Bulletins. *Annali di Geofisica*, **28**, 267-285.

Uski, M., 1990. Event detection and location performance of the FINESA array in Finland. *Bull. Seism. Soc. Am.*, **80b**, 1818-1832.

THE NATURE OF SEISMOACOUSTICAL NOISE AND OF THE EVENTS REGISTERED BY OCEAN BOTTOM SEISMOGRAPHS

S.A.Boldyrev, S.M.Zverev
(Institute of Physics of the Earth, RAS, Moscow)

Abstract

General results of OBS seismological observations, undertaken by IPE, are discussed. The specific features of bottom background nois, observed by OBS in frequency range 3-25 Hz, are effected by the influence of bottom currents, and by the presence of hydro-acoustical waves in OBS records.Some attempts are suggested to promote the effectivity the OBS observations, and to use its results for seismoacustical monitoring of nearbottom processes (water currents, volcanism, hydrotermal vents and so on) and to use earthquake T-phase for theoretical and applied studies of World Ocean.

The oceanic researches using ocean bottom seismographs (OBS) need great organizing efforts and expenses. At the same time, numerous experiments with OBS have already given vast information wich are not used enough now. In the present report, an attempt is made to get a summary and to obtain a quantitative estimate of the contribution of various sources in the generation of noise back-grounds registered on different oceanic structures from the point of view of the improvement the efficiency of marine deep seismic survey and seismological studies. The typical disturbancies are discussed here along with the methods of their analysis. However, numerous phenomena of the OBS records are still unapparent for our perception because they appear to be beyond the frames of the events expected. We can suggest that it would be possible to find out an explanation, at least for several phenomena, if we enlarge the circle of problems which is being to solve with the OBS data and if we appeal to scientists of adjacent specialities for discussing the problems close to marine seismology.

Since 1970, the Institute of Physics of the Earth (IPE), Russian Academy of Sciences, carrieys out investigations with the OBS of its own design which allows one to register oscillations in a range of 3 to 25 Hz. During these 20 years, observations were held in almost 350 points of the World Ocean, with total duration exceeding 30 000 hours, mostly aimed for seismic waves observation from explosive and airgun sources by deep seismic sounding experiments. The list of publications with some results of this experiments is given at the end of article.

The influence of currents and hydroacoustical oscillations are the main conditions that the OBS work under. The most intense low-frequency
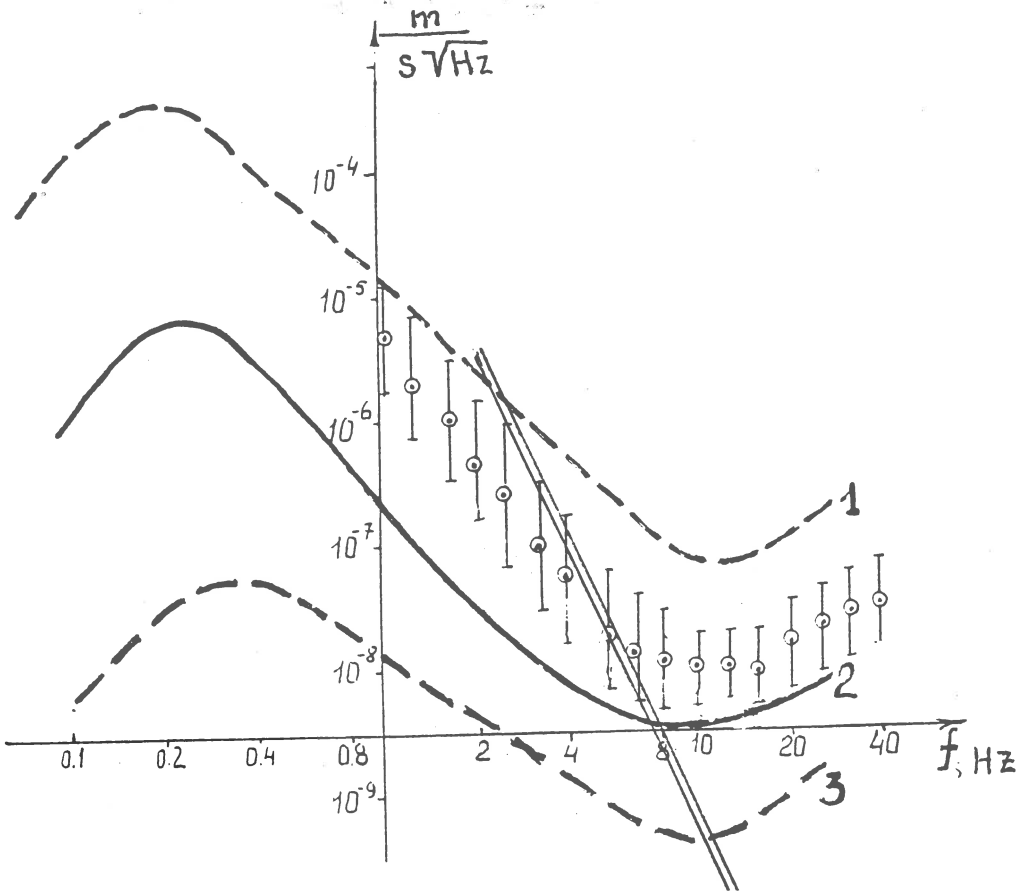
Fig.1 Seafloor noise (vertical component) spectra for the OBS-experiments of IPE and generalized world-ocean spectrum - maximal (1), average (2) and minimal (3) level [Ostrovsky, 1982]. Dubbled line shows the relative spectrum of disturbances generated by the bottom currents (IPE-data).

ДС-1

ДС-2

20dB

ДС-4
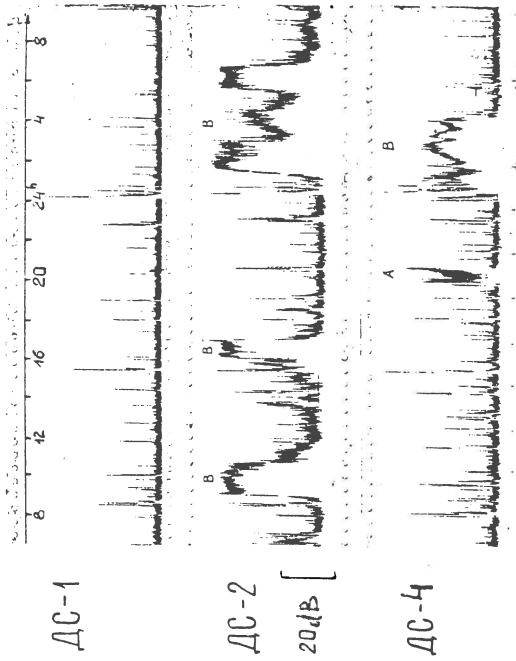
Fig.3 Fragment of seismogramms OBS (Fig.2). Short impulses are records of waves from local shocks. The long-time disturbancis type B (5-8 hours) are supposed induced by landslides in soft sedimants on bottom's slope.

Australia
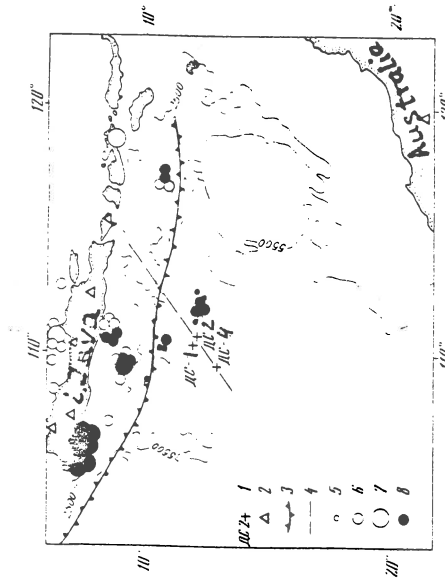
Fig.2 Location map of the Roo Rise (dotted line). The cross indicate land OBS; the circles - epicenter of earthquakes, registered by OBS. Dark circls - earthquakes, caused T-phase.

Fig.5 Variation of R-parameter of oscilations for f=8 Hz and 15 Hz depending on oscillation speed (E). Arrows shows values E of signal for R=1 ("earthquake's noise").

Fig.4 The distribution of time-interval numbers with various R-parameter (pulse-period to pulse ratio) for the various levels of amplitude seismic signal (A).

background disturbancies in the records of the OBS of our Institute design were induced by sea currents. Fig.1 shows a generalized spectrum of the oceanic bottom noise (Ostrovsky, 1982) in comparison with the averaged noise spectrum after our data as well as a relative spectrum of random noises emerging due to the currents taking place near the bottom. With the increasing frequency from 3 till 15 Hz, the intensity abates up to 30 dB per octave. The main contribution is brought by the periodic disturbances which are probability dependent on the phases of lunar-solar tides. The absence or abnormally small thickness of sediments may be an evidence of strong near-bottom currents. In tectonically activated zones, for example Roo Rise (Fig.2), large earthquakes may cause near-bottom flows accompanying landslides in soft sediments on the slopes of oceanic bottom along with the background disturbances of a kind that is shown in Fig.3 (type B).

Submarine earthquakes, as well as the P- and S-waves, often generate hydroacoustical oscillations (T-phase). Due to them, the duration of the OBS records exceeds the duration of the similar records on land. The duration depends in turn on the energy of the source and on the epicentral distance, the topographic features of the bottom in the area of origination and propagation of the signal.

In 1979, more than 1000 earthquakes were registered with OBS within the 2000-km radius area in the Roo Rise during 170 hours of observation (Fig.2). Many of these shocks generated intense hydroacoustical oscillations. The ratio of time, then signal exceed the fixed amplitude level, to the common time of observation (the R-parameter) was calculated for a series of two-hours temporal intervals that the observational period was divided into. The earthquake waves caused the bottom vibrations with frequencies up to 15 Hz whose amplitudes A exceeded 5 nm in average during 5 minutes (R=0.03, on Figure 3) while being more than 50 nm during approximately 15 seconds (R=0.002).

The dependence of the mean value of the R parameter on the intensity of seismic pulses, R(E), for frequencies of 8 and 15 Hz at the OBS site is shown in Fig.4. Within a broad dynamical range, ten to thousand nm/s, the alteration rate of the R parameter appear to be inversely proportional to the amplitude logarithm, dR=0,5/dlgE. The values of R(E) for the range of small E values where R=1 represent the noise level generated by local earthquakes. For the frequencies of 8 and 15 Hz, these values were equal to 3 and 5 nm/s, respectively, i.e. they coincide approximately with the mean value of seismic noise at the bottom. As for the signal structure recorded with a vertical seismograph in the Roo Rise, the T-phase, due to its long duration, constitutes up to 80% of the energy of oscillations registered.
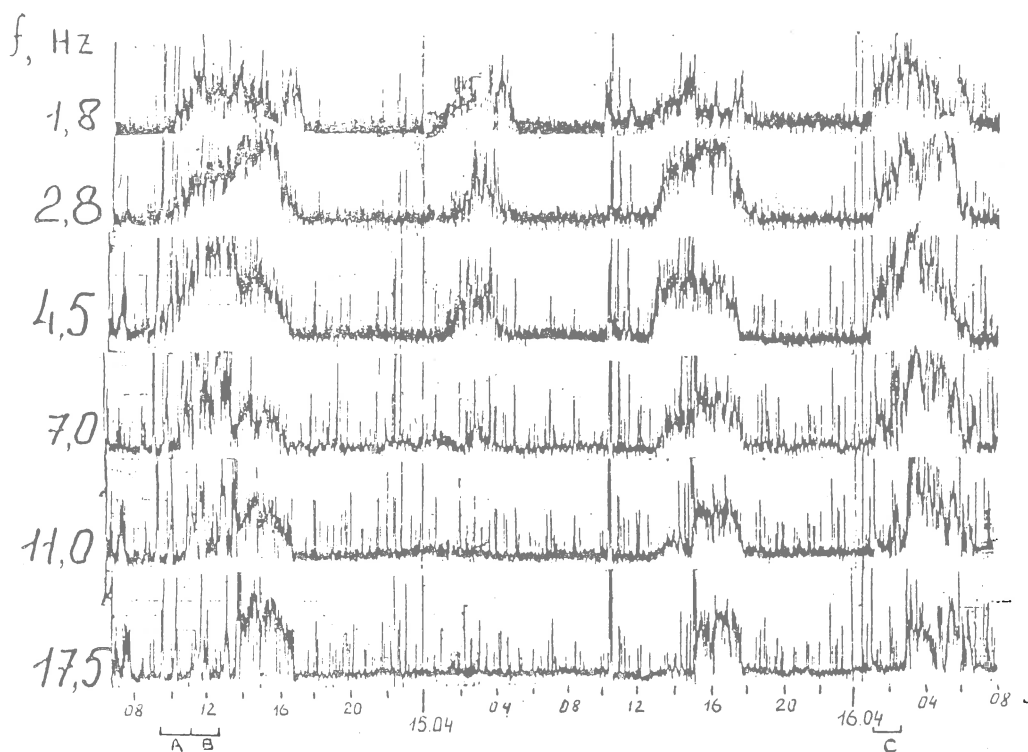
Fig.6 Bending lines of seismic noise in different frequency bands registrated by OBS at Gabon foult zone of MAR. Short impulses are records of waves from local shocks, most strong of them coincide with frequential-temporal alterations of seismoacoustical noise. Low-frequency component (1-5 Hz) predominate in the initial part of disturbances. In the final phase containance of high-frequentcy component (f>7 Hz) increases. Sources of disturbances, so as epicenters of accompaning shocks are situated in the central rise of the Gabon Fault MAR - in a neovolcanic zone.

The high seismic activity of the Roo Rise, especially in its eastern part (Fig.2), and the steepness of its slopes may evidence of intense recent vertical movements within this region. The observation with the OBS reflects not only the seismological aspect of the tectonic evolution of those structures but also the concurrent hydrological effects which we should take into account when the registering station installation. Under similar conditions, it is useful to consider the high-frequency range (f>15 Hz) when seismic studies with the controlled sources are made.

The frequency-temporal variations of the random noise registered near the neovolcanic morphostructures of Gabon foult (Mid-Atlantic Ridge) and their interconnection with the seismoacoustical waves from local earthquakes (Fig.6) are similar, in many respects, to the properties of seismic fenomena which accompany the activation of subaerial volcanic areas. The largest earthquakes precede the disturbances of the background and the alteration of its frequency composition. We assume, that it is possible to identify the nature of the random noise with the OBS groups to determine their source locations, and to estimate quantitatively the development and energy of the generating processes (particularly, those of submarine volcanoes and hydrotherms).

The peculiarities of oceanic hydroacoustical wave propagation constitute one of the main problems of the applied knowledge, and at a low-frequency range (less than 100 Hz), earthquakes seem to be unique sources of intense oscillations. The ocean water is virtually transparent for sound and the hydroacoustic oscillations propagate at long distances without noticeable attenuation. That is why the spectral-and-temporal features of the T-phase records, which emerge while the propagation of P-waves, could determine the peculiarities of the sound transformation in the bottom rocks and the dissipative properties of the lithosphere. The T-phase recording data can be used for the energy estimation of the earthquake sources and for the determination of frequency-dependent attenuation of the P-waves at the generation region of the hydroacoustical oscillations.

The peculiarities of the T-phase variation recorded by an OBS group at the epicentral distances more than 5000 km can reflect the generation and propagation conditions of the hydroacoustical oscillations.Some example is shown on Fig.8 where the experimental records are supplied by the theoretical curves 1 and 2, calculated for the cases when T-phase generated on several bottom features (see Fig.7). The times, shapes and intensities of hydroacoustic oscillation radiation in morphostructures of South Atlantic are estimated by the supposition that the coefficient of compression wave transformation from solid into a liquid is similar in both these areas. The rear front of the T-phase pulse appears as an exponent, $A(t)/A(T)=exp[k(t-T)]$. The factor "k" is equal to -0.014 and does not depend on frequency in

Fig.8 Temporal variations of T-phase levels for frequency of 3.2, 5.0 and 8.0 Hz (the curves are positioned arbitrarily on vertical). 1 and 2, fragments of the curves of T-phase calculated for various zones of radiation (see Fig.7).

Fig.7 Supposed areas of the T-phase radiation (solid lines) for the 82.03.10 earthquake. The asterisk denotes its epicenter. The arrow indicates the direction to receiver.

Fig.10 The T-phase spectra of the 82.03.10 earthquake (dash lines) and hose of background noise (solid lines) recorded by the OBS for the paths not crossing (a) and crossing (b) the MAR.

Fig.9 The MAR topography in the OBS deployment region (c) and (d) compared with the maximum amplitudes of T-phase (light circles) and background noise (dark circles) at frequences 3.2 (a) and 8.0 Hz (b).

the range of 2 to 25 Hz. It may reflect the medium quality (Q) in an epicentral area.

In the diagrams of Fig.9, there is shown the variation of the T-phase level and of the background unperturbed at two frequency components for the records of stations with different depths of installation, when the wave paths to several stations being intersecting the submarine ridge. The intensity variations of 2-20 Hz T-phase maxima and those of background correlate with the floor topography: amplitudes of both the hydroacoustic oscillations and microseismic noise increase with the elevation of floor relief (Fig.9). It allows us to suppose that the noise in frequency band studied is composed by the hydroacoustic oscillations of various origin, and its intensity depends on the nearness of a receiver to the submarine sound channel. This regularity is seen on the background of a screening influence of the Mid-Atlantic Ridge: in the right-hand branch of the graph (Fig.10) the T-phase levels vary considerably relative to those of the background contrasting with the rays crossing the MAR where the T-phase intensities are weakly differentiated. The crest areas of the MAR manifest their selves in a kind of scattering sound that may depend not solely on the complex topography of the sea floor but also on the temperature inhomogeneities of sea water above the MAR rift zone and its neovolcanic features. The definite similarity of the T-phase and noise background in the South Atlantics suggests that the seismic background at the bottom is formed due to a combination of the shipping noises, storm microseisms, and seismoacoustical random noises propagating in a fluid medium.

Waves of submarine earthquakes contribute considerably to the formation of the noise background, however, the minimum level of the seismic noise is lower in many cases than the level of oceanic own noise, and only signals from individual large earthquakes exceed this background. The studies of the bottom regions where the high efficiency in the transformation of the bottom vibrations into the hydroacoustical oscillations take place, is important not only from the point of view of comparative seismicity. It is noticed that the essential share of the oceanic shipping noises get into the sound channel due to scattering sounds by the bottom, like when the T-phase generation. Since the bottom can disturb itself on a large area during earthquakes, we can try to solve the problem of the estimation of the shipping contribution in oceanic noises with taking into account that the low-frequency noises come together from some thousand-kilometer environs.

677

The main results of earthquakes investigation by means OBS of the Institute of Physics of the Earth RAS published on the next articles (in Russian):

1. Boldyrev S.A., Spirin A.I., 1980. Study to South-Kuril earthquakes by ocean-bottom seismic stations// Vulcanologia i seismologia, No.5, P.48-60
2. Boldyrev S.A., 1981. An upper limit of sources in seismomofocal zone of kuril-kamchatka earthquakes// Isvestiya AN USSR, Fizika Zemly, N.4, P.25-32.
3. Boldyrev S.A., Kadykov I.F. 1983. Seismometric observations in the Indian Ocean by means of ocean-bottom seismograph//In: S.A.Boldyrev & S.M.Zverev (Eds.) Seismologicheskie issledovaniya Mirovogo okeana, "Nauka", Moskow, P.134-149
3. Boldyrev S.A.(Ed.), 1989. Kuril seismological experiment 1988 (KURSE-88)//Yujno-Sahalinsk, 25 p
4. Boldyrev S.A., 1993. Bottom seismological observations at Angola-Brazil geotraverse (South Atlantic)// Vulkanologia i seismologia, N 6, P.58-71.
5. Kosminskaya I.P.,Rykunov L.N.,Krasil'schikova G.A., Mihota G.G., Yarochevskaya G.A., 1977. Deep structure of earth's crust and seismicity// In: V.V.Belousov (Ed.) Iceland and mid-oceanic ridge. Structure of the bottom ocean. Moskow, "Nauka", P.50-73
6. Kadykov I.F.,1986. Acoustic of underwater earthquakes// Nauka, Moskow, 126 pp
7. Karp B.Ya., Boldyrev S.A.,1990. Soviet-Japan geophysical experiment 1990//Izvestiya AN USSR, Fizika Zemli, N.6, P.107-108
8. Zverev S.M, Akimov G.N., Novikov V.S. et al.,1978. Instruments for depth-seismic sounding and investigations of local earthquakes. In: Z.I.Aranovich (Editor) "Seismicheskie pribory", No.11, Nauka, Moskow, P.75-78
9. Zverev S.M., Yaroshevskaya G.A., Tulina Yu.V. et al., 1986. Deep-seismic sounding the undercrust lithosphere of South Atlantic// Doklady AN SSSR, 289, No.2, P.322-327
10. Zverev S.M.(Ed), 1988. Autonomous bottom seismical apparatus// VINITI, N.6857-B88, Moskow, 174 p.

Resume

General results of OBS seismological observations, undertaken by IPE, are discussed.

The specific features of bottom background nois, observed by OBS in frequency range 3-25 Hz, are effected by the influence of bottom currents, and by the presence of hydroacoustical waves in OBS records.

Some attempts are suggested to promote the effectivity the OBS observations, and to use its results for seismoacustical monitoring of nearbottom processes (water currents, volcanism, hydrotermal vents and so on) and to use earthquake T-phase for theoretical and applied studies of World Ocean.

Conclusion.

The main aim to ctudy an OBS background noise we suppose to creation the data bank, containing the data about frequency components, intencities, polarization of noise oscilations. Statistical analisys of noise space-temporal variations allow to try the zonning of ocean bottom to find he best places and times for OBS deployment, and to choose the optimal frequency band for the artifition sourses seismic experiments. The study of interrelations of the bottom noise parameters variations with the geomorphological, geological, hydrological, climatic and another fenomena allow to estimate the possible sourses of bottom noises, and to extend the possibility to use the noise for the theoretical and appliad investigations the seismoacoustical waves propagation in the real media.

PRIMARY AND SECONDARY MICROSEISMS FORMED OFF THE COAST OF NORWAY.

Jack Darbyshire

Unit for Coastal and Estuarine Studies, Marine Science Laboratories
Menai Bridge, U.K.

Abstract.

Large microseisms of the primary kind with the same frequency as the sea wave frequency and the secondary type with double the sea wave frequency have been recorded by various workers off the coast of Norway. Secondary microseisms can only be formed by the interference of of sea waves moving in opposite directions and in most of the cases cited, this could only have been brought about by coastal reflection. It is difficult to see how this can come about with a severely indented coast like that of Norway. A previous investigation has shown that though the coast is indented, the continental shelf edge is much more regular and reflection is possible here. This work is summarized in this paper and an alternative approach to estimate the microseism activity is suggested which is easier to use when dealing with coastal generation.

Primary microseisms do not need wave reflection but depend on the sea wave activity being very large over a small area and there is then an analogy with a pulse in time, with the wave number spectrum rather than the frequency spectrum being spread over a wide range which can encompass that of the ground seismic wave with the same frequency as the sea wave. An investigation along these lines shows that this effect is much more marked with the narrow steep shelf off the coast of Norway than with the broader shelf off the coasts of the British Isles.

1.Introduction.

Large microseisms of the primary kind with the same frequency as the incident waves and the secondary type with double the wave frequency have been recorded off the coast of Scandinavia by various authors, e.g. Tabulevich et al. (1990) and Bâth et al (1987). Secondary microseisms can only be formed by the interference of sea waves moving in opposite directions as shown by Longuet-Higgins (1950). In most of the cases cited this could only have been brought about by coastal reflection. At first sight, it is difficult to see how such magnitudes could be obtained with such an indented coast. A previous investigation by Darbyshire (1992) has shown, however, that the continental shelf contours for Norway, are much more regular and involve a very steep gradient so that reflection is possible. The work is summarized in this paper but an alternative approach is made to calculate the microseismic activity which is easier to apply when dealing with coastal wave interference.

Primary microseisms do not need wave reflection but depend on the sea wave activity being appreciable only over a small area. In this case there is an analogy with a pulse in the time domain with the wave number spectrum rather than the frequency spectrum being spread over a wide range which can encompass the wave number corresponding to the ground seismic wave corresponding to the frequency of the sea wave.

An investigation on these lines shows that this effect is much more marked over the narrow and steep continental shelf off Norway than is the case with the broader shelf off the British Isles.

2a. Secondary microseisms.

This part of the work has been described in more detail by Darbyshire (1992). Tabulevich et al. (1990) have shown sets of microseisms for 21-28 October 1983 recorded at many stations ranging from near the coast of Norway to 3000 km. away. They all showed similar characteristics, having a dominant period of about 7 s. By an analytical method, they were able to locate three sources which acted at different times but the first two were situated off the coast of Norway.

It was decided to investigate further and hindcast the wave directional spectra off the Norwegian coast and off the Scottish coast as shown by the squares of 300 km. side in Figure 1. For the southern square off the Norwegian coast, all the wave energy within directions 292.5° to 277.5° were taken and half the values for 315° to 277.5° and 270° to 255° and for the two northern squares the full value for 315° to 300° and half for 337.5° to 322.5° and 292.5° to 277.5°. For the Scottish coast, the straight sum of the values for 292.5° to 277.5° and 270° to 255° were taken. The energies for each period within these direction ranges were squared over the period interval desired. In the first instance only energies corresponding to periods higher than 14 seconds were considered. The values for the Scottish square and the sum of the values for the Norwegian squares are shown in Figure 2 for 22-27 October 1983 as well as the energy values for over 7 second period for the microseisms recorded at Menai Bridge, North Wales. There is a clear correspondence between the three sets,all showing two peaks of maximum activity. The activity off Norway is the more dominant at the first peak at 22-23 October whilst the activity off the Scottish coast is more dominant at 25-26 October. These results could be related to two storms at 23 and 25 October when the first gave strong winds off the Norwegian coast and the second strong winds off the Scottish coast. As would be expected, the microseisms recorded in North Wales, agreed better with the wave activity off Scotland but the first storm had an appreciable effect.

It was next decided to sum up all the energy square values for the three squares off Norway,take the square root and compare the results with the observatons given by Tabulevich et al (1990), for Pulkovo and Obinisk. These two sites were roughly equidistant from the Norwegian coast and and showed approximately equal amplitudes. The results are compared in Figure 3. The wave values have been scaled to match the observed microseism values. There is good agreement, both sets showing two maxima which are within six hours of each other.

The results shown in Figures 2 and 3 leave no doubt that the microseisms were generated off the coast of Norway. A detailed analysis of the three - dimensional wave spectra over a large area of the North Atlantic failed to show the presence of any wave activity moving in opposite directions and so the microseisms must have been caused by coastal reflection.

At first sight it is difficult to see how waves can be reflected off such a severely indented coast as that of Norway. An examination of the shelf characteristics, however, shows that off the land, the contour lines are much more regular and there is a very steep gradient beteen the contours. The contour lines for 30 and 200 metres are shown in Figure 4 and

are seen to be almost parallel to each other and to the general drift of the coast for for a large distance.

The reflection coefficient can be calculated by extending Lamb's formula (1932) for the case of a waves propagating over a discontinuity in depth, to the case of a continuously varying depth. It turns out that if x is the distance travelled by the waves from a region of constant or very large depth, c the wave velocity and k the wave number at that point, after having traversed a total distance l the reflection coefficient is given by

$$R = \int_0^l \exp(2kix)(1/2c)(dc/dx)dx \qquad (1)$$

This integral can be evaluated numerically from the bathymetric charts. The calculation was done along two transits D and C starting at 17 km. off the shore. The transit lines are within the areas of wave hindcasting. The reflection coefficients varied from 0.25 for 20 s. waves to 0.37 for 14s. waves for transit C, and for the same periods from 0.13 to 0.26 for transit D. It was decided that an overall value of 0.20 would be acceptable.

It was then possible to use the formula given by Longuet-Higgins,(1950) for microseisms caused by coastal reflection. We have

$$\delta^2/2 = [1.02 \times 10^{-15} (\Lambda/r).\Sigma a\ R^2/4]/(dT.d\theta) \qquad (2)$$

where $\delta^2/2$ m² is the variance of the microseisms, $a^2/2$ m² is the variance of the sea waves, R the reflection coefficient, Λ is the area of microseim generation , r the distance of the generating area from the point of measurement, $d\theta$ the angle range and dT the period range used in calculating the wave components.

For 23 October, 1983, $\Sigma a^2/4$ was 1.5 m , r= 1.7 x 10^6 m. (for Pulkovo and Obinisk), dT= 2s. and $d\theta=\pi/8$.

Hence $\delta^2/2 = 11.4 \times 10^{-22} R^2$ (3)

Savarenski et al (1961) gave an experimental distance decay factor , λ of 7 x 10^{-7} m^{-1} for amplitude and this has to be doubled for energy. Thus using this for a distance of 1700 km.

$$\delta^2/2 = 10.55 \times 10^{-23}\ R^2 \qquad (4)$$

The area of generation is difficult to estimate. As all the values for the three squares have been added up, only the area of one square can be taken into account. There may be, however, some effect due to the squares seaward of these. It was decided as a conservative estimate to take = 90000 km²., then taking R as 0.2

$$\delta^2/2 = 3.798 \times 10^{-13}\ m^2 \qquad (5)$$

Hence the standard deviation is
          $\delta/2 = 0.616\ \mu$ (6)

The significant height would be $3\sqrt{2}$ times this and = 2.613 μ. This somewhat lower than the value given in the previous paper. It is rather low but is of the right order of magnitude.

2b. An alternative approach to secondary microseisms.

An alternative approach to the calculation of coastal microseism intensity was suggested by Darbyshire and Okeke (1969),following Hasselmann.(1963) but applied when the depth is less than 1000m. This considers that for a case where we have interference of waves moving in opposite directions but with a slightly different period, there could be formed a long wave with the same wavelength as the ground Rayleigh wave with the mean wave period value. In the two-dimensional case, the vector wave number difference can have any direction so the ground wave activity created will be isotropic. These waves can then supply energy to the ground waves which will then increase until the energy intake is balanced by the attenuation due to damping. The coupling between the waves would not be a close one as sea waves are not self-coherent over large distances. They are in fact only highly auto-correlated over a length L_g which is of the order of two or three wavelengths. The waves in these small lengths can be considered as acting independently and if the fetch is F there would be F/L_g such contributions to the ground wave energy.

The wave activity is contained between wave periods T_1 and T_2 and angles θ_1 and θ_2 and the angular range is considered small enough for all the waves to be reflected equally.

It is possible to obtain a steady state solution to this interaction and it is assumed that this state is reached for the distances normally dealt with.

With these assumptions one can obtain a formula for the microseism variance. It has the advantage that it only requires the wave intensity at and the length of the coastal generating area along the coast.

$$\tfrac{1}{2}\delta^2 = \sum_2^1 \sum_{T_2}^{T_1} \; 0.0028 \; R^2[P(T,\theta)]^2 .2\emptyset \qquad (km.s) \qquad (7)$$

where $P[T,\theta]$ is the (wave energy)^2 contained within the period and direction intervals. In the case considered these were 2s. and $22\tfrac{1}{2}°$. $\emptyset$ is the angle subtended by the affected coastline at the point of measurement,in radians, and was $\pi/4$ in this case.

Thus

$$\tfrac{1}{2}\delta^2 = 0.0028 \times .5 \times 10^{-12} \times 1.57 = 2.198 \times 10^{-15}R^2 \qquad (8)$$

If R = 0.2, and the attenuation due to distance is .092 for a distance of 1700 km. then

$$\tfrac{1}{2}\delta^2 = 8.088 \times 10^{-18} \; km^2 = 8.088 \times 10^{-12} \; m^2 \qquad (9)$$

Hence the standard deviation $\delta/\sqrt{2} = 2.84 \; \mu$.
The significant wave height would be $3\sqrt{2}$ of this = 12.04μ.

This value is rather higher than the observed value of 9μ and shows that a lower reflection coefficient would have been sufficient.

3. Primary Microseisms.

Various investigators,such as Bâth and Kulhânek,(1987), Ostrovski and Korhonen (1990) have published results indicating the presence of strong primary microseisms in Scandinavia. Bâth and Kulhánek cite one instance where the primary peak on the spectrum is bigger than the secondary one. On the contrary, in Great Britain, as shown by Hinde and Hatley (1965), Darbyshire and Okeke, (1969) and Darbyshire (1990), the primary activity is very low,being barely above background level, the spectral energy values

683

being about 50 to 100 times less than the secondary ones

Some understanding of this effect can be obtained if we investigate the mechanism by which these primary microseisms are formed. This has been done by Darbyshire and Okeke (1969). In the secondary case, the long water wave of the same length as the ground wave is caused by interference of waves moving in opposite directions. A different mechanism occurs in the primary case. Here the wave activity off the shore starts at zero at the water-line, increases up to the breaker point and then vanishes more slowly as the bottom pressure dininished with increasing depth, being negligible at a depth of half a wavelength. The wave activity at the bottom is thus concentrated within a limited distance and we have the case of an interrupted sine wave, where the smaller the distance involved, the wider the resulting spectrum. Thus due to this effect there could be an appreciable amount of energy at the wave number corresponding to the ground wave.

In this case, the parent wave and the ground wave have the same direction and it is assumed that the pressure function is given by:

$$p/(g_w)=(\exp-\alpha x)\cos(\sigma t+k_o x) \text{ for } x>0 \tag{10}$$
$$\text{and} \qquad =(1+x/d)\{\cos(\sigma t+ k_o x)\} \text{ for } -d<x<0$$

where k_o is the sea wave number, d is the width of the breaking zone and $\alpha=\pi/d_2$ where d_2 is the distance from the breaking point to the point where the depth is more than half a wavelength. The point of breaking is taken to be the origin.

If α is $<<1/d$ then as shown by Darbyshire and Okeke (1969)

$$S_M(\sigma)=0.052(1-\cos k_o d)d^{-1}k_o^{-4}\alpha^2 g^2 \ W^2 \ S^{-2} \ S_w(\sigma) \quad \text{(km,s,units)} \tag{11}$$

where $S_M(\sigma)$ represents the microseism energy per unit frequency and $S_w(\sigma)$ represents the wave energy per unit frequency.

$S_M(\sigma)$ varies from 0 to 2, depending on the value of k_o and d and its mean value is:

$$S_M(\sigma)=0.052d^{-1}k_o^{-4}\alpha^2 g^2(\rho_w/\rho_s)^2 S_w(\sigma) \quad \text{(km,s,units)} \tag{12}$$

In the case of the Norwegian coast, values of α can be found from Figure 3 and the steepness of the coast leads to relatively high primary microseism activity. k_o the wave number depends on the period and the depth but as most of the pressure effect is concentrated near the breaking point, a close approximation can be obtained by using the value of k_o at the breaking point.

This equals $2\pi/\{T.\sqrt{(gh)}\}$ where h is the depth at breaking.
Then we have:

$$S_M(\sigma)=3.33 \times 10^{-5} \ T^4 g^4 h^2 \alpha^2(\rho_w/\rho_s)^2 S_w(\sigma) \quad \text{(km,s,units)} \tag{13}$$

Table 1 shows the results for the coast of Norway.

Table 1
Ratio of primary microseism variance to wave variance.
for the coast of Norway

Period (s)	a (km^{-1})	d_1 (km)	$S_M(\sigma)/S_W(\sigma) \times 10$
2	39.26	0.1	2.85
3	18.47	0.1	5.08
4	8.06	0.1	2.38
5	5.82	0.1	3.09
6	3.79	0.1	2.65
7	3.21	0.1	3.86
8	2.14	0.1	2.98
9	1.60	0.1	2.86
10	1.40	0.1	3.59
11	1.37	0.1	5.51
12	1.31	0.1	7.78
13	1.28	0.1	11.10
14	1.16	0.1	13.08
15 .	0.98	0.1	12.98
16	0.85	0.1	13.28
17	0.63	0.1	9.51
18	0.38	0.1	4.40
19	0.30	0.1	3.66
20	0.25	0.1	3.26

Table 2 shows the coresponding results for the area south west of Cornwall.

Table 2
Ratio of primary microseism activity to wave activity
for the western approaches.

Period	$a \times 10^2$ (km^{-1})	d	$S_M(\sigma)/S_W(\sigma) \times 10$
2	628	0.1	38.58
3	314	0.1	53.25
4	105	0.1	19.91
5	39	0.1	7.97
6	20	0.1	4.86
7	9.5	0.1	2.44
8	1.89	0.1	0.186
9	1.23	0.1	0.141
10	1.11	0.1	0.195
11	1.05	0.1	0.281
12	0.99	0.1	0.391
13	0.99	0.1	0.583
14	0.90	0.1	0.688
15	0.90	0.1	0.971
16	0.90	0.1	1.342
17	0.90	0.1	1.817
18	0.90	0.1	2.418
19	0.90	0.1	3.169
20	0.79	0.1	3.135

The values in Table 2 are three orders of magnitude less than those in
Table 1. The formula does not work too well here because there is no
uniform gradient throughout but a smaller gradient followed by a steep one
as the edge of the shelf is reached. The distances d_2 involved here are are
bigger and more likely to have reached the steady state than those in Table
1. However, the results do show that primary activity should be
considerably greater off the coast of Norway than in the western
approaches.

4.Conclusions.
The nature of the depth contours and gradients off the coast of
Norway can explain both the large secondary microseism activity and the
appreciable primary activity which has been observed in Scandinavia.

References.
(1) Bâth,M. and Kulhánek,O.,1987. Long period microseisms:Literature
    Review, Analysis of Umeá records.Rep.No.2-87,Seismological Dept.,
    Uppsala,43 pp.
(2) Darbyshire,J. and Okeke,E.O.,1969. A study of primary and secondary
    microseisms rescorded in Anglesey. Geophys. J.R. Astron.Soc.,17:63-82
(3) Darbyshire J.,1990. Analysis of twenty storms during the winter of
    1987-1988. Phys.Earth Planet.Inter.,63:181-195.
(4) Darbyshire, J.,1992. Microseisms formed off the coast of Norway.
    Phys.Earth.Planet.Inter.,73:282-289.
(5) Hinde,B. and Hatley,A., 1965. Nature,Lond.,205,1100.
(6) Hasselmann,K.,1963,Rev. Geophys.,1,177-210.
(7) Lamb H., Hydrodynamics,Cambridge Univ. Press, 1932, 738 pp.
(8) Longuet-Higgins,M.S., 1950. A theory of the origin of microseisms.
    Philos.Trans.R.Soc.London Ser. A,243:1-35.
(9) Ostrovsky,A.A. and Korhonen,H., 1990, On correlationof the energies of
    primary and secondary storm microseisms. Phys.Earth Planet.Inter.,
    63:196-208.
(10)Savarenski,E.F.,Rykonov,L.N.,Proskuryakova,T.A. and Prosvirnin,V.M.,
    1961. The influence of the Scandinavian relief on the propagation
    of microseisms. English translation in Annals of the International
    Geophysical Year, Vol 11.Pergamon,London, pp 439-444.
(11)Tabulevich,V.N.,Drugova,L.A. and Troshina,G.M.,1990. On observations
    of storm microseismic observations of the U.S.S.R. Phys Earth Planet.
    Inter.,63:209-218.

List of Figures.

Figure 1. Areas of wave hindcasting.
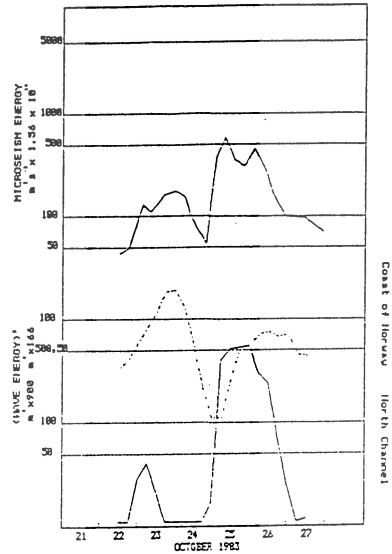
Figure 2. Comparison of
microseism and
hindcasted wave
activity. Oct.
21-27 1983
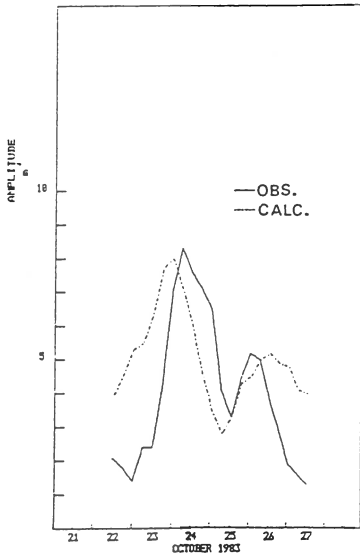
Figure 3. Comparison of
microseism and
predicted wave
amplitudes.
Oct. 21-27 1983.
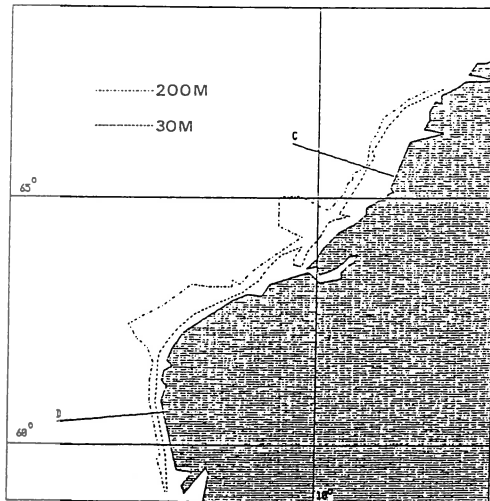
Figure 4. Depth contours off the
coast of Norway.

Synthetic Amplitude-Distance Curves of the Earth's Mantle P Waves

V. Červený, J. Janský

Institute of Geophysics, Charles University, Prague
Ke Karlovu 3, 121 16 Praha 2, Czech Republic

Abstract

The synthetic amplitude-distance curves of P waves for the PREM and IASP91 models of the Earth's mantle are studied. The amplitudes are taken from synthetic seismograms, computed by the WKBJ method. This method allows to atribute various pecularities of the amplitude-distance curves under given conditions (e.g. source depth, source-time function) to the velocity-depth distribution of a given model and thus to contribute to the better seismological understanding of the observed amplitude-distance curves. For a given model, the level and form of amplitude-distance curves of P waves depend on various factors, mainly on the depth of the source, on the prevailing period of the source-time function and on the radiation pattern. At certain range of epicentral distances, especially for shallow sources, the amplitude-distance curves have an oscillatory character. This oscillatory character is caused by the interference of various upper mantle phases. The influence of the mantle model, source depth, source-time function and radiation pattern on the synthetic amplitude-distance curves of vertical displacement of P waves is discussed.

Introduction

The synthetic amplitude-distance curves of seismic body waves propagating within the Earth's mantle have a rather complicated character. They depend not only on the structure of the mantle, but also on the characteristics of the source (depth, source-time function, radiation pattern) and on the recorded component of the seismic wave field (vertical, horizontal, transverse).

In our paper, we shall study the synthetic amplitudes of the vertical component of the displacement vector of P waves. Under the amplitude of these waves, we shall understand a maximum value of the vertical displacement component within a specified time window of the length of DT, measured from the effective first arrival. The time interval DT may be chosen in various ways, so that the amplitudes can also depend on it.

Both the PREM and IASP91 models of the Earth's mantle that we use in computations, represent the layered structure, each layer being defined by two neighbouring interfaces. Among many types of P waves that propagate in such a structure, we will consider only a selected group of elementary waves: the refracted (direct) waves that propagate from the source to the receiver without any reflection, and primary reflected waves that propagate from the source to the receiver being only once reflected upwards at its deepest point, i.e. at one of the

model interfaces.

It is obvious that several elementary waves may arrive at the receiver within the specified time window of the length *DT*. For short source-time functions, these elementary waves may be separated, at least partially. For longer source-time functions, individual elementary waves are not separated and form an interference group of waves. At different epicentral distances the number of interfering waves within the time window under consideration may be different.

In this paper we compute and discuss the amplitude-distance curves in the time domain. We compute the synthetic seismograms of the interfering wave complex and measure the maximum displacement within the chosen time window from them.

The other possibility of computation of the amplitude-distance curves, i.e. the computation in the frequency domain, has been extensively studied recently, see e.g. Duda et al. (1989), Duda and Yanovskaya (1993). In our paper we do not consider this approach.

The WKBJ method, see Chapman (1978), Dey-Sarkar and Chapman (1978), Chapman et al. (1988), that we use for the computations, is very fast and efficient and its accuracy is usually fairly high, see Chapman and Orcutt (1985). It is based on the ray expansion of the complete wave field into elementary waves. The complete WKBJ synthetic seismograms are calculated as a superposition of synthetic seismograms corresponding to individual elementary waves. The WKBJ method is especially suitable for computation in tasks of global dimensions, where some other methods, e.g. the method of finite differences, are often not practically applicable.

The amplitude-distance curves will be evaluated for different source depths, different source-time functions and radiation patterns. Such computations may contribute to the better understanding of observed amplitude-distance curves.

Comparison of some synthetic and observed amplitude-distance curves will be published in Červený and Janský (1994). Fairly good mutual similarity of their form has been found there.

Approximation of the model and the travel times

In this paper, we shall consider the 1-D, radially symmetric models PREM and IASP91 of the Earth's mantle, see Dziewonski and Anderson (1981) and Kennett and Engdahl (1991). The relevant distributions of *P* wave velocity *v* within the mantle are shown in Fig.1. In the PREM model, the velocity was changed in the depth range 0-3 km to enable the continental crust to be extended up to the surface.

The PREM mantle model contains four *P*-velocity interfaces below the Mohorovičic' discontinuity. They are situated at depths of 220km, 400km, 670km and 2891km (core-mantle boundary). The IASP91 mantle model contains three *P*-velocity interfaces below the Mohorovičic' discontinuity. They are situated at depths of 410km, 660km and 2889km. Thus, the IASP91 mantle model contains one interface less. The lack of this interface is compensated by a higher velocity gradient at corresponding depth range. The mantle interfaces as well as the depth

sections with increasing velocity gradient have an important influence on the form of amplitude-distance curves.

The computation was done using the Earth Flattening Approximation (EFA), see Müller (1977). The relation

$$z = (-1/b)\ln(v/a), \qquad (1)$$

where z denotes the depth, recomended in Chapman at al.(1988), is used for the velocity-depth distribution between individual grids.

In our computations, only elementary refracted and reflected waves are considered, i.e. we do not take in consideration e.g. reflections and conversions of P wave in the crust, the pP waves, etc.

For PREM mantle model, for sources situated below the Mohorovičic'discontinuity but above the first mantle interface at 220km, we obtain four elementary reflected waves, reflected at individual mentioned interfaces. Similarly we obtain four elementary refracted waves with minima of the ray situated between individual interfaces. Let us denote the reflected waves by letters R, and the refracted (direct) waves by letter D with an index which gives at what model layer the given wave bottoms.

Fig.1 The velocity-depth distribution of P waves in the crust and mantle of the PREM and IASP91 models.

For IASP91 mantle model, for sources situated below the Mohorovičic' discontinuity, but above the first upper mantle interface at 410km, we obtain three elementary reflected waves and three elementary refracted waves.

For the source situated below some of the mantle interfaces, certain of elementary waves do not exist. For example, for model PREM and for a source situated at the depth of 700 km, only one reflected wave ($R4=PcP$)) and one refracted (direct) wave ($D4$) exists.

Only waves that arrive in the first arrival or close to it, depending on the length of source-time function and on the chosen length DT of the time window under consideration, may contribute to the resulting amplitude-distance curve of P waves.

The reduced travel times of our elementary waves for the models PREM and IASP91 and source depth of 33km (36km for IASP91) and 500km are shown in Fig.2 for the epicentral distance range up to 5000 km. (The wave PcP, that belongs from

690

our point of view among the *P* waves, is not shown, being out
of the chosen figure frame.) Starting from certain epicentral
distance that depends on the model and source depth (e.g. from
3400km for PREM and source depth 33km), the amplitude-distance
curve is formed practically by the wave *D* from the deepest
layer only. Due to the smooth and monotonous velocity-depth
distribution in the deep mantle, the amplitude-distance curves
of *P* waves display there simple and regular behaviour up to
the beginning of the diffraction. For this reason, we
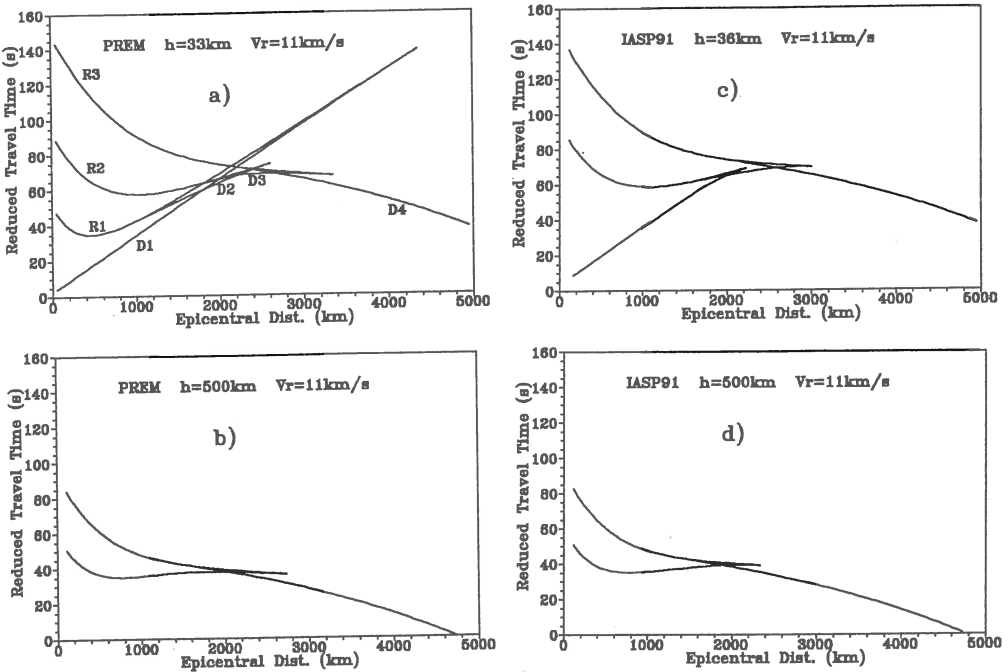
Fig.2 The reduced travel times illustrate the influence of
the model and of the source depth on the *P* elementary waves.
a), b) - model PREM, c), d) - model IASP91. *D* and *R* on Fig.2a
denote refracted (direct) and reflected waves respectively.
The indexes give the mantle layer, in which the given wave
branch (elementary wave) bottoms.

concentrate our attention to distances less than 4000km only
in further computations.

Interference effects among individual elementary waves will
play an important role mainly in such cases when at least two
elementary waves have amplitudes close to each other.

Computation of synthetic seismograms.

To evaluate the WKBJ synthetics, the computer program
WKBJ3 written by Chapman (version April 1981) is used. The
program is based on an efficient integration over the
horizontal slowness *p*. We supplemented the program WKBJ3 by
a wave attenuation algorithm, directional radiation pattern

and convolution with the source-time function.

A point source, with a symmetric isotropic radiation pattern, is considered in most of our computations in this paper, with the exception of one part, where the double-couple radiation pattern is considered. In all cases, we consider only sources situated below the Mohorovičic' discontinuity.

The source time function used in our computations is represented by a Gabor signal

$$f(t) = \exp[-(2\pi t/T)^2/\beta^2]\cos(2\pi t/T+\delta), \qquad (2)$$

with three free parameters: T (prevailing period), δ (initial phase shift), and β (relative width of the signal). The Gabor signal is non-causal, and for $\delta=0$ it is symmetric with respect to $t=0$. The computed travel time corresponds, by a definition, to the maximum of the Gaussian envelope.

The dissipation effects corresponding to the quality factors Q of the PREM model are introduced into the synthetics for both models in an approximate way, using multiplicative factor $\exp(-\pi t^*/T)$ for each elementary wave. Here t^* is given by the relation $t^* = {}_s\!\int^r (vQ)^{-1}ds$, ($v$ being the propagation velocity) and T is the prevailing period of the signal. The integral is evaluated along the ray of the elementary wave under consideration, from the source s to the receiver r. The values of v and Q, of course, vary along the ray.
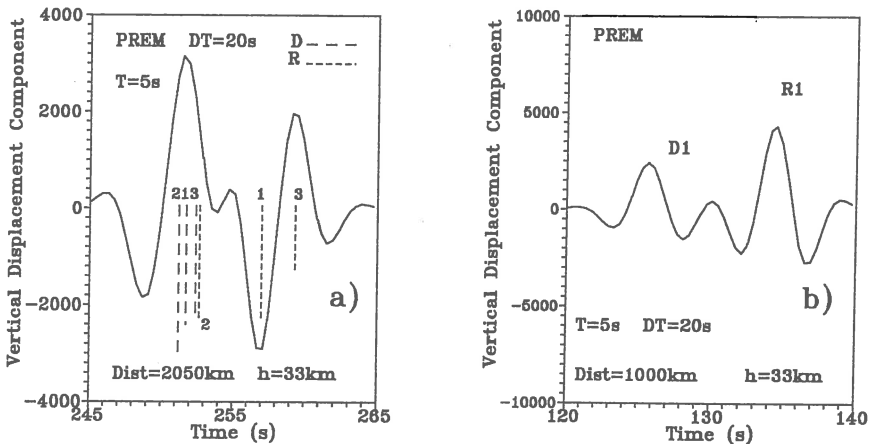
Fig.3   a) Synthetic seismogram formed by the interference of 6 P elementary waves. The dashed lines show the position and size of the maximal displacement in the individual waves.

b) Synthetic seismogram formed by 2 P elementary waves for time window DT=20s. The maximal displacement belongs to the second impulse. For smaller DT, e.g. DT=10s the maximal displacecement would be taken from the first impulse.

We shall now present two examples of synthetic seismograms. We shall consider the model PREM, a normal depth source (33 km), the source-time function (2) with the prevailing period T=5s, the width β=4 and the initial phase shift δ=0. The

length of the time window DT=20s is used.

By first example, we demonstrate the situation in which the individual elementary waves are not mutually separated and form an interference complex. We consider the receiver situated at the epicentral distance of 2050km. Three reflected wa-waves $R1$, $R2$, $R3$ and three refracted waves $D1$, $D2$, $D3$ arrive at the receiver within the time window under consideration in this case, see Fig.2. The resulting synthetic seismogram is presented on Fig.3a, where the position of the dashed lines give the arrival times, and their lengths show the amplitudes of vertical displacement of individual waves. We see that the amplitudes are rather close to each other in this case.

The second example, see Fig.3b, demonstrates the influence of the time window width. Different time window will produce different maximal displacement.

Amplitude-distance curves

In this section, we shall present the amplitude-distance curves of P waves for different situations and thus demonstrate the dependence of this curves on the model, source depth, prevailing period of the source-time function and on the source radiation pattern.

In all cases, the presented amplitudes correspond to the vertical component of the displacement, and the vertical axes in the figures display the decadic logarithm of the amplitude, not the amplitude itself.

Influence of the model

Figure 4a shows the P amplitude-distance curves for models PREM and IASP91 for the range of epicentral distances of 200 -4000km. Source depth is 33km (36km for IASP91), T=5s, DT=20s, β=4 and δ=0. The fast, but monotonous decrease of both curves at short epicentral distances is followed by significant os-cillations at epicentral distances between 1000 and 3000km.
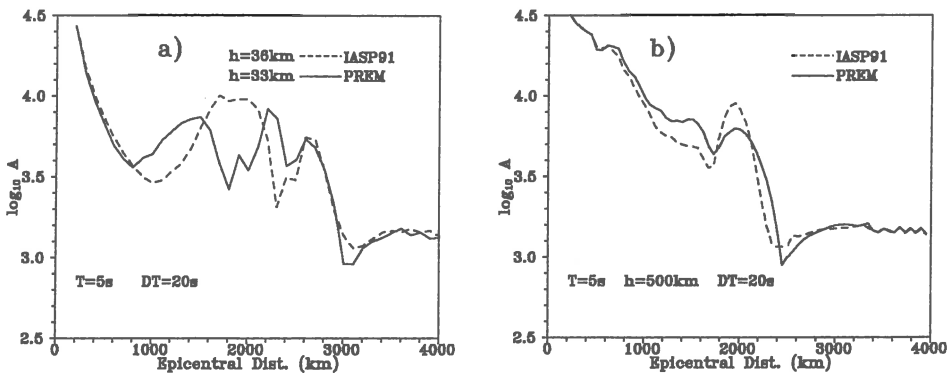
Fig.4 Comparison of synthetic amplitude-distance curves for models PREM and IASP91 for shallow a) and deep b) source. The mutual differences tend to decrease with increasing source depth.

The oscillations are caused by interference of several elementary waves (compare Fig.2). Behind the epicentral distance of about 3400km, only one refracted wave arrives inside the time window of 20s, so that the resulting amplitude-distance curves are smooth there. The difference between both amplitude-distance curves is remarkable. It is caused mainly by the absence of the discontinuity at the depth close to 200km in the IASP91 model. The first oscillation for model PREM at distance close to 1400km is due to the critical region of the wave reflected at the 220km interface. The first oscillation for model IASP91 at distance close to 1600km is due to the velocity gradient increase at the depth of 120km.

Figure 4b shows again *P* amplitude-distance curves for the PREM and IASP91 models, this time for the source depth 500km. (*T, DT, β, δ* are the same as in Fig.4a). Here the difference between both curves is not so remarkable as in Fig.4a and the number of oscillations is less because the number of generated elementary waves is less for such source depth.

Figure 5 shows how the elementary waves that bottom in individual model layers contribute to the resulting amplitude-distance curve for model IASP91, given on Fig.4a.

Fig.5 Contributions to the IASP91 amplitude-distance curve, produced by waves that bottom in individual layers of the model.

Influence of the source depth

To demonstrate the strong influence of the depth of the source on the amplitude-distance curves, we present in Fig.6 the synthetic amplitude-distance curves for three source depths, namely for 33km, 300km and 700km. The model is PREM, *T*=5s, *DT*=20s, *β*=4 and *δ*=0. We see the remarkable simplification of synthetics with increasing source depth, due to the decrease of the number of generated and hence interfering waves. The waves *D*1, *R*1 do not exist for source depth of 300km and the waves *D*1, *D*2, *D*3, *R*1, *R*2, *R*3 do not exist for the source depth of 700km.
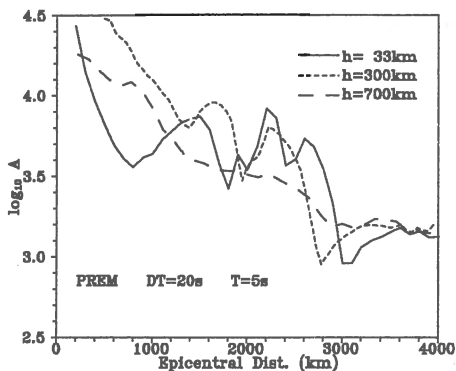
Fig.6 Synthetic amplitude-distance curves for different source depth.

Influence of the source-time function

The influence of the prevailing period T of the source-time function on the synthetic P amplitude-distance curves for model PREM is demonstrated in Fig.7a, where the periods $T=2s$ ($DT=10s$), $T=5s$ ($DT=20s$) and $T=20s$ ($DT=50s$) are considered, $h=33km$, $\beta=4$ and $\delta=0$. We see that the level of amplitudes depends on the prevailing period due to the frequency dependent attenuation. In addition, the situation in the interference region is also frequency dependent. The number of oscilations increases with decreasing period.

The influence of the prevailing period T of the source-time function on the amplitude-distance curve for IASP91 model for $T=2s$ and $T=5s$ is shown on Fig.7b for the source depth of 36km and on Fig.7c for the source depth of 500km.

The influence of other source-time function parameters, like slightly different β or δ in the Gabor signal, or the use of the Berlage signal (with the same prevailing period) on the amplitude-distance curves is less remarkable and is therefore not given here.

Fig.7 Synthetic amplitude-distance curves for models PREM a) and IASP91 b), c) for different prevailing periods T of the source-time function. The osillations simplify with increasing T.

Influence of directional radiation pattern

Additional complications in the amplitude-distance curves may be caused by the directional radiation pattern of the source. We shall give here only a simple example of this case, using the double-couple radiation pattern. Such a radiation pattern is specified by several parameters, see Aki and Richards (1980). For our computations, we have used fixed rake (90°), strike (90°) and radiation azimuth (90°) and show only the influence of two different dips, namely of 30° and 60°, on the amplitude-distance curve. The moment value for the double-

-couple radiation (the same for both dips) was chosen so that the average level of the double-couple amplitude-distance curves agree approximatly with the level of the amplitude-distance curve for symmetric isotropic radiation. Both corresponding amplitude-distance curves are compared with the curve for symmetric isotropic radiation in Fig.8. All three curves are computed for model PREM, $T=5$s, $DT=20$s, $\beta=4$ and $\delta=0$.
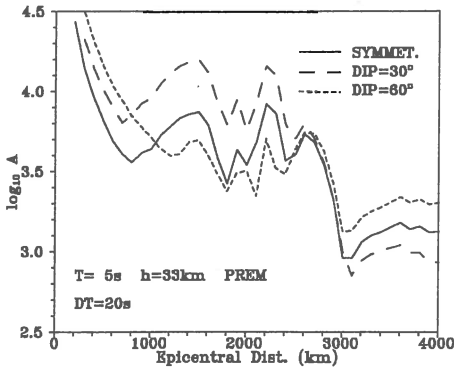
Fig.8 Comparison of synthetic amplitude-distance curves for symmetric isotropic radiation and for double couple radiation pattern for two dips, namely 30° and 60°. The rake= =90°, strike=90° and azimuth= =90° are the same for both dips

Conclusions

The computation of the amplitude-distance curves of P waves for the PREM and IASP91 models of the Earth's mantle by the WKBJ method has shown interesting results. It yields a link between various pecularities of the amplitude-distance curves and the velocity-depth distribution at depths responsible for these pecularities. In such a way, such computations increase our physical understanding of observed amplitude-distance curves.

The model structure, i.e. its velocity and Q-factor depth distributions, predestinates the basic form of amplitude-distance curves. This is demonstrated on the PREM and IASP91 Earth's mantle models. Their velocity-depth distributions differ significantly in the upper-most part of the mantle. This difference results in the different form of their amplitude-distance curves in the epicentral distance range up to 3000km. On the contrary, both models are almost identical for depths over 700km. This is reflected in practically identical amplitude-distance curves for epicentral distances over 3000 km, see Figs.1 and 4a.

The shape of the amplitude-distance curves is also considerably influenced by the source depth, prevailing period of the source-time function and by the directional radiation pattern of the source. The influence would be weaker for very simple models, without interfaces and with gentle velocity gradient decrease with depth (to prevent the generation of caustics).

Examples of amplitude-distance curves of P waves for deeper sources show (Figs.4b, 6) that the amplitude-distance curves for larger depth sources are considerably simpler than for normal depth sources. The reason is that the number of elementary waves, causing the interference oscillatory effects in the amplitude-distance curves, is decreasing with the increasing depth of the source.

The amplitude-distance curves of P waves depend also on the source-time function, especially on its prevailing period.

There are two effects related to the prevailing period. The first effect is general, but smooth. For shorter periods, the general level of amplitudes is lower due to the higher dissipation. The second effect is limited to certain range of epicentral distances, where the prevailing period of the source time function influences strongly the existing mutual interference of individual elementary waves and thereby the resulting oscillatory character of the amplitude-distance curves. This effect is most distinct for shallow sources and for epicentral distances close to 1000km - 3000km, see Fig.7.

Complex directional radiation pattern of the source can strongly influence the form of amplitude-distance curves. This is demonstrated in Fig.8, by changing the dip in the double--couple radiation pattern. Thus, the observed amplitude-distance curves for certain source regions can have their own characteristic features if some prevailing source mechanism exists there.

References

Aki, K. and P.G. Richards, 1980. Quantitative seismology. W.H. Freeman, San Francisco, 105-121.

Červený, V. and J. Janský, 1994. *P* and *PKP* amplitude-distance curves. Acta Geophysica Polonica, in press.

Chapman, C.H., 1978. A new method for computing synthetic seismograms. Geophys. J. R. Astr. Soc., 54, 481-518.

Chapman, C.H. and J.A. Orcutt, 1985. The computation of body wave synthetic seimograms in laterally homogeneous media. Rev. of Geophys., 23, 105-163.

Chapman, C.H., Chu Yen-Yi and D.G. Lynnes, 1988. The WKBJ seismogram algorithm. In: Seismological algorithms, D.J. Doornbos, Editor, Acad. Press Ltd., London, 47-74.

Dey-Sarkar, S.K. and C.H. Chapman, 1978. A simple method for the computation of body-wave seismograms. Bull. Seism. Soc. Amer., 68, 1577-1593.

Duda, S.J., T.B. Yanovskaya, E.N. Its and R. Nortmann, 1989. Preliminary reference calibrating functions for body-wave magnitudes: refracted *P*-waves. Tectonophysics, 166, 189-203.

Duda, S.J. and T.B. Yanovskaya, 1993. Spectral amplitude-distance curves for *P*-waves: effects of velocity and *Q*-distribution. Tectonophysics, 217, 255-265.

Dziewonski, A.N. and D.L. Anderson, 1981. Preliminary reference Earth model. Phys. Earth Planet. Int., 25, 297-356.

Kennett, B.L.N. and E.R. Engdahl, 1991. Traveltimes for global earthquake location and phase identification. Geophys. J. Int., 105, 429-465.

Müller, G., 1977. Earth-flattening aproximation for body waves derived from geometric ray theory - improvements, corrections and range of applicability. J.Geophys., 42, 429 -436.

CONCEPT FOR A NEW "MANUAL OF SEISMOLOGICAL OBSERVATORY PRACTICE"

By Peter Bormann

GeoForschungsZentrum Potsdam (GFZ)
Telegrafenberg A 17, D-14473 Potsdam, Germany
Department of Disaster Research

Abstract

The paper develops a concept for a new updated version of the "Manual of Seismological Observatory Practice". It should reflect - besides the still operational classical instrumentation and procedures - the significant technological and methodological changes which have taken place in the field of seismological sensors, networks, data acquisition, storage, analysis and communication since the last manual was published in 1979. It should be complemented by a concise and coherent problem-oriented and motivating introductory chapter on observatory seismology, its scientific base and rationale, its goals and requirements with respect to seismological research, seismic hazard assessment and risk mitigation and current international projects such as ISOP, GSHAP et al.. The new manual should be complemented by a comprehensive index and by annexes providing all needed basic aid materials and reference data such as seismological tables and diagrams, algorithms and programs, typical "master recordings" etc. The bulk of the new manual should not be printed as a book but rather be organized as an on-line data base comprising job-oriented self-explanatory data/instruction sheets, algorithms and programs with needed cross- and literature references. Any user with Internet access could then browse through it with key words given in the index. Others may request printouts so as to compile for themselves an easy-to-update and task-oriented loose-leaf collection of data/instruction sheets. Such a structure would enable expeditious upgrading, authorization and compilation of the new manual step by step according to priority needs as identified by IASPEI. It would also allow to better address and harmonize the different needs of both the still analog "classical" and the "modern" digital community without bothering about an all-comprising printed manual which might become too bulky or unbalanced, take too long a time to complete and be to rigid for quick updating in keeping with changing needs and practices.

Introduction

Both the Commission on Practice (CoP) of the International Association of Seismology and Physics of the Earth's Interior (IASPEI) and a workshop organized by the International Seismological Observing Period (ISOP) project have identified recently an urgent need to produce a new edition of the "Manual of Seismological Observatory Practice" (Willmore, 1979) since "... Existing documents and publications are clearly inadequate to guide routine practice in the 1990s at seismological observatories acquiring digital data" (Bergmann and Sipkin, 1993, Sipkin and Bormann, 1994). In view of this CoP decided at its Wellington meeting in January 1994 to establish a new Working Group on Manual of Seismological Observatory Practice chaired by the author and G. Choy. The meeting of the European Seismological Commission (ESC) in Athens in September 1994 was to be used for establishing an initial membership of this Working Group and for presenting first ideas on this matter at a workshop session.

The paper analyses the contents and approach of the old manual with respect to the current status, requirements and developments of observatory seismology, identifies the main user groups who should benefit from the new manual and proposes a list of contents, structure and ways of accessibility to and presentation of the information contained in it. This concept will be submitted to the XXI IUGG General Assembly in July 1995 for discussion and agreement with a broader audience and, after approval, be realized in close co-operation of the Manual WG with other working bodies of IASPEI such as the Federation of Digital Seismograph Networks (FDSN), with the IASPEI Commission on Practice and its Subcommissions on Seismogram Analysis and Interpretation, Earthquake Size, Microseisms and Reporting Standards and with the ESC Subcommissions on Data Acquisition, Theory, and Interpretation and Engineering Seismology, respectively.

Besides this, it will be indispensable for the success of such an undertaking that it is carried out in close consultation and with active support of the relevant international and regional seismological data centers. One of them would need to be identified as being the most suitable one for establishing, maintaining and continuously updating - under the guidance and auspices of IASPEI - a manual data base which should allow for free on-line access by any user.

ORIGIN, STRUCTURE AND CONTENTS OF THE OLD MANUAL

The last version of the "Manual of Seismological Observatory Practice", edited by P.L. Willmore, was published as paperback Report SE-20 by the World Data Center A for Solid Earth Geophysics in Boulder, USA, in September 1979 and reprinted in 1982. The manual arose from a resolution of the United Nations Economic and Social Council. In response to it the Committee for the Standardization of Seismographs and Seismograms of the IASPEI specified in 1963 the general requirements of such a manual as follows:
- To act as a guide for governments in setting up or running seismological networks;
- To contain all necessary information on instrumentation and procedure so as to enable stations to fulfil normal international and local functions;
- Not to contain any extensive account of the aims or methods of utilizing the seismic data, as these were in the province of existing textbooks.

The first edition of the manual along these lines, with considerable sections being already rewritten in the course of its preparation, was published in 1970 by the International Seismological Centre with the financial assistance of UNESCO. A sustained demand for copies and suggestions for new material prompted the Commission on Practice of the IASPEI in 1975 to decide the preparation of a second edition. It should also ensure a balance of representation between major Eastern and Western areas of practice. This resulted in the manual version of 1979 in which the *basic duties of seismological observatories* were envisaged as follows:
- To *maintain equipment* in continuous operation, with instruments calibrated and adjusted to conform with agreed standards;
- To *produce records* which conform with necessary standards for internal use and international exchange;
- To *undertake preliminary readings* needed to meet the immediate requirements of data reporting.

The *"final" interpretation* of seismic records was considered to be an *optional activity* for which the manual should provide some *introductory background material.* On the other hand the manual was considered to

provide also the information needed by observatory personnel when they are occasionally required to collect and classify *macroseismic observations.* In general the international team of authors "... sought to extract the most general principles from a wide range of world practice, and to outline a course of action which will be consistent with those principles."

Already at that time it became obvious that there exist significant regional differences in practice and that the subject as a whole was rapidly advancing. Since this implied the need for continuous development it was decided to make up the book in loose-leaf form and to identify chapters with descriptive code names so as to allow for easy reassembling, updating and insertion of new chapters.

Following these recommendations the 1979 version of the manual was broken down into the following main chapters:
- General introduction;
- The organization of station networks;
- Instruments;
- Station operation;
- Record content;
- The determination of earthquake parameters;
- Reporting output;
- Macroseismic observations;
- International services.

But this modern concept was only partially achieved and no updating or addition of new chapters happened after the 1979 manual edition.

MERITS AND SHORTCOMINGS OF THE OLD MANUAL

The old manual is still the most comprehensive and concise compilation of arguments, facts, formulae, data tables, diagrams and instructions relevant for classical analog seismological stations, seismogram evaluations and data reports based on mostly narrow-band seismographs with photographic or paper recordings. Therefore, for the personnel at the many stations of this type still being in operation around the world, especially in developing countries and the territories on the former Soviet Union, this manual is still a very suitable guide to observatory seismology. This is even more true when taking into account that these operators are often the only local "experts in seismology" although many of them never had a proper education in seismology. They rather graduated in a technical discipline or in physics, geology or geophysical prospection, have to specialize themselves on-the-job and to do their duty without being in direct contact with the global seismological community and up-to-date techniques or expertise.

But even for this classical user group a new edition of the manual requires upgrading and complementation. *Major shortcomings* of the 1979 edition are:
- The original concept of loose-leaf publication suitable for easy up-dating has not been realized;
- Several manual chapters mix background information, often needed for the understanding of other chapters as well, with instructions how to carry out specific tasks;
- Seismological practice related to single stations, the analysis of teleseismic events and to global data exchange is overemphasized on the expense of procedures relevant for local and regional events and network data;
- Digital seismological practice is not elaborated at all;
- The practice at seismic arrays and network centers is only marginally discussed;
- Many illustrations are now either outdated or no longer relevant;

- Representative selections of "master" recordings from standard seismographs for typical distance and depth ranges and response characteristics of seismographs are missing;
- There is no index available which would significantly ease the search for needed definitions, background information or specific instructions.
- The manual is lacking a concise but none the less comprehensive introductory chapter which could arouse the interest of station operators and seismogram analysts, stimulate their job motivation by providing the needed interdisciplinary problem awareness together with the basic background information required from the outset before any specified job can be properly executed and understood in its context and interrelatedness with others. This shortcoming is mainly due to the early decision of the IASPEI Committee that the manual *"... would not contain any extensive account of the aims or methods of utilizing the seismic data since these were in the province of existing textbooks".* Such a position is reasonable with respect to elaborations on specific research methods of using seismic records or data for the investigation of the Earth structure or of seismic source processes or with respect to earthquake statistics and hazard assessment. But such a self-limitation is in my view not appropriate with respect to the urgent need to explain also to observatory personnel the aims of such methods and how much their applicability and the reliability of their results depend on the continuity, completeness, compatibility, reliability and accuracy of seismological observatory data. Only with such an understanding of the "why", "what for" and "what happens if not" the needed motivation to execute the "tedious" daily routine work with keen interest, awareness, care and greatest precision possible can grow.

In this context we have to be aware that most textbooks in seismology are addressing either students or researchers. They are either too general or too academic/theoretical and rarely related to the needs of the routine practitioners and their professional background for *understanding the aims and requirements* of seismological data acquisition. And if they do, as Kulhaneks "Anatomy of Seismograms" (1990), they are in most cases still too limited in scope with respect to observatory duties and too expensive for station operators in developing countries.

PROPOSED CONCEPT AND CONTENTS OF THE NEW MANUAL

1. The new manual should be a rather complete and self-explanatory reference source *("cook and recipe book")* aimed at providing the necessary background information and problem awareness as well as the needed specific instructions for the self-reliant execution of any "routine" or "pre-research" job by the technical and scientific staff at seismological stations, observatories, networks, network centers or arrays in charge of analog, digital or hybrid data acquisition, processing and analysis/evaluation of original seismic recordings, of documenting and reporting seismic parameter and/or wave form data to relevant national and international agencies, data centers or the public and, occasionally, also of assessing and classifying earthquake damages. It should also cover the tasks of selecting suitable sites for both individual and network/array stations and give some guidance with respect to the appropriate design, construction, equipment and installation of such stations.

2. The new manual *should not cover* the often highly automated procedures at international seismological data centers. These normally neither record nor analyse seismic records themselves but use the parameter or waveform reports of stations or networks/arrays. Such centers typically

dispose of the expertise and the scientific-technical environment and international connections needed to execute their job self-reliantly.

3. The manual should serve, in particular, the needs of the many seismological station operators and seismogram analysts in developing or less developed smaller countries. They do often not dispose of the qualified manpower at their seismic stations/centers or of the scientific-technical expertise within the country so as to *assure that all necessary tasks can be properly executed without external guidance or help* within the scope and with the quality required for fulfilling their national and international obligations according to given standards and procedures.

4. Currently there exist analog, digital and hybrid stations with a clear trend to more and more digital ones. Therefore, *all techniques of data acquisition and processing at seismological observatories need to be covered* by the new manual.

5. Digital techniques in seismology are much more diverse and versatile, and up to now much less standardized than analog ones. Consequently, *the new manual will* necessarily *become much bulkier* if its new and broader scope as outlined in paras 1., 3. and 4. is accepted.

6. The different degree of complexity and amount of instructions, algorithms or reference data needed for the self-reliant execution of the various jobs in present-day and future observatory seismology might result in a rather *unbalanced representation* of the various topics covered by the new manual. On the other hand, it is to be expected that practically *no single user/observatory will ever need all the information* which has to be contained in the new manual because of the multitude of potential user groups and their specific requirements.

7. To produce the new manual as a book of so wide a scope would take a very long time. This would unneccessarily delay the circulation of urgently needed up-dated or new instructions for station operators and would not allow subsequent easy up-dating and complementation. It is recommended, therefore, also taking paras 4. and 5. into account, that *the bulk of the new manual should* not be published as a book but *be organized as an IASPEI authorized on-line data base* at an international data center with assured Internet access by users for consultation. Those who do not yet have an Internet connection may order outprints of the information required for the execution of their jobs.

8. In order to achieve the goals outlined above as good as possible the new manual should consist of 3 main parts:

- *Long-term manual introduction* which outlines the scope, terms of reference, philosophy and scientific-technical and social background of observatory seismology. It aims at creating the needed problem awareness and sense of responsibility with respect to the precision and reliability with which the routine tasks have to be executed and may *be produced in printed form* for all potential users. This introduction should be complemented by an extensive index to guide the search for any specific piece of information.

- Data/instruction sheets which provide under key word entries detailed definitions of terms, descriptions of specific jobs, recommended procedures, relevant algorithms and reference data as well as a guide to suitable software, e.g. such made available as IASPEI software library volumes or IASPEI shareware, together with necessary cross or literature references for further readings. These data/information sheets should be contained in the recommended manual on-line data base at world or regional seismological data centres/services. Users may browse through it with keywords as provided by the manual index. Such data/instruction sheets may be subject to more frequent changes or complementation. Therefore, they should not

become obligatory part of the printed manual introduction and guide. But, in case of missing data links to the manual data base users may request printouts of sheets relevant to their task and complement their manual themselves by a loose-leaf collection in alphabetical order of key word entries (dictionary type). This would enable a high degree of flexibility, quick and easy updating, replacement or complementation of data sheets and avoid unnecessary waste of paper and printing capacity.

- The third part of the manual should consist of annexes, providing a complete documentation of all required reference data such as travel-time tables, master event recordings etc. which are too bulky to be included into the introductory part or an individual data sheet or which need to be referred to in several manual chapters or data sheets. Also these annexes could be consulted via on-line access to the data base or their content be copied to user computers for integration into application programs or be provided as printouts to users who do not yet avail of these possibilities.

9. For the printed manual introduction and guide the following list of contents is proposed:
- Preface
- Objectives, scope and requirements of seismological observatory practice
- Seismic waves and Earth models
- Seismic source processes and parameters
- Seismic noise and signal-to-noise improvement
- Seismographs: principles, theory, calibration and parameter determination
- Seismological stations, networks and arrays: site selection, installation, equipment and configuration
- Recording, handling and storage of analog data
- Acquisition, preprocessing, handling and storage of digital data
- Routine analysis of analogue seismological recordings
- Routine analysis of digital seismological recordings
- Reporting outputs and data exchange
- Macroseismic observations
- Index

PROPOSED PROCEDURES AND SCHEDULE OF WORK

Phase A

It comprises the time span from the XXIV General Assembly of the ESC in Athens and the XXI General Assembly of the IUGG at Boulder. At the Athens meeting some of the basic ideas of the general concept and several specific topical proposals with respect to the scope, contents and structure of the new manual were discussed for the first time and several European colleagues showed interest in joining the project. At the same time scepticism was voiced, especially from colleagues involved in digital seismological data acquisition and analysis and their automation, whether the drafting of a new manual was meaningful and managable at all if it was to include digital practices and formats as well. The latter were still so diverse, often not yet well understood or compatible and not suitable or not yet ripe for global standardization. As a result of these discussions the modified concept presented here was drafted. It will be circulated amongst those who have already indicated their interest in contributing to the IASPEI WG "Manual of Seismological Observatory Practice" but also amongst the chairmen and active members of all working bodies of IASPEI and the ESC which are relevant for seismological observatory practice. Their comments and proposals with respect to this preliminary draft are kindly invited.

As a next step in this first phase a meeting of the Manual WG is planned at the XXI IUGG General Assembly in Boulder. It will be open to anybody interested in this task. The meeting aimes at getting a feedback on this draft concept, at agreeing on the principal philosophy and structure of the manual and on matters/instructions of urgency which should be dealt with first. Complementary to this, all working bodies of IASPEI with competence in any important subject to be addressed by the new manual should be invited by the Secretary General of IASPEI and by the chairman of the IASPEI Commission on Practice to comment on this draft, to identify priority issues from their point of view and to propose manual chapters or data/instruction sheets for which they see fit to elaborate drafts.

Parallel to this the chairman of CoP might investigate prior to the Boulder meeting whether the WDC A, which was responsible for issueing the last versions of old the manual, would be prepared to establish and maintain the proposed on-line manual data base. On the basis of these general discussions and clarifications the CoP should at decide or recommend at the Boulder meeting:
- whether or not the here proposed, or a modified concept for a new manual should be pursued;
- which priority items should be dealt with first;
- what key subjects should be taken up by which SCs and WGs of CoP in consultation and close co-operation with the Manual WG;
- which other working bodies of IASPEI, besides those of CoP, should be invited to join in this effort of producing a new manual under the auspices of IASPEI;
- whether the matter of producing the manual, authorizing it and keeping it constantly up-to-date in accordance with changing needs and developments should be considered a permanent obligation of CoP in the future.

Phase B

When these points have been clarified and respective decisions/recommendations have been made, the real working phase on the manual itself can start. It is proposed that the author, in collaboration with other members of the working group as formed at the Boulder meeting, prepares - on the basis of the old manual, of more recent training materials as published for the annual international Potsdam training courses on seismological practice and of other drafts related to specific items of the manual (e.g. Musson et al., 1994) - a *first preliminary draft* for the introductory part of the manual together with an index. This may be complemented by drafts of some closely related topical data/information sheets which could later serve as models for other sheets.

These drafts should be circulated amongst European and other interested seismologists prior to the XXV General Assembly of the ESC in Reykjavik, Iceland, September 1996, requesting comments, changes and additions as well as complementary or alternative draft proposals to be presented at a manual workshop in Reykjavik. The author would then compile, on the basis of these various proposals, a second preliminary draft for world-wide circulation within the seismological observatory and data center community prior to the XXIX General Assembly of IASPEI at Thessaloniki in Greece, 1997. If the work proceeds well, the introductory part to the new manual might be ready for approval already at this meeting and could be prepared for publication afterwards.

In the time span between the Boulder and Thessaloniki meetings of IASPEI it should already be possible to arrange at the WDC A or elsewhere the data annexes of the on-line manual data base in a format suitable for access and

use by observatory personnel. Additionally, data/instruction sheets should be drafted for topics which CoP might consider to be of high priority. This could be the case, e.g., with respect to the notification, analysis, measurement protocols and the ways of analysis and reporting of ISOP events (Bergman and Sipkin, 1994). But it may also concern general instructions with respect to new kinds or formats of parameter and wave form reports to seismological data centers. These might soon become necessary in connection with new hardware and routines currently being introduced at the National Earthquake Information Center (NEIC) at Boulder.

Additionally, there are several other topics relevant to the manual where during the last few years major progress was made and a high degree of international consensus has been reached already. This applies, e.g., to the practice of analysing and classifying macroseismic observations. Recently, the Working Group on Macroseismic Scales of the ESC, has produced a very well documented new European Macroseismic Scale 1992 (Grünthal 1993). It is a significantly up-dated and complemented version of the MSK scale in which - for the first time - the usage of the macroseismic scale is made explicit. This reduces the chances of wrong intensity assignment through misunderstanding of procedures. Meanwhile it has been widely circulated and tested under different conditions and aspects. Its application has also yielded many new experiences with respect to the relationship between macroseismic and instrumental earthquake parameters such as the location of earthquake epicenters. A partially revised and further improved final version will be presented at the forthcoming Eleventh World Conference on Earthquake Engineering in Acapulco, June 1996. It is recommended that this version becomes part of the new manual. Musson et al. (1994) have already made well founded detailed proposals with respect to the reorganization and new contents of the respective chapters and sections in the manual. Therefore, this redrafting could be accomplished as well within the second phase until 1997.

Phase C

This third phase, stretching from 1997 to 1999, should aim at completing the manual by finishing the bulk of its data/instruction sheets, by integrating them into the manual data base, by arranging for the full on-line access of users and by issueing sets of related printouts to users without Internet connection.

Phase D

This *long-term follow-up phase* consists of continuous maintaining, up-dating and complementing of the on-line manual data base under the supervision and with the authorization of the IASPEI Commission on Practice. In order to ease this task, for each data item, instruction sheet or chapter the names of responsible author(s) should be given together with their address, e-mail, fax and phone numbers. This would allow users to approach the author(s) for clarifications or more detailed information if needed. Additionally, it would enable other colleagues to send comments, corrections, amendments or alternative versions to the author(s) and IASPEI for consideration and, if necessary, for inclusion into the data base after harmonization with other entries and authorization by IASPEI. This kind of easy and direct feed-back from users at observatories and from the wider seismological community would enable to keep the manual always up-to-date.

CONCLUSIONS

A "Manual of Seismological Observatory Practice" is an essential aid and guide for the qualification and international harmonization of seismological practice. Since the last issue of such a manual in 1979 seismological practice has been revolutionized in many aspects, especially by the large-scale introduction of digital data aquisition and processing techniques. Nowadays, triaxial broad-band recordings of very large dynamic range allow to replace whole complexes of classical seismographs working in different frequency and sensitivity ranges by just one instrument. On the other hand, telemetred station networks may reduce the tasks of data acquisition, processing, analysis and archiving in a given country to one or only a few central station(s). Additionally, quite a number of small-scale regional seismic arrays have been put into routine practice in recent years . They apply rather different procedures of data processing and analysis, produce very useful complementary data and allow the detection of rather week events or the discrimination and identification of seismic phases which are not well defined in classical records.

Besides this, more and more nations complement their networks of permanent seismic stations by digital mobil systems for seismic data acquisition which often have to be deployed or their data be analysed by the same personnel working with the permanent seismic networks. These developments necessitate - and at the same time enable - significant changes in the kind of data to be reported to the global and regional seismological data centers, in the procedures applied and data products produced.

All these new aspects, techniques and methods are not yet or not sufficiently reflected in the old manual. The production of a new manual under the auspices of IASPEI is considered, therefore, as a matter of high priority. The paper proposes both a new list of contents as well as a new structure and format for this new manual. It should be organized as an on-line data base and be accessible by any user via Internet.

It is proposed to realize this task as a joint effort of all relevant working bodies of the IASPEI and ESC under the guidance of the IASPEI Commission on Practice and its WG on Manual of Seismological Observatory Practice. The work should be accomplished in three phases between 1995 and 1999 according to the general decisions taken and the priorities set by IASPEI at the XXI General Assembly of the IUGG at Boulder in 1995. After the establishment of the on-line manual data base its maintenance, up-grading, up-dating and completion in accordance with changing needs and possibilities of seismological observatory practice and the requirements of international data exchange and co-operation should be considered as a permanent obligation of the IASPEI Commission on Practice.

REFERENCES

Bergman, E.A. and S.A. Sipkin, 1993. Measurement protocols for routine analysis of digital seismic data. Paper produced at the workshop "Measurement Protocols for Routine Analysis of Digital Data" organized by the International Seismological Observing Period (ISOP) project and the IASPEI Commission on Practice, Golden, Colorado, 29 Nov.- 01 Dec. 1993, 8 pp., also contained as Annex 3 in Sipkin and Bormann, 1994.

Grünthal, G. (Ed.), 1993. European Macroseismic Scale 1992 (up-dated MSK-scale). Conseil de L'Europe Cahiers du Centre Européen de Géodynamique et de Séismologie, Vol. 7, Luxembourg, 79 pp.

Kulhánek, O., 1990. Anatomy of seismograms. Developments in Solid Earth Geophysics Vol. 18, Elsevier, Amsterdam-Oxford-New York-Tokyo, 178 pp.

Musson, R.M.W., G. Grünthal and M. Stucchi, 1994. Modern macroseismic practice: Recommendations for updating the manual of seismological observatory practice. Paper presented at the XXIV General Assembly of the European Seismological Commission, Session SC-B6, Athens, 19-24 September 1994, 7 pp.

Sipkin, S.A. and P. Bormann, 1994. Memorandum and minutes of the Commission on Prac-Practice meeting of IASPEI on 18 Jan. 1994 at Wellington, New Zealand. Issued in Denver, 11 April 1994

Willmore, P.L. (Ed.), 1979. Manual of Seismological Observatory Practice. Report SE - 20, World Data Center A for Solid Earth Geophysics, Boulder, 165 pp.

MODERN MACROSEISMIC PRACTICE: RECOMMENDATIONS FOR UPDATING THE MANUAL OF SEISMOLOGICAL OBSERVATORY PRACTICE

R.M.W. Musson [1], G. Grünthal [2] and M. Stucchi [3]

1 British Geological Survey
West Mains Road
Edinburgh EH9 3LA
UK

2 GeoForschungsZentrum Potsdam, Dept 1
Telegrafenberg A 17
D - 14473 Potsdam
Germany

3 Consiglio Nazionale delle Ricerche - Istituto di Ricerca sul Rischio Sismico
Via Ampère 56
I - 20131 Milano
Italy

ABSTRACT

In the fifteen years since the Manual of Seismological Observatory Practice was published, there have been significant advances in macroseismic methods as well as in methods of recording and interpreting instrumental data. In the first case it is necessary to report the further development of intensity scales, especially the latest version of the MSK scale (1992), now known as the European Macroseismic Scale (EMS). This scale breaks new ground in that for the first time the usage of the scale is made explicit, thus reducing the chances of wrong intensity assignment through misunderstanding of procedures.

In the second case, there is a considerable amount of new experience in the application of macroseismic data to specific problems, such as equivalences between macroseismic data and other earthquake parameters, including the location of earthquake epicentres from macroseismic data, and this should be reflected in an updating of the appropriate sections of the Manual.

INTRODUCTION

The Manual of Seismological Observatory Practice was first published in 1979 under the editorship of Willmore (1979). On account of the considerable developments in seismological techniques in the following fifteen years, a revision is now necessary. The advances that spring to mind most readily are the considerable changes in instrumental monitoring from the days of paper chart recorders to the latest radio-telemetered digital broadband networks. However, although macroseismic investigations are less driven by technology and are an older method of study altogether, there have been advances in this field as well, and the macroseismic section of the Manual of Seismological Observatory Practice needs updating as well. The purpose of this paper is to offer some suggestions in this regard, dealing with a topic at a time, following the original section layout, which had

three main divisions: 1. Definitions of intensity; 2. The organisation of macroseismic observation; 3. Isoseismal maps. This layout of the chapter is not the best, however, and we conclude with a suggestion for a revised order of contents which we believe to be more pertinent and logical.

DEFINITIONS OF INTENSITY

1 - Intensity

The definition of intensity given in the Manual of Seismological Observatory Practice is "a measure of the effect of an earthquake upon natural objects, artificial structures, and human observers in a given locality". We prefer the definition given in the EMS scale: "a classification of the severity of the ground shaking on the basis of observed effects in a limited area" (Grunthal 1993). The use of the word "classification" is more precise since no measuring, in the same sense as instrumental measuring, is actually done. Various attempts to produce an "intensity meter" have never succeeded.

1.1 - Intensity scales

There have been various revisions to the two major intensity scales since 1979. The so-called Modified Mercalli scale (actually based on Sieberg's scale of 1912), since its 1956 edition prepared by Richter (1958), has been further revised by Eiby (1965), Brazee (1978), Principia (1982), NZSEE (1991) and Dengler and McPherson (1993), although none of these modifications have attained the status of a standard, except perhaps that of Eiby on a regional basis. That of Brazee has been used more widely, but many studies continue to use the 1956 version or even the two 1931 versions (Wood and Neumann 1931). Further revisions may be planned (Algermissen 1993 pers. comm.).

The MSK intensity scale underwent minor revision in 1981 (Ad-hoc Panel 1981) and a complete overhaul in 1992 (Grunthal 1993), including a name change to European Macroseismic Scale (EMS). This new version is radically different from all previous intensity scales in its approach. In addition to the tradional list of diagnostics (the "core scale") there are a number of additional modules or annexes to give further guidance to the user. As well as a series of guidelines on the basic application of the scale, there are sections of illustrative photographs and drawings to demonstrate damage types, worked examples, a discussion of the application to buildings with anti-seismic design features, and a new approach to building type (in which building condition is explicitly taken into account) and effects on nature.

There is quite inadequate discussion in the Manual of Seismological Observatory Practice at present in *how to actually use an intensity scale to assign an intensity*. The guidelines and examples laid out in the EMS are, so far as we know, the first time that this topic has been fully discussed in the literature. Some of this discussion should certainly be carried over into the new Manual.

1.1.1 Modified Mercalli Intensity Scale of 1956

Until a new standard version of this scale is produced, the 1956 text remains the best.

1.1.2 MSK Intensity Scale (1964)
This should be replaced by the core scale from the European Macroseismic Scale.

1.1.3 Accuracy of assessment
The existing text in the Manual of Seismological Observatory Practice is over-optimistic about the accuracy that can be obtained. It is greatly to be doubted whether greater accuracy than one degree can be defined or obtained. If it were possible to distinguish in the field an intensity between, say, 5 and 6, then it would be necessary to define in the scale a description of intensity 5½. In effect, one posits the existence of a 23-degree intensity scale, which could never be written. The division of the MM/MSK/EMS scales into twelve degrees reflects the smallest changes in shaking severity that can practically be distinguished with good observational data. Where the data are less good, it is often necessary to express intensity as a range. The expression "5-6" (or "V-VI"; the use of Roman numerals is optional) is best considered as meaning that the intensity was 5 or 6, or, in a wider sense, more than 4 and less than 7. This subject is discussed at length in the EMS guidelines.

1.1.4 Equivalence between scales
It is rightly pointed out by Ambraseys et al (1983) that translating numbers from one intensity scale to another cannot be done in a reliable manner, particularly (in our opinion) in view of the different ways in which scales have been implemented by different workers (who may have had different definitions of intensity in mind). It is therefore preferable to return to the original data. If conversion is unavoidable, the table given in the Manual of Seismological Observatory Practice is as good as any, but could do with some minor modifications, particularly with regard to which scales are represented.

1.2 Relationship between intensity and earth-motion parameters
This section needs to be updated to take into account more recent work. It should also be more cautiously worded. The correlation between intensity and peak ground acceleration is extremely poor for several reasons (eg the duration of strong shaking has a major impact on the level of damage observed) and shows a scatter of two orders of magnitude. Recently observed extremely high peak accelerations, approaching and even exceeding 2g, have not been accompanied by correspondingly high intensities. More sophisticated approaches to the subject other than simple equivalences are now being sought.

THE ORGANISATION OF MACROSEISMIC OBSERVATIONS
2.1 Earthquake questionnaires
In the Manual of Seismological Observatory Practice three different sample questionnaires are given, but there is little discussion of questionnaire design. This a subject that has been studied in depth in the social sciences, but most seismologists have no contact with this literature. Some points need to be made, for instance:

i) The form a questionnaire takes is partly predicated by its intended recipient. Cultural factors come into play. In some countries there exist local officials who are able to fill in a questionnaire on behalf on a whole community; in other countries it is necessary to address questionnaires to private individuals who will

710

answer for themselves only. The amount and form of detail given to damage reports will vary to reflect regional seismicity and local construction types.

ii) Questionnaires that consist of a number of boxes to be ticked are easy to process, but data may be distorted or lost if the options given to the respondent do not match his or her actual experience. Textual descriptions attached to the questionnaire can help.

For about five years a collection of different macroseismic questionnaire designs has been made by the Seismological Survey of Slovenia (Cecic 1989) which could be drawn upon for examples of more recent questionnaires in use than those presented in the Manual of Seismological Observatory Practice.

2.2 Local emergency procedure

This section needs to be made more generally applicable. What, for instance, is meant by "central office"? The issues covered here go largely beyond matters of macroseismic procedures and are thus beyond the scope of this paper. What is perhaps intended, or at least would be an improvement, would be a discussion of macroseismic field investigations and damage surveys *per se*. The use of questionnaires is generally only applicable for intensities up to 6; beyond this it is really advisable to investigate the earthquake damage in the field.

2.3 UNESCO emergency missions

This section is similarly beyond the scope of this paper. Its relevance to observatory practice may be questioned.

ISOSEISMAL MAPS

3.1 Smoothing the data

This aspect of macroseismic practice is given very brief coverage, which should be expanded. One fundamental point that is missing is that one should not, ideally, assign intensity for each individual observation received, but for a place (eg a town or village) one should assign one intensity value on the basis of all the data for that place. Certainly this is the intention behind the MSK and EMS scales. These issues are discussed at some length in the guide to the EMS scale, and some of this discussion could profitably be brought forward into a revised Manual of Seismological Observatory Practice.

The drawing of isoseismal maps is a practice that varies very much from worker to worker, and to date there is no single technique to be regarded as standard or correct (Cecic 1992). An isoseismal map is different from other types of contour map in that it is not directly an expression of a continuous surface. For this reason, the attempts that have been made so far to use automatic contouring programs to produce isoseismal maps have not been very successful. Some of the problems involved with applying trend surface analysis to macroseismic data are discussed by de Rubeis et al (1992). Other problems regarding the reliability of isoseismal maps are discussed by Berardi et al (1990).

An isoseismal is a line enclosing an area within which the intensity is predominantly the same value. The word "predominantly" is open to interpretation, and isoseismals can be smoothed to a greater or lesser degree according to individual taste in the amount to which re-entrants and outliers are to be accepted.

This degree of variation in practice is actually quite acceptable, since it has a functional dimension. The degree of complexity desirable in an isoseismal map varies with the purpose for which it will be used. If it is to be used towards microzonation studies, complexity, to show small-scale intensity variations with local geology, is desirable as long as the data are good enough to maintain it. If the purpose is to study attenuation, then isoseismals with a greater degree of smoothing might be appropriate.

3.2 Further treatment of macroseismic data
3.2.1 Seismic zoning maps
The issues under discussion in this section veer off into the subject of seismic hazard and microzonation, both of which have undergone very considerable technical development since 1979. Their relevance to observatory practice is questionable.

3.2.2 Estimation of focal depth
The work of Sponheuer (1960) referred to here is still the basis of modern practice, but the prevalence of computing resources means that other ways of applying the technique are available. The discussions in Burton et al (1985) and Musson (1994) are relevant.

3.2.3 Relationship between intensity and magnitude
Relationships between maximum intensity and magnitude need to be approached with caution, and are absolutely unreliable if they do not include any depth term. It is now agreed to be generally preferable to use isoseismal areas to estimate magnitude from macroseismic data, and there are a number of recent studies that can be referred to, including Greenhalgh et al (1988), Johnston (1993), Frankel (1994) and Musson (1994).

OTHER ISSUES
a) Epicentral determination from macroseismic data
One topic not mentioned in the Manual of Seismological Observatory Practice is the determination of epicentre from macroseismic data. This may have been from the assumption that observatories would always be using instrumental locations; but there are times when the macroseismic location may actually be more accurate than the instrumental one (eg for small earthquakes well outside the nearest network), and of course, for historical earthquakes, location from macroseismics is inevitable. The main criteria to be used are the centre of the highest isoseismal and the centre of the overall felt area. Where these are significantly different it may be necessary to consider if one or the other is distorted by factors such as local geology, irregular population distribution, etc. The observation of felt foreshocks and/or aftershocks may also be useful. The way in which some seismologists interpret such data is discussed in detail by Cecic and Stucchi (1994).

Much interest in macroseismic methods since 1979 has been stimulated by the upsurge in studies of historical seismicity. While these may be outside routine observatory practice, some mention may be in order. A review is given by Stucchi and Albini (1991).

b) Intensity attenuation

The attenuation of earthquake intensity is also not considered in its own right, although it comes into both focal depth determination and seismic zonation mapping. Since intensity directly relates to effects (including damage), unlike other ground motion parameters, it is very useful to use in seismic hazard studies, particularly where these are designed to be of benefit to planners and insurers. Classically, intensity attenuation may be expected to be of the form

$$I = a + b\,M + c\,\log R + d\,R \qquad\qquad (1)$$

where c is attenuation due to geometric spreading and d is anelastic attenuation. Values of a, b, c and d should be determined regionally from macroseismic observations and can then be used to predict the likely effects of any given earthquake in the future. This may be particularly useful in the first stages of responding to a major earthquake that has just occurred.

This is a simplification inasmuch that intensity attenuation is rarely uniform in all directions, isoseismals more often approximating to ellipses. Attempts have been made to model anisotropic intensity attenuation, either parametrically (eg Caputo et al 1973) or non-parametrically (eg Heidari 1987), but the predictive power of such models depends on the extent to which the azimuth of elliptical elongation of isoseismals is a regional constant.

c) Reorganisation of the chapter

We propose a reorganisation of the chapter along more logical and clearer lines. The three subdivisions reflect three themes: the definition of intensity (by means of intensity scales); the gathering of macroseismic data; and the processing and uses of macroseismic data. The proposed scheme is as follows:

1 Intensity and intensity scales
   1.1 EMS Scale
   1.2 MM56 Scale
   1.3 Accuracy of assessment
   1.4 Equivalence between scales
2 Collection of macroseismic data
   2.1 Macroseismic questionnaires
   2.2 Field investigations
3 Processing of macroseismic data
   3.1 Assessing intensity from data
   3.2 Isoseismal maps
   3.3 Determination of earthquake parameters from macroseismic data
      3.3.1 Epicentral intensity
      3.3.2 Macroseismic epicentre
      3.3.3 Macroseismic magnitude
      3.3.4 Estimation of focal depth
   3.4 Intensity attenuation
   3.5 Relationship with ground motion parameters

CONCLUSIONS

A problem that has been repeatedly identified in the past with macroseismic studies is the incompatibility and inconsistency of investigations by different workers. We believe this is due in no small part by the lack of adequate guidance in proper macroseismic methods. Confronted with the bare outlines of a macroseismic scale, different workers may variously assign intensities by taking the maximum observation, the modal observation, or some private system of their own, giving quite different results.

A major aim in the formulation of the EMS was to improve this situation by giving clear guidelines as to how this intensity scale was to be used. This initiative needs to be followed by the new Manual of Seismological Observatory Practice.

REFERENCES

Ad-hoc Panel, 1981. Report on the Ad-hoc Panel meeting of experts on up-dating of the MSK-64 intensity scale, 10-14 March 1980, Gerl. Beitr. Geophys., 90, 261-268.

Ambraseys, N.N., E. Banda, J. Irving, D. Mallard, C. Melville, T. Morse, R. Muir Wood, D. Munoz, L. Serva, D. Shilston, E. Surinach, and J. Vogt, 1983. Notes on historical seismicity, Bull. Seis. Soc. Am., 73, 1917-1920.

Berardi, R., L. Magri, and M. Mucciarelli, 1990. Do different experts and computer programs agree on the interpretation of the same intensity map?, Proc. XXII ESC General Assembly, Barcelona, 17-22 Sept 1990, 371-376.

Burton, P.W., R. McGonigle, G. Neilson, and R.M.W. Musson, 1985. Macroseismic focal depth and intensity attenuation for British earthquakes, in: Earthquake engineering in Britain, Telford, London, 91-110.

Brazee, R.J., 1978. Reevaluation of Modified Mercalli intensity scale for earthquakes using distance as determinant, NOAA Tech. Mem EDS NGSDC-4.

Caputo, M., V. Keilis-Borok, T. Kronrod, G. Molchan, G.F. Panza, A. Piva, V. Podgaezkaya, and D. Postpischl, 1973. Models of earthquake occurrence and isoseismals in Italy, Ann. Geophys., 26, 421-444.

Cecic, I., (ed) 1989. First AB Workshop on Macroseismic Methods, May 9-11, 1989, Seismological Survey of Slovenia, Ljubljana.

Cecic, I., (ed) 1992. Second AB Workshop on Macroseismic Methods, October 15-18, 1990, Seismological Survey of Slovenia, Ljubljana.

Cecic, I. and M. Stucchi, 1994. Do seismologists agree upon epicentre determination from macroseismic data? *this volume*.

Dengler, L. and R. McPherson 1993. The 17 August 1991 Honeydew earthquake, North Coast California: a case for revising the Modified Mercalli scale in sparsely populated areas, Bull. Seis. Soc. Am., 83, 1081-1094.

Eiby, G.A., 1965. The Modified Mercalli scale of earthquake intensity and its use in New Zealand, N.Z. Jnl of Geol. and Geoph., 9, 122-129.

Frankel, A., 1994. Implications of felt area-magnitude relations for earthquake scaling and the average frequency of perceptible ground motion, Bull. Seism. Soc. Am., 84, 462-465.

Greenhalgh, S.A., D. Denham, R. McDougall, and J.M.W. Rynn, 1988. Magnitude-intensity relations for Australian earthquakes, Bull. Seism. Soc. Am., 78, 374-379.

Grünthal, G., (ed), 1993. European Macroseismic Scale 1992 (updated MSK Scale), Cahiers du Centre Européen de Géodynamique et de Séismologie no 6, Luxembourg.

Heidari, M., 1987. Statistical methods of earthquake attenuation, PhD thesis, Dept. Civ. Eng., MIT, Cambridge MA.

Johnston, A., 1993. The stable continental region data base, in: The earthquakes of stable continental regions: Assessment of large earthquake potential, EPRI Report TR-102261.

Musson, R.M.W., 1994. Macroseismic magnitude and depth for British earthquakes, Bull. Seism. Soc. Am., *in press*.

NZSEE 1991. A revision of the Modified Mercalli seismic intensity scale: Report of a study group of the New Zealand Society for Earthquake Engineering, Bull. N.Z. Nat. Soc. for Earthquake Eng., 25, 345-357.

Principia Mechanica Ltd 1982. British earthquakes, PML, London.

Richter, C.F., 1958. Elementary seismology, WH Freeman, San Francisco.

Rubeis, V. de, C. Gasparini, A. Maramai, M. Murru, and A. Tertulliani, 1992. The uncertainty and ambiguity of isoseismal maps, Eq. Eng. and Struct. Dyn., 21, 509-523.

Sieberg, A., 1912. Über die makroseismische Bestimmung der Erdbebenstärke, Gerl. Beitr. Geophys., 11, 227-239.

Sponheuer, W., 1960. Methoden zur Herdtiefenbestimmung in der Makroseismik, Freiberger Forschungshefte C88, Akademie Verlag, Berlin.

Stucchi, M. and P. Albini, 1991. New developments in macroseismic investigation, Proc. Mexico-EC Workshop "Seismology and Earthquake Engineering", Mexico City, Apr 22-26, 1991.

Willmore, P.L., 1979. Manual of Seismological Observatory Practice, World Data Centre A for Solid Earth Geophysics Report SE-20.

Wood, H.O. and F. Neumann 1931. Modified Mercalli intensity scale of 1931, Bull. Seis. Soc. Am., 21, 277-283.

KINEMATIC PARAMETERS OF SEISMIC FIELD FOR RECONSTRUCTING VELOCITY STRUCTURE

L.B.Slavina, G.A.Belyankin
Institute of Physics of the Earth, RAS, Moscow

ABSTRACT
An algorithm and a technique for numerical determination of compressional velocity within a region of earthquake have been developed. Compressional travel times from local earthquakes with varying depth of focus have been analyzed to show that the technique can be used for constructing a three - dimensional velocity field.

INTRODUCTION
The objective of the present investigation is the restoration of a medium 3D velocity structure at the foci cluster of earthquakes after the data of a regional net of seismic stations that records the first arrival of the P- and S-waves of local earthquakes.

The velocity field is an important characteristic of the medium, its constant constituent part on whose background the preparation of strong events proceeds.

The 3D velocity structure reflect dense inhomogeneities in the medium and make an objective basis for quantitative estimates of its strain-stress state parameters.

GENERAL FEATURES OF THE METHOD
The problem of the velocity determination can be reduced to the approximation of the observational data on the basis of formulae which link the propagation times of seismic waves and their velocities. The algorithm is based on the restoration of the

wave front within a limited volume where the velocity changes only slightly.

The method of calculation is differentiated. It makes use of differences of travel times from the near sources. Every point of the medium has thus got its own value of the velocity.

The application of the approach proposed allows one to estimate quantitatively the velocity distribution within the area of weak earthquake origination. For the Caucasus, this area is in a range of depth lesser than 30 km; for the Carpathians, 0 to 170 km; for the Kamchatka region, 0 to 250 km; and for the Mediterranean region, 0 to 80 (100) km.

The algorithm and software elaborated by us differ from those adopted in seismic tomography (Aki, 1977; Nolet, 1987) which make use of the residuals from a standard hodograph revealed in experimental data of travel times which tend to be characteristical for the medium throughout the propagation path of a ray on its travel from the source to the receiver.

The accuracy of tomographical drawings depends on the density of covering the medium studied with such rays. Making use of different stations increases the discrepancy owing to medium differencies under individual stations.

In our approach (Slavina,1992, 1993), we have used two following principles:

1) the differency of travel times Δt from a couple of closely situated sources must be recorded at the same station;

2) the reciprocity law was applied that is adopted in seismic prospection: the source and receiver change places.

The stability of restored velocity field depends on the density of source distribution for weak earthquakes by square and depth.

Due to non-uniformity of the seismicity distribution, a problem arises of data smoothing. The stability depends also on the method and accuracy of the hypocenter determination. Therefore, the absolute values calculated for velocities may differ for various initial data sets, but the morphological features
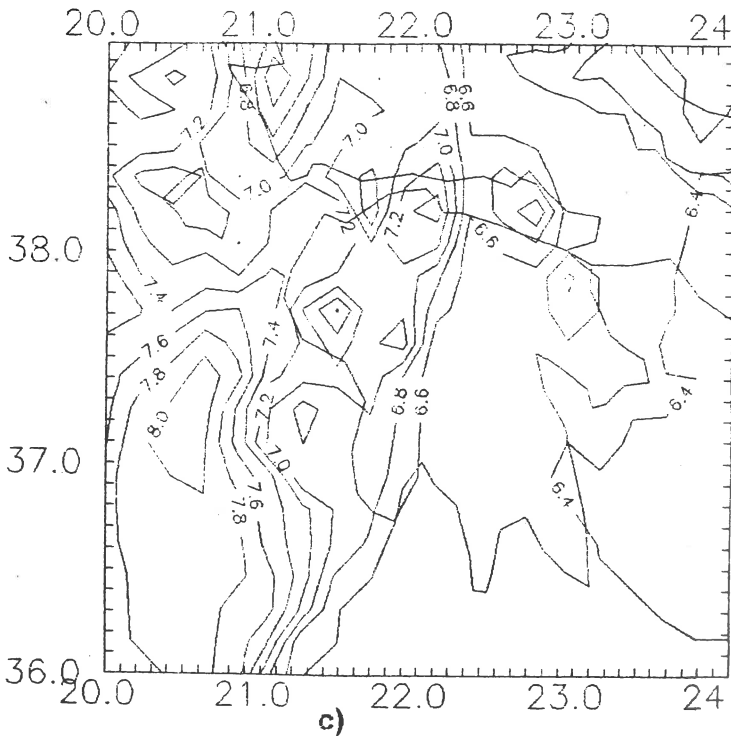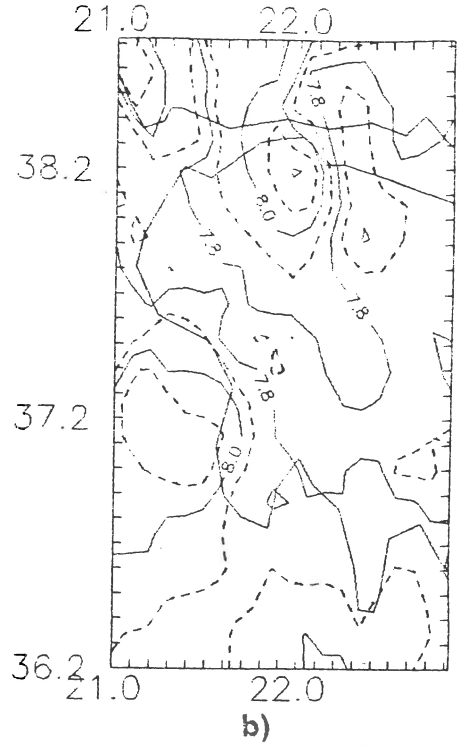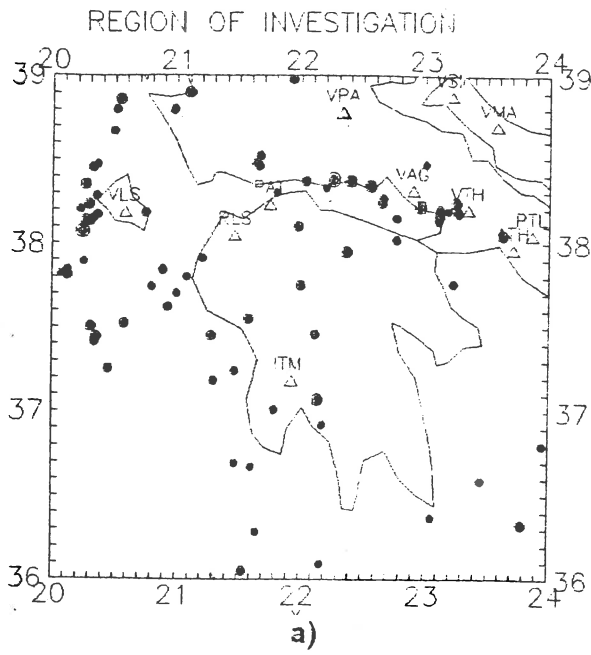
Fig.1. Greek region velocity structure **a)** The region of investigation. Filled circles are the strong earthquakes (M>5) of 1964-1988 temporal interval. **b)** Horizontal velocity section at the depth 45 km. **c)** Horizontal velocity section at the depth 75 km.
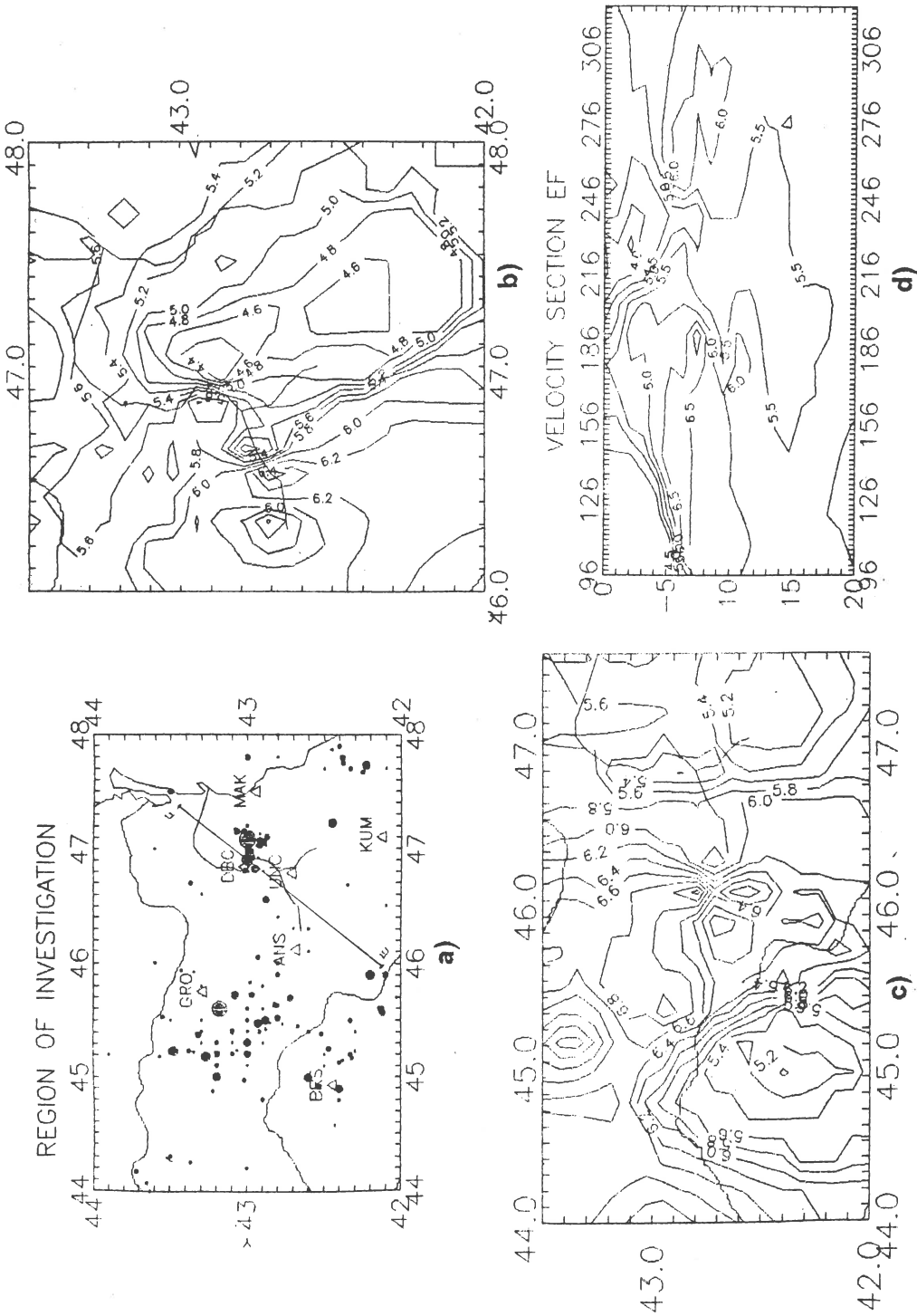
Fig.2. Northern Caucasus region velocity structure **a)** The region of investigation. Filled circles are the strong earthquakes (K>11) of 1978-1994 temporal interval. **b)** Horizontal velocity section at the depth 5 km. **c)** Horizontal velocity section at the depth 10 km. **d)** Vertical velocity section EF (see fig.2a).

revealed of the medium (locations of zones of high and low velocity values) are valid.

The methodics limitations include:

- the necessity of data smoothing;

- the fact that the velocity can be estimated in the epicenter clustering zones only.

The merits of this approach include in turn the possibility of the construction of a 3D velocity distribution model for any zone of earthquake occurring without applying sources controlled and expensive works.

THE BASIC RESULTS

The main result is the possibility of obtaining maps at different levels of the velocity fields for different depth intervals and velocity cross-section in every direction.

As an example, velocity models for the Northern Caucasus are shown for two depth intervals, 5 and 10 km (fig. 2b,2c), and for vertical cross-section (fig. 2d). The velocity field of the Northern Caucasus is non-uniform, with alteration of the segments of high and low values of velocity. The main tendency is eastward the lowering of the velocity toward the Caspian Sea. Interesting are the gradient zones that can be interpreted as steps or faults. One of them is associated with well known in geology Bujnaksk step. But geological data cannot show us the depth of this step. Our results show that this step have about 4 km by depth and vertical angle of fail. Some of strong earthquakes such as in 1992 are associated with this step.

The comparison of seismicity and velocity field allows us to definite probable strong event locations.

The approach under development was applied to the computation of models for the Mediterranean region of Greece and the Creete Island. Preliminary results after the calalogue and ISC bulletins data for 1964-1987 where the regional Greek net are not represented completely.

The figures 1b and 1c show maps of velocity distributions for the levels of 45 and 75 km. The velocity field is nonuniform, with high and low velocity segments altered.

We plan to continue this work in future with coloboration with our greek colleagues.

CONCLUSION

The calculation of a three-dimensional velocity field according to this technique does not demand on special observations using controlled sources. As a result,new data about velocity structure of medium in the focal zone including transition zone between Eurasian continent and Caucasus, Carpatian, Greece and Creat arc were obtained. The focal zone has a very complex structure and morphologically consists of high and low velocity areas.

REFERENCES

Aki K., Christofferson A., Husebye E.S. (1977) Determination of the three-dimensional seismic structure of the lithosphere. *J. Geophys. Res* **82**, 277-296.

Nolet G. (1987) Seismic tomography with applications in global seismology and exploration geophysics, D.Reidel Publishing Company, Dordrecht, Holland.

Slavina L.B., Pivovarova N.B., (1992) Three-dimensional velocity models of focal zones and refinement of hypocenter parameters. *Physics of the Earth and Planetary Interiors* **75**, 77-88.

Slavina L.B., Pivovarova N.B. (1993) A Three-Dimensional Velocity Model of the Kamchatka Benioff Zone. *Journal of Earthquake Predicton Research* **2** .549-570.

3-D VELOCITY STRUCTURE OF THE UPPER CRUST OF PYRGOS REGION (SOUTHERN GREECE)

G. Stavrakakis*, G. Drakatos*, D. Papanastassiou*, G. Karantonis* and J. Louis**

* Geodynamic Institute, National Observatory of Athens
** Geophysics - Geothermy Division, University of Athens

Abstract

On March 26, 1993, a moderate earthquake of $M_s = 5.5$ struck the city of Pyrgos, located in the Western part of Peloponnesus (Southern Greece). In this seismic zone, no earthquakes of $M_s = 6.0$ have occurred in the mainland up to now, whereas larger shocks have occurred at the coast off the city of Pyrgos.

The above mentioned main shock was followed by a severe aftershock activity lasted for about two months. More than 800 aftershocks in the magnitude range of $2.0 \leq M \leq 4.9$ have been recorded by a temporary seismic network of eight (8) stations, installed in the broad epicentral region by the Geodynamic Institute of the National Observatory of Athens.

Two data sets of well located earthquakes, recorded at least at seven stations, have been selected in order to be used for the determination of the 3-D velocity structure of the upper crust of Pyrgos area with application of two different inversion techniques.

The results are presented in terms of velocity distribution contour maps and show a very good agreement with studies of seismic hazard assessment in the same region.

Introduction

The west coast of Peloponnesus (Figure 1a) is an area of the Hellenic arc system with relatively high seismic activity. This area is undergoing the consequences of the subduction of the African plate beneath the Eurasian plate along the Hellenic trench located offshore. The compressional regime of the area is well documented by interdisciplinary work (**McKenzie, 1978; Angelier et al., 1982; Hatzfeld et al., 1990**).

The basement formations consist of Jurassic - Cretaceous limestones and Eocene - Oligocene flysch. These formations are faulted, due to lateral eastward compression, mainly by steep reverse faults having almost N-S directions and dipping towards the east. It is important to

Ionion Sea   Katakolo   Alfios R.

Pio-Pleistocene deposits   Eocene - Oligocene Flysch

Miocene conglomerates   Jurassic - Cretaceous
and sands   Limestones

b

STRONG EVENTS   7 Events
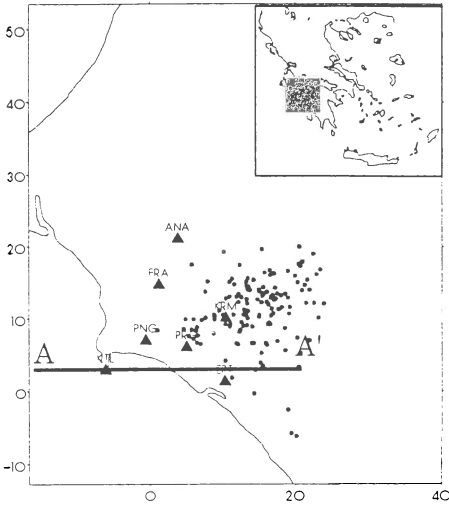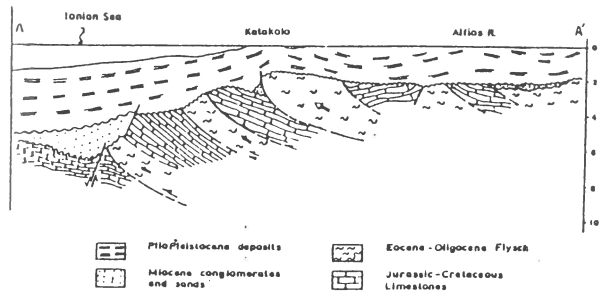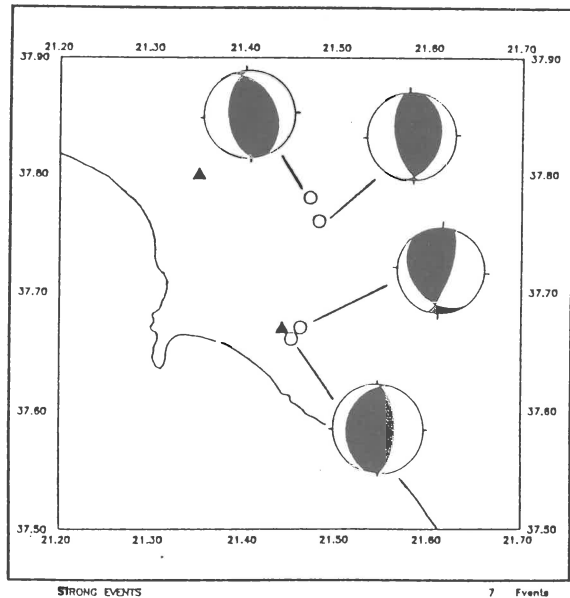
c

Figure 1. (a) Study area and location map, (b) geological
cross section and (c) focal mechanisms.

723

note that, during the Quaternary, the Triassic evaporites used these faults to emigrate and create neodiapirism into the corresponding sediments, (**Nikolaou, 1988**). The plain of Pirgos is covered by alluvial uncosolidated deposits which consist of mixed phases of clay, silt, sand and gravel with vertical and lateral variations.

The above mentioned srtucture is shown in Figure 1(b), where an east-west trending geological cross section is presented. The geology of the area is reconstructed ' according to **Monopolis and Bruneton (1982)** and the geological maps of the Institute of Geology and Mineral Exploration.

On March 26, 1993 a series of earthquakes occurred in the area of Pirgos (W. Peloponnesus). The shocks caused serious cumulative damages in the area of Pirgos and its environs but no fatalities. The stronger aftershocks occurred on March 26, with M_s=4.7, on March 30, M_s=4.6 and on April 29, M_s=4.9 The fault plane solutions of the above metnioned earthquakes are shown in Figure 1(c).

Following the main shock, the Seismological Institute of the National Observatory of Athens installed a seismic network consisting of 8 stations. Over 800 aftershocks were recorded for a time period of 2 weeks. Their spatial distribution defined a cluster having an NNE - SSW direction while almost all the epicentres were located at depths between 5 and 25 km.

The aim of this study is to contribute in the knowledge of the velocity structure of the area using 3-D inversion techniques. Two different methodologies (**Aki & Lee, 1976; Thurber, 1986**) are evaluated, and the results are compared with previous seismotectonic and seismic hazard studies.

Data and Method

From the above mentioned total number of recorded events two different data sets were prepared for the application of 3-D inversion. The selection of data was carried out with attention to the requirements of each method. The main criteria for the selection of events are the number of recording stations and the accuracy of the parameter determination.

For the method of **Aki & Lee** 140 well located earthquakes were selected, which are included in the area with dimensions 40 x 32 km, with coordinates of the SW corner 37 37' N - 21 23' E. Attention was given in the spatial distribution of events. The crust of the study area was divided in four layers, each one of 5 km thickness. Each layer was divided into 4 x 4 rectangular blocks. The block size was 10 x 8 km in NS and EW directions, respectively. The initial velocity values for each layer was 6.11, 6.56, 7.28 and 7.65 km/s. Several applications of the method with different inversion parameters were carried out in order to improve the quality and the reliability of the results. Finally,

the whole block configuration was shifted by half block size towards SW, in order to obtain slight variations of the velocity in the horizontal direction.

The same criteria were used for the preparation of a second data set for the application of **Thurber**'s method. The study area was altered slightly, with dimensions 16 x 20 km (measured from the same origin). The final data set consists of 90 events, including events and stations from the surrounding area. The initial velocity model is parameterised in terms of a grid of 5 x 5 x 3 nodes, in EW, NS and vertical directions, respectively. The nodes lay on three horizontal planes at 2, 5, ,9 and 14 km depth. The initial velocity values for the nodes of the first, the second and the third layer are 4.10 km/s, 6.40 km/s and 7.28 km/s, respectively. The spacing between the nodes of the first plane (depth 0 Km) is 4 Km in the X (EW) and 5 Km in the Y (NS) directions. Like in the previous case, several applications of the method, using different inversion parameters each time, were carried out, in order to improve the reliability of the results.

Results and Discussions

In Figure 2, the results of the inversion are shown, following the method of **Aki and Lee (1976)**. The results are shown in terms of a velocity contour map for each layer separately. Each map consists of curves of equal velocity values extracted after superposition of both block configurations (the initial and the shifted one).

In Figure 3, the results of the inversion are shown, following the method of **Thurber (1986)**. The results are presented again in terms of contour maps.

Both figures show similar velocity distribution. The difference in the geometry of the contours can probably be explained by the fact that the results of the Aki's method refer to blocks of 5 km thickness, whereas the results of the Thurber's method refer to layers of nodal points at particular depths. The velocity values however, are in good agreement with other geophysical (**Voulgaris, 1991**) and seismic hazard studies (Figure 4) in the region.

References

Aki, K. and W.H.K. Lee, 1976. Determination of three-dimensional velocity anomalies under a seismic array using first P arrival times from local earthquakes 1. An homogeneous initial model. *"J. Geophys. Res.", 81: 4381-4399.*
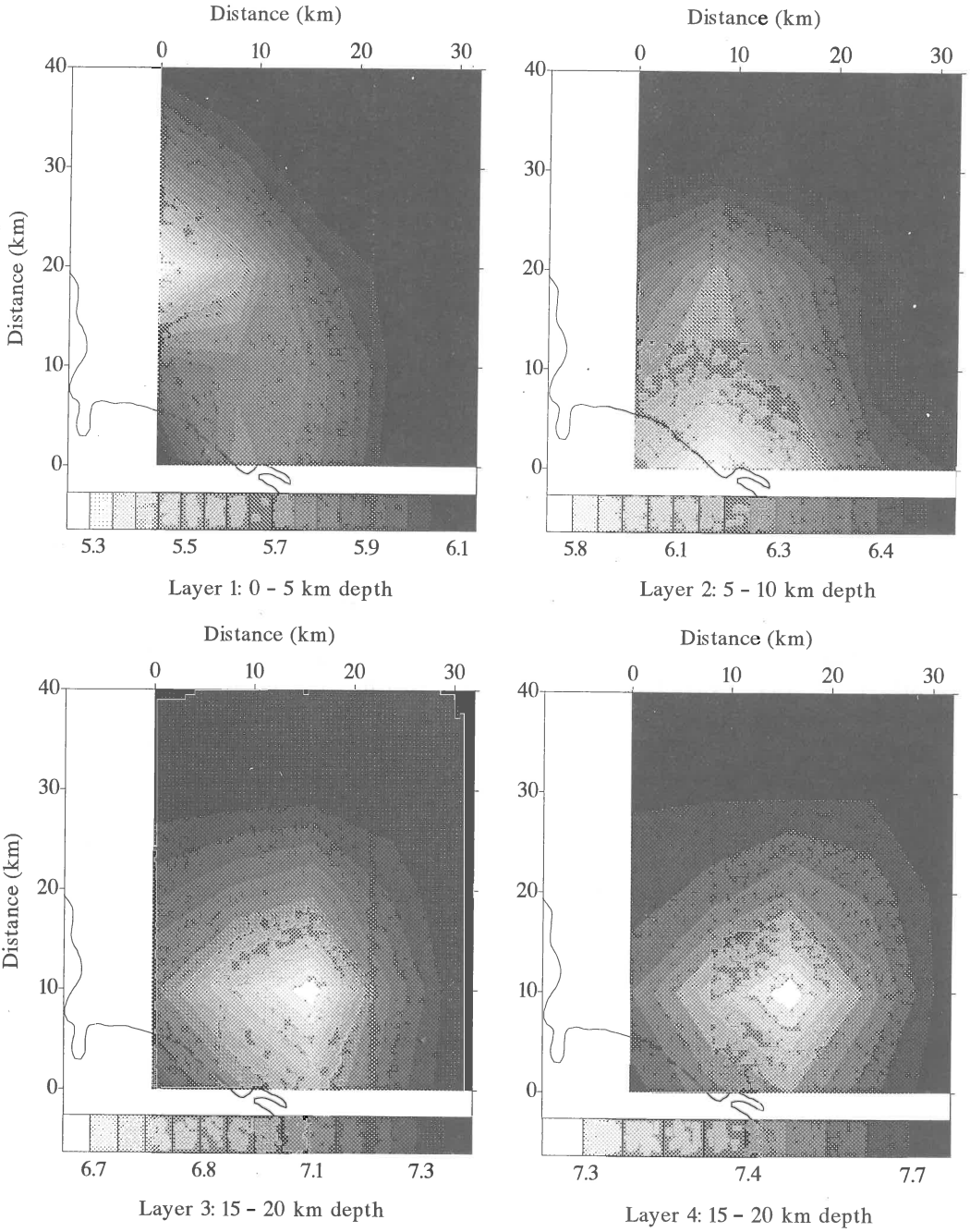
Figure 2. Velocity contour maps presenting the results
of the Aki & Lee method (velocity in km/s).
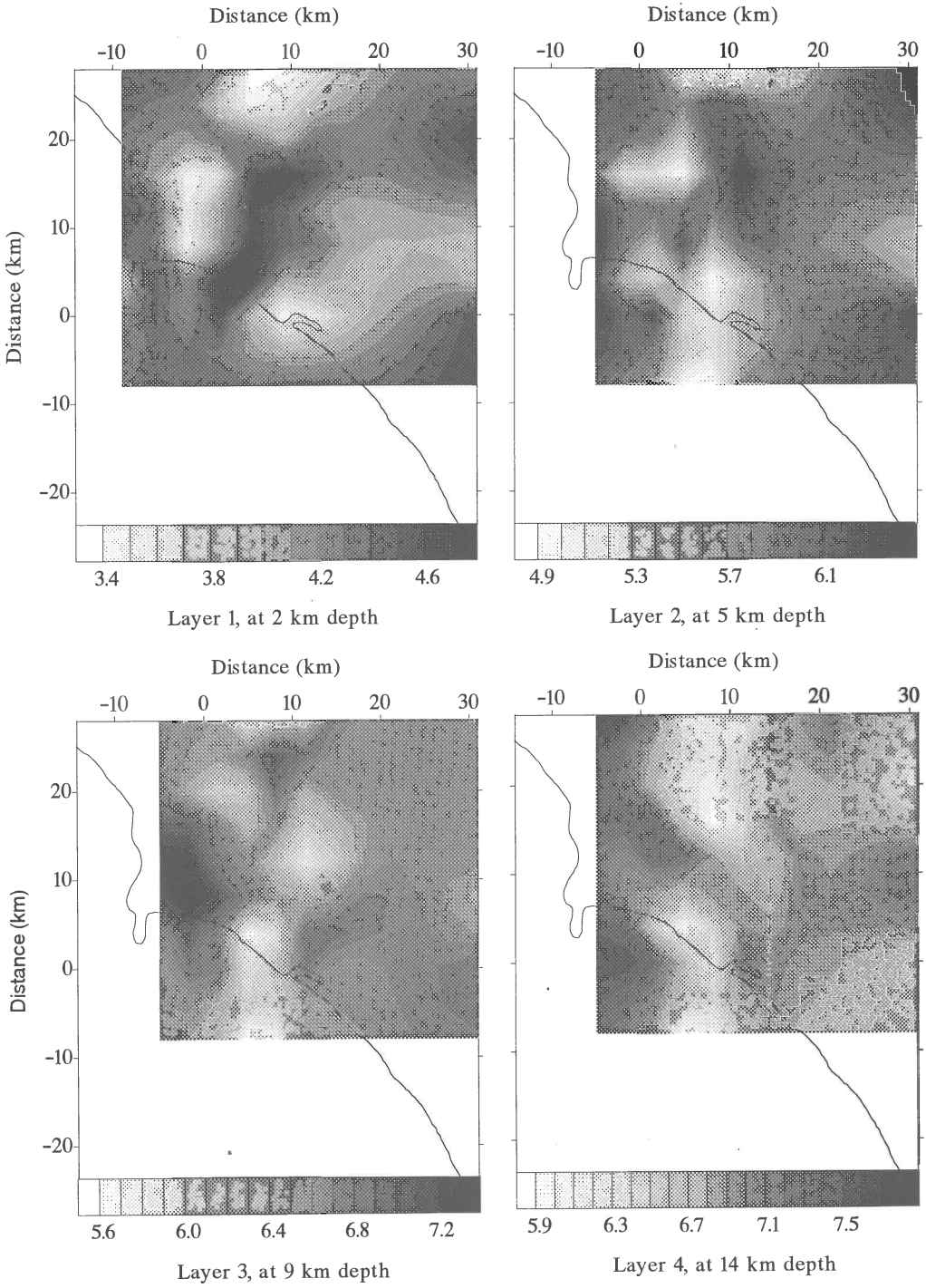
Figure 3. Velocity contour maps presenting the results of the
Thurber's method (velocity in km/s).
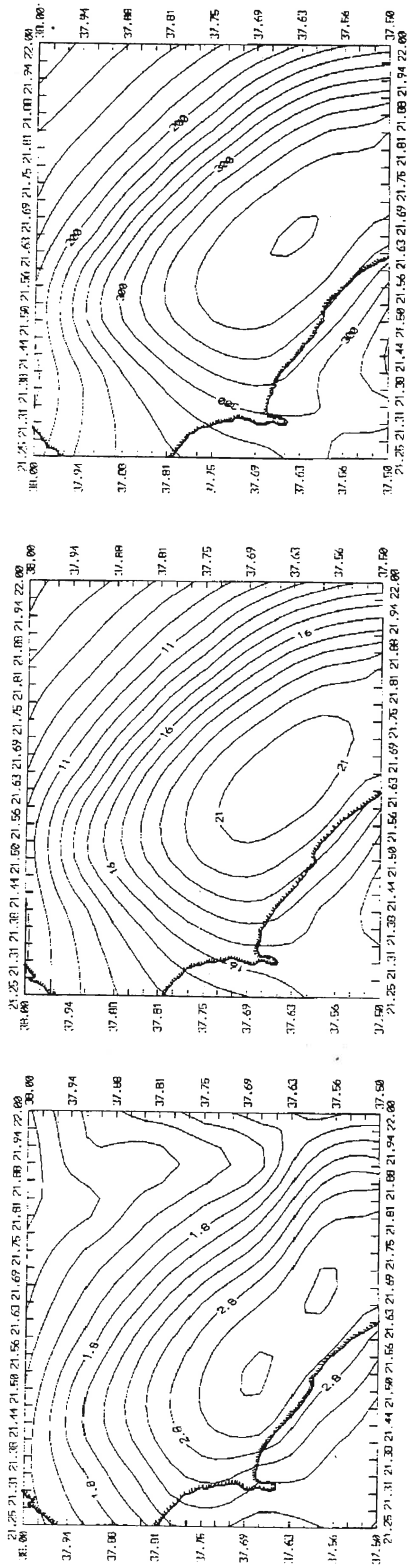
Figure 4. Maximum values of (a) seismic displacement in cm, (b) seismic velocity in cm/sec and (c) seismic acceleration in gals, with probability 90% not to be exceeded the next 50 years.

728

Angelier, J., Lyberis, N., Le Pichon, X., Barrier, E., Huchon, P., 1982. The neotectonic development of the Hellenic Arc and the sea of Crete: a synthesis. *Tectonophysics, 86, 159 - 196.*

Hatzfeld, D., Pedotti, G., Hatzidimitriou, P., Makropoulos, K., 1990. The strain pattern in the western Hellenic arc deduced from a microearthquake survey. *Geophys. J. Int., 101, 181 - 202.*

Mckenzie, D., 1978. Active tectonics of the Alpine-Himalayan belt: the Aegean sea and surrounding regions. *Geophys. J. R. Astr. Soc., 55, 217-254.*

Monopolis, D. and Bruneton, A., 1982. Western Greece. Its outline deduced from drilling and geophysical data. *Tectonophysics, 83, 227-242.*

Nikolaou, K., 1988. Neodiapyric movement of the Triassic evaporites in Zakynthos and Strofades islands. *Bull. Geol. Soc. Greece, 20, 83-99.*

Thurber, C.H., 1986. Nonlinear earthquake location: Theory and examples. BSSA, V 75, pp 779 - 790.

Voulgaris, N., 1991. Examination of the structure of the earth's crust in the area of Zakynthos - NW Peloponnesus (W. Greece). *Ph. D. Thesis, Univ. of Athens, 224 pp.*

3-D VELOCITY STRUCTURE IN NORTHERN PELOPONESSUS (GREECE) FROM INVERSION OF LOCAL EARTHQUAKE ARRIVAL TIMES.

N. Voulgaris[1], G. Drakatos[2], K. Makropoulos[1] and J. Drakopoulos[1]

[1]Geophysics-Geothermy Department, University of Athens
[2]National Observatory of Athens, Seismological Institute

Abstract

In the present study, the three dimensional P-wave velocity of the upper crust in the northern Peloponessus area was obtained using the methods for iterative simultaneous inversion of hypocentral parameters and velocity structure, developed by Aki and Lee and by Thurber. Application of both methods in the same area was adopted, in order to test the overall reliability of the obtained results, as well as compare the velocity structure solutions. Furthermore, the dependency of the results (velocity structure and resolution) from the model parameterisation was also tested, by using two different approaches while implementing Thurber's method.

Evaluation of the results obtained by both methods, talking into account their limitations, indicate important velocity variations for the topmost layer (0-6km) probably due to the existence of neogene sedimentary basins and flysh deposits in the area, while velocity variations at deeper layers (6-12km and 12-18 km), appear in close agreement with the main geological and tectonic features of the area and the general trend of the Hellenides.

Introduction

Three dimensional simultaneous inversion methods, using observed travel time data to examine the crustal velocity of a given area and minimise earthquake location uncertainties was first applied in seismology by Aki and Lee in 1976. Since then, the method has grown in popularity among seismologist and several variations of this initial approach have been developed adopting different model parameterisation techniques, formulations of the forward problem and inversion methods. Among them, the one developed by Thurber in 1986 offers greater flexibility for constructing the three dimensional model and improved ray-tracing techniques for the calculation of the forward problem. Both methods have been applied in order to investigate the crustal velocity structure in the northern Peloponessus area and compare the obtained results.

The study area is located in central Greece and as it can be seen from figure 1 the region is dominated by the NNW-SSE overthrusts created by the compressional tectonics of the Alpine orogeny, affecting the limestone and flysch formations. A number of important E-W trending faults (figure 1) is superimposed on the above tectonic
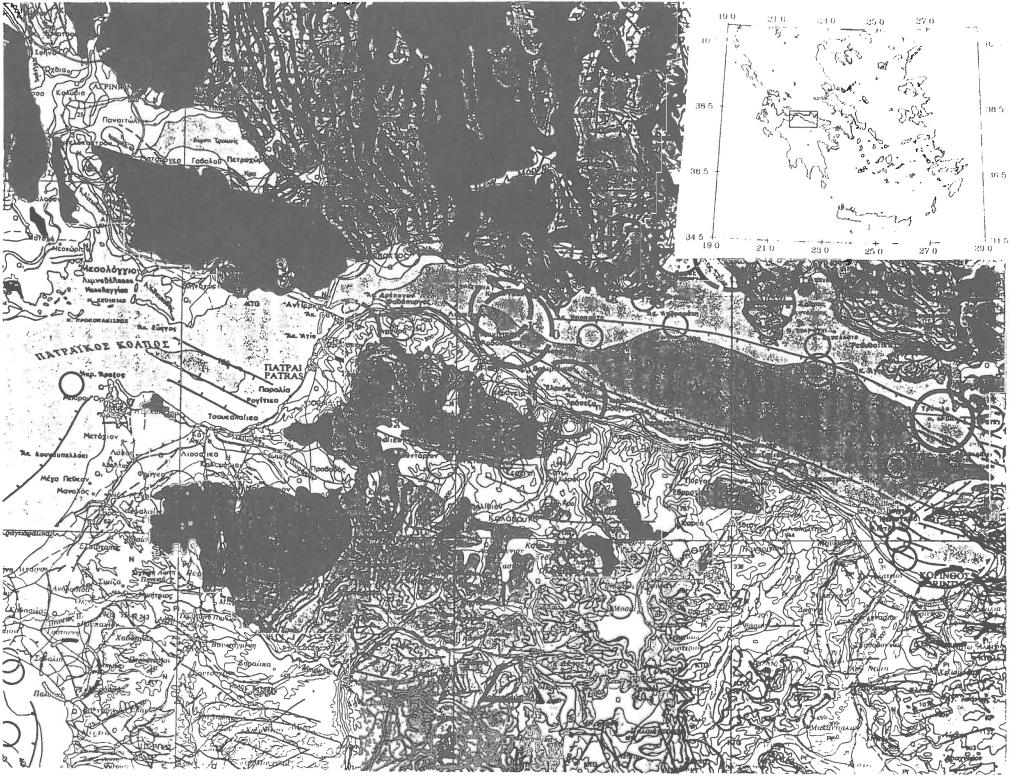
Figure 1. Geological and tectonic setting of the study area

structures representing the post-alpine extensional tectonic episodes in the area of the Hellenic arc. The deposition of relatively less consolidated Neogene and Plio-Quaternary sediments in the area is also associated these extensional features.

In present times, tectonic activity in the area is expressed by normal and strike-slip motion along E-W trending faults, indicating a nearly N-S extension (Hatzfeld et al, 1990).

Data and Method

In the summer of 1986 a dense seismographic network of 46 portable stations was installed in the area of Central Greece and Peloponessus, in order to obtain more detailed information about the tectonics of Western Hellenic arc. During the seven week period that the network remained in operation more than 1000 events were recorded. Initial epicenter location was carried out using the program HYPO 71 (Lee and Lahr, 1972) and finally a data set of 437 best located events was compiled (Hatzfeld et al, 1990).

In order to implement the method of Aki and Lee (1976), 139 earthquakes were selected from the final dataset, on the basis of their spatial distribution and number of observations. The dimensions of the investigated area were 192x128 km, oriented almost

731
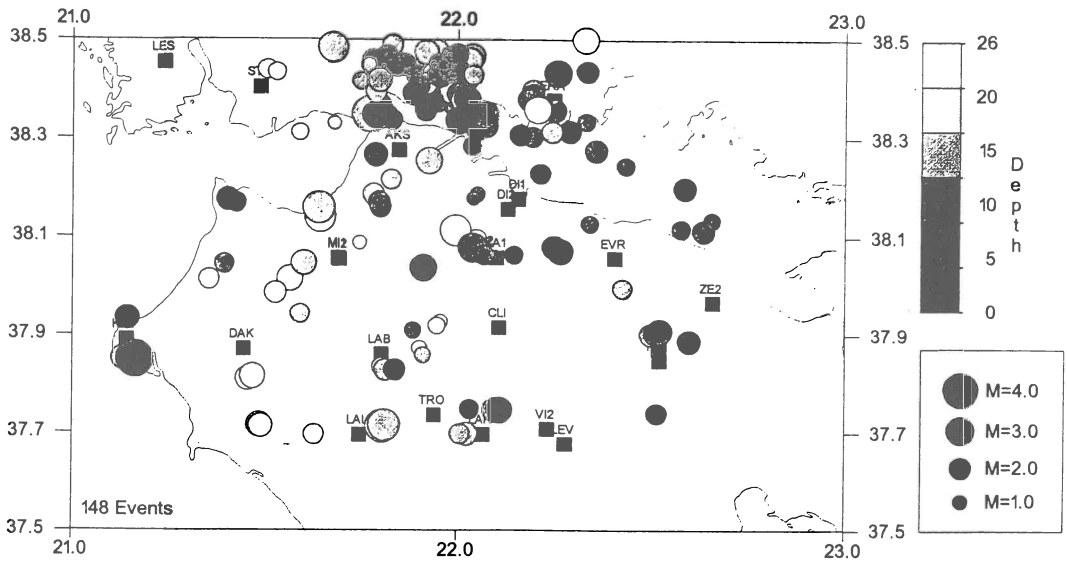
Figure 2. Station and epicentre location in the study area.

parallel to the predominant tension axis of the broader region. In order to model the crustal structure of the area, four horizontal layers, with a thickness of 6 km each were used. Each layer was divided into 8x8 rectangular blocks with a block size of 24x16 km, along the E-W and N-S directions respectively. A total of 25 stations located in the above mentioned region were used (figure 2.). Initial velocity values of, 5.2, 5.9, 6.1 and 6.4 km/s were assigned to the first, second third and fourth layer, respectively.

The ray paths from each event to all stations were traced and travel times through each block calculated. The data were inverted 5 times, using different inversion parameters each time in order to improve the quality and the reliability of the solution. The resolution and covariance matrices were computed. Furthermore, in order to obtain slight variations of the velocity and to improve the resolution in the horizontal direction, the whole block configuration was shifted by half block size to the NE and solution, resolution and covariance matrices were computed again.

Next, in order to verify and test the stability and reliability of the obtained results, a second data set was prepared, as input for Thurber's (1986) method of iterative simultaneous inversion for three-dimensional velocity structure and hypocenter parameters, using travel time residuals.

Ninety earthquakes were selected on the basis of their spatial distribution and number of observations. The number of available observations per event ranged from 8 to 19. The inclusion of stations and earthquakes outside the modelled area was necessary

to improve the ray path distribution within the modelled area. However, this must be taken into account while interpreting the results, since the peripheral velocity grid points include ray paths from the surrounding area.

The crustal structure of the region was parameterised by assigning velocity values at the intersections (grid points) of a three dimensional grid (figure 3, model A). The grid spacing was 12km along the EW and 13 along the NS directions. The initial velocity values were 3.5, 5.8, 5.95 and 6.2 km/s at depths of 2, 6, 11 and 17 km respectively. The velocity at a given point along a ray path and the corresponding partial derivatives were computed by linearly interpolating between the surrounding eight grid points. Using this method, the resulting velocity model displays gradual velocity variations as opposed to the sharp discontinuities shown by block type parameterisation. The ray paths from each event to the corresponding stations were traced as parts of circular arcs and according to Thurber's (1986) approximate ray tracing method the arc with the fastest travel time was selected as the true ray path. Observed and calculated travel times were used in the inversion and finally the solution, resolution and covariance matrices were computed.
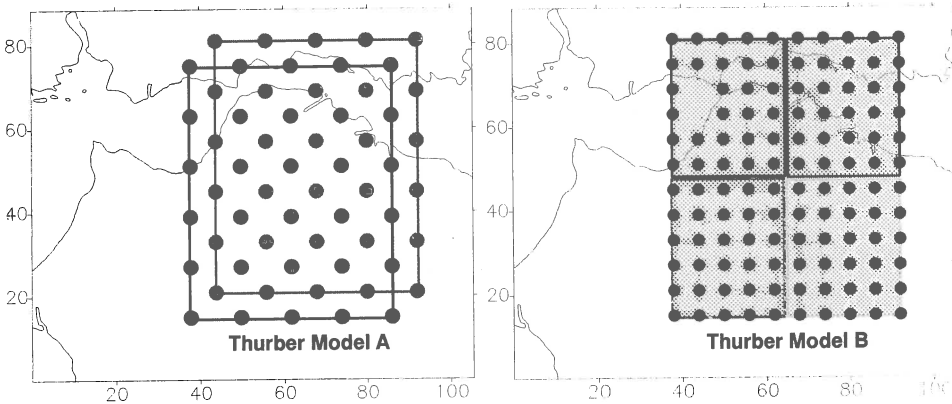
Figure 3. Crustal model definiton for the implementation of Thurber's (1986) method (cases A and B).

In addition, in order to test for a possible resolution enhancement, the study area was divided in four equal rectangular blocks, and each one of them was parameterised using the same grid point technique (figure 3, model B). Inversion was again applied, leading to the computation of a second set of solution, resolution and covariance matrices.

As in the previous case, in order to detect slight variations of the velocity in the horizontal direction, the whole configuration has been shifted by 6km in a NE direction.

Results and Discussion

The results of inversion using the Aki and Lee (1976) method, are presented in figure 4 in terms of velocity contour maps, for each of the first three layers separately. For the calculation of the velocity contours, the results of both (initial and shifted) block configurations have been used.

In the first (upper) layer (0 - 6 km) important variations of velocity can be observed. This could be partly attributed to the influence of the various geological formations of the area, characterised by a large thickness of recent sedimentary and flysch formation units (Nikolaou, 1988). The sharp velocity variations which appear in the peripheral blocks however should be attributed to the poor ray coverage in these areas inherent in the method.

In the other two (deeper) layers (6-12km and 12-18 km)the velocity variations are not so pronounced and appear to correlate well with the general NNW - SSE trend of the Hellenides, which dominates the geotectonic regime of the region.

In figures 5 and 6, the results of the inversion obtained from the implementation of Thurber's (1986) method are presented both for Model A and Model B parameterisations. As it can be seen, the results obtained using Model B display very sharp and numerous velocity variations, while model A results appear to be in good agreement with those of the previous method in the same area. The poor image of model B results, is probably related to the high degree of parameterisation of the modelled area due to the dense grid network, as opposed to the relatively limited data set. This results to a significant decrease in resolution. Hence, it is obvious that Model B parameterisation should be avoided as it will provide unreliable results.

References

Aki, K. and W.H.K. Lee, 1976. Determination of three-dimensional velocity anomalies under a seismic array using first P arrival times from local earthquakes 1. An homogeneous initial model. "J. Geophys. Res.", 81: 4381-4399.

Drakatos, G. and J. Drakopoulos, 1991. 3-D Velocity Structure beneath the crust and upper mantle of Aegean sea region. PAGEOPH, Vol. 135, No 3, pp 401 - 420.

Hatzfeld, D., Pedotti, G., Hatzidimitriou, P., Makropoulos, K., 1990. The strain pattern in the western Hellenic arc deduced from a microearthquake survey. Geophys. J. Int., 101, 181 - 202.

Lee, W. H.. K. and Lahr, J. C., 1972. Hypo 71 (revised), a computer program for determining hypocenters, magnitude and first motion pattern of local earthquakes, US Geological Survey Open File Report 75-311.

Le Meur, H. 1994. Tomographie tridimensionnelle a partir des temps des premieres arrives des ondes P et S., application a la region de Patras (Grece), Ph.D. Thesis, Universite de Paris VII, 304 pp.

Makris, J., 1976. A dynamic model of the Hellenic arc decided from geological data. Tectonophysics, 36, 339 - 346.
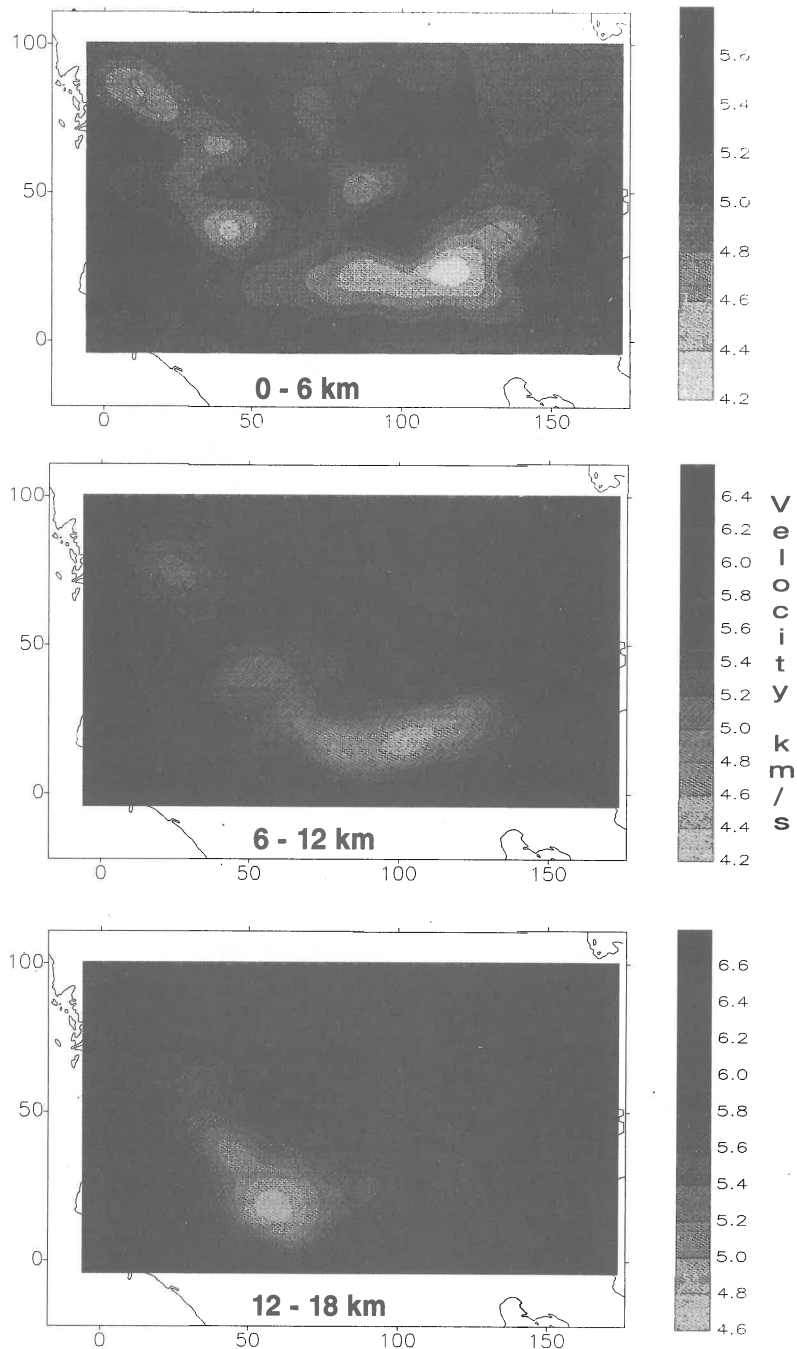
Figure 4. P-wave velocity (km/s) distribution in the study area obtained by the implementation of the Aki and Lee (1976) method for the layers 0–6, 6–12, and 12–18 km.
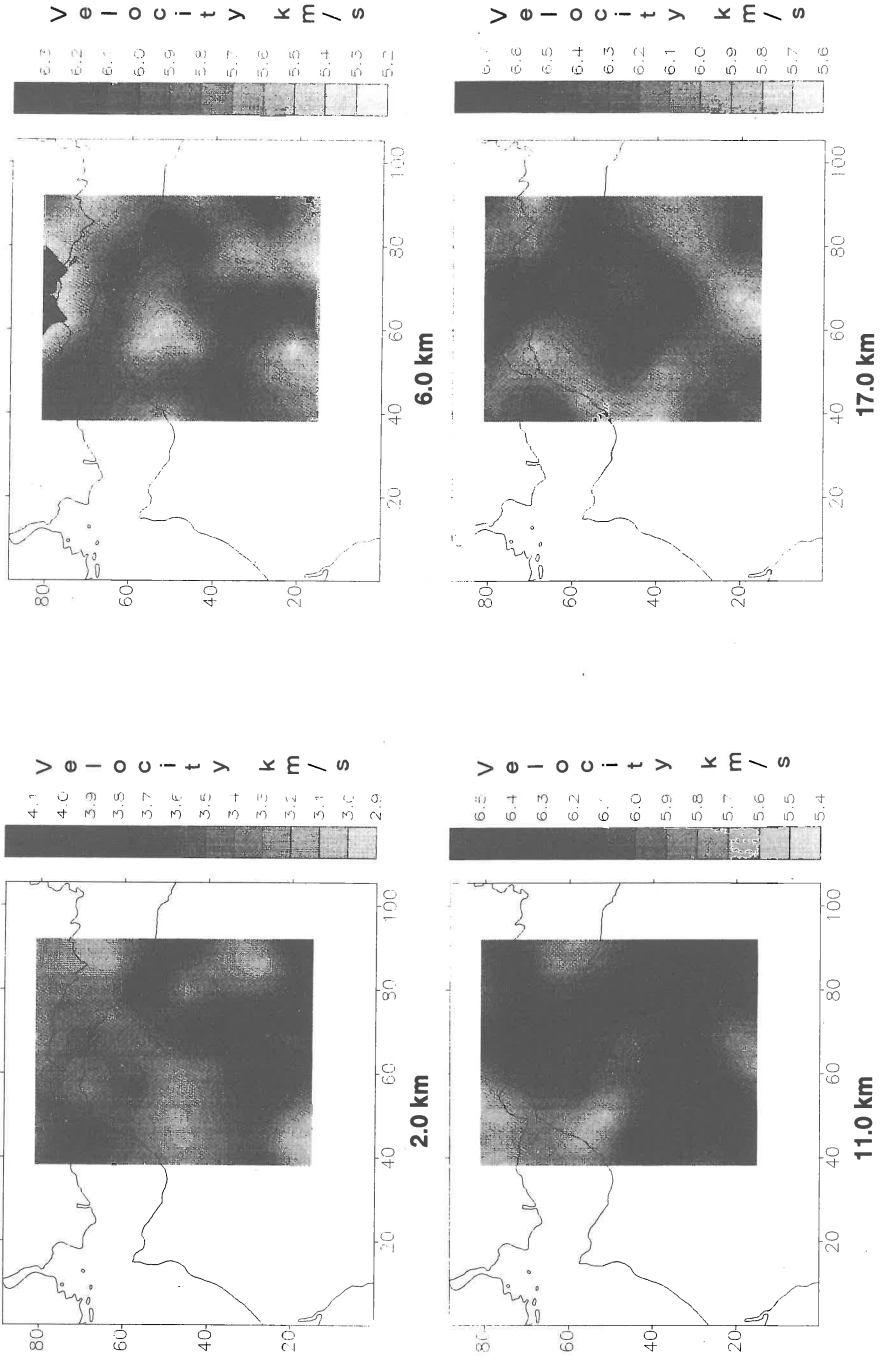
Figure 5. P-wave velocity (km/s) distribution in the study area obtained by the implementation of Thurber's (1986) method (Model A) at depths of 2, 6, 11 and 17 km.

Thurber Model B
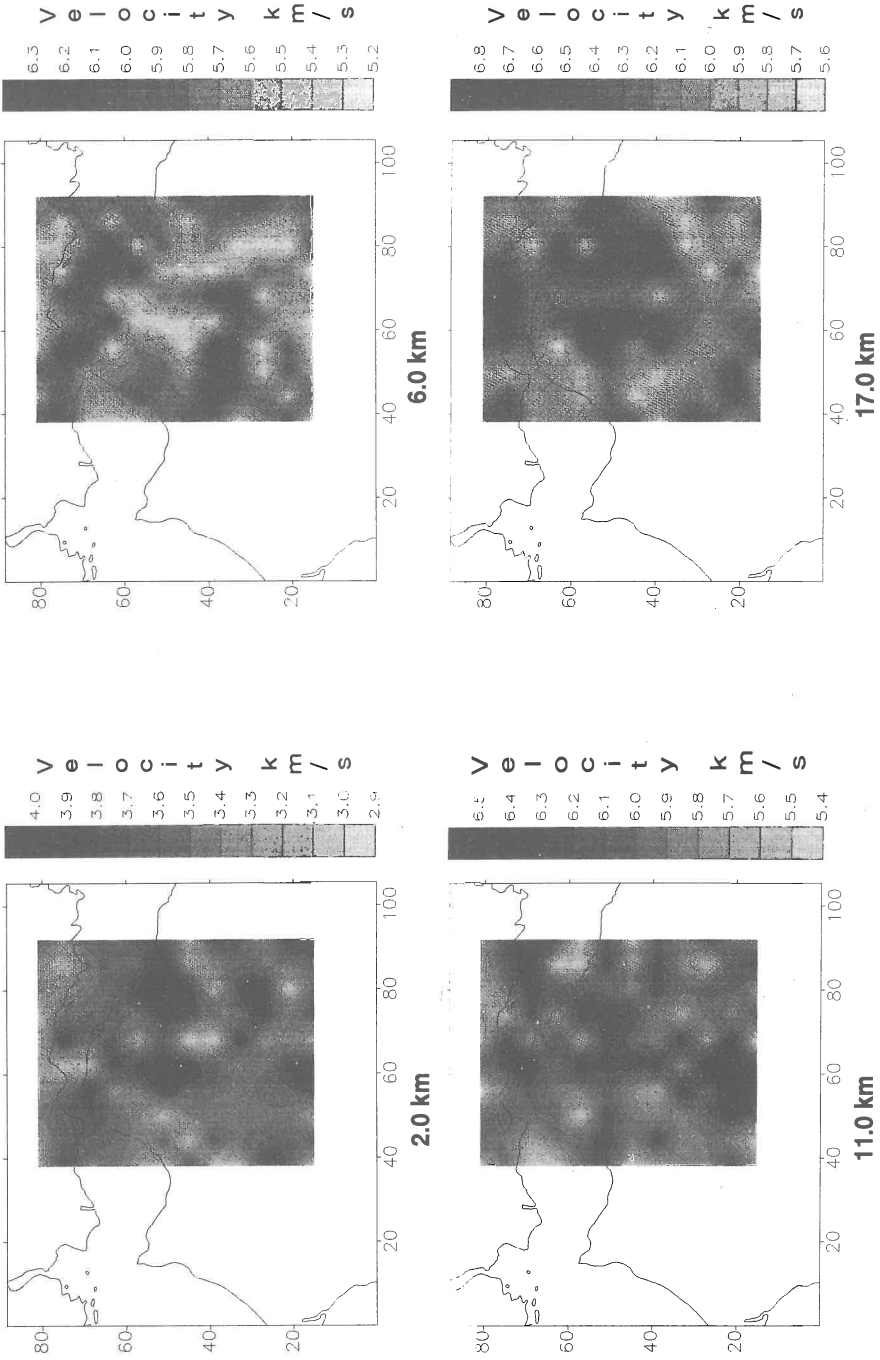
Figure 6. P-wave velocity (km/s) distribution in the study area obtained by the implementation of Thurber's (1986) method (Model B) at depths of 2, 6, 11 and 17 km.

Nikolaou, K., 1988. Neodiapyric movement of the Triassic evaporites in Zakynthos and Strofades islands. Bull. Geol. Soc. Greece, 20, 83-99.

Thurber, C.H., 1986. Nonlinear earthquake location: Theory and examples. BSSA, V 75, pp 779 - 790.

Voulgaris, N., 1991. Examination of the structure of the earth's crust in the area of Zakynthos - NW Peloponnesus (W. Greece). Ph. D. Thesis, Univ. of Athens, 224 pp.

ACTIVE FAULTING AND 3-D VELOCITY STRUCTURE AT STENO DAM-SITE AREA (NW GREECE) AS DETERMINED BY TOMOGRAPHIC INVERSION OF P-WAVE TRAVEL TIMES

Ioannis Louis, J. Drakopoulos and K. Pavlou

University of Athens, Geophysics & Geothermy Division
Panepistimiopolis Ilissia, 15784 Athens, Greece.

Abstract

As part of the geophysical-geological investigations for the construction of a hydroelectric project at Steno (Epirus area) in north-western Greece, an array of 15 portable seismic stations was installed around Steno site to monitor the background seismicity of the broader area. During the two years recording period a total number of 1014 local earthquakes with magnitude greater than 1.7 and focal depths in the range 0-35 Km were determined. 272 of these events, uniformly distributed in the target area, were finally selected for the construction of the 3-D velocity structure.

The relocated events and the 3-D seismic structure, simultaneously determined with tomographic inversion techniques, are in a good agreement with the surface geology and the complex tectonics of the area. Thus, a fairly good correlation seems to exist between the slightly relocated (0-3 Km) epicenters and the details of the surrounding velocity structure as with the shallow low velocity areas and the gaps in the surface faulting. The almost diffuse seismicity pattern, obtained initially with the 1-D velocity model and station corrections, is now significantly constrained. Instead, some lineaments in the seismicity are now apparent.

There is a strong evidence that the major faults in the broader area of Steno are seismically active while the observed linearities in seismicity pattern increase the probability that some minor faults are active as well.

The advantages of using a reliable 3-D velocity model are discussed and the conclusions support the results of previous investigators (King et al., 1983; Papazachos and Drakopoulos, 1985; Kiratzi et al., 1987).

Introduction

One of the most useful techniques for the investigation of the crustal structure in seismically active zones has been the method of simultaneous inversion for seismic structure and hypocenters (SSH). Since its original conception by Aki and Lee (1975), many technical variations and

velopments have made it practicable to image complex geological structures both on regional and local scale, given reasonably well distributed seismicity and seismological stations (Thurber and Aki 1987; Eberhard Philips 1989). 3-D tomography has been applied in active well instrumented areas such as the Geysers (Eberhard-Philips and Openheimer, 1984; O' Connell and Johnson, 1991), Long Valley (Kissling 1988; Romero et al., 1993), Loma Prieta (Foxal, 1992), Irpinia Earthquake (Amato and Selvagi, 1993), Lesvos island (Louis et al., 1994), Aegean Sea (Louis et al., 1995) yielding smooth velocity models with adequate resolutions. This study targets to contribute in the knowledge of the velocity structure of the area using 3-D inversion techniques. The SSH method proposed by Aki and Lee was employed and the results are compared with previous seismotectonic studies of the region.

Background

Northwestern Greece plays an important role in most of the geodynamical models of current deformation in the Aegean. This region of north western Greece lies near the transition area between a zone of active subduction located just south of the Ionian islands at the Hellenic trench and a region where continents collide in Apulia and northern Greece. Significant tectonic activity in the region created folds and thrust faults that generally strike northeast-southwest or more rarely, northeast. The study area shows complex tectonics in the sense that normal and thrust faulting have been reported not far apart from one another(figure 3a and b).

In the area west of the region examined, King et al. (1983) attributes the variation in the fault plane's solution to local inhomogeneities in the stress field producing localized extension and main tectonic features. Complicated patterns of both the seismicity and the focal mechanism characterize the area where no clear general pattern about its deformation was shown (King et al. 1983; Kiratzi et al.,1987).

During the period November 1982 to October 1984 the Public Power Corporation (PPC) of Greece established and operated a network of 15 portable seismographs to monitor the seismicity of the Steno area where a dam is to be constructed. Over 1000 local seismic events were recorded and analysed (Papazachos and Drakopoulos 1985) for a time period of two years. Figure 1 shows the aerial distribution of the seismic sources. The network configuration established and the two major tectonic lines of the area are shown in figure 2.
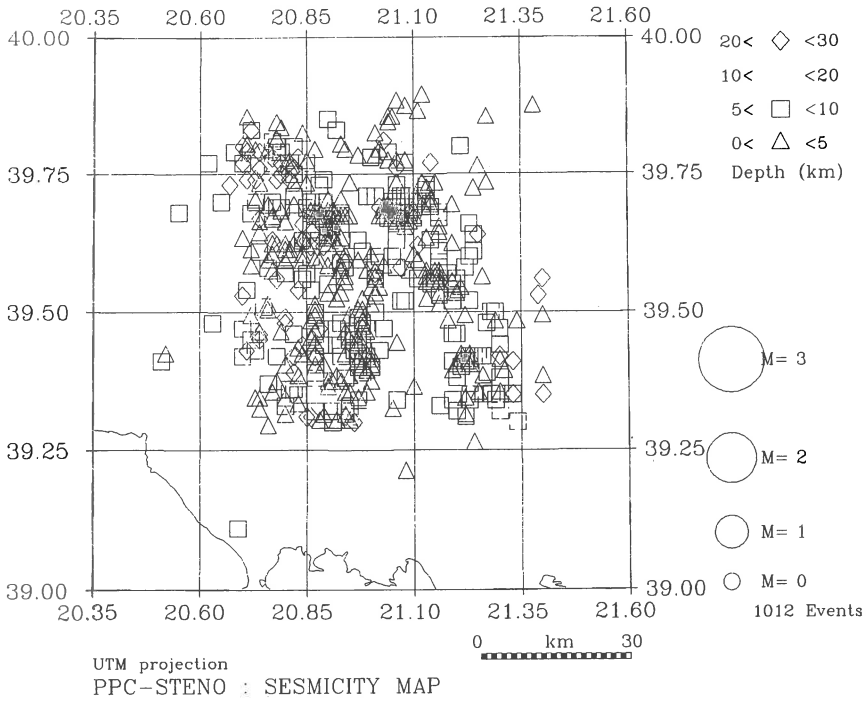
Figure 1. Location map and map view of the seismicity recorded by the PPC seismological network.
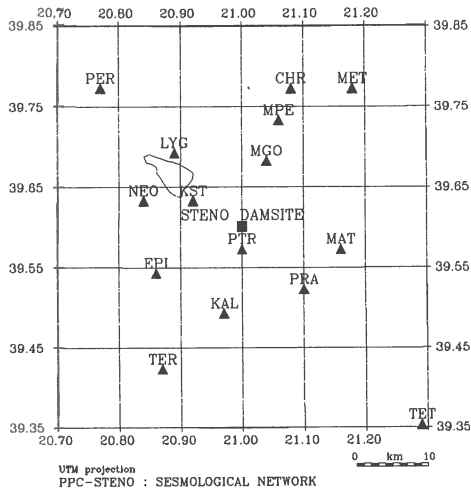
Figure 2. Map showing the seismological network configuration, the Steno dam site.
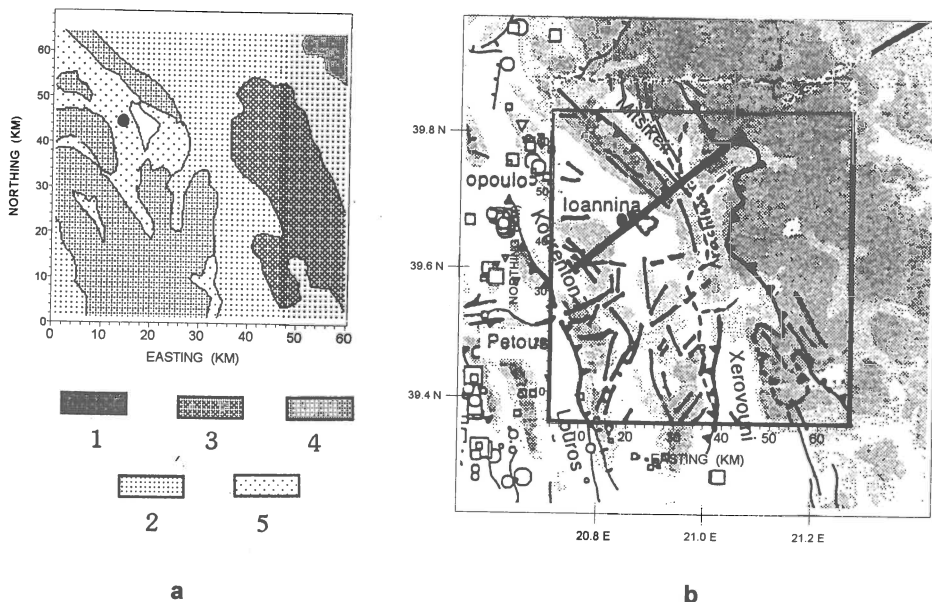
Figure 3. Simplified geology map (a) (IGME, 1989) and the tectonic structure of the area (b) (Hatzfeld et al., 1995; IGME, 1989).
1=Basic and ultra-basic igneous rocks, 2=Flysch formations, 3=Olonos-Pindos limestones locally alternate with cherts and schists, 4=Ionian zone limestones and dolomites, 5=Alluvial deposits.

In this study we present a detailed three-dimensional velocity model for the greater area of Steno damsite, determined from local earthquake arrival times using 3-D inversion techniques. The velocity structure and the seismicity simultaneously analysed are based on the advantages of using a reliable 3-D velocity model and give a better understanding of the active tectonic processes in this seismically active region.

Data acquisition and processing

The seismic recorders used in this experiment were all Sprengnether MEQ-800 instruments. The first arrivals were picked using magnifying lens with an estimated accurancy better of 0.1 s for P-waves. The data for this analysis consist of direct P-wave arrival times for local earthquakes recorded during the operation of the PPC network. A total number of 1014 local earthquakes with focal depths ranging from 0 to 35 km were determined. Among them we excluded all events whose rays did not lie entirely within the target model.

The final data set selected for the simultaneous inversion of hypocenters and velocity structure included 3224 phases recorded at 15 stations from 272 high quality seismic events. Care was taken to ascertain that these selected

events were well distributed both in epicentral distance and in depth. This way we improve the spatial distribution of the data set, and in the mean time we conserve the most important events, that is the larger and deeper events with more phases.

The initial event location was carried out using the program HYPO71 (Lee and Lahr, 1975). Particular attention was also paid at the determination of the velocity model.

Method of Inversion

The inversion technique used to compute the three-dimensional velocity structure is that originally developed by Aki & Lee (1976). In this method the earth beneath the seismic array is divided into plane layers and each layer is divided into rectangular blocks. An average P-wave velocity is assigned to each layer. Linear equations relating the observed relative residuals to the average fractional slowness perturbations within the blocks are inverted to calculate the slowness perturbations within the blocks.

The study area is a block of 70X70X18 km with coordinates of its south-western corner 39.4°N - 20.7°E. This volume was parameterized with a grid of cells with constant velocity, as required by the inversion algorithm. The number of grid cells is selected with attention to the total number of data in order to achieve a reliable solution. Thus the crust of the study area was divided into five layers and each layer into 10X10 rectangular cells. The cell size for all layers was 7X7 km in NS and EW directions. The vertical cell size for the first three layers was 3 km. Due to poor ray sampling with depth a vertical cell size 4.5 km was used for the last two layers in order to achieve a reliable solution. Only blocks that were sampled by at least 20 rays were included in the inversion; less frequently sampled blocks were constrained to have zero slowness anomaly. The whole inversion procedure used can be summarised as follows :

Model parametarization.
Important factor for the successful application of the methodology is the use of a realistic initial reference velocity model. Both 1-D and 3-D crustal models for the study area have been investigated. The choice of the geometry of the models and the number of layers and blocks was based on such factors as getting optimal ray coverage. For this purpose a number of tests were run using the inversion algorithm with a grid of 1X1X5 blocks. Among several models we selected the best fit half-space by observing the weighted mean residual for P phases and the associated weighted standard deviations. Information from relevant seismic experiments (Hatzfeld et al. 1990) were also considered. The following half space was found to best meet these criteria:

Velocity (Km/s)	Top of the layer (Km)
5.2	0.0
6.0	3.0
6.2	6.0
6.7	9.0
6.8	13.5
7.0	18.0

Hypocenter location.

The initial hypocenters location was routinely determined by using the standard location techniques such HYPO71 (Lee & Lahr, 1975) and an homogeneous starting crustal velocity model.

Application of the inversion technique.

Application of the damped least squares inversion and computation of the velocity perturbations to the initial model. The best damping value was determined by performing preliminary one-iteration runs with different damping parameters. With a selected value of 60 s² / (Km/s)² for the damping parameter a 40% improvement in the travel time residuals (0.25s) was achieved after five iterations. The final velocity model, well-resolved to a depth of 13 km within the area of investigation, is shown in figure 4.

Relocation of the hypocenters.

Earthquakes were relocated with the updated 3-D velocity model. The rms residuals for the locations of the hypocenters in the space ranged from 0.1 to 0.5s with an average of 0.3s. Most of the rms residuals are larger than the estimated reading error of 0.1s and this is attributed probably to the unmodelled velocity variations prevailing particularly near the surface layer.

Final inversion model and interpretation

The results of the tomographic inversion are presented by means of velocity distribution contour maps (figure 4) and in terms of a cross section (figure 7). Since poor ray sampling for the cells below the predominat hypocentral depth (~13 km) prevents the computation of the velocity anomalies we only present here the lateral velocity variations at 3, 6, 9 and 13.5 km depths

The velocity structure

The most striking feature in the velocity structure is the lateral velocity variation in the upper 3 km. The velocities in this layer are strongly influenced by the surface geology (figures 3a and 4a). In particular the P-wave velocity for

the area east and west of Arachthos river (figure 4a) ranges from 5 to 5.3 km/s. According to the geology (figure 3a) this area is covered by the flysch formation and its velocity appears to be overestimated. This overstimation is probably attributed to the initial model parameterization. Thus the initial velocity for the first layer (5.2 km/s) and the vertical block size (3 km) adopted, leaded to a suppression of the shallow (<1 km) and lower velocity structure.
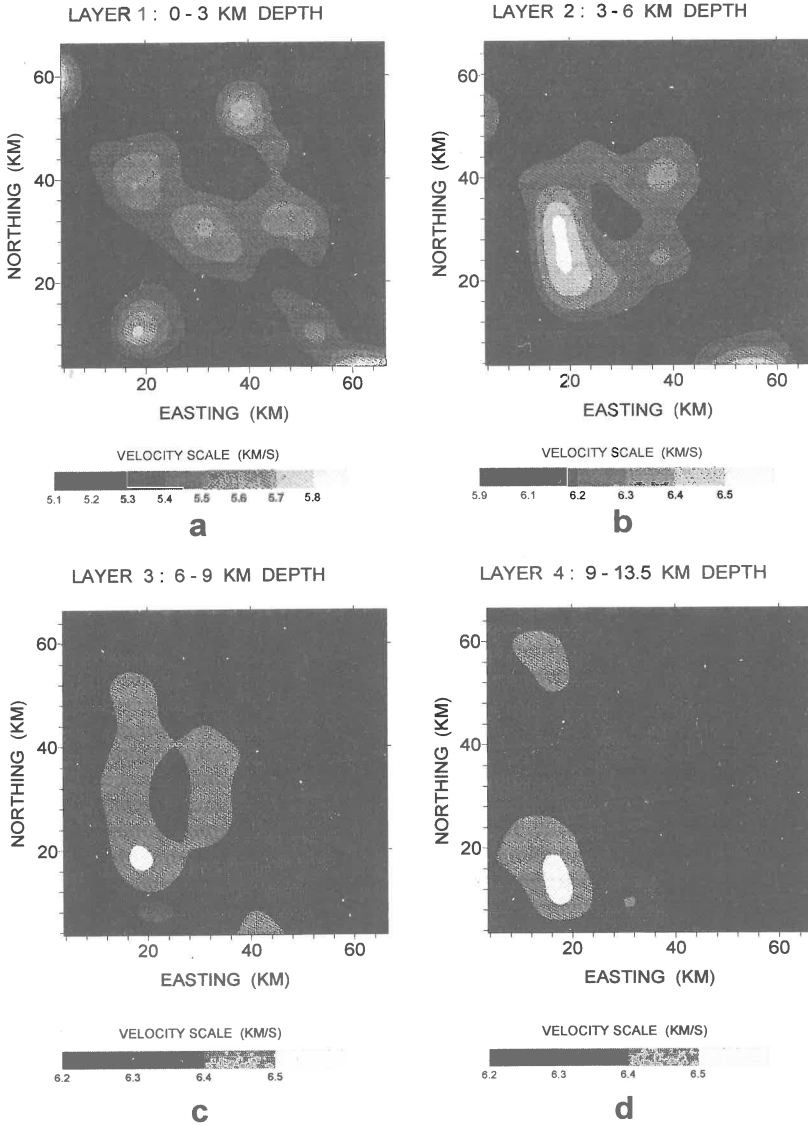
Figure 4. Velocity distribution contour maps.

The location and strike of the boundaries between high and low velocity regions seen in figure 4a and b correspond approximately to the position of the three major tectonic lines of Pindos thrust fault, Mitsikeli - Xerovouni trend and Kourenton fault, trending NW-SE (figures 4a and 3b).

The velocity structure becomes more uniform below the depth of 6 km. The diffuse low-velocity regions extended east and northeast of Arahthos river for the first 6 km depth (figure 4a and b) and west of the river at greater depths (figure 4c and d) are fictitious and correspond to unresolved areas due to a poor ray sampling. The low-velocities observed in the northern, southern and western part of the central area (figure 4a) may be possibly explained by the presence of the Triassic eveporites. An evidence for the latter explanation is the almost total absence of seismicity in the above areas (figure 6a).

The seismicity pattern
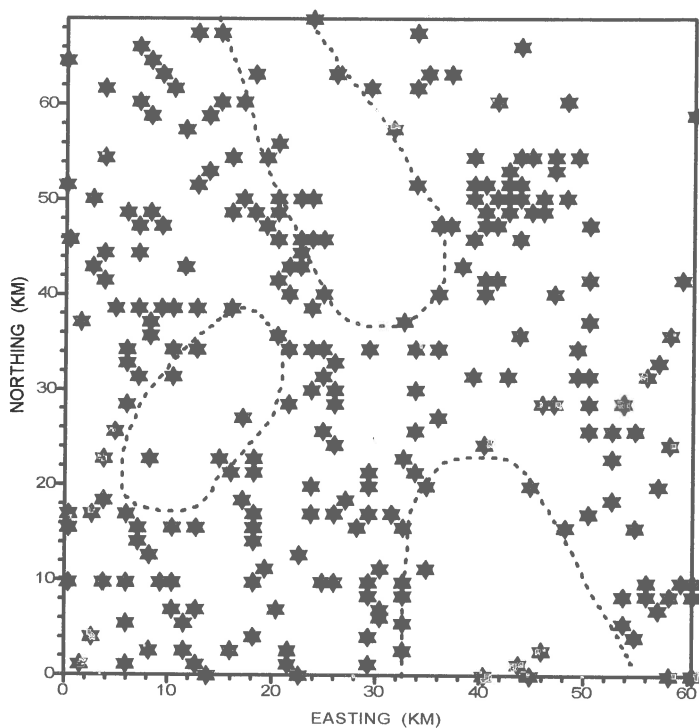
Figure 5. Map view of the relocated events

Figure 5 is a map view of the relocated events. The seismicity pattern varies along the length of the fold structure. The most dense concentration of

seismic sources extends along the main tectonic structures of the area. Thus a dense concentration of epicenters is observed along a curved strip zone striking NS over high-velocities and coinciding with Mitsikeli and Xerovouni faults (figure 6a). In the same figure similar linear concentrations are observed over high-velocity strip zones coinciding with Pindos thrust fault and Kourenton and Louros tectonic structures as well.
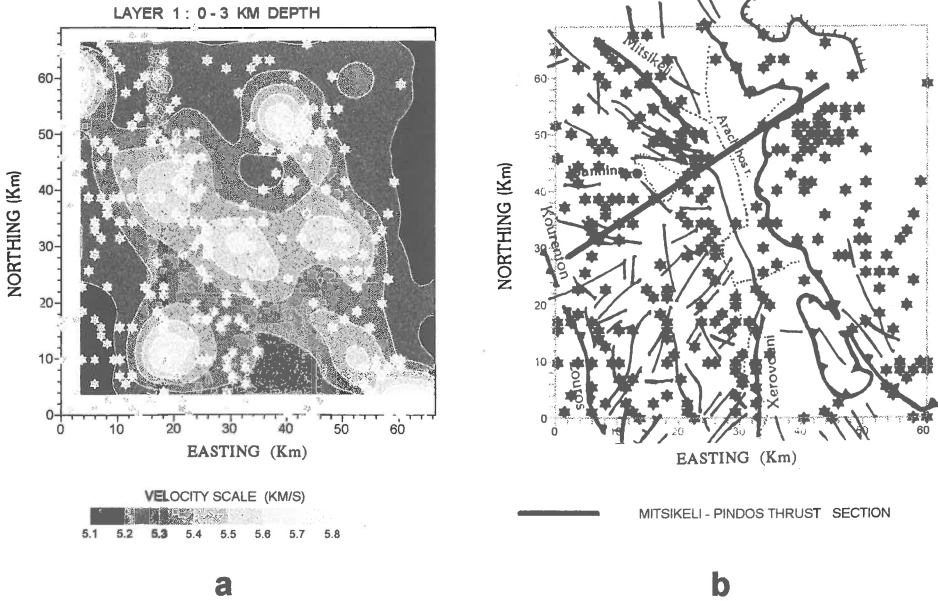
Figure 6. Surface layer velocity variation and seismicity (a) and tectonic structure and seismicity (b).

Minor diffuse seismicity is also concentrated in a SW-NE direction over the high-velocity blocks crossing the Mitsikeli-Xerovouni and Pindos tectonic structures (figure 6a). Looking in figure 5 a great tectonic activity with a considerable number of small faults is observed in the above area.

The aseismic regions in the study area are explicitly observed over the low-velocity zones. They are characteristic the seismic gaps observed over the northern, southern and western part of the central area in figure 5 (areas enclosed by dotted line), possibly attributed to the presence of the Triassic evaporites as it was discussed earlier.

The Mitsikeli - Pindos cross-section

Looking at the cross-section of figure 7, perpendicular to the Mitsikeli and Pindos main tectonic structures, we can see three clusters of seismic sources.
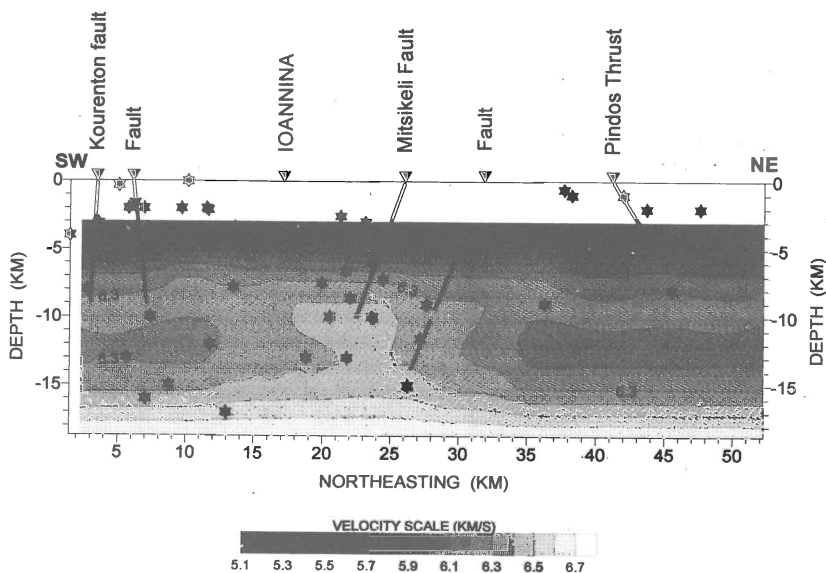
Figure 7. Cross - section of hypocenters and velocity model across Kourenton - Mitsikeli - Pindos thrust. The seismicity is concentrated beneath the main tectonic structures, giving thus evidence that the above faults are still seismically active.

The central cluster is observed over the main velocity anomaly, forms a strip zone dipping SW and coincides with the Mitsikeli fault. There is also a good correlation between the second cluster observed in the northeast end of the section, its location and the position of the Pindos thrust fault. A more diffuse seismicity pattern occurs in the southwest end of the section where the Kourenton fault occurs. It is evident that all of the tectonic structures discussed are still seismically active. Mitsikeli fault seems to concentrate the higher seismic activity. The continuous seismic activity observed along the strip zone Mitsikeli - Xerovouni gives evidence for a possible extension of Mitsikeli fault towards the Steno damsite area.

Summary and Conclusions

The prominent velocity anomalies apparent in the three dimensional model show a remarkable correlation with the surface geology and tectonic structure. It is obvious the correlation between seismicity pattern, velocity distribution and the location of Mitsikeli, Xerovouni, Kourenton and Pindos main tectonic structures which leads to the conclusion that they are still seismically active.

Further to this obvious correlation, with the 3-D velocity model and the relocation of the seismic sources obtained for the study area, some of the

748

secondary features in the seismicity pattern are now more detailed delineating thus a seismically active set of minor faults.

There is strong evidence of a possible extension of the Mitsikele fault towards SE where the Steno dam site area is located.
The results is in agreement with other geophysical and seismotectonic studies in the region.

References

Aki, K., and W.H.K. Lee, 1976. Determination of three-dimensional velocity anomalies under a seismic array using P arrival times from local earthquakes 1. An homogeneous initial model. *J. Geophys. Res., 81, 4381-4399.*

Amato, A., and G. Selvagi, 1993. Aftershock location and P-velocity structure in the epicentral region of the Irpinia earthquake. *Annali di Geofisica, xxxvi, 3-15.*

Eberhart-Phillips, D., and D.H. Oppenheimer, 1984. Induced seismicity in The Geysers geothermal area, California. *J. Geophys. Res., 89, 1191-1207.*

Eberhart-Phillips, D., 1989. Active faulting and deformation of the Coallinga anticline as interpreted from three-dimensional velocity structure and seismicity. *J. Geophys. Res., 94, 15565-15586.*

Foxall, W., 1992. Heterogeneous slip and rupture models of the San Andreas fault zone based upon three-dimensional earthquake tomography, *Ph. D. thesis, Dep. Of Geol. And Geophys., Univ. of Calif., Berkeley.*

Hatzfeld, D., Pedotti, G., Hatzidimitriou, P., and K. Makropoulos, 1990. The strain pattern in the western Hellenic arc deduced from a microearthquake survey,. *Geophys. J. Int., 101, 181-202.*

Hatzfeld, D., Kassaras, I., Panagiotopoulos, D., Amorese, D., Makropoulos, K., Karakaisis, G., and O. Coutant, 1995. Microseismicity and strain pattern in northwestern Greece. *Tectonics, vol. 14, No 4, 773-785.*

King, G., Tselentis, A., Gomberg, J., Molnar, P., Roecker, S., Sinvhal, H., Soufleris, C., and J. Stock, 1983. Microearthquake seismicity and active tectonics of northwestern Greece. *Earth and Planet. Sci. Lett., 66, 279-288.*

Kiratzi, A., Papadimitriou, E., and B. Papazachos, 1987. A microearthquake survey in the Steno dam site in northwestern Greece. *Annales Geophysicae, 5B, (2), 161-166.*

Kissling, E., 1988. Geotomography with local earthquake data. *Rev. Geophys., 26, 659-698.*

Lee, W., and J. Lahr, 1975. HYPO71 (revised) : a computer program for determining hypocenter, magnitude , and first motion pattern for local earthquakes. *U. S. Geol. Surv., Open-file Rep., 75-31, 113pp.*

Louis, I., Delibasis, N. and G. Apostolopoulos, 1994. Passive seismic tomography and 3-D velocity structure of the uppermost crust below Lesvos island, Greece. *Expanded Abstracts, 64th Annual meeting and technical exhibition of the Society of Exploration Geophysicists, Los Angeles, October, 23-28, pp. 795-798.*

Louis, I., Karantonis, G., Makropoulos, K., and D. Hatzfeld, 1995. Tomographic images of P-wave velocity distribution at the central Aegean Sea area, Greece. *Expanded Abstracts, 4th International Congress of the Brasilian Geophysical Society and the 1st Latin American Geophysical Conference, Rio De Janeiro, Brasil, August, 20-24, pp. 1083-1086.*

O' Connell, D.R., and L.R. Johnson, 1991. Progressive inversion for hypocenters and P-wave and S-wave velocity structure : Application to The Gaysers, California, geothermal field. *J. Geophys. Res., 96, 6223-6236.*

Papazachos, B., and J. Drakopoulos, 1985. Final report of the seismic activity in the Steno area. *Public Power Corporation of Greece, 53 pp.*

Romero, A., McEEvilly, T., Majer, E., and A. Michelini, 1993. Velocity structure of the Long Valley Caldera from the inversion of local earthquake P and S travel times. *J. Geophys. Res., 98, 19869-19879.*

Seismotectonic Map of Greece. *I.G.M.E. 1989 .*

Thurber, C.H., and K. Aki, 1987. Three-dimensional seismic imaging. Annu. *Rev. Earth Planet. Sci., 15, 115-139.*

KNOWLEDGE-BASED SYSTEMS FOR SEISMOGRAM INTERPRETATION

Claudio Chiaruttini

Department of Naval Architecture, Ocean and Environmental Engineering
University of Trieste, Trieste, Italy
and
Department of Georesources and Territory
University of Udine, Udine, Italy

Abstract

This article reviews the issues in the application of knowledge-based systems (KBS) to seismic event analysis: seismic knowledge representation, integration of numerical signal-processing and logical reasoning based on qualitative and heuristic knowledge, interpretative strategies, selective focus-of-attention control, blackboard system architecture, uncertainty handling. A distinguishing feature of these systems is an efficient interpretative strategy based on step-wise refinement of solution hypotheses and error correction. As an example, the design of SNA2, a KBS for the interpretation of records from a local network, is illustrated in some detail. Experience proves that the KBS technology is mature to be routinely employed in seismic observatories. Success rates up to 90%, when compared with a seismic analyst performance, are attainable. Low detection thresholds may be safely used when combining traditional signal-processing with logical reasoning. Explicit representation of domain knowledge allows to explain in natural language the system reasoning chain. Artificial intelligence techniques offer the possibility to improve the quality of automatic seismogram interpretation greatly. They are particularly appealing in the frame of the ISOP project, since they allow to code, preserve and disseminate the knowledge of expert seismic analysts.

Introduction

The advent of automatic analysis of seismic records assures timely processing of the large amount of data collected daily by seismic networks. However, the ability of most automatic systems is limited to the bare needs of picking first arrivals and evaluating event location and magnitude. It is now well known—and deprecated—how computer-intensive seismology had the side-effect of reducing the quality of seismic event catalogues and data bases, with respect to the time of human analysis. A further negative impact of automation was the reduction in number of skilled interpreters, who are the real repositories of seismological practice. The spread of the awareness of the limits of routine seismic signal analysis is the reason for the ongoing ISOP project, aimed at the improvement of the quality of seismic data analysis. Artificial Intelligence (AI) provides techniques that may be profitably applied to these problems.

In the cognitive sciences, two are the principal paradigms to model intelligence. The first one is known as *declarative* or *symbolic*. It is focussed on *explicit* representation and manipulation of knowledge (Barr and Feigenbaum, 1981). These techniques are well suited whenever the interpretation principles can be expressed in a symbolic form, and especially when a mathematical theory on the application domain exists. An appealing

751
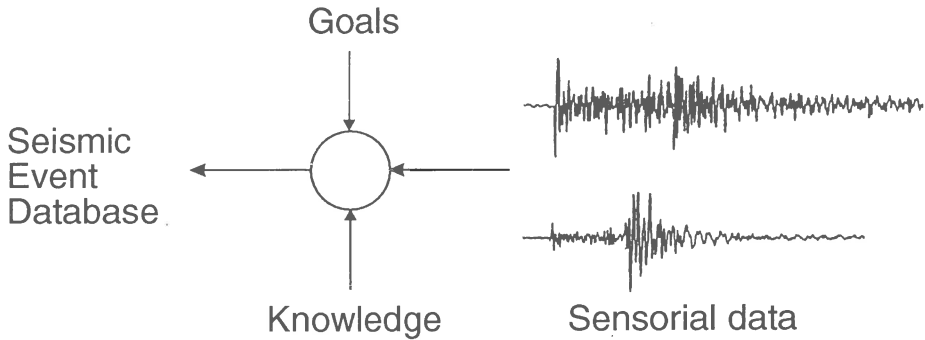
Figure 1: Seismogram interpretation as a perceptual activity.

property of this approach is the possibility to explain the reasoning steps. Knowledge-based systems (KBS) of this kind have been designed and tested successfully in seismology (Chiaruttini *et al.*, 1989; Bache *et al.*, 1990; Roberto and Chiaruttini, 1992; Bache *et al.*, 1993).

The second paradigm is *connectionist*, and attempts to mimic how the brain is organized and works (see, e.g. Pao, 1988). A distinguishing feature of artificial neural networks is the abstraction ability, which makes them able to learn from examples. However, once a net is trained, knowledge is encoded *implicitly* in the synapses weights, and can hardly be explained in symbolic terms. Interestingly, this resembles some behaviour of human experts, when they can give correct answers, although they may have difficulty in giving a straightforward explanation of their reasoning. Examples of application of neural networks to seismology are given by Dowla *et al.* (1990), Dysart and Pulli (1990), Dai and MacBeth (1994). Symbolic and connectionist AI constitute complementary approaches, that future automatic systems will most probably need to integrate.

Another approach to seismogram interpretation, based on "mental images", was proposed by Joswig (1993, 1994). Pictorial representations of signals (adapted sonograms) are used as knowledge-base. This approach shares aspects of both the above paradigms. Like declarative AI, it makes use of an explicit knowledge representation, although of analogue rather than symbolic nature; at the same time, like connectionist AI, it uses directly a set of representative seismic signals.

The scope of this article is the review of issues in the application of declarative KBS to seismology: seismic knowledge representation, integration of numerical signal-processing with logical reasoning based on qualitative and heuristic knowledge, interpretative strategies, selective focus-of-attention control, blackboard system architectures, uncertainty handling. Examples are taken from the design and test of SNA2, a KBS for interpretation of records from local networks (Chiaruttini *et al.*, 1989; Roberto and Chiaruttini, 1992).

Knowledge and knowledge representation

Seismogram interpretation may be defined as a perceptual activity, by which visual information on waveform is converted into a data-base of seismic events (Figure 1). According to Newell (1981), the key attribute of intelligent interpreters is rationality, meaning the use of *knowledge* to fulfill some goal. In the declarative paradigm of artificial

Event

part-of

Trace

part-of

Seismogram

part-of   *part-of*

Background Noise

part-of

Transient Noise

part-of

Phase

Is-a   *Is-a*   *Is-a*

Pg-phase   Sg-phase   ...-phase
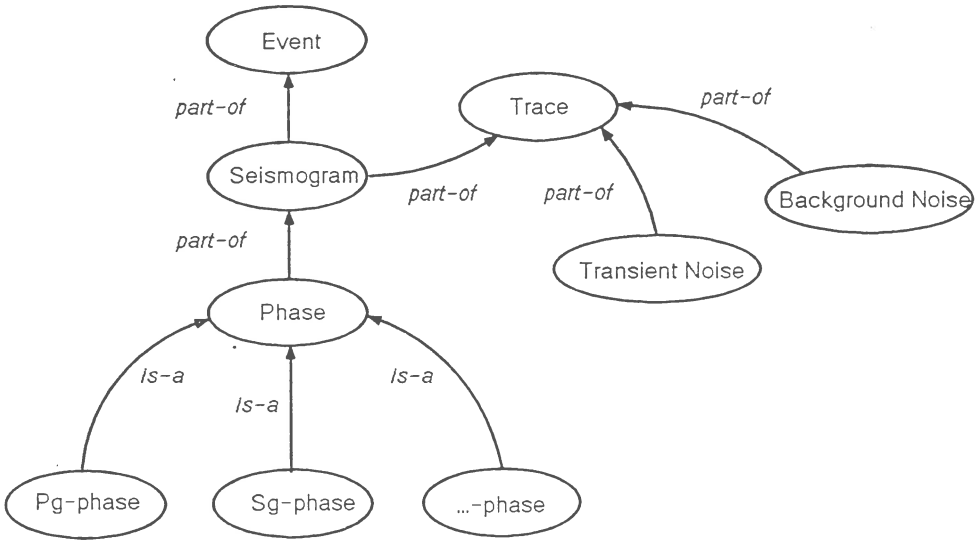
Figure 2: Semantic net with the most relevant seismological objects and the relations among these.

intelligence, knowledge is modelled by a set of explicitly defined concepts (or objects) and a set of procedures that manipulate them (Barr and Feigenbaum, 1981). Loosely speaking, concepts are the static part of knowledge and procedures are the dynamic part.

To make knowledge available to an automatic agent, a suitable representation technique is needed. As an example, consider the *semantic net* in Figure 2: a directed graph where the nodes are objects and edges are binary relations among them. **Part-of** links form the part-to-whole decomposition hierarchy, **is-a** links form the taxonomical classification hierarchy.

The dynamic part of knowledge consists of procedures to instantiate and manipulate objects. They include all numerical procedures routinely used for phase picking, event location, and so on. Expert knowledge consists not only of numeric computational tools; an essential part is logical in nature and allows to infer new information from established facts. A commonly used representation of this kind of knowledge is by means of antecedent-consequent pairs termed *rules*. The following "compatibility rule":

> if the arrival time difference of a phase at two stations
>   is greater than the travel time between the two
> then the arrival times are incompatible

illustrates how well a known mathematical property of wave propagation can be translated into inferential knowledge. Theory is not all with expert knowledge; a large part of the ability of skilled interpreters is heuristic in nature and acquired by practice. This also can be represented by rules whenever precise symbolic statements can be given. Rules can be easily coded with commercial expert systems shells or with specific languages, like OPS5, which was used for SNA2. The efficiency of this approach is demonstrated in seismology by the performance of IMS and of SNA2, which we will discuss later.
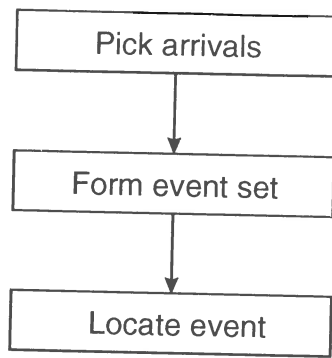
Figure 3: Data-driven strategy for seismogram interpretation.

The interpretative strategy

The most straightforward interpretative strategy is *data-driven*, as in Figure 3. Data are processed to extract phase arrival times and waveform attributes, then phases are grouped within association windows to form event sets, and finally the event parameters are computed. Although correct in principle, this strategy is faced with the problem of combinatorial explosion and leads to algorithms that are impractical, but for small networks and a very limited number of events occurring within an association window. As an example, consider k stations, all recording the first arrivals of n events within the association time window. There are as much as $(n!)^{k-1}$ ways to form event sets taking one onset from each station. To compute the optimal solution—i.e., the one with the least location errors—for 10 stations and as few as 3 events one should search through a space in excess of 10^7 possible associations.

To obtain feasible algorithms, it is necessary to restrict the search space using additional information, like amplitude and frequency of phases. Frequently, *a priori* expectations are used to generate acceptable solutions, the correctness of which is *checked* against the data. This constitutes a *model-driven* strategy, where data are used to validate or reject models (i.e.: hypotheses) of the world. Once a test is not passed, the cause of failure can be analyzed to obtain clues to "debug" the hypothesis and generate a better one. The *generate-test-and-debug* (GTD) paradigm of problem-solving (Fig. 4) results in efficient strategies for sampling the solution space.

The GTD paradigm lends itself to step-wise refinement of the solution. To do so, we need to perform tests at a greater level of detail than the previous hypothesis generation. As an example, consider the way SNA2 behaves in the analysis of an event (Fig. 5). After preliminary arrival picking, one seismogram per station is selected within an association time window, compatibility analysis is applied to each onset time pair, incompatible pairs are inspected to sort out the miss-picks most likely responsible for the fault. The set of correct, mutually compatible, picks constrains the possible arrival-time intervals on wrong traces. A sensitive detection algorithm is applied in the predicted time-intervals to prove or disprove the signal onset hypothesis. A more complete account of the SNA2 interpretative strategy is given by Chiaruttini *et al.* (1989) and by Roberto and Chiaruttini (1992).
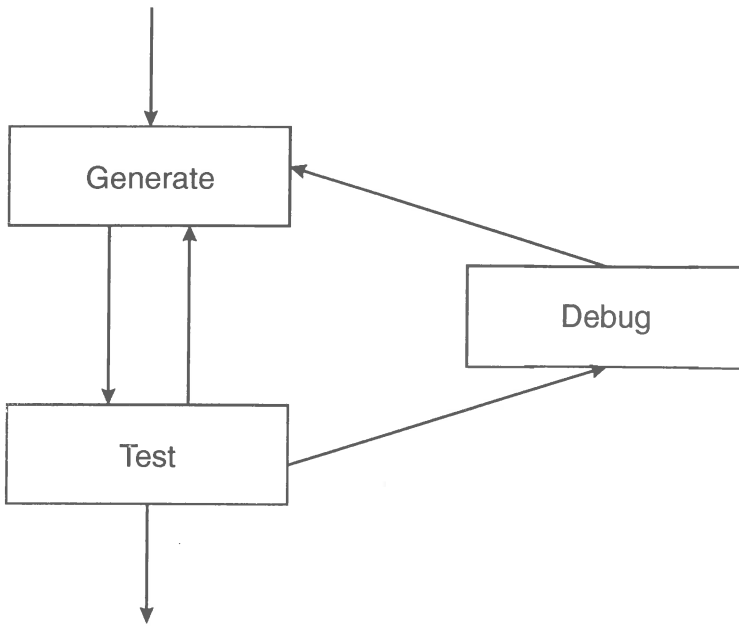
Figure 4: The *generate-test-and-debug* (GTD) paradigm of problem-solving.

Another critical point for the efficiency of a system lays in the focus-of-attention control. Interpretation activity flows through instantiation of a whole set of objects (see Fig. 2). The selection of the object on which attention should be currently focussed is a key point in the strategy. One could, for instance, focus on details, and extract all possible information about individual phases before attempting to locate the event. Needless to say, this strategy may be wasteful, if bursts of noise are fully analysed before coincidence analysis reveals what they are. On the contrary, having a gross event location may help in labeling phases, and dictate the use of analysis procedures specific for the event distance-class.

<center>Blackboard architecture</center>

The *blackboard model* (Engelmore and Morgan, 1988) is a well established architectural principle for the design of KBS. It assumes the distinction between domain objects and procedures: the former are instantiated in a volatile memory (the *blackboard*), the latter form the set of *knowledge sources* (KS), modules which manipulate the blackboard. Each KS has an activation condition, which is to be satisfied before it can be executed. The system activity then flows in a KS activation-execution cycle under the control of a scheduler. When multiple KS are activated, a conflict is said to occur. Conflicts are solved by the scheduler, which selects the KS to execute according to the some strategy.

The strategy of SNA2 is defined assigning the knowledge sources increasing priority levels for tasks generating, testing, and debugging hypotheses, in the order (Fig. 6). Within each category, priority is further split according to the aggregation level of the target objects (**part-of** relation). Inferences on events and phases have high and low priority respectively. This allows the scheduler to follow the GTD cycle; furthermore, the

<center>755</center>
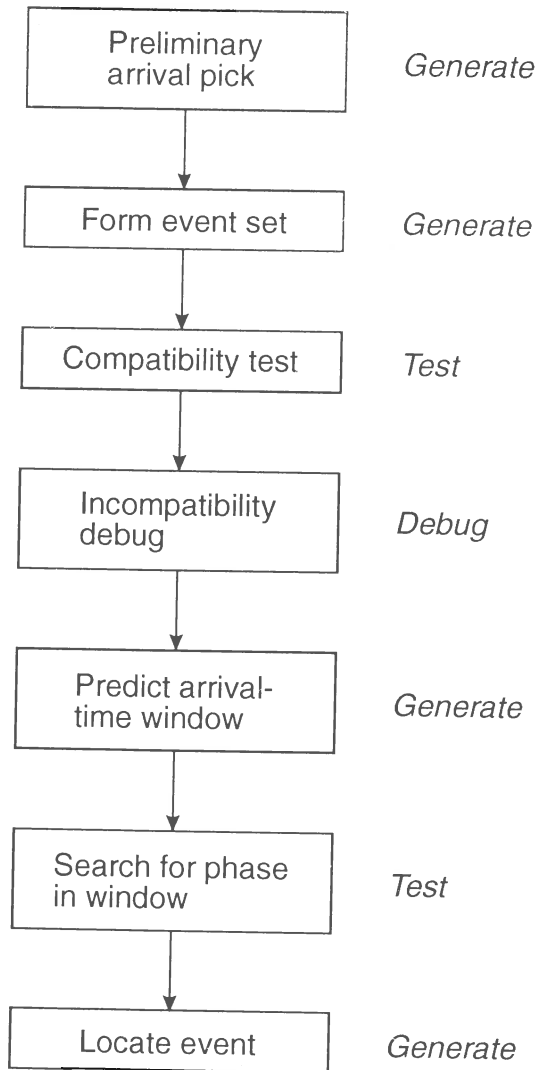
Figure 5: A procedure based on the GTD paradigm used by SNA2 for event analysis.

PRIORITY   TASK TYPE   AGGREGATION LEVEL

high ↑   Debug

                                 Event
                                 Trace
       Test   Seismogram
                                 Phase

low | Generate
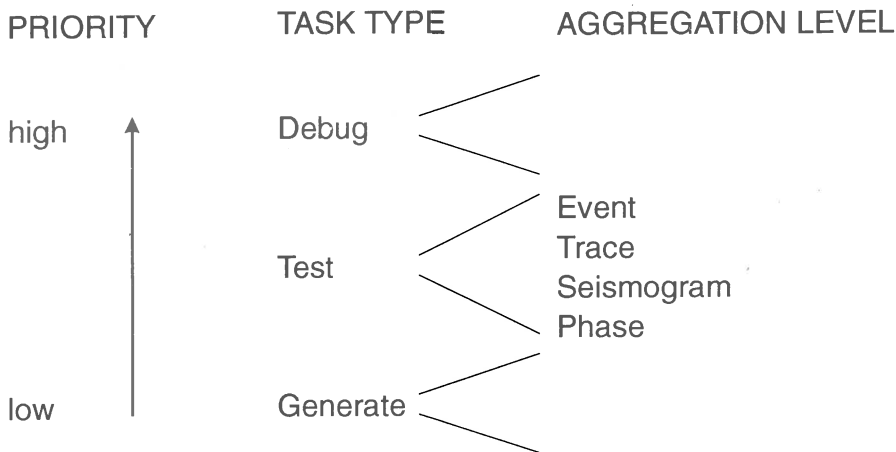
Figure 6: Priority level for the KS scheduling strategy in SNA2.

system attention is preferably focussed on the interpretation context (i.e., the event) rather than on details (like phase attributes). SNA2 uses extensively the step-wise refinement of interpretation. This adds efficiency to the system, allowing to quickly dismiss noisy records and to spend time extracting waveform details only after the presence of a seismic event has been ascertained.

Uncertainty handling

The argument of uncertainty is two-fold. First, data are incomplete and affected by noise. Second, knowledge itself is often uncertain, and different experts may eventually draw different conclusions from the same evidence. Handling uncertainty is an essential part of a KBS. Several approaches have been proposed, and here, again, the problem is a balance between correctness and tractability. Bayesian theorem on posterior probability is a theoretically firm ground to make inferences, although, in practice, approximations are needed to avoid combinatorial explosion. At the opposite, the efficient method of "certainty factors" is based on heuristics and is difficult to justify theoretically. Ng and Abramson (1990) give a thorough review of the most popular methods.

Seismological knowledge is largely based on the theory of elastic waves, so we deemed unnecessary to introduce knowledge uncertainty in the design of SNA2. Uncertainty in data and conclusions is dealt with by rating the clarity of signals and events in three levels: clear, probable, and possible signals, plus positive noise. The reasoning strategy of SNA2 embeds step-by-step inclusion of data with decreasing rating, low-rate signals being forbid to invalidate the results obtained with high-rating data.

Experience with SNA2

The SNA2 was designed to analyse records from local networks and was implemented to run on VAX/VMS platforms. OPS5 production system language was used for the control modules and logical reasoning, Fortran 77 for numerical processing, and C language for the graphic user interface.

The capability of SNA2 in the analysis of first arrivals is illustrated in Figure 7 with

E V E N T   D I S P L A Y

EVENT #   1 is LOCAL   and rated CLEAR

Magnitude   : 2.487000
Epicentre latit. and longit.: 46.36900 13.03
                       +/- 10.00000   K

Recorded at Stations:

CAE RCL UDI BOO ZOU BUA BAD MPRI COLI

SELECT: Event (number or N(ext), Reasoning (R), Seism.
        Back to CBH Menu (X)

R E A S O N I N G   C H A I N

Ev	Sei	Ph	Tr	
	CAE	PG		The FIRST ARRIVAL phase TYPE was INFERRED, based on the Seismogram distance class.
	CAE	PG		The TIMES of these PHASES are INCOMPATIBLE.
	UDI	PG		
	CAE	PG		The TIMES of these PHASES are INCOMPATIBLE.
	RCL	PG		
	CAE	PG		FIRST Phase may be TOO EARLY and SECOND TOO LATE, having number of incompatibilities with later and earlier Phase
	RCL	PG		
	CAE	PG		The FIRST ARRIVAL was searched and FOUND by the Detector
				- End of Reasoning Chain

SELECT: More (Return), Again (A), Skip n Reasoning Steps (+/- number),
        Back to Hypothesis Display (X)

TAL
COLI
UDI
CAE
RCL
MPRI
DRE
BAD
BUA
BOO
ZOU

0   10   20   30   40   50
                                          Time (sec)

Exit this menu

Figure 7: An example of first-arrival analysis by SNA2. Correct preliminary picks are indicated by thick arrows; thin arrows indicate wrong initial hypotheses in stations UDI and CAE.

a local event recorded in 1987 by the North Eastern Italy Seismometric Network run by OGS (Udine, Italy). Preliminary picks, correct within 1 s, obtained by a cursory detection algorithm (Chiaruttini, 1991) are indicated by thick arrows. Initial wrong detections on the noisy traces of UDI and CAE were recognized by compatibility analysis and corrected using a sensitive detector, according to the procedure in Figure 5. An approximate location of the event is given in the upper-left panel of Figure 7.

The ability to *explain* reasoning is a distinguishing feature of KBS, which rests on the symbolic representation of knowledge. This feature provides the user with the possibility to understand deeply the performance of the system, thus gaining confidence in its results. Also system debugging and maintenance is greatly eased. An example of explanation, in natural language, is shown in the upper-right panel of Figure 7, containing the reasoning chain on the CAE station.

Tests show that SNA2 is highly efficient and reliable. The step-wise hypothesis refinement strategy allows to quickly reject noisy records and use time-consuming algorithms only for real seismic events. The integration of numerical processing with logical reasoning assures the possibility to test and correct interpretative hypotheses. In this way, the problems caused by detection false alarms are greatly reduced. SNA2 was successfully tested with detection thresholds as low as 1.5 in signal-to-noise-ratio, still keeping correct interpretation rates of nearly 90% of cases.

Conclusion

KBS can be designed to perform with success rates not too far from those of expert seismologists. Knowledge representation in a symbolic form allows to use theoretical knowledge, as well as heuristic knowledge that can be expressed in a symbolic form. The possibility to provide explanations of reasoning is important in three respects at least. First, the expert user can easily validate the system performance. Second, system debugging and maintenance is greatly simplified. Third, systems of this kind can be used to train human interpreters. The KBS technique is therefore appealing in the frame of the ISOP project, since it allows to encode, preserve, and disseminate the knowledge of expert seismic analysts.

Acknowledgements

References

Bache, T.C., S.R. Bratt, J. Wang, R.M. Fung, C. Kobryn, and J.W. Given, 1990. The Intelligent Monitoring System. Bull. Seism. Soc. Am., 80, 1507-1526.

Bache, T.C., S.R. Bratt, H.J. Swanger, G.W. Beall, and F.K. Dashiell, 1993. Knowledge-based interpretation of seismic data in the Intelligent Monitoring System. Bull. Seism. Soc. Am., 83, 1507-1526.

Barr, A. and E.A. Feigenbaum, 1981. The Handbook of Artificial Intelligence, vol. 1. Pitman.

Chiaruttini, C., 1991. Focus-of-attention techniques in the automatic interpretation of seismograms. Pageoph, 135, 61-75.

Chiaruttini, C., V. Roberto, and F. Saitta, 1989. Artificial intelligence techniques in seismic signal interpretation. Geophys. J. Int., 98, 223-232.

Dai, H. and C. MacBeth, 1994. Split shear-wave analysis using an artificial neural network?. First Break, 12, 605-613.

Dowla, F.U., S.R. Taylor, and R.W. Anderson, 1990. Seismic discrimination with artificial neural networks: preliminary results with regional spectral data. Bull. Seism. Soc. Am., 80, 1346-1373.

Dysart, P.S. and J.J. Pulli, 1990. Regional seismic event classification at the NORESS array: seismological measurements and the use of trained neural networks. Bull. Seism. Soc. Am., 80, 1910-1933.

Engelmore, R.S. and A.J. Morgan, Editors, 1988. Blackboard systems. Addison-Wesley.

Joswig, M., 1993. Single-trace detection and array-wide coincidence association of local earthquakes and explosions. Computers & Geosciences, 19, 207-221.

Joswig, M., 1994. Knowledge-based seismogram processing by mental images. IEEE Trans. Syst. Man Cybern., 24, 429-439.

Newell, A., 1982. The knowledge level. Artif. Intell., 18, 87-127.

Keung-Chi Ng and B. Abramson, 1990. Uncertainty management in expert systems. IEEE Expert, April issue, 29-48.

Pao, Y.H., 1988. Adaptive Pattern Recognition and Neural Networks. Addison-Wesley.

Roberto, V. and C. Chiaruttini, 1992. Seismic signal understanding: A knowledge-based recognition system. IEEE Trans. Signal Proc., 40, 1787-1806.

SEISMOMETRY IN GERMANY - DEMONSTRATED BY THE EQUIPMENT OF THE SEISMOLOGICAL STATION JENA/MOXA (1900 - 1975)

Unterreitmeier, E.[*], Kowalle, G.[**]

[*] GeoForschungsZentrum Potsdam, Germany
[**] GTU Ingenieurbüro Knoll, Teltow, Germany

Abstract

Seismometric research and development as well as the production of seismometers have a long and successful tradition in Germany. The seismic stations which at the beginning of the century were an integrated part of the faculties of natural sciences have been equipped with instruments developed at these institutions.
Jena is an old town with university located in Thuringia, within the central part of Germany. The history of the seismological station Jena is very similar to that of other German stations, but it has also some peculiarities. So after the Word War I the Reichsanstalt für Erdbebenforschung has been shifted to Jena. One of the tasks of this institution beside regular providing of seismological recording was the development and test of new instruments. So working at Jena KRUMBACH, MARTIN, and MEISSER have introduced new ideas into seismometry.
Based on the records and bulletins of the seismological station Jena/Moxa the history of instrumentation is presented. Some general trends of the development of seismometry can be demonstrated by the historical equipment of this station. It's a great luck the most of the historical instruments of this station could be preserved.
This tradition has been continued by the Institute Earthquake Research and Soil Dynamics at Jena and Central Institute for Physics of the Earth. Starting in the sixties TEUPSER and latter UNTERREITMEIER have developed new instruments, which were used not only at Moxa but also at several other stations in GDR, Eastern Europe, and Cuba. Now Moxa station is equipped with very broad band instruments, too, and integrated into the German Broad Band Network.

1. Introduction

For more than 90 years the history of the seismological station Jena/Moxa is embedded into the development of seismometry and seismological research in Germany. It can be treated as the standard situation that at the end of the 19th century at most universities seismological studies have been performed. Mostly at this base the development of permanent seismological and geophysical research has been started. Within the Faculty of Physics of the University of Jena the first seismological studies have been undertaken in 1899. In the cellar of the Physical Institute temporary observations by means of REBEUR-EHLERT pendulum have been performed. In Germany the idea that most of seismological tasks can be solved only by organizing a network of observatories has been formulated firstly by REBEUR(1894). In Germany the well-known geographer G. GERLAND has done a enormous work for creating a national seismological network (GERLAND, 1904, 1905). He proposed to organize the German network consisting of two levels of stations (Tab. 1). The first order stations within the

761

network had to be equipped with excellent seismographs and clocks for recording regional and global seismicity. The second order stations had to be equipped with instruments giving the possibility for monitoring local and regional seismic activity. GERLAND proposed 11 seismological districts consisting first and second order stations.

Table 1. German Seismological Network (1904/05) as proposed by GERLAND

district	first order station	second order station
1	Aachen (1905)	Koblenz (+)
		Trier (+)
		Marburg (-)
		Fulda (+)
2	**Strassburg (**)**	Kolmar (+)
		Metz (+)
		Mühlhausen (+)
		Hohenheim (-)
		Ravensburg (-)
	Karlsruhe (Durlach)	Heidelberg (*)
		Freiburg (*)
3	Darmstadt (+)	Gießen (+)
		Fulda (+)
4	München (1905)	Nördlingen (+)
		Passau (+)
		Bamberg (-)
5	Göttingen (1903)	Clausthal (+)
6	Hamburg (1904)	Rostock (+)
		Helgoland (1905)
7	Leipzig (1902)	Plauen (1905)
		Freiberg (+)
8	Jena (1902/1905)	Meiningen (+)
9	Breslau (1905)	Bromberg (-)
		Görlitz (+)
		Glatz (+)
		Zabrze (+)
10	Königsberg (1905)	Stettin (1905)
11	Potsdam (1902)	

(*)   working in 1905,
(**)   Main station of the German Empire
(+)   planning stage in 1905
(-)   no activities in 1905

He also proposed additional stations outside the German Empire at Samoa Islands (Apia - temporary geophysical observatory), in China (Kiautschou) and in Eastern Africa (Daresalam). In the frame of this proposal firstly Jena has been mentioned as a first order station.

2.   History of the seismological observatory Jena/Moxa

Jena is located in Thuringia in the central part of Germany. It is a place with an old university where in the end of the 19th century optical industry and mechanics had strong development.

This development has been reflected into the research fields of the University of Jena, too. So in the Physical Institute there has been a concentration on optics, astronomy, and development of precise scientific instruments.

In 1899 first temporary seismological investigations have been performed in the laboratories of the Physical Institute. In 1989 in Jena an astronomical observatory has been established. In 1904 in the cellar of the observatory the permanent Seismological Observatory Jena has been established. There the REBEUR-EHLERT horizontal pendulum and a WIECHERT seismometer (seismic mass M = 1200 kg) have been installed. At this time STRAUBEL has started his experiments with a long-period seismometer developed by himself. With the work of STRAUBEL the director of the station at the Jena station the fruitful tradition to combine seismological observations with the development of new instruments has been established. Looking to the bulletins of Jena station one can recognize that there was a steady progress in performing seismological observations. The World War I interrupted the development. Due to the lack of well-trained staff and funding only a minimum of routine observations for the time period 1916 - 1923 could be performed. Practically there was no chance for installing new equipment.

In 1926 the Main Seismological Observatory of Germany together with the Reichsanstalt für Erdbebenforschung have been shifted from Strasbourg to Jena. A new building containing the seismological observatory, the seismological service, and research departments has been given to the Reichsanstalt. The equipment of the station has been modernized. So vertical and horizontal WIECHERT-seismometers with 1200 kg and 15000 kg seismic mass, respectively, have been installed. Within the Reichsanstalt a sophisticated mechanical workshop has been established, too. Beginning at this time seismological equipment has been developed by seismologists working in this institution. KRUMBACH, MEISSER, MARTIN should be mentioned in this context. The improvement of conventional instruments was the second field of activities. Especially attention was drawn to the problem of seismometer damping, to the quality of recording, and to the time service. In every of these fields there were elaborated new technical solutions which have been applied not only at Jena station but also at most other German seismological observatories. For example, at the end of the 1920s and the beginning of the 1930s the time service of Jena-station has had such a quality that the seismological station has been the reference station for post service in Thuringia.

The World War II has interrupted the development of Jena station again. Only in 1949/1950 new equipment could be installed at Jena station. In the end of the 1950s a fruitful period of instrumental research at Jena begun. In 1960 the long period electrodynamic seismometer HSJ-I developed by TEUPSER and co-workers has been taken into permanent exploitation. In 1965 the corresponding horizontal seismometer HSJ-I has been introduced into the permanent seismological observations. In 1968 and 1970 the new short period vertical and horizontal seismometers have been permanently installed at Jena/Moxa.

In 1964 due to the increasing noise level and higher resolution of the seismometric equipment the seismological station Jena had to move to Moxa. At Moxa-station there were not only realized excellent conditions for performing seismological observations, but also a test laboratory for seismometric research has been established. Especially remarkable are the investigations of the influence of different noise sources on the seismometric equipment and the quality of observations (TEUPSER, UNTERREITMEIER). In 1972 the first electronic seismograph with active electronic elements (VSJ-I/E) has been installed for systematic research. In 1975 a newly developed triaxial electronic seismograph EDS-1 has been introduced into the observatory. This large inventory of seismometers has been used successfully for producing high quality seismograms. It is interesting to mention that looking to the seismographic equipment of the station Jena/Moxa one can recognize the principal trend of reducing the seismic mass of the pendulum (Fig.1), increasing the detection capability.

Most of the instruments were installed for several tens of years and have worked simultaneously. So always a comparison of records of different types of instruments is available up to recent time.
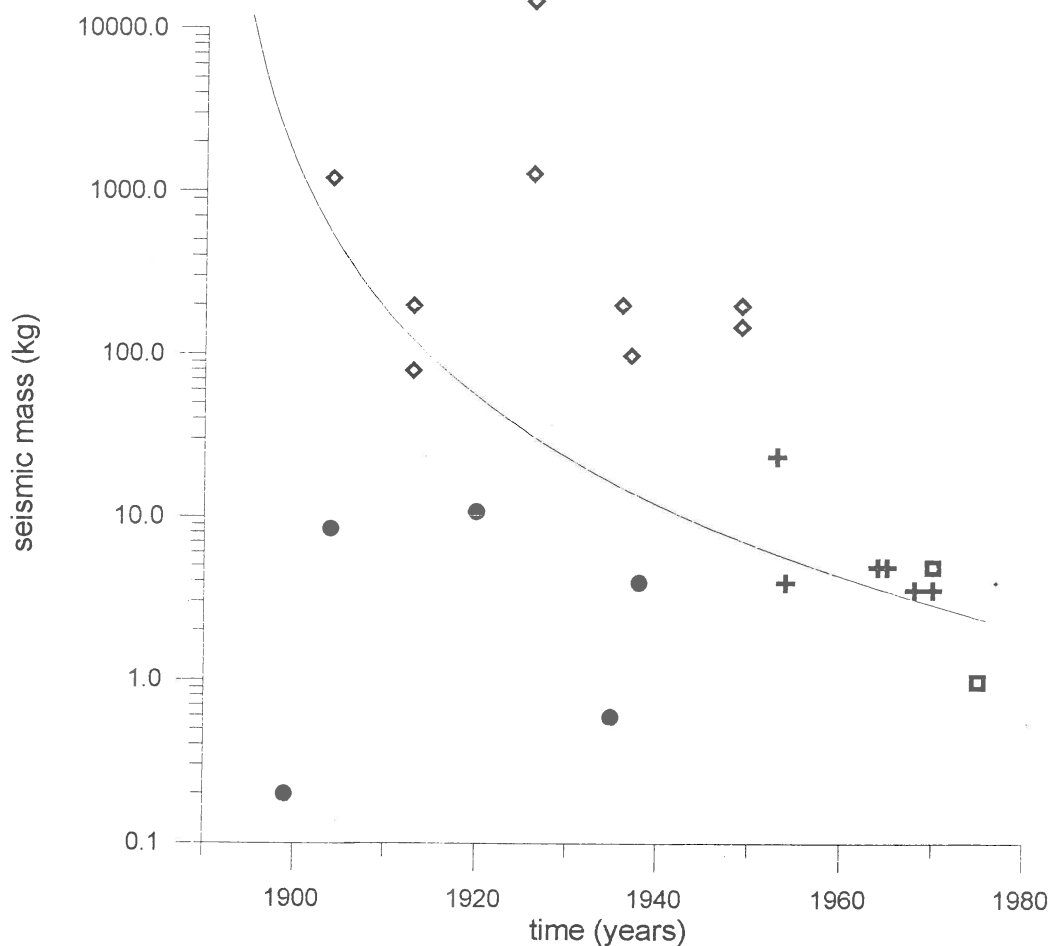
Fig.1. Change of the seismic mass of seismometers used at Jena/Moxa station. The data are taken from table 1 and indicate the year of installation of the seismometer at Jena/Moxa. Black dots represent optical recording, diamonds mechanical, crosses electrodynamical and squares electronic recording seismometers. The line represents a assumed trend in changes of the seismic mass over time.

Fig.2 shows the characteristics of seismographs being installed and in operation in 1968. There were working parallel mechanical (WIECHERT, MAINKA) and electrodynamical (mod. KRUMBACH, KIRNOS, HSJ/VSJ-I and II), as well as broad-band seismographs of the type SSJ-I.
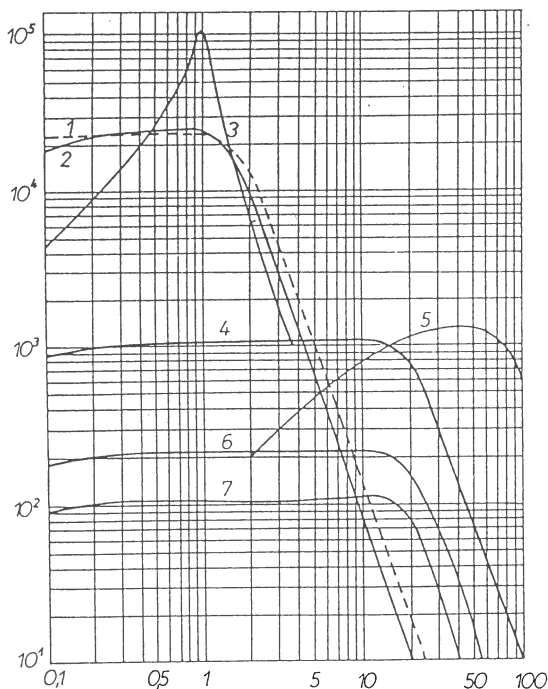
1 — Modified Krumbach Seismograph (Z-component)
2 — Seismograph Kirnos Modernised-III (SKM-III) (NS-, EW- and Z-component)
3 — Seismograph Type Jena II (Z-component)
4 — Seismic Station Apparatus Type Jena I/1000 (SSJ-I/1000) (NS-, EW- and Z-component)
5 — Seismic Station Apparatus Type Jena I/L (SSJ-I/L) (NS-, EW- and Z-component)
6 — Seismic Station Apparatus Type Jena I/200 (SSJ-I/200) (NS-, EW- and Z-component)
7 — Seismic Station Apparatus Type Jena I/100 (SSJ-I/100) (NS-, EW- and Z-component)
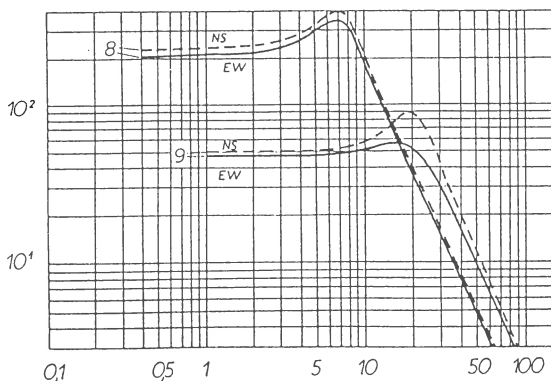
8 — Wiechert Seismograph (NS- and EW-component)
9 — Mainka Seismograph (NS- and EW-component)

Fig.2. Amplitude charachteristics of seismographs of the station Moxa (MOX) for the year 1968 (upper part - electrodynamic seismographs, lower part - mechanical seismographs) (STEZNER et al, 1973).

3. History of equipment

It is obvious that all the instruments have their own history. In Tab.2 there are shown not only the date of installation and the main parameters of the seismometers of the seismological station Jena/Moxa but also the current status of them.

Tab.2 Seismometers installed at Jena and Moxa station (1900 - 1975)

instrunent	Dates	Component	T_e [sec]	$\varepsilon : 1, \alpha_s$	V_0	type	M[kg]	State
Rebeur-Ehlert	1900-1926	3 H	(12)	1: // (3:)	-	opt	(0.2)	loss
Wiechert	1904-	2 H	10	4:	200	mech	1200	Moxa
Straubel	1904-1926	Z	6.6	4:	2030	opt	8.5	loss
Wiechert (probably 1926 to Hof)	1913- (1926)	2 H Z				mech mech	200 80	Deutsches Museum München
Wiechert	1926-1964	Z	5	3.5:	120	mech	1300	loss
Large pendulum	1926-1964	H (EW)	(1.4)	3.1:	2200	mech	15000	loss
Large pendulum	1935-1964	H (NS)	2.1	(5:)	2200	mech	1500	loss
Mainka	1936-1971	H (EW)	28	5:	25	mech	200	Museum Ranis
Krumbach	1937-1967	2 H	3	(4:)	100	mech	100	loss
Krumbach	1937-1967	2 H	(20)	(4:)	(5000)	opt	4	Museum Ranis
Mainka	1949-1971	H (NS)	23	5:	23	mech	200/150	loss
Galitzin	1953-1954	Z	(20)	-	-	el.dyn	(24)	Museum Ranis
Krumbach	1955-1971	Z	2.4	0.82	2000	el.dyn	4	Museum Ranis
HSJ-I	1960-	H (2)	20/30	0.5	950	el.dyn	5	Moxa/ Ranis
Krumbach/mod	1964-1968	Z	2.2	0.54	23 K	el.dyn	(5)	Museum Ranis
SKM/III	1965-	2 H, Z	1.5	0.5	20 K	el.dyn	(5)	Moxa
VSJ-I	1965-	Z	20/30	0.5	1500	el.dyn	5	Moxa
Strain	1967-	2 H	$T_o=50$	$\alpha_o=0.6$	V*=60			Moxa
VSJ-II	1968-	Z	1	0.5	44 K	el.dyn	3.6	Moxa
VSJ-II	1970	Z	0.23	0.35	300 K	el.dyn	3.6	Moxa
VSJ-I/E	1972- (1980)	Z	20	0.7	(25 K)	electron	5	private

opt	instrument with optical recording
mech	instrument with mechanical recording
el.dyn	instrument with electrodynamic recording
electron	instrument with electronic recording (active + possible feed back)

From Tab.2 it is obvious that in 1964, when Jena station has been moved to Moxa, a whole collection of seismometers has been removed from its permanent exploitation. It is worthy to state that more than 50 % of the old equipment could be preserved. In 1971/72 at the castle Ranis a special seismological branch of the historical museum could be organized by means of the old equipment of Jena/Moxa, Potsdam and Collm stations (UNTERREITMEIER, SCHACHE, 1983; UNTERREITMEIER, 1994). But nevertheless there were also historical instruments replaced by modern ones with scrapping the older ones. Fig. 3 shows the copy of the document of scrapping. So practically some instruments are partly or fully lost. For

example the unique STRAUBEL-seismometer could be preserved only partly, and other instruments are lost fully.

Fig.3. Copy of the receipt for scrapping metal (aluminium and brass) of historical seismometer (1970).

4.   Conclusions

The history of seismological equipment of the observatory Jena/Moxa represents the history of seismometry in Germany. Most of the typical seismometers have been installed at Jena/Moxa, too. Together with the scientific and instrumental progress the equipment of seismological stations changes more or less continuously. The parallel operation of new and older (historical) instruments is one of the most important experiences of maintaining the seismological station Jena/Moxa. This practise gave the possibility to compare the records of both types of instruments, to develop procedures for determining seismologically relevant parameters by means of records of different instruments which are compatible. This is very important due to the fact that seismology has to collect data about natural phenomena in a uniform manner over very long periods of time. So often the problem arises to convert older data into new formats and to derive parameters from historical records.

Also possible malfunctions of instruments could be detected by means of parallel recording very quickly. Further, the combination of maintaining seismological observations and instrumental research and development has shown very fruitful results.

In case that instruments within an observatory should be replaced by modern ones one has to check very carefully what to do with the instruments to be replaced. From the experience of operation the seismological station Jena/Moxa there are the following possibilities:

*   parallel operation of both types of instruments for a certain time period,
*   keeping the instruments in special stocks in the institution or in a museum, and
*   scrapping.

The solution of the problem should take into consideration the given situation, whether the instrument is of historical interest or not, is the instrument an unique one or not, should it be preserved for reconstruction of historical data or not.

5. References

GERLAND, G. (1904): Über Verteilung, Einrichtung und Verbindung der Erdbebenstation im Deutschen Reich. Beiträge zur Geophysik, vol. VI, 464 - 480.

GERLAND, G. (1905): Denkschrift über die Durchführung der vom Kuratorium der Kaiserlichen Hauptstaion für Erdbebenforschung beschlossenen Organisation des seismischen Beobachtungsdienstes in den deutschen Bundesstaaten und den Schutzgebieten. Mit Anlage I - III und 3 Karten. Beiträge zur Geophysik, vol. VII, 415 -437.

GERLAND, G. (1905): Jahresbericht des Direktors der Kaiserlichen Hauptstation für Erdbebenforschung für das Rechnungsjahr 1904. Beiträge zur Geophysik, vol. VII, 493 -522.

STELZNER, J., GÜTH, D., WEYRAUCH, J. (1973): Seismological Bulletin 1968. Station Moxa (MOX). Veröff. ZIPE.

UNTERREITMEIER, E. (1994): Grundzüge der historischen Entwicklung der Seismometrie zwischen 1879 und 1989 in Deutschland und anderen Ländern. Z. geol. Wiss., 22, 429-446.

UNTERREITMEIER, E., SCHACHE, K. (1983): Das Seismologische Kabinett im Museum Burg Ranis. Neue Museumskunde, 26, (1/83), 21 - 25.

STRONG MOTION INSTRUMENT NETWORKS

Christoph Kündig
GeoSys AG, Kanalstrasse 11, 8152 Glattbrugg, Switzerland

1. Abstract

As soon as more than one Strong Motion Instrument is implemented in a structure the question of the Network principle rises up. There are four principle Network configurations:

A Independent Recording Network
B Interconnected Recording Network
C Local Recording Network
D Central Recording Network

For each of the above principles, the specifications and advantages are pointed out and typical applications are shown. Based on the following modules: Sensor, Recorder, Center and Interconnection, the different system parameters are discussed. The key comparison parameters as common triggering, common sampling and common timing and options such as modem communication and time synchronisation are explained.

2. Introduction

Usually in a particular application one or several independent recording stations are placed at different sites. As example to show four different approaches of instrumentation a dam instrumentation is taken as base. There are six sensor sites in and around the dam: 3 at the crest, 2 at the basement and one free field site.

Site 1 = Crest Left
Site 2 = Crest Middle
Site 3 = Crest Right
Site 4 = Bottom Gallery
Site 5 = Bottom Downstream
Site 6 = Free Field
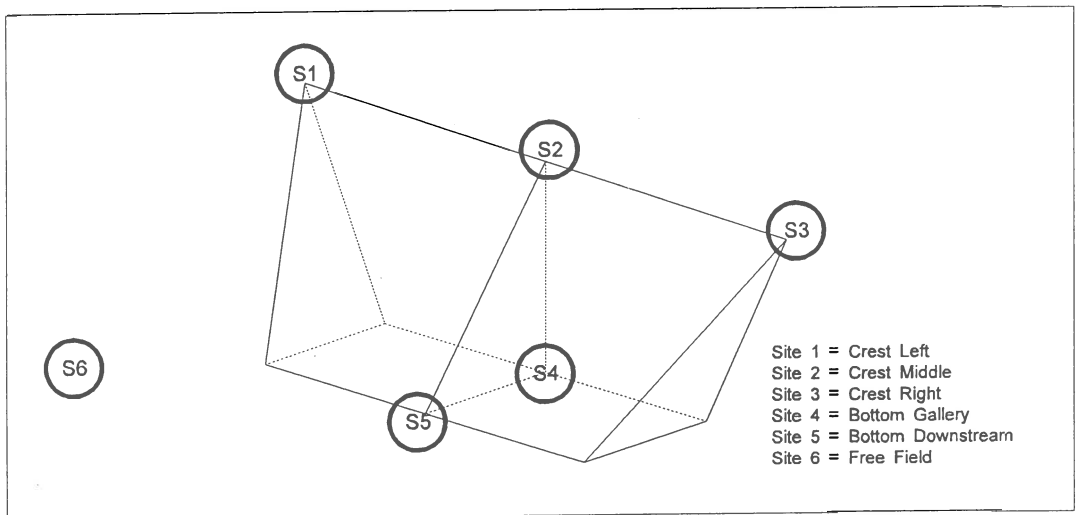
Table 1: Logic Line Network and Communication Network

The user is just interested to have information about the vibration occurring at the sites. The four different instrumentation approaches are:
- Independent Recorders
- Interconnected Recorders
- Local Recording Network
- Central Recording Network

769

Every approach has it advantages and disadvantages. The final decision about the network approach which has to be implemented has to be done by the user. Different physical implementation possibilities and limits or specification (common sampling, common triggering, common timing) of the application usually lead to one preferable solution.

3. Independent Recording Network
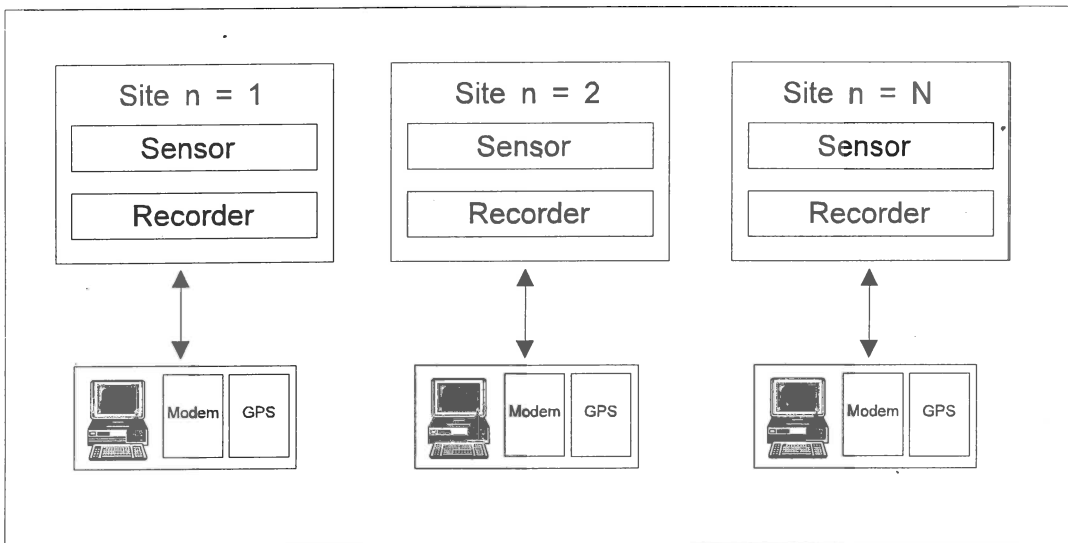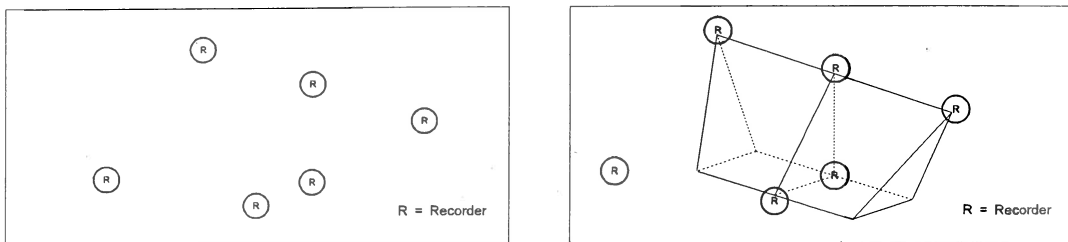
Table 2: Topology of Independent Recording Network

One or several independent recorders with internal or external sensor are placed on site. In case of an event each recorder records independently the time history of the event. An exact correlation between the individual recordings can be provided only if each of the recorder is connected to a time reference such as a GPS receiver. In this case common sampling and common timing is based on UTC-time. There is no common sampling and common triggering available. There is not any logical connection between the different recorders for triggering, therefore false triggering caused by local human induced seismic noise may occur.

The parameters settings and the data retrieval have to be performed on the site of each recorder. If several accelerometers are used, the reliability of the monitoring is quite high. A malfunction of a recorder affects only one location. Error and warning messages are visible on the site of each accelerometer, a malfunction will be recognised as soon as an on site check has been done.

Connected to every recorder as options are also are also the GPS Receiver for accurate real time (UTC), a modem as well as an automatic dial up system which can be connected to the Network Center to get external access and control of the system. An integration of one or several recorders in the local security system is possible.

4. Interconnected Recording Network
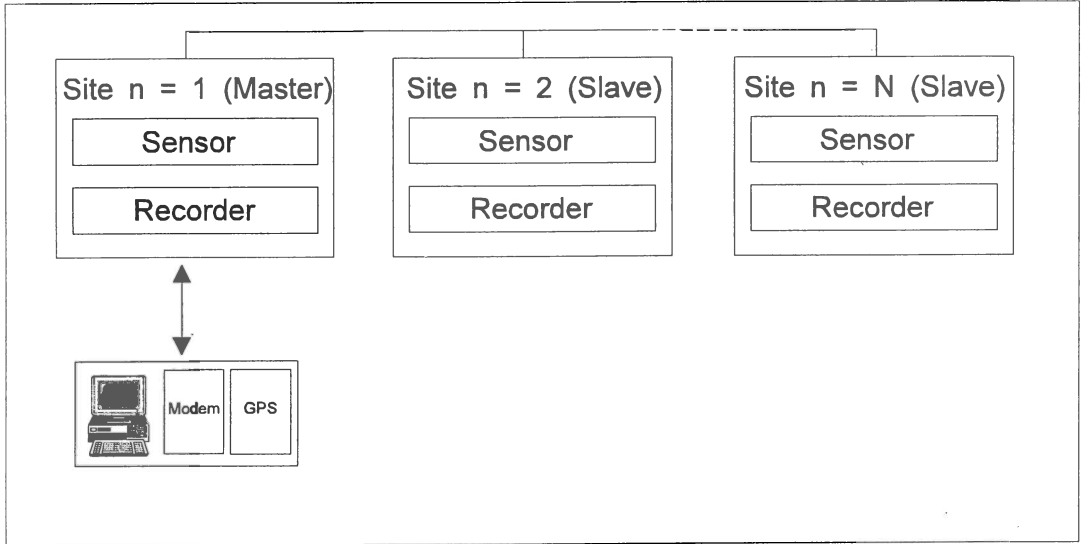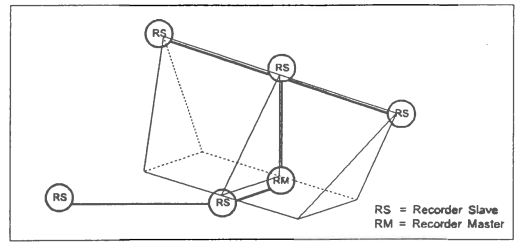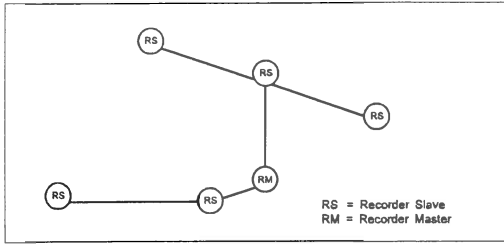
Table 3: Topology of the Interconnected Recording Network

Several independent recorders with internal or external sensors are placed on site. They are logically connected together with one twisted pair cables but galvanically isolated against each other. This is a favourable and cost effective solution for many applications.

Each recorder works and records independently. The data are stored locally in every recorder. The array gives additional common trigger in the simplest form. All interconnected recorders will start recording as soon as any authorised recorder in the array reaches its trigger level. The internal trigger capability of any recorder can also be disabled, so it starts recording only with external network trigger command.

For common time and common sampling one instrument of the array (master) is enabled to synchronise and update the internal clock of each recorder (slave) via network. A time source like DCF, Omega or GPS connected to the master controls the time system of the whole array and allows therefore easier correlation with recordings made at other arrays or at individual recorders. A local output is available for each recorder to activate an alarm.

This network approach supports fully common trigger, common timing and common sampling. The setting of parameters and data retrieval must be performed on the site of each recorder.

The reliability of the monitoring network is high. A malfunction of a recorder affects only one location in the array. If a malfunction in the master recorder occurs or the network is interrupted, every other recorder will perform as a stand-alone recorder, thus recording if the instrument recording trigger level is reached.

The interconnection between the stations can be carried out in ring, star or in net topology. Distances between the stations from up to 2 km can easily be realisable.

Connected to the master recorder as options are also the GPS Receiver for accurate real time (UTC), a modem as well as an automatic dial up system which can be connected to the master of the recorders to get external access and control of the system. An integration in the local security system is possible.

5. Local Recording Network

A network Center (GNC) takes control of an array of individual recorders with internal or external sensors. The data is recorded locally e.g. Local Recording (LR).
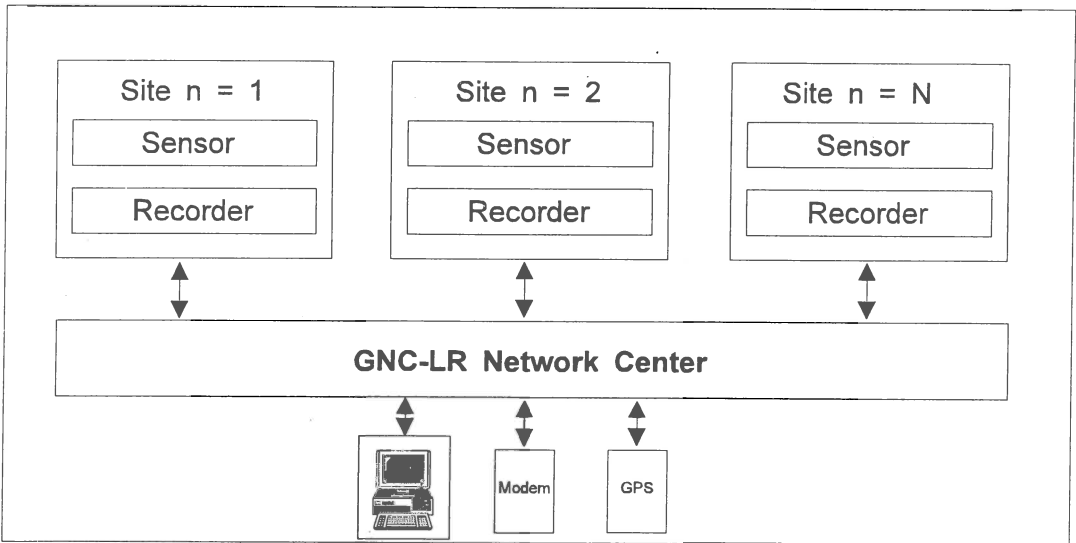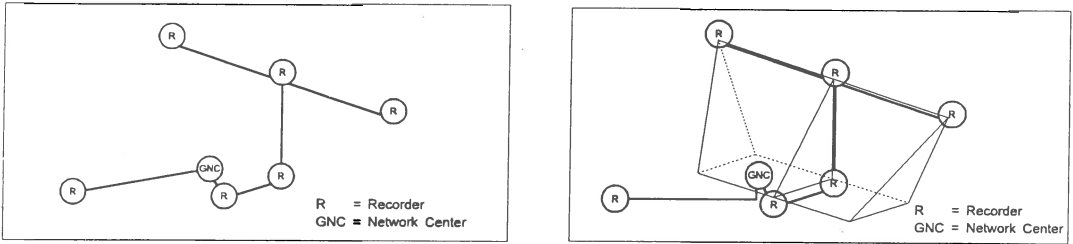
Table 4: Local Recording Network

The GNC-LR Network Center enforces common trigger only if a logical combination of individual instrument triggers is satisfied. It allows central programming, monitoring and data retrieval of every recorder in the array. Furthermore it gives on-line surveillance, common sampling and time synchronisation for the whole array. A malfunction of one recorder affects only one location in the array.

If a malfunction in the GNC-LR Network Center occurs or the network is interrupted, every recorder will perform as a stand-alone unit. The status of every recorder is indicated on-line on the GNC-LR Network Center. The interconnection between the recorders and the Network Center can be carried out in a star or a net topology or in any mixed combinations.

Optionally an Alarm Output can be defined in a way similar to recording trigger, thus allowing the personnel to be informed immediately on the intensity of an earthquake or can perform any other security circuits. Lightning and over voltage protection is used for the sensors, the recorders as well as for the Network Center unit.

Connected to the GNC-LR as options are also the GPS Receiver for accurate real time (UTC), a modem as well as an automatic dial up system which can be connected to the Network Center to get external access and control of the system. An integration in the local security system is possible.
The power for the on site recorder can be provided through the interconnection network.

6. Central Recording Network

Sensors installed on site are connected to the Network Center (GNC) where the centralised recording takes part (Central Recording, CR).
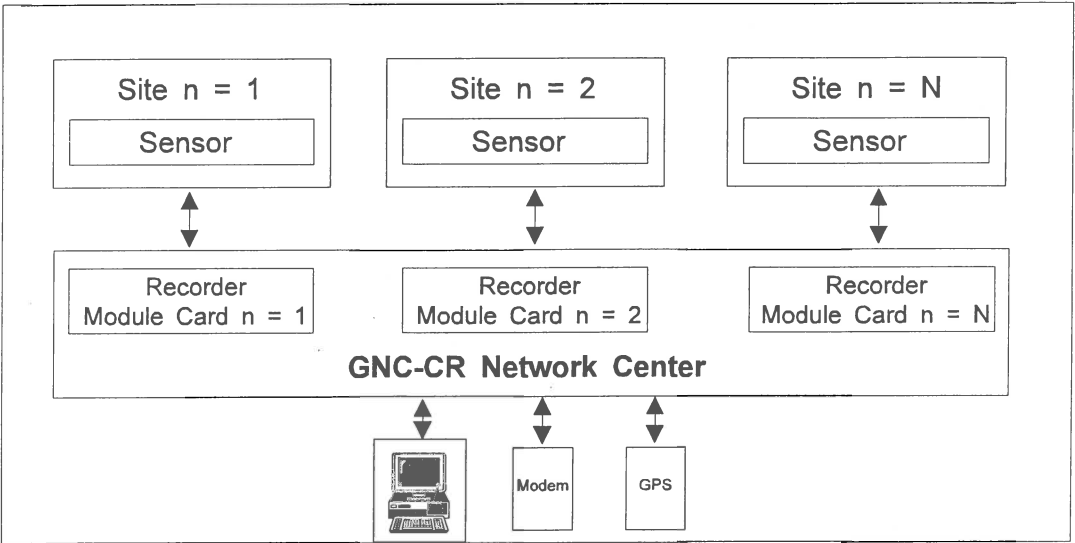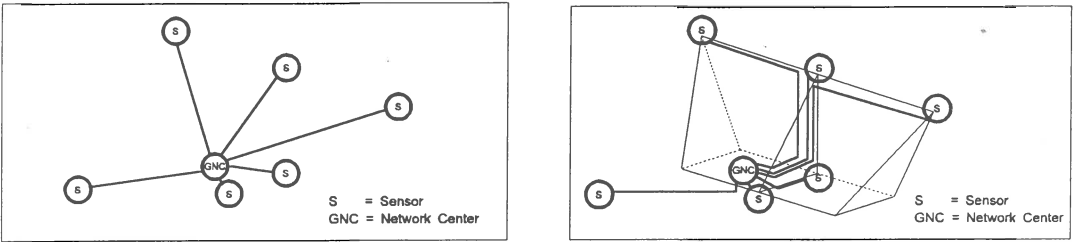
Table 5: Central Recording Network

The signal of every accelerometer in the network is converted and transmitted continuously by an industrial standard 0...20 mA current-loop to the Network Center. Within the GNC-CR Network Center Recorder Module Cards are included which fulfil the recording capability within the GNC-CR Network Center. The GNC-CR Network Center enforces common trigger only if a logical combination of individual station triggers is satisfied. The data are stored on the central recorder. Based on the principle approach, the accelerometers are interconnected in a star topology, e.g. every accelerometer has to have its own connection to the GNC-CR Network Center.

The Central Recording Network gives on-line surveillance, common trigger, common sampling and time synchronisation. The status of every station is indicated on-line in the central recorder.
Optionally an Alarm Output can be defined in a way similar to recording trigger, thus allowing the personnel to be informed immediately on the intensity of an earthquake or can perform any other security circuits. Lightning and over voltage protection is used for the sensors, the recorders as well as for the Network Center unit.

Connected to the GNC-LR as options are also GPS Receiver for accurate real time (UTC), a modem as well as an automatic dial up system which can be connected to the Network Center to get external access and control of the system. Even an integration in the local security system is possible.

Network Type	Interconnected Recording Network	Interconnected Recording Network	Local Recording Network	Central Recording Network
Common Timing	NO	YES	YES	YES
Common Sampling	NO	YES	YES	YES
Common Trigger	NO	YES	YES	YES
Logical Array Trigger	NO	NO	YES	YES
Local Alarm Option	YES	YES	YES	NO
Central Alarm Option	NO	NO	YES	YES
Data Transfer / Parameter Setting / Status Control	NO	NO	YES (Optional)	YES
Local Data Storing	YES	YES	YES	NO
Central Data Storing	NO	NO	YES (Optional)	YES
Central Power Supply Option	NO	YES (Optional)	YES (Optional)	YES
Central Station needed	NO	NO	YES	YES
Galvanic Isolation (Site - Center)	NO	YES	YES	NO
Maximal Number of Stations in the Network	UNLIMITED	60 Axes	60 / 180 Axes	60 / 180 Axes
Interconnection	NO Interconnection	1 twisted pair (2 wires) / 'High'/'Low' or 2 Fibre Optic lines	2 twisted pairs (2 x 2 wires) / RS-485 or 2 Fibre Optic lines	Analog Current Loop
Network Protocol	-	Coded Time and Trigger Information	RS-232	-

Table 6: Features of the four network principles

7. Physical Implementation of Interconnecting Hardware Consideration

Signal Interconnection

After having the network principle defined the physical implementation has to be defined. As long as there is a distance between the sensors and the recorders the analogue sensor signal must be transmitted to the recorder. The direct voltage transmission is adequate for short distances. For longer distances either differential voltage or commercial transmission must be used. The differential voltage transmission asks for high impedance inputs therefore it is obvious that the noise impact has to be considered. Widely used in the industry is the current transmission 0 .. 20 or 4 .. 20 mA. This transmission system is immune against noise impacts and also different line resistors are compounded by the current driver.

Principle	Low Signal '0'	High Signal '1'	max. Distance	Galvanic Isolation	# of Masters	# of Slaves	Signals
RS-232	< 10 V	> 10 V	30 m	Optional	1	1	TxD, RxD, GND
Digital Current loop	< 10 mA	> 10 mA	1000 m	Integrated	1	1	Send, Receive, GND
RS-485	U1 > U2	U1 < U2	1000 m	Optinal	Unlimited	Unlimited	A1, B1 B1, B2
Fibre Optic	now light	light	2000 m	Integrated	1	1	Transmit Fibre, Receive Fibre
Analog Current Loop	0 (4) mA	20 mA	1000 m	Optional	1	1	Signal, GND
Direct Voltage Transmission	- 5 V - 10 V + 0.5V	+ 5 V + 10 V + 4.5 V	5 m	Optional	1	1	Signal GND
Differential Voltage Transmission	(- 5 - Vref) V (- 10 - Vref) V (+ 0.5 - Vref) V	(+ 5 - Vref) V (+ 10 - Vref) V (+ 4.5 - Vref) V	100 m	Optinal	1	1	Signal, Reference

Table 7: Comparison between the different physical network interconnections

8. Network Terms

- **Common Timing**
  The Master station in the Logic Line Network or the Central station in the Communication network provides the time information to the network. This information is used by all the stations within the network to synchronise their internal time to the network time. This time synchronisation is a permanent task for the Master / Central station. The stations within the network permanently check their synchronisation status. In case of not having the network time information available, the Slave station bases on the internal real time clock. The time of the last successful synchronisation is available in the status information of the Slave station and is written into every event header.

  To be able to send the time information to the network, the Maser / Central station base either on their internal Real Time Clock or on an external Time Code Receiver (GPS, DCF-77, etc.). At this point the question has to be answered whether in addition to the common time within the network also the network time has to be synchronised to the absolute time.

- **Common Sampling**
  The common sampling is a result from the common timing. Every stand alone unit generates the sampling clock based on the internal real time clock. Having the internal real time clock precisely synchronised to the network time, common sampling within the network is provided.

- **Common Triggering**
  With the three flags 'Internal Trigger', 'Network Trigger Input' and 'Network Trigger Output' the behaviour of every station can be defined precisely as it is needed in the particular application. A network station located at a noisy place (traffic vibrations) can be configured to only accept triggers coming from the network.

  Every station bases on the following logic trigger algorithm.
  1. The station triggers if an internal trigger condition is fulfilled and the 'Internal Trigger' flag is set.
  2. The station transmits an active trigger message to the network if an internal trigger condition is fulfilled and the 'Network Trigger Output' flag is set.
  3. The station triggers if an active trigger message arrives from the network and the 'Network Trigger input flag is set. If a station is not synchronised to the network it still records based on the specified internal trigger condition.

GNCNETW1.DOC

- **Logical Array Trigger** (only in Communication Network)
Within the Central station some network trigger conditions can be defined. Examples: 'A network trigger is only given if at least three stations have triggered' or 'if station 5 and 7 have triggered stations 1 to 4 have to trigger as well'. This network trigger conditions depend on the particular application and the specific implementation.

- **Local Alarm Option**
If the Alarm Option is implemented in the stations they are fully working also if the station is in a network.

- **Network Alarm Option** (only in Communication Network)
The Network Alarm is working similar to the Logical Array Trigger. Based on the information coming from the different stations and based on predefined Alarm Conditions, a Network Alarm is provided by the Central station. This feature is needed in nuclear power plants for 'OBE' (Operation Base Earthquake) and 'SSE' (Save Shut-down Earthquake) alarms.

- **Data Transfer / Parameter Setting / Status Control** (Communication Network)
Within the Communication Network all the communication is fully supported by the Central station. Data can be transferred from any station to the Central station and all the stations can be configured through the network interconnection. Very useful is the only Status Control.

- **Centralised Data Storing Option** (Communication Network)
Generally data is stored within every station. To increase the data storing redundancy the stations transfer automatically after recording an event the data to the Central station. Data are stored in the Central station as well.

- **Centralised Power Supply Option**
There are applications where power is not on every station site available. In this case the power can be provided from the Central station through the network. A cable with two more wires for power will be needed. Due to security reason on the network interconnection only 48 VAC is available (voltage of public phone). Within the station the galvanic isolation is realised and the voltage is transformed to the level needed for the switched power supply.

Central Station (Communication Network)
The Central station provides data transfer, parameter setting and status control within the network in addition to common timing, common sampling and common triggering. Two user programmable alarm outputs, modem interconnection, time receiver, centralised data storing and status printer are some of the options supported by the Central station.

- **Galvanic Isolation**
There are differences in the ground potentials which have to be considered. The only solution is to make sure that all the recorders have a galvanic isolation against each other. Both network types, the Logic Line and the Communication Network can be realised with a single twisted pair interconnection or with a two fibre optic interconnection. In the case of twisted pair cables, the galvanic isolation is realised by optocouplers and in the case of a fibre optic interconnection the galvanic isolation is given by the fibre approach itself.
In any case the stations have to be connected to the local Ground (Protection Earth) and in the case of twisted pair interconnection cables a sufficient over voltage protection has to be installed.

Over Voltage Protection
Over voltage protection prevents damages and disturbances caused by electrostatic discharges and lightning. The fibre optic interconnection approach needs no over voltage protection of the interconnection lines. Nevertheless a standard over voltage protection for the station's power supply is recommended.

- **Software**
All the necessary parameter and configuration settings of a Logic Line Network can be done by the 'FieldView' program. The 'NetView' program supports the additional functions of the Communication Network.

The recorded data can be evaluated by the 'CloseView' program. This is a dedicated evaluation program designed for earthquake and civil engineering data analysis. Features like response spectrum, single and double integration, CAV etc. are implemented.

10. How to specify a Strong Motion Network?

To make it easier for network designers in a check-list, most of the points which have to be considered are listed:

1. **Network type**
   - Based on table 1 you have to select the Network type. Is a Logic Line Network suitable for your application or do you like to have the advantages of a Communication Network?
   - Specify your principle needs as Common Timing, Common Sampling, Common Triggering, ...

2. **Network topology**
   - How many stations have to be interconnected
   - Where are they located (dam, field, building)
   - What's the maximum distance between the Master / Central station to a station

3. **Interconnection**
   - Twisted pair (two lines), simple and cost effective (select cable with a total cable resistor of 100 Ohm)
   - Fibre optic (two lines), more difficult to install and expensive
   - Centralised Power supply option for stations without local AC Power needed?

4. **Master / Central station features and options**
   - Time Code receiver required?
   - Central station with Modem?
   - Central station with Status Printer Option?
   - Central station with Common Alarm Output option?
   - Central station with Centralised Data Storing option?

5. **Miscellaneous**
   - Galvanic isolation from the Master / Central station to all the other station in the network
   - Over voltage protection (at least 1.5 kW (1 ms))

11. Cost Comparison

Table 8 shows the cost comparison between the different networks.
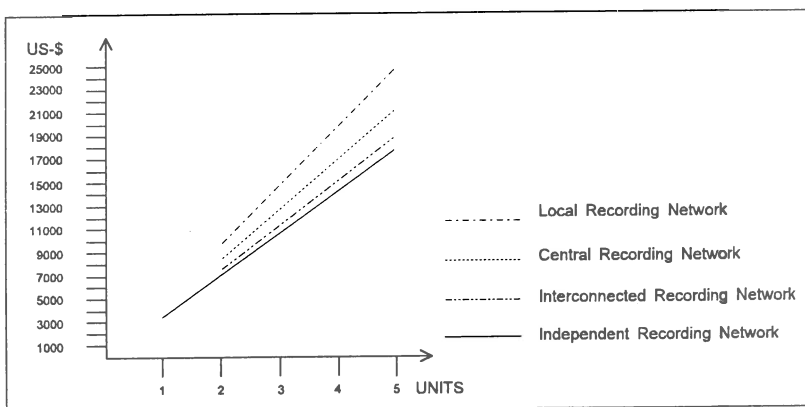
Table 8: Cost comparison between the different networks

Independent and interconnected network have a small cost difference. Having an interconnected network where you get common sampling, timing and triggering the costs are about 5 % higher than with independent recorders.

The cost of a local recording network compared to independent recorders is 40 % higher and the cost of the central recording network compared to independent recorders is 20 % higher.

The higher redundancy given by the central recording network has to be paid by higher cost.

Both, central and local recording networks are more comfortable to operate and easy to service especially when many sensor sites are connected to the system.

New Fast Digitization and Correction Procedures of the Greek Strong Motion Records

V.N. Margaris

Institute of Engineering Seismology and Earthquake Engineering, (ITSAK), 1 Hapsa Str., 54626, Thessaloniki, Greece.

Abstract

The majority of the available strong ground-motion data have been obtained by processing measurements made with analog accelerograms. Each step of the process to generate information such as ground velocity, displacement and response spectra introduces errors which can significantly affect the reliability of the results obtained. Although low-cost, modern digital accelerograms are now available, it will be tens of years before analog accelerographs are completely replaced by the digital ones. For these reasons, some current developments in data processing of strong-motion accelerograms continue with the assumption that most of the acceleration data available will be on analog films. On the other hand, the advancements of the PC's hardware, impose the adaption of the digitization and correction procedure of strong ground-motion data in this computer environment. Using this hardware and software facilities a typical triaxial film accelerogram can be accurately digitized and processed in a short time. In order to adopt this new methodology some tests have been carried out at ITSAK. A comparison of three applied digitization techniques manual digitization by ITSAK, fully automatic digitization by ENEA, Italy, and an automatic digitization by KINEMETRICS are presented. Strong-motion accelerograms with different durations have been digitized and processed with these aforementioned techniques. For the correction of the accelerograms, the same digital filters were utilized and comparisons on time and frequency domain are accomplished. The results from the above three techniques are in good agreement for frequency range 0.4 - 20 hz.

Introduction

A great number of strong-motion data has been collected by various accelerogram networks which have been installed in all over the world. A significant number of strong-motion records have recorded in USA, Japan, Italy, Greece and elsewhere (Borcherdt et al., 1984, Papastamatiou et al., 1986, Basili, 1987). These strong-motion data have been used in many applications in Seismology and Earthquake Engineering.

Very early, the digitization and correction procedures have been recognized as important techniques in order to use these strong-motion data. From the beggining of 1970, significant research has been carried out in digitizing and correcting strong-motion accelerograms (Trifunac, 1971, 1972). The early work relied on manual digitization of the triaxial analog accelerogram. Applying this technique, many errors were included in the corrected accelerogram (Trifunac et al., 1973). Significant efforts were made in order to digitize the strong-motion data automatically (Trifunac and Lee, 1979, Basili, 1987). Although some very reliable digital strong-motion instruments have been installed in the strong-motion networks, it will be a long time before analog accelerographs are completely replaced by the digital ones.

Because of advancements of the hardware and software, the digitization and

correction procedures can now be carried out on personal computers (Lee and Trifunac, 1990, Converse and Brady, 1992).

In Institute of Engineering Seismology and Earthquake Engineering (ITSAK), the manual digitization procedure was applied (Margaris, 1986, Margaris et al., 1989). On the other hand, some Greek strong-motion data were automatically processed, based on a joint project with ENEA, Italy. Comparison of both techniques has been carried out, presenting interesting results (Papastamatiou et al., 1989). Recently a scanner-based film accelerogram digitization system (Nigbor and Kodama, 1990) has been installed in the Institute. In order to apply the scanner-based procedure using a PC, some comparisons with the previous techniques were made, using accelerograms of the ITSAK data bank.

Data Used

Two strong-motion records from two earthquakes which occurred in Greece, were selected in order to compare the results of the three digitization techniques. The first record is the main aftershock of a strong seismic sequence, which occurred in the SE Messinia district near the village of Pelekanada (Oct. 10, 1984). The surface-wave magnitude of this strong earthquake is $M_s=5.0$ and the epicentral distance $R_e=13$ km (Anagnostopoulos et al., 1985).

The second well - known earthquake occurred near the city of Kalamata (Sept. 13, 1986), causing intensive damage in the epicental and surrounding areas. The surface-wave magnitude of this earthquake is $M_s=6.2$ and the epicental distance is $R_e=9$ km (Papazachos et al.,1988, Margaris et al., 1990). The selection of these strong-motion records was based on the different record length of these accelerograms. The different total record length of each accelerogram supposes some modifications in the digitization procedures. In Table 1, the main seismological data of these two earthquakes are included.

Table 1. The main seismological information of two selected
strong motion records.

STN COD.	DATE OF EARTHQ.	M_s	R_e (km)	TOTAL DUR. (sec)
PEL84-1	Oct. 25, 1984	5.0	13.0	20.5
KAL86-1	Sep. 13, 1986	6.2	9.0	32.0

The aforementioned accelerograms were digitized using three different digitization techniques. In the first technique, the accelerograms were manually digitized and corrected based on the routine procedure applied in IT-SAK (Margaris et al., 1989). The films of both records, were magnified by 4 times and were digitized. After an overlapping check of the magnified films with the digitized ones, the correction procedure was carried out, obtaining corrected acceleration and response spectum values.

The same accelerograms were processed at ENEA, Italy. The two records were digitized based on a photoscanning machine and were processed by the routine procedure which is applied there (Basili, 1987). Corrected acceleration and response spectrum values were obtained by this technique.

A scanner - based film accelerogram digitization software was adopted in order to process the data in a PC computer using scanlaser facilities. The accelerograms were digitized, and corrected acceleration and response spectrum values were derived. The digitization procedure of the (KAL86-1) accelerogram was made in two part because the length of the record is longer of the active area of the scanner. It is noteworthy to mention that the corrections in the three proposed techniques have been carried out by the same digital filters. The equally-spaced time interval of the processings were the same, Dt=0.01 in

all procedures applied. Also, for the manual digitizer the resolution is about 100 points/cm, for the automatic photoscanning digitizer is about 450 points/cm and for scanner-based digitizer is about 350 points/cm. For the comparison, horizontal and vertical (higher frequencies) component of each accelerogram, were adopted.

The corrected peak acceleration and peak displacement of the two processed accelerograms for the horizontal and vertical components are presented in Table 2. In Figure 1 and 2 the corrected acceleration and displacement time histories of the two accelerograms (PEL84-1) and (KAL86-1) are presented. The prefix MANUAL, AUTO and KINE are referred to ITSAK, ENEA and KINEMETRICS strong motion data processings respectively.

Table 2. The corrected values of the peak acceleration and peak displacement of the two accelerograms processed by three different techniques (MANUAL=ITSAK), (AUTO=ENEA) and (KINE=KINEMETRICS) and for horizontal and vertical components

| PROCESS | HORIZONTAL COMP. | | VERTICAL COMP. | |
	a_H (cm/s^2)	d_H(cm)	a_V(cm/s^2)	d_V(cm/s^2)
PEL84-1				
MANUAL	178.	0.56	85.	0.22
AUTO	176.	0.55	122.	0.18
KINE	167.	0.51	76.	0.18
KAL86-1				
MANUAL	264.	5.74	168.	1.13
AUTO	268.	5.34	178.	1.43
KINE	265.	5.70	188.	2.44

In order to study the differencies in the frequency contents of the corrected time histories, response spectra of the Pseudo velocity and the spectral displecement for damping D=0.05, were calculated. In Figure 3 and 4 the response spectra of Pseudo velocity and dispacement of the two earthquakes are shown.

Discusion

Comparing the corrected acceleration and displacement time histories some similarities and some differencies as well, can be observed. For the accelerogram with a small record length (PEL84-1), the similarities in the horizontral acceleration components in the time and frequency domain are obvious. Significant variations can be seen in the vertical time histories of this record especially in the character of the waveforms due to the applied digitization techniques. Enriched low-frequency motion in the manual digitization procedure especially in the high-frequency vertical component, it is something that can be expected (Trifunac et al., 1973).

The same good aggreement in the horizontal acceleration components in the time and frequency domain can be observed in the second accelerogram (KAL86-1) as well. Important differencies can be seen in the corrected peak-displacement values in the high-frequency vertical component. Some differencies can be observed in the scanner - based digitization procedure. In time domain and especially in displacement time history, some unexpected high displacement values are presented in time 22-24 sec, close to the point at which two segments has been selected digitizing the accelerogram. Also, in the frequnecy content, a significant variation of the spectral displacement values is observed in higher than 0.4 hz.
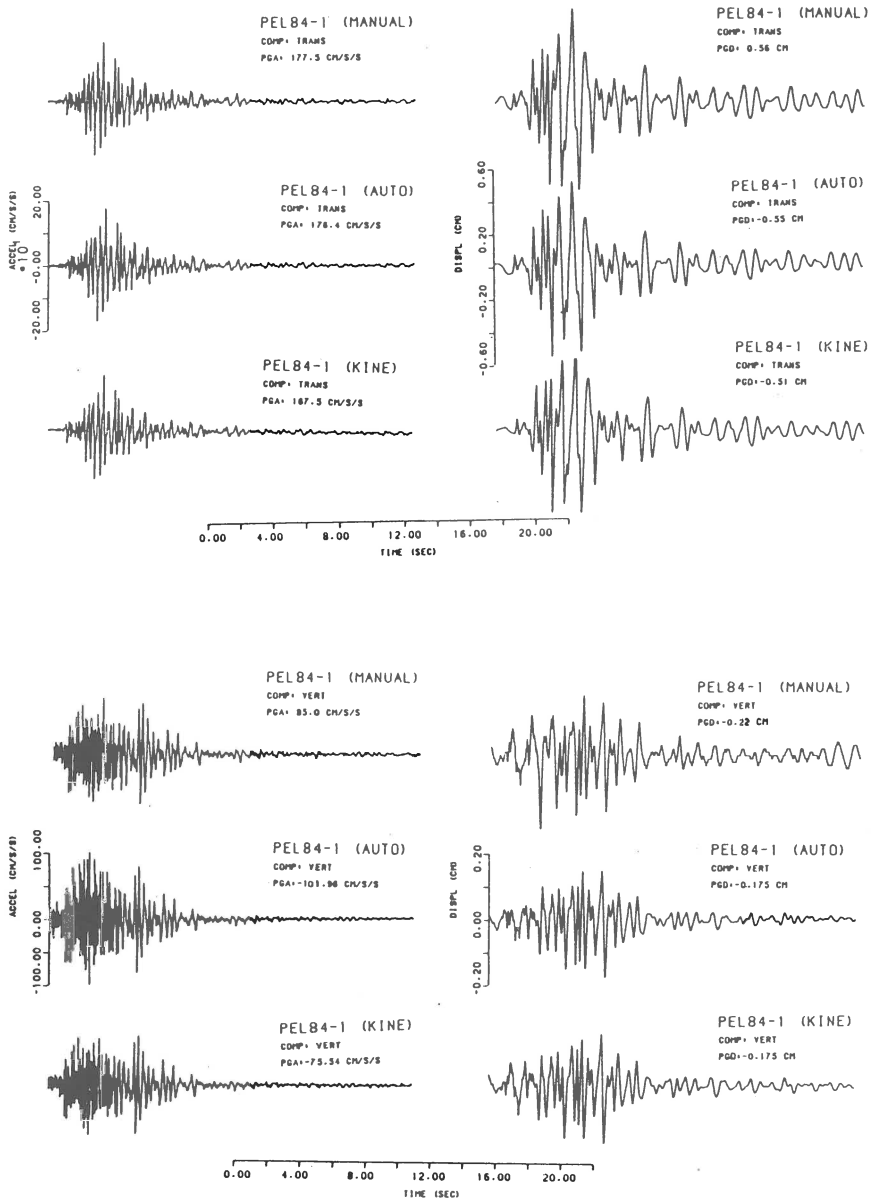
Figure 1. The corrected time histories of acceleration and displacement from the Pelekanada earthquake (Oct 25, 1984), of the horizontal and verical components (PEL84-1).
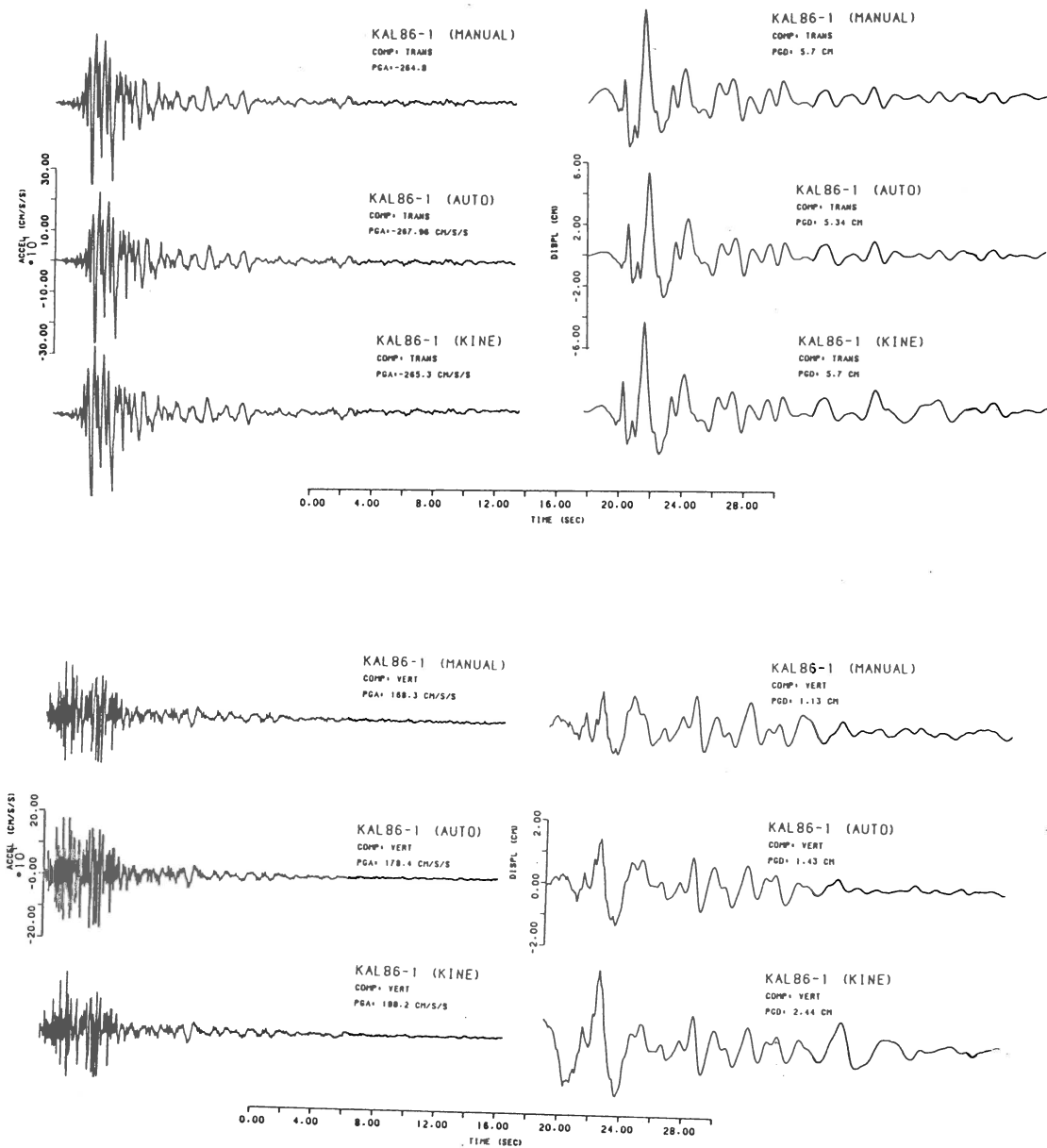
Figure 2. The corrected time histories of acceleration and displacement from the Kalamata earthquake (Sept 13, 1984), of the horizontal and verical components (KAL86-1).
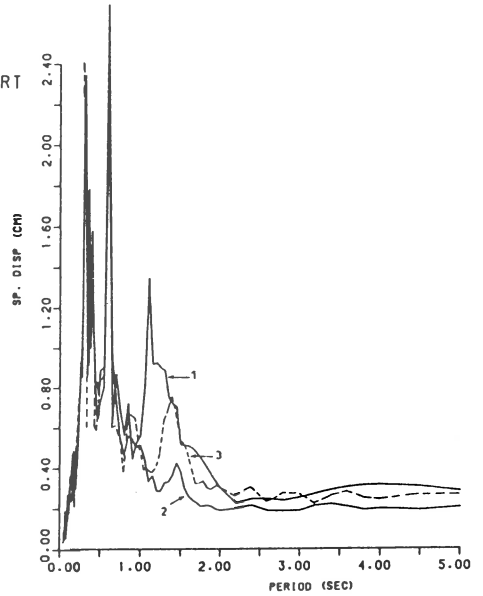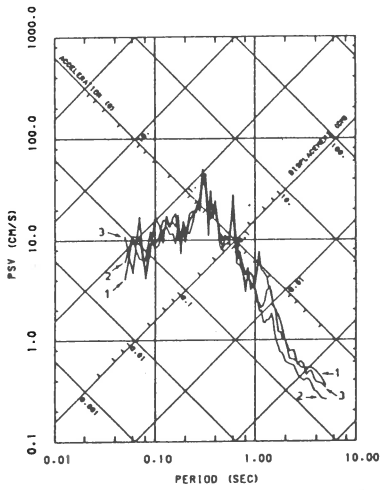
Figure 3. The response spectra of the pseudovelocity and the spectral displacement of the Pelekanada earthquake (PEL84-1), for the horizontal and verical components of three different data processings (ITSAK=1, ENEA=2 and KIMETRICS=3).

784

KAL86-1
COMP: TRANS
DAMP: 0.0
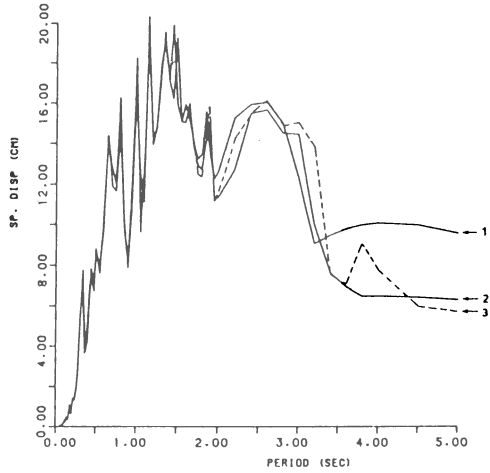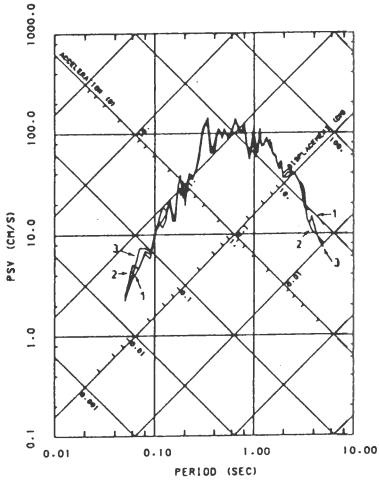
KAL86-1
COMP: VERT
DAMP: 0.0
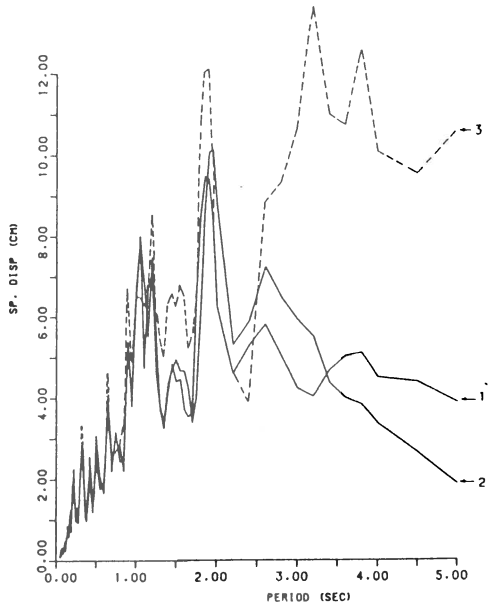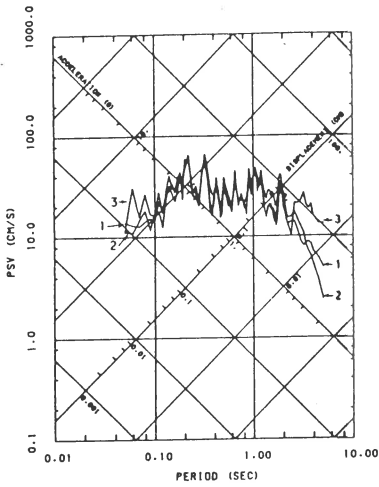
Figure 4. The response spectra of the pseudovelocity and the spectral displacement of the Kalamata earthquake (KAL86-1), for the horizontal and verical components of three different data processings (ITSAK=1, ENEA=2 and KIMETRICS=3).

References

Anagnostopoulos, S.A., V.N. Margaris, N.P. Theodulidis, E.E. Vorrias and A.I Marinos, 1985. Strong ground motion bulletins of the ITSAK network, Inst. Eng, Seism. Earthq. Eng., Rept. ITSAK: 85-1, 1-41.

Basili, M., 1987. Data acquisition and processing in strong motion seismology. Strong Ground Motion Seismology, (Erdik, M.O. and Toksoz, M.N. edits), Reidel Publ. Co, 251-331, 1987.

Borcherdt, R.D., J.G., Anderson, C.B. Crouse, N.C. Donovan, T.V. McEvilly, and A.F. Shakal, 1984. National planning for the acquisition of strong -ground motion data, Earthq. Eng. Res. Inst., Publ. No. 84-08, 1-57.

Converse, A. and G. Brady, 1992. BAP: Basic strong motion accelerograms processing software; Version 1.0, Unit. Stat. Dep. of the Inter. Geol. Surv., Open-File Report:92-296A, 1992.

Lee, V.W. and M.D. Trifunac, 1990. Automatic digitization and processing of accelerograms using PC, Univ. of South. California, Dept. of Civ. Eng., Rept No. 90-02.

Margaris, V.N. 1986. Digitizing errors and filters, Inst. of Eng. Seism. Earthq. Eng., Rept. ITSAK:1-43.

Margaris, V., D. Papastamatiou and N. Theodulidis, 1989. ITSAK: Strong motion data processing, Inst. of Eng. Seism. Earthq. Eng., Rept. ITSAK: 89-2, 1-27.

Margaris, V., A. Marinos, N. Theodulidis, E. Vorrias and A Akritidis, 1990. ITSAK strong motion bulletin (1986-1988), Inst. Eng. Seism. Earthq. Eng., Rept ITSAK: 90-1.

Nigbor, R.L. and D.A. Kodama, 1990. Scanner-based film accelerogram digitization system user's manual, KINEMETRICS /Systems, 1.1-6.2.

Papastamatiou, D., V. Margaris, N. Theodulidis and A. Marinos, 1989. Experimental strong motion seismology in the area of Greece, Proc. 1st Hell. Geophys. Congress, Athens, 521-534, 1989.

Papazachos, B., A. Kiratzi, B. Karakostas, D. Papagiotopoulos, E. Scordilis, and D.M. Mountrakis, 1988. Surface fault traces, fault plane solution and spatial distribution of the aftershocks of the September 13, 1986 earthquake of Kalamata (Southern Greece), Pageoph, 126, 55-68.

Trifunac, M.D., 1971. Zero baseline correction of strong-motion accelerograms, Bull. Seism. Soc. Am., 61, 1201-1211.

Trifunac, M.D., 1972. A note on correction of strong-motion accelerograms for instruments response, Bull. Seism. Soc. Am., 62, 401-409.

Trifunac, M.D. and V.W. Lee, 1979. Automatic digitization and processing of strong motion accelerograms, Dept. of Civil Eng., Univ. of Sout. Calif. Rept. No:79-15, I and II.

Trifunac, M.D., F.E. Udwadia, and A.G. Brady, 1973. Analysis of errors in digitized strong-motion accelerograms, Bull. Seism. Soc. Am., 63, 157-187.

SAPS - A COMPLETELY AUTOMATED AND NETWORKED SEISMOLOGICAL ACQUISITION AND PROCESSING SYSTEM

MIHNEA CORNELIU ONCESCU[1], MIHAELA RIZESCU[2], KLAUS-PETER BONJER[1] and WOLFGANG BRÜSTLE[3]

[1] Geophysical Institute, Hertzstrasse 16, 76187 Karlsruhe, Germany
[2] National Institute for Earth Physics, P.O. Box MG-2, 76900 Bucharest-Magurele, Romania
[3] Seismological Service, Geological Survey of Baden-Württemberg, Albertstr. 5, 79104 Freiburg, Germany

A PC-based digital data acquisition and processing system was developed and implemented on two PCs linked by a peer-to-peer LAN. Sixteen channels are sampled with a rate of 200 Hz. The acquisition is *continuously* performed in sequenced files on one PC using the IASPEI-released XRTP software. The length of these 'elementary' file is set to 1.5 minutes. The second PC runs a program to automatically organize the following processing steps: i) moving the raw data from the first to the second PC; ii) filtering the data for running a 'Rex Allen'-like picker (Allen, 1978) for P waves on each elementary file; iii) concatenating 3 consecutive elementary files if the detection criteria are fulfilled; iv) decoding a fast time code (Lennartz-style); v) discriminating between local and teleseismic events; vi) plane-wave method localization and m_b determination for teleseisms; vii) picking S waves, determining coda duration and locating local events with a new location program HYPOPLUS; viii) conversion of PC-SUDS into GSE format and 'feeding' a Data Request Manager with phases, locations and waveforms; ix) sending phases and location, *via* e-mail, in minutes after a detection, and a 'health status' every hour to the system manager; x) plotting the raw data, the picks and printing the location results; xi) archiving data and results locally and on a remote workstation. Conversion into other formats are possible using the CONVSEIS program package of Oncescu and Rizescu (1994).

Being modular, the system is flexible for extensions and upgrading. Loss of data is avoided by using large hard disks as temporary data buffers and file mirroring on different disk drives.

The following requirements were considered in developing this system: *i)* it should be of low cost to have a wide acceptance, *ii)* it should be reliable to permit unattended operation for weeks, *iii)* it should be upgradable, both in hardware and in software, *iv)* it should be of very high performance, both in the speed of computation and in the accuracy of results, and *v)* it should be completely automated and networked to permit quasi real-time exchange of earthquake information. The first three requirements led us to adopt the PC open architecture, while the last two led us combine some existing acquisition, picking, plotting or networking software with a newly developed package of 18 programs and 10 batch files for complete on-line processing of seismological data from a local telemetered seismic network. Our programs handle the PC-SUDS file format (Ward, 1989; Banfill, 1993). The commercial software we adopted is: MS-DOS v6.2 operating system, FTP Software v2.3 for e-mails, ftp and clock setting, Kirschbaum Netz v2.01 for the 'peer-to-peer' LAN, XRTP v1.22 IASPEI-released A/D program, AUTOPICK, DEMUX, SUDSJOIN and SUDSPLOT for SUDS file picking, demultiplexing, concatenating and plotting (Banfill, 1993). The quasi real-time automatic exchange of earthquake information is of great importance for alerting authorities and specific rescue or relief organizations in case of strong earthquakes, preventing in the same time false alarms.

The event file length is initially given by the length of three elementary files (e.g. 270 seconds) and finally the first 60 seconds are cut (a value used in our application), so that a minimum pre-event time can be set at 90 - 60 = 30 seconds. The minimum event duration is set by the length of the elementary file (e.g. 90 seconds) in case the detections occured at the end of the current elementary file and the maximum event duration is twice that value (e.g. 180 seconds) in case the detections occured at the beginning of the current elementary file.

The hardware requirements are minimal: both PCs could be 486/40 MHz machines with minimum 4 MB RAM, eventually with VESA-Local-Bus, two fast hard disks, VGA card and monitor, serial and parallel ports. For the A/D conversion one Data Translation DT2824 PGH card is needed, one HP LaserJet 4ML laser printer, for the Ethernet connection one 16 bit Ethernet card, two Arcnet cards or two additional parallel ports for the 'peer-to-peer' local area network (LAN) and one uninterruptible power supply unit for both machines ($\approx$500 VA).

The whole processing stage takes less than 2 minutes, so at its end it is just the right time to start moving the last acquired elementary file (1.5 minutes long) from PC1 to PC2.

Several automations were implemented to increase the autonomy and the safety of the system. On PC1, if, for any reason, the acquisition disk becomes full (in case of a breakdown of PC2), the acquisition is started on a second disk drive. On PC2 the clock is synchronized every hour from time services offered across the external Ethernet. The system manager receives every hour a 'state-of-health' message from the system. In the same time, PC2 checks periodically (also every hour), if the link with the workstation is functioning and keeps a corresponding logfile and it also checks the link with PC1 to avoid possible conflicts when trying to move the next elementary file. Moreover, PC2 controls the sending of e-mail, preventing those coming from 'simultaneous' picks to be sent and retrying (again every hour) to send the mail that, for any reason, failed to be sent.

After a succesful testing period, SAPS was transfered from the Geophysical Institute of Karlsruhe University to the Seismological Service of the Geological Survey of Baden-Württemberg, Germany, where the data of the telemetered network operating in the Upper Rhinegraben are now recorded. It was also recently installed, still without e-mail sending and DRM activities, at the National Institute for Earth Physics in Bucharest, Romania, for the on-line acquisition and processing of the telemetered data from the seismic network operating in the Eastern and Southern Carpathians.

Allen, R.V., 1978, Automatic earthquake recognition and timing from single traces: Bull. Seism. Soc. Am., v. 68, p. 1521-1532.

Banfill, R., 1993, PC-SUDS Utilities, IASPEI Software Library Supplement #1, Menlo Park,California.

Oncescu, M.C. and Rizescu, M., 1994, Conversion program package for seismological digital data on PCs, Computers & Geosciences, v.20, p.193-196.

Ward, P., 1989, SUDS - Seismic Unified Data System: USGS Open-File Report 89-188, Denver, Colorado.

LOCAL WEST BOHEMIAN SEISMOLOGICAL NETWORK WEBNET

F.Hampl[1], T.Fischer[2], J.Horálek[1], A.Boušková[1], P.Jedlička[1], T.Jíra[2] and M.Brož[2]

[1] Geophysical Institute, Academy of Sciences, Boční II/1401, 141 31 Praha 4, Czech Republic
[2] Institute of Rock Structure and Mechanics, Academy of Sciences, V Holešovičkách 41, 182 09 Praha 8, Czech Republic

EXTENDED ABSTRACT

1. REGION UNDER STUDY

The frontier region between the Czech Republic and Germany, comprising the territories of West Bohemia, SE Saxony and NE Bavaria, is characteristic in repeated occurrences of earthquakes swarms. Its area covers more than 1000 km^2. Intensive swarms re-occur in this region with a period of roughly from 10 to 20 years (Kárník et al., 1986), the most recent intensive earthquake swarm having occurred here at the turn of the years 1985 and 1986. Based on continual observations of local stations it was found that this region displays permanent seismicity (Horálek et al., 1995a). In the interval between two intensive swarms, seismic energy is released here in the form of a large number of shallow micro-earthquakes, mostly with magnitudes M_L<2.5. The foci of most micro-earthquakes cluster in six focal zones, four of which are located on the territory of West Bohemia, and the remaining two in Germany, specifically in Saxony and Bavaria (Fig. 1). The depths of the foci differ from zone to zone, generally ranging from 6 to 15 km. The seismicity of the region as a whole displays the distinct character of earthquake or micro-earthquake swarms. Further information and details can be found in Horálek et al., (1995b).

2. PURPOSE AND CONCEPT OF THE WEBNET NETWORK

To understand the nature of seismotectonic processes and to be able to construct a model of the seismic regime in the region concerned, the following studies are required: a detailed mapping of the individual focal zones and their links with tectonic faults, determination of the seismic energy released in the individual zones, determination of the space-time energy-release distribution, determination of foci migration, and evaluation of the effective anisotropy parameters of the upper crust and their variations in time, based on S-wave splitting analysis. Homogeneous, digital, three-component seismograms, recorded in a magnitude range of M_L= -0.5 to M_L=5, from the largest possible number of local stations, suitably deployed within the whole epicentral region, are required for these studies.

The WEBNET seismological network was established by the Geophysical Institute in cooperation with the Institute of Rock Structure and Mechanics (formerly the Institute of Geotechnics) of the Academy of Sciences for the purpose of creating a homogeneous database
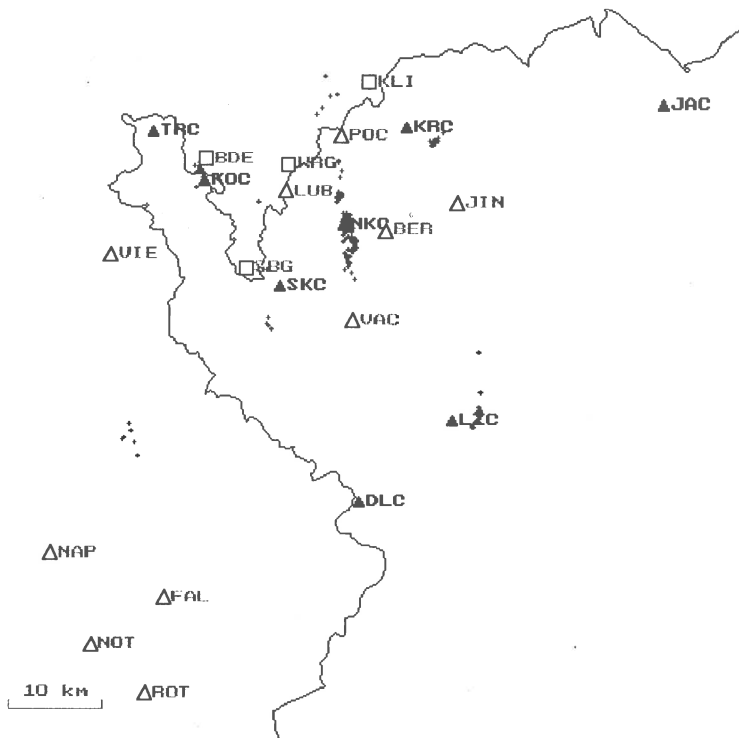
Figure 1. Distribution of the hitherto identified focal zones (1 through 6) and the positions of the local seismic stations in the seismically active region of West Bohemia, SE Saxony and NE Bavaria. The WEBNET stations are marked with black triangels and their station code is underlined. The other digital stations are marked by white triangles. The analogue stations are shown as white squares.

of local observations in the area of West Bohemian earthquake swarms, which would best conform to the requirements mentioned.

WEBNET consist of eight digital seismic stations. Four of them, NKC, KRC, KOC and LZC are located directly in the epicentral zones in West Bohemia for the purpose of fixing the depth of hypocentres, and of recording reliably even very weak micro-earthquakes (events with magnitudes $M_L \geq -0.5$). The remaining four stations, SKC, DLC, TRC and JAC, are located outside the focal zone to ensure the best possible areal and azimuthal coverage of the studied region with respect to the other digital stations which were already operating within the region.

3. WEBNET CONFIGURATION AND DATA

WEBNET is in fact formed by two subnetworks (subnets A and B) with data telemetring to a common recording centre, and by two autonomous stations. The WEBNET configuration is shown in Fig. 2. Two different types of seismographs and data acquisition systems are used in WEBNET, but the response characteristics, the dynamic ranges, sampling frequencies and the triggering threshold level are either the same or very similar at all WEBNET stations.
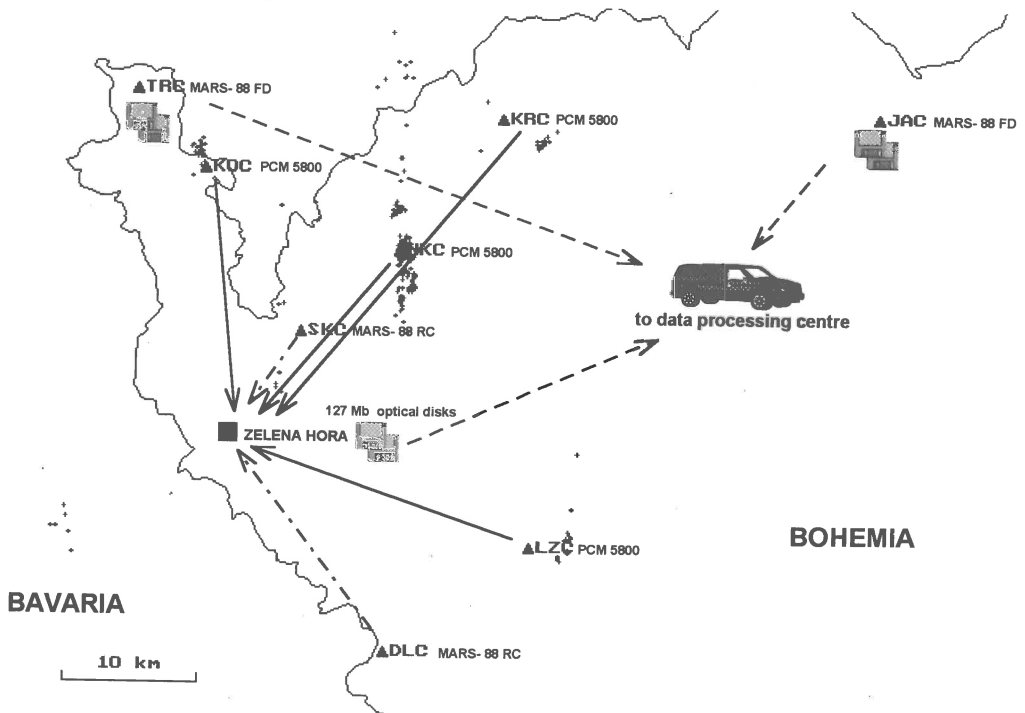
Fig. 2. The WEBNET configuration. The arrows indicate the data flow from the stations to the Zelená Hora data acquisition centre. The data flow from subnet A is indicated by solid arrows, that from subnet B by dot-dashed arrows.

The network is arranged with a view to the instrumental equipment available in the GI and IRSM or the purpose of establishing the network.

Subnet A, which comprises station NKC, KRC, KOC and LZC (stations located in the focal zones) is equipped with 5800 PCM data acquisition systems with UHF telemetry by Lennartz Electronic. The seismographs at the remote stations consist of a three-component set of SM-3 seismometers and a 5800 PCM encoder. The seismographs operate with a frequency response proportional to the ground velocity in the 0.5-600 Hz frequency band. In view of the frequency content of the observed events, these seismographs are sufficiently broadband for recording local earthquakes with magnitudes M_L from -0.5 to 5. The dynamic range of the records is 120 db with the resolution of 60 db (10 bits). The ground velocity corresponding to LSB is 10 nm/s. The sampling frequency used is 250 Hz. The remote stations are telemetrically connected with the 5800 PCM mixer acquisition system in the data acquisition centre. Data transmission from the remote stations to the 5800 PCM mixer is continual, and the overall bit rate is 80 kbit/s.

Subnet B, which is made up only two stations, SKC and DLC, is equipped with the seismograph system consisting of a Radio Control MARS-88 acquisition system and a LE-3D seismometer by Lennartz Electronic. The seismograph systems are operated at a frequency characteristic proportional to the ground velocity in the 1-80 Hz frequency band, and with regard to the events observed are also broadband. The corner frequency of 80 Hz is given by

the sampling frequency of 250 Hz used. The dynamic range of the record, which is equal to the resolution, is 96 db (16 bits). The ground velocity corresponding to LSB is 10 nm/s. Data retrieval and transmission from the remote stations to the data acquisition centre are controlled by an HP-370 central network computer with a MARS-gateway via bidirectional UHF telemetry.

   The data acquisition centre consists of a 5800 PCM mixer (data acquisition system of subnet A), an HP-370 / MARS-Gateway (central controlling data acquisition system of subnet B) and of a PC 386 with a removable 128 MByte magneto-optical disk which serves as the common recording device for the data from subnets A and B (Fig. 3). Communications of the PC with the 5800 PCM mixer are via HP-IB. The teleseismic data, transmitted from the stations of subnet A, are stored practically in real time on the magneto-optical disk in ESSTF
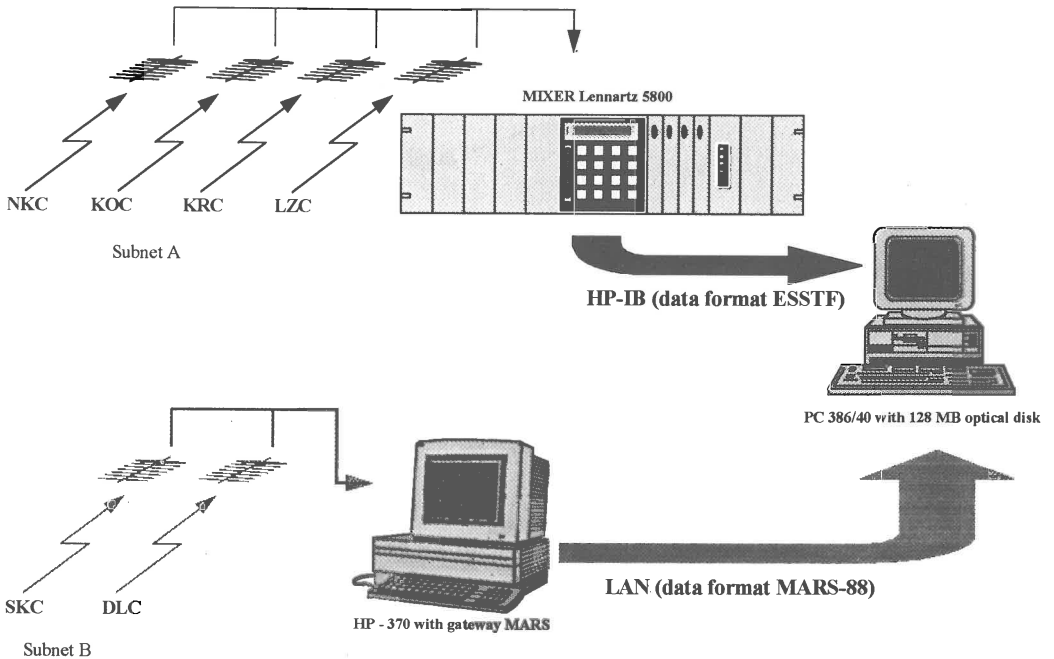
Figure 3. Block diagram of the Zelená Hora data acquisition centre.

data format (European Seismic Standard Tape Format). Communications of the PC with the central HP-370 computer are effected via the local computer network (LAN).The seismic data transmitted from the stations of subnet B, are temporarily buffered on the HP-370 hard disk and, at the time when there is no communication between the PC and the 5800 Mixer (i.e. when subnet A is not triggered) the data are transferred to the magneto-optical disk where they are stored in the MARS-88 format.

   Besides this, the data acquisition centre is equipped with an analogue drum recorder. Since the 5800 PCM mixer, operated at the bit rate of 800 kbit/s, provides an output for only one component from any subnet A station, the vertical component of station NKC (which operates in the seismically most active zone) is monitored continually to provide instantaneous information on activity.

The data acquisition centre is located in the premises of the TV tower Zélená Hora near Cheb. The aerial systems are located at height of about 100 m. This guarantees reliable UHF telemetry in a very vertically varied terrain, characteristic of West Bohemian earthquakes swarm region.

Both subnets, A and B, operate in trigger mode. At the subnet A stations and at the subnet B stations, respectively, the trigger algorithm STA/LTA (short-term average/long term average) and STA/LTA combined with the STA/Threshold Level is used. The level of seismic noise at the subnet A stations and the parameters of the STA/LTA detector used enable reliable detection of all events with magnitude above -0.7 recorded at stations in the epicentral zone in which the event occurred. In order to record even very weak seismicity (i.e. microearthquakes with magnitudes of at least $M_L \geq -0.5$) in the region of the West Bohemian earthquake swarms, coincidence between stations is not applied either in subnet A, or subnet B to trigger the recording. Besides, if the trigger in subnet A is activated, the trigger in subnet B is also automatically activated.

Autonomous stations TRC and JAC are equipped with seismographic system consisting of a floppy disk MARS-88 data acquisition system and LE-3D seismometer. The frequency response, sampling frequency, dynamic range and ground velocity corresponding to LSB, and the data format are identical with those of subnet B.

4. PROCESSING OF OBSERVATIONS

Off-line processing of observations from the WEBNET is carried out in the WEBNET Laboratory at the Geophysical Institute in Prague. The magneto-optical disks from the Zelená Hora data acquisition centre and the floppy disks from the autonomous stations TRC and JAC are sent approximately once a weak (by mail, or occasionally by car) for processing to the WEBNET Laboratory. For analysing the seismograms of local events and for advanced processing of seismic data, Fischer developed a high-performance database-oriented interactive program, SeisBase, run on a PC (Fischer and Hampl, 1995). SeisBase provides for three levels of processing: (a) primary processing, (b) visualization of seismograms, phase picking and wave-form analysis, (c) processing of selected data..

(a) In primary processing, records from subnets A and B from the autonomous stations are automatically associated on the basis of trigger time coincidence. This enables rapid retrieval of true seismic events from among the large number of spurious triggerings which occur because the network is highly sensitive. The coincidence combination of records creates a new sequence of events in order of trigger times, as if the events were recorded in a homogeneous network.

(b) Apart from the basic routines such as determining the onset times of the individual phases and amplitudes by means the cursor, SeisBase also enables the integration, filtration (low-pass, high-pass, band-pass and band-stop f filters are available) and rotation (transformation of Z-, N- and E-components to Z-, R- and T-components), as well as polarization analysis (polarization, filtration, ZxR-product and polarization diagrams) of seismograms. It is also possible to carry out spectral analysis and correlation analysis of wave forms. The results of the seismogram analyses are stored in the appropriate database tables.

(c) As regards quantitative processing of selected data (data obtained by interpreting seismograms) SeisBase contains programs for localizing hypocentres and for their 2-D and 3-D mapping in the region, for determining the mechanism of earthquake foci (fault plane solution)

and for constructing histograms. A detailed description of SeisBase can be found in Fischer and Hampl, (1995).

The complete WEBNET database, containing wave forms of seismic events and the appropriate tables, is stored on CD ROM disks.

ACKNOWLEDGEMENTS

REFERENCES

Fischer, T. and F. Hampl, 1995. Seisbase 4.6 - a database oriented program for routine multi-station seismograms analysis. This volume.

Horálek, J., A. Boušková, and F. Hampl, 1995a. Local seismic observatios at stations Nový Kostel and Skalná, and their interpretation: Period 1986-93. Studia Geophys. Geod., 39, 148 - 161.

Horálek, J., A. Boušková, F. Hampl, and T. Fischer, 1995b. Seismic regime of the West-Bohemian earthquake swarm region: Preliminary results. This volume.

Kárník, V., Z. Schenková, and V. Schenk, 1987. Time pattern of the swarm of December 1985--March 1986 in West Bohemia. In: Earthquake swarm 1985/86 in Western Bohemia, D. Procházková, Editor,Geophys. Inst. of Czechosl. Acad. Sci.,Praha, 328 - 342.

SATELLITE SEISMIC NETWORK

Calderoni G. *, De Simoni F.M. *, Merucci L. *, Saracino C. *

* Istituto Nazionale di Geofisica, Via di Vigna Murata, 605

00143 Rome - Italy

Abstract Argo Project represents the first digital seismic network with data transmission by satellite in Europe. Argo Project is financed by the Italian Civil Defence Department and connects two independent networks used for Emergency Communication and Environmental Data Collection respectively, with the following institutions: Control Centre of the Civil Defence Department, the Istituto Nazionale di Geofisica (*ING*) and the volcanological and hydrogeological centre. Argo satellite network is based on a stellar model which is characterized by a centripetal data traffic. The multiple data flows coming from the Peripheral Stations are sent via satellite to the Fucino Operational Centre (Master Station) and retransmitted by a satellite relaunching to the above mentioned operational centres. Seismic and self-potential data flows coming from *ING* Peripheral Stations distributed on the whole country are transmitted to the *ING* data processing centre where a Digital hardware configuration provides the highest reliability of the acquisition process through the duplication of the machines in a *VAXcluster* environment. The access to the Satellite Data Network is based on *X.25 protocol* and is managed by the software communication product *Packetnet System Interface Access*. The efficiency and reliability of the whole satellite network has been tested. Due to the high performances of the satellite communications, the stability of the error-control mechanism in the transmitted data by means of *X.25 protocol* and the continuous hardware and software development, the European Community (*CEE*) has financed the Argo Project expansion in Spain and in Greece.

Introduction

Argo Project represents the first European digital seismic network with data transmission via satellite. Argo Project is financed by the Italian Deptment of Civil Defence, and deals with a heavy data traffic concerning Civil Defence activities on the national territory, and environmental data collection (Fig. 1.). The Argo satellite network is based on a stellar model: a Master Station, located in Central Italy, acts as the central node in the satellite communication with the Peripheral Stations. The Master Station carries out the following tasks: controls the conditions of the network stations; assigns a permanent capacity of transmission to each single station, in order to provide a continuous data transmission; sends a time mark reference necessary to the timing of the acquired data. The data flows coming from each Peripheral Station, located on the whole national territory, are sent to the satellite and then to the Master Station, which forwards them again, by a satellite relaunching, to the Istituto Nazionale di Geofisica (as far as seismic data are concerned) and to other qualified centres (as far as volcanological and hydrogeological data are concerned).

Probe Interface Card

In each Peripheral Station the physical interface between the sensors and the satellite transmission system is represented by the electronic board *Probe Interface Card (PIC)*.

The PIC supplies the following kind of data in *X.25* packets (Fig. 2.): a) IS1 containing 150 bytes of seismic data, acquired by a seismic sensor (S13), sampled at the frequency of 100 Hz and forwarded once every second; 40 bytes of digital data and 8 samples per minute available for low frequency analog signal, forwarded once every minute. b) IS2 containing 240 bytes of digital seismic data, acquired by a very broad band seismic sensor (VBB), forwarded once every half a second and 40 bytes of digital data and 8 samples per minute available for low frequency analog signal, forwarded once every minute. c) IV2, containing (90 x 3) bytes of seismic data, acquired by a set of three seismic sensors, sampled at the frequency of 120 Hz and forwarded once every half a second; and 7 samples per minute available for low frequency analog signal forwarded once every minute.
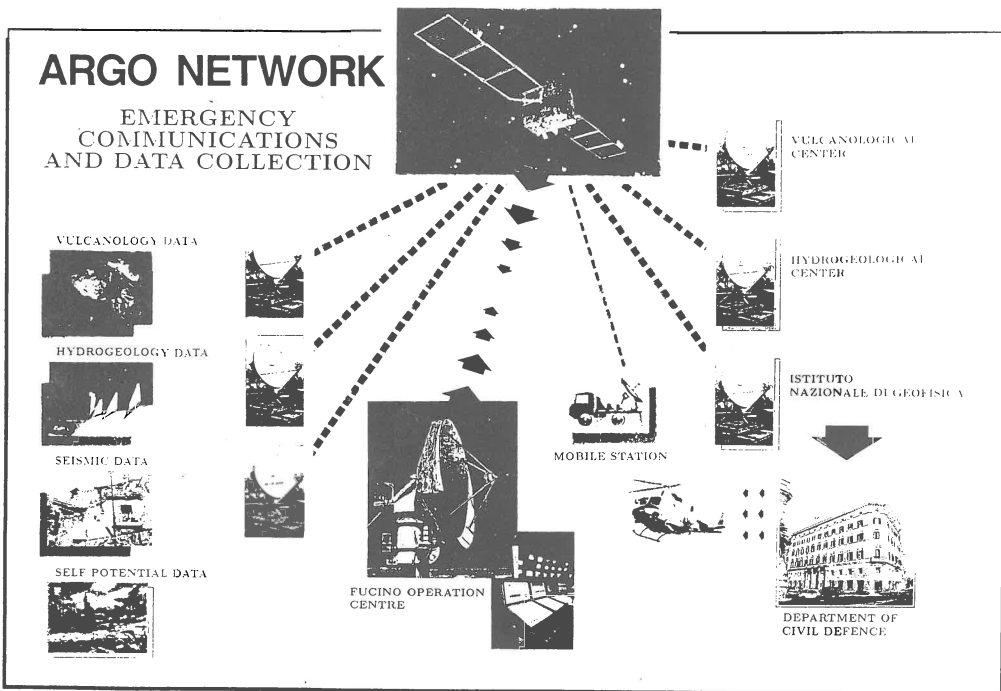
Figure 1. Configuration of Argo data network.

field A   field B
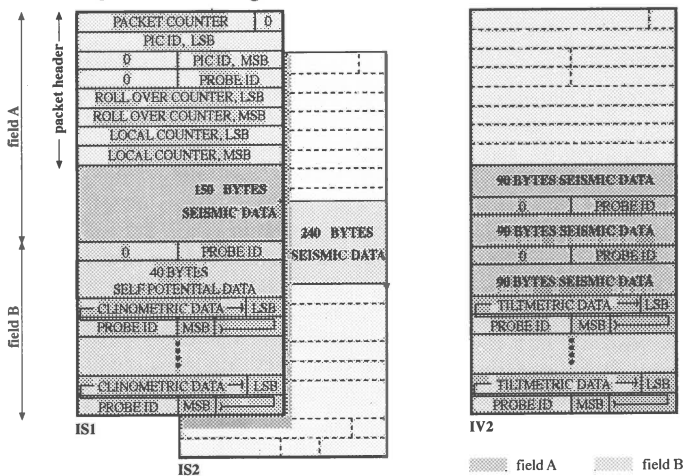
Figure 2. *X.25* data packets generated by the PIC.

Hardware

The seismic data processing centre is based at the Istituto Nazionale di Geofisica. To achieve the maximum hardware reliability, the system has been configurated in a *VAX-cluster* environment, and the main components duplicated - namely the mail computer, the disks, their controllers and the computers that interface *X.25* lines, on which are forwarded all the data coming from Argo network. Figure 3. shows a schematical but complete hardware architecture of the system.

Software

The software can be divided in two different sections, respectively dealing with data acquisition and events detection (Fig. 4.). Acquired and digitalized seismic signals are forwarded from the Master Station to the *ING* processing centre, where is based the data acquisition software, using the *X.25* protocol and a specific software product, the *Packetnet System Interface Access (PSI)*, which handles the *X.25* data communication on Digital hardware.
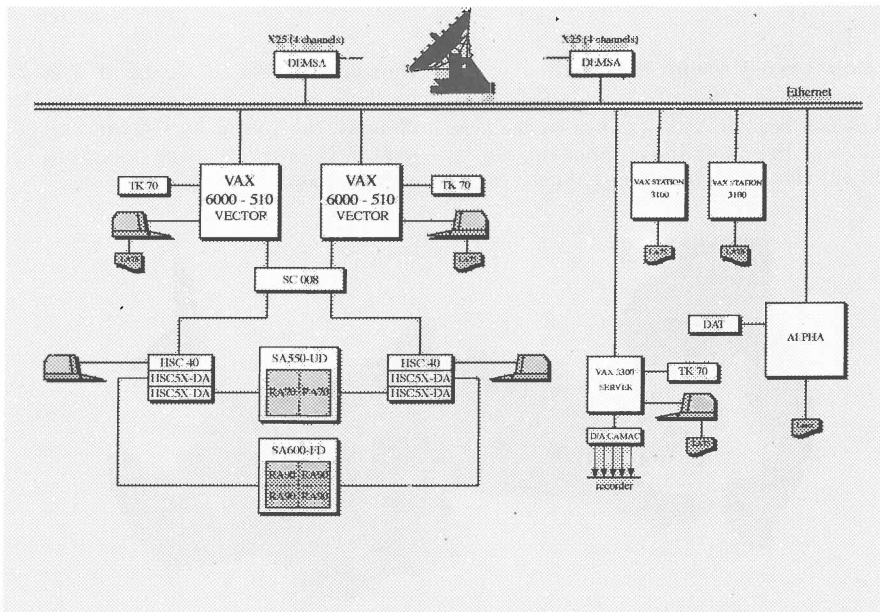
Figure 3. Hardware configuration.

The main functions of the software are: to give a chronological reconstruction, according to each station, of the acquired data; to carry out an on line and an off line analysis; to supply graphs and tables of the recorded signals.

The main purpose of this software realization is to develop a system able to process all the data of seismological relevance coming from the network, in order to optimize the parameters determining the trigger condition, determining in this way the useful signals and memorizing in a data base only the most important events. The selected data, ordered according to their original station and synchronized according to the time, can be forwarded to the D/A CAMAC helycorder, which directly interfaces with the analogical recorders.

The result obtained by a satellite communication is the loss of the original sequence of transmission; to recreate the chronological order of the samples that can be only compared with the absolute time, it is necessary the use of time marks of reference. To this end, the Master Station forwards to each Peripheral Station a time mark, given every 360 ms found in the X.25 data packet, generated by the PIC card; besides, in each Peripheral Station a Local Counter with a time vernier function divides each 360 ms interval into 8 of 45 ms, with 19.24 μs per step. These time marks are not absolute time references, as all the Peripheral Stations have a different geographical position, and as both the time counters cyclically take the same values. In the data processing centre it is used a time mark signal, using a DCF, which allows the reconstruction of the absolute time of the acquired data, through the comparison between the two time marks given by the network with the decoded DCF time.

Figure 4. Software.

797
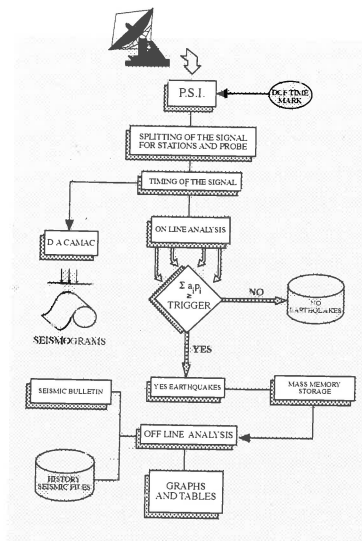
Southern Europe Network

The efficiency and reliability of the whole satellite network has been tested. Thanks to the high performances of the satellite communications, to the stability of the error-control mechanism in the transmitted data by means of *X.25 protocol*, and to the continuous hardware and software development, the European Community (*CEE*) has financed the Argo Project expansion both in Spain and in Greece (Fig. 5.).
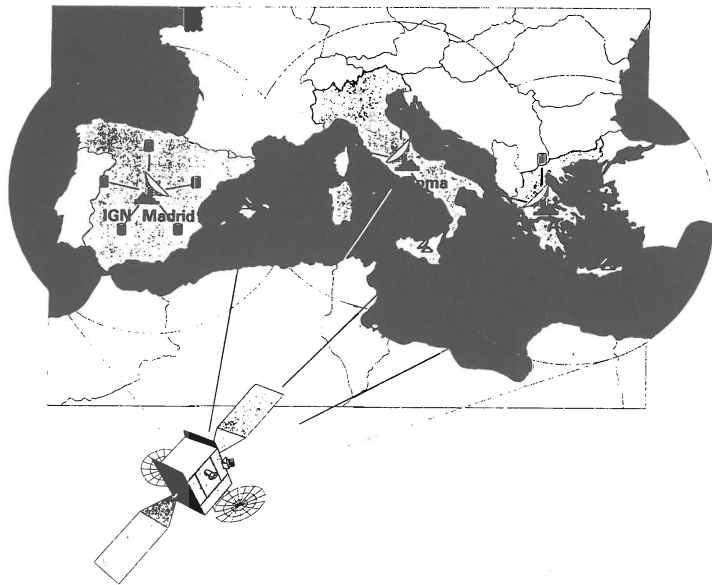
Figure 5. Southern Europe Network.

The Southern Europe Network relies upon an extension of the Argo technology and involves the countries of Greece, Spain and Italy and their national seismic networks.

The results expected from this project are:

- the creation of a distributed system for the real-time monitoring of the network area seismicity;
- The creation of an infrastructure and the study of common methods for the determination, the selection and the exchange of seismic data among European countries via satellite link.
- The creation of a common database, storing a suitable choice of the data representing the main seismic events monitored by the Southern Europe Network stations.
- The analysis of at least 10 important seismic events with the highest magnitudes occurred in this century, based on the original instrumental tracks from stations located in several countries.
- The elaboration of a tridimensional kinematic model of the Mediterranean Sea.

Conclusions

The realization of the Argo Project opens new perspectives to the optimization of the satellite seismic network. To exploit thoroughly this new communication system via satellite, some important developments have been considered to realize a flow inversion in the communication between Remote Stations and *ING*, sending some telecontrolled messages in an 8 bits word concerning, for instance, the calibration and the diagnostic processes of each remote station. Moreover, to optimize the management of the satellite channel, it has been thought to realize intelligent stations, able to perform autonomously the trigger analysis, simply sending the useful signals and increas-

798

ing the points of detection; in fact, taking into accounts the maximum daily time of the seismic data production, which is equal to about 16 hours, the data flow will be reduced of about 50% of their present value. Argo Project, then, even if in its preliminary phase of installation, already takes into account a dynamic and continuous hardware and software development, aiming to improve the seismic signal quality.

Acknowledgments

References

Calderoni, G., B. De Simoni, and C. Saracino, 1992. Progetto Argo. *Istituto Nazionale di Geofisica*, **542**.

De Simoni, B., R. Di Giovambattista, 1988. Sviluppo della rete sismica nazionale centralizzata. *Atti del 7° Convegno Nazionale del Gruppo Nazionale di Geofisica della Terra Solida*.

Urbini, G., 1990. Misure e considerazioni sul segnale marcatempo DCF77. *Istituto Nazionale di Geofisica*, **527**.

A NEW ALGORITHM BASED ON SIGNAL SPECTRAL ANALYSIS FOR SEISMIC EVENT DETECTION

Giuseppe Cagnetti, Massimo Maffucci: ENEA

ABSTRACT: An advanced algorithm based on signal spectral analysis for seismic event detection is shown herein. Some interesting results of a research work based on the analysis of many digital seismic recordings from the spectral valuation point of view are presented, with the aim to characterize the real seismic signal in respect of noise of various origin this to realize intelligent algorithm to implement on new generation digital data acquisition systems.

GENERAL DESCRIPTION

For seismic characterization and monitoring of the territory, radiotransmitted or local acquisition sensing networks are realized to record possible seismic events.

Independently by the recorded physical unity (acceleration, speed, field displacement or structure displacement), seismic signals can be classified in two different categories, micro-earthquakes (the intensity can be recorded only by instrument) and those relative to high-intensity events (more than 4° degree of Mercalli scale); generally first category is recorded with seismometer and the second with accelerometer.

Micro-earthquakes recorded are utilized, principally, to characterize geographical areas from the seismic activity point of view and to discover seismogenetic areas.

The earthquakes of highest intensity recorded with accelerometers (strong motion accelerometers) are instead used to study the dynamic behaviour of structures like bridges, dams, railways, monuments during an earthquakes.

Monitoring of seismic events "strong motion" type, with acceleration higher than 10 mg, today is made with acquisition systems that record the events on electronic digital mass-memory. In these conditions a continous high resolution recording of seimic signals coming from the sensors needs a high quantity of memory resources, to avoid that in these systems is provided a trigger that operates on the base of various logics:

-threshold: the acquisition start when a fixed signal level is exceeded;

-STA/LTA (short term average/long term average).

These techniques have two problems:

-they don't permit the recording of low level microearthquakes (that are very interesting for the scientific research);
-they can do to start the recording on not-seismic signal.

ALGORITHM PDZ (Poles in Detection Zone)

Here are described some results of a study, in the field of seismic signal recognition, aimed to realize dispositives that processing in real time an accelerometric signal can recognize a seismic event on the base of its particular and unique characteristics (we want to underline that the results don't take in account the characteristic of the terrain where the sensor are installed, in fact the developed method is based only on the signal characteristics).

The algorithm PDZ constructs with the seismic incoming signal an autoregressive model, with which is possible to have a spectral estimation of the signal power spectral density and on the base of the poles position on the complex plane of the function $F(jw)$, that represents the estimator response, then it decides if the signal is relative to an earthquake or not. The power spectral density (PSD) of a signal, gives a measure of the distribution of its power in function of its frequency and it permits to individuate the main spectral components. In the

practical application are employed digital method, spectral calculation algorithms for a finite signal samples. These algorithms are the Discrete Fourier Transform (DFT) and the Fast Fourier Transform (FFT); the second has the advantage in respect of the first to reduce the necessary operation number from a quantity proportional to N^2 to another proportional to $\log_2 N$. To analyze the signal spectrum as above, don't take great advantages in the calculation of statistical properties of a signal class. In fact FFT needs a number of parameters equal to the signal samples. The spectral estimation methods permit under correct conditions to have a corrispondence between the signal PSD and the coefficient of a rational function that approximate the signal in the frequency domain. It is in this way that can be reduced the parameter numbers that we need to characterize the signal.

The initial hypothesis is that the accelerometric signal could be approximate by a series obtained making pass a white signal through a linear, causal and stationary filter modellizable like a rational transfer function with poles only:

$$F(jw)=1/H(jw)$$

with $H(jw)$ polynomial in e^{jw} of p order.

The variance values of accelerometric signal and the filter coefficients are the parameters to utilize. Among the various methods to determine the estimator coefficients, it has been chosen Burg algorithm.

The possible actions relative to this study (ordered in a preference scale) are the following:

-To record an earthquake;
-Don't record a false alarm;
-To record a false alarm;
-Don't record an earthquake.

The first two actions are wanted and the acquisition system start to record only if the input signal is an earthquake. the third and the fourth are unwanted but they can happen with a lower probability than the previous two. The cost associated to the fourth action is higher than the third, infact is best to record a false alarm that don't record an earthquake.

When we face a decision problem it needs to understand the structure and the characteristics of the elements in game. First we choose the dimension n of the sample and the characteristic to utilize. Analizing recording of false alarm and earthquakes the considered characteristic is the autocorrelation function of the sample x and the parameter to estimate are the spectral estimator poles associated to the same sample. In fig. 1 is shown an earthquake accelerogram and in fig.2 is shown the normalized (in respect of the maximum) estimate of autocorrelation. From the figures we can observe that the value of autocorrelation, after the first 1000 samples go down under 0.1; then samples with distance greater than 1000 positions are uncorrelated and not useful for the characterization of the signal. This result has been confirmed by the analysis of a high number of accelerograms, relative to earthquakes and false alarms then we have chosen 1024 for n (number of samples).

Computing the sample x FFT and evaluating the spectrum maximus, it is possible to find frequency components relative only to earthquakes. In this case being the dimension of the parameter equal to that of the sample an automatic implementation is very complex. Then starting by the sample series $\{x(n)\}$ we attempt to extrapolate a characteristic z of m<n dimension without loss of information in respect of x. The order of the estimator is connected to the risolution of estimate spectrum; if m is the order of the estimator, we need m+1 autocorrelation function sample to evaluate the estimated spectrum. Evaluating the estimator poles position in the complex plane and finding one in the detection zone the dimension of the parameter is reduced from n=1024 to m=7, this reduce too much the complexity of the results interpretation. Moreover because the estimator poles are represented on the complex plane with module and phase, the recognition problem is reduced to find the pole with minimal phase different by zero.

Observing the poles position on the complex plane of recordings of earthquakes, we have found that the seismic events have a pole couple that falls inside at a zone near the real positive axis. To this zone has been given the name "Detection Zone", by which the algorithm takes the name. The analysis of a high number of earthquakes has shown that the angular amplitude of this zone is about 17°. From this analysis is moreover emerged the known characteristic of a seismic signal that the maximum energy is concentrated under 16 Hz. In fact also the trigger logic circuits, today in use in accelerometric acquisitors, have a low pass filter with the target to increase the probability to detect only seismic events.

Flow-chart in fig.3 shows the decision procedures of the algorithm PDZ. A series of tests have shown that the best parameters to utilize PDZ are:

-Samples number n=1024;
-Estimator order p=7
-Trigger angle ø=15°

The choose to take the first 1024 samples of signal (about 5s at 200 Hz of sampling frequency) is giustified by the above mentioned fact that samples with distance more than 1000 can be considered uncorrelated. Instead for the choose of the estimator order (p=7), we need to remind that the prediction error minimum FPE is joined to the prediction error variance by mean of proportionality relation. Whereas the prediction error variance decreases if p grows, the proportionality coefficient (equal to the ratio $\{m+p+1\}/\{m+p-1\}$) grows. The consequence is that FPE has an absolute minimum point when p change.

After the the calculation of values of the parameters were calculated the estimator coefficients for all the events studied. The figure 4 shows the location on complex plane of the Burg 7 order estimators poles, obtained from a series of earthquakes accelerograms. The figure 5 instead shows the same situation for false alarm accelerograms. Comparing the two figures we can observe the difference in poles location for earthquakes and false alarm. Moreover because for each pole with phase ø it corresponds a spectrum peak with frequency $\emptyset f_C/180°$ (where f_C is the sampling frequency), we have that in seismic signal spectrum is ever present a low frequency component in the detection zone. Then it is possible to recognize an earthquake by a false alarm, thank to property that belong only to the power spectral density of an earthquake accelerogram. PDZ algorithm on the base of the above mentioned criterions avoids to record false alarms, also if these have a high low frequency power contents (a traditional acquisitor with threshold trigger logic with a low pass filter could record surely), but with with the first peak above the detection frequency.
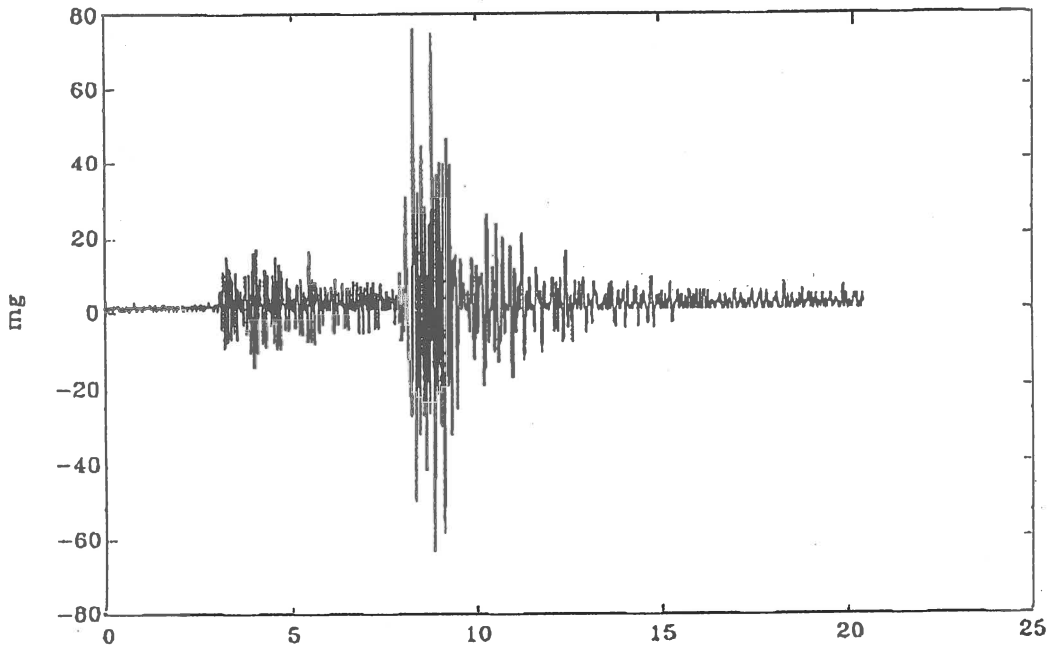
Fig. 1 Earthquake accelerogram
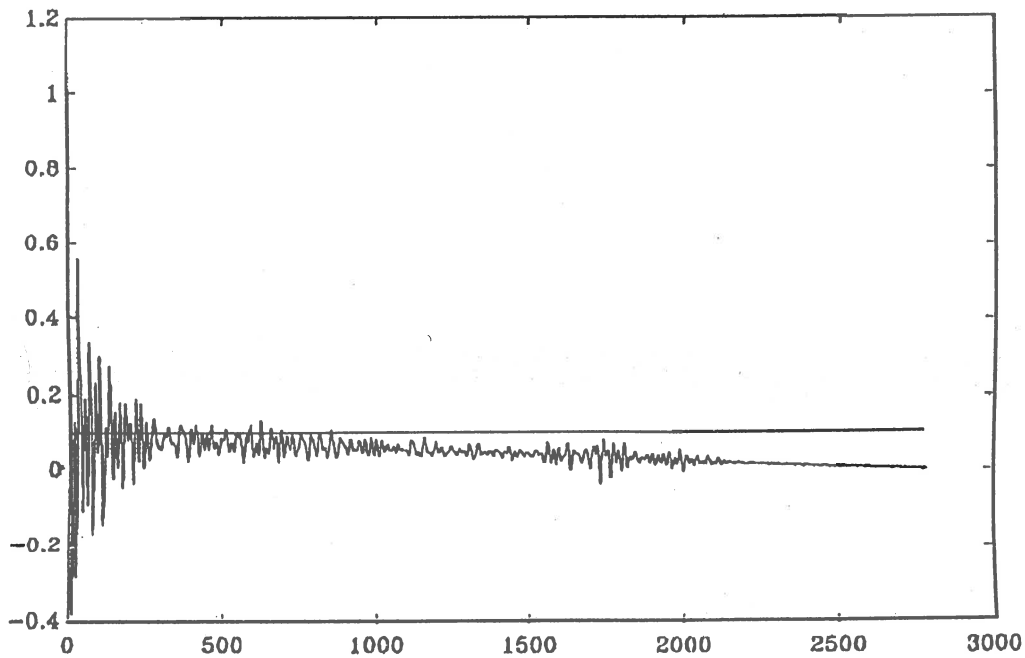
Fig.2 Estimate of autocorrelation
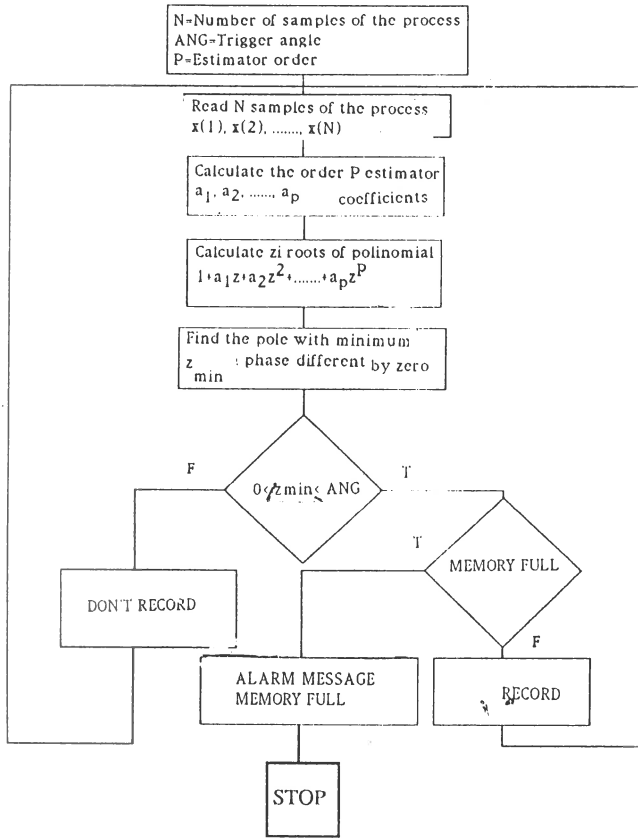
Fig. 3 PDZ algorithm
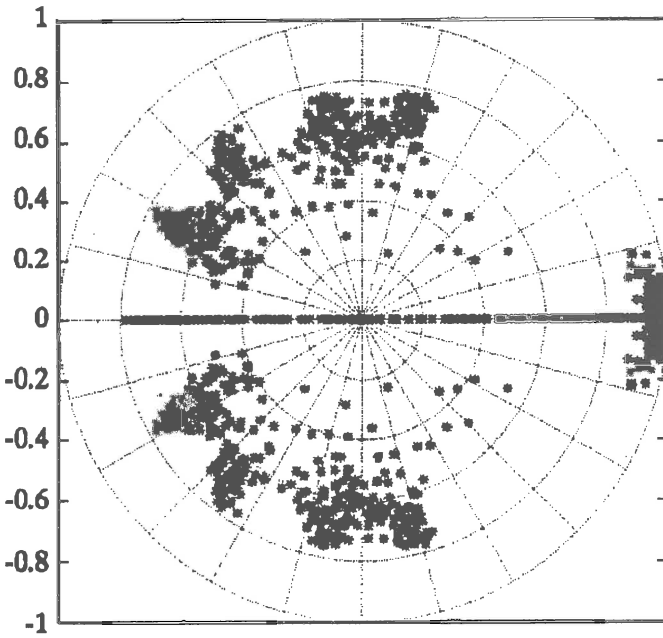
Fig 4 Burg poles estimator in the complex plane for an earthquake.
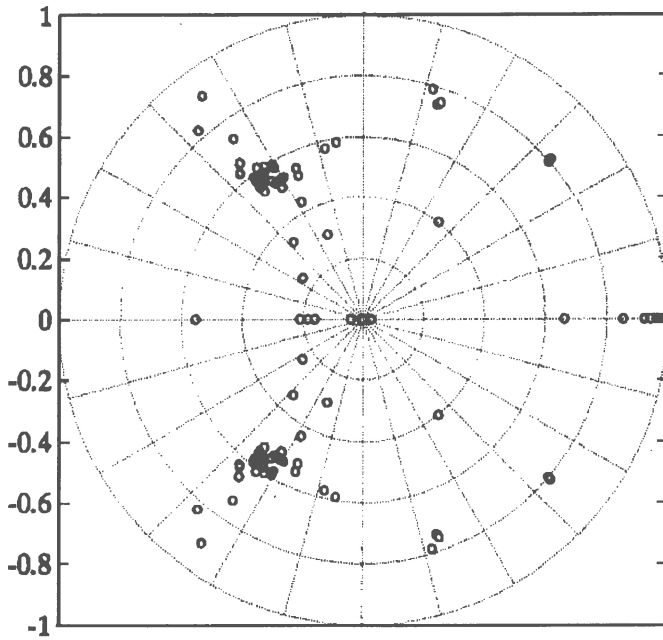
Fig. 5 Burg estimator poles in the complex plane for a false alarm.

CODISMA II: THE NEW MULTICHANNEL ACCELEROMETRIC DATA ACQUISITION SYSTEM. A TEST CAMPAIGN ON A REAL SIZE SPECIMEN OF ARCH.

Massimo Maffucci , Fausto Vitiello: ENEA
Francesco Pirilllo, Marco Stella: Oerlikon Contraves

ABSTRACT

CODISMA II, the new multichannel accelerometric data acquisition system developed by ENEA and Contraves Italiana is shown herein. This system is an advanced multichannel (up to 48), 16 bit, digital data acquisition equipment developed on the experience of the previous CODISMA I. It has been designed and builted on modern DSP concepts and it has available all the state of art of trigger logics. Moreover is described the test campaign on real size specimen of arch, that has been held at the laboratories of ENEA Casaccia research centre in Rome.

GENERAL DESCRIPTION

ENEA (Italian National Agency for New Technology, Energy and the Environment) has long experience in the field of seismic monitoring; at first seismic investigations were aimed by ENEA at the identification of safe places for nuclear power plants. Later the activities have been aimed also for other plants and for seismotectonic researches. For many years, ENEA has designed, realized and managed local-acquisition and radio-transmitted (by radio-relays or by satellite) seismic and accelerometric arrays, acquiring in this way wide know-how in the field of seismic instrumentation. ENEA has realized and still manages various seismic and accelerometric networks (Seismic:Southern Latium and Tosco-Emiliano Appenine. Accelerometric: Val Nerina and archaeological monument in Rome with the first triaxial version of Codisma), this has permitted to our Agency to acquire a large experience in the vibrational field, with the aim to realize advanced instrumentation to validate new research methodologies to prevent vibrational damage of archaeological monuments and civil buildings.

TEST CAMPAIGN DESCRIPTION

CODISMA II, is the new multichannel accelerometric data acquisition system developed by ENEA and Oerlikon Contraves on the base of the experience of previous triaxial version CODISMA employed on the italian territory in many vibrational recording campaigns and accelerometric networks.

To test the compliance of specifics with the features of real protoytpe it has been held, at the laboratories of ENEA Casaccia (Rome) research centre, a test campaign on a real size specimen of arch, builted by the same laboratories, with the double aim to test the new instrument on structure (see fig. 1) and to acquire seismic simulated data on a real size specimen of arch, to improve knowledge regarding structural responses to vibrations. This research has been made with the aim to allow the development and increase of the quality of methods and technologies for the maintenance and the restoration of monuments and civil buildings after earthquakes and vibrational stress. The test has been held as it follows:

-The arch specimen (tuff bricks) mounted on shaking table has been shaken with two different types of signals: One type (TEST) constitued by recordings of real seismic events (see fig. 2a for the input and fig. 2b for the output on structure) and another (CHARACTERIZATION) constitued by a random signal 60s long, with frequency range from 4 to 30 Hz and with maximum acceleration of 0.015 g. All the signal have been applied to the table were monoaxial

-LINEAR PHASE: It has been applied to the specimen a sequence of CHARACTERIZATION (Latitudinal, Longitudinal, transverse) followed by a TEST up to reach an acceleration of 0.06 g.

-NOT LINEAR PHASE: It has been applied to the specimen a sequence of CHARACTERIZATION followed by a TEST up to reach an acceleration of 0.3 g.

The two different phases give the complete response of the structure before damaging and after the first damaging.

SENSORS

The employed accelerometric sensors (see fig. 3, fig.5a and fig. 5b) connected with CODISMA II have been N°8 (Monoaxial) FBA-11 Kinemetrics and N°1 (Triaxial) FBA-13 Kinemetrics, all force-balance type.

DATA ANALYSIS

A first elaboration of the data recorded has been performed by the operator directly in field with the software provided which displays the time history and the frequency response. Afterwards data were examined by dedicated software to obtain informations about ground velocity and displacement. On the basis of this information it is possible to carry out studies concerning dynamic behaviour of structure under investigation.

New knowledge which is being gained, increases the ability to restore damaged monuments and to made them stronger with respect to vibrational action.

The data, after elaboration, are inserted into a dedicated digital bank, and so the recordings and the results are made available on an international scientific computer network.

FUTURE IMPLEMENTATIONS ON THE SYSTEM

At present CODISMA II records seismic data in its memory; in the future for networks applications a centralized management, performed via radio, will be implemented. To this end, it is possible to use the Codisma II RS232C interface that permits connection with standard radio-modem. In this way will be possible to connect each instrument to an acquisition centre by digital radio-relay link; it will be possible, performing a polling interrogation (automatical at prefixed hour, after an event, on request) of each data acquisition site, to transmit data directly to acquisition centre.

Moreover advanced software will be implemented; the new software will be based on spectral analysis of the acquired signals and it will be possible to record lower level vibrations.

CONCLUSIONS

Protection from earthquakes begins with knowing them. To this end it is necessary to carry out the study of seismic waves in earth layers and the analysis of the dynamic behaviour of the structures.

At present protection and prevention standards need monitoring networks which are designed to characterize seismic areas and to perform specific analysis of typical structures such as monuments, bridges & dams. Then precision and reliability of collected data are the first step towards the validity of earthquakes models and for the ability to find solutions for the effects of earthquakes and vibration.

Valid monitoring needs high quality instrumentation, able to acquire data in severe environmental conditions (it has been tested, shaking it with an acceleration higher than 1g) with high reliability and precision. CODISMA II is an accelerometric data acquisition system which has been designed to satisfy this requirement.

CODISMA II

CODISMA II is a 16 bit multi-channel data acquisition system. Although optimized for both seismic and strong-motion applications, the CODISMA II smart architecture and accurate design make it suitable for a very wide range of applications.

Built as a PC-based system, CODISMA II combines a well-known and reliable hardware-software platform with the most advanced DSP techniques to achieve superior performances and an extraordinary ease of use. Virtually anything in CODISMA II can be set or read by user via a standard RS-232 interface. By connecting a PC to CODISMA II it is possible to see how our software-controlled menu-driven configuration is light years ahead of all those boring and cryptic FORTRAN-like user interfaces.

FEATURES

Programmable input gain (+- 1.25 V to +- 10V F.S) and sampling frequency (10 Sps to 500 Sps), technique of oversampling and up to 16 Mb RAM (with data retention) are among the unique features of CODISMA II. Other features are:

-ATL (Advanced trigger logic). A very wide range conditions can be tested: STA, LTA, channel weights, thresholds are all under control;

-SCFS (Software -controlled Filter shaping) lets you choose the most suitable filter shape for your application. Triple FIR filter stage (two for main data stream plus one trigger filter) for each channel exceeds equivalent single-stage 5000-tap performances;

-SDAA (Simultaneous Data Acquisition Architecture) allows elimination of time skews between channels and lets system performances be independent of the number of channels intalled. This

means it is possible to drive a second CODISMA II achieving up to 48 zero-skewed input channels, and all at the maximum sampling frequency;

-Single supply voltage (24 Vdc typical, 10 to 30 Vdc range) and a built-in +-15 Vdc power supply for sensors in conjunction with seismic data retention capabilities (up to 30 days continously) erase the problem of power blackouts.

CODISMA II can be configured and left to collect data for lenghty periods.

GLOBAL SPECIFICATIONS

Channels	6, 12, 18, 24
Channel-to-channel skew	None
Main processor (CPU)	80286 20 MHz
Main operating system	MS-DOS
Signal processor	One 24 Mips DSP every six channels
Main communication interface	Serial RS-232 standard
Data rate	115 kbaud
Trigger I/O interface	TTL compatible
Display	LCD 8 rows x 32 columns
Memory	4Mb to 16 Mb (from 13' to 52' recording time @ 12 channels, 200 Sps)
Pre-event memory	1 to 20 s
Post-event memory	1 to 90 s
STA (Short Time Average)	0.5 to 3 s
LTA (Long Time Average)	60 to 300 s
External time reference interface	DCF-77 time code
Internal time reference	Compensated Xtal oscillator
Internal time reference precision	2×10^{-6}
Internal time accuracy	+-1 ms
Output data rate	10, 20, 40, 100, 200, 400, 500 Sps

INPUT CHANNELS SPECIFICATIONS

Input impedance	120 kΩ
Full scale	+-1.25V, +-2.50V, +-5.00V, +-10.0V
Sensitivity	+-1V/G to +-10V/G
A/D conversion	16 bit, 8000 Sps (oversampling)
Decimation and antialiasing filter	Double linear-phase cascaded FIR (64x256 taps)
Low-pass trigger filter	Linear-phase FIR (32 taps)
Signal filter band-width	Software selectable (depending on output data rate): 1, 3, 5, 10, 30, 40, 50, 60, 70, 80, 90, 100, 120, 130, 140, 150, 160, 180 Hz.
Pass-band ripple	None
Trigger filter band-width	Software selectable (depending on signal band-width): all-pass, 5, 10, 12.5, 16, 20, 25, 32, 40 Hz.

SHAKING TABLE FEATURES

FREQUENCY RANGE	0.5-50 Hz
Max Displacement	+-12.5 cm
Min Displacement (readble by the transducer)	1/10 mm
Max acceleration	5 g
Min acceleration	table noise
Max load	10 t
Dimensions	4x4 m
Freedom degrees	6
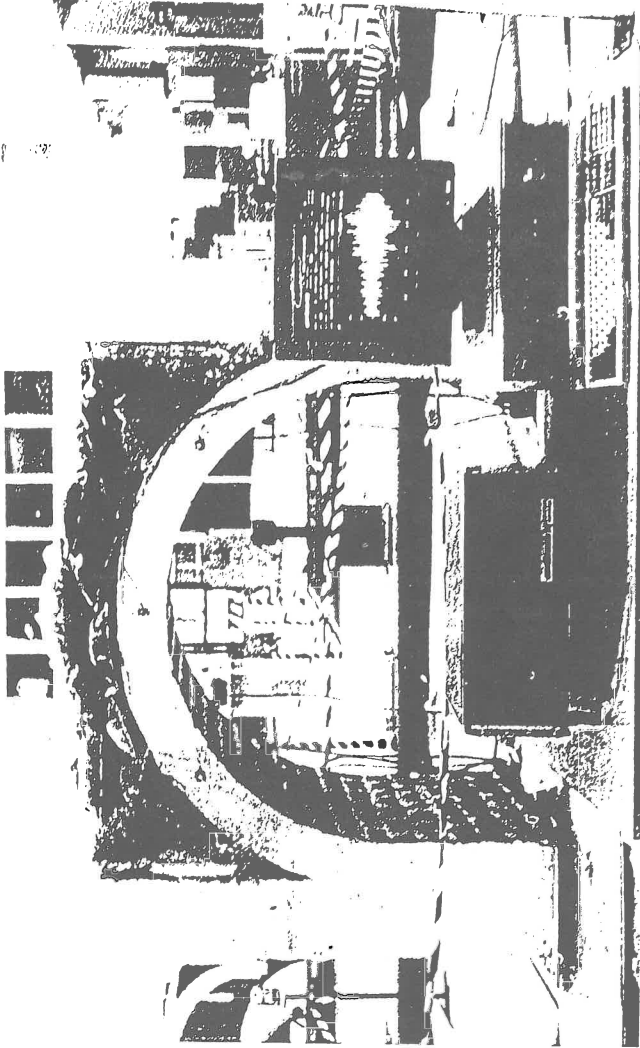
FIG. 1 CODISMA II UNDER TEST
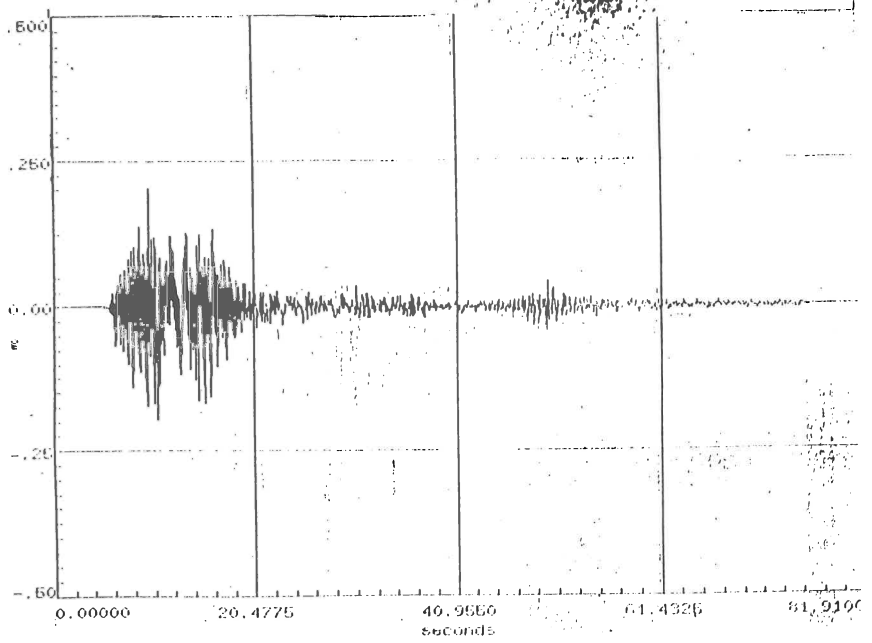
FIG. 2A TABLE INPUT (VERTICAL)

LOCALITY: ENEA: Prove su arco   ALTITUDE :   10 mt.
SERIAL NUMBER: 1   LATITUDE :   0° 0' 0"
OPERATOR ID. : 1002   LONGITUDE: 0° 0' 0"

EVENT Nbr.:   19   PRE-EVENT: 5 sec.   POST-EVENT: 20 sec.

SPS: 200   CUT-OFF FREQUENCIES: SIGNAL = 70.00 Hz   TRIGGER = 16.00 Hz

SSA GAIN: SSA1= +/-2.5 V   SSA2= +/-2.5 V   SSA3= +/-10.0 V SSA4= +/-10.0 V

DATE: 28-Jul-1993   TIME: 11:16:20.142   LENGTH: 2' 17.90   TRIGGER: IN
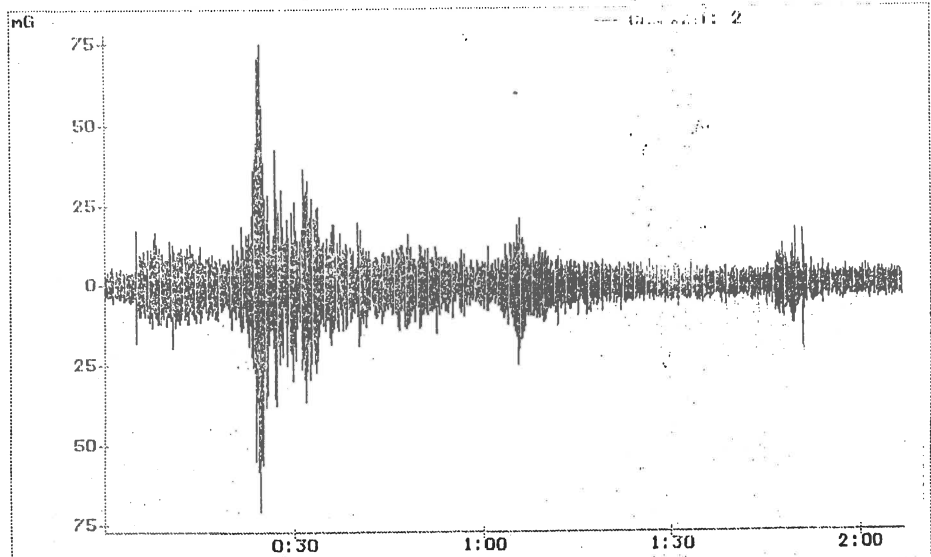
FIG. 2B OUTPUT ON STRUCTURE RECORDED BY
CODISMA

810
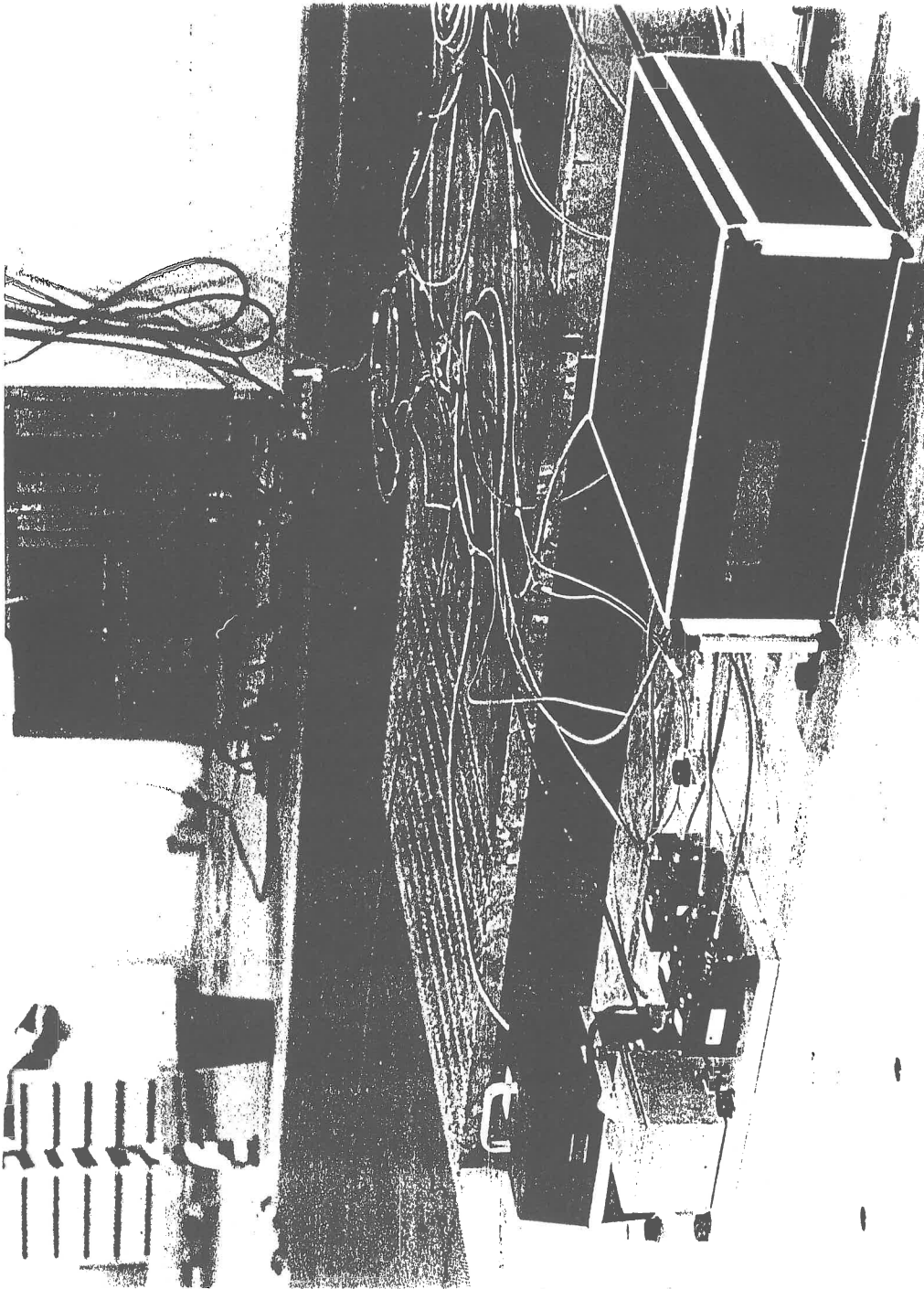
FIG. 3 CODISMA II MOUNTED ON SHAKING TABLE, UNDER VIBRATIONAL TEST.

FIG. 4 SIGNAL ACQUIRED BY CODISMA II WITH
THE TABLE EXCITED WITH A REAL SEISMIC
EVENT RECORDING.
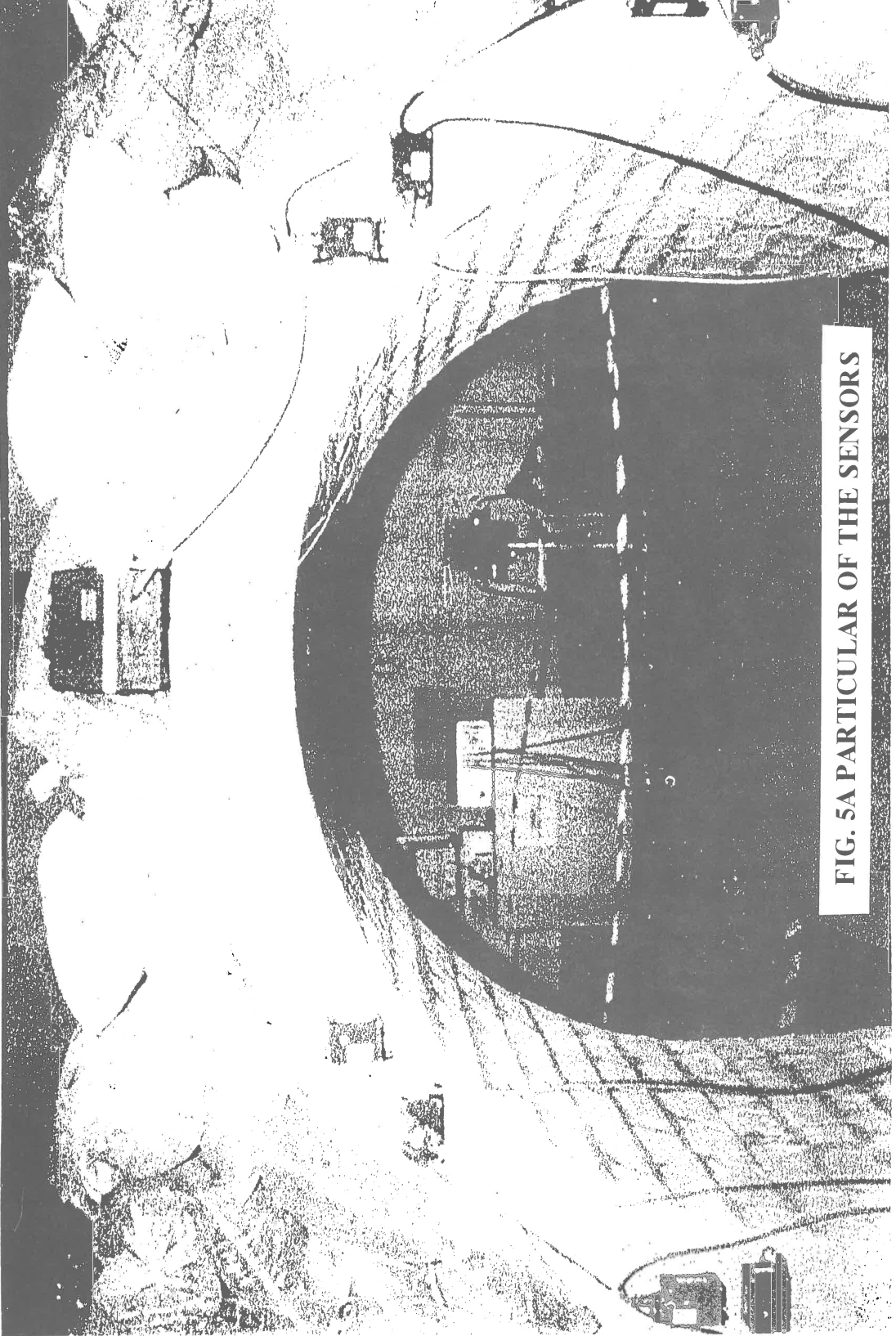
FIG. 5A PARTICULAR OF THE SENSORS

FIG. 5B PARTICULAR OF THE SENSORS
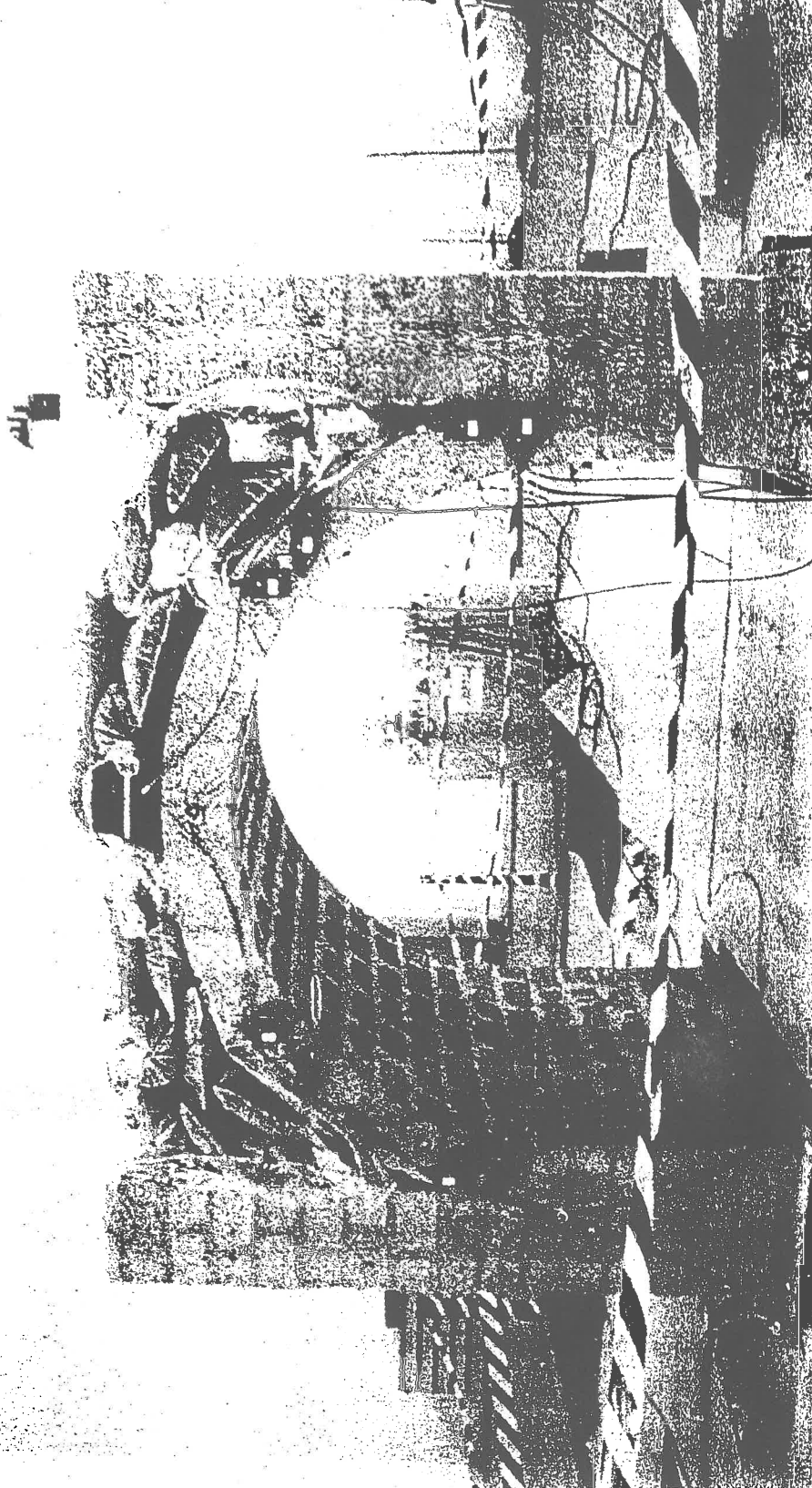
B8-20-1629
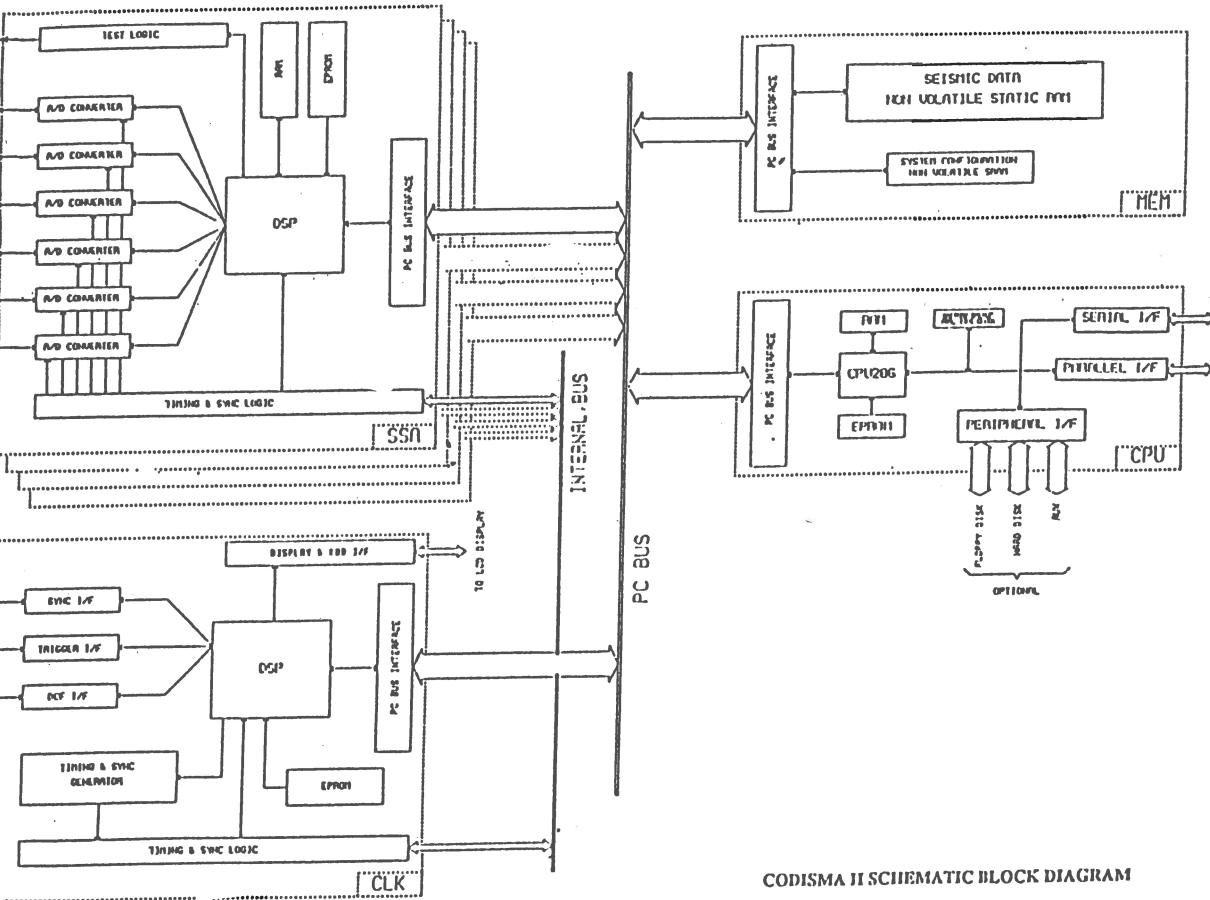
CODISMA II SCHEMATIC BLOCK DIAGRAM
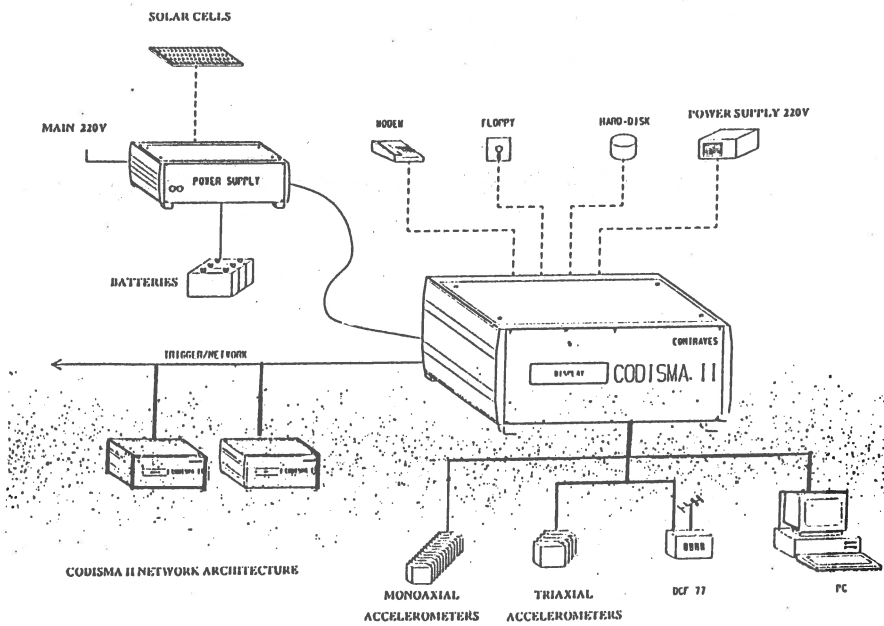
CODISMA II NETWORK ARCHITECTURE

815

Design of the future oriented seismological and strong motion networks in Slovenia

Bojan Uran

Ministry of Environment and Physical Planning,
Geophysical Survey of Republic of Slovenia, Kersnikova 3, 61000 Ljubljana, Slovenia

Abstract

This paper presents some points of view, which we should consider in the phase of developing seismological and strong motion networks. We emphasize internetworking, modularity and upgradeability of the system as a whole, including the data storage, archival and presentation. Frame relay is proposed as the backbone of the network, connecting intelligent instruments. Data base system and GIS tools are also included.

Introduction

We want to develop a modern, high performance and relatively cheap permanent system for earthquake monitoring all over the Slovenia. It should cover both strong motion instruments and seismographs and allow us to migrate to newer technologies in the future. Internetworking and data exchange with other seismological institutions is also very important.

Recent advances in electronics, computer sciences and telecommunications have strong influence also on the seismological instrumentation. More powerful and cheap processors allow us to set up quite different hardware and software types as we used to do a decade ago. Networking is the key issue, allowing us to connect different type of computer.

Another major issue is the standardisation. ISO OSI standards with the seven layers model for communications and the TCP/IP suite form two frameworks, which allow us to connect different equipment from different manufacturers and it will still work together. De facto standards, like the PC ISA (Industry Standard Architecture), with a huge amount of companies, producing boards, software and other accessories, cuts the prices for the hardware and software. Our investments are safer, because we do not depend just on one manufacturer. Because of the standardisation, there are always upgrades to newer and better technologies, not making our equipment totally obsolete.

Collecting digital data became so simple, which we can bury ourselves in huge amounts of data. That is certainly not our intention so we will pay great attention on data bases for data storing and archival and GIS tool for data presentation and correlation with other spatial data.

We used experiences from other seismological networks, like BUG, SIL and many others. Our solution uses frame relay as the backbone of the WAN network and is digital from the beginning. More attention is paid also on the completeness of the system, incorporating data base system and presentation tools.

Hardware

Central station is shown in Figure 1. It will consist of an Ethernet local area network and different kind of workstations. We have now a Silicon Graphics Indigo workstation, Novell Netware server and a few PC graphic workstations, which can work either under DOS or as Xwindows terminals. TCP/IP and Novell's IPX protocol are concurrently supported on the Ethernet. A router will serve for connection to the Internet.
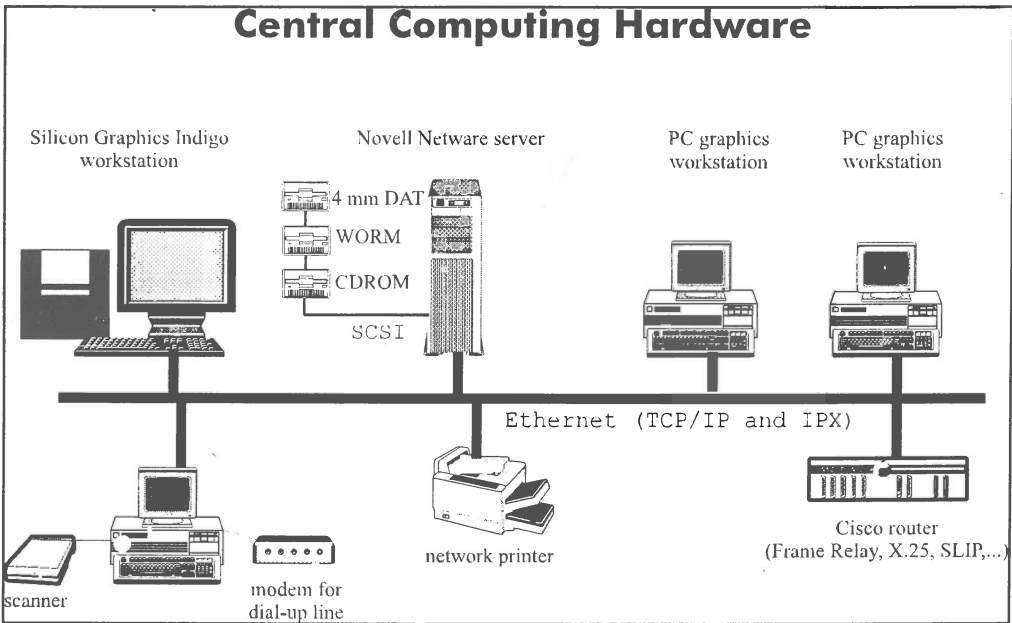
Figure 1: Central computing facilities.

Storing and archival of huge amounts of seismological data demands different kinds of devices. Hard disks are the main media, with 4 mm DAT as the backup and for short term storage. WORM disk is for the archiving. CD-recordable can also serve the same purposes. It is even more practical not only for archiving, but for distribution of our own data. CDROM is now a usual part of computers. All devices are on SCSI.

A modern instrument, schematically shown on Figure 2, should consist from a good sensor with high dynamic range and broad band characteristics to cover the whole frequency band of events with high fidelity. Amplifier stage and analog to digital conversion are the first steps in the measurement chain. They are also the most critical ones, because we can introduce much of the noise and decrease the quality of the system. 24 bit A/D converters are necessary for seismographs. From that point on, there are no bigger differences between an ordinary computer and the seismograph.

When we have data in the digital format, the things become simpler and do not differ much from networking of whatever kind of computers. We can indeed loose some data because of the malfunctioning of hardware, but nowadays mass storage devices are quite reliable. Redundancy as mirroring, duplexing or even RAID arrays are quite common and the prices are sinking. Hard disk is the choice of preference for the temporary data storage in a ring buffer in the instrument,
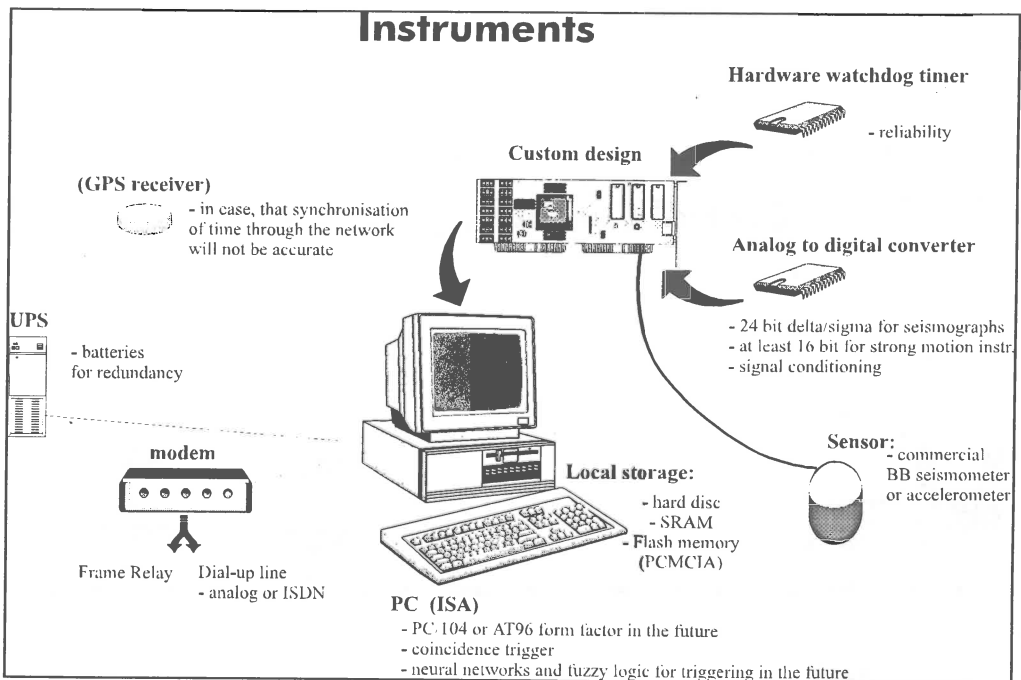
Figure 2: Our vision of a smart instrument.

because of the high capacity and low price. Flash memory or SRAM is more expensive and more suitable for really harsh environment.

Uninterruptable power supply with additional batteries serves as the power source and guaranties the work of the instrument in every condition. Another important part of the instrument is the hardware watchdog timer, which resets the instrument to a known state in case of malfunctioning. Modern processors are powerful enough to simultaneously handle the data acquisition, storage and communications.

Accurate time functions are also very important in seismology. GPS receivers offer the possibility of very precise synchronisation with UTC. Their prices are sinking so we plan to use them. Another possibility for synchronisation of time is through the network, but we should first tests the accuracy and repeatability of it.

Big ring buffers and smart trigger algorithms on a single instrument, with the coincidence triggering for the whole system, insure the integrity of data and decrease the amount of data that should be transferred and processed on the central computer. We will try to use neural networks and fuzzy logic to improve the trigger algorithms, recognise events and help in data preparation and phase picking.

WAN Networking

Frame relay technology will serve as a backbone in the WAN network, as shown in the Figure 3. It started as a protocol for packet switching service as a part of the ISDN. Later frame relay became an independent standard. It is intended for packet data transmission in wide area networks, is fully digital and allows us to use also copper wires. Transmission speeds are 64 kbps on a single channel. We can combine different number of channels up to the maximum

transmission speed of 2.048 Mbps. Each user of the frame relay network has a guaranteed bandwidth. In our case we will use that bandwidth for cyclical transfer of status data or data from a stream of very low frequency. In case of events, frame relay allows us to increase the bandwidth on demand, so we can transfer our actual earthquake data very fast. Dual use of the bandwidth means also lower cost for the data transmission. On the other hand, it demands smarter instruments with bigger ring buffer, more sophisticated trigger algorithms on a single instrument and coincidence trigger for the whole system. Transmission is faster then with X.25, because it uses just OSI layers 1 and 2. Transit delays are also low so we hope to synchronise the time over the network. Interconnection of different nodes of the network is fast and we can have permanent virtual circuits.
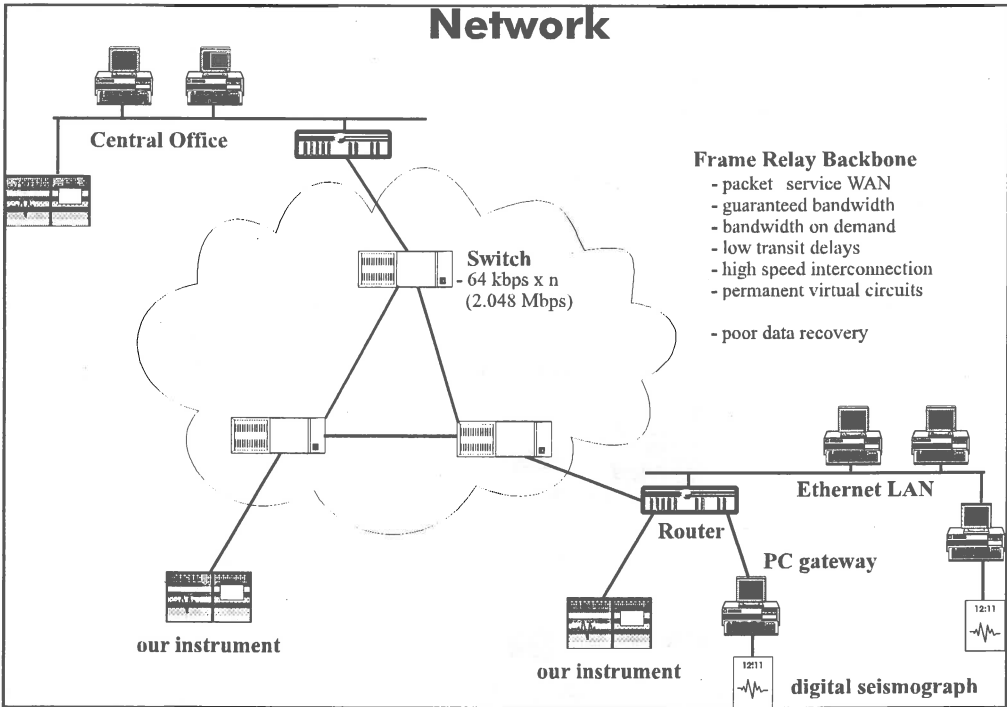
Figure 3: WAN network.

Poor data recovery is the only minus of the frame relay in comparison with the X.25. The application must take care of the integrity of data. In case of X.25, the data recovery is built in the OSI layer 3, making the protocol less efficient.

ATM will replace other technologies in the future. With the frame relay and the switches we are prepared for a smooth transition to ATM.

There are many possibilities to connect an instrument to the frame relay. First is a direct connection with the frame relay board to the switch. That is the less cost-effective solution, because we take and pay for the whole bandwidth. Others are through a local area network, with shared access. Then we need router and network interface card for the instrument. For digital seismographs, which do not have this possibility, we will use a PC computer as a gateway between the network and the seismograph, adapting the hardware and software differences. The entry points to the frame relay network will be all over the country, so we will have plenty of possibilities

to find suitable locations for seismographs and strong motion instruments near the entry points. We should take care for connections between the actual locations and the entry points. Leased lines, ISDN, RF digital telemetry and spread spectrum are some solutions for these short distance connections.

Software

SQL with its additions for handling the huge amount of raw binary data is the choice of preference. We intend to use client-server and distributed data base architectures (Figure 4). Client-server architecture is the logical choice, because of the nature of the data collection and later interpretation and archival. We need all the data of an event on a single computer. Distributed data base model is also very promising, especially for the data in the ring buffer. Data can be on heterogeneous servers, we can have replication of data and the best of all, we do not have to take care of the integrity of data. Replications and redundancy are already built in.
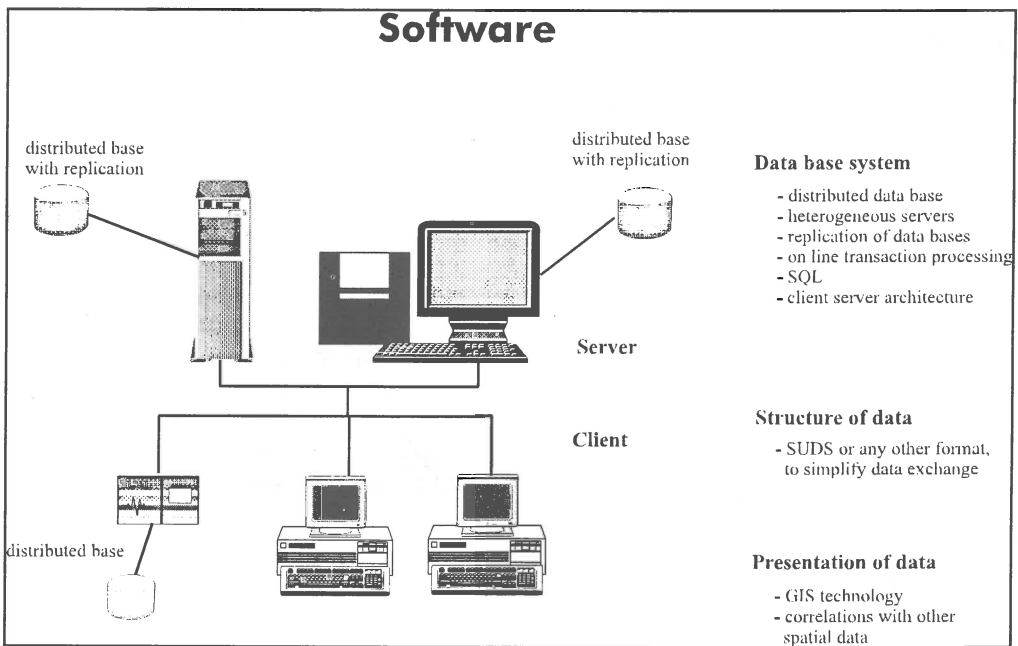
Figure 4: Software-the power of the system.

The structure of data is not figured out yet. There are many different and incompatible data formats, but none of them as a firm, well-established standard. SUDS, SEED or perhaps the GSE formats of the AutoDRM are the most probable choices. It should allow us to store the raw, processed data and catalogues. We will definitely not introduce our own format, but will use the format and possibly also the structure of the data base tables, which will simplify data exchange with seismological centres in the neighbourhood.

Geographical information systems are developing very fast. In Slovenia, as the benefit of its small size, we have already many spatial data in GIS (geodetical, geological, tectonical and geophysical maps, digital model of relief and satellite photos among others). The use of the same reference model and structure of the seismological location data greatly simplifies data presentation

and correlation with other spatial data.

We will allow seismological community to use our data through Internet. World Wide Web (WWW) server on our central location will hide the complexity of the system and limit unauthorised access of the other resources. Access will be possible to the raw and processed data, locations, catalogue and maps, located on our SQL server.

Conclusions

Global networking is influencing also seismological community. Seismologists in Slovenia want to participate in this process with the data from our seismological and strong motion networks of loosely coupled digital stations. Intelligent instruments are one of the key points. They should partially process data and send just the actual earthquake data to the central station for the final processing. Fault tolerance in the form of redundancy and independence of individual segments is built into the solution. Frame relay network is a fast, cost-effective and open solution for interconnection of instruments. Powerful data base and GIS presentational tools are also important issues in the system, freeing the seismologist from the tedious task of handling of huge amounts of data and letting them more time to work on the actual studies of earthquakes. Our experiences with the setting up and operation of the system will be presented elsewhere.

THE SEISMOGEOGRAPHICAL REGIONALISATION FOR GERMANY. - THE PRIME EXAMPLE OF THIRD LEVEL REGIONALISATION.

G.Leydecker (1) and H.Aichele (2)

(1) Dr.Günter Leydecker, Bundesanstalt für Geowissenschaften und Rohstoffe, Stilleweg 2, D-30655 Hannover
(2) Dr.Helmut Aichele, Seismologisches Zentralobservatorium, Krankenhausstrasse 1-3, D-91054 Erlangen

ABSTRACT
At first Gutenberg and Richter subdivided the earth surface into 51 seismic regions, later Flinn and Engdahl suggested a computer orientated regionalisation scheme of 728 regions. As even this concept seems to be too coarse for modern research the IASPEI Working Group on Regionalisation was founded with the aim to subdivide the existing regions into local regions, called level 3 regions.

For this concept the territory of the Federal Republic of Germany was subdivided with respect to seismic activity, geological development and tectonic features, defining also regions with very low seismicity. This strategy is called "seismogeographical regionalisation". The new regions were named, following the appropriate conventions. Now experts of neighbouring countries should continue this work, especially by reviewing borderline areas.

INTRODUCTION
For the automatic printout of readable epicenter listings and descriptive epicenter locations with modern seismic data management systems it is indispensible to have a uniform, systematic method for regionalizing the earth's surface so that seismic data can be efficiently retrieved by event location. Based on the seismic regionalisation of Gutenberg and Richter (1954) with 51 seismic regions, which was found to be too coarse for modern research, Flinn and Engdahl (1965) and Flinn, Engdahl and Hill (1974) suggested a computer orientated regionalisation scheme which divides the earth surface into 728 regions, called the Flinn-Engdahl (FE) Regions. This scheme became the international standard and is used by all agencies performing geophysical data management systems and global earthquake location.

The Flinn-Engdahl Code (F-E Code) was designed before the concept of plate tectonics was well developed. The borderlines of its regions were defined by integer values of latitude and longitude. This results in a rough approximation of boundaries, especially of political ones. Therefore the F-E Code is inadequate or in some details incorrect (i.e. Aichele and Peterschmitt 1977; Young and Pooley, 1986).

In 1985 the IASPEI-Commission on Practice established a Working

Group with the mandate to correct and modernize the original F-E Code This group decided at its meeting in Vancouver (1987):

1. to keep the present F-E Code unchanged, except for correcting a few errors (Young 1988; Young and Wiens 1990; Young, Aichele and Presgrave 1993; Young and Presgrave 1995), and to review all region names (without changing the region boundaries)

2. to subdivide the existing regions into local regions.

With this local regions it should be possible to solve the present problems and to develop a uniform, flexible regionalisation system to fulfil future requirements for seismic data management systems. The new scheme is named the level 3 regionalisation and consequently level 2 means the Flinn-Engdahl and level 1 the Gutenberg-Richter concept.

The IASPEI Working Group on Regionalisation started to develop general guidelines for the design of the third level regionalisation parallel to examples. Individual members of the Working Group were assigned to coordinate the different areas of the globe.

The region of Europe, defined as the area of interest by the European Seismological Commission (ESC), a regional commission of the IASPEI, can be described as followed:

westwards: to the Mid-Atlantic-Ridge, north of 30°N
northwards: to the Arctic Ocean
eastwards: to the Urals and the regions bordering the
          Caspian Sea, the Black Sea and the Mediterranean
          Sea
southwards: to the regions bordering the Mediterranean Sea.

In this tectonically complex area, which is additionally divided into many states, good examples can be found to demonstrate the difficulties in further regionalisation but also to represent its practical solution.

THE EXAMPLE FEDERAL REPUBLIC OF GERMANY (BEFORE 1990)
The former Federal Republic of Germany (FRG) is situated in the centre of the European area and forms the western part of the level 2 Flinn-Engdahl Region 543 "Germany", the political name of a political entity which did not exist in this shape even at the time when the FE regions were introduced. As Europe is divided into many states of large differences in size, all adjacent level 2 regions have geopolitical names (e.g. Austria, Switzerland, France etc.). For seismic events occurring in areas crossed by state borders, which could only very roughly fitted by the coarse region boundaries, this can lead to misinterpretation of data, retrieved by event location procedures.

This can best be demonstrated at the southwestern part of the region under consideration. Here the Upper Rhine Graben forms

a well defined seismotectonic unit. A reliable continuous ob-
servation of this area including hypocenter determination of
microearthquakes with high accuracy, is very important because
of its dense population and with many facilities, highly
sensitive against seismic hazard. Additionally the epicenter
of the strongest earthquake that occurred in Central Europe,
the Basel earthquake of 1356 that took about 300 victims, was
located at or close to the southern end of the Upper Rhine
Graben.

The area (Fig.1) is crossed by the border between France and
the FRG, which follows the river Rhine, and by the borderlines
between France and Switzerland as well as Switzerland and FRG.
From the level 2 FE-regionalisation system the area includes
the boundaries between the regions 538 "France", 543 "Germany"
and 544 "Switzerland", those following by definition integer
values of latitude and longitude and missing therefore the true
borderlines. When using only this level 2 in an automatic re-
gion association program all kinds of misleading results may be
produced.

The third tier of local regions should avoid errors in region
names caused by the coarseness of the level 2 region defini-
tion, and should allow an efficient retrieval of earthquake
data by association with tectonic or at least geographical
features. For the example described above this was achieved by
introducing a local area as a third tier, defined by a polygon
and taking the complete tectonic feature into consideration.
It is named "Upper Rhine Graben."

The third tier regionalisation for the entire FRG was done
according to the following basic rules, developed by the IASPEI
Working Group:

   - a local region is a closed linked list of polygon vertices
   defined by latitude and longitude

   - a local region containing FE region boundaries is defined
   as complete polygon without regarding these boundaries.
   (The subdivision of a local region by a FE region boundary
   is to be handled by computer algorithms.)

   - the level 3 regionalisation is multilayered with the top
   layer consisting of political borders defined separately.
   The Working Group is to define the second and subsequent
   layers of polygons defining seismotectonic and/or local geo-
   political regions.

   - a local region can have two names, a seismotectonic name
   and a geopolitical name, with the minimum requirement being
   either name.

To avoid misinterpretation and misunderstanding the Working
Group on Regionalisation issued the following important notice
(Working Group on Regionalisation, Further interim report to
the Commission on Practice, IASPEI, meeting of 21 August 1991):

"Level 3 Regionalisation is based on seismicity and tectonic features. It is being designed to provide a clear and precise description of a geographical point. It is <u>not</u> designed for use with seismic hazard or risk and the maps are not maps of seismic hazard or risk."

A starting point for the regionalisation of the FRG was the coarse division made by Ahorner, Murawski and Schneider (1970) (Fig.2). This scheme did not fulfil the requirement of closed polygons, and it was too coarse in respect to the actual knowledge about the seismicity of the country. This can be seen by combining the Fig.2 with the epicenter map plotted with historical and actual earthquakes (Fig.3) from the reference earthquake catalogue of the FRG (Leydecker 1986). Another sub-division of the area (Fig.4) by Ahorner and Rosenhauer (1983) was designed for seismic risk analysis purposes. Here, for example, the Rhinegraben area is subdivided into the valley, filled with sediments, and separated from the graben shoulders, because of different soil response. This subdivision seems to be not adequate for the purpose in discussion. In general the regionalisation of Ahorner and Rosenhauer is too fine for our purpose.

THE FEDERAL REPUBLIC OF GERMANY (AFTER 1990)
The work on a local example for the third tier of seis-mogeographic regionalisation has been started in 1988 after the IASPEI decisions of the Vancouver meeting. This work, however, was unexpectedly influenced by the global political changes in 1989. With the unification of the former German Democratic Republic (GDR) with the Federal Republic of Germany this new state fitted much better the region 543 which had been clairvoyantly introduced as level 2 region by Flinn and Engdahl in 1965. For the former GDR similar preparatory work as described for the former FRG was performed and documented (Grünthal 1988). This subdivision was made for the eastern part of the state and not at all coordinated with the western part

As a result the seismologists of all seismological observatories of the country, experts for the local seismicity of the different regions, decided a new regionalisation. The regions were defined with respect to seismicity and under con-sideration of geological development and tectonic features. In this way also regions with very low seismicity could be subdi-vided. This strategy is called "<u>seismogeographical regionali-sation</u>". The result is shown in Fig.5. The names of the re-gions are given in table 1. The numerical values of latitude and longitude of the polygon vertices are submitted to the Wor-king Group for further coordination and are available on diskette by the authors of this paper.

The plot of epicenters of damaging earthquakes together with the new seismogeographical regions in the same map (Fig.6) illustrates, that our subdivision of the Federal Republic of Germany complies with the seismicity. However it also shows

that in Northern Germany with its very low seismic activity, especially geological and tectonic features had to be taken into consideration in order to avoid too large regions.

NAMING THE LOCAL REGIONS

nalysing the names of the level 2 regions, we can distinguish hree kinds of names:

1. political names (e.g. France, Switzerland),
2. geotectonic names (e.g. Carlsberg Ridge, Mid Atlantic Ridge),
3. geographical names (e.g. Mediterranean Sea, Aleutean Island).

These different categories of names led to different kinds of confusion. A thorough analysis of the level 2 region names resulted in renaming many regions without changing their boundaries. Together with this name revision the conventions for choosing a region name were redefined, and seismologists working on the regionalisation for local regions should adhere as closely as possible to this conventions (Young et al. 1993). For FRG we strictly followed the convention, which clarifies the use of directional suffix "ern", the avoidance of generic names, the clarification of words (e.g. region, border region) and the use of hyphen.

FURTHER PROCEDURES

At its meeting in Istanbul the IASPEI Working Group on Regionalisation decided to accept this Third Level Regionalisation of the FRG "as the Working Group's primary example" (IASPEI Report to the Commission on Practice, Working Group on Regionalisation, Meeting of 31 August 1989). The elaboration of this example, because of the above described development, took much more time than previously expected. At three meetings of seismologists working at the seismological observatories of FRG, the presented result has been developed and continuous reports were given to the IASPEI Working Group at its meetings in Barcelona (1990), Vienna (1991) and Prague (1992).

Now, after the Working Group has developed the prerequisites for the Level 3 Regionalisation with the German example, the local experts of other countries are requested to submit level 3 subdivisions of the regions of their responsibility to the Working Group. Special care should be taken for those regions containing borderline areas, and cooperation between experts of neighbouring countries should result in commonly agreed level 3 region proposals.

It is expected that this work leads to a homogeneous system of third level regionalisation for the entire globe. Then this system than will be submitted to the IASPEI for acceptance and after that made available to the data centers and interested institutions for implementation and further use.

REFERENCES
Ahorner,L.,Murawski,H. and G.Schneider, 1970. Die Verbreitung von schadenverursachenden Erdbeben auf dem Gebiet der Bundesrepublik Deutschland, Zeitschr.f.Geophys. 36, 313–343.

Ahorner,L. and W.Rosenhauer, 1983. Erdbebenzonenkarte. -- Chap. 9 in Hosser et al.: Abschlußbericht zum Forschungsvorhaben "Realistische seismische Lastannahmen für bauliche Anlagen mit erhöhtem Sekundärrisiko". Im Auftrag des Inst.f.Bautechnik, Berlin (Aktenzeichen IV/1-5-377/82).

Aichele,H. and E.Peterschmitt, 1977. Refinement of geographical and seismic regionalisation, Publ.Inst.Geophys.Pol.Acad.Sc., A-6, 117.

Flinn,E.A. and E.R.Engdahl, 1965. A proposed basis for geographical and seismic regionalisation, Rev.Geophys., 3, 123–149.

Flinn,E.A., Engdahl,E.R. and A.R.Hill, 1974. Seismic and geographical regionalisation, Bull.Seism.Soc.Am., 64, 3, II, 771–993.

Gutenber,B. and C.F.Richter, 1954. Seismicity of the earth and associated phenomena, Princeton University Press, Princeton New Jersey.

Grünthal,G., 1988. Erdbebenkatalog des Territoriums der Deutschen Demokratischen Republik und angrenzender Gebiete von 823 bis 1984, Zentralinstitut für Physik der Erde, No.99, Potsdam.

Henger,M. and G.Leydecker (eds.), 1987. Erdbeben in der Bundesrepublik Deutschland 1982, Bundesanstalt für Geowiss. und Rohstoffe, Stilleweg 2, D-30655 Hannover.- ISSN 0723-3465 -- The earthquake data for the following years till 1990 are taken from the same publication serie.

Leydecker,G., 1986. Erdbebenkatalog für die Bundesrepublik Deutschland mit Randgebieten für die Jahre 1000–1981, Geol. Jahrbuch E 36, pp 83, Hannover, ISSN 0341-6437. -- The expanded earthquake catalogue for the years 800–1990 for all events, respective till 1994 for damaging earthquakes, is available on diskette.

Young,J.B. and C.I.Pooley, 1986. Classifiers of seismic and geographical regionalisation, AWRE report No. 06/85 (January 1986).

Young,J.B., 1988. A proposal for additional regions for the Flinn-Engdahl Regionalisation scheme, Geophy.J., 93,

583-586.

Young,J.B. and D.A.Wiens, 1990. A further proposal for additional regions for the Flinn-Engdahl Regionalisation scheme, Geophy.J.Int., 103, 759-762.

Young,J.B., Aichele,H. and B.W.Presgrave, 1993. Region name conventions in the Flinn-Engdahl Regionalisation scheme, Geophy.J.Int., 114, 411-413.

Young,J.B. and B.W.Presgrave, 1995. The political subdivision of Northwest Africa and Southeast Asia in the Flinn-Engdahl Regionalisation scheme (sent to GJR).

Table 1: Names of the Seismogeographical Regions for
the Federal Republic of Germany and Borders

ALTMARK
BAVARIAN ALPS, Austria-Germany-Switzerland border region
BAVARIAN MOLASSE BASIN, Austria-Germany border region
BOHEMIAN MASSIF, Austria-Czech Republic-Germany border region
CENTRAL SAXONY, Czech Republic-Germany-Poland border region
CENTRAL THURINGIA
EASTERN NETHERLAND BLOCK, Germany-The Netherlands border region
EASTERN RHENISH MASSIF
EASTERN WUERTTEMBERG
EIFEL MOUNTAIN REGION, Belgium-Germany-Luxembourg border region
FRANKONIAN JURA
HARZ AREA
HESSIAN DEPRESSION
HUNSRUECK, Luxembourg-Germany border region
KREFELD BLOCK, Germany-The Netherlands border region
LAKE CONSTANCE AREA, Austria-Germany-Switzerland border region
LOWER RHINE AREA, Belgium-Germany-The Netherlands border region
MIDDLE RHINE AREA
MUENSTERLAND
NORTHEASTERN GERMANY, Germany-Poland border region
NORTHERN BLACK FOREST
NORTHERN FRANKONIA
NORTHERN LOWER SAXONY AND HOLSTEIN, Germany-The Netherlands
                                    border region
NORTHWESTERN GERMANY, Denmark-Germany border region
PFALZ - SAAR AREA, France-Germany border region
RINGKOEBING - FYN HIGH, Denmark-Germany border region
RUHR COAL MINING DISTRICT
SAAR MINING DISTRICT, France-Germany border region
SOUTHERN BLACK FOREST, Germany-Switzerland border region
SOUTHERN HARZ MINING DISTRICT
SOUTHERN LOWER SAXONY
SWABIAN JURA
SWISS JURA, Germany-Switzerland border region
TEUTOBURGER WALD
TEXEL - IJSSELMEER BLOCK, Germany-The Netherlands border reg.
UPPER RHINE GRABEN
VENN AREA, Belgium-Germany border region
VOSGES MOUNTAIN REGION, France
VOGTLAND REGION, Czech Republic-Germany border region
WERRA POTASH MINING DISTRICT
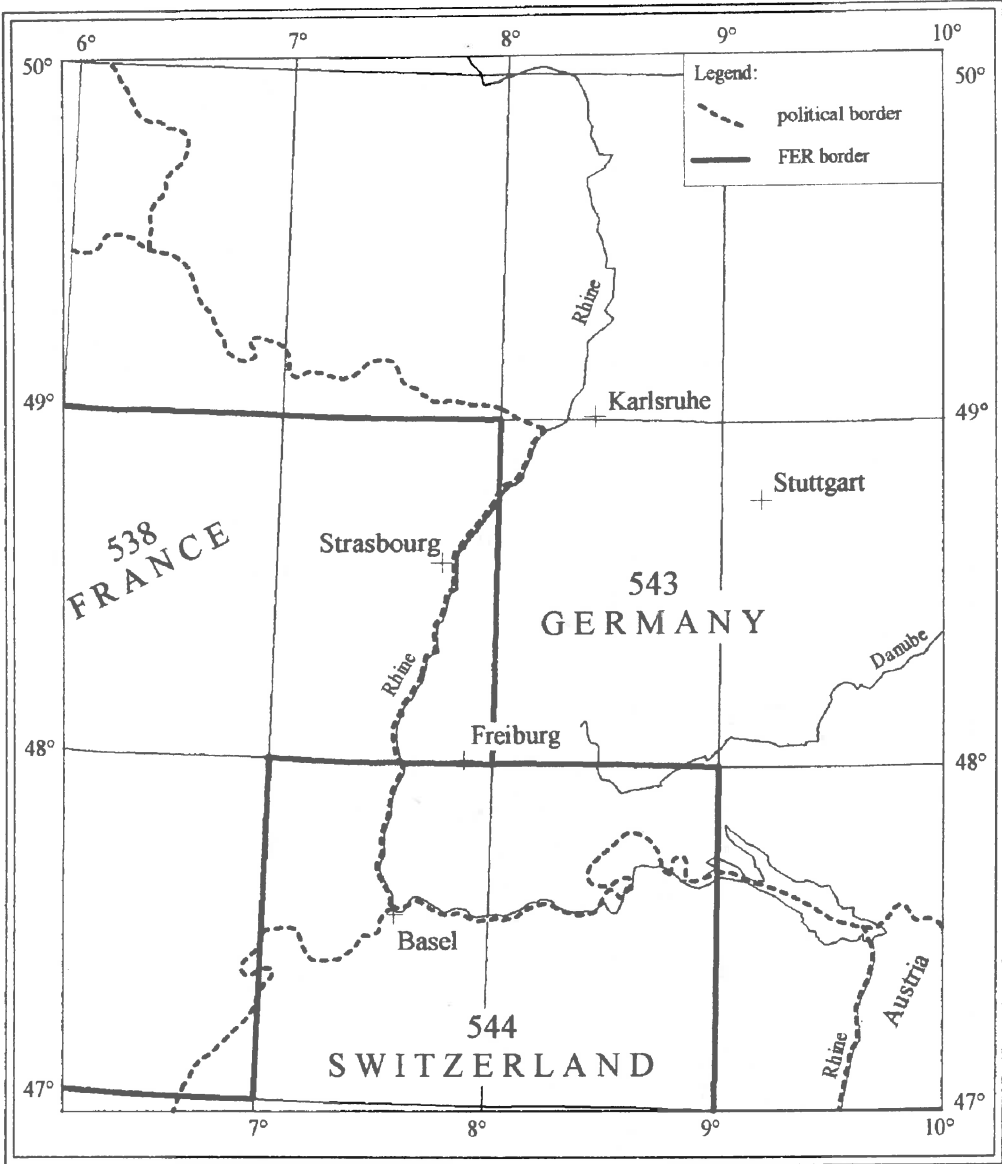
Fig. 1: The Southern Upper Rhine area, an example for the problems with the level 2 Flinn-Engdahl Regionalisation.
Given are numbers and names of the three Flinn-Engdahl Regions (FER) covering this area.
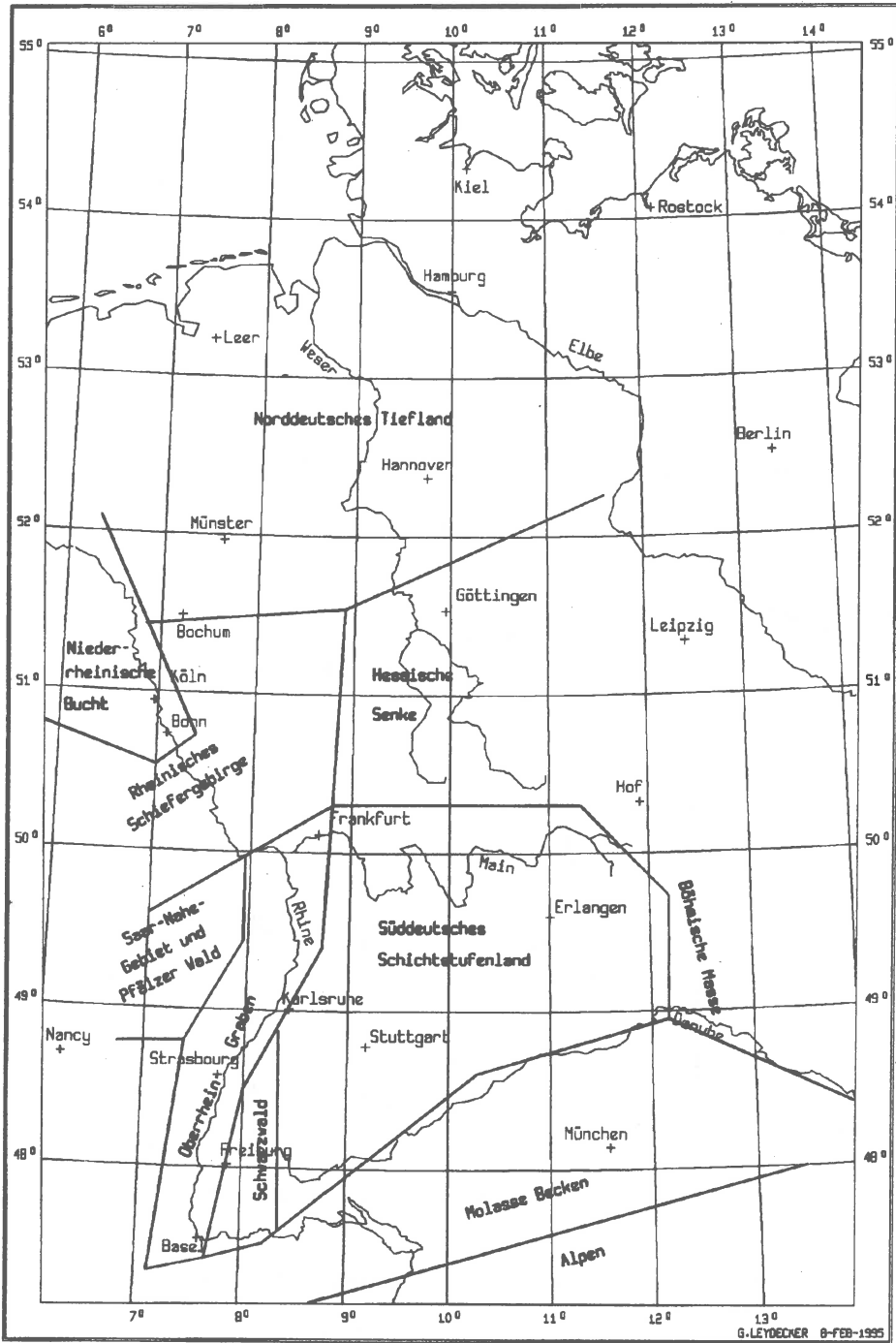
Fig. 2: The first seismogeographical regonalisation of the Federal Republic of Germany (after Ahorner, Murawski & Schneider 1970).
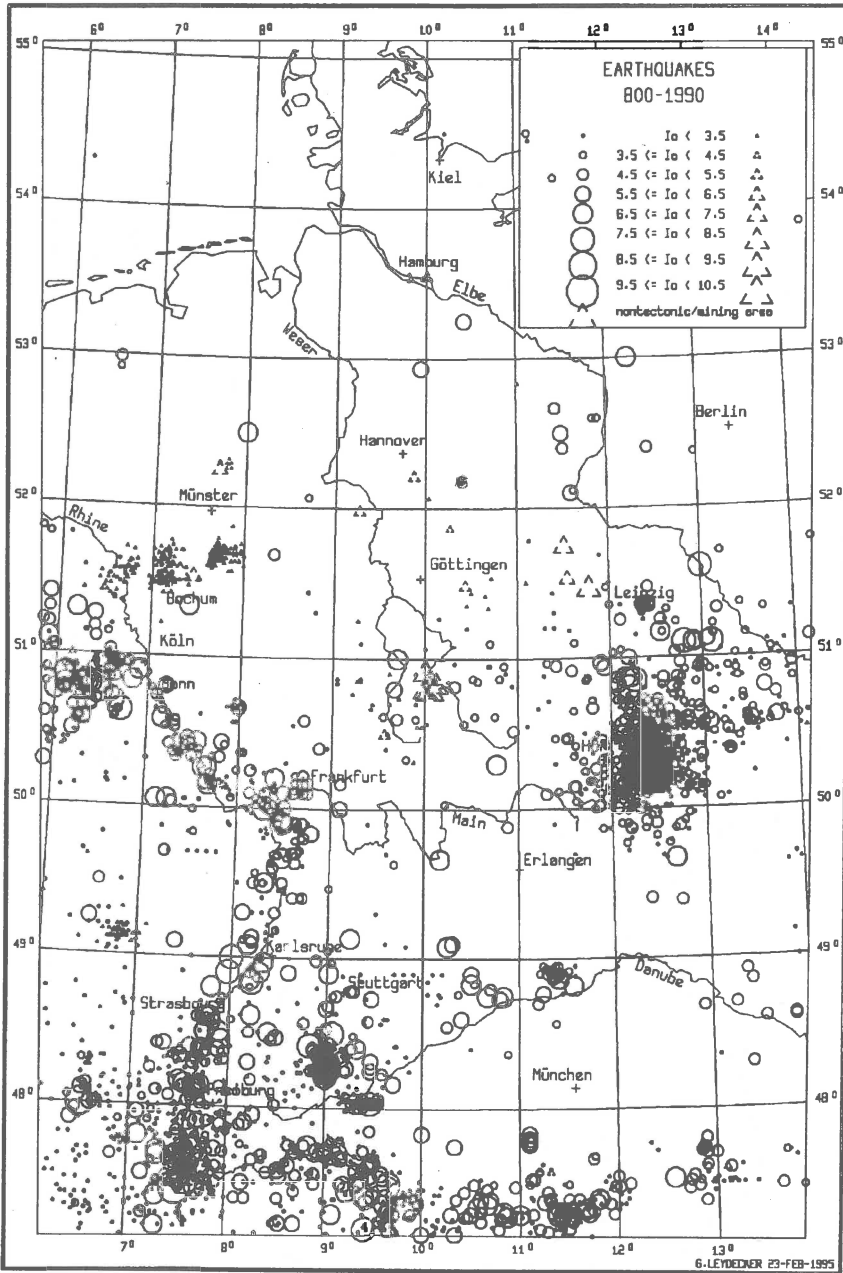
Fig. 3: Earthquake epicenters in Germany for the years 800-1990
     (Grünthal 1988; Henger & Leydecker 1987; Leydecker 1986).
     The size of the earthquake symbols is related to epicentral
     intensity Io (MSK-1964).
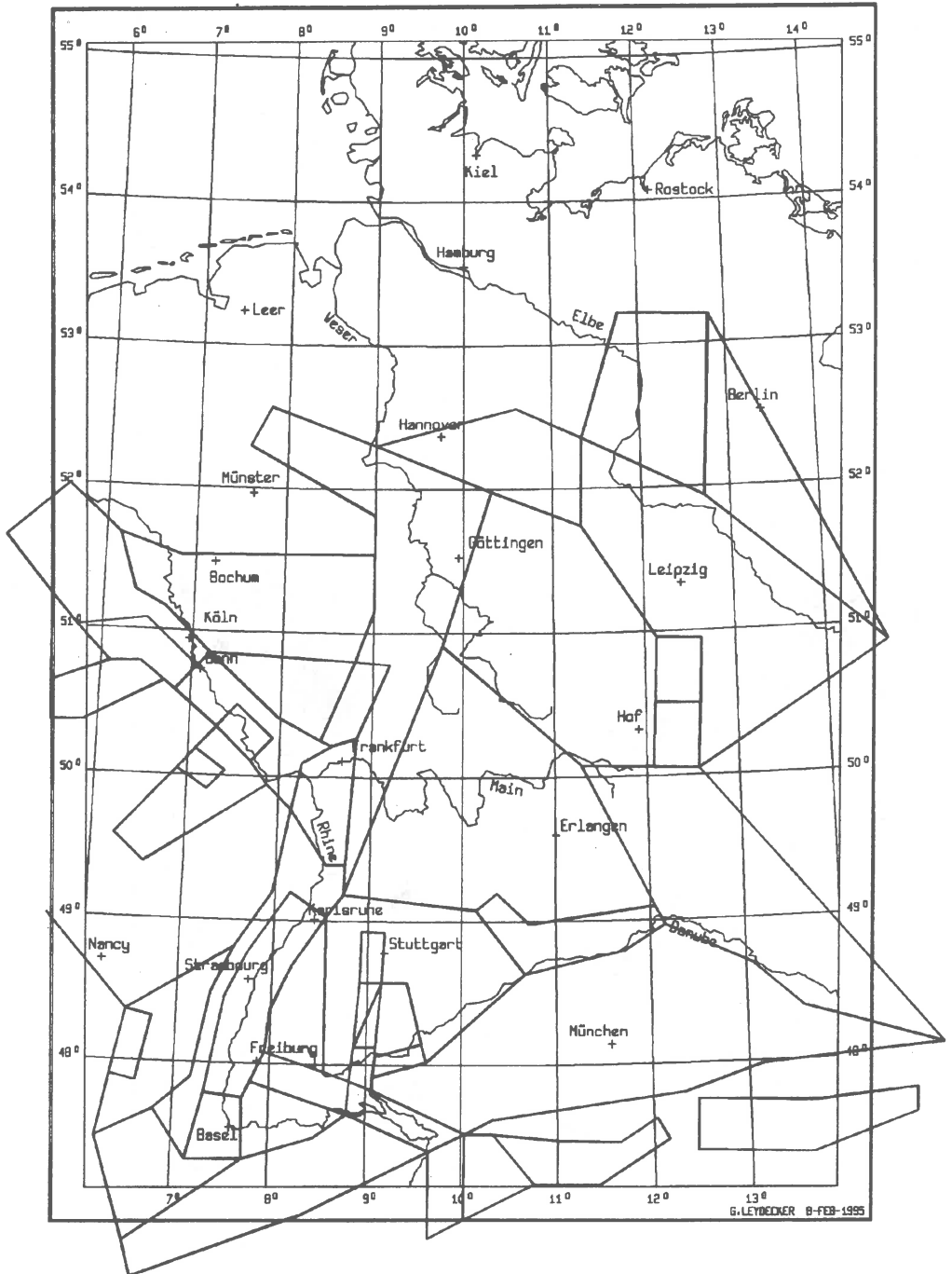
Fig. 4: The regionalisation of Federal Republic of Germany for
seismic risk analysis (after Ahorner & Rosenhauer 1983).
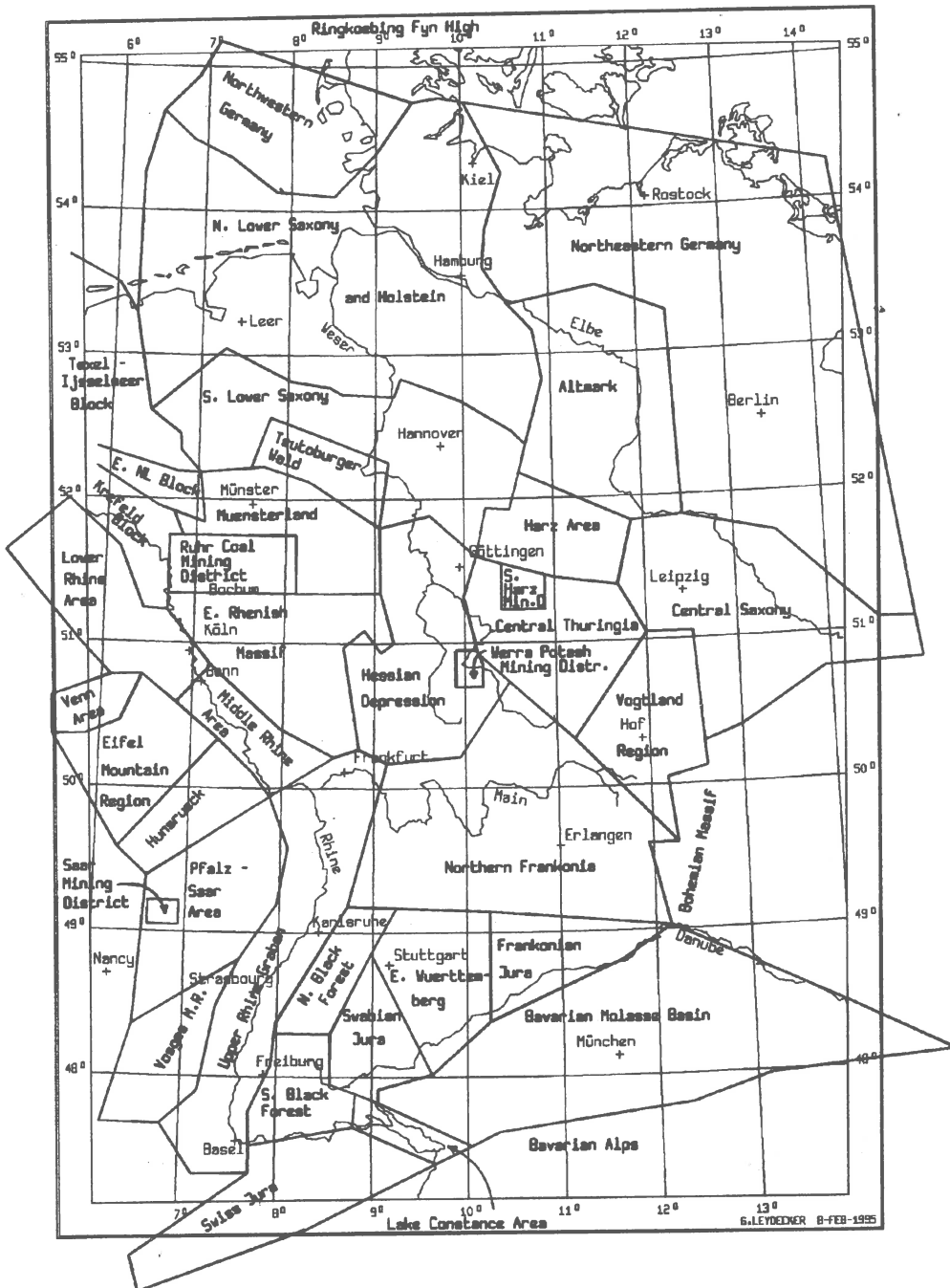
Fig. 5: The new seismogeographical regionalisation of the Federal Republic of Germany following the level 3 concept. For exact names of the regions see table 1.
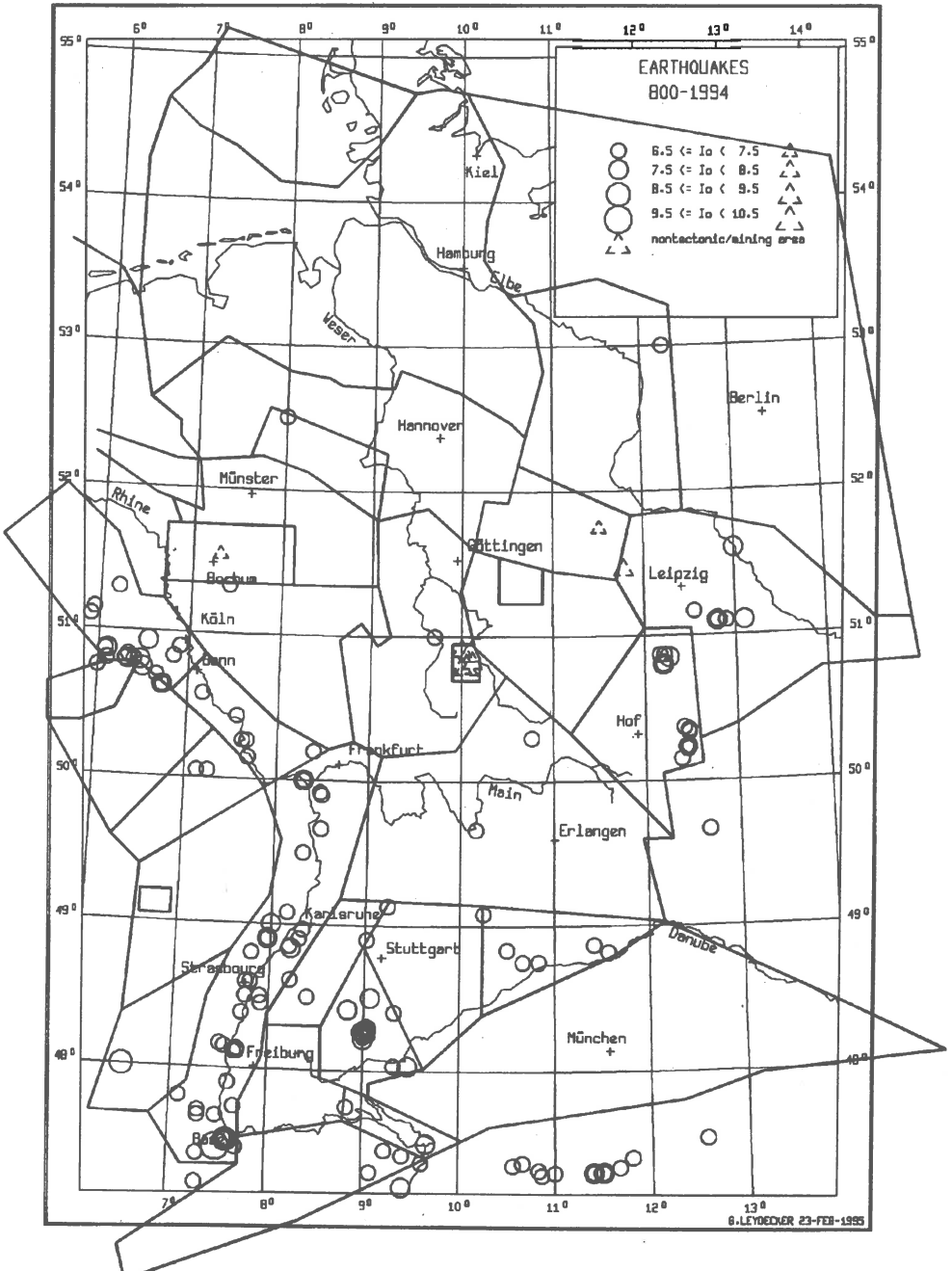
Fig. 6: Earthquakes in Germany with intensities Io>=VI-VII for the years 800-1994 (Grünthal 1988; Henger & Leydecker 1987; Leydecker 1986), together with the new seismogeographical regions.

SOURCE PARAMETERS OF MICROEARTHQUAKES IN THE NAFPAKTOS REGION, CENTRAL GREECE, RECORDED BY A DIGITAL NETWORK.

G.Chouliaras[1] , G.Stavrakakis[1], J.Drakopoulos[1], K.Makropoulos[2]

1.Geodynamic Institute, National Observatory of Athens,
  Athens 11810, Greece.
2.Geophysics-Geothermy division, University of Athens,
  Athens 15784, Greece.

Abstract
    The seismic source parameters, seismic moment M_o, source dimension r and shear-stress drop $\Delta\sigma$, are calculated for a set of 35 microearthquakes recorded by a local network of portable, three component, digital seismographs. These source parameters are expressed in terms of two spectral parameters namely the long-period spectral level Ω_o and the spectral corner frequency f_c. The calculations are based on P and S waves and two different spectral models are compared, that of Brune to that of Madariaga.
    The results show that moments, magnitudes, and corner frequencies are linearly related and that the P-wave corner frequencies are consistently larger than those of S-waves. Also it is observed that the calculated stress drops of Brune's model are consistently lower than those calculated using the Madariaga model.

Introduction
    On April 12 1994 three Lennartz MARS-88 three component digital seismographs were installed in the region of Nafpaktos, Greece, inorder to monitor the microseismic activity of the area for a period of ten days.
    The seismicity of the region of interest from the catalogues of Makropoulos et al.(1989), and the bulletin of Geodynamic Institute of N.O.O.A, reveals that the largest events of this century have occured in 1975 June 30 and 1975 December 21, both of magnitude Ms=5.5. Focal mechanism studies by Drakopoulos and Delibasis (1992) for these events indicate dip-slip faulting with a reverse vertical motion for the first event and a normal vertical motion for the second. In general all the seismotectonic evidence of the region points to a N-S extensional regime and around Nafpaktos this results in ENE-WSW faulting (Melis et al. 1989).

Data and methodology
    The microseismicity of the region was monitored for ten days by three portable Lennartz 3-component digital seismographs employing the Lennartz L-4 seismometers with a sampling rate of 125 Hz and filters between 5 and 10 HZ.
    In addition the readings from the permanent seismological stations of the National Observatory of Athens in RLS, EVR and VLS were used in some cases in the location of the events with

the Hypo 71 program.

According to Brune's model (1970, 1971), the near field displacement spectrum is controlled by the spectral level Ω_0 and the corner frequency f_c. Once we determine these two parameters from the displacement spectra the seismic moment M_0, the source radius r and the stress drop Δ_s can be calculated:

SEISMIC MOMENT : $M_0 = \dfrac{4 \pi \rho \Omega_0 (\alpha,\beta)^3 \kappa}{R_{\theta\phi}}$ (Keilis-Borok, 1960)

SOURCE RADIUS : $r = 0.37 \beta/f_c$ (Brune 1970,1971)

$r = 0.32 \beta/f_c$ (Madariaga, 1976)

STRESS DROP : $\Delta_\sigma = 0.44 M_0/r^3$ (Keilis-Borok, 1960)

Where α= P-wave velocity = 6.0 Km/sec

β= S-wave velocity = 3.4 Km/sec

$R_{\theta\phi}$= Radiation pattern correction factor= 0.35 for P
= 0.25 for S

κ= Free-surface correction factor = 0.56

ρ= Average density = 2.64 g/cm^{-2}

In order to obtain the two important spectral parameters Ω_0 and f_c, representing the low frequency spectral level and corner frequency, respectively, we used the PITSA software package for spectral analysis and applied the same procedure to the recordings of the P and the SH and SV components of the S wave, of each recorded event for each station. For each event the true ground displacement spectra were calculated for each station and the geometric average value of M_0 and r was used instead of the arithmetic mean.

Results

From a total of 35 recorded seismic events, 26 were succesfully located using arrival data from at least three stations with trustworthy residuals. The magnitude range of these events ranged between Md=1.6-2.6, the epicentral distance from our digital stations ranged from 0.5 to 18 km and their depth ranged from 6 to 28 km (Figure 1). From these 26 events, 22 were chosen as appropriate for spectral analysis based on their low noise content. An example is shown in figure 2.

The results from the performed spectral analysis on the P and S waves are shown in figure 3. We observe, that the range of seismic moments for our data is found to be between 8.08×10^{19} dyne-cm and 1.04×10^{18} dyne-cm while the stress drops for that data set ranges between 1 and 60 bars and is in general less than 10 bars. The stress drops of the Madariaga model are consistantly larger than those of the Brune model, nevertheless there is an increase of stress drop with moment in the Brune model.

The moments imply a linear log moment-magnitude relationship which is similar for both P and S wave data and this is shown in figure 4.

The corner frequency for the S-waves are consistantly lower than that of the P-waves. Also, linear log corner frequency-magnitude relation exists for both P and S wave data in figure 5.

Plots of log seismic moment relative to log corner frequency in figure 6 show a clear relation between moment and corner frequency for both P and S wave data eventhough the slopes are different and the intercepts are different suggesting errors in

the assumed radiation pattern

References

Brune, J, N., 1970. Tectonic stress and the spectra of seismic shear waves from earthquakes. J. Geophys. Res., 75, 4997-5009.

Brune, J, N., 1971. Correction to tectonic stress and the spectra of seismic shear waves from earthquakes. J. Geophys. Res., 76, 5002.

Drakopoulos, J. and Delibasis, N., 1982. The focal mechanism of earthquakes in the major area of Greece for the period 1947-1981. In: Seismol. Lab. Univ. Athens, Publ.2, 1982, pp 72.

Keilis-Borok, K, V., 1960. Investigation of the mechanism of earthquakes. Soc. Res. Geophys., 4, A.G.U., Consultants Bureau, New York, pp 201.

Madariaga, R, C., 1976. Dynamics of an expanding circular fault. Bull. Seism. Soc. Am., 66, 639-666.

Makropoulos, K., Drakopoulos, J. and Latousakis, J., 1989. A revised and extended earthquake catalogue for Greece since 1900. Geophys. J. Int., 98, 391-394.

Melis, S, N., Brooks, M. and Pearce, G, R., 1989.A microearthquake study on theGulf of Patras region, western Greece and it's seismotectonic interpretation. Geophys. Journal 98, 515-524.
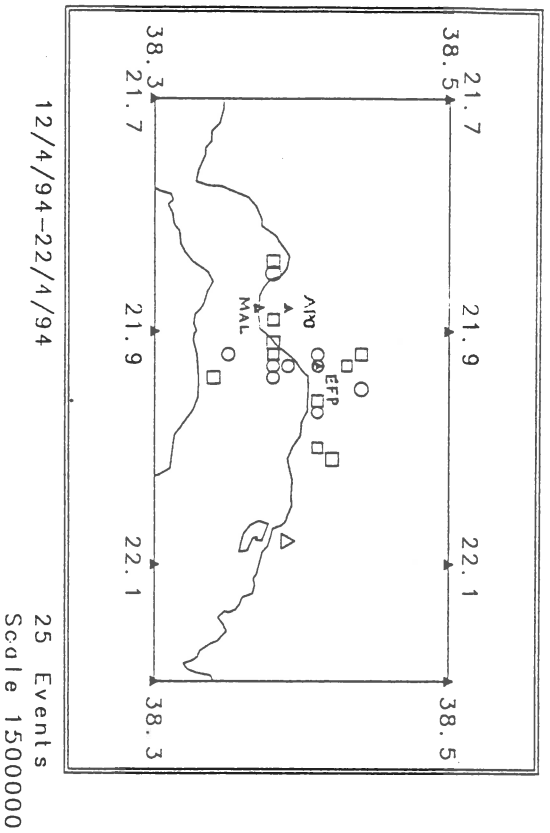
Figure 1. Map of Náfpaktos region and the recorded seismicity of this study. APO, MAL and EFP are the recording sites.

TIME [sec]

1.2409.2

-11736.0
156.77

-177.49

0.0   2.0   4.0   6.0   8.0   10.0   12.0   14.0   16.0   18.0   20.0

(1)
(2)
(3)

100
10
1
0.1
0.01
0.001
0.0001

1
10
100

FREQUENCY [Hz]
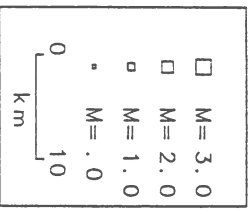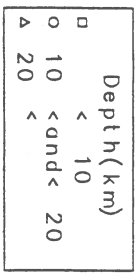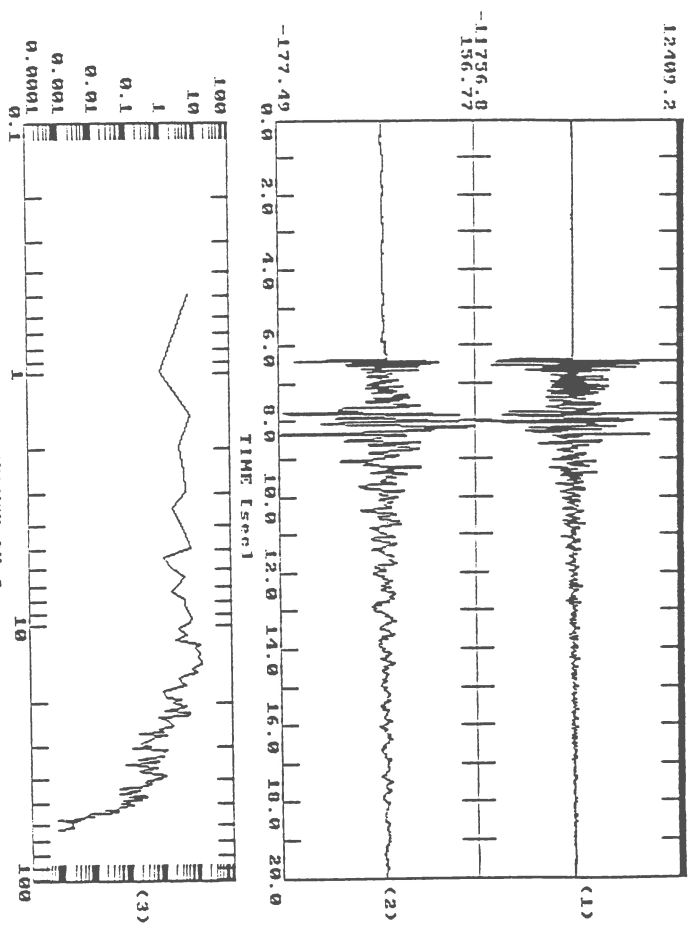
EFP-Z 21/4/94 23:49, Md=2.4, r=0, z=6, km

P-WAVE RESULTS

Md	Mo	Fc	DSb
2.1	1.76	26.3	10.0
1.8	1.74	28.5	12.9
1.9	.23	24.5	1.1
2.1	5.24	24.0	23.1
1.9	.13	27.0	.8
1.8	.87	20.0	2.2
1.7	.18	27.0	7.0
1.8	.11	23.5	2.8
2.2	.73	22.5	6.2
2.3	2.47	22.0	12.6
2.4	2.07	24.0	59.5
2.1	.25	27.5	1.6
1.6	.10	29.0	.8
1.8	.82	26.0	4.5
2.4	.91	23.0	3.4
2.2	.90	26.0	5.4
2.0	.40	16.5	.6
1.8	.25	24.0	1.1
2.0	1.22	18.5	2.4
2.2	2.26	25.0	11.6
2.6	3.76	17.5	29.0
2.4	1.19	24.5	41.7

S-WAVE RESULTS

Md	Mo	Fc	DSb	DSm
2.1	1.03	15.0	7.0	10.8
1.8	1.07	13.0	4.8	7.4
1.9	.14	17.0	1.4	2.1
2.1	.29	17.0	2.9	4.4
1.9	.32	14.0	1.8	2.7
1.8	.02	20.0	.4	.6
1.7	1.02	15.0	1.1	10.6
1.8	.76	14.8	.8	9.7
2.2	3.73	14.5	7.6	38.9
2.3	4.77	14.0	15.4	45.8
2.4	2.91	13.5	14.5	25.0
2.1	.14	18.5	1.8	2.7
1.6	.13	17.0	1.3	2.1
1.8	2.04	17.0	20.4	32.7
2.4	1.58	14.0	8.8	13.6
2.2	.97	13.0	5.3	8.3
2.0	.95	14.0	5.4	8.2
1.8	.27	15.0	1.9	2.9
2.0	1.52	14.0	8.3	13.0
2.2	1.47	14.5	9.0	15.3
2.6	8.08	11.0	21.6	34.5
2.4	4.69	15.0	31.9	48.9

Figure 3. Results of the spectral analysis Md is the duration magnitude, M_0 is the seismic moment ($M_0 \times 10^{19}$ dyn-cm) Fc is the corner frequency in Hz, DSb is the stress drop from Brune's model in bars and DSm is the stress drop from Madariaga's model in bars.

P—wave

Y=1.28 + 16.24

S—wave

Y=1.52 + 15.79
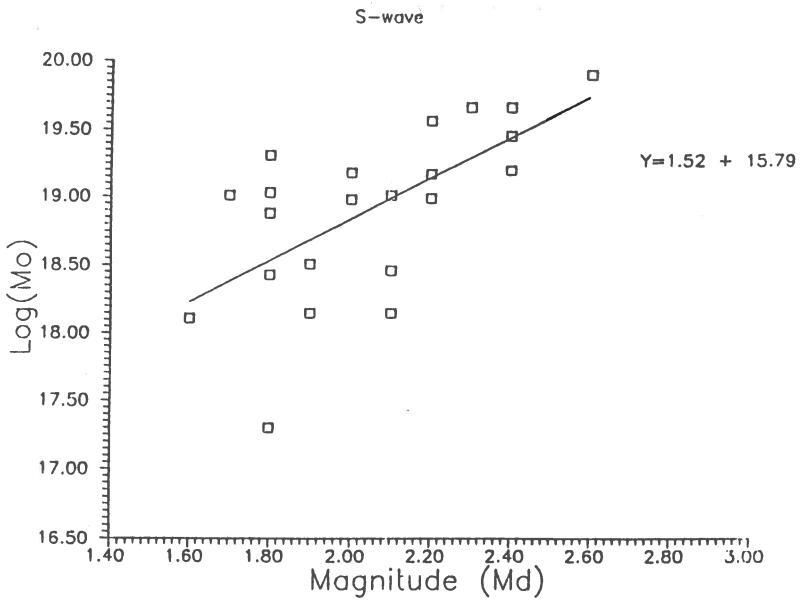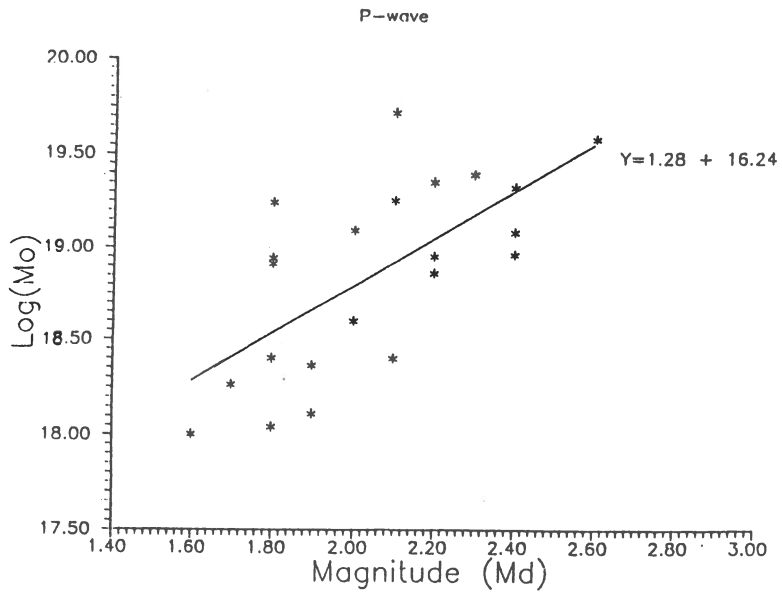
Figure 4. Log Mo vs Md for P and S waves.
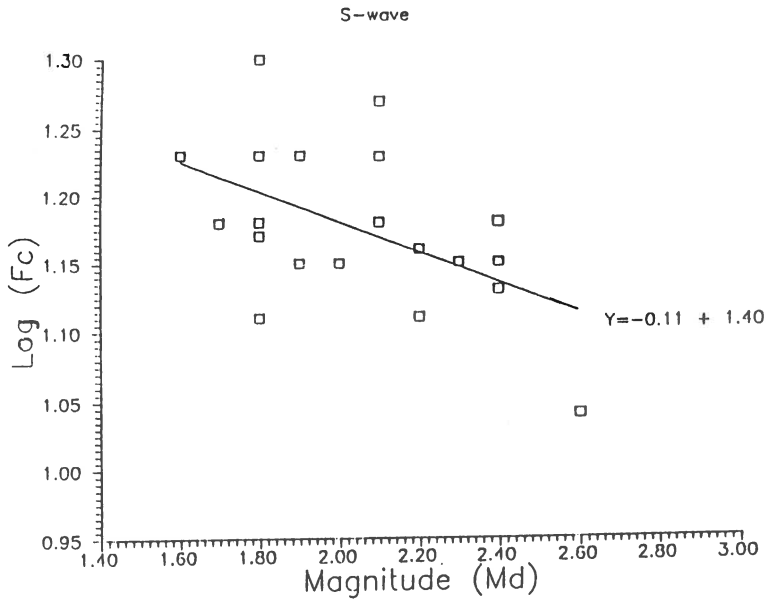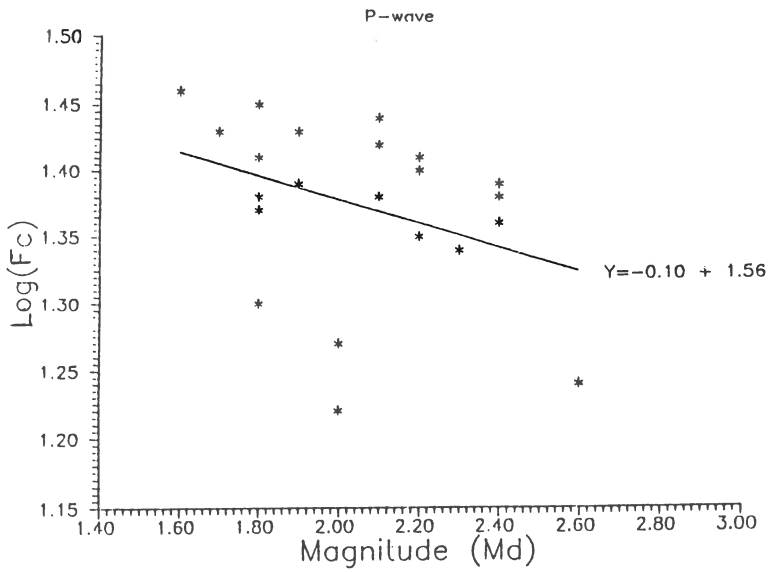
Figure 5. Log Fc vs Md for P and S waves.
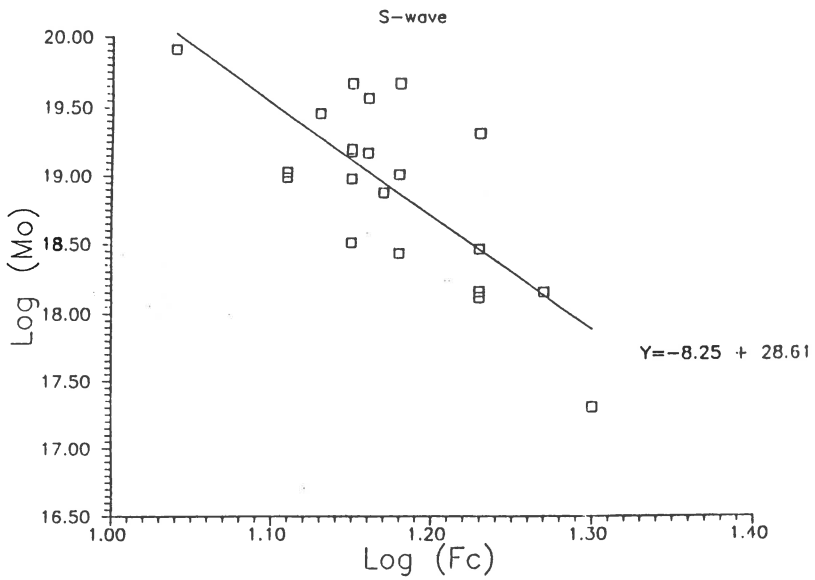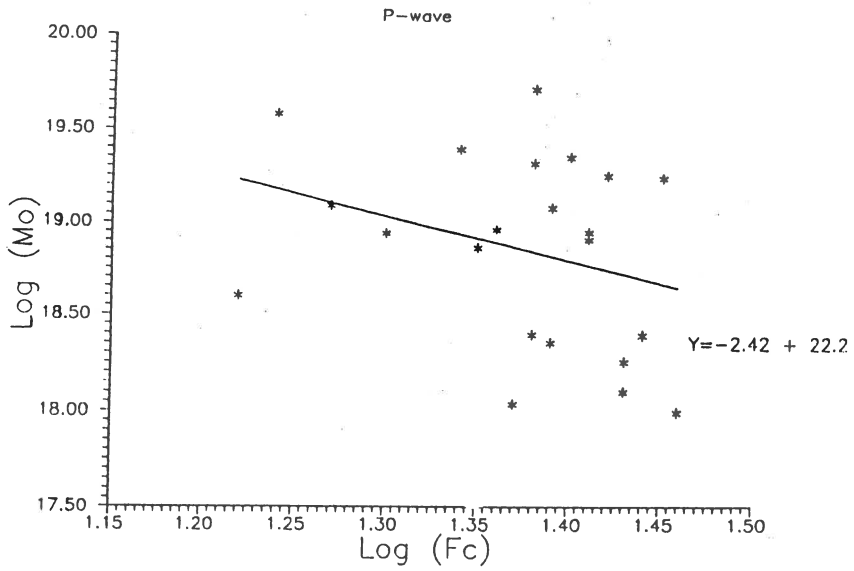
Figure 6. Log Mo vs Log Fc for P and S waves.

SCALING OF THE PARAMETERS OF THE VRANCEA SUBCRUSTAL SEISMIC SOURCE

Radulian Mircea and Mihaela Popa

National Institute for Earth Physics
P.O.Box. MG-2, Bucharest-Magurele, ROMANIA

The main purpose of the paper are: (1) to get as good as possible informations on Vrancea subcrustal source by using relative deconvolution technics; (2) to determine scaling relations between source parameters by using an extended set of digital data. To this aim we benefitted by a relative high number of digital waveforms locally recorded and by the confined hypocentral volume, which is characteristic for Vrancea REGION: The relative deconvolution technics offer the possibility to eliminate the focus-site effects without making any assumption about them.

Data consist of digital waveforms of earthquakes with h > 60 km and M_L > 2.5 recorded between 1982-1992 by the Romanian telemetered network. By visual examination a set of 101 events with relative similar waveform patterns was selected. We made the study on groups of events of events located as close as possible.

Analysis of the observed first pulse duration separately on depth intervals reveals the fact that the path effects effectively control the recorded waveforms for magnitudes less than a minimum value which depends on the particular focus-site path. Deconvolutions in frequency and time domains are performed on different depth intervals. An example of average P and S corrected source spectra for the depth interval between 120 and 140 km is given in Fig.1. The the same depth interval obtained at three stations by using empirical Green functions are represented in Fig.2.

For the entire subducting plate the deconvolution points out simple source time functions with Brune's ω^{-2} high-frequency decay in amplitude spectrum. A clear tendency of the source duration to decrease in the lower part of the slab is emphasized which determines consequently a separation on depth of the scalings of the seismic moment with source radius and stress drop (Fig.3 and Fig.4). Static stress drops are systematically higher in the lower part of the slab (II) as compared with the upper part (I). The moment-radius scaling indicates a self-similarity of the source over a large magnitude range (4.0-7.4).

REFERENCES

Boatwright, J., 1980. A spectral theory for circular seismic sources: simple estimates of source dimensions, dynamic stress drop and radiated energy.Bull.Seismol.Soc.Am., 70: 1-28
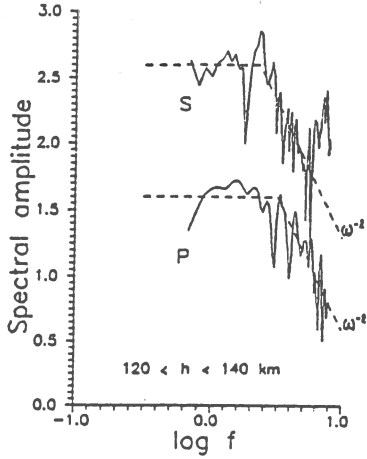
Fig.1:Average corrected
P and S source spectra for
the depth interval between
120 and 140 km
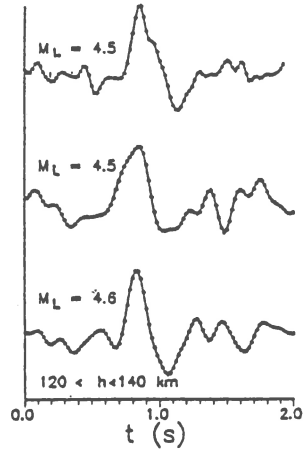
Fig.2:The deconvolved pulses
obtained for three events
occurred within the depth
interval between120 and 140 km
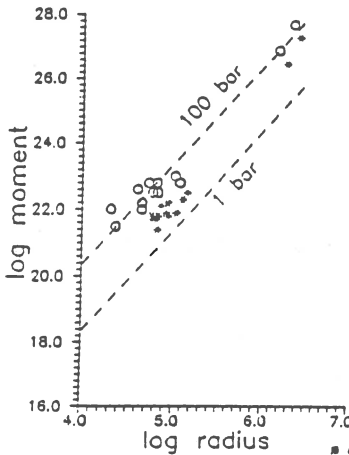
Fig.3:Seismic moment - source
radius scaling

■ upper slab (I)
○ lower slab (II)
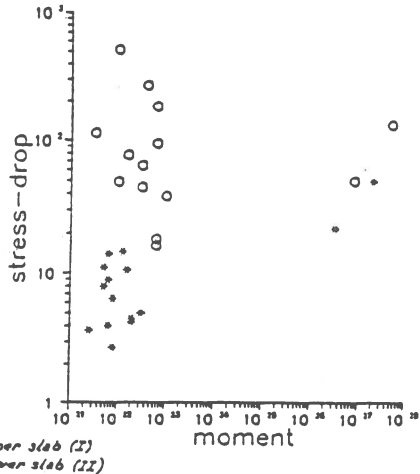
Fig.4:Stress drop - seismic
moment scaling

SOURCE PARAMETERS OF LARGE AND SMALL EARTHQUAKES IN CORINTH GULF (C. GREECE)

P. Papadimitriou[1], J. Kassaras[1], A. Rigo[2], H. Lyon-Caen[2], D. Hatzfeld[3], K. Makropoulos[1] and J. Drakopoulos[1]

[1] Department of Geophysics, University of Athens, Athens, Greece
[2] Institute de Physique du Globe, Department of Seismology, Paris, France
[3] LGIT-IRGM, Observatory of Grenoble, Grenoble, France

ABSTRACT

The gulf of Corinth is one of the most seismically active grabens in the world. High seismic energy release characterizes the area during the last decade, with the occurrence of several strong earthquakes along the gulf. The activity starting in the eastern part of the gulf with the 1981 Alkyonides' sequence. These shallow events produced surface faulting striking in E-W direction and formed an antithetic faulting system. In July-August 1991, a dense network of digital stations was installed around the western margins of the gulf, recording an important microearthquake activity. About 5000 events were recorded having magnitudes less than 3.5, among which 2000 were located. The seismicity was concentrated around Aigio, where two major parallel faults are observed, striking E-W and dipping toward the north: the Aigion and the Eliki faults. The northern margin is also characterized by high activity around the Naupactos and Eupalio area, where the observed faults are of small scale. The depth distribution varies mainly from surface to 12 km. However, an important activity is located beneath, between 12 and 25 km depth. The depth distribution of several events beneath 20-25 km and down to 50 km, may probably consist evidence of an active subduction taking place. About 500 fault plane solutions were computed, the majority revealing normal faulting with a mean E-W direction. Furthermore, strike-slip and reverse mechanisms are also observed.

On November 18, 1992, a moderate earthquake of magnitude 5.9 occurred near Galaxidi, followed by low aftershock activity, which was recorded by a temporary local network installed after the mainshock. The source parameters of the mainshock calculated using teleseismic body wave recordings, indicate shallow earthquake and normal faulting, a pattern also revealed by the aftershock's analysis.

The combination of reliable seismological data obtained over the last 15 years with geodetic studies in the area, indicate that the main deformation occurs along major faults located in the vicinity of the southern margin of the gulf, dipping toward the north. The northern margin, although characterized by high activity level, does not reveal evidence of major scale active structures.

INTRODUCTION

The gulf of Corinth, a WNW-ESE trending, 120 km long and 25 km wide active asymmetric graben, is one of the most active areas in the Mediterranean region (Higgs, 1988; Roberts & Jackson, 1991), with a history of repeated large earthquakes and a high level of background seismicity (Papazachos & Papazachos, 1989; Makropoulos & Burton, 1981; Ambraseys & Jackson, 1990). The high activity of the area is expressed in tectonics, topography, geomorphology (i.e uplift of the coastline relative to sea level) (Vita-Finzi & King, 1985; Doutsos & Piper, 1990; Doutsos & Poulimenos, 1992). The gulf of Corinth graben is surrounded by faults, the larger of them located along the southern shore of the gulf dipping toward the north, while the northern shore is a southward faulted flexure (Keraudren and Sorel, 1987), which affect Quaternary and recent formations, activated since lower Pliocene time (Mercier et al., 1976; 1989). Historical resources reveal that large earthquakes occurred along the Gulf of Corinth. The first earthquake reported in the area occurred in 373 BC
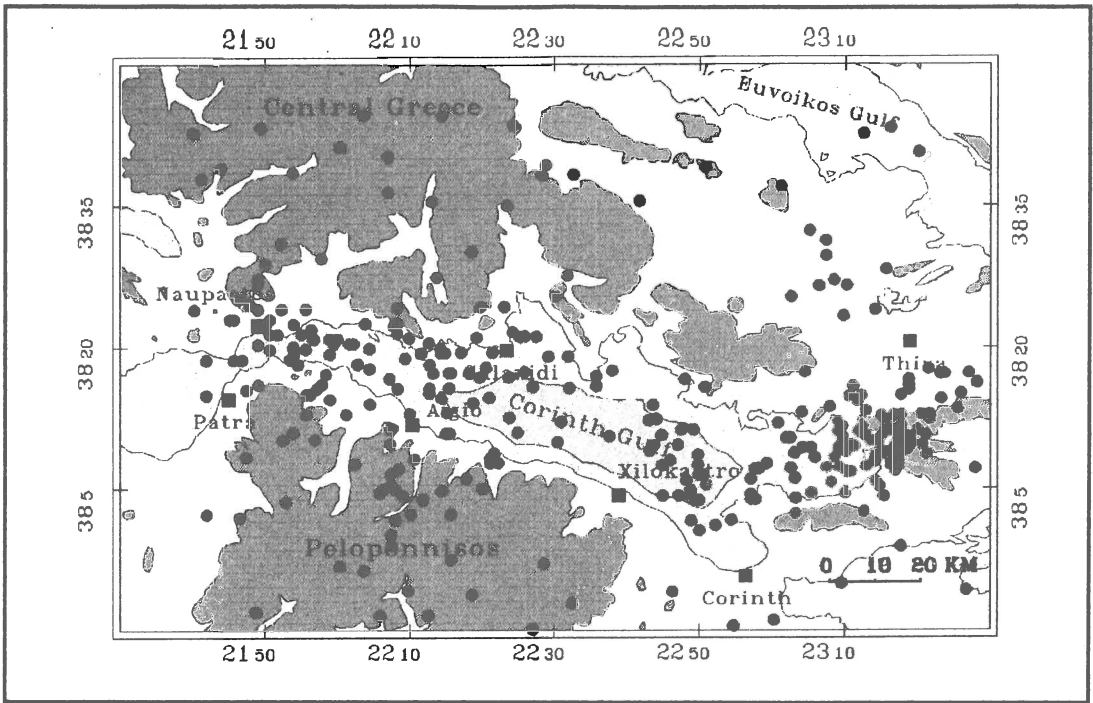
Figure 1. Seismicity map during the period 1964-1994, with a magnitude M$_s$≥4.5

and completely destroyed the city of Eliki. On February 21, 1858 the old town of Corinth collapsed by an earthquake. This event forced the people to rebuild a new town near the sea that was destroyed again on April 22, 1928 by another earthquake (Sieberg, 1932). On December 26, 1861, an earthquake occurred near the city of Aigion producing an E-W surface rupture of about 13 km long, with a 100cm coseismic slip, dipping toward the north (Schmidt, 1867). After the installation of the WWSSN network, two moderate shallow events occurred in the area; the first near Eratini on July 6, 1965, and the second near Antikyra on April 8, 1970. These events reveal normal faulting in E-W direction (McKenzie, 1972; P. Papadimitriou, 1988).

On February 24, 1981, a large earthquake occurred in the eastern part of the gulf (near Alkyonides islands) followed by two large events. Following these events, a temporary network of 14 MEQ-800 stations was installed, in order to record the aftershock activity. In 1991 and for a period of two months, a temporary network of 60 digital stations was installed in the western Gulf of Corinth, around Rio-Antirrio to monitor the micro-earthquake seismic activity. On November 18, 1992, an earthquake occurred near the city of Galaxidi and a temporary digital network was installed in the area in order to record the aftershocks. In this paper, data concerning the recent activity over the period 1981-1992 are used to discuss the seismic regime and the evolution of the gulf.

SEISMOLOGICAL EXPERIMENTS

The gulf of Corinth has been extended as a result of back-arc spreading behind the southwestward Hellenic trench (Le Pichon et al., 1982). Extensional deformation continues today and events are spread over the entire area (fig. 1). During the period 1981-1992 three temporary networks were installed around the gulf of Corinth to record the aftershocks (for the cases of the February 24, 1981 and November 18, 1992 events) or the seismic activity
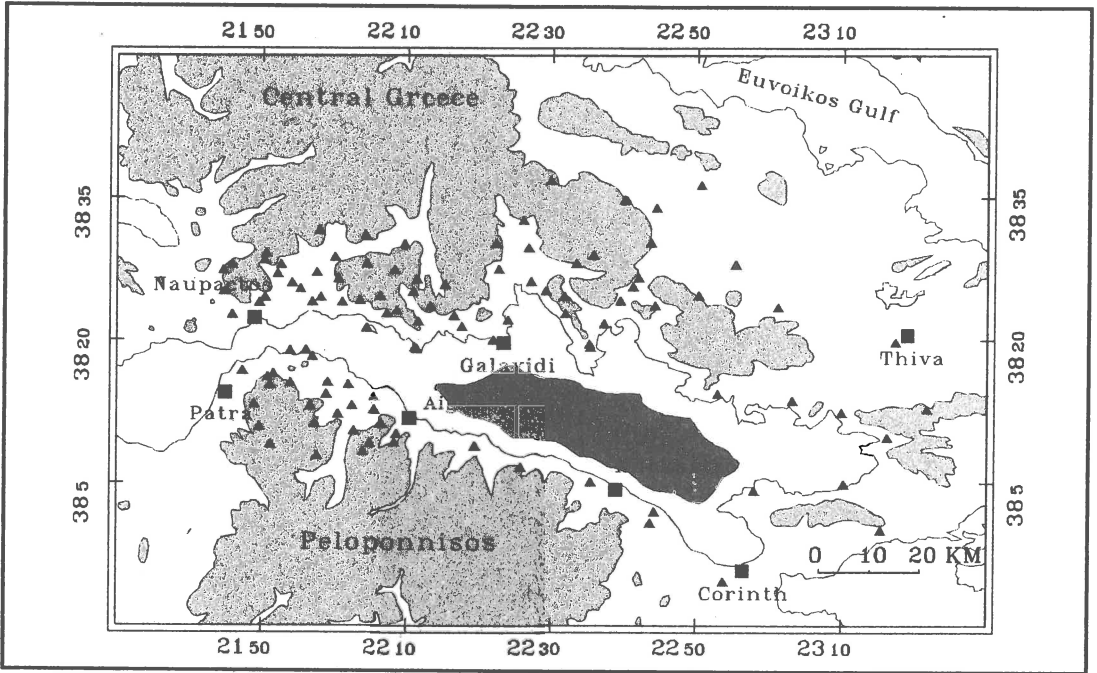
Figure 2. Map of the temporary stations installed during the three seismological experiments., in 1981, 1991 and 1992.

of the area (July-August, 1991). The location of the stations during the three experiments is presented in figure 2. For each experiment we discuss the data separately.

Corinth experiment (1981)

On February 24, 25 and March 4, three earthquakes of magnitudes M_s=6.7, 6.4 and 6.4 respectively, occurred in the eastern part of the gulf of Corinth (fig. 3). Surface breaks with a northward-dipping slip vector, were observed on the southern margin of the gulf following the first and second event and further fresh faulting with a southward dip, appeared later on the northern side of the gulf as a result of the March 4 event. By March 4, a network of 14 MEQ-800 portable smoked-paper seismographs was installed in the area. The array remained operational for five weeks and at the same time, studies of surface faulting, shoreline changes and morphology, were carried out.

The source parameters of the three large earthquakes were calculated using teleseismic body-waveform inversion. Synthetic modeling of the long period P- waveforms of WWSSN records was used by Jackson et al., (1982). Won Young et al., (1984), applied the same technique on GDSN long period records. Bezzeghoud et al., (1986) and P. Papadimitriou, (1988), used Kikuchi and Kanamori (1982) method on broad-band signals obtained from the short period GDSN records, reshaping the instrument response and applying a broad-band Butterworth filter. The main difference of this technique compared to the others is the calculation of the source time function, which in this case is a complex source, probably due to the complexity of stress relaxation on the fault surface. The focal depths of the events are determined between 8 and 10 km and the fault plane solutions indicate normal faulting striking E-W.
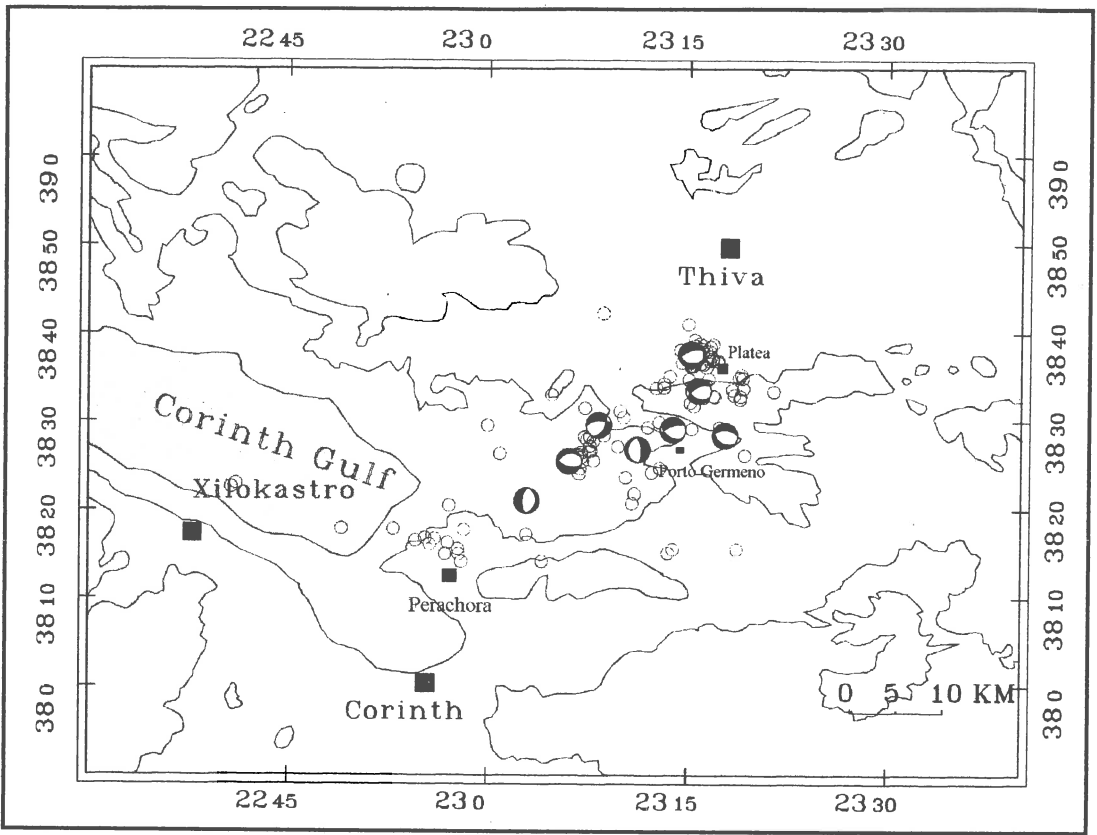
Figure 3. 1981 Corinth experiment, 133 selected aftershocks and 8 focal mechanisms.
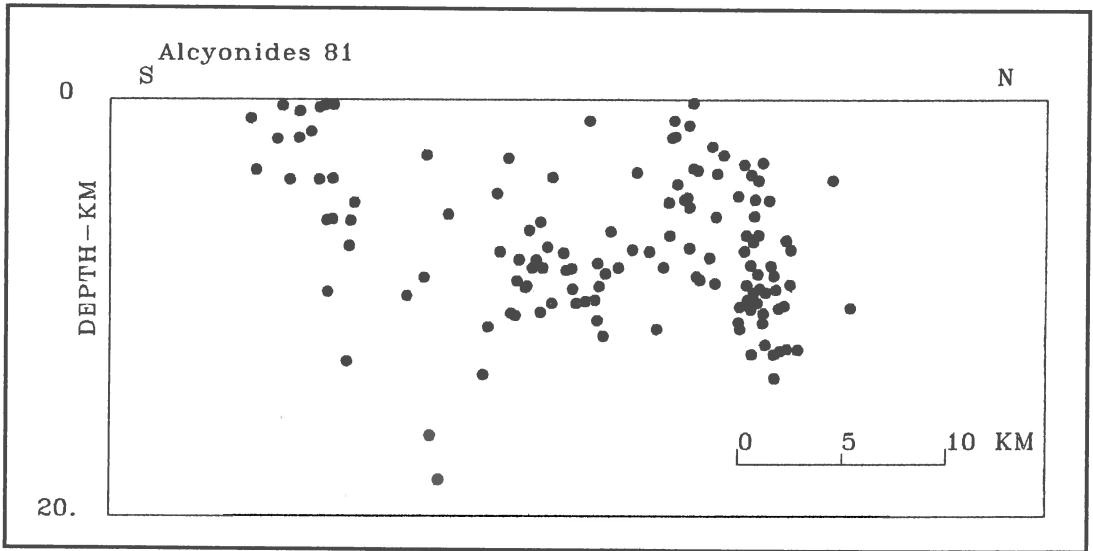
Figure 4. 1981 aftershocks, cross-section in NE-SW direction

Figure 3 presents 133 selected aftershocks located with an accuracy of ±2 km in epicenter and ±4 km in depth, 26 of them providing reliable fault plane solutions (P.Papadimitriou, 1982; King et al. 1985). In the figure, only 8 representative focal mechanisms are plotted for clarity reasons. The events are predominantly concentrated between the north dipping faulting, associated with the first two earthquakes and the south dipping faulting, associated with the third event, while a cluster lies in the footwall southeast of the third earthquake. The events form a zone 60 km long and 20 km wide and are distributed in three clusters; one in Perachora peninsula (southern cluster), one west of Porto Germeno (central cluster) and another near Platea (northern cluster). A longitudinal cross-section in NE-SW direction is presented in figure 4. The distribution in depth varies essentially between surface and 10 km, with a few events located deeper than 10 km. The aftershock activity is apparently greater in the northeast than it is in the southwest. A percentage of this pattern is probably an artifact due to the station's distribution, which allows a greater selectivity where the higher concentration is observed, however, apart from that, the above effect is certainly real. Reliable fault plane solutions computed by projecting upward-going rays in a lower hemisphere focal sphere are displayed in figure 3. Normal faulting is indicated by all the fault plane solutions, in agreement with the source parameters of the three large earthquakes, although a slight component of left or right lateral horizontal shear is also present, probably due to an internal deformation occurring between the two parallel main fault segments activated by the three large events.

Rio-Antirrio experiment (1991)

During the summer of 1991, a dense network of 60 portable digital seismographs was installed for a period of two months (July-August), in the western part of the gulf of Corinth, around the Rio-Antirrio and Aigio area. The stations were equipped with 1 or 2Hz seismometers. A number
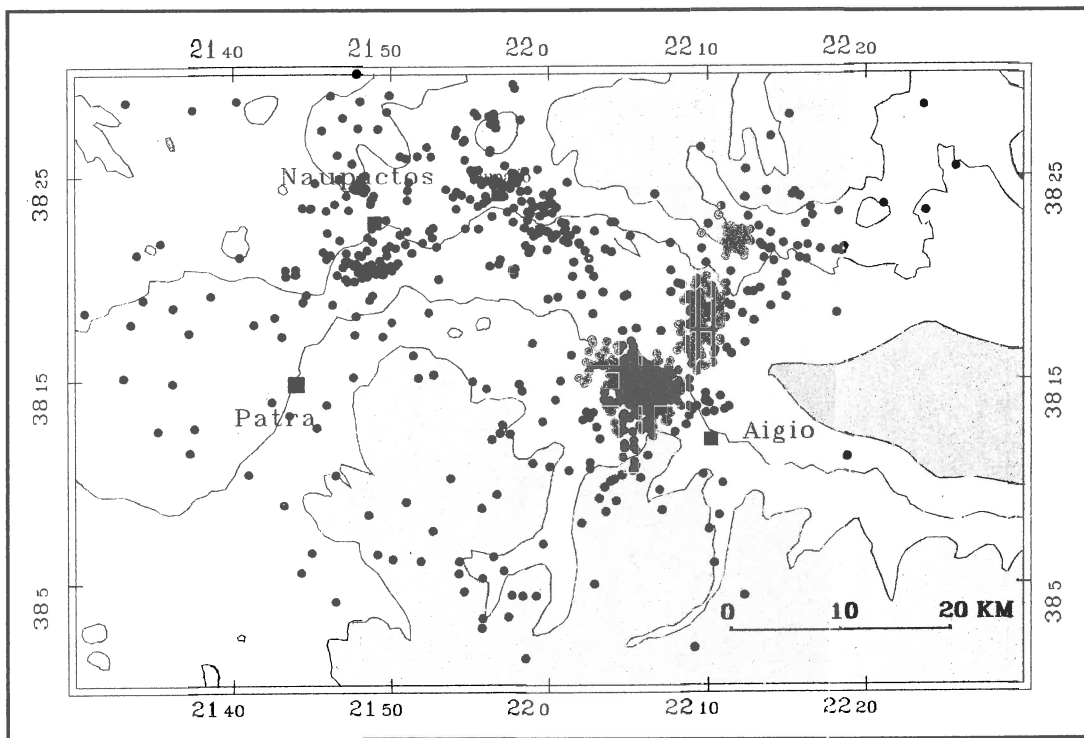
Figure 5. 1991 Rio-Antirrio experiment, all the events.
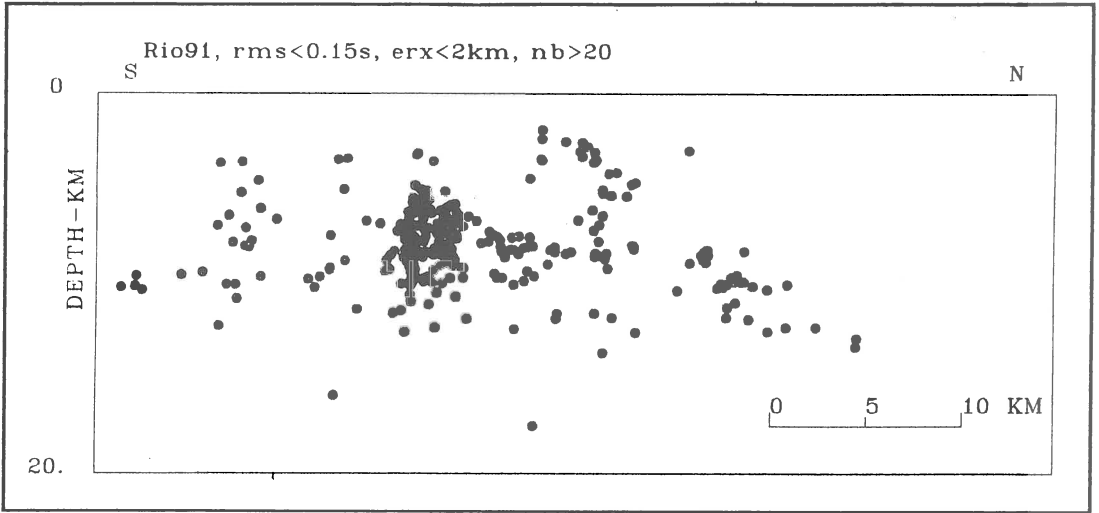
Figure 6. 1991, Rio-Antirrio experiment, cross-section in N-S direction.
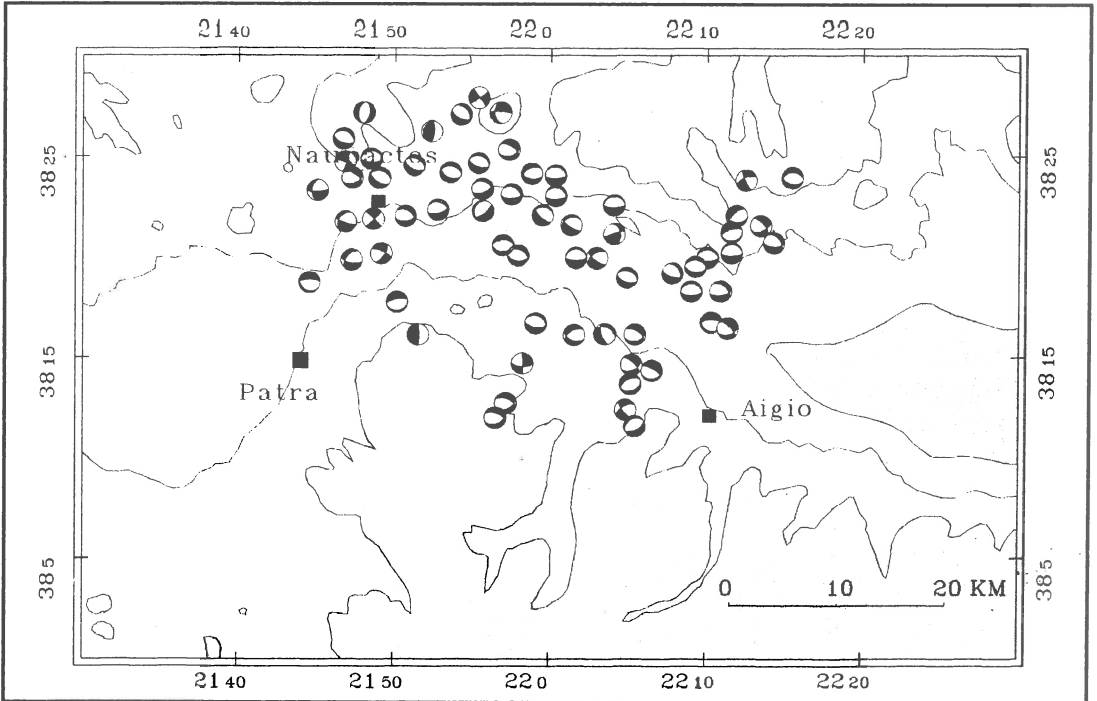
Figure 7. 1991 experiment, selected fault plane solutions.

of about 5000 events was recorded. The time-reading precision is estimated ±.05sec for the P-waves and ±0.1sec for the S-waves. During the month of July, 1300 events (analyzed in this study) were located while 600 of them located with a precision of about ±1 km in epicenter and ±2 km in depth.

    Figure 5, presents the location of all the events. The seismicity is distributed beneath the sea and for a few kilometers inland, on both margins of the gulf. The events form essentially three clusters, the most important one near the town of Aigion (eastern cluster), one near Eupalio (central

cluster) and another near Naupaktos (western cluster). A cross-section in N-S direction (fig. 6) shows a focal depth distribution essentially between 2 and 12 km, distinguishing three groups; one located southern dipping north, one central located under the town of Aigio, dipping vertically and one northerner, located under the sea and the northern margin of the gulf, dipping north. An absence of seismicity within the two first kilometers of the crust is observed becoming more significant in the south. This effect is not an artifact of calculation and could be related to the rheological properties of the shallow crustal layers.

More than 300 focal mechanisms were computed using P-waves' first motion polarities. Figure 7, shows the distribution of 65 focal mechanisms where the two nodal planes are very well constrained (the deviation for both nodal planes being less than 10°). Normal faulting is indicated by the major part of the fault plane solutions, although some present varying amounts of left or right-lateral strike-slip component. Some strike-slip and reverse focal mechanisms are also observed. This pattern is in agreement with the one proposed by Rigo et al., (1993; 1995) who additionally used S-waves' horizontal polarization directions to invert the fault plane solution parameters.

Galaxidi experiment (1992)

On November 18, 1992, an earthquake of M_s=5.9 occurred in the central part of the gulf of Corinth near Galaxidi. No surface ruptures were observed on either sides of the gulf. In order to
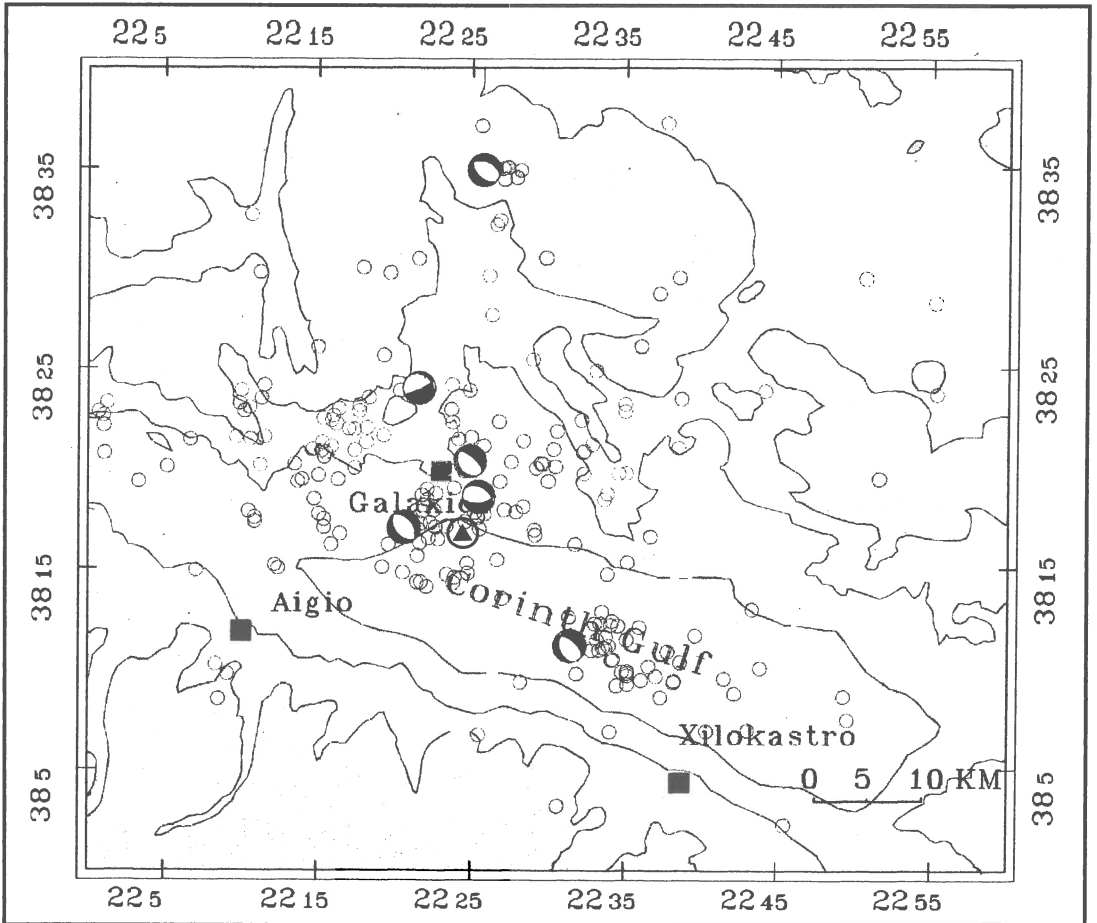
Figure 8. 1992 Galaxidi experiment, epicenters and selected focal mechanisms.

study the aftershock sequence a network of 35 portable seismographs was installed in the area for a period of 10 days.

The source parameters of the main shock were determined by body wave analysis. The inversion of the ground displacement was obtained from teleseismic records of the worldwide broad-band stations (Briole et al. 1993). Similar results were obtained by Karakaisis et al. (1993) using long period body waves inversion and records from the WWSSN network. The centroid depth is calculated at 8±2 km and the obtained fault plane solution represents normal faulting with: strike=80°±10°, dip=60°±5° and rake=-95°±10°. The calculated seismic moment is 5.2×10^{17} Nm and it is clearly released by two different sub-events represented in the source time function by two identical lobes with a total duration of 4 seconds.

The installation of the temporal network started on November 22, and remained operational for 10 days. 255 events have been located, from which 195 have more than 6P and 1S readings, RMS <0.5sec and location error both in epicenter and depth smaller than 5 km (Kementzetzidou et al., 1993; Karakaisis et al., 1993). Figure 8 shows the distribution of all the microearthquakes and the location of the big event. The seismicity recorded during this experiment is spread between Aigio and Xilokastro. Around the epicentral zone of the main shock we can distinguish three clusters: one near Xilokastro (eastern cluster), one near Galaxidi (central cluster) and one near Eratini (western cluster). A cross section (fig. 9) trending in the N-S direction (perpendicular to the Aigion fault) clearly shows that the depth distribution is dipping toward the north, while varying between 4 and 14 km.

Six lower hemisphere focal mechanisms, located around the epicentral area, are presented in fig. 8, indicating normal faulting in E-W and SE-NW directions.

DISCUSSION

Figure 10 presents the focal mechanisms of the most important earthquakes occurred in the gulf of Corinth and for which the fault plane solutions were calculated by body wave inversion methods. We remark that the focal mechanisms of the large and small events show a homogeneous
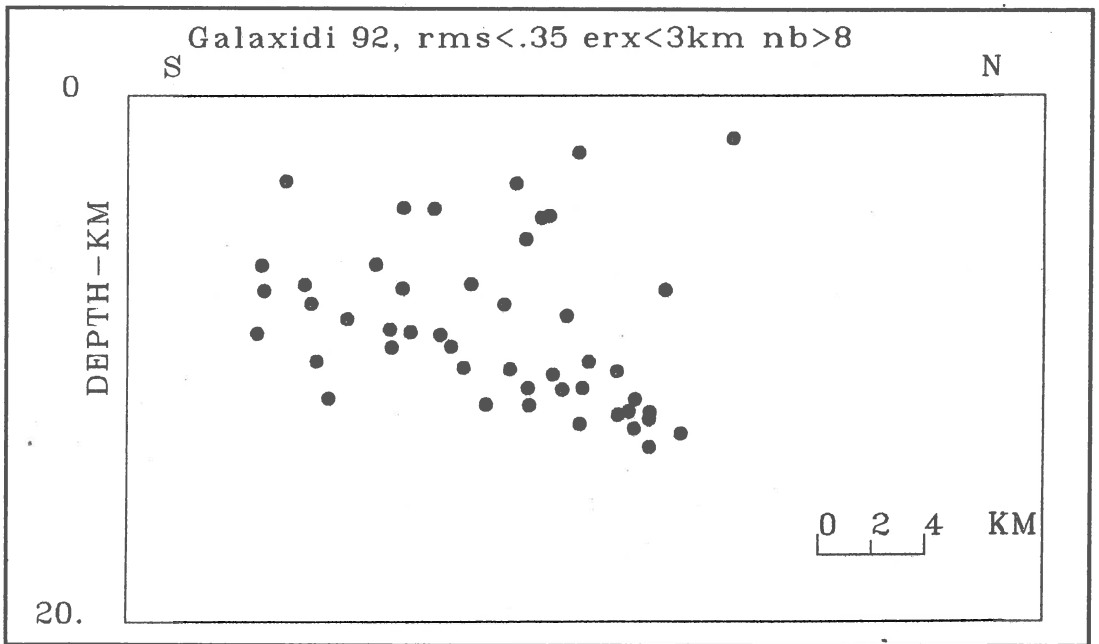
Figure 9. Galaxidi 1992 experiment, cross-section in N-S direction.
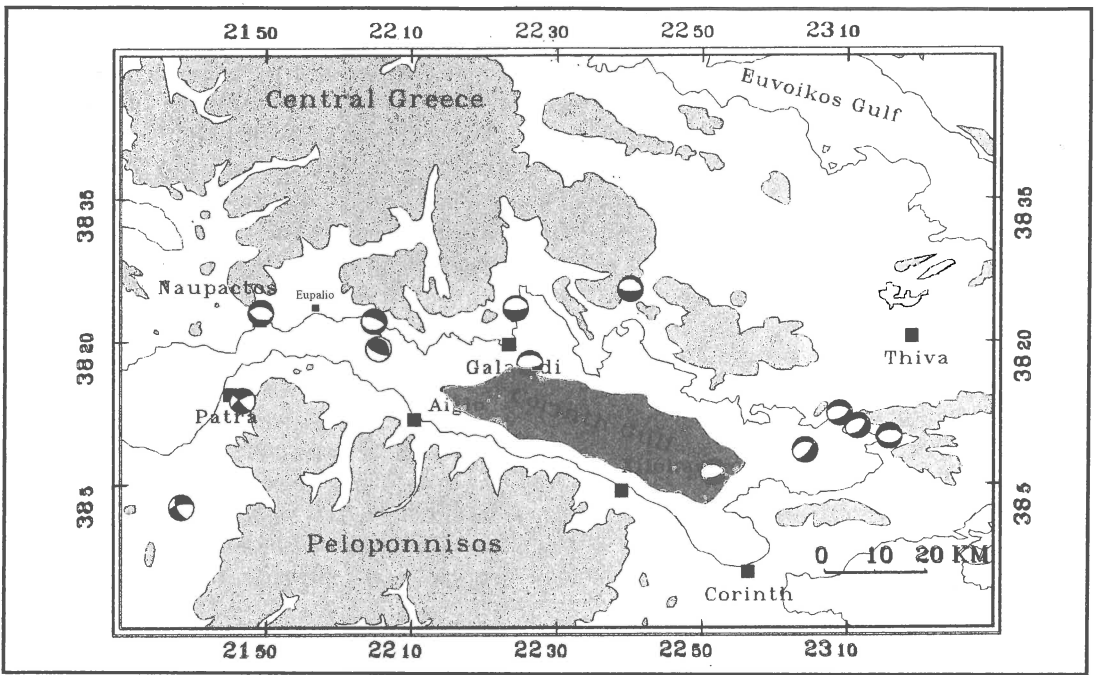
Figure 10. All the available fault plane solutions calculated by body wave inversion.
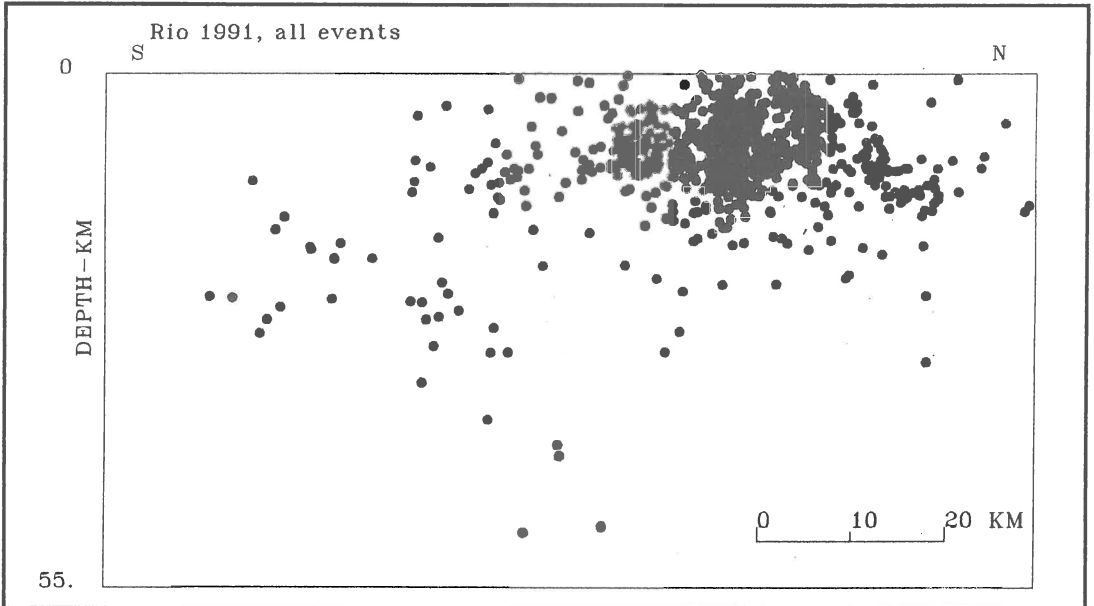
Figure 11. Rio-Antirrio 1991, cross-section in N-S direction.

stress pattern that indicates normal faulting in E-W direction and N-S extension. The depths of the large events calculated by body wave inversion methods were located near the seismogenic layer at 8-12 km depth. The focal depths of the aftershocks of the large events determined by HYPO71 (Lee

& Lahr, 1975) were located between surface and 15 km. Similar pattern was obtained using the data of Rio-Antirrio experiment. Nevertheless, some differences appear between the western and eastern part of the gulf. The depth distribution of the seismicity in the western and central part of the gulf, starts after the first superficial layer estimated between 2 and 4 km. At the eastern part, activity is observed above this depth. We remind that during the 1981 Corinth earthquake sequence, surface breaks were observed, while during the 1992 Galaxidi earthquake this was not the case.

Another remark concerning the focal depth distribution is an important seismic activity between Aigio and Patras beneath 15 km depth (figure 11), during the 1991 Rio-Antirrio experiment. Two different configurations can be distinguished; the first one concerns the subduction zone which is defined by the depth distribution extended between 10 and 50 km. Several deep events have been located there during another microerthquake campaign (Hatzfeld et al., 1990). The second concerns the seismic activity located between 15 and 25 km. This phenomenon is also observed in the eastern part of the Gulf where some of the focal depths are located between 15 and 20 km.

Concerning the focal mechanisms of large and small events, we observe a homogeneous pattern between Aigio and Corinth that is defined by normal faults striking E-W. The area between Aigio and Patras presents an unhomogeneous pattern, while a superposition of mechanisms indicating normal, strike-slip or reverse faulting can be seen. The reliability of the available data in the specific area, does not allow at the moment a further investigation of the stress field distribution. In order to proceed in this analysis, we need more reliable focal mechanisms in the western part of the gulf which can be probably obtained by the S-wave polarization method. This work however exceeds the purpose of this paper, constituting the subject of another presentation.

CONCLUSION

The analysis of the data collected during the three experiments combined to historical data, indicate that the main faults in the area are situated along the southern part of the gulf. The seismic activity is associated with the active extension of the gulf that is also apparent in the bathymetry, topography and morphology which define an asymmetric graben characterized by antithetic faults. An example of this is the 1981 Corinth earthquake sequence: the two large events occurred on the 24th and 25th of February and were located on the major north-dipping faults while the third one, on March 4, was located on the northern, south-dipping fault. However, the western part of the gulf doesn't follow the same pattern. The existence of a major antithetic fault system is not evident as only small antithetic faults are reported. The Galaxidi earthquake sequence and the Rio-Antirrio microseismicity showed the existence of a main fault system dipping to the north.

The focal mechanisms of the large and small shallow (0-15 km) events define a homogeneous extensive stress field with a N-S direction. Nevertheless, an important seismicity beneath 15 km depth located between Aigio and Patras shows a more complex pattern with strike-slip and reverse types of faulting.

REFERENCES

Ambraseys, N.N. & Jackson, J.A., 1990. Seismicity and associated strain in central Greece between 1890 and 1988, *Geophysical Journal International*, **101**, 663-708.

Bezzeghoud, M., Deschamps, A., Madariaga, R., 1986. Broad-band modelling of the Corinth (Greece) earthquakes of February and March 1981. *Ann. Geophys.*, **4**, B, 295-304.

Briole, P., Deshamps, A., Lyon-Caen, H., Papazissi, K. & Martinod, J., 1993. The Itea (Ms~5.9) earthquake of November 18, 1992. Characteristics of the main shock inferred from body waves and ground displacement analysis, Proceedings of the 2nd Congress of the Hellenic Geophysical Union, Florina, 5-7 May 1993, Greece, 297-308.

Doutsos, T. & Piper, J.W., 1990. Listric faulting, sedimentation and morphological evolution of the Quaternary eastern Corinth rift, Greece: First stages of continental rifting, *Geological society of America Bulletin*, **102**, 812-829

Doutsos, T. & Poulimenos, G., 1992. Geometry and kinematics of active faults and their seismotectonic significance in the western Corinth-Patras rift (Greece), *Journal of Structural Geology*, **14**, 689-699.

Jackson J. A., J. Gagnepain, G. Houseman, G.C.P. King, P. Papadimitriou, C. Soufleris and J. Virieux, 1982. Seismicity, normal faulting and the geomorphological development of the Gulf of Corinth (Greece): the Corinth earthquakes of February and March 1981, *Earth and Planetary Science Letters*, **57**, 377-397.

Hatzfeld, D., Pedotti, G., Hatzidimitriou, P. & Makropoulos, K., 1990. The strain pattern in the western Hellenic arc deduced from a microearthquake study, *Geophys. J. Int.*, **101**, 181-202.

Higgs, B., 1988. Syn-sedimentary structural controls on basin deformation in the Gulf of Corinth, Greece, *Basin Research*, **1**, 155-161.

Karakaisis, G., Karacostas, B., Scordilis, E., Kiratzi, A., Diagourtas, D., Papadimitriou, P., Voulgaris, N. & Ziazia, M., 1993. The spatial distribution of the aftershocks and focal mechanism of the Galaxidi (Central Greece) earthquake of November 18, 1992, Proceedings of the 2nd Congress of the Hellenic Geophysical Union, Florina, 5-7 May 1993, Greece, 309-317.

Kementzetzidou, D., Bernard, P., Bouin, M.-P., Dervin, P., Diagourtas, D., Hatzfeld, D., Karakaisis, G., Karacostas, B., Nothard, S., Papadimitriou, P., Scordilis, E., Smith, R., Voulgaris, N. & Ziazia, M., 1993. Proceedings of the 2nd Congress of the Hellenic Geophysical Union, Florina, 5-7 May 1993, Greece, 349-357.

Keraudren, B. & Sorel, D., 1987. The terraces of Corinth (Greece) - A detailed record of eustatic sea-level variations during the last 500,000 years, *Marine Geology*, **77**, 99-107.

Kikuchi, M., & Kanamori, H., 1982. Inversion of body waves. *Bull., Seism. Soc. Am.*, **72**, 491-506.

King, G.C.P., Ouyang, Z.X., Papadimitriou, P., Deshamps, A., Gagnepain, J., Houseman, G., Jackson, J.A., Soufleris, C. & Virieux, J., 1985. The evolution of the Gulf of Corinth (Greece): an aftershock study of the 1981 earthquakes, *Geophys. J. R. astr. Soc.*, **80**, 677-693.

Le Pichon, X., Lyberis, N., Angelier, J. & Renard, V., 1982. Strain distribution over the east Mediterranean ridge: a synthesis incorporating new sea-beam data, *Tectonophysics*, **86**, 243-274.

Lee, W.H.K. & Lahr, J.C., 1975. HYPO71 (revised): a computer program for determining hypocenter, magnitude, and first motion pattern for local earthquakes, *Open-File Rep. US geol. Surv.*, 75-311, 113.

Makropoulos, K.C. & Burton, P.W., 1984. A catalogue of seismicity in Greece and adjacent areas, *Geophysical Journal of the Royal Astronomy Society*, **65**, 741-762.

McKenzie, D., 1972. Active tectonics of the Mediterranean region, *Geophysical Journal of the Royal Astronomy Society*, **30**, 109-185.

Mercier, J.L., Carey, E., Philip, H. & Sorel, D., 1976. La neotectonique plio-quaternaire de l'arc egeen externe et de la mer Egee et ses relations avec la sismicite, *Bul. Soc. Geol. Fr.*, **18**, 159-176.

Mercier, J.L., Sorel, D., Vergely, P. & Simeakis, K., 1989. Extensional tectonic regimes in the Aegean basins during the Cenozoic, *Basin Research*, **2**, 49-71.

Papadimitriou P., 1982. Les seismes de Corinthe (1981): Etude des repliques. Stage du DEA, Paris.

Papadimitriou P., 1988. Etude de la structure du manteau superieur de l'Europe et modelisation des ondes de volume engendrees par les seismes egeens, Ph. D. thesis, Univ. of Paris.

Papazachos B. & K. Papazachos, Earthquakes in Greece, Ziti publications, Thessaloniki, Greece, 1989.

Schmidt, J. F. Πραγματεία περί του γενομένου τω 1861ω Δεκεμβρίω 26η (14η). 52 σελ., Αθήνα, 1867.

Sieberg, A., 1932. Die Erdbeben, in B. Gutenberg's Handbuch der Geophysik, vol. 4, Borntraeger, Berlin.

Roberts, S. C. & Jackson, J., 1991. Active normal faulting in central Greece: An overview. In: *The Geometry of Normal Faults* (Eds A.M.Roberts, G.Yielding & B.Freemann), Geological Society Special Publication, **56**, 125-142.

Rigo, A., Lyon-Caen, H., Armijo, R., Bernard, P., Makropoulos, K., Papadimitriou, P. & Deschamps, A., 1993. Fault plane solutions of microearthquakes and tectonic analysis in the western part of the Gulf of Corinth (Greece), Proceedings of the 2nd Congress of the Hellenic Geophysical Union, Florina, 5-7 May 1993, Greece, 275-285.

Rigo, A., Lyon-Caen, H., Armijo, Deschamps, A., Hatzfeld, D., Makropoulos, K. & Papadimitriou, P., 1995. A microseismicity study in the western part of the Gulf of Corinth (Greece): Implications for large-scale normal faulting mechanisms. (In press).

Vita-Finzi, G. & King, G.C.P., 1985. The seismicity, geomorphology and structural evolution of the Corinth area, *Philos. Trans. R. Soc. London*, Ser. A, **314**, 379-407.

Won Young, K., Kulhanek, O., & Meyer, K., 1984. Source process of the 1981 Gulf of Corinth earthquake sequence from body wave analysis. *Bull. Seism. Soc. Am*, **74**, 459-477.

A METHOD TO DETERMINE FOCAL MECHANISMS IN THE PRESENCE OF ANISOTROPY

Karnassopoulou, A.K.[1,2], Booth, D.C.[1] and Pearce, R.G[2].

[1]British Geological Survey, Murchison House, West Mains Road, Edinburgh EH9 3LA.
[2]Department of Geology and Geophysics, Edinburgh University, Edinburgh EH9 3JW.

ABSTRACT

The waveforms of body wave signals carry information about both the source and the path. Frequently in seismology there is difficulty in separating the effects of the path from the source, when interpreting waveforms. Therefore, when the polarisations of the S waves are analysed, the observed polarisation characteristics might be due to the source radiation, or to the passage of the wave through a seismically anisotropic medium, or to a combination of both. Any attempt to determine source or path parameters should therefore consider the possibility that both the source and path may contribute to the observations, and take both into account.

In this study, a method that provides reliable focal mechanisms as well as an independent means to detect the existence of anisotropy has been developed. A data set from Arkansas, an intraplate region, is used for the first application of the methodology because of the simple waveforms, typical of intraplate regions. The Relative Amplitude Moment tensor Program (RAMP) (Pearce and Rogers, 1989) is used to determine focal mechanisms.

The procedure followed to determine the focal mechanisms and take into account the effect of anisotropy, where it exists, was the following: Firstly, earthquakes which had at least three station recordings, with steep raypaths (angle of incidence less than the critical angle, which is 35° for a plane wave striking the free surface of an isotropic halfspace, and for a Poisson's ratio of 0.25) were selected in order to avoid phase conversions of the SV component at the surface, which would result in elliptical particle motion. Then the horizontal components are rotated to the radial and transverse directions, and particle motion diagrams are plotted for specified time windows in order to identify the shear-wave onset and measure the shear-wave onset polarisation. The polarisation of the identified shear-wave onset is measured in the horizontal plane (Radial-Transverse), which is valid for steep raypaths. The traces are subsequently rotated to the geographical polarisation direction 'X' and its orthogonal direction 'Y'. The P- and S-wave polarities and amplitudes, as measured in the above directions, are used as input for RAMP, assuming a double-couple source mechanism. If the measured polarisation represents the polarisation excited by the source, then the above measurements should contribute to the determination of a valid focal mechanism. However, if the shear wave has entered an anisotropic region resulting in shear-wave splitting (a review of the shear-wave splitting phenomenon as diagnostic of seismic anisotropy is given in Crampin and Lovell, 1991), the measured polarisation of the shear-wave onset does not represent the source polarisation and it is controlled by the symmetry that the anisotropic region displays. Therefore, no focal mechanism is expected to be determined. In this case, the 'Y' component is advanced towards the 'X' component to remove the time delay, and determine the focal mechanism. The time delay between the two components can be deduced from the particle motion diagrams. New shear-wave amplitude measurements are incorporated in the procedure of determining focal mechanisms. Using this procedure it should be possible to conclude

whether anisotropy exists and to determine valid focal mechanisms by taking into account the presence of anisotropy.

In Figure 1, the seismograms, the measurements and the resulting focal mechanism for one earthquake are shown. In this case, the measurements made on the 'X' and 'Y' directions gave no mechanisms compatible with the data but provided a valid focal mechanism when the 'Y' component was advanced towards the 'X' component. The focal mechanism agrees with the composite one that was derived from P-wave first motions recorded on three smoked-drum recorders (Johnston, 1982) and it also agrees with the composite focal mechanism derived from impulsive P-wave first motions of a cluster of earthquakes to which this event belongs (Chiu *et al.*, 1984). Therefore, the technique using both the P- and S-wave information from the seismograms may be adequate for determining the focal mechanisms of single events, and the need to depend on composite focal mechanisms may be reduced.
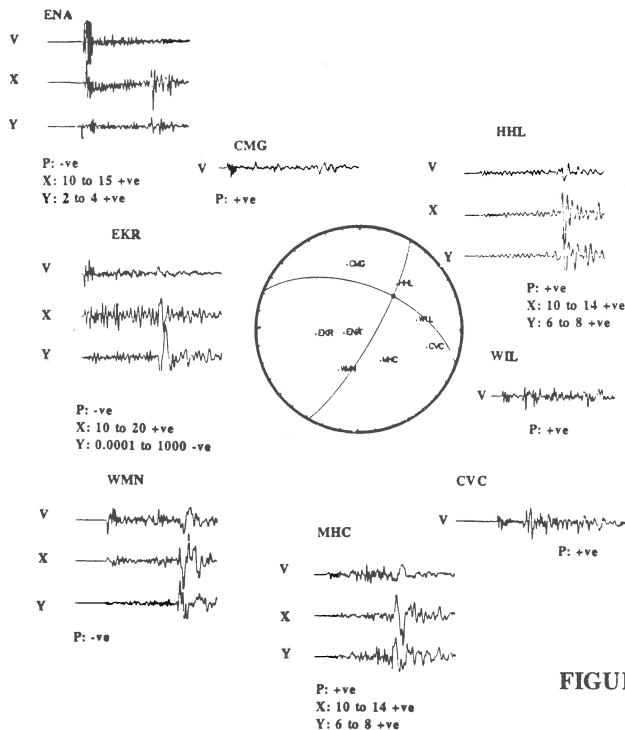
FIGURE 1

References

Chiu, J.M., A.C. Johnston, A.G. Metzger, L. Haar and J. Fletcher, 1984. Analysis of analog and digital records of the 1982 Arkansas earthquake swarm. Bull.Seism.Soc.Am., 74, 1721-1742.

Crampin, S. and J. Lovell, 1991. A decade of shear-wave splitting in the Earth's crust: what does it mean? what use can we make of it? and what should we do next? Geophys.J.Int., 107, 387-407.

Johnston, A. and A. Metzger, 1982. The central Arkansas earthquake swarm. In: TEIC special report #8, part 1, 12 January-12 July 1982, Tennessee Earthquake Information Center.

Pearce, R.G and R.M. Rogers, 1989. Determination of earthquake moment tensors from teleseismic relative amplitude observations. J.Geophys.Res., 94, 775-786.

ROBUSTNESS OF SOURCE MECHANISM DETERMINATION FROM FIRST MOTION POLARITIES AND WAVEFORM INVERSIONS.

Kravanja S.([1]), Suhadolc P.([1]), Panza G.F.([1,2]), Russi M.([3])

([1]) Istituto di Geofisica e Geodesia, Università degli Studi di Trieste, Via dell' Università 7, 34123 Trieste, Italy.
([2]) International Centre for Theoretical Physics, Miramare, Trieste, Italy.
([3]) Osservatorio Geofisico Sperimentale, 34016 Opicina, Trieste, Italy.

Introduction

We analyse some $M_d > 3$ events from the Friuli (NE Italy) seismic area in order to estimate the robustness of fault plane solutions. The digital records are provided by the Osservatorio Geofisico Sperimentale of Trieste (OGS) North-Eastern Italy Network (Fig. 1).
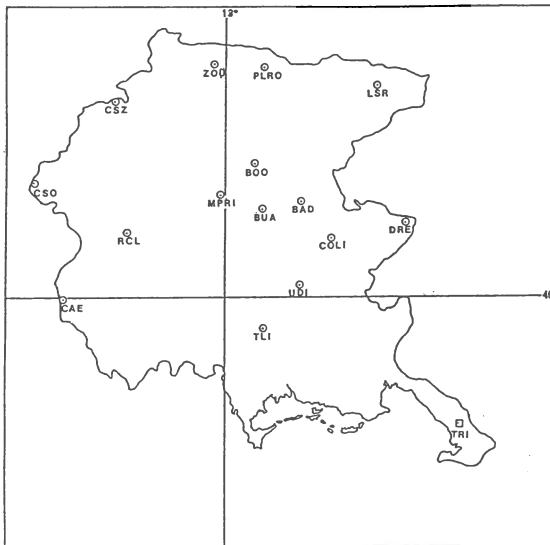
Fig. 1. North-Eastern Italy seismometric network in the Friuli region.

Fault plane solutions are computed by two methods: by P-wave first-motion polarities and by waveform inversion. In the first method we perform two steps: the hypocentral location and the fault plane solution

computation. We estimate the stability of the hypocentral location with respect to the used structural model and to the use of two different location algoritms.

In the waveform inversion the dominant part of the signals is used, and we invert for hypocentral location, fault plane solution, source time function and seismic moment of the event (Mao et al., 1994). Another inversion algorithm (Sileny et al., 1992) is used to check the stability of the solution.

Methods

We consider two different location algoritms: the well-known Hypo71 (Lee and Lahr, 1975) and a nonlinear algorithm Hypogen proposed by Bondar (1993) and based on a genetic process. Both algorithms use a 1-D flat parallel-layer structural model.

For the fault plane solution computation the Brilliger et al. (1980) probabilistic method is used. The stability of this algoritm depends of course on the number of available polarities and their distribution on the equatorial plane.

In both computations two structural models are considered similar to the models FRIUL7A (Panza and Suhadolc, 1987) and FRIUL7W (Mao et al., 1992); the only difference is the elimination of the low-velocity channel.

The waveform inversion is limited to the dominant part of the signal and it allows us to retrieve the source time function. Green functions for point-like sources are computed with the multimode summation in layered anelastic media (Panza, 1985; Panza and Suhadolc, 1987; Florsch et al., 1991) for frequencies up to 10 Hz, although we use, in the analysis, only frequencies up to 5 Hz. The misfit between synthetic and observed seismograms is computed with the L_2 norm.

The Mao et al. (1994) method assumes a double couple source and uses damped least squares to invert the matrix of partial derivatives of synthetic seismograms. The Sileny et al. (1992) method considers the complete seismic moment tensor and uses the Green functions of the single moment tensor elements to retrieve the values of these elements; a simple inversion permits to estimate the best structural model and hypocentral depth from an "a priori" fixed range.

Discussion of results

The epicentral distances of the used events are in the range of 10-50 km and typically about 10 stations are considered.
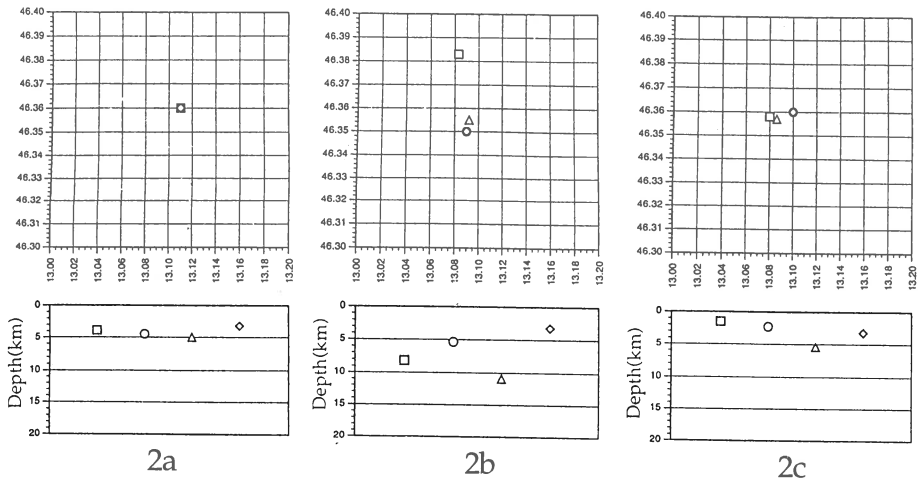
Fig. 2. Epicentral and hypocentral location with employed algoritm and structural model. (a): February 4, 1988 at 19:36; best case. (b): February. 1, 1988 at 14:21; worst case. (c): February 1, 1988 at 11:22; standard case. Symbols: □ HYPO71, FRIUL7A; △ HYPO71, FRIUL7W; O HYPOGEN, FRIUL7A; ◇ HYPOGEN, FRIUL7W.

Fig. 2 shows the stability of the hypocentral solution with respect to the two considered structural models. In the best case (Fig. 2a) the variation in depth is less than 2 km, while in the worst case (Fig. 2b) the variation in depth is around 8 km, associated to an epicentral uncertainty of about 3 km. In general, the variation of the epicentral location is about 1 km, while the depth variation is around 3-5 km (Fig. 2c).

An example of the variation of the fault plane solutions is shown in Fig 3. For the event shown on the top row all fault plane solutions are consistent with each other, while for that on the bottom row there is a large difference in the strike of the nodal planes in one of the solutions.

The cause of the small variations between the solutions for event 1 has to be found in the different parameters of the two structural models. For event 2, the difference between the hypocentral locations is the main responsible for the large difference in the nodal planes orientations.

For waveform inversion, assuming structural model FRIUL7W we first analyse an event occurred on December 27, 1987, in Friuli (Fig 4), using the Mao et al. (1994) method applied to four stations; we use Hypo71 agorithm for the starting hypocentral location. The results are reported in Fig. 4. A small difference between the final and the initial hypocentral depth (0.2km) is noted, while fault plane solution is consistent with the observed polarities. In the source time history the largest peaks have a duration of about 0.3 seconds. These results are

863
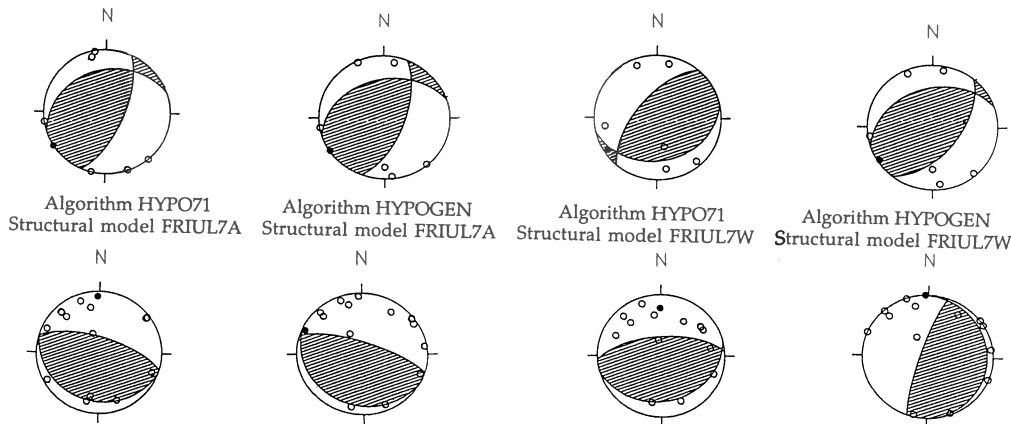
Fig. 3. Top: Event 1 of February 1, 1988, at 11:22. The different solutions are consistent with each other. Bottom: Event 2 of February 1, 1988, at 14:21. Note the different strike of the nodal planes in the solution retrieved when FRIUL7W structural model is used with algorithm HYPOGEN.
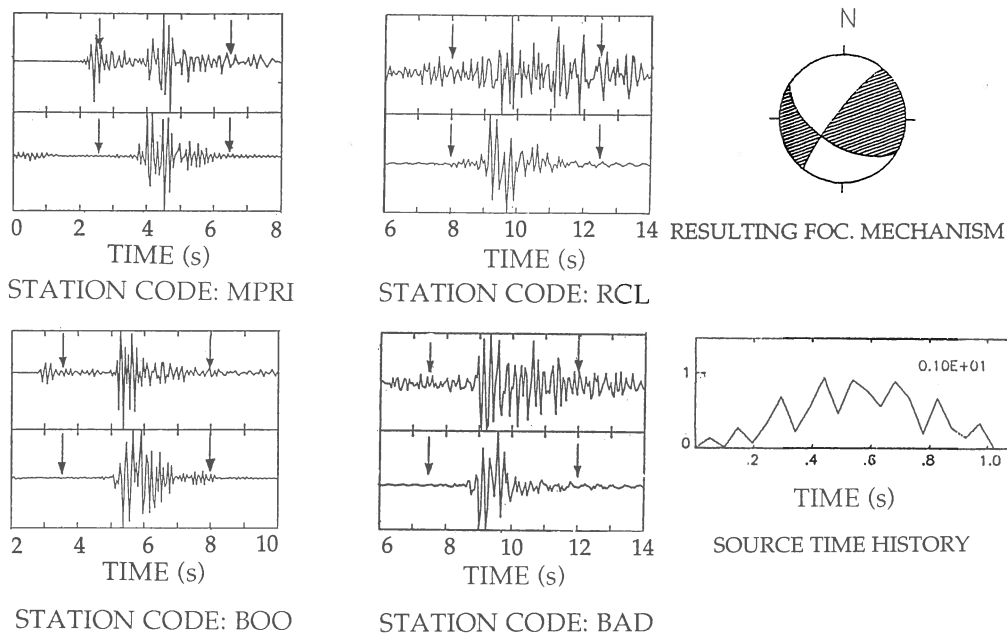
Fig. 4. Waveform inversion with Mao et al. (1994) method of the event on December 27, 1987, at 00:21. Epicentral coordinates: 46.306°N, 12.922°E. Depth: 7.2 km. Seismic moment $M_0 = 4.48 \times 10^{12}$ Nm. Upper seismograms are real signals; lower seismograms are synthetic signals. The arrows indicate time windows inverted. The number inside the box of the time history of the source indicates the value of the maximum.
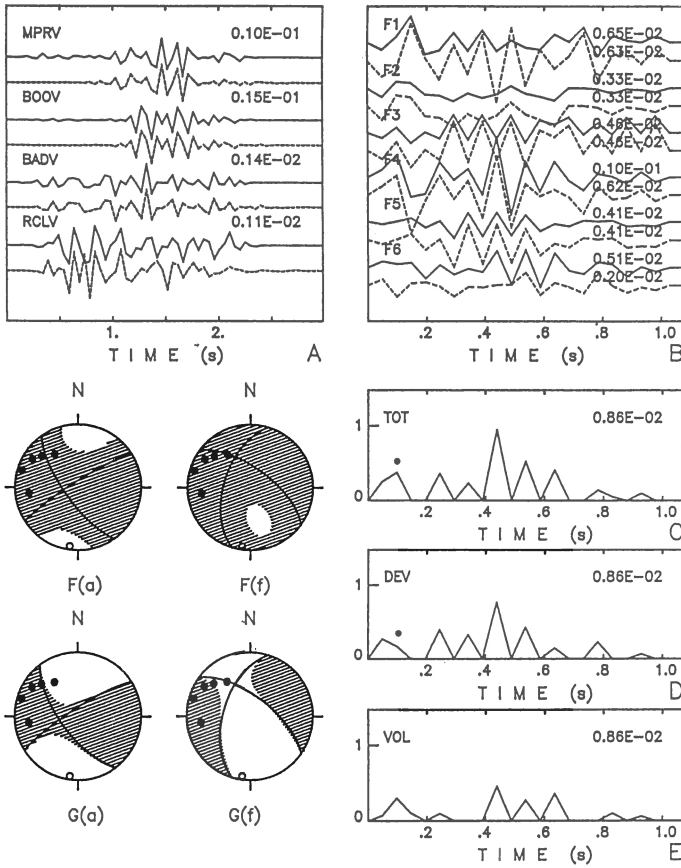
Fig. 5 Waveform inversion with the Sileny et al. (1992) method of the event on December 27, 1987, at 00:21. Epicentral coordinates: 46.306°N, 12.922°E. Depth: 7.7 km. Seismic moment $M_O=2.40 \times 10^{12}$Nm. A) real seismograms (continous lines) and synthetic seismograms (dashed lines). B) Full moment tensor derivatives (continous lines) and deviatoric component derivatives of moment tensor (dashed lines). C), D), E) Total, deviatoric, and volumetric components of source time function. The number inside the box of the time history of the source indicates the value of the maximum. F(a) Fault plane solution retrieved from all time history of the full moment tensor. F(f) Fault plane solution retrieved from the full moment tensor at 0.1s from origin time. G(a) Fault plane solution retrieved from all the time history of the deviatoric component of the moment tensor. G(f) Fault plane solution retrieved from the deviatoric component of the moment tensor at 0.1s from the origin time.

essentially confirmed when applying the Sileny et al. (1992) method (Fig. 5), which validates the assumption of a double couple for this event (the retrieved volumetric component is negligible).

The waveform inversion has been applied to the event 2, since the fault plane solutions obtained from the polarities show major unconsistencies. Fig. 6 shows the solution obtained with Mao et al. (1994) method. This solution is not consistent with that retrieved with the polarities, but it is rather consistent with the focal mechanisms retrieved for the event 1, with the same epicenter and a minor difference in the focal depth. Since only three polarities (two almost nodals) are unconsistent with the mechanism obtained with the waveform inversion, we are lead to believe that the mechanism shown in Fig. 6 is the more reliable one.

STATION CODE: MPRI STATION CODE: DRE RESULTING FOCAL MECHANISM

STATION CODE: COLI STATION CODE: RCL SOURCE TIME HISTORY
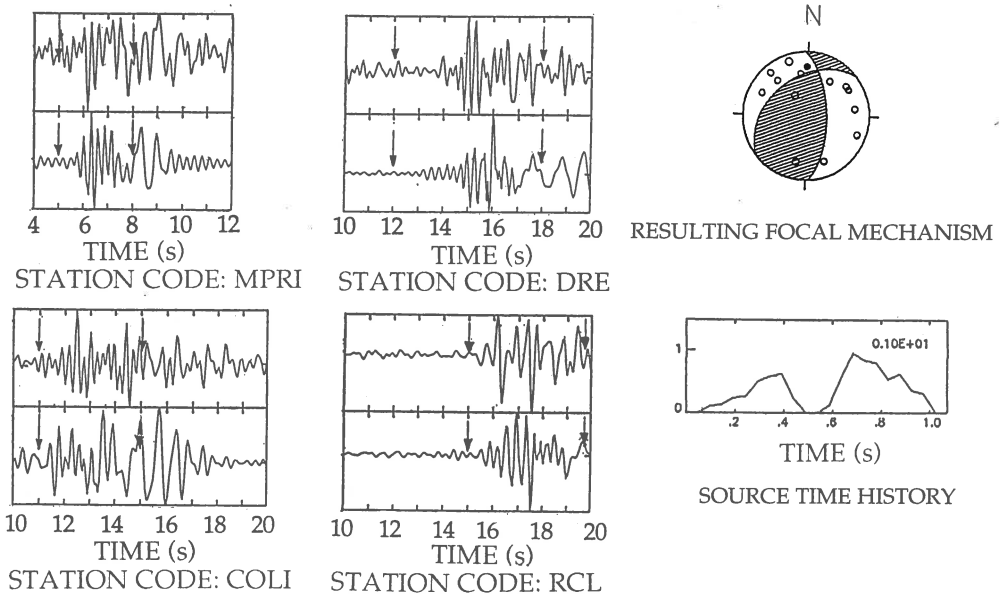
Fig. 6. Waveform inversion with Mao et al. (1994) method, of the event on February 1, 1988, at 14:21. Epicentral coordinates: 46.365°N, 13.121°E. Depth: 3.2 km. Seismic moment $M_O=6.90 \times 10^{13}$Nm. Upper seismograms are real signals; lower seismograms are synthetic signals. The arrows indicate time windows inverted. The number inside the box of the time history of the source indicates the value of the maximum.

Conclusions

The preliminary analysis made on some Friuli events in order to assess the robustness of the fault plane solution detreminations needs to be implemented with more waveform inversions, in order to get a better statistics. The stability of fault plane solutions retrieved from first

motion analysis depends on signal to noise ratio in the recorded signals, on the structural model, the depth of the source and the number and distribution of recording stations. The waveform inversion allow us to retrieve a more reliable fault plane solution and information about the source time history.

References

Bondar I., 1993. Hypocenter determination of local earthquakes. Seismol. Obser., Geodetic and Geophys. Res. Inst., Hungarian Acad. Sci., Budapest, preprint.

Brillinger D.R., Udias A. and Bolt B.A., 1980. A probabilty model for regional focal mechanism solutions. Bull. Seism. Soc. Am., 70, 149-170.

Florsh N., D. Fäh D., Suhadolc P. and Panza G. F., 1991. Complete synthetic seismograms for high-frequency multimode SH waves. In: El Escorial workshop proceedings, A. Udias and E. Buforn, Editors, Pageoph 136, 529-560.

Lee W.H.K., J.C. Lahr, 1975. HYPO71 (revised): a computer program for determining hypocenter, magnitude and first motion pattern of local earthquakes. U.S. Geol. Surv. Open-File-Rpt., 75-311.

Mao W.J. and P. Suhadolc, 1992. Simultaneous inversion of velocity structures and hypocentral locations: application to the Friuli seismic area NE Italy. Pageoph, 138, 267-285.

Mao, W.J., Panza G.F., and Suhadolc P., 1994. Linearized waveform inversion for source mechanism and time-space rupture process from local and near-regional events. Geophys. J. Int., 116, 784-798.

Panza, G. F. and P. Suhadolc, 1987. Complete strong motion synthetics. In: Seismic Strong Motion Synthetics, B. A. Bolt, Editor, Computational Techniques 4, Academic Press, Orlando, 153-204.

Sileny J., G.F. Panza and P. Campus, 1992. Waveform inversion for point source moment tensor retrieval with variable hypocentral depth and structural model. Geophys. J. Int., 109, 259-274.

SOME PARAMETERS AND SCALING RELATIONS
FOR SINAIA (ROMANIA) SEQUENCE OF MAY-JUNE, 1993

Dumitru Enescu, Emilia Popescu, Mircea Radulian

National Institute for Earth Physics
P.O. Box MG-2, Bucharest, Romania

Abstract

A particular sequence of crustal earthquakes (h < 10km, M_L ≤ 5.1) occurred in the south-western extremity of the Eastern Carpathian Arc Bend (Sinaia region) starting with May 4, 1993. The main shock (M_L = 5.1) appeared on May 23 after a significant foreshock activity, extended on a 20-day time interval. The location of the events delineates an epicentral area of about $380km^2$, elongated on a NW-SE direction, in agreement with the fault plane solution of the main shock and the seismotectonics of the region. The digital recordings of the Romanian telemetered network are analyzed in order to estimate the source parameters and the scaling relations between them. An empirical deconvolution technic and the spectral ratio method are used to this purpose. The scaling of the stress drop reveals continuous increase with the earthquake size. The results emphasize the role of the hierarchical structure of the inhomogeneities in the source region in describing the earthquake generation process.

INTRODUCTION

The presence of earthquake sequences in a given seismic zone offers a large base of generally well constraint data allowing refined analyses on scaling and estimation of the source parameters. A particular sequence of crustal earthquakes occurred starting with May 4, 1993 in Sinaia region, situated south-west of Eastern Carpathian Arc Bend. It was accompanied by a substantial increase of the seismic activity in the region till the end of the year. This is the most unusual seismic activity related to Sinaia area as far as we are informed from historical and instrumental data. The present paper aims to carry out an extended analysis of the digital data available for this seismic sequence in order to determine the source parameters and to outline the scaling characteristics of the source.

OBSERVATION DATA

The data set consists of digital waveforms recorded by the Romanian telemetered local network. The seismic stations belonging to this network which are used are plotted in Fig. 1. They have all S13 instruments (vertical component of velocity) with a natural period of 1s and a useful frequency bandwidth between 0.2 and 15Hz. The frequency of digitization is 50 Hz. The data are cut-up at 15Hz by an antialiasing filter.
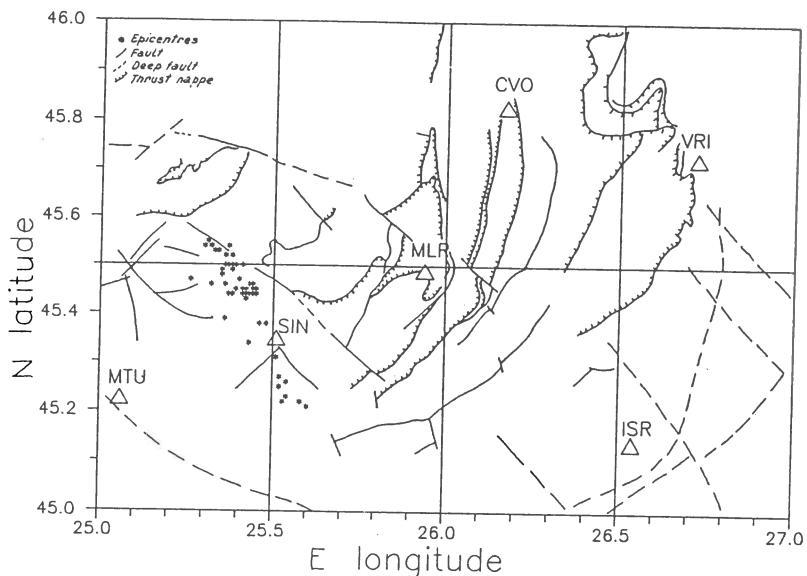
Fig. 1. Seismotectonic map of the Sinaia region. The seismic stations are represented by triangles.
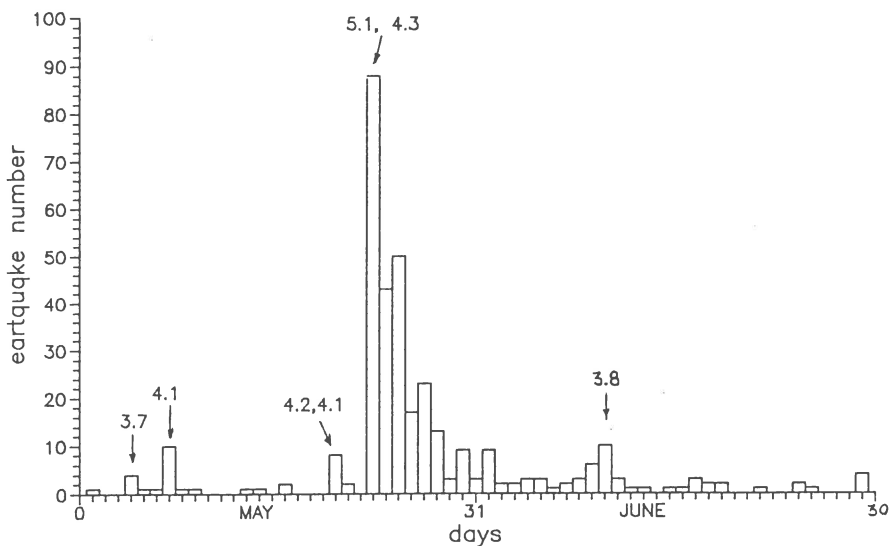
Fig. 2. Distribution of time occurrences of the events. The arrows mark the time occurrences of the strongest eartquakes of the sequence.

The best available recordings are from MLR station which is a high-gain station situated close enough ($\Delta \sim$ 45Km) from the epicentral area. Unfortunately, the station SIN which lies closest to the epicenter has started to work only since 24th of May. Moreover, the recordings at this station are clipping for a local magnitude as low as 2.5. The MTU station is another station situated not too far from the epicentral area ($\Delta \sim$ 40Km), but it has a high level of local noise.

LOCATION EVENTS

A number of 345 events with magnitude $M_L > 1.5$ are identified directly by visual examination on analog seismograms recorded at station MLR. The histogram of time occurrences is presented in Fig. 2. The largest shock ($M_L =$ 5.1) was preceded by a relative significant foreshock activity, spanning around 20 days. Three of the four earthquakes of the sequence with $M_L \geq 4.0$ (excepting the main shock) are foreshocks. They could be related to the somewhat higher stress level within the foreshock interval as compared with the aftershock interval.

From the total number of identified earthquakes, a number of 55 events are located, by using at least 6 arrival times. The configuration of the seismic stations that are mainly used to locate the events together with the resulted epicenters are represented in Fig. 1. The distribution of the epicenters can be approximated by an ellipse with the great axis oriented on a direction N 30° W and the area of roughly 380 km^2. The crustal model of Enescu et al. (1992) is used to locate the sequence. A fixed value of 5 km was imposed for the depth of all events.

FAULT PLANE SOLUTION FOR THE MAIN SHOCK

The fault plane solution for the largest shock of the sequence is determined by using 14 P wave polarities (Fig. 3). The principal axis of compression stress (P axis) is nearly vertical, while the principal axis of tensional stress (T axis) is nearly horizontal. One of the nodal planes is oriented N25°W, roughly coincident with the great axis of the epicentral distribution (Fig. 2). For this reason we choose this plane as faulting plane. The faulting is neither of strike-slip type, nor dip-slip type. The slip component on dip direction shows a normal faulting, while the slip component on strike indicates a left lateral motion on fault.

The fault plane solution and the epicentral distribution are in good agreement with the tectonics of the region, which is characterized by a system of normal faults striking mainly from NW to SE and doubled by a secondary system of faults directed on a normal direction (Fig.1).
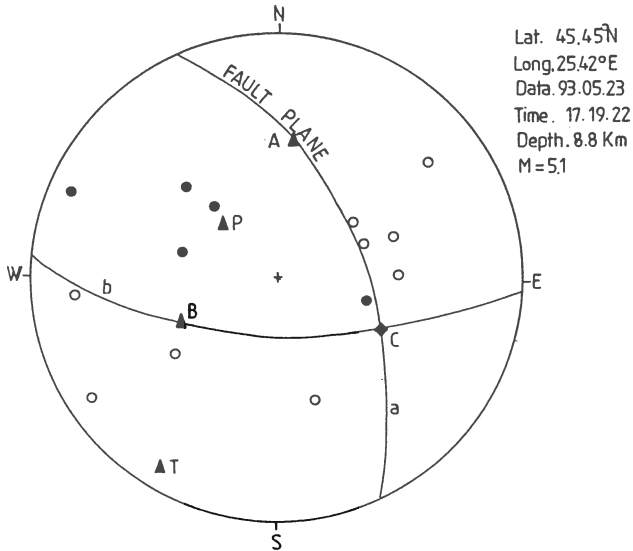
Fig. 3. Fault plane solution for the main shock. Full circle = tension, empty circle = compression.
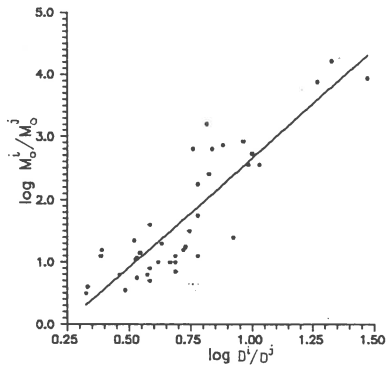
Fig. 4. Regression line of the distribution of seismic moment ratios versus total duration ratios for different pairs (i,j) of events; i stands for events with ML > 2.9, while j for events with ML < 2.5.

SEISMIC MOMENT

First of all, we determine a scaling relationship between seismic moment M_0 and local magnitude M_L of the type:

$$\log M_0 = cM_L + d \tag{1}$$

In order to consider the events as small as possible we prefer to use the total duration D (.as measured on seismogram) instead of magnitude. By using the MLR recordings and the magnitude values computed by Radu and Enescu (1993), the following equation is obtained between local magnitude and total duration:

$$M_L = 2.3\log D - 1.6 \tag{2}$$

Since the difference between first arrivals of S and P waves is almost constant ($T_{S-P} \cong 6.5s$) for all sequence events, it is included in relation (2) as a simple additive constant. Relation (2) helps us to estimate in the following the seismic moment values for the smallest events by using only readings of duration at MLR station.

The slope c of the relation (1) is determined by using spectral ratios between different pairs of events. For a pair (i,j) we can write from (1):

$$\log (M_0^i / M_0^j) = c(M_L^i - M_L^j) \tag{3}$$

or, equivalently:

$$\log (M_0^i / M_0^j) = 2.3c \log (D^i / D^j) \tag{4}$$

If the foci for a given pair of events are about the same and the recording station is the same, the ratio $M_0^i / M_0^j \cong \Omega_0^i / \Omega_0^j$, where Ω_0 is the long period level of the displacement amplitude spectrum. The ratio M_0^i / M_0^j thus obtained versus the ratio D^i / D^j is represented in Fig. 4. The slope value of the regression line is 3.5, implying c = 3.5 / 2.3 = 1.5.

To determine the free term of equation (1) we choose three reference events of magnitude around 2.2. The corresponding seismic moments are computed from P wave spectra after correcting them for instrument, geometrical spreading, attenuation and free surface response. A quality factor Q = 200 = constant was considered to correct for inelastic attenuation. The average value of the seismic moment for the three reference events is $<M_0> = 10^{18}$ dyne cm, and the average duration $<D> = 30s$.

We introduce these values in (4) and put $M_0^j = M_0$ and $D^j = D$. Finally, we come back to log moment - magnitude relationship:

$$\log M_0 = 1.5M_L + 14.5 \tag{5}$$

RUPTURE DURATION

To estimate the rupture duration in the source the empirical deconvolution proposed by Frankel and Kanamori (1983) is used. It refers to a pair of events (main and Green) with close enough hypocenters and recorded by the same station. In these conditions, if the Green event is sufficiently small, it is a good approximation of the Green function (empirical Green's function) and is almost entirely controlled by path effects.If $\tau_{1/2}^S$ is the half width of the

source time function of the main event, $\tau_{1/2}^G$ is half width of the observed Green event and $\tau_{1/2}$ is the half width of the observed pulse for the main event, than:

$$\tau_{1/2}^S \cong \tau_{1/2} - \tau_{1/2}^G \qquad\qquad (6)$$

Therefore, the difficult task to get the source time function, is simply carried out by measuring the pulse width of the first P wave (velocity) recorded at station for the main and Green earthquakes. The pulse width in velocity corresponds to the half width of the displacement pulse. It is practically given by the difference between the first onset and first zero crossing of the recorded trace. The method has the great advantage of being applicable even for clipping traces, extending this way the useful magnitude range.

The observed pulse widths for events with $M_L > 2.9$ are deconvolved by (6) There are chosen only impulsive waveforms with high signal/noise ratio. The plot of observed $\tau_{1/2}$ dependence on seismic moment for MLR station (Fig. 5) emphasizes the increase of $\tau_{1/2}$ with increasing M_0. This means that the signal radiated by the source is still noticeable in the recorded seismograms even for magnitudes smaller than $M_L = 3.0$. However, we can assume that for the smallest earthquakes ($M_L < 2.5$) the pulse width is controlled first of all by the path effects and consequently these events can be approximated by empirical Green's functions.

Several studies (e.g. , Frankel, 1982; Anderson, 1986) demonstrated that the first shallow layers (h < 3 Km) below the free surface cause a strong attenuation of the high frequencies leading to significant distortions in the observed displacement spectrum (corner frequency) and in the time domain (pulse width). In this case, the recorded seismograms are not relevant as concerns the source information.

It is likely that the $\tau_{1/2}^G$ value in equation (6), for a given focus-station configuration, and a given instrument response, is a specific value, roughly a minimum constant threshold value as suggested by Frankel and Kanamori (1983). In our case, for MLR station, we took the value $\tau_{1/2}^G = 0.06s$. With this value, the corrected $\tau_{1/2}$ values for earthquakes with $M_L > 2.9$ are given in Table 1.
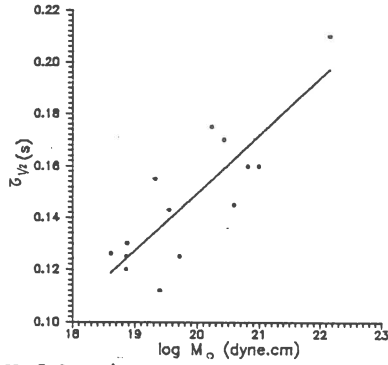
Fig. 5. Half width of the first P pulse measured on MLR seismograms as function of the seismic moment.
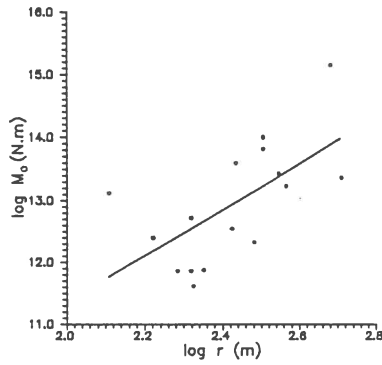
Fig. 6. Scaling relation of the seismic moment (in N m) with the source radius (in m).
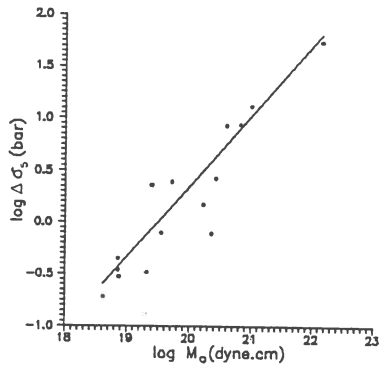
Fig. 7. Scaling relation between static stress drop and seismic moment.

Table 1 Source seismic parameters computed for several earthquakes of the Sinaia sequence (May-June, 1993).

	Data	Time	ML	Mo(dyne.cm)	r(m)	Δσs(bars)	τ1/2(s)
1.	1993 0504	03:41	3.7	3.52e+19	265	0.80	0.083
2.	1993 0504	04:43	3.3	7.20e+18	208	0.35	0.065
3.	1999 0507	10:13	3.2	5.21e+19	208	2.50	0.065
4.	1993 0507	11:47	4.1	3.90e+20	271	8.50	0.085
5.	1993 0520	17:21	4.2	9.94e+20	319	13.00	0.100
6.	1993 0520	23:10	4.1	2.70e+20	351	2.70	0.110
7.	1993 0520	23:15	2.6	4.05e+18	211	0.19	0.065
8.	1993 0523	17:19	5.1	1.35e+22	479	54.00	0.150
9.	1993 0523	18:01	3.5	1.30e+20	128	27.00	0.040
10.	1993 0523	18:33	3.8	1.70e+20	367	1.50	0.115
11.	1993 0523	19:24	4.3	6.51e+20	319	8.7	0.100
12.	1993 0523	20:44	2.9	7.50e+18	224	0.30	0.070
13.	1993 0523	21:35	3.2	2.13e+19	303	0.33	0.095
14.	1993 0523	22:32	3.3	2.54e+19	166	2.30	0.052
15.	1993 0525	16:25	3.0	7.20e+18	192	0.45	0.060
16.	1993 0610	12:16	3.8	2.31e+20	511	0.76	0.160

STRESS DROP SCALING

For a simple circular source model, the source duration is related to the source radius r by the relation (Boatwright, 1980):

$$r = \tau_{1/2} \, v \, / \, (1 - v/\alpha \, \sin\theta) \qquad (7)$$

where v is the rupture velocity, α is the velocity of the P wave and θ is the take-off angle in the focus (angle between the normal to the fault plane and the outgoing seismic ray). Table 1 contains also the radius values estimated by using the deconvolved $\tau_{1/2}$ values. We considered in equation (7) a rupture velocity $v = 0.8\beta$, the seismic wave velocities in the source region, $\alpha = 5\,km/s$ and $\beta = 2.65\,km/s$, and an average take-off angle $\theta = 45°$. The scaling of the seismic moment with the source radius is plotted in Fig. 6 and is given by:

$$\log Mo = 3.7 \log r + 3.98 \qquad (8)$$

where Mo is measured in N m, while r is in m.

The radius values are subsequently used to determine the static stress drop values $\Delta\sigma$ following Brune (1970):

$$\Delta\sigma = 7/16 \, Mo \, /r^3 \qquad (9)$$

Stress drop estimations are also given in Table 1. The scaling of the stress drop with the seismic moment is represented in Fig. 7. It shows a continuous increase of the stress drop with increasing seismic moment for earthquakes with magnitudes in the range $2.9 < M_L < 5.1$, which is approximated by the regression line:

$$\log \Delta\sigma = 0.68 \log Mo - 13.22 \qquad (10)$$

According to Frankel's model (1991) the slope of the line in equation (10) is equal with 3+H, where H is the exponent of Hurst and it represents a measure of the way the distribution of the stress on the fault is scaled. For the usual case in which the stress drop is assumed constant (independent of the

earthquake size), H = 0 and log M_0 ~ 3 log r or M_0 ~ r^3. This is the classic case characterized by a high-frequency decay of the type ω^{-2} in the displacement amplitude spectrum. The deviations of the H exponent from zero value can be ascribed to a power-like scaling of the stress distribution on fault as expressed by (Frankel, 1991):

$$\Delta\sigma \ \alpha \ r^H \text{ or } \log \Delta\sigma = H \log r + C \qquad (11)$$

In the case of Sinaia sequence the seismic moment scaling with radius implies a Hurst coefficient H ≅ 0.7 and hence an increase of the static stress drop with radius given by $\Delta\sigma$ ~ $r^{0.7}$ and, correspondingly an increase of the seismic moment like that given by relation (10).

CONCLUSION

The estimation of the seismic source parameters for the Sinaia sequence by using the digital waveforms locally recorded within the time interval of May-June 1993 allowed the analysis of the scaling relations between the seismic moment, source dimension and stress drop. To get the seismic moment values we use the scaling with the local magnitude. This is determined by making use of the spectral ratio method. The source dimension is retrieved from the rupture duration in the focus, which is estimated by measuring the pulse width of the first P wave in the recorded seismogram and following the empirical deconvolution technic of Frankel and Kanamori (1983). This deconvolution is very efficient since is simple and allows the use of clipping seismograms.

The source radius and the static stress drop are computed for a Brune-type circular source model (1970). The resulted scaling relations reveals significant increases of the radius and stress drop with increasing seismic moment. These are interpreted in terms of an hierarchical distribution of stress inhomogeneities on the fault (Frankel, 1991). The value of the Hurst coefficient H = 0.7 suggests the presence in the focal region of a relative high number of large scale inhomogeneities as compared with the small scale ones. This feature is expected to be pointed out also in other characteristics of the seismic process, like frequency-magnitude distribution, seismic wave attenuation, high-frequency radiation of the source, stress drop scaling with rupture surface at foreshocks and aftershocks etc.

REFERENCES

Anderson J.G., 1986. Implications of attenuation for studies of the earthquake source, in "Earthquake Source Mechanics", S.Das, J.Boatwright and C.H.Scholz editors, A.G.U. Monograph 37, 311-318.

Boatwright J., 1980.A spectral theory for circular seismic sources: simple estimates of source dimensions, dynamic stress drop and radiated energy. Bull.Seism.Soc.Am. 70, 1-28.

Brune J.N., 1970. Tectonic stress and the spectra of seismic shear waves from earthquakes. J.Geophys.Res. 75, 4997-5009.

Enescu D., E. Popescu and M. Radulian, 1993. Preliminary study of the sequence of earthquakes occurred in Sinaia region, May-June 1993. Report CFP 39.92.1/1993, Bucharest (in Romanian).

Frankel A., 1991. High-frequency spectral falloff of earthquakes, fractal dimension of complex rupture, b value, and the scaling of strength on fault. J.Geophys.Res. 96, 6291-6302.

Frankel A. and H. Kanamori, 1983. Determination of rupture duration and stress drop for earthquakes in southern California. Bull.Seismol.Soc.Am., 73, 1527-1551.

Radu C. and D. Enescu, 1993.Seismic activity on the Romania territory during 1993. Report CFP 39.92.1/1993, Bucharest (in Romanian).

CRUSTAL MICROEARTHQUAKE SEQUENCES IN THE VICINITY
OF THE VRANCIOAIA STATION (ROMANIA)

Emilia Popescu, Mircea Radulian and Olivia Bazacliu

National Institute for Earth Physics
P.O. Box MG-2, Bucharest, Romania

Abstract
The seismic zone around Vrâncioaia station is characterized by a continuous seismic activity consisting mainly of small crustal earthquakes with magnitudes $M_S \leq 4.0$. They are occurring both as isolated events or grouped in swarms of tens or hundreds events.

The present study is an attempt to use the digital data in order to determine the characteristics of the seismic source in this specific region. The computed source parameters for seismic events with magnitudes in the range $0.6 \leq M_D \leq 2.4$ are in a good agreement with the values estimated for microearthquakes in other crustal zones.

A systematic monitoring of this seismic activity, including the estimation of the source parameters, could provide significant information related to the Vrancea region microseismotectonics.

INTRODUCTION
The Vrâncioaia station is situated to the northeastern extremity of the Vrancea seismic region . The seismic activity in the proximity of Vrâncioaia station ($\Delta < 10$km) consists mainly of small shallow earthquakes which are occurring both as isolated events or grouped in swarms of tens or hundreds events (Radu et al., 1979; Jianu, 1990; Popescu and Bazacliu, 1992).

It is hopeful that a systematic monitoring of this seismic activity , including the estimation of the source parameters, could provide significant information related to the Vrancea region seismotectonics. This paper is an attempt to value all the information available from the waveforms recorded by the Romanian telemetered local network. To this aim, an extended analysis of the source parameters in time and frequency domains is carried out for two sequences and two singular events generated in the neighbourhood of Vrâncioaia (VRI) station, for which digital data are available.

Since the high-frequency content which prevails in the microearthquake waveforms is very sensitive to the path effects, it is essentially to appeal to relative methods, like spectral ratios, in order to recover source characteristics.

OBSERVATION DATA
The data set consists of digital velocity recordings from short period ($T_0 = 1$s) S-13 seismometers (vertical component),

digitized at a sampling frequency of 50Hz and high-cut at 15Hz by an antialiasing filter. The existence of two gain channels extends the dynamic range of the system with 40db.

The studied earthquakes are presented in Table 1. Two of them are singular events (occurred on 17th and 19th May 1992, M_D=2.4 and M_D=2.1, respectively) and the others belong to two swarms, one of them containing 19 microearthquakes produced on December 7-8, 1991 ($1.0 \leq M_D \leq 1.8$) and the other 58 microearthquakes produced on May 23-24, 1993 ($0.6 \leq M_D \leq 2.24$), in the vicinity of VRI station.

Table 1. The used events and some of their parameters

Nr	Date (y / m / d)	Time (h: m: s)	M_D	M_0 (dyne cm)
1	1991 12 07	18:13:45	1.40	3.97e+16
2		18:14:12	1.00	2.99e+16
3		18:49:00	1.80	1.77e+16
4		19:51:30	1.40	5.67e+16
5		22:19:41	1.40	2.92e+16
6		22:55:46	1.40	4.48e+16
7		23:43:10	1.20	
8		23:43:37	1.60	1.12e+17
9		23:46:18	1.20	2.57e+16
10		23:48:08	1.40	4.99e+16
11		23:51:17	1.00	
12	1992 12 08	00:01:53	1.00	
13		00:04:12	1.00	
14		00:55:57	1.00	1.75e+16
15		00:57:09	1.30	5.15e+16
16		03:56:26	1.50	7.02e+16
17		09:08:14	1.40	
18		14:08:47	1.60	
19		16:42:40	1.40	
20	1992 05 17	03:09:44	2.40	1.13e+18
21	1992 05 19	02:42:17	2.10	7.32e+16
22	1993 05 23	07:35:51	1.80	1.70e+17
23		09:53:49	1.40	5.20e+16
24		10:02:47	1.85	1.98e+17
25		10:06:00	1.00	1.60e+16
26		10:40:46	1.60	9.40e+16
27		10:44:20	1.33	4.20e+16
28		11:44:36	1.52	7.40e+16
29		12:08:15	1.33	4.20e+16
30		12:08:38	1.00	1.60e+16
31		12:18:40	1.80	1.70e+17
32		12:20:14	1.80	1.70e+17
33		12:22:32	1.52	7.40e+16
34		13:43:41	1.00	1.60e+16
35		14:07:20	1.00	1.60e+16
36		15:47:56	1.90	2.30e+17
37		16:41:29	1.33	4.20e+16
38		17:52:28	1.40	5.20e+16
39		18:44:35	1.00	1.60e+16

40		21:31:09	1.10	2.10e+16
41		22:34:11	1.97	2.80e+17
42		23:18:13	1.52	7.40e+16
43	1993 05 24	23:19:19	1.10	2.10e+16
44	1993 05 24	00:56:36	0.86	1.00e+16
45		01:31:30	0.86	1.00e+16
46		01:33:40	1.97	2.80e+17
47		01:43:25	1.52	7.40e+16
48		01:45:24	0.60	4.80e+15
49		02:00:44	1.30	3.90e+16
50		02:13:18	1.17	2.60e+16
51		02:16:23	1.17	2.60e+16
52		02:24:17	1.00	1.60e+16
53		02:28:11	0.73	7.10e+15
54		02:32:21	1.33	4.20e+16
55		02:34:48	1.63	1.00e+17
56		02:39:20	1.17	2.60e+16
57		02:45:35	1.68	1.19e+17
58		03:24:54	1.52	7.40e+16
59		04:01:11	1.26	3.40e+16
60		05:00:54	1.10	2.10e+16
61		05:42:16	1.86	2.00e+17
62		05:42:28	1.86	2.00e+17
63		05:42:38	1.86	2.00e+17
64		05:43:00	1.26	3.40e+16
65		05:43:20	2.24	6.30e+17
66		05:46:07	1.33	4.20e+16
67		05:48:32	1.52	7.40e+16
68		06:11:09	2.13	4.50e+17
69		06:11:28	1.97	2.80e+17
70		06:15:18	1.86	2.00e+17
71		07:01:00	1.52	7.40e+16
72		07:12:15	1.33	4.20e+16
73		07:41:00	1.17	2.60e+16
74		08:10:26	1.52	7.40e+16
75		08:18:40	1.33	4.20e+16
76		08:36:26	1.17	2.60e+16
77		12:26:54	1.50	7.00e+16
78		12:27:05	1.77	1.56e+17
79		22:16:56	1.17	2.60e+16

The magnitude M_D is evaluated from the total duration of the recorded seismogram (τ) and the difference between S and P wave arrival times (t_{S-P}) by the following relation:

$$M_D = -0.87 + 2.00 \lg \tau + 0.029 t_{S-P} \qquad (1)$$

The events are generally recorded at only one station (VRI), so that an accurate location is not possible. Even for the greatest earthquake of 17th May, for which seven arrival times (P and S) are identified, the depth is poor constraint. However, a good estimation of the hypocentral distance for all data is obtained by:

$$R \cong t_{S-P}(\alpha\beta)/(\alpha-\beta) \qquad (2)$$

where $t_{S-P} = 1.5s$, $\alpha = 3.5 km/s$ is the P wave velocity in the shallow crust, and β is the S wave welocity. For $\beta = \alpha/\sqrt{3}$, R = 7km. Consequently, a depth of 5km is a rough estimation of the real focus.

TIME DOMAIN ANALYSIS

The seismic ground motion U(t) at the Earth's surface can be expressed as a convolution of the source time function S(t), path response P(t), instrument response I(t), and noise N(t) :

$$U(t)=S(t)*P(t)*I(t)*N(t) \qquad (3)$$

The observed waveforms are corrected for noise and instrument to determine the ground displacement. Sample windows of noise prior to P wave arrival time are considered in order to determine a Wiener optimum filter for removing the noise:

$$\Phi(f) = \frac{|U_0(f)|^2}{|U_0(f)|^2+|N(f)|^2} \qquad (4)$$

where f is frequency, $\Phi(f)$ - Wiener filter, $|U_0(f)|^2$ - power spectrum of the true signal (without noise), and $|N(f)|^2$ - power spectrum of the noise. A simple estimation of the power spectrum $|U_0(f)|^2$ is given by:

$$|U_0(f)|^2 \approx |U(f)|^2-|N(f)|^2 \qquad (5)$$

where U(f) is the observed spectrum. Finally, the signal is high-pass filtered (f>1Hz) in order to remove the low frequency noise.

The corrected displacements are presented in Fig. 1a, b, c. All the seismograms are normalized to the maximum amplitude to facilitate their comparison. From the total number of events 22 earthquakes are selected (12 belonging to the swarm produced on December 7-8, the two singular events of 17th and 19th May 1992 and 8 microearthquakes belonging to the swarms produced on May 23-24) with signal to noise ratio greater than 3. Following their waveform patterns, the events are clasified into two specific types: I (Fig 1a) and II (Fig 1b and 1c). The both types are present in the swarm of December 1991. The swarm of May 1993 is entirely characterized by type II, while events of 17th and 19th May 1992 are type I-like.

When comparing the seismograms, two significant phases are emphasized, one after the P and other after S wave arrivals, for both types I and II events. This indicates a rather complex structure of the upper crust in the Vrâncioaia region.

The existence of two unipolar pulses in the type I seismograms is attributed to the source complexity (the rupture is characterized by two main episodes which appear like two subevents). However, it is not excluded the possibility that the second pulse to be generated by a conversion at a local inhomogeneity in the source region.

The area under the first motion displacement is a measure of the seismic moment, and the pulse width is related to the source duration or to the source dimension. Following Boatwright (1980), the seismic moment is given by:

$$M_0[dyne.cm]=4\pi[\rho_0\rho v^i]^{1/2}(v_0^i)^{5/2}\frac{R}{F^i}\overline{u_i} \qquad i=P \text{ or } S \quad (6)$$

where:
- ρ_0 and ρ - densities at the source and receiver, respectively; $\rho=\rho_0=2.5g/cm^3$;
- v_0^i , v^i - velocities at the source and
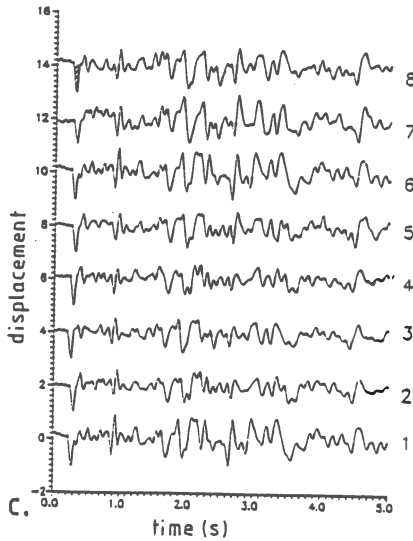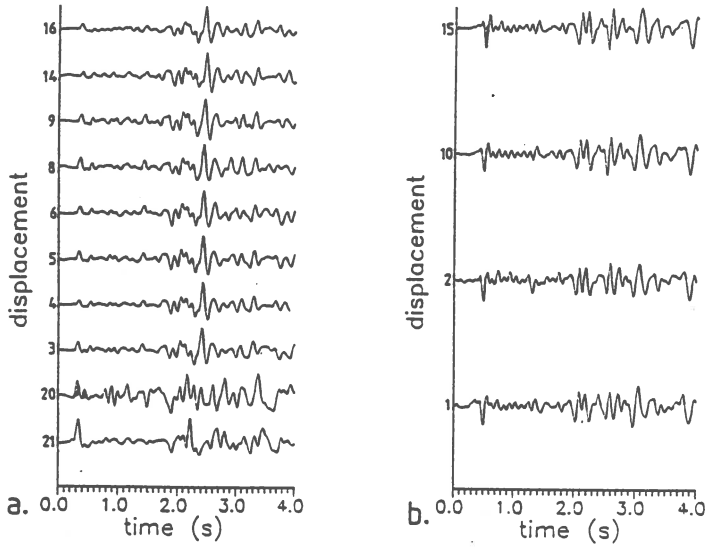
Fig. 1. Displacements corrected for instrument and noise; a and b for sequence produced in December 1991 and the·two singular events and c for sequence occurred in May 1993. Traces are normalized and shifted along the vertical axis.

Typical P pulse areas used to seismic moment estimation are reprezented as dashed areas.

receiver, respectively; $v_0^i = v^i$, $v^P = 3.5$km/s and $v^S = 2$km/s;
  - R - hypocentral distance ≈ 7km;
  - F^i - radiation pattern which includes a free surface
correction at the receiver ($F^P \approx 1.0$, $F^S \approx 1.2$);
  - u_i - area under the displacement waveforms;
    To estimate the area $\bar{u}$, the pulse shape is approximated by
a triangle. Several typical cases are represented in Fig. 1a,
b, c. For complex events the both subevents are considered.
The moment value does not depend on the attenuation; this one
flattens the displacement pulse without changing its area. The
empirical moment-magnitude relation in time domain is given by
equation (7) and represented in Fig. 2a:
$$\log M_0 = (1.30 \pm 0.08) M_D + (14.60 \pm 0.13) \qquad (7)$$
    For the magnitude range analyzed, $0.6 \leq M_D \leq 2.4$, there are no
significant variations in the pulse widths ($\tau_{1/2}$ around 0.1s).
There are several possible factors leading to this constancy:
  - (i)   - existence of a minimum area for earthquake
generation;
  - (ii)   - high frequency cut-off due to the site
attenuation;
  - (iii) - high frequency cut-off due to the limited
bandwidth of the recording instrument.
    To answer which is the real cause of the similarity in the
width of the displacement pulse, it is necessary to apply
relative methods, like spectral ratios or empirical Green
deconvolution which make possible the remove of the path
effects.

FREQUENCY DOMAIN ANALYSIS

    A simultaneous analysis of the source parameters is carried
out in the frequency domain. To this purpose, time windows of
0.5 to 1.5 seconds are extracted from the recorded velocity
waveforms and Fourier transformed. Seismic moment is evaluated
from the low-frequency level Ω_0 of the displacement amplitude
spectrum (Brune, 1970), after correction for instrument
response, noise and attenuation (by using a Q value
independent of frequency determined by Popescu and Bazacliu,
1992). The seismic moment is computed by:

$$M_0 [\text{dyne.cm}] = \varepsilon_i \frac{4\pi\rho v_0^i (v^i)^2 \, R\Omega_0^i}{F^i} \qquad i = P, S \qquad (8)$$

which is the equivalent of equation (6) in the frequency
domain. The constants $\varepsilon_P = 1.4$ and $\varepsilon_S = 2.0$ are average factors
introduced to compensate for using in (8) of only vertical
components. They are estimated for P and S waves in the
hypothesis of an incidence angle of 45^0 at the station.
Moment-magnitude relation is given by relation (9) and is
repesented in Fig. 2b.
$$\log M_0 = (1.29 \pm 0.10) M_D + (14.91 + 0.17) \qquad (9)$$
$$r = 0.96, \quad \sigma = 0.17$$
The estimations of the seismic moment for all the events are
presented in Table 1.
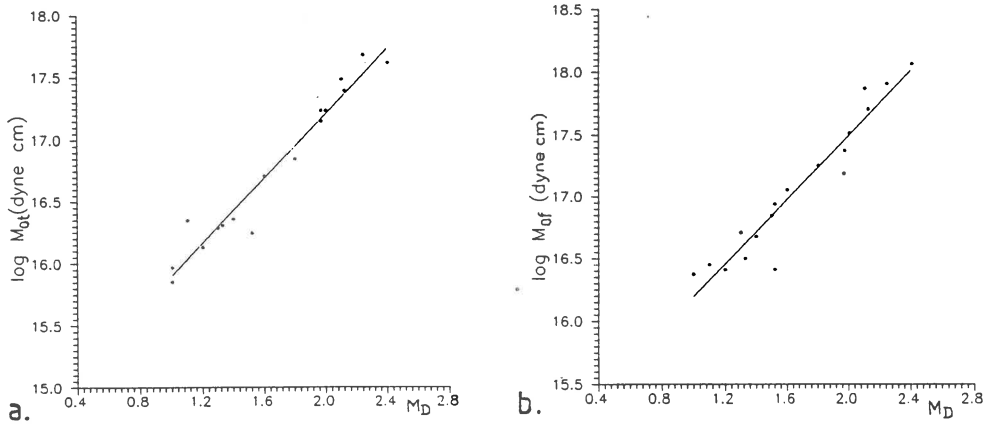
Fig. 2. Moment-magnitude relations for both, time (a) and frequency (b) domain values.
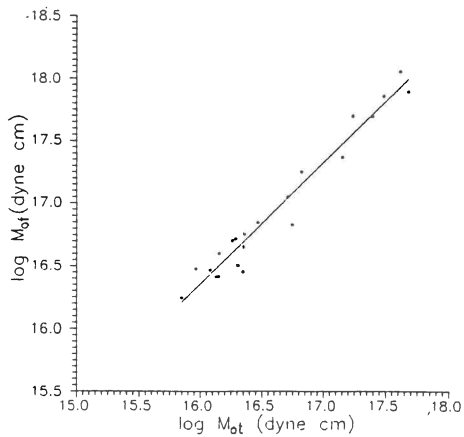
Fig. 3. Linear regression between the seismic moment values determined in frequency and time domains.

The spectral and time determinations are linearily correlated as can be seen in Fig. 3, the linear regression is given by:

$$\log M_0^f = (0.98 \pm 0.05) \log M_0^t + (0.71 \pm 0.96) \qquad (10)$$
$$r = 0.98, \quad \sigma = 0.12$$

For earthquakes generated around the same focus and recorded at the same station, with the same focal mechanism, the spectral ratios effectively remove all the effects which are not related to the source. The convolution operation (3) in the time domain turns to a multiplication in frequency domain:

$$U(f) = S(f) P(f) I(f) N(f) \qquad (11)$$

The ratio between the spectra of two events 'a' and 'b' reduces to the ratio of the corresponding source spectra:

$$r(f) = \frac{U_a(f)}{U_b(f)} = \frac{S_a(f)}{S_b(f)} \qquad (12)$$

Let's event 'b' be greater than event 'a' ($M_b > M_a$). If its corner frequency f_b falls within the bandwidth of the S13 instrument ($1Hz \leq f_b \leq 12Hz$) then f_b could be identified in the plot of r versus f at the intersection of a low-frequency constant level ($f < f_b$) and a high-frequency linear increase ($f > f_b$), as schematically shown in Fig. 4.

The spectral ratios for the greater event of 17th May ($M_D = 2.4$) and three of the smallest events ($M_D \approx 1.4$) are averaged and plotted in Fig. 5. No any increasing trend can be detected in the reliable frequency bandwidth (1–10Hz). It is likely that the f_b value lies around or passes beyond the highest frequency of the instrument bandwidth, f_h. The limitation of this one makes impossible any inference regarding the source duration or corner frequency. The including in the analysis of earthquakes with magnitudes greater than $M_D \approx 3.0$ is urged in order to point the lower magnitude threshold from which the computation of source duration, dimension and stress drop is reliable.

CONCLUSION

The extension in the last years of the digital data to microearthquakes with magnitudes as small as $M_D \approx 0.6$ substantially enlarges the possibility to study the seismotectonics in the Vrancea region. The present study is a first attempt to utilize these data to determine the characteristics of the seismic source in this seismic region.

The analyses in time and frequency domain provide reliable estimates of the seismic moment which can be subsequently introduced in scalings of seismic source over a broader magnitude range. For the seismic events considered in this paper ($0.6 \leq M_D \leq 2.4$), the seismic moment values range in the domain $10^{15} - 10^{18}$ dyne cm, in good agreement with evaluations for microearthquakes in other crustal regions (e.g.,Cranswick et al.,1985).

Unfortunately, the limited bandwidth of the present instrumentation makes impossible the determination of the source dimension and consequently of the stress-drop for this magnitude range. From this point of view, our results claim
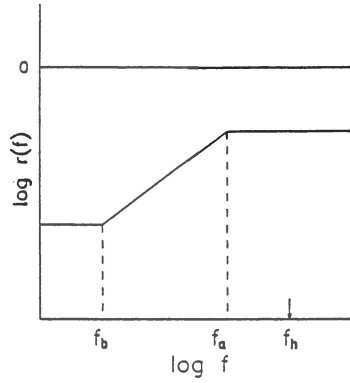
Fig. 4. Theoretical spectral ratio for events a and b with Mb > Ma; fa, fb are corner frequencies; fh is the high limit of the instrument bandwidth.
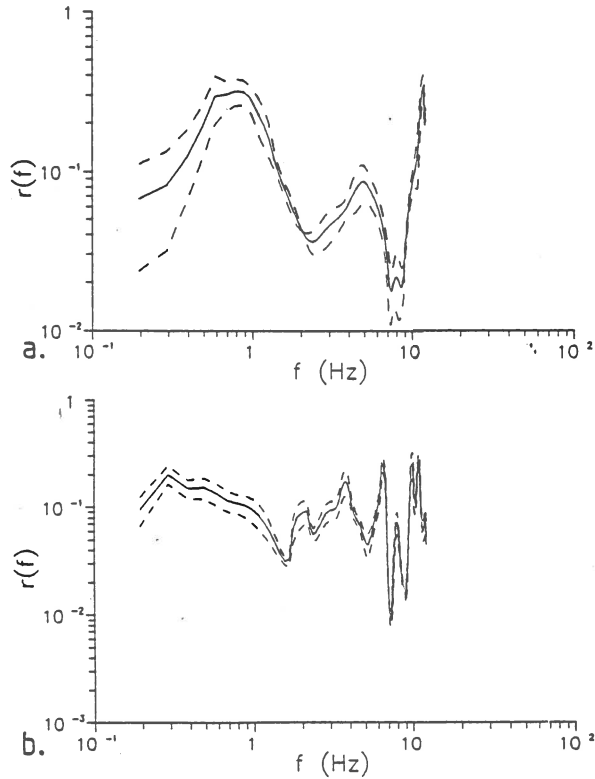
Fig. 5. Observed spectral ratio obtained by averaging four ratios for the following pairs of events: 4/20, 5/20, 6/20, and 9/20 for P wave (a) and for S wave (b); dashed lines represent the standard deviations from the average curve (solid line).

886

attention on the importance of installing broad - band instruments in the region and on the extension of the magnitude range in order to get reliable source parameters determinations. In the same time, this extension of data will make possible detailed studies on the local structure based on more numerous recordings and synthetic seismograms.

REFERENCES

Brune, J.N., 1970. Tectonic stress and the spectra of seismic shear waves from earthquakes. J. Geophys. Res., 75, 4997-5009.

Boatwright, J., 1980. A spectral theory for circular seismic sources: simple estimates of source dimension, dynamic stress drops, and radiated energy. Bull. Seism. Soc. Am., 70, 1-28.

Cranswick, E,, R. Wetmiller and J. Boatwright, 1985. High frequency observations and source parameters of microearthquakes recorded at hard-rock sites. Bull. Soc. Am. 70,, 735-755.

Jianu, D., 1990. On the seismic swarm occurred in May 11th 1975. Proc. XXIInd Gen. Ass. of ESC, Barcelona, 1990, 697-701.

Popescu, E. and O. Bazacliu, 1992. On the sequence occurred on 7 - 8 December, 1991, in the adjacent zone of Vrîncioaia station (in Romanian). Internal Report 30.92.1, 25p., 1992.

Radu, C., G. Polonic, and V. Winter, 1979. On the earthquake swarm recorded at Vrîncioaia station on 2 - 5 July, 1977 (in Romanian). Seismological investigations on the March 1977 earthquake. Ed. Cornea I. and C. Radu.

A COMPLEX STUDY OF SEISMIC DOUBLETS AND MULTIPLETS OCCURRED IN ROMANIA USING ANALOGIC AND DIGITAL DATA FOR 1988-1991 PERIOD

Zina Malita, Iren Adelina Ivan

National Institute for Earth Physics, P.O.Box MG-2, 76900 Bucharest, Magurele, Romania

Abstract

A seismic doublet can be defined as an ensemble of two earthquakes satisfying the following conditions:
- the magnitudes must be in the same range,
- the rupture zones must be contiguous,
- the interoccurrence time, Δt, must be greater than the increasing time of each individual event, but shorter than the return time.

Vrancea seismic zone favors the appearance of the doublets and multiplets due to its special structure. We have established the energetical and hypocentral parameters: v, l, h, M and E of the studied doublets and multiplets. We have also determined the source parameters M, r, Ds, D and the fault plane solutions. In this study we have used the seismic data of the Romanian earthquake catalog (1988-1990) which fulfill the following conditions:
- $M \geqslant 3.0$,
- the difference between the magnitudes let be less than 0.5,
- the distance between the rupture zones let be less than 10 Km,
- the interoccurrence time let be less than 10 days.

10 doublets and 10 multiplets situated within 45.18 N - 46.17 N and 26.44 E - 27.35 E coordinates have been chosen under the conditions mentioned above.

Introduction

A seismic doublet can be defined as an ensemble of two earthquakes satisfying the following conditions: the magnitude must be in the same range, the rupture zones must be contiguous, the interoccurrence time Δt must be greater than the increasing time of each individual event, but shorter than the return time. (Marza V. et al. 1985). Using Das and Scholz (1981) model we consider that the stopping of the rupture process is produced in the moment when the rupture of the first earthquake, during its propagation reaches a high resistance zone (physic or geometric inhomogeneity) or in a zone were the lubrication is not enough (or does not exist) for the slip on the fault plane to exceed the friction. The increase of the tension during the time interval Δt from the stopping phase of the first rupture can overpass the strength of the barrier an it is possible the occurrence of the second earthquake.

The term "doublet" differs from the term "multiple event", when $\Delta t \rightarrow 0$, i.e. the barrier is broken before reaching the static equilibrium. Only some seismic zones favor the occurrence

of doublets and multiplets due to their special tectonic structure, and the Vrancea seismic zone is one of these zones.

Hypocentral and energetic parameters of doublets and multiplets

The data were obtained using the arrival time of p and s waves, measured on the analog and digital recordings. The localization of these events contain the data, the origin time, the epicentral coordinates (latitude ϕ and long λ), the focal depth h and the magnitude M_D.

The M_D magnitude was obtained using the oscillation time D:

$$M_D = -0.87 +2 \log D +0.0035 \, K \, (s\text{-}p) \tag{1}$$

for: K = 8.4 in the case of normal earthquakes

K = 10.5 in the case of intermediate earthquakes.

The energy delivered by each earthquake was determined using Gutenberg and Richter relation (1956):

$$\text{Log } E = 2.9 +1.92 \, M_D - 0.024 \, M_D^2 \tag{2}$$

Doublets and multiplets source parameters

The source parameters were calculated from the digital recordings of the telemetered Romanian seismic network using the SEIS89 program and the Madariaga source model. This model is based on the following formulas:

$$M_0 = \frac{4\pi\rho_h v_o v_h^2 R \Omega_o}{\mathcal{R}} \tag{3}$$

$$r = \frac{3h v_h}{\pi F_c} \tag{4}$$

$$\Delta\sigma = \frac{7M_o}{16r^3} \tag{5}$$

$$D = \frac{M_o}{\pi\mu_h r^2} \tag{6}$$

Were:

M_0 = the seismic moment;

v_0 = seismic wave velocity at the surface;

v_h = p or s seismic wave velocity in the source;

c = transfer coefficient at the free surface;

$\mathcal{R}$ = source radiation pattern;

R = hypocentral distance;

Ω_o = Low level frequency;

r = source ray;

$\Delta\sigma$ = stress-drop;

D = final fault dislocation;

μ_h = rigidity modules;

F_c = corner frequency.

We have used the velocity and density local model determined by V. Raileanu (1993) and the K.E. Bullen (1963) global model. The quality factor of the medium is $Q_0 = 108$ and $N = 0.88$ for Vrancioaia seismic station.

Fault plane solutions for the studied doublets and multiplets

We have studied the focal mechanism using the program realized by M.C.Oncescu (1980) based on the signs of the first arrivals recorded at the Romanian telemetered and analog seismic stations and on the signs communicated by NEIC in Earthquake Data Report. We have obtained the "a" and "b" fault plans parameters strike direction, dip direction and slip direction. The main axes: pressure axis P and the tension axis T are characterized by the strike- and dip parameters. For the graphic representation of the fault plane solution we have used the stereographic projection in the Wulff diagram and the STEREO program .

Discussions

In this study we have used data from the Romanian earthquake's catalogue (1988 - 1992) fulfilling the following conditions:
-Md $\geqslant$ 3,
-the difference between the magnitudes < 0.5,
-the distance between the rupture zones < 10 Km,
-the interoccurrence time < 10 days.

Using these conditions we have chosen 10 doublets and multiplets presented in Table 1 situated in a zone limited by: 45.18 and 46.17 North and 26.44 and 27.35 East.

Table 1 - The catalogue with the earthquakes identified as doublets and multiplets

No	Data	Time	Lat. N	Long. E	h (Km)	M_D	E (J)	Δt	ΔM
1.	1989.02.26	02:50:11	45.18	27.10	4.0	4.2	3.467 10^9	57.5 min	0.5
	1989.02.26	03:47:42	45.18	27.10	8.0	3.7	4.786 10^9		
	1989.02.26	04:38:27	45.16	27.05	2.0	3.4	1.413 10^9	50.8 min	0.3
2.	1989.05.07	20:25:56	45.00	27.03	26.0	3.4	1.413 10^9		
	1989.05.07	21:01:34	44.94	27.04	18.0	3.7	4.786 10^9	35.6 min	0.3
3.	1989.08.18	06:28:19	45.98	26.68	9.0	3.5	2.138 10^9	0.96 hours	0.4
	1989.08.18	07:26:24	45.96	26.69	10.0	3.9	1.047 10^{10}		
	1989.08.18	11:42:20	45.96	26.66	9.0	3.7	4.786 10^9	4.3 hours	0.2
4.	1989.08.18	11:50:06	45.79	26.90	5.0	3.0			
	1989.08.18	13:21:28	45.76	26.88	5.0	3.0		1.5 hours	0.0
5.	1989.08.18	07:41:32	46.02	26.62	17.0	3.0	3.978 10^8	4.4 hours	0.3
	1989.08.18	12:06:22	45.96	26.66	5.0	3.3	9.333 10^8		
	1989.08.18	13:15:41	45.96	26.64	8.0	3.2	6.310 10^8	1.2 hours	0.1
	1989.08.18	14:29:33	45.99	26.63	16.0	3.1	4.169 10^8	1.2 hours	0.1
6.	1989.12.08	20:37:48	45.56	27.04	25.0	3.6	3.162 10^9		
	1989.12.09	06:15:23	45.63	27.02	25.0	3.5	2.138 10^9	9.6 hours	0.1

No	Data	Time	Lat. N	Long. E	h (Km)	M_D	E (J)	Δt	ΔM
7.	1990.06.20	11:53:56	45.71	26.79	99.0	3.8	$7.079\ 10^9$	5.8 days	0.4
	1990.06.26	07:54:18	45.81	26.72	107.0	4.2	$3.467\ 10^{10}$		
	1990.06.29	20:07:19	45.76	26.80	94.0	3.9	$1.047\ 10^{10}$	3.5 days	0.1
8.	1990.07.12	04:24:12	45.86	26.81	88.0	3.3	$9.333\ 10^9$		
	1990.07.13	01:51:52	45.85	26.80	80.3	3.1	$4.169\ 10^8$	21.5 hours	0.1
9.	1990.11.11	10:53:19	45.92	27.26	0.0	3.7	$4.786\ 10^9$		
	1990.11.11	10:54:07	46.05	27.13	6.2	3.7	$4.786\ 10^9$	0.8 minute	0.0
10.	1990.12.20	13:03:26	45.75	26.68	79.2	3.5	$2.138\ 10$		
	1990.12.21	19:09:15	45.79	26.81	75.8	3.1	$4.169\ 10$	2.3 days	0.4

From those 10 doublets and multiplets we have choosen 4 multiplets, with the corresponding parameters represented in Table 2.

Table 2 - Source parameters for the analyzed multiplets

No	Data	Time	ρ g/cm^3	V_s Km/s	Δ Km	M_0 Nm	r m	$\Delta\sigma$ N/m^2	D m
1.	1989.02.26	02:50:11	2.37	2.138	64.684	$1.22\ 10^{14}$	$4.35\ 10^2$	$6.46\ 10^5$	$1.89/10^2$
	1989.02.26	03:47:42	-	-	-	-	-	-	-
	1989.02.26	04:38:27	-	-	-	-	-	-	-
2.	1989.08.18	06:28:19	-	-	-	-	-	-	-
	1989.08.18	07:26:24	2.50	2.425	52.936	$6.94\ 10^{13}$	$5.18\ 10^2$	$2.19\ 10^5$	$5.61/10^3$
	1989.08.18	11:42:20	2.50	2.425	52.062	$6.83\ 10^{13}$	$5.18\ 10^2$	$2.15\ 10^5$	$5.52/10^3$
3.	1989.08.18	07:41:32	2.55	2.527	57.486	$1.90\ 10^{13}$	$3.26\ 10^2$	$2.40\ 10^5$	$3.50/10^3$
	1989.08.18	12:06:22	2.37	2.138	52.062	$1.08\ 10^{13}$	$2.76\ 10^2$	$2.25\ 10^5$	$4.17/10^3$
	1989.08.18	13:15:41	-	-	-	-	-	-	-
	1989.08.18	14:29:33	2.55	2.527	54.510	$5.19\ 10^{13}$	$4.76\ 10^2$	$2.11\ 10^5$	$4.19/10^3$
4.	1990.06.20	11:53:56	3.25	3.452	35.100	$1.99\ 10^{13}$	$4.90\ 10^2$	$7.42\ 10^4$	$6.82/10^4$
	1990.06.26	07:54:18	3.38	4.589	39.381	$1.46\ 10^{14}$	$8.10\ 10^2$	$1.20\ 10^5$	$1.83/10^3$
	1990.06.29	20:07:19	-	-	-	-	-	-	-

The depth of these earthquakes is between 10 Km and 147 Km. The interoccurrence times have values between 0.8 minutes and 10.3 days. The maximum differences between the magnitudes is 0.5 (1988 December 25/ 1988 December 25 and 1990 September 02/ 1990 September 13). The studied earthquakes have the magnitudes between M = 3.4 (1989 February 26) and M = 4.2 (1990 June 26) and MS = 4.9 in the case of the doublet from November 1993.

The source parameters were calculated only for the digital recordings of the seismic telemetered network. The number of seismic events with source mechanism solutions is not very large because we have chosen only the earthquakes with at least 7 signs for the first movement. For the multiplets presented in Table 2, we have represented in Figure 1 to 4 the focal mechanism.
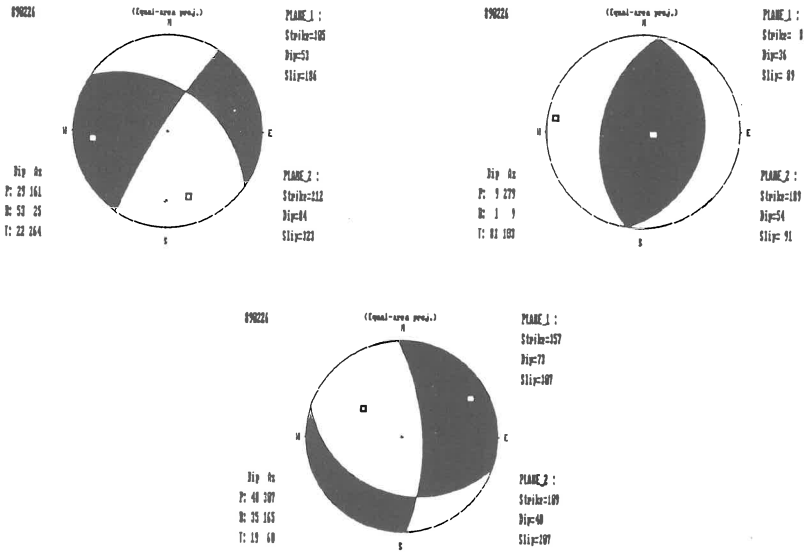
Fig. 1 - Focal plane solution for the multiplet from 26th of February 1989

For the first two events, the nodal planes "b" are orientated to NV, and the nodal planes "a", are orientated for the first one to NE and for the second to SE. T axis is horisontal for the first event and vertical for the second but both of them are toward SE-NV. P axes is horizontal for both events but the directions are different: SV-NV and NV-SE. The fault for the first event is strike slip and for the second is thrust. The last event of this multiplet has the nodal plane "a" dipping to NE and the "b" plane is dipping to SV. T axis is horizontal (NE-SV) and P axis is vertical (NV-SE). The fault is dip slip.
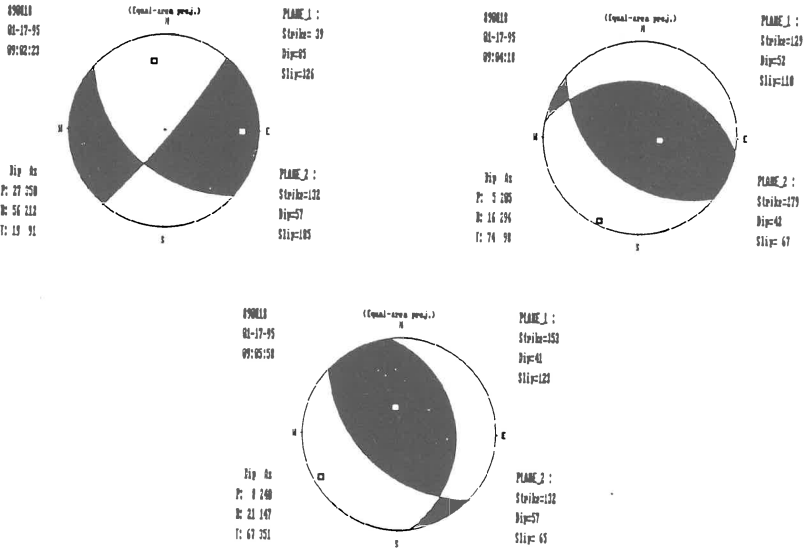
Fig. 2 Focal plane solution for the multiplet from 18th of August 1989

For the first two events, the nodal planes "b" are orientated to NE and SE, and the nodal planes "a", are orientated for the first one to SV and for the other to NE. T axes is vertical for the 2 events but for the first one it is acting toward NE-SV and at the other toward NV-SE. P axis is horizontal for both events but the directions are different: SV-NE and SE-NV. The fault type is trust for the both events. The last event of this multiplet has the nodal plane "a" dipping to NE and the "b" plane is dipping to NV, T axis is horizontal (SV-NE) and P axis is vertical (SE-NV). In this case we have normal faulting.
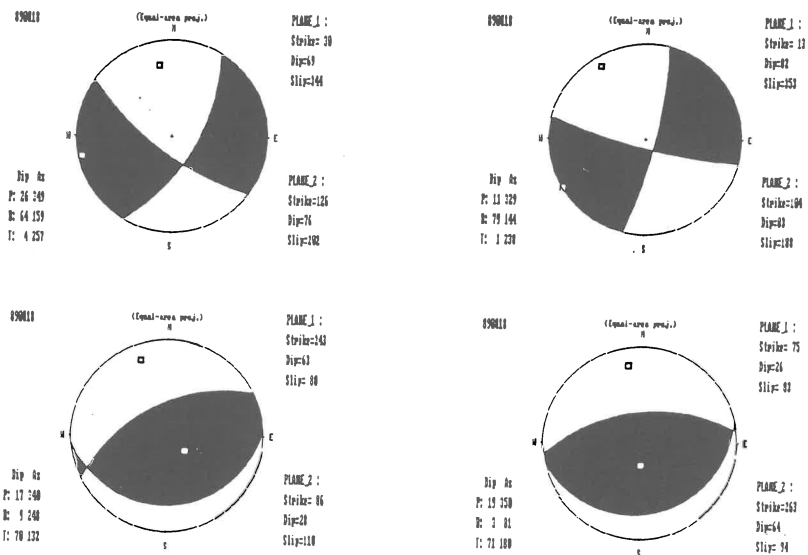
Fig. 3 Focal plane solution for the multiplet from 18th of August 1989

For the first two events, the nodal planes "b" are dipping SV, and the nodal planes "a" are dipping to SE. T axes is horizontal for the two events and is acting toward SV-NE. P axis is horizontal for both events but the directions are different: N-S and NV-SE. The fault type is dip slip for the both events.
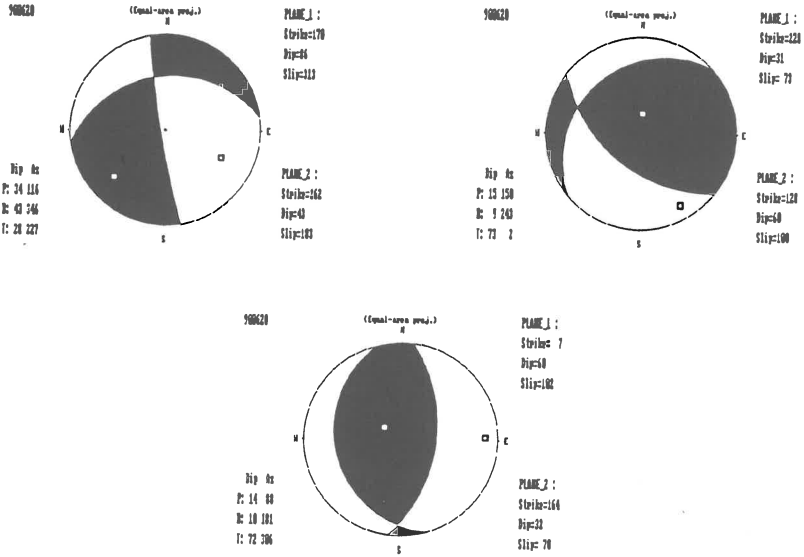
Fig. 4 Focal plane solution for the multiplet from 20/26/29 June 1990

The nodal plane "a" of the first event is dipping to SV, and the "b" plane to NV. T axis and P axes are horizontal toward SV-NE and SE-NV. In this case we have strike slip fault. For the second event the nodal plane "a" is dipping to NV and the nodal plane "b" is dipping to SV. The T axis is vertical (NE-SV) and the P axis is horizontal (SV-NE). We have reverse faulting. For the last event the "a" plane is dipping to SE and the "b" plane is dipping to SV. The T axis is horizontal (NE-SV) and the P axis is vertical (NV-SE). In this case we have normal fault.

Generally both nodal planes are oriented NV-SE but there are some exceptions too. Some of the earthquakes were produced by dip slip and others by strike slip. From the point of view of focal stress some earthquakes have the T axis almost vertical and the P axis almost horizontal toward the direction NE-SV or NV - SE. The others have the T axes almost horizontal toward NE-SV or NV - SE and the P axis in an almost vertical plane. The wave forms of the events from the same doublet or multiplet recorded at the same station have the same shape when the focal mechanisms are similar.

Another remark is that the wave forms from one event recorded at two Romanian stations: MLR and VRI can be different due to the filter effect of the propagating medium and to the source radiation pattern.

References

Bullen, K.E., 1963. An Introduction in the Theory of Seismology, M.A., Sc.D.,F.R.S. Cambridge University Press.

Das, S., and C.H. Scholtz, 1981. Theory of Time-dependent Rupture in the Earth J. Geophis. Res. 86,6039-6051.

Gutenberg, B., and C.F. Richter, 1956. Magnitude and Enery of Earthquakes. An. di Geofis., 9, 167-198.

Malita, Z., and I.A. Ivan, 1993. Complex Study of Doublets and Multiplets occurred in Romania during 1991-1992, C.E.P. Technical Report, 30.92.1/1993, Bucharest.

Marza, V., V. Burlacu, and A. Pantea, 1985. Vrancea Seismic Doublet - 01 August, 1985, in CEPS Technical report 8054/1984, Chapter 4, pp. 12-28, Bucharest.

Oancea, V., and O. Bazacliu, 1988. Source Factor Using Seismic Attenuation from Coda waves. Seismological Investigations in Europe, Proc. of XIX General Assembly of the ESC, Moscow, October 1984, pag. 279-285.

Raileanu, V., C. Diaconescu, D. Mateciuc, and M. Diaconescu, 1993. Velocity Crustal Models under the Romanian Telemetred Seismological network. National Congress of Physics, Constanta, September 1993.

Radu, C., and A. Utale, 1988, 1989, 1990, 1991. The Seismic Activity in Romania. C.E.P. Reports, Bucharest, Romania.

SOURCE INVERSION WITH SEISMIC WAVEFORMS, APPLICATION TO THE WESTERN IBERIAN MARGIN

J.F.Borges[1][2] and A.J.S.Fitas[1][2]

[1]Departamento de Física da Universidade de Évora, Largo dos Colegiais, 2,
7000 ÉVORA, PORTUGAL
[2]Centro de Geofisica da Universidade de Lisboa, R. da Escola Politécnica,
1200 LISBOA, PORTUGAL

Abstract
The Iberian Portuguese margin has a considerable seismic activity associated to important tectonic faults set: Messejana fault, Tejo Low Valley Fault, Nazare Fault. Also there is seismic activity which is difficult to correlate with known tectonic accidents.

All these accidents which are present in the sea, they are located at the west side of the Portuguese Seismic Network. This location turns to be difficult the source mechanism determination of moderate seismic events because of the poor azimutal coverage and of the use of the first motion directions which are few.

The aim of the present work is to develop a source inversion method that may conjugate information of first motion directions provided by analogical records and the wave form of the body waves provided by high quality digital stations.

Introduction
We can describe a general seismic source with a moment tensor $[M_{ij}]$ by 6 independent elements. If we are interested in a deviatoric double-couple source the trace and determinant of $[M_{ij}]$ are zero.

The response to arbitrary oriented double couple source, W_{in}, in the station i it can be found by a linear combination of five elementary Green's functions, G_{jn}, depending on time, which corresponds to the focal mechanisms of fig. 1 (Kikuchi, 1991).

$$W_{in}(t,p) = \sum_{j=1}^{5} a_j G_{ijn}(t,p) * f(t) \tag{1}$$

$f(t)$ is the source time function, the value n corresponds to the three components of the seismogram (vertical, radial and tangential) and the parameter p represents the localisation of the source. The coeficients of the linear combination can be found by

$$
\begin{aligned}
a_1 &= M_{12} \\
a_2 &= \frac{1}{3}(M_{11} + M_{33} - 2M_{22}) \\
a_3 &= M_{23} \\
a_4 &= M_{13} \\
a_5 &= \frac{1}{3}(2M_{33} - M_{11} - M_{22})
\end{aligned}
\tag{2}
$$

and M_{ij} is function of the strike parameters of the fault (ϕ, δ, λ) (Aki and Richards, 1980). If the three parameters of the fault are known it is possible to calculate the moment tensor, and then, by (2) and (1), we can find the response of the source.
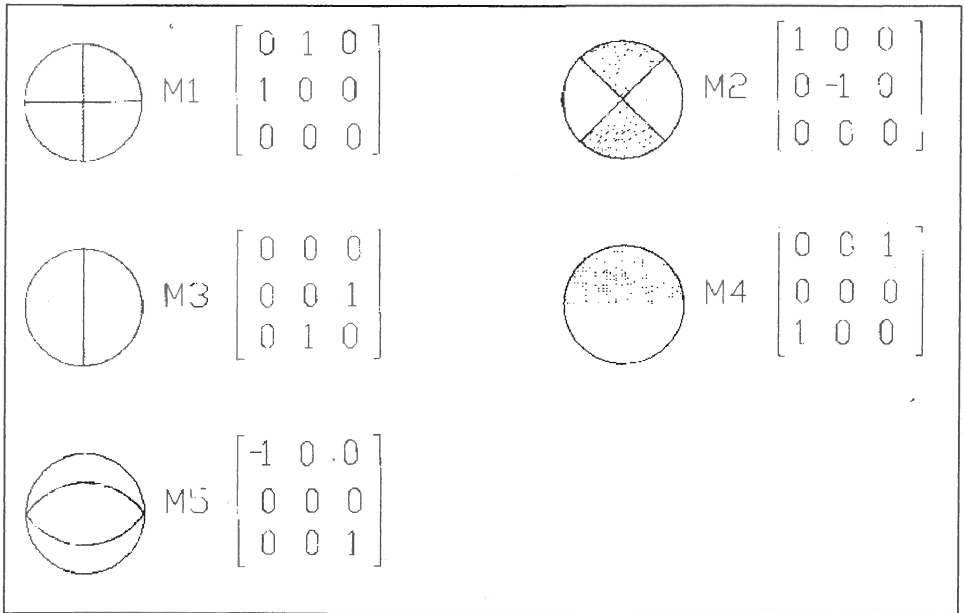
Fig. 1. Elementary moment tensor for the base system

Inversion method

Taking in consideration that the errors between observed seismogram, X_{nij} , and the synthetic seismogram, Wnij, are gaussian and independent, the probability density function which represents the information we have is

$$fdp(x/m) = k\prod_{n=1}^{3}\prod_{i=1}^{N}\prod_{j=1}^{Np} \exp(-(X_{nij} - W_{nij})^2/\sigma^2)$$

(3)

where m is the model parametersn Np is the number of points of the time serie and σ is the standard deviation.

The relation between the data and thge parameters of the source are a nonlinear function.We have adopted a method of grid search in whole parameter space in order to find the best mechanism for n stations which corresponds to the maximum of the previous function. This method of inversion was used because the function is highly nonlinear and there were only three parameters to find.

The complete parameter space for the source is ($0\leq\phi\leq360$, $-180<<\lambda\leq1\leq80$, $0\leq\theta\leq90$), and the search can be accomplished in two steps. First, we use a regular grid spacing of 10° and we determine the most significative maximum, then we use a finer grid of 2° to calculate the global maximum.

We have adopted the representation of de probability function in three distinct plans which are associated to the couple strike-slip, strike-dip and dip-slip. This representation gives us the possibility of having a global image of the solutions.

In order to compute the synthetic Green's functions we have used the reflectivity method developped by Kennett (1979) for a stratified model. The synthetic seismogram of an arbitrary source was determined by the application of expression (1). Using this approach we were able to compute the seismograms for every orientation of the source in a reasonable computing time.
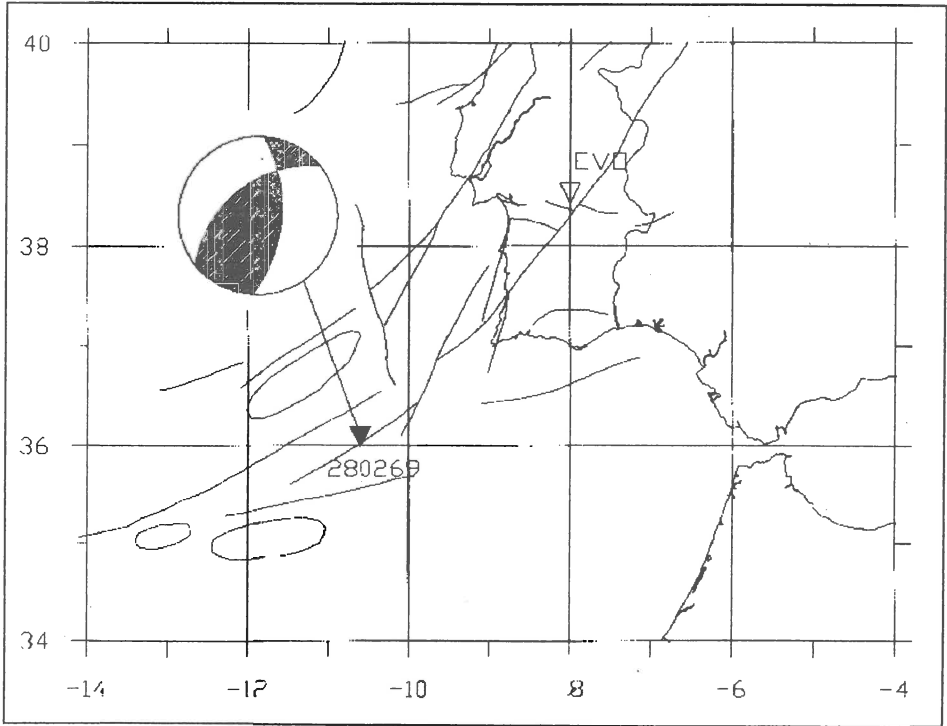
Fig. 2. Location of the event of 69/02/28 which is used in this application

Application

· In this section we discuss the application of this method to synthetic data of the earthquake occurred on February, 16, 1969. This event, with a magnitude 8, was well recorded by a large number of stations in all the world and its focal mechanism was published by several authors. We have adopted the solution of Buforn (1985). The solution of the first nodal plane NP1 for the strike, dip and rake is 4.2/54/58 and for NP2 the best solution is 231/47/126. The depth of the event is 22Km..

The synthetic seismogram for this source and the Green's functions was obtained using the kennett algorithm for a rang of frequenties, 0.1 to 2Hz. The velocity model is the best for the location of the events in this region.

In order to test the method, with noise contamination and simulating lateral heterogeneities of the medium, we have introduced a model of noise suggested by Kennett (1985). For this model each value of the seismogram in the frequency-slowness domain is multiplied by a factor $1+c(r_1+ir_2)$ where r_1 and r_2 are random numbers with a uniform distribution on the interval (0,1). The values of c controls the level of noise. For our application we have considered the value of 0.1 which corresponds to a maximum variation of the amplitude of 10%, and a maximum variation of phase of $\pi/20$.

We have inverted the seismogram without noise (seismogram A in the fig. 4) and the seismogram with noise (seismogram B of the same figure). The results of this two inversions are almost the same.

The best solution obtained by this method are 7/50/55 for NP1 and 222/23/124 for NP2. As we can see by the analysis of the fig.4, the inverted mechanism deviates very little from the origina mechanism.
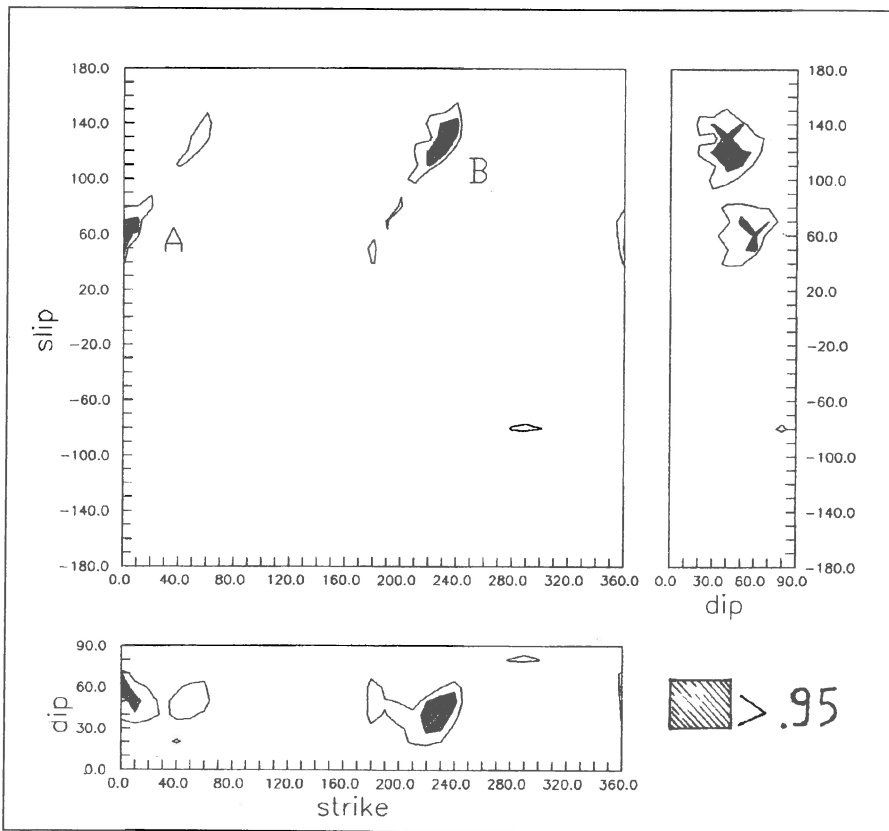
Fig. 3. Inversion results (grid search with intervals of 10°)

Conclusions

In the above tests with synthetic sesimograms and with noisy syinthetic data we have the indication that it is possible to determine the focal mechanism solution of the source using the body waves recorded in one single station.

This method works very fast in a PC computer and it can be used to have first solution of a fochal mechanism, with the condition of previous calculation of the Green´s fuctions.

It is possible to improve this method using also the wave polarities. The probability density function for the wave polarities is known, Brillinguer (1980), so the final fdp is the product of both functions: polarity information and body wave information.
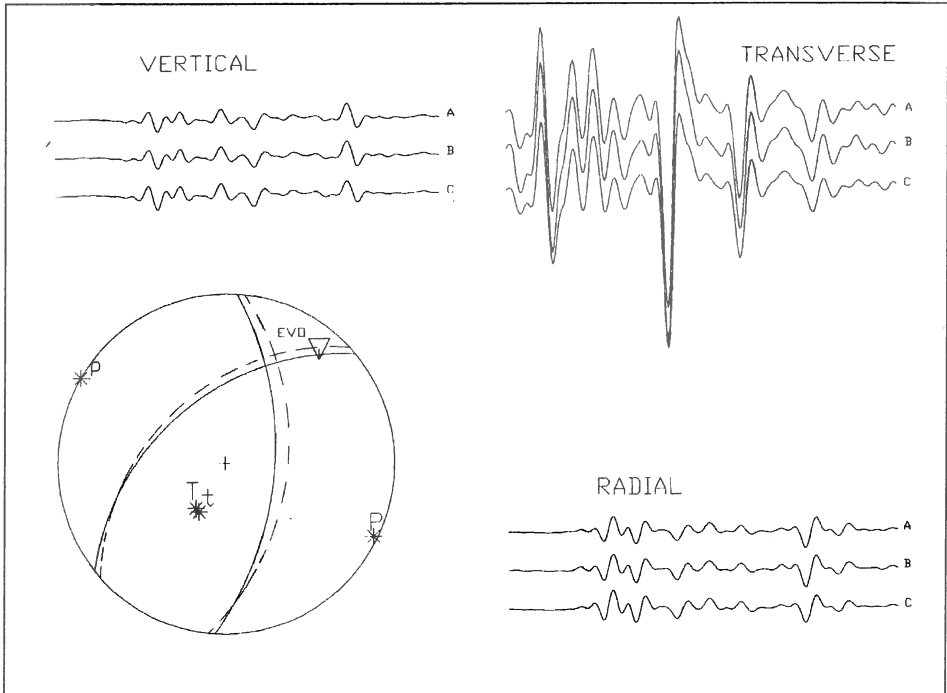
fig.4 Trace A- synthetic seismogram used as input; Trace B- synthetic seimogram with noise used as input; trace C- synthetic seismogram generated by the final solution. Mechanism used as input (projection with continuos line), mechanism inverted from the seismogram with noise (projection with dashed line).

References

Aki, K., Paul G. Richards; 1980. "Quantitative Seismology, Theory and Methods". W. H. Freeman and Company.

Brillinger, D.R., A. Udías, B. A. Bolt; 1980. "A Probability Model For Regional Focal Mechanism Solutions". Bull. Seismol. Soc. Am., **70**, N° 1, pp. 149-170.

Buforn, E, Mezcua, J, Udias, A. (1988). "Seismicity and source Mmechanisms and tectonics of the Azores-Gibraltar plate Bondary, Tectonophysics, **152**, pp. 89-118.

Doornbos, Durk J.; 1988. "Seismological Algorithms *Computational Methods and Computer Programs*". Academic Press

Doornbos, Durk J.; 1988. "Seismological Algorithms *Computational Methods and Computer Programs*". Academic Press

Kikuchi, Masayuki, H. Kanamori; 1991. "Inversion of complex body waves III". BSSA, **81**, pp. 2335-2350.

Kenett, B.L.N; 1985. "On regional S". BSSA, **75**, pp. 1077-1086.

Zollo, Aldo, Pascal Bernard; 1991. "Fault Mechanisms from Near-Source Data: Join Inversion of S polarizations and P Polarities". Geophys. J. Int., **104**, pp. 441-451.

BODY WAVE MODELLING AND SOURCE PARAMETERS DETERMINATION OF THE 23 MAY 1994 CRETE EARTHQUAKE

P. Papadimitriou, J. Kassaras, K. Makropoulos, J. Drakopoulos
Department of Geophysics, University of Athens, 15784 Athens, Greece

ABSTRACT

The Hellenic Trench, convergence zone between Eurasia and Africa, is characterized by a rate of about 6cm.yr^{-1}. Several moderate earthquakes have been located in the south and southwest of Crete, along the Hellenic trench. The focal depths vary between surface and 60 km and the mean slip-vector direction is N22°. The focal mechanisms of these events indicate mainly reverse faulting.

On May 23, 1994 an earthquake of Ms=6.2 occurred near the northern coast of Crete. In this region no large events have been recorded during the last thirty years. Therefore the estimation of the source parameters by teleseismic body wave analysis could not be performed. The only available seismological data for the area of northern Crete, other than the earthquake catalogues, have been provided by microearthquake studies in southern Aegean sea. The recent earthquake of Crete is one of the largest teleseismically recorded in the area. Body wave modelling is applied in this study to determine the source parameters of the earthquake. The determined fault plane solution indicates thrust mechanism with a low angle NE dipping plane and a focal depth at 80km. Considering source parameters calculated also by body wave modelling and microearthaquake results from the experiment of 1988, we conclude that the recent earthquake occurred in the Wadati-Benioff zone, the dip of which is estimated 32° toward the NE, within the African lithosphere and in the bending zone where the frictional process yields an important shear field.

INTRODUCTION

The African and Eurasian lithospheric plates are converging at about 1cm/yr with a N-S orientation (Argus et al.,1989). The Hellenic Trench subduction system, belt of rapid deformation due to the convergence between the two plates in the eastern Mediterranean region, has been a subject of various recent discussions, which attempt to describe the geometry of the motion. McKenzie et al., (1978), based on slip vectors of earthquakes' fault plane solutions and field data, suggest that the convergence rate is at least 70mm/yr in a N202° direction. Le Pichon and Angelier (1979), estimate an average rotation rate of 2-3°/ Myr, predicting velocities of about 10mm/yr at the western edge of the trench, increasing to about 40mm/yr eastwards. Jackson and McKenzie (1988), estimated the convergence velocity of about 100mm/yr and the age of subduction to 5Myr, in agreement with Mercier et al. (1976). Ekstrom and England (1989), calculated the seismic moment release, estimating the azimuth of the velocity vector south of Crete at 163°.

The inferred from seismicity Benioff zone (Comninakis and Papazachos 1980; Martin 1988; Besnard 1991; Hatzfeld and Martin 1992), is not parallel to the trench, dipping gently in the west beneath Peloponnesus steepening 200km from the trench, while being steeper beneath the sea of Crete (Hatzfeld et al. 1993a). Taymaz et al., (1990), calculated the source parameters of teleseismically recorded intermediate moderate earthquakes located near Crete by body waveform modelling, estimating that the slab is striking about N280°, dipping about 35° towards the northeast, while the relative motion between the two plates constrained by the slip vectors azimuth is N25±12°.

Most of the reliably determined fault plane solutions of moderate intermediate earthquakes are located along the trench, while in the north of it there is no evidence for large events during the

last decades. The only focal mechanisms computed at the north of the trench concern microearthquakes recorded during a two months' experiment in the Aegean in 1988 (Hatzfeld et al. 1993a; Hatzfeld et al. 1993b; Besnard 1991). The May 23, 1994, moderate earthquake near the northern coast of central Crete, is the only large event in the specific area, for which the source parameters can be teleseismically determined. In this paper, considering the most reliable intermediate earthquake data available for the area of Crete (ISC locations M>5; best located events and focal mechanisms obtained during the 1988 microseismicity campaign; focal mechanisms computed by waveform inversion methods; the results of the recent Crete earthquake analysis), we are attempting to contribute to the definition of the slab geometry and the stress field distribution of the area of Crete.

DATA AND METHODOLOGY

Body wave inversion applied on teleseismic recordings of IRIS data center distribution is used to determine the source parameters of the May 23, 1994, Crete earthquake. The shape and amplitude of the body waves recorded at epicentral distances between 15 and 90° are compared with synthetic waveforms. For epicentral distances between 15 and 30° we use the Gaussian Beam Sum-
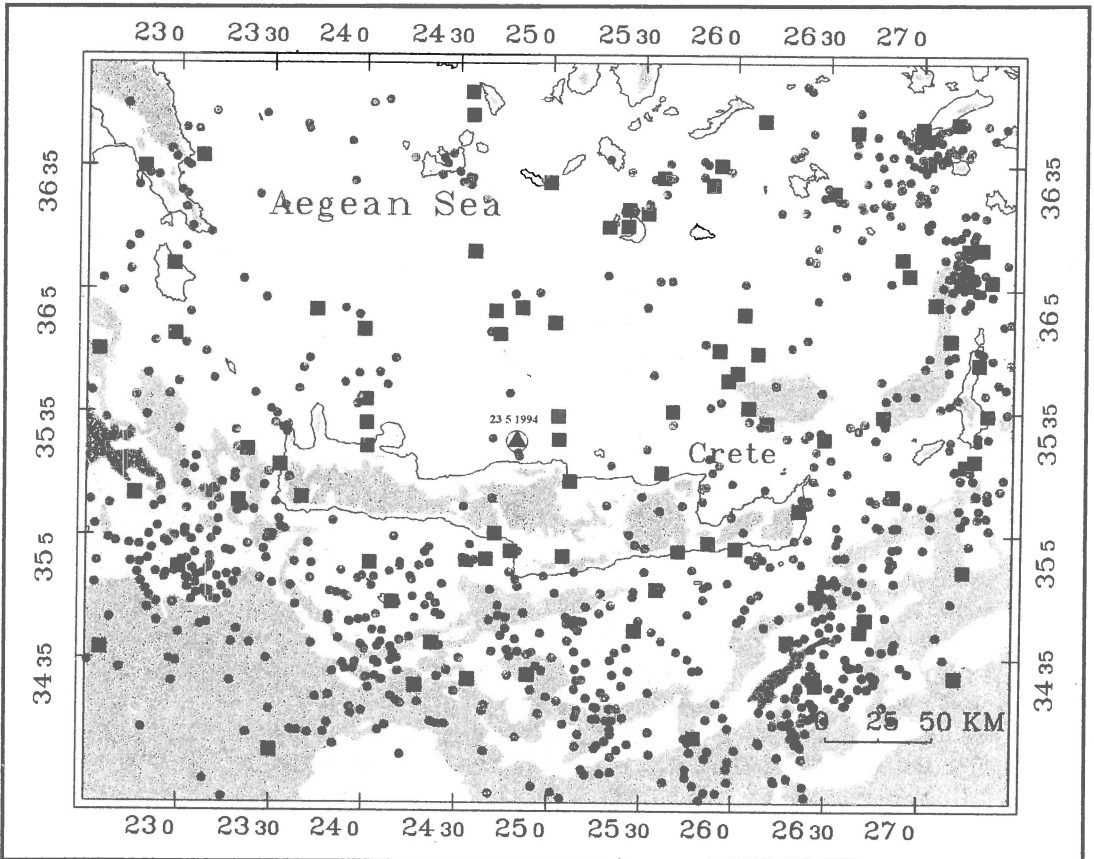
Figure 1. Map of large earthquakes occurred in the area until 1994. Historical data until 1963 are plotted in squares, while circles denote ISC locations during 1963-1994, M>4. The larger symbol represents the epicenter of the under study event.

904

mation Method (GBS) and the EΠ86 velocity model (P. Papadimitriou, 1988). At these distances no standard methods are valid due to the presence of the upper mantle triplications. The GBS method calculates the Green's function, which represents the response of the upper mantle, as proposed by Madariaga and Papadimitriou (1985), using a constrained velocity structure. For epicentral distances between 30 and 90° we use standard methods. The synthetic seismograms are composed by generating direct (P or S) and reflected at the free surface (pP and sP or sS) phases radiated by a point source, assuming a ray propagation in a homogeneous half-space medium (the body waves travel mostly in the lower mantle and the Green's function is simulated as a delta function).

The determined source parameters are compared with those concerning earthquakes located in the surrounding area, estimated by using also modelling techniques (P. Papadimitriou, 1990; Taymaz et al., 1990; Beiber et al., 1990). In addition, source parameters from microearthquake studies (Hatzfeld et al., 1993a,b; Chabalier et al., 1992) are considered, to discuss about the geometry of the slab and the role of the recent earthquake occurred on May 23, 1994.

Hypocentral Location				
Lat.: 35.50	Long.:24.78		Depth: 80km	
Station	Distance	Azimuth	I_h	I_o
ESK	27.60	324.6	42.0	28.8
CCM	85.85	314.6	21.5	15.3
CHTO	66.69	83.0	28.5	20.0
COL	79.77	356.8	23.8	17.0
KONO	26.11	342.4	42.3	29.0
MAJO	85.33	47.9	21.6	15.4
PAB	23.40	288.6	45.3	30.8

Table 1. Hypocenter location of the 23/5/1994 event, the epicentral distances in degrees, azimuths and the angles of incidence-emergence for each station used.

DETERMINATION OF SOURCE PARAMETERS

We retrieved teleseismic digital records from IRIS data center distribution to determine the source parameters of the event. Synthetic seismograms were composed using displacement waveforms sampled at 4 points per seconds. Because of high frequencies presence in the content of the observed seismograms, for each record we deconvolved the instrument response and applied a broad-band Butterworth filter. The May 23, 1994, Crete earthquake has a moderate magnitude and thus, only seven recordings being of good quality are used (table 1), the three of them reported at epicentral distances less than 30°. Synthetic seismograms are generated for a given epicentral distance, depth and focal mechanism and then they are compared to the corresponding observed ones. The best fit between the observed and calculated seismograms is obtained by direct matching.

The body wave modelling is presented in figure 2. The final solution reveals thrust faulting in a depth of 80km and a trapezoidal source time function of 5 seconds duration. The fitting between the observed and the synthetic seismograms is well established at 80km depth, where the pP and sP reflected phases are very clear. The fault plane solution is essentially constrained by the PAB, ESK and CHTO stations because they are situated very close to the nodal planes which control the shape and the amplitude of the direct and reflected phases. In figure 2, we also indicate the epicentral distance for each station in degrees and the value of the seismic moment. The mean value of the seismic moment of the earthquake is 3.2×10^{24} dyn-cm.
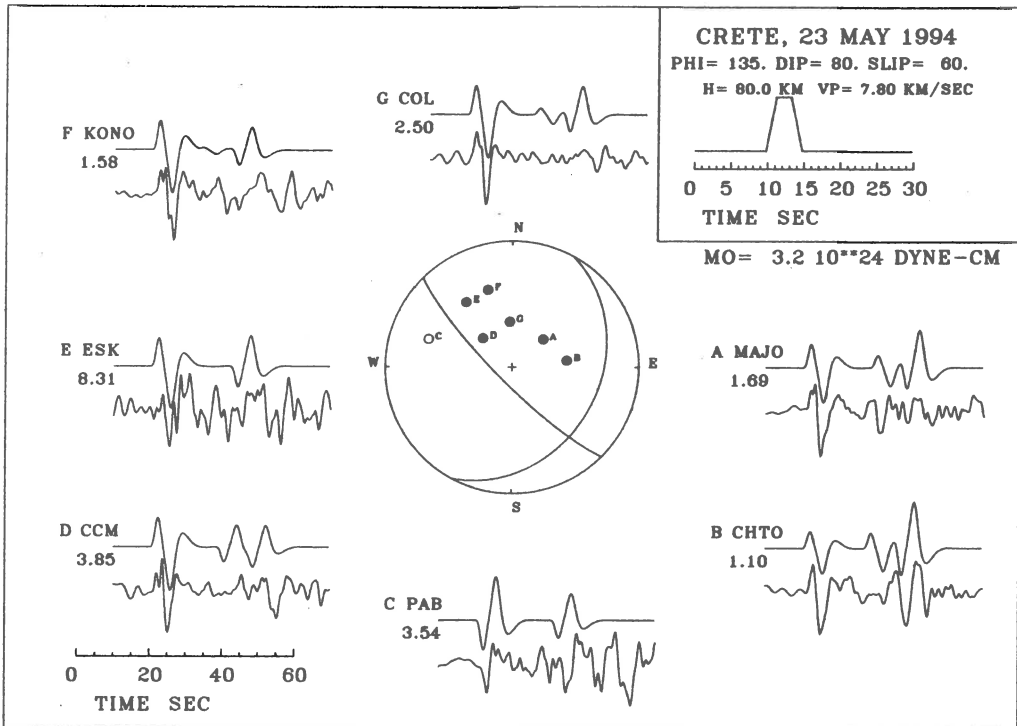
Figure 2. Broad band observed (lower plotted) and synthetic (upper plotted) P waveforms, recorded at teleseismic distances, of the May 23, 1994, Crete earthquake. The synthetics were calculated for a fault plane with strike=135°, dip=80°, rake=60° and focal depth h=80km. The source time function is simple trapezoidal with a duration of 5secs., and the seismic moment M_o=3.5x10^{24} dyn-cm.

DISCUSSION

In figure 1, the locations of large earthquakes occurring in the area of Crete until 1994 (historical and ISC catalogues data, M>4) are plotted. In 1988, a temporary network of 82 portable seismographs was installed for seven weeks over the islands of the southern Aegean Sea and Peloponnesus (Hatzfeld et al., 1993a). During this period, 766 events were recorded, among which 72 have been located deeper than 40 km, with 47 of them located better than 20 km (Hatzfeld et al., 1993b). Comparing the distribution of large events (fig. 1) and microearthquakes (fig. 3), we obtain a similar pattern, with the majority of the epicenters being located along the trench.

The focal mechanisms constrained by modeling methods (Lyon-Caen et al., 1988; Kiratzi & Langston, 1989; P. Papadimitriou et al., 1990; Taymaz et al., 1990; Beiber et al., 1990) and CMT solutions are presented in figure 4. In this figure, we additionally plot fault plane solutions of the 1988 experiment microeartquakes located north of Crete, determined by using first motion P-waves' polarities (Hatzfeld et al., 1993b). The selected micro-earthquakes are included in this paper because their depth distribution exceeds the depth of large earthquakes limited at 40-60 km, except in the case of the 23rd of May, 1994, earthquake, for which the depth is estimated at 80 km. Another reason for using the small events is their higher location precision, as they are recorded by a local
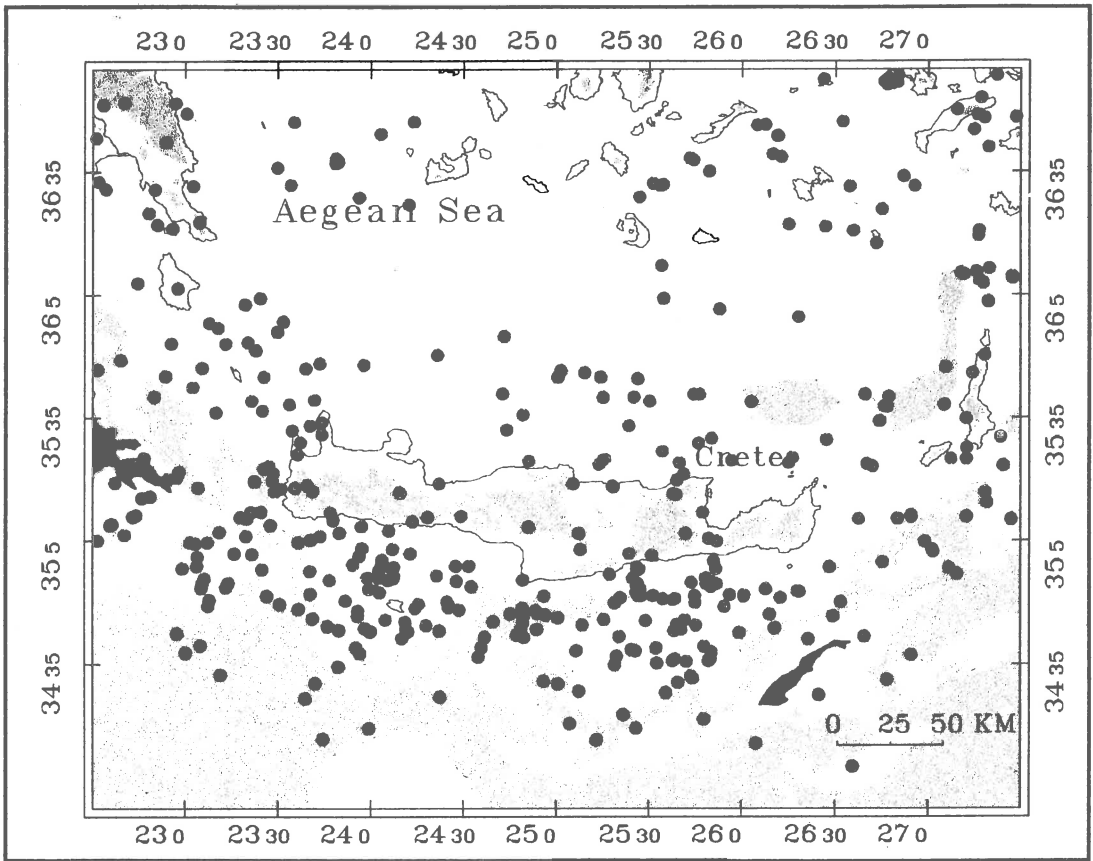
Figure 3. 1988 experiment, microearthquakes' locations.

network, compared to the locations included in the ISC catalogues, estimated using teleseismic recordings. The microearthquake activity reveals only a part of the brittle deformation in time and space, thus it is obvious that the rupture mechanisms of large events could be different and more complex.

The distribution of focal mechanisms along the Hellenic Arc present a complex pattern (figure 4). Normal faulting in N-S direction is observed along the southern edge of the Aegean with a depth distribution from surface to 20 km (Hatzfeld et al., 1993a; Chabalier et al. 1992). This crustal deformation represents an extension parallel to the arc above the subduction zone (Lyon-Caen et al., 1988). Along the Hellenic arc, reverse focal mechanisms are observed with a depth distribution between 20 and 60 km. Taymaz et al., (1990), distinguish the reverse type of mechanisms in three groups: a) low-angle thrust faulting trending in E-W direction b) high-angle reverse faulting trending in E-W direction and c) high-angle reverse faulting with strike-slip motion. The slip vector of groups a and b have both a similar NE direction and nodal planes dipping north. In this configuration, the low-angle thrust mechanisms could be associated to a frictional interface between the subducting African plate and the overriding Aegean lithosphere with the high-angle reverse faulting representing splay faulting off this master thrust surface. Fault plane solutions constrained by P-wave first motion polarities located at a depth between 40km and 130km have approximately similar mechanisms with a and b groups.

A cross section across the Trench, in N22° direction is presented in figure 5.
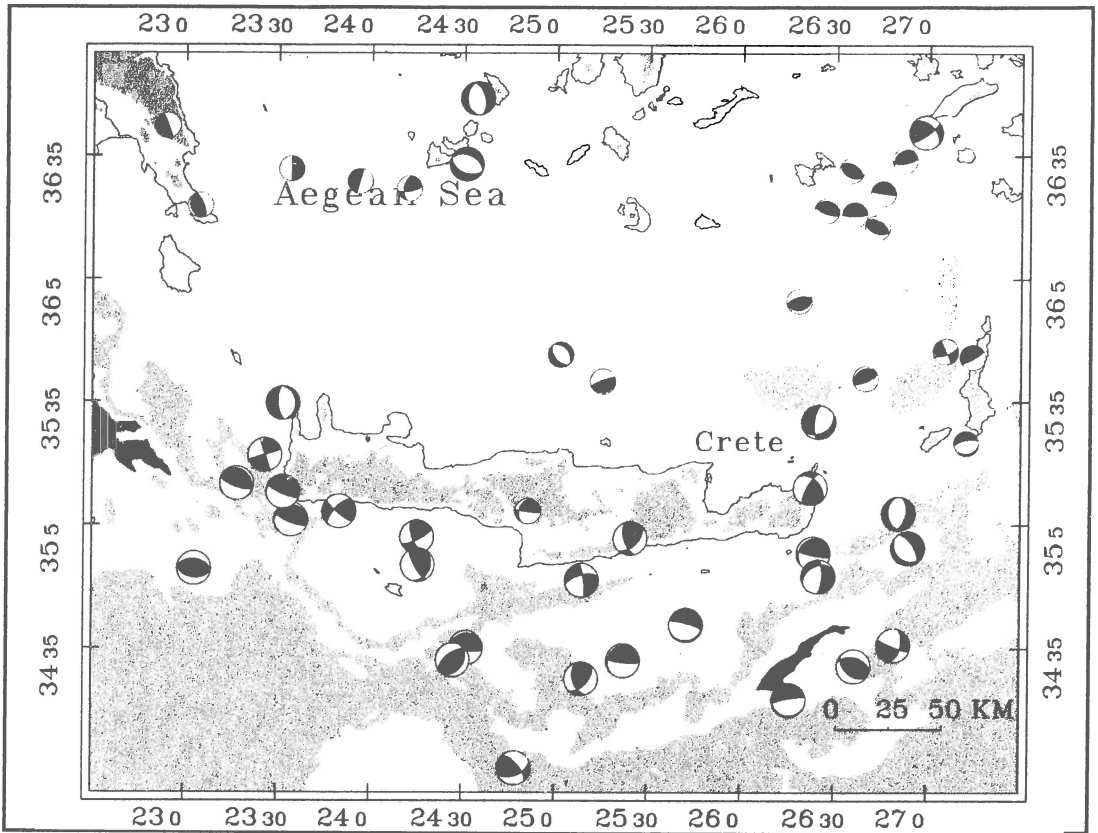
Figure 4. Fault plane solutions available for the area (see text). The large events are represented with the larger focal sphere.

The deep-focus May 23, 1994 earthquake occurred in the Wadati-Benioff zone within the lithospheric slab descending into the mantle. The earthquake is located in the bending zone where the frictional process yields an important shear field. The focal mechanism fits the shallow dipping Wadati-Benioff zone, for wich the dip is estimated at 32° towards the NE. The N-S trending T-axis is aligned to the subducted slab, while the E-W trending P-axis is parallel to the strike of the Hellenic arc south of Crete.

CONCLUSION

The source parameters of the May 23, 1994 Crete earthquake were calculated using teleseismic body-wave analysis by the application of GBS method and the EΠ86 velocity model. The focal mechanism of the event reveals thrust faulting with a N-S trending T-axis, aligned to the subducted slab and an E-W trending P-axis, parallel to the Hellenic arc south of Crete. The depth of the source was estimated in 80 km, within the subducted lithosphere. The considered source parameters for large earthquakes in the area estimated by body wave modeling and those obtained by microeartquake analysis, well define a shallow dipping, of 32° towards the NE, Wadati-Benioff zone. According to this configuration, the studied event occurred within the frictional zone, where the largest intermediate earthquakes along the Hellenic arc were produced during the last years.
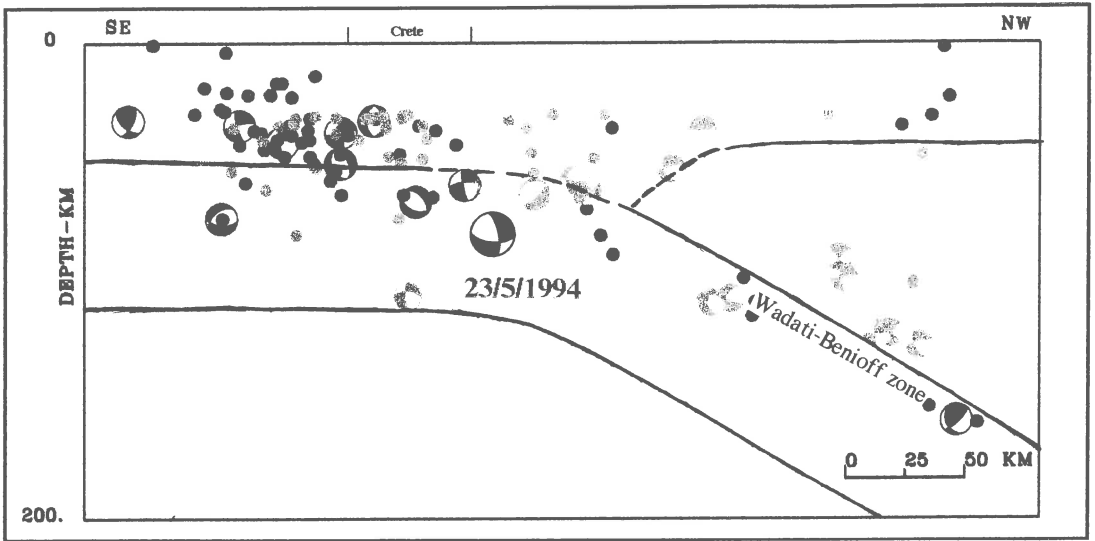
Figure 5. Cross section across the trench, in N22° direction. ISC locations, 1963-1994, M>5 and focal mechanisms constrained by waveform inversion methods (see text), are denoted in black. The microearthquakes' hypocenters located during the 1988 experiment, (z>30km, erx<20km), are denoted in gray.

REFERENCES

Beiber M., Wyss M. and Kind R., 1990. Inversion of source parameters for subcrustal earthquakes in the Hellenic Arc, *Geophys. J. Int.*, **103**, 439-450.

Besnard, M., 1991. Sismotectonique de l'arc égéen, résultats d'une campagne de microsismicité, *Thèse*, Universitè J. Fourier, Grenoble.

Chabalier, J.B., Lyon-Caen, H., Zollo, A., Deschamps, A., Bernard, P. & Hatzfeld, D., 1992. A detailed analysis of microeartquakes in westrem Crete from digital three-component seismpgrams, *Geophys. J. Int.*, **110**, 347-360.

Comninakis, P. E. & Papazachos, B. C., 1980. Space and time distribution of the intermediate focal depth earthquakes in the Hellenic arc, *Tectonophysics*, **70**, T35-T47.

Ekstrom, G. & England, Ph., 1989. Seismic strain rates in regions of distributed continental deformation, *J. geophys. Res.*, **94**, 10231-10257.

Jackson, J. A. & McKenzie, D., 1988. The relationship between plate motions and seismic moment tensors, and the rates of active deformation in the Mediterranean and the Middle East, *Geophys. J. Int.*, **93**, 45-73.

Hatzfeld, D. & Martin. Ch., 1992. The Aegean intermediate seismicity defined by ISC data, *Earth planet. Sci. Lett.*, **113**, 267-275.

Hatzfeld, D., Besnard, M., Makropoulos, K., Hatzidimitriou, P., Panagiotopoulos, D., Karakaisis, G., Deschamps, A. & Lyon-Caen, H., 1993a. Subcrustal microearthquake seismicity and fault plane solutions beneath the Hellenic arc, *J. geophys. Res.*, **98**, 9861-9870.

Hatzfeld, D., Besnard, M., Makropoulos, K. & Hatzidimitriou, P., 1993b. Microearthquake seismicity and fault plane solutions in the southern Aegean and its geodynamic implications, *Geophys. J. Int.*, **115**, 799-818.

Kiratzi, A.A. & Langston, C.A., 1989. Estimation of earthquake source parameters of the May 4, 1972 event of the Hellenic arc by the inversion of waveform data, *Earth Planet. Inter.*, **57**, 225-232.

Le Pichon, X. & Angelier, J., 1979. The Hellenic arc and trench system: a key to the neotectonic evolution of the Eastern Mediterranean region, *Tectonophysics*, **60**, 1-42.

Lyon-Caen, H., Armijo, R., Drakopoulos, J., Baskoutas, J., Delibasis, N., Gaylon, R., Kouskouna, V., Latoussakis, J., Makropoulos, K., Papadimitriou, P., Papanastassiou, D. & Pedotti, G., (1988). The 1986 Kalamata (S Peloponessus) earthquake: detailed study of a normal fault, evidences for east-west extension in the Hellenic Arc, *J. Geop. Res.*, **93**, 14967-15000.

Madariaga, R., & papadimitriou, P., 1985. Gaussian Beam modelling of upper mantle phases, *Ann. Geophys.*, **6**, 799-812.

Martin, Ch., 1988. Géométrie et cinématique de la subduction égéene, structure en vitesse et atténuation sous le Péloponnése, *Thése*, Université J. Fourier, Grenoble.

Mercier, J. L., Carey, E., Philip, H. & Sorel, D., 1976. La néotectonique plio-quaternaire de l'arc égéen externe et de la mer Egée et ses relations avec la sismicité, *Bull. Soc. Géol. France*, **7**, 355-372.

McKenzie, D. P., 1978. Active tectonics of the Alpine-Himalayan belt: the Aegean Sea and surrounding regions, *Geophys. J. R. astr. Soc.*, **55**, 217-254.

Papadimitriou P., 1988. Etude de la structure du manteau superieur de l'Europe et modelisation des ondes de volume engendrees par les seismes egeens, Ph. D. thesis, Univ. of Paris.

Papadimitriou P., Makropoulos K., Drakopoulos J. and Deschamps A., 1990. Source parameters determination of the 21st of June 1984 moderate earthquake in western of Crete (Greece), proceedings of XXII General Assembly of the ESC.

Taymaz, T., Jackson, J. A. & Westaway, R., 1990. Earthquake mechanisms in the Hellenic Trench near Crete, *Geophys. J. Int.*, **102**, 695-732.

THE THEBES FRACTURE ZONE (NEAR ATHENS)

Papazachos,B.C.*, Mountrakis,D.**, Karakaisis,G.F.*, Panagiotopoulos,D.G.* and Hatzidimitriou,P.M.*

* Geophysical Laboratory, University of Thessaloniki, Thessaloniki 54006, Greece
** Dept. of Geology and Physical Geography, University of Thessaloniki, Thessaloniki 54006, Greece

ABSTRACT

On the basis of instrumental and historical seismological data, supported by geomorphological and geological information, a fracture zone which has an almost east-west direction and a total length of about 60 Km has been identified in central Greece. It connects the northern end of the southern Evoikos gulf with the Alkionides gulf (eastern part of the Corinth gulf) following the Libadostras and Asopos river valleys. Strong historical and present century earthquakes generated in this zone caused destruction in Thebes and other cities and villages located in the zone. Such earthquakes affected also Athens which is located in a distance of only 40 Km from the central part of the zone. Five strong earthquakes ($M_S \geq 6.0$) occurred in this zone during the last one and a half century (1853, 1893, 1914, 1938, 1981). Macroseismic data were used to define the rupture area for each of these shocks. It is found that these five rupture areas trend parallel to the zone and cover the whole fracture zone. A reliable fault plane solution for the last of these earthquakes and geological information shows that this is a fracture zone of normal faulting. Information, based on seismicity quiescence and migration of seismic activity, indicates that there is a high probability for a strong earthquake ($M_s \geq 6.0$) to occur in the eastern or central part of the zone during the next decade (1995-2004).

INTRODUCTION

There are two very well known fracture zones of shallow earthquakes in central Greece which affected Athens in the past and very propably will affect this big city also in the future. The first of these zones is the fracture zone of the northern Evoikos gulf where the last destructive earthquake occurred on 27 April 1894 (38.7°N, 23.0°E, M_S =7.0) and the other is the fracture zone of the Corinthiakos-Saronikos gulfs where the last destructive earthquake occurred on 24 February 1981 (38.1°N, 22.9°E, M_S = 6.7). Both these earthquake affected seriously Athens too.

There is, however, a third fracture zone in central Greece, which is closer to Athens (40 Km north of Athens) but is not well known, although this zone is very active too. This zone has an almost east-west direction, is slightly curved to the north and joins the northern end of the southern Evoikos gulf with the Alkionides gulf (eastern end of Corinthiakos gulf). The largest city in this zone is Thebes, which is located in the central part of the zone and has been repeatedly destroyed by its earthquakes. This is the reason why we call it "Thebes Fracture Zone".

The purpose of this paper is to define accurately this fracture zone, to determine its seismotectonic properties by the use of seismological, geomorphological and geological information and to examine its potential for the generation of a strong earthquake.

THE LAST LARGE EARTHQUAKES OF THE ZONE

There are several cases of historical earthquakes for which evidence exists that their epicenters are in this zone (e.g. 1321, 1694). Accurate information are available for all strong earthquakes ($M_S \geq 6.0$) which occurred in this zone during the last one and half century. There are five such earthquakes for which their dates, origin times, epicenters, surface wave magnitudes, M_S, and the value and place of maximum macroseismic intensity (I_o), are known (Table 1). The source for this information is the book of Papazachos and Papazachou (1989) but
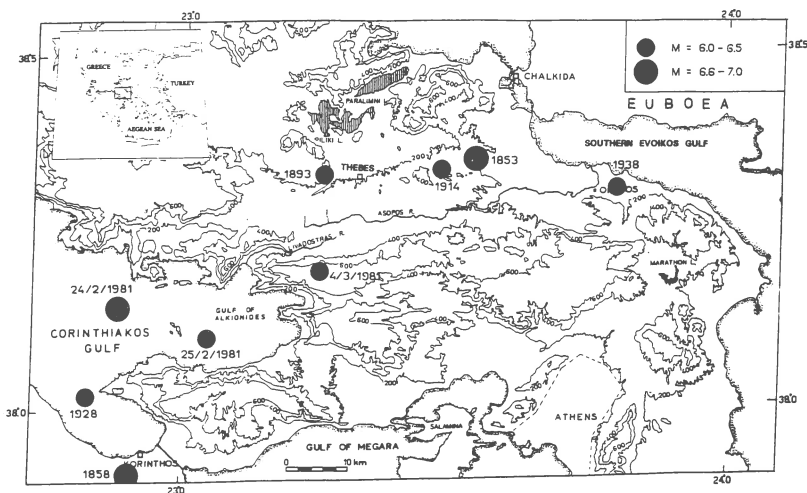
Fig. 1. The epicenters of the strong mainshocks ($M_S \geq 6,0$) since 1853 in the Thebes zone on a topografic map.

Table 1. Information on the most recent strong ($M_S \geq 6.0$) earthquakes in the Thebes fracture zone.

Date	Origin Time	Epicenter	M_S	I_o
18. 8.1853	08:30	38.35°N, 23.52°E	6.8	(X, Thebes)
27. 5.1893	22:02	38.33°N, 23.26°E	6.0	(VIII,Thebes)
17.10.1914	06:22	38.33°N, 23.48°E	6.1	(VIII,Thebes)
20. 7.1938	00:23	38.29°N, 23.79°E	6.0	(VIII,Oropos)
4. 3.1981	21:58	38.19°N, 23.25°E	6.3	(IX, Plataees)

some minor modifications were made on the basis of additional information concerning macroseismic observations (Ambraseys and Jackson, 1990) and instrumental data (Papazachos C.; 1994). All these five earthquakes are very shallow (h ~ 10Km).

Figure (1) shows a topographic map of the broader area (part of the topographic map published by the National Statistical Service of Greece) where the

epicenters of all strong earthquakes ($M_S \geq 6.0$) which occurred in this area during the last 150 year are depicted by circles of sizes according to their magnitudes.
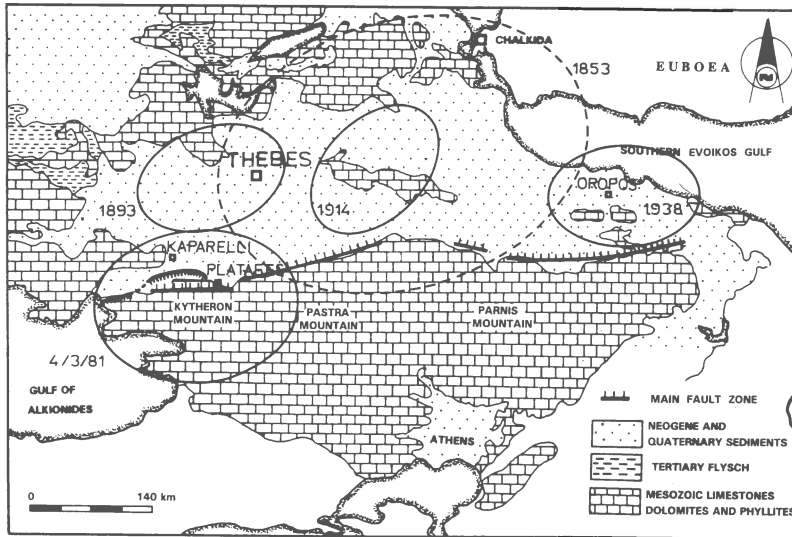
Fig. 2. The rupture areas of the five earthquakes on a geological map, showing the main E-W fault zone and the neotectonic graben of Thebes.

The relation of the spatial distribution of the five earthquakes listed in Table (1) with the geomorphology of the area is obvious. These five earthquake epicenters are distributed in an almost east-west direction and follow the valleys of Livadostras and Asopos rivers in the northern feet of the Kytheron-Pastra-Parnis mountain range.

The 1853 shock is the largest ($M_S = 6.8$) known earthquake of the zone. It destroyed Thebes and caused very serious damage in Chalkida. It also affected Athens. The 1893 shock caused damage in Thebes and in the villages west of this city and the 1914 shock caused damage in the same city and in the villages east of the city. The 1938 shock caused damage in the eastern part of the zone, while the 1981 earthquake occurred in the southwesternmost part of the zone and destroyed the villages Kaparelli and Plataees. This last earthquake is considered as the second largest aftershock of the strong main shock ($M_S = 6.7$) which occurred on 24 February 1982 in the Alkioneds gulf (Papazachos et al., 1981) where also the largest aftershock occurred on 25 February 1981 (see fig.1). Therefore, the earthquake of 4 March ($M_S = 6.3$) occurred in the boundary of the fracture zone of the east Corinthiakos gulf and of the Thebes fracture zone.

THE RUPTURE AREAS OF THE LARGE EARTHQUAKES

The rupture area (or rupture zone) of an earthquake is the area around its fault which is deformed before the generation of the earthquake and supplies the seismic wave energy. This area can be defined by several methods which depend on the available data. Determination of the spatial distribution of aftershock foci, mapping of the surface fault traces, location of the tsunamogenic source and definition of the meizoseismal area (area of maximum macroseismic intensity) are some of the simpler

913

but very effective such methods (Kelleher et al., 1972; Papazachos et al., 1993). The length of the maximum horizontal dimension of a rupture area of an earthquake is considered to be equal to its fault length, L. For the shallow earthquakes in Greece, this length can be calculated by the relation:

$$logL = 0.51M_S - 1.85 \qquad (1)$$

where L is measured in Km and M_S is the surface wave magnitude (Papazachos and Papazachou, 1989).

The rupture zones of the five strong earthquakes listed on Table (1) have been basically defined by the use of macroseismic intensity data and the results where checked by the use of other information (distribution of aftershocks, surface fault traces, tsunami) when such data were available.
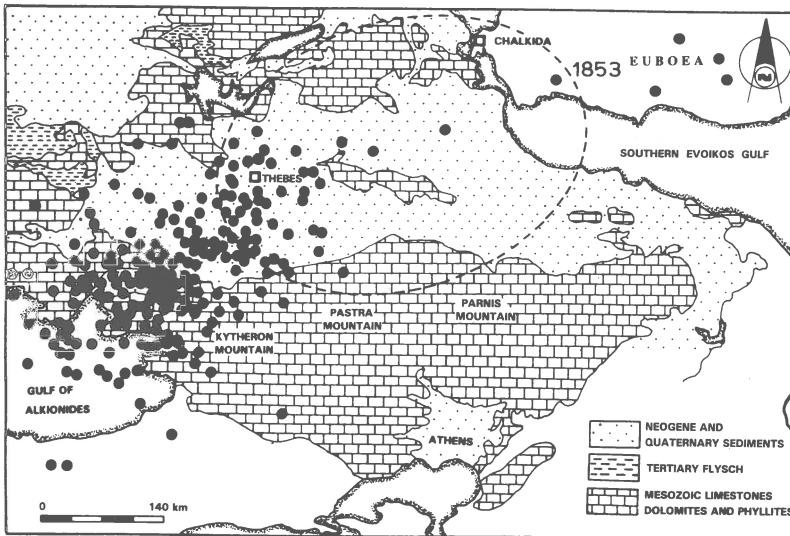
Fig. 3. Epicenters of the small earthquakes ($M_s \geq 4,0$) which occurred in the area during the period 1981-1993 and the rupture area of the 1853 earthquake.

As rupture area for each of the last four strong earthquakes (1893, 1914, 1938, 1981) has been considered the synthetic isoseismal which has maximum axis given by the relation (1). These synthetic isoseismals have been determined by the application of a method suggested by C.Papazachos (1992) on the available macroseismic data. It uses all observed values of the macroseismic intensity of an earthquake and takes into consideration the anisotropic radiation, the geometric spreading and the anelastic attenuation. This method has been proved very effective for determining the rupture areas since its results are in very good agreement with the results of other methods (Papazachos et al., 1993). In previous cases (Papazachos et al., 1985, 1993) as well in the present four cases, the isoseismal of intensity VIII (in MKS scale) defines well the rupture area. Several sources of macroseismic information were used in the present study (Ambraseys and Jackson,1990; Papazachos and Papazachou,1989).

914

The rupture areas for these four earthquakes are shown by solid elliptical lines on a geological map in figure (2). For the rupture area of the 1981 earthquake, there are also information concerning its surface fault trace (Papazachos et al., 1981) and accurately located aftershocks (Papazachos C., 1994). The observed fault trace for the 4 March 1981 shock is also drown in figure (2). This fault trace and almost all well located aftershocks are in the rupture area determined by the macroseismic method.

For the 1853 earthquake there are no enough macroseismic data to apply the above mentioned method for defining its rupture area. There are, however, some very reliable other information which can be used to accuratly locate its rupture area. As we have already mentioned, this earthquake destroyed Thebes and caused very serious damage in Chalkida. It also caused a tsunami in the southern Evoikos gulf (Papazachos and Papazachou, 1989). This clearly shows that Thebes and a part of the Evoikos gulf are in the rupture area of this earthquake and that Chalkida is in or very close to this rupture area. Based on this information and taking its maximum dimension equal to that given by the relation (1) and its ellipticity equal to the mean ellipticity calculated for the other four shocks, the rupture area of the 18.5.1853 shock was defined and is represented by a dashed elliptical line in figure (2). Its two largest aftershocks (on 29 and 30 September) caused very serious damage in Chalkida which indicates that the rupture started in the western part of the fault and migrated to the east. Such a procedure, in which the rupture from the focus of the mainshock, which is usually located close to the one end of the fault, propagates to the other end of the fault where the largest aftershock occurs is a very usual phenomenon for shallow earthquakes in Greece (Karakaisis et al., 1985). It is interesting to note that a surface fault trace was observed in the eastern end of this rupture zone (between Chalkida and Eretria) during a strong earthquake in ancient time, as it mentioned by Strabo in its Geographica.

Figure (2) shows a very interesting relation between the geology of this fracture zone and the distribution of the rupture areas of the five earthquakes. The rupture areas of these five shocks (1853, 1893, 1914, 1938, 1981) cover the Livadostras-Asopos valeys and the whole geological graben of Thebes which is filled in by Neogene and Quaternary. The Thebes graben has been formed in Neogene times (probably in late Miocene) by a main fault zone trending E-W and dipping to the North (fig. 2) which is shown on the seismotectonic map of Greece (IGME, 1989). The fault zone consists of several neotectonic faults along the same fracture line in the northern feet of the Kytheron-Pastra-Parnis mountain range, in the boundary between the bedrock (Mesozoic carbonates and phyllites) and the Neogene and Quaternary deposits of the graben.

Based on one available fault plain solution for this zone, which is that of the 4 March 1981 (Papazachos et al., 1984), and on the fact that the active stress field in central Greece is tensional with the maximum tensional component being horizontal and having an almost north-south direction (Papazachos and Kiratzi, 1992), we can safely conclude that this graben is composed of the hanging walls of the normal faults which caused these earthquakes. It is not known, however, if the first four of these earthquakes were generated on the main normal fault zone which dip to the north or on antithetic normal small faults which dip to the south. The earthquake of 4 March 1981 was generated on a fault which dips to the south (see fig.2).

EVIDENCE FOR THE SEISMIC POTENTIAL OF THE ZONE

The city of Thebes has been repeatedly struck by high seismic intensities (see Table 1) which indicates that a strong barrier exist close to this city. This is propably a geometric barrier since this fracture zone is slightly bent to the north with a maximum benting just east of Thebes. A further evidence for the existence of this barrier is the fact that the microseismic activity which followed the 1981 seismic sequence in the Alkionides gulf migrated to the northeast and reached the area of Thebes where it stopped.

Figure (3) shows the spatial distribution of the small earthquakes ($M_S \geq 4.0$) which occurred in this area between 1981 and 1991 and the rupture area of the 1853 earthquake. It is observed that this microseismic activity covers the western part of this fracture zone but it did not affect its eastern part where the 1853 earthquake occurred. It means that the eastern part of the zone is a seismic gap of the second kind, according to the term used by Mogi (1979), where a strong earthquake may occur.

A migration of the strong earthquake seismic activity from the Alkionides in 1981 (see fig.1) towards the Thebes seismic zone in the future is probable because such eastward migration of seismic activity in central Greece has been observed in the past. Such an example is the migration of the epicentrers of the strong earthquakes in the Thebes zone during the period 1893-1938 (see fig. 1).

The maximum magnitude of the expected earthquake will be equal to 6.8 if this earthquake breaks the whole central and earthern part of the fracture zone or smaller (e.g. 6.0) if it breaks part of it. For an earthquake with that magnitude the probability for its occurrence in the eastern or central part of the zone can be calculated by the time predictable model (Papazachos and Papaioannou, 1993) and is equal to 0.57, if we do not take into account the 1981 earthquake which is located in the westernmost part of the zone.

CONCLUSIONS

Historical and instrumental seismological data, supported by geological and geomorphological information, shows the existence of a very active fracture zone 40 Km north of Athens, the so called Thebes zone, which has an almost east-west direction and joins the eastern part of the Corinthiakos gulf (Alkionides gulf) with the northern part of the southern Evoikos gulf. This zone is a neotectonic graben with Neogene and Quaternary sedimentary deposits which is formed by the hanging walls of the normal faults which produce earthquakes with magnitudes up to 6.8.

Observations, concerning quiescence of recent small earthquakes and eastward migration of strong earthquakes, indicate that the occurrence of a strong earthquake can occur in the eastern or central part of the zone. The maximum magnitude of this earthquake is equal to 6.8. The probability for the occurrence of an earthquake with M>6.0 in this zone during the decade 1995-2004 is 0.57. This earthquake will affect seriously the cities and villages in the zone. It will also affect Athens since its epicenter will be in a relatively short distance from this very large city.

REFERENCES

Ambraseys, N. N. and Jackson, J. A. 1990. Seismicity and associated strain of central Greece between 1890 and 1988. Geophys. Jour. Intern., 101, 1-46.

IGME, 1989. Seismotectonic map of Greece with seismological data. Institute of Geology and Mineral Exploration(IGME).

Karakaisis, G. F., Karacostas, B. G., Papadimitriou, E. E., Scordilis, E. M. and Papazachos, B. C. 1985. Seismic sequences in Greece interpreted in terms of barrier model. Nature, 315, 212-214,.

Kelleher, J. 1972. Rupture zones of large south America earthquakes and some predictions. Jour. Geophys. Res., 77, 2087-2103.

Mogi, K. 1979. Two kinds of seismic gaps. Pageoph, 117, 1172-1186.

Papazachos, C. B. 1992. Anisotropic radiation modelling of macroseismic intensities for estimation of the attenuation structure of the upper crust in Greece. Pageoph, 138, 445-469.

Papazachos, C. B. 1994. A study of the crust and upper mantle in Southeastern Europe by inverting seismic and gravimetric data. Phd. Thesis, University of Thessaloniki, 204pp.

Papazachos, B. C., Comninakis, P. E., Mountrakis, D. M. and Pavlides, S. B. 1981. Preliminary results of an investigation of the February-March 1981 Alkyonides gulf (Greece) earthquakes. Proc. Intern. Symp. Hellenic Arc and Trench, Athens, April 1981, 2, 47-87.

Papazachos, B. C., Comninakis, P. E., Papadimitriou, E. E. and Scordilis, E. M. 1984. Properties of the February-March 1981 seismic sequence in the Alkyonides gulf of central Greece. Annales Geophysicae, 2, 537-544.

Papazachos, B. C., Koutitas, Ch., Hatzidimitriou, P. M., Karacostas, B. G. and Papaioannou, Ch. A. 1985. Source and short-distance propagation of the July 9, 1956, southern Aegean tsunami. Marine Geology, 65, 343-351.

Papazachos, B. C. and Papazachou, C. B. 1989. The earthquakes of Greece. Ziti Publications, Thessaloniki, 356pp.

Papazachos, C. B. and Kiratzi, A. A. 1992. A formulation for reliable estimation of active crustal deformation and its application to central Greece. Geophys. Jour. International, 424-432.

Papazachos, B. C. and Papaioannou, Ch. A. 1993. Long term prediction in the Aegean area based on a time and magnitude predictable model. Pageoph, 140, 593-612.

Papazachos, B. C., Hatzidimitriou, P. M., Karakaisis, G. F., Papazachos, C. B. and Tsokas, G. N. 1993. Rupture zones and active crustal deformation in southern Thessalia central Greece. Boll. Geof. Teor. ed Appl., 139, 363-374.

GEOLOGICAL ESTIMATES OF SEISMIC HAZARD PARAMETERS ALONG THE GREAT SUMATRAN FAULT ZONE (INDONESIA)

Olivier BELLIER and Michel SEBRIER

URA-CNRS - Géophysique et Géodynamique Interne, Bât. 509, U. Paris-Sud, 91405 ORSAY Cedex, FRANCE

ABSTRACT

The 1650-km-long Great Sumatran Fault (GSF) is a NW-trending dextral strike-slip fault that parallels the trench and approximately follows the magmatic arc, from the Andaman sea to the Sunda Strait. To characterise the deformation parameters along the Sumatran Arc, accurate estimates of the long-term slip rates have been conducted, using geomorphic features analysed on SPOT images. Theses long-term dextral slip rate decreases southward along the GSF from about 23±2 mm/yr (2°N) to 6±4mm/yr (5°S). Thus, seismic hazard has to be expected higher in northern Sumatra than in southern Sumatra. This study permits to expect also a distribution of seismic deformation throughout the arc domain. Morphological and paleoseismic observations conducted in southernmost Sumatra support a minimum recurrence interval of 400 year for the maximum expected earthquake of Mw=7.3, calculated using the method of the seismic moment. Therefore, in northern Sumatra, one should expect that such size comparable earthquake may have a minimum recurrence interval of the order of 150 years. A large scale segmentation map complemented by major earthquake ruptures have been realised. This provides evidences of several major releasing stepovers and two restraining bends which permit to individualised 18 major fault segments with lengths ranging between 45 and 200 km. The northward increase of the segment lengths could be correlated with the slip rate increase, and corresponds to a northward seismic hazard increases that agrees with the historical seismicity.

INTRODUCTION

Paleoseismology and seismic hazard studies are very difficult to perform with significant results in and around moderate seismicity area under wait temperate climate as for example in European and Mediterranean countries : in France, in North Spain and Italy, in Belgium... To get experiences of this kind of study in wait area, we begun to perform analyses along the Great Sumatran fault which is an active fault system in a wait tropical area. When we begun this analyses, it was probably one of the first paleoseismologic study in wait tropical region.

The 1650-km-long Great Sumatran Fault (GSF) is one of the major strike-slip fault system in the world. Global modelling proposed maximum horizontal slip-rates ranging between 40 and 60 mm/yr [Jarrard, 1986; Mc Caffrey, 1991] along the GSF. Consequently, it could be one of the faster fault, in the world. However, the segmentation characteristics, long-term as well as instantaneous slip-rates and seismic hazard parameters are very poorly constrained in spite of recent active tectonics studies [e.g., Sieh et al, 1991; Bellier et al., 1991; Sébrier et al., 1992; 1993; Bellier and Sébrier, 1994]. The GSF is a NW-trending dextral strike-slip fault zone, that parallels the trench and approximately follows the Sumatran magmatic Arc, from North to South, from the Andaman Sea back-arc basin to the Sunda Strait extensional domain (Figure 1). Off Sumatra, the N3°-20°E-trending convergence [DeMets et al., 1990; McCaffrey, 1991] is oblique and, mechanically, has to be accommodated both by subduction (convergence component normal to the trench) and strike-slip deformation (convergence component parallel to the trench) [Fitch, 1972; Beck, 1983]. Most of this strike-slip deformation appears localised on the GSF [Fitch, 1972; Jarrard, 1986; Mc Caffrey, 1991]. In order to constrain the geometry and segmentation of this major active fault, and to precisely analysed its seismic hazard, we realised a large scale segmentation map based on morphologic and topographic characteristics. We complemented this segmentation map reporting the major earthquake ruptures on the basis of an historic seismicity study, since 1835. Although several damaging historical earthquakes are known [e.g, Katili and Hehuwat, 1967; Deverchère and Louat, 1993; Beaudoin et al., 1995], few teleseismic epicentres appear to be located on this fault. Unfortunately, this could indicate that the fault has a dominantly strike-slip mechanical behaviour and is nearly locked between major seismic events. In order to evaluate whether or not the GSF has a high seismic potentiality, the long-term slip rate has to be accurately calculated. To calculate this key parameter, we performed an along strike survey of the GSF System with SPOT images. Our purpose was to detect any evidence of fault offsets in order to determine slip-rate along the fault zone. At the same time we performed trench observations across the southernmost segment (Semangka Valley) of the GSF to constrain the superficial source parameters of the active fault; i.e., fault geometry, fault kinematics, slip value per event, and recurrence interval between major events.

Figure 1 : Regional geodynamic framework of the Sumatran Arc where we represent the Great Sumatran Fault and Mentawaï Fault Zones.

Inset at bottom left : SW-trending cross-sectional sketch across the Sunda Arc subduction (Sumatran segment). 1: Fore-arc and back-arc basins; 2: continental crust and subcrustal lithospheric mantle; 3: oceanic lithosphere. G.F.Z. : Great Sumatran Fault and M.F. : Mentawaï Fault.
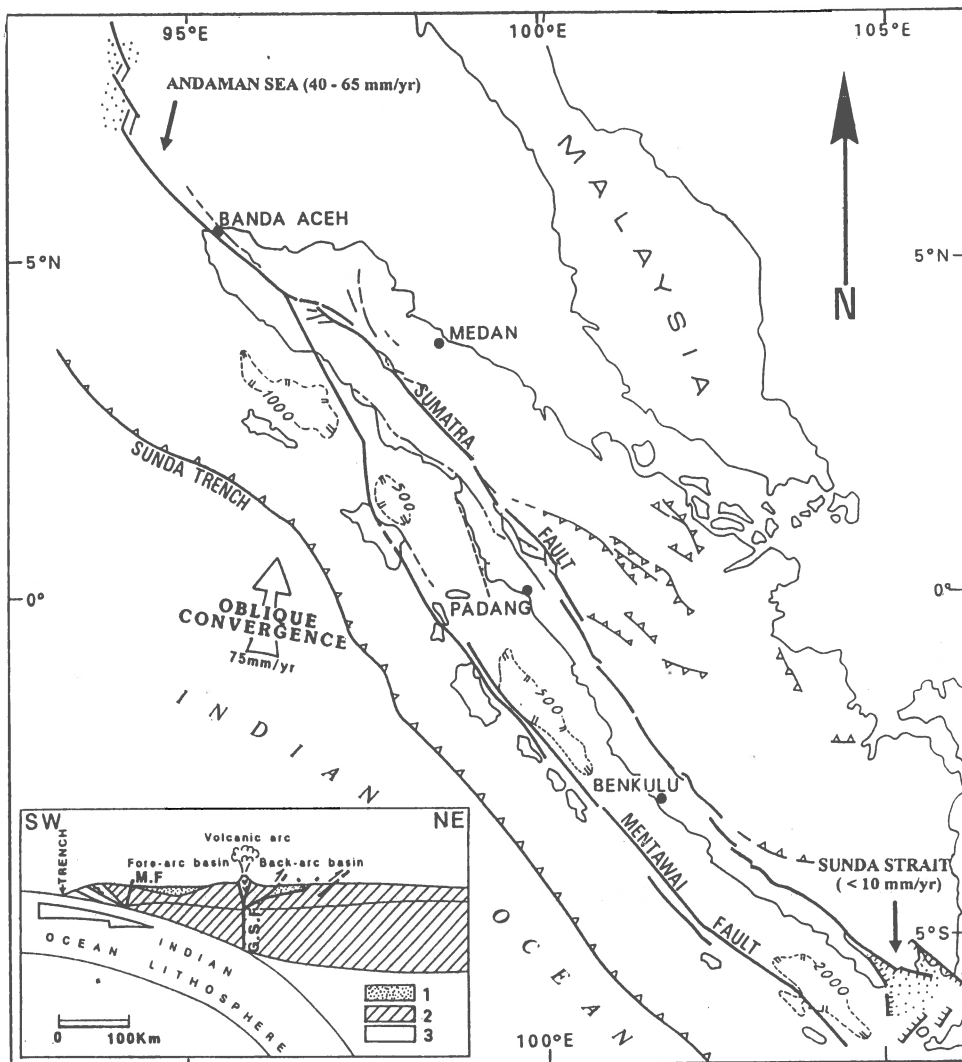
PALEOSEIMOLOGY IN SOUTH SUMATRA : TRENCHING OBSERVATIONS

In order to define precisely the slip rate and recent seismic history of the GSF, we excavated four trenches in its southernmost part (Figure 2), where the strike-slip movement changes to oblique-normal faulting. Thus, we could expect to analyse more easily dip-slip evidence than strike-slip in a trench excavated under wet tropical conditions. The trenches were located at the foot of the 800-m high, east-facing escarpment that limits the Semangka Valley to the West. All the trenches were excavated at the base of triangular facets not affected by landslides and out of reach of major alluvial fans. In order to avoid water table problems the excavations were performed at the end of the dry season. The trenches were 20 to 25 m long, and up to 4.6 m deep. They exposed a colluvial wedge in fault contact with a relatively unweathered bedrock and a thin slope wash (Figure 2). The occurrence of only one paleosoil indicates that in wet tropical climate the degradation rate of organic material is faster than seismic recurrence. Scarp heights and slip vectors on major fault planes allow us to better constrain the dextral slip rate of the southernmost GSF and confirms a maximum velocity of about 10 mm/year.

Expected $M_W$max on the Semangka segment (southernmost Sumatra) : Trenching observations [Sébrier et al., 1992; 1993; Pramumijoyo, 1991] permitted us to estimate the parameters that are necessary to calculate of the maximum expected magnitude ($M_W$max). In order to calculate $M_W$max, we used the method of the seismic moment (Mo) [Brune, 1968; Hanks and Kanamori, 1979; Kanamori, 1983].

-> $Mo = \mu.D.L.h$

-> $M_W = (\log(Mo) - 16.1)/1.5$

(μ, shear modules $= 3.10^{11}$ dynes/cm^2; D, fault displacement; L, fault length; h, fault width)

Taking D = 2 m, L= 65 km, and h = 20 km (for values see Sébrier et al. [1992; 1993]), we obtained :

->$Mo = 1.092 \times 10^{27}$

-> $M_W$max = 7.3

Estimation of the recurrence interval in southernmost Sumatra : In southernmost Sumatra, along the Semangka fault segment of the GSF System, we calculated a maximum dextral slip-rate of about 10 mm/year and estimated a maximum magnitude $M_W$max = 7.3. Considering the estimated slip per major event D $\approx$ 2 m, a minimum recurrence interval of 400 years was deduced from these estimates [Sébrier et al., 1992; 1993]. Since the fault displacement is not only due to major events this 400 years recurrence interval must be considered as a lower bound value. Therefore, in northern Sumatra, one should expect that such size comparable earthquake may have a minimum recurrence interval of the order of 150 years.

The 14 February 1994 Liwa earthquake (M_W =6.88) occurred at 17:07 GMT and reactivated part of the Ranau-Suwoh segment that we recognised and mapped as an active 65±2 km long segment of the south GSF [Bellier et al., 1991; Bellier and Sébrier, 1994]. It caused deaths and damages, but field study did not report seismic surface rupture. The rupture has not been transmitted up to the surface owing to the rheological characteristics of the Quaternary Ranau Tuff that extensively covers the region. The seismogenic depth (18±3 km) and the reactivated segment length (25±1 km) have been given by the preliminary results of the aftershock study [Deverchère et al., 1994]. Knowing these values and the seismic moment ($M_o = 2.1 \ 10^{26}$ dyne.cm, Harvard GMT solution), we deduced a co-seismic displacement of about 1.6 ± 0.3 m.

RIGHT-LATERAL DISPLACEMENT OF THE GREAT SUMATRAN FAULT

Even if the GSF is one of the major structures of the Sumatran overriding plate, no accurate slip rate have been reported and this slip parameter is crucial to elucidate seismic deformation mechanism associated to oblique convergence. In order to analyse the active deformation detailed mapping and morphological analysis of the surface fault traces with high resolution SPOT images have been developed (pixel sizes being 10 m for Panchromatic and 20 m for Multispectral mode images, respectively). This image analysis further completed by stream offsets reported on topographic maps permitted us to accurately calculate the right-lateral strike-slip rate along of the GSF.

Previous estimates of the dextral slip rate of the Great Sumatran Fault : The slip rate of the GSF has been either indirectly estimated from global plate motions and opening rate of nearby basins. Assuming that the strike-slip motion along the GSF could accommodate the trench parallel component of the oblique convergence between the Indo-Australian and Eurasian plates, the theoretical maximum slip rate of the GSF estimated by global modelling should range between about 40-60 mm/yr [Jarrard, 1986; McCaffrey, 1991]. The other indirect estimate may be deduced opening rate of the both Andaman Sea back-arc basin and of the Sunda Strait. Previous offshore studies showed that the Andaman Sea back-arc basin opening rate is of at least 40 mm/yr during the last 10-13 Ma [Curray et al., 1979]. In addition, the Sunda Strait opening rate is less than 10 mm/yr during the last 6 Ma [Lassal et al., 1889]. As the Andaman opening motion should be transferred to the Sunda Strait extensional area by the GSF, these first estimates from offshore studies suggest a difference of the fault slip rate between northern and southern Sumatra; i.e., between the Andaman sea and the Sunda Strait

Figure 2 : Structural map from the Lake Ranau to the Semangka Bay deduced from structural interpretations of SPOT (K/J: 278/360 (7/16th 1989) and LANDSAT (133/64 and 133/63) images. Arrows along the Semangka fault point to trenche locations.

Inset right represent an example of trench section across the Semangka fault segment (southernmost Sumatra - 5°10'S). a, paeosoils; b, colluvium; c, weathered (Oligocene?) volcanic substratum; d, fault planes observed in the trench.

Inset at bottom left : Interpretation of a detail view of K/J-278/360 SPOT image showing offsets, from North to South, of the caldera rim, of a lineament, and of streams; arrows pointing to the horizontal offsets.
1: Major active faults of the SFZ; 2: Minor active faults; 3: Minor active faults with a dominant normal component (hatchured on the downthrown block); 4: Quaternary alluvial and volcano-sedimentary deposits; 5: Volcanoes; 6: Caldera rims of Ranau and boundary of the Suwoh caldera cluster.
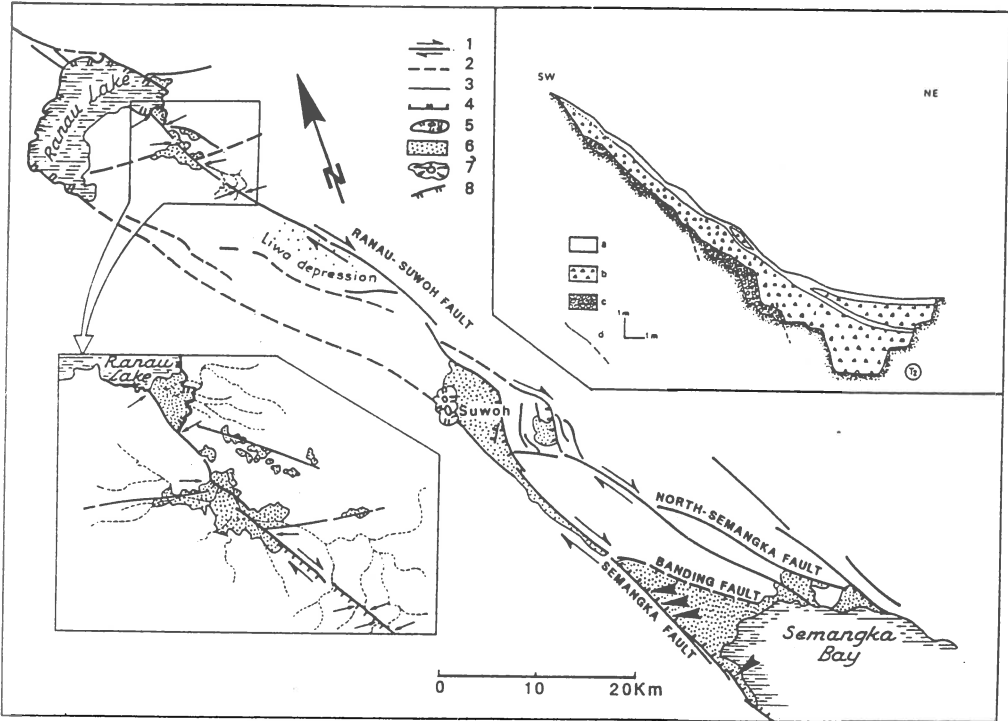
domains, it is thus necessary to accommodate at least 30 mm/yr of lateral displacement. Morphological characteristics of major fault scarps [Pramumijoyo, 1991; Sébrier et al., 1992; 1993] also support a low slip rate of about 10 mm/yr for the southernmost segment of the GSF. In addition, recent neotectonic study in northern and central Sumatra suggests a variation of the GSF slip rate from 11 mm/yr in central Sumatra (lat. 1°S) to 28 mm/yr in northern Sumatra (lat. 2°N) [Sieh et al., 1991].

Slip rate of the Great Sumatran Fault near the Toba Lake (2°N) : At about 2°10'N, the strike-slip motion along the GSF has right-laterally offset streams incising the Toba Tuffs (Figure 3). We measured 7 stream offsets range from 500 m to 1660 m ± 30 m [Detourbet et al., 1993]. The paroxysmal volcanic event that formed the Toba caldera has produced the Toba Tuffs by 73000±4000 years [Chesner et al., 1991]. The estimated rate of dextral displacement deduced from the maximum stream offset (1660 ± 30 m) affecting the 73000±4000 year tuffs is 23±2 mm/yr. This rate is more accurate, in close agreement but slightly lower than 28 mm/yr previously proposed in the same region by Sieh et al. [1991].

Slip rate of southern Great Sumatran Fault, near Ranau Lake (5°S) : High resolution SPOT images confirmed the GSF right-lateral strike-slip displacement (Figure 2) and supported a low slip rate for the southernmost segments of the GSF. Those offsets along the GSF include right-lateral offset streams ranged between 200 m and 500 m±30 m which allow us to calculate a 6±4 mm/yr slip rate [Bellier et al., 1991]. This result is significantly lower than the slip rate of 23±2 mm/yr estimated in north Sumatra suggesting a north-westward slip rate increase between 5°S and 2°N.

Slip rate in Central Sumatra between 1°N and 4°S : Katili et Hehuwat [1967], documented right-lateral stream offsets of small tributaries of the Upper Gadis (about 0.5 to 1°N), Seblat (about 3° to 3.5°S), Ketahun (about 3.5°S to 4°S) and Musi (about 4 to 4.5°S) Rivers (see Figure 2 in Katili and Hehuwat, [1967] page 10). These offsets located between the Ranau Lake and the Toba Lake regions along the GSF are mainly incising Quaternary volcanic tuffs and in some part bedrocks. Unfortunately, these morphologic markers are not datable and the tuffs do not give accurate ages up to present and thus do not permit to calculate directly a slip rate. In order to constrain slip rates on active strike-slip faults, morphological relationship between drainage offset pattern and strike-slip fault has been investigated [Gaudemer et al., 1989]. Using this method, we estimated slip rate for the Central GSF, between the Toba and Singkarak Lakes, from the Gadis River tributary stream offsets, and between Singkarak and Ranau Lakes from Seblat, Ketahun and Musi tributary stream offsets.

Methodology : river offsets across active strike-slip fault : The Gaudemeret al.'s method [1989] considers that for a given strike-slip fault, there is a linear correlation between the apparent horizontal stream offsets (d), and the length (L) of the river upstream from the fault, such as d = α . L. Thus, while stream offsets (d) increase with time (t) proportionally with the slip rate (v), the river upstream lengths (L) increase with time (t) proportionally with upstream erosion rate (a); it is generally accepted by geomorphologists than a river can increase its length with time by headward growth of its upper reaches, this progression being a slow and continuous process up to the basin perimeter [see references in Howard, 1971; Schumm et al., 1987; Gaudemer et al., 1989]. Because both offsets and upstream rivers increase with time, we can exposed the following relations :

$$L = a . t, \qquad d = v . t, \qquad \text{and} \qquad d = \alpha . L => \text{Consequently} : v = d/L . a = \alpha . a$$

" α" is the slope of the "apparent offset vs. upstream length" deduced from the linear interpolation deduced from the best-fitting (least-squares criterion) line that passes through the origin, such as :

$$d = \alpha . L \text{ and } \Sigma \varepsilon_i^2 = \Sigma (d_i - \alpha . L_i)^2 .$$

We calculated slope uncertainty taking into account to the uncertainties of the apparent offset (d) and upstream length (L), and the dispersion of the points d/L. The upstream increase rate "a" is of about some centimetres per year and expresses the influence of various factors : climate, lithology, base level variation. Then, in a given area, where "d" and "L" are measured, if "t" is known, "v" can be calculated as well as "a". Assuming that in a wet tropical region and for a similar rock type "a" should be constant, once "a" is calibrated "v" can be estimated in an other area from "d" and "L" measurements without knowing "t".

Slip rate along the Central Great Sumatran Fault between 1°N and 4.5°S : The Gaudemer's method applied to the stream offsets near Toba, permitted to calculate the slope " α" (=0.497±0.021) determined by linear interpolation. With the slip rate value (v=23±2 mm/yr), we calculate further the calibrated "a" parameter 46±6 mm/yr. Once calibrated, we used it to calculate a slip rates with stream offsets reported by Katali and Hehuwat [1967]. For northern Central Sumatra (0.5° to 1°N), they reported 7 stream offsets ranging between 360 m to 1030 m±80 m. The "a" value calibrated on the Toba Tuffs being of 46±6 mm/yr and the "a" (=d/L) value determined by linear interpolation being of 0.351, a dextral slip rate of 17±6 mm/yr can be calculated for this region.

For southern Central Sumatra (between 3°S and 4.5°S), we reported 18 stream offsets ranging between 260m to 1600m±80m. The "a" value for Sumatra being 46±6 mm/yr and the "a" (=d/L) value being of 0.231±0.073 we deduce from the stream offsets in this region a dextral slip rate of 11±5 mm/yr. This rate is of the same order but slightly higher than the slip rate calculated just south around the Ranau Lake (where v = 6±4 mm/yr. At about 1°S, Sieh et al. [1991] proposed a 11 mm/yr slip rate. In any case, even if these last estimated

Figure 3 : Sketch of the Sumatran arc deformation where we reported the horizontal slip rates along the Great Sumatran Fault.
Inset right represents the example of stream offsets observed along the GSF trace south of the Toba lake.
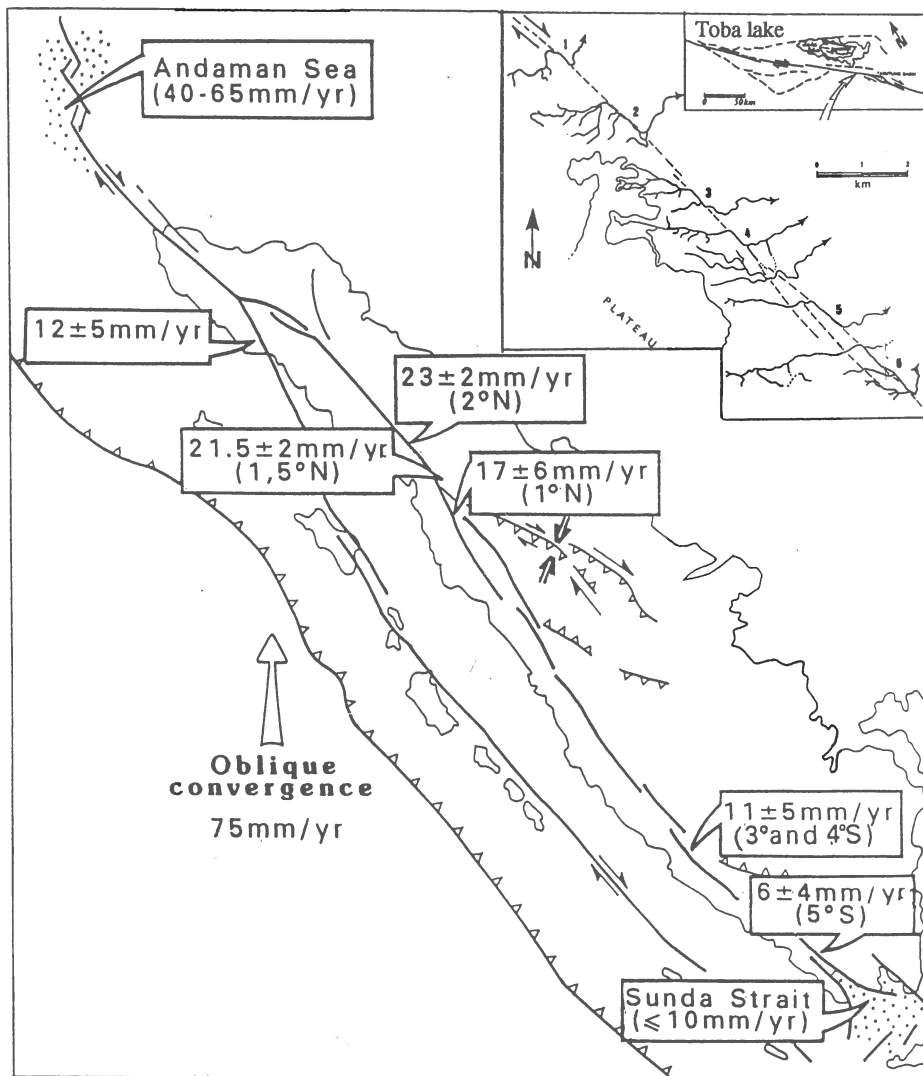
slip rates for the South-Central part of Sumatra are not very precise, the results seems enough accurate to estimate the tendency of the slip rate variation along the fault zone. These rates are intermediates between 6±4 mm/yr calculated around Ranau Lake and 23±2 mm/yr rate around the Toba Lake region (about lat. 2°N). If the estimated rate of 11 mm/yr at 1°S is correct, the more significant change is about at 1°S -1°N.

Estimation of the slip rate along the Batee fault : On a SPOT image, we reported only 3 right-lateral stream offsets (at about 4°20'). Unfortunately the offsets and upstream length are inaccurately determined. Thus, for this stream network, we consider that the uncertainties are of about ±250. These offsets range between 1160 to 5600±250 m. The "a" (=d/L) value of 0.232±0.093 have been determined by linear interpolation. Using the "a" value of 46±6 mm/yr, calibrated on the Toba Tuffs near to the Batee fault, a dextral slip rate of 12±5 mm/yr could be preliminary estimated for this fault.

Discussion on the Great Sumatran Fault slip rate : Precise offset measurements performed thanks to SPOT image analysis and channel networks deduced from topographic maps allow us to estimate the long-term dextral slip rate of the GSF. In the Toba region, the estimated rate of displacement is 23±2 mm/yr at about 2°N. The slip-rate in the Ranau region, South of Sumatra (about 5°S), is of about 6±4 mm/yr. In central Sumatra the determined slip rates are intermediate: 11±5 mm/yr at about 3°-4°S, 11 mm/yr at 1°S, and 17±6 mm/yr at 1°N (Figure 3). These estimations suggest that the dextral slip rate increases northward along the GSF between 5°S and 2°N. This increase appears very significant between 1°S and 1°N. However, these rates are less than the maximum rate estimated by global modelling for northernmost GSF 40-65 mm/yr, and thus is still too low to accommodate the whole parallel component of the convergence.

SEGMENTATION AND HISTORIC SEISMICITY OF THE GREAT SUMATRAN FAULT

In order to constrain the geometry and the segmentation of this major active fault, and to precisely analysed its seismic hazard, we realised a large scale segmentation map based on morphologic-topographic characteristics and on major geometric discontinuities (stepovers and bends) [e.g., De Polo et al., 1989; Crone and Haller, 1993], using SPOT images as well as topographic and geologic maps [see Beaudouin et al., 1995]. We complemented this segmentation map reporting the major earthquake ruptures [Beaudoin, 1995] on the basis of an historic seismicity study since 1835 [Gutenberg et Richter, 1954; Untung et al., 1985; Katili and Heuwat, 1967; Deverchère et Louat, 1993; Deverchère et al., 1994] (Figure 4). We provide evidences of several major releasing stepovers and two restraining bends which permit to define 18 major fault segments with lengths ranging between 45 and 200 km. On the basis of this analysis, two regions may be distinguished : a Northern (segments S9 to S19) and a Southern (segments S1 to S8). In fact, the northern fault system presents both longest segments (e.g., 200 km length for S12, S14, S18), and several parallel traces. This is well developed South of Toba lake (around 2°N) where a 40 km wide crustal scale overstep is observed. Another major geometric feature of the northern GSF is the presence of a 200 km-long restraining bend which is situated between 3° and 5°N. We also emphasised a northward decrease of the number of releasing stepovers, which are more numerous southward. Consequently, the tectonic regime along the GSF is considered to be dominantly transtensional, but northern part appears more transpressional. The maximal magnitudes, calculated using the seismic moment empirical method [e.g., Kanamori, 1983] are ranging between 6.8 and 7.7 [Beaudouin et al., 1995]. Segment length being the fundamental parameter for constraining this estimates, magnitudes are higher in the North (Mw=7.7 for segment length of 200 km). These values show that earthquakes of high magnitudes are possible along the GSF. This is confirmed by historical seismicity (M= 7-7.5 in 1933 and 7.6 in 1943, see Figure 4). Mw 8 earthquakes seem to be able to occur only for a stepover rupture. Northward increase of segment lengths appear to be correlated with an increase of the slip rate. Consequently, maxi·   ·n magnitudes are higher and seismic recurrence shorter in North than in South of Sumatra. This suggests a northward increase of seismic hazard, which is in good agreement with historical seismicity showing more earthquakes in the North. However, we report two atypical regions. A 300-km-long seismic gap extending between 3°N and 5°N is characterised by about 120 to 200-km long segments with high slip-rates. This gap seems to correspond with the huge restraining bend that should be presently locked. These data suggest that this zone has an high potential for a major seismic event. In contrast, the Liwa region (near 5°S) suffered two major earthquakes during the XXth century on a short and low slip rate segment. In conclusion, we provide evidences of several major releasing stepovers and two restraining bends which permit to individualised 18 major fault segments with lengths ranging between 45 and 200 km. Additionally, we evidence a northward increase of the segment lengths and complexities, that could be correlated with an increase of the slip rate. Consequently, this could be interpreted as a northward increase of seismic hazard agreeing with the historical seismicity. Our analyses also report a 300-km-long seismic gap which extends between 3°N and 5°N. This gap is characterised by about 120-200-km long segments with high slip-rates that seems to correspond apparently to a locked restraining bend. These data suggest that this zone has an high potential for seismic hazard.

924

Figure 4 : Map of major historical earthquake (M≥6 or Intensity≥VIII) ruptures occured on the Great Sumatran Fault since 1835. Rupture zones are approximately represented by dashed zones on the active segmentation map (after Beaudouin et al. [1995]).
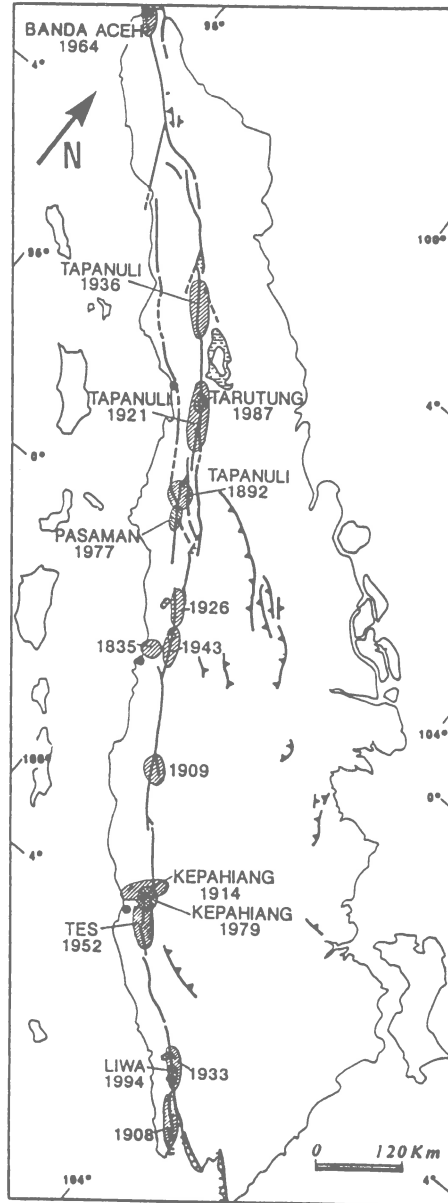
CONCLUSION

To define precisely the slip rate and recent seismic history of the South GSF, we excavated four trenches in its southernmost part, where the strike-slip movement changes to oblique-normal faulting. The trenches exposed a colluvial wedge in fault contact with a relatively unweathered bedrock and a thin slope wash. The occurrence of only one paleosoil indicates that in wet tropical climate the degradation rate of organic material is faster than seismic recurrence. Scarp heights and slip vectors on major fault planes allow us to better constrain the dextral slip rate of the southernmost GSF and confirms a maximum velocity of about 10 mm/year. Morphological and paleoseismic (trenching) observations conducted in southernmost Sumatra support a minimum recurrence interval of 400 year for the maximum expected earthquake of Mw=7.3, calculated using the method of the seismic moment. Taking into account the northward increase of the slip rate, a shorter recurrence interval of the order of 150 years has to be expected in northern Sumatra (for seismic event of $M_W$max = 7.3). Nevertheless, those estimated recurrence intervals should be longer if part of the slip on the GSF System is due to creeping slip.

In order to characterise the seismic hazard parameters along of the GSF, accurate estimates of the long-term dextral slip rates of the GSF have been conducted from stream offsets observed on SPOT images and topographic maps. These estimated slip rates are of about 23 ± 2 mm/yr (2°N), 17 ± 6 mm/yr (1°N), 11 ± 5 mm/yr (between 3° and 4°S), and 6 ± 4mm/yr (5°S); this last one being similar to the slip-rate calculated from field observations. Thus, the dextral slip rate increases northward along the GSF. Consequently since, seismic hazard is roughly a direct function of the slip rate, this difference in slip rate suggests that seismic hazard has to be expected higher in northern than in southern Sumatra; i.e., for similar sized earthquake the recurrence interval should be shorter in northern than in southern Sumatra. The northern slip rate is still too low to accommodate the whole trench parallel component of the convergence which is of about 40-65 mm/yr in northernmost GSF. To accommodate slip rate deficiency and the rate variation between northern and southern Sumatra, we suggest that a combination of fore-arc and back-arc domain deformation : 1, slip transfer to the Mentawaï Fault zone localised in the western forearc [Diament et al., 1991; Zen, 1993], 2, northwestward stretching of the fore-arc platelet [McCaffrey, 1991] and, 3, shortening within the back-arc domain. This implies that the active deformation is not only localised along the GSF, but it is distributed across throughout the arc domain from the fore-arc to the back-arc. Consequently we deduce seismic hazard distribution throughout the arc domain.

To constrain the segmentation of this major active fault and to precisely analysed its seismic hazard, we realised a large scale segmentation map complemented by the major earthquake ruptures on the basis of an historic seismicity study. We provide evidences of several major releasing stepovers and two restraining bends which permit to individualised 18 major fault segments with lengths ranging between 45 and 200 km. Additionally, we evidence a northward increase of the segment lengths, that could be correlated with the increase of the slip rate. Consequently, this could be interpreted as a northward increase of seismic hazard clearly confirmed by the historical seismicity. Our analyses also report a 300-km-long seismic gap (between 3°N and 5°N) which is characterised by an about 120-200-km long locked restraining bend; this zone has an high potential for seismic hazard.

In order to assess the instantaneous deformation along the GSF, we performed both terrestrial and GPS geodetic measurements within two suitable zones: the Ranau Lake-Liwa area (5°S) and the Singkarak Lake-Padang area (0°30'S) [Duquesnoy et al., 1992; Kasser et al.,1993]. This geodetical field work will permit to determine if there is some creeping-slip along the GSF System and whether or not the slip is distributed across the fault over a wide zone.

REFERENCES

Beaudouin, Th., O. Bellier and M. Sébrier, 1995. Segmentation et aléa sismique sur la Grande Faille de Sumatra (indonésie). C. R. Acad. Sci. Paris .

Beck, Jr M.E., 1983. On the mechanism of tectonic transport in zones of oblique subduction. Tectonophysics, 93, 1-11.

Bellier, O., M. Sébrier and S. Pramumijoyo, 1991. La Grande Faille de Sumatra : Géométrie, cinématique et quantité de déplacement mises en évidence par l'imagerie satellitaire. C.R. Acad. Sci. Paris, 312, 1219-1226

Bellier, O. and M. Sébrier, 1994. Relationship between tectonism and volcanism along the Great Sumatran Fault zone deduced by SPOT image analyses. Tectonophysics, 233, 215-231.

Brune, J., 1968. Seismic moment, seismicity and rate of slip along major fault zones. J. Geophys. Res., 73, 777-784.

Chesner, C.A., W.I. Rose, A. Deino, R. Drake and J.A. Westgate, 1991. Eruptive history of earth's largest quaternary caldera (Toba, Indonesia). Geology, 19, 200-203.

Crone, A.J. and K.M. Haller, 1991. Segmentation and the coseismic behavior of Basin and Range normal faults: examples from east-central Idaho and southwestern Montana, U. S. A. J. Struct. Geol., 13, 2, 151-164.

Curray, J.R., D.G. Moore, L.A. Lawver, F.J. Emmel, R.W. Raitt, M. Henry and R. Kieckhefer, 1979. Tectonic of the Andaman sea and Burma. Mem. Am. Ass. Petrol. Geol., 29, 189-198.

De Mets C., R.G. Gordon, D.F. Argus and S. Stein, 1990. Current plate motions. Geophys. J. Int., 101, 425-478.

Detourbet, Ch., O. Bellier and M. Sébrier, 1993. La caldera volcanique de Toba et le système de faille de Sumatra (Indonésie) vue par SPOT. C. R. Acad. Sci. Paris, 316, 1439-1445.

DePolo, C.M., D.G. Clark, B.D. Slemmons and A.R. Ramelli, 1991. Historical surface faulting in the Basin and Range province, Western North America: implication for fault segmentation. J. Struct. Geol., 132, 123-136.

Deverchère, J. and R. Louat, 1993. Evaluation du risque sismique lié à la grande faille de Sumatra. Public. ministère de l'environement. 29 p.

Deverchère, J., M. Sebrier, M. Diament and H. Harjono, 1994. Le séisme de Liwa (Sumatra, Indonésie) du 15 février 1994. Coopération scientifique Franco-Indonésienne. Public. Ministère de l'environement. 48 p.

Diament, M., H. Harjono, K Karta, C. Deplus, D. Dahrin, M.T Jr. Zen, M. Gérard, 0. Lassal, A. Martin and J. Mallot, 1992. Mentawaï fault zone off Sumatra : A new key to the geodynamics of Indonesia. Geology 20, 259-262.

Duquesnoy, T., O. Bellier, M. Kasser and M. Sébrier, 1992. Etude géodésique de la partie centrale et méridionale de Sumatra (Indonésie) : contribution à l'étude sismotectonique de la faille de Semangka, Rep. Coopération Scientifique Franco-Indonésienne. 107p.

Fitch, T.J., 1972. Plate convergence, transcurrent faults, and internal deformation adjacent to Southeast Asia and western Pacific. J. Geophys. Res., 77, 4432-4460.

Gaudemer, Y., P. Tapponnier and D.L. Turcotte, 1989. River offsets across active strike-slip faults, Annales Tectonicae , 3, 2, 55-76.

Gutenberg, B. and C.F. Richter, 1954. Seismicity of the earth, Princeton University Press, Princeton, New Jersey, 310p.

Hanks, T., and H. Kanamori, 1979. A moment magnitude scale, J. Geophys. Res., 84, 2348-2350.

Howard, A.D., 1971. Simulation of stream networks by headward growth and branching. Geogr. Annal., 3, 29-50.

Jarrard, R. D., 1986. Terrane motion by strike-slip faulting of forearc slivers. Geology, 14, 780-783.

Kasser, M., O. Bellier, Th. Duquesnoy and M. Sébrier, 1994. Geodetic survey of the Great Sumatran Fault, Annales Geophysicae, Suppl. I, 12, 65.

Katili, J. A. and F. Hehuwat, 1967. On the occurence of large transcurrent faults in Sumatra, Indonesia. Journ. of Geosciences, Osaka City Univer., 10, 1-1, 5-17.

Lassal, O., P. Huchon and H. Harjono, 1989. Extension crustale dans le détroit de la Sonde (Indonésie). Données de la sismique réflexion (campagne du Krakatau). C. R. Acad. Sci. Paris, 309, 205-212.

Mc Caffrey, R., 1991. Slip-vectors and stretching of the Sumatra fore arc. Geology, 19, 881-884.

Pramumijoyo, S., 1991. Néotectonique et sismotectonique de la terminaison méridionale de la grande faille de Sumatra et du détroit de la Sonde (indonésie). Thèse Université Paris Sud, 215p.

Schumm, S.A., M.P. Mosley and W.E. Weaver, 1987. Experimental fluvial geomorphology. John Wiley, New York, 413p.

Sébrier, M., O. Bellier, S. Pramumijoyo, H. Harjono and M.T. Zen, 1992. Trenching observations acros the southernmost part of the Great Sumatran Fault System (Indonesia), Eos Trans. AGU, 73(14), 193.

Sébrier, M., O. Bellier, S. Pramumijoyo, and H. Harjono, 1993. Geological estimation of seismic hazard parameters on the Great Sumatran Fault. The Indonesian-French volcanological workshop, proceedings, Ed.Wimpi S. Tjetjep,159-173.

Sieh, K., J. Rais and Y. Bock, 1991. Neotectonic and paleoseismic studies in West and North Sumatra. AGU Fall Meeting, EOS, 72(44), 460.

Untung, M., N. Burg, E. Kertapati, Undang and C. R. Allen, 1985. Rupture along the Great Sumatran fault, Indonesian, during the earthquakes of 1925 and 1943. Bull seism Soc Am., 75, 313-317.

Zen, M.T. Jr., 1993. Deformation de l'avant-arc en réponse à une subduction a convergence oblique: exemple de Sumatra. Thesis Univ. Paris VII, 317p.

PARAMETERS OF TYPICAL FAULTS IN THE ACTIVE REGIONS OF THE AEGEAN AND SURROUNDING AREAS

Constantinos B. Papazachos and Anastasia A. Kiratzi

Geophysical Laboratory, University of Thessaloniki
GR-54006, GREECE

ABSTRACT

Eighty six reliable fault plane solutions of strong shallow earthquakes and instrumental as well as historical seismicity are used to accurately define the basic parameters of seismic faulting and the rate of crustal deformation in several regions of the Aegean and surrounding area.

Along the coastal area in northwestern Greece and west Albania, compressional crustal seismic (brittle) deformation at a rate of 4 mm/yr and in a N48°E causes thrust faults with a strike slip component. These faults strike parallel to the coast (strike=334°, dip =31°, rake=109°). In the convex side of the Hellenic arc (Zante-south of Crete-Rhodos) compressional seismic deformation at a rate of about 1cm/yr in a N34°E direction causes low angle thrust faults with an almost constant strike direction all along the arc (strike=300°, dip=25°, rake=96°). These two thrust zones are separated by the Cephalonia transform dextral fault (strike=45°, dip=61°, rake=173°) where slip takes place at a rate of 3 cm/yr, which the highest slip rate observed in the whole Aegean area. Along the whole external thrust area vertical crustal shortening takes place at a mean rate of 1 mm/yr.

In a tensional zone along the Hellenides mountain range (Pindos-Peloponnesus-Crete), horizontal extension, at a rate of 2 mm/yr and in a N108° E direction, generates normal faults with a small strike slip component. These faults strike almost parallel to the mountain range (strike=7° , dip=34° , rake=-98°). In a curved long zone, which includes south Bulgaria, north and central mainland of Greece, the south Aegean volcanic arc and southwest Turkey, extension at a rate of 5 mm/yr and in a N14°W direction generates normal faults with a small strike slip dextral component. These faults strike in an ENE direction (strike=72°, dip=47°, rake=-98°). In central western Turkey, an extension of the same value (5 mm/yr) acts in a N8°E direction and generates normal faults with a small strike slip dextral component. These faults strike in an almost east-weest direction (strike=93°, dip=47°, rake=-96°). Along the western part of the northern Anatolia fault zone, dextral strike slip motion with a normal component (strike=79°, dip=64°, rake=147°) takes place at a rate of 2 cm/yr, while in the north Aegean fault zone the motion takes place in strike-slip dextral faults (strike=48°, dip=86°, rake=-174°) at a rate of 1 cm/yr. Vertical thinning of about 1 mm/yr takes place in the Aegean Sea and surrounding countries.

The direction of maximum extension in the Aegean area shows an anticlockwise rotation of about 100° from east to west especially in the northern part of the area. It has a N26°E direction in the northwestern Anatolia, an almost north-south direction in northern Aegean, a N14°W in central Greece and a N72°W in the Hellenides mountain range of western Greece.

INTRODUCTION

The Aegean sea and surrounding area (figure 1) lies on the most active part of the Africa-Eurasia collision zone. The eastern Mediterranean lithosphere, which is the front part of the African lithosphere, is subducted beneath the Aegean along the Hellenic arc, which results in high shallow seismicity (magnitudes up to M_S=8.2) with thrust faults along the Hellenic arc and intermediate depth seismicity which forms a well defined Benioff zone in southern Aegean (Papazachos and Comninakis, 1971; Papazachos, 1990). However, the seismicity is not confined in the collision zone but expands in the back-arc Aegean area (Aegean sea, mainland of Greece, Albania, southern Yugoslavia, southern Bulgaria, Asia Minor), where it is expressed mainly with normal faults. Dextral strike-slip motion is observed in the North Anatolian fault and its continuation in the northern Aegean, especially along the North Aegean trough. This tectonic setting is attributed to the combination of an extension pattern due to the "roll-back" forces of the subduction and the westrward movement of Turkey.

This complicated tectonic image motivates for a detailed study of the seismic faults and velocity rates of the active crustal deformation. A lot of work has been done already, but the results are sometimes very controversial. For instance, along the convex side of the Hellenic arc values from 3 to 30 mm/yr have been calculated (Jackson and McKenzie, 1988 a, b; Papazachos et al., 1992). For the inner part, extensional velocities of the order of 3 to 30 mm/yr have been calculated (Tselentis and Makropoulos, 1986; Jackson and McKenzie, 1988b; Ekstrom and England, 1989; Ambraseys and Jackson, 1990; Papazachos, et al., 1991a, 1991b; Papazachos and Kiratzi, 1992; Papazachos et al., 1992) with an extreme of 60 mm/yr (Jackson and McKenzie, 1988a).

In the present paper, we present the parameters (strike, dip, rake) of the typical faults and the corresponding rate of crustal deformation in the active regions of the Aegean and surrounding area ($34^{o}N$-$43^{o}N$, $18^{o}E$-$30^{o}E$).

METHOD OF ANALYSIS AND DATA

The method of analysis proposed by Papazachos and Kiratzi (1992) is used, which is based on the formulation of Kostrov (1974) and its expansion by Jackson and McKenzie (1988a). Briefly, the strain rate, $\dot{\varepsilon}$, and the velocity tensor, U, are calculated by the following equations:

$$\dot{\varepsilon}_{ij} = \frac{1}{2\mu V} \dot{M}_o \bar{F}_{ij} \quad i,j = 1,2,3 \tag{1}$$

$$U_{ii} = \frac{1}{2\mu\, l_k l_j} \dot{M}_o \bar{F}_{ii} \quad i \neq k, k \neq j, j \neq i, \ i = 1,2,3 \tag{2}$$

$$U_{12} = \frac{1}{\mu\, l_1 l_2} \dot{M}_o \bar{F}_{12} \tag{3}$$

$$U_{i3} = \frac{1}{\mu\, l_1 l_3} \dot{M}_o \bar{F}_{i3} \quad i = 1,2 \tag{4}$$

where μ is the bulk modulus ($=3*10^{11}$ dyn/cm^2), V is the seismogenic volume (a parallelepiped prism with length, l_1, width, l_2, and depth extent, l_3), $\dot{M}_o$ is the seismic moment rate as it is determined from Molnar (1979), and F is the tensor calculated by:

$$\overline{F} = \frac{\dot{M}}{\dot{M_0}} = \frac{\sum_{n=1}^{N} M^n / t}{\sum_{n=1}^{N} M_0^n / t} = \frac{\sum_{n=1}^{N} M_0^n \cdot F^n}{\sum_{n=1}^{N} M_0^n} \qquad (5)$$

The reference system in equations (1) to (5) is the zone's $0l_1l_2l_3$ system, so a rotation of $\overline{F}$, usually calculated in the North-East-Down system, is necessary. In the present paper, $\overline{F}$ was calculated as a simple average of the F^n tensors.

Two separate data sets are used: a) A set of fault plane solutions deduced either from recent instrumental data or from past reliable field observations to determine the stress field, which defines the "shape" of the deformation and b) all the available complete instrumental and historical data to calculate the moment rate released in each area which is consequently used for the determination of the "size" of the strain. The zonation of Papazachos and Papaioannou (1993) which separates the studied area in 68 seismic sources was adopted, shown in figure 2
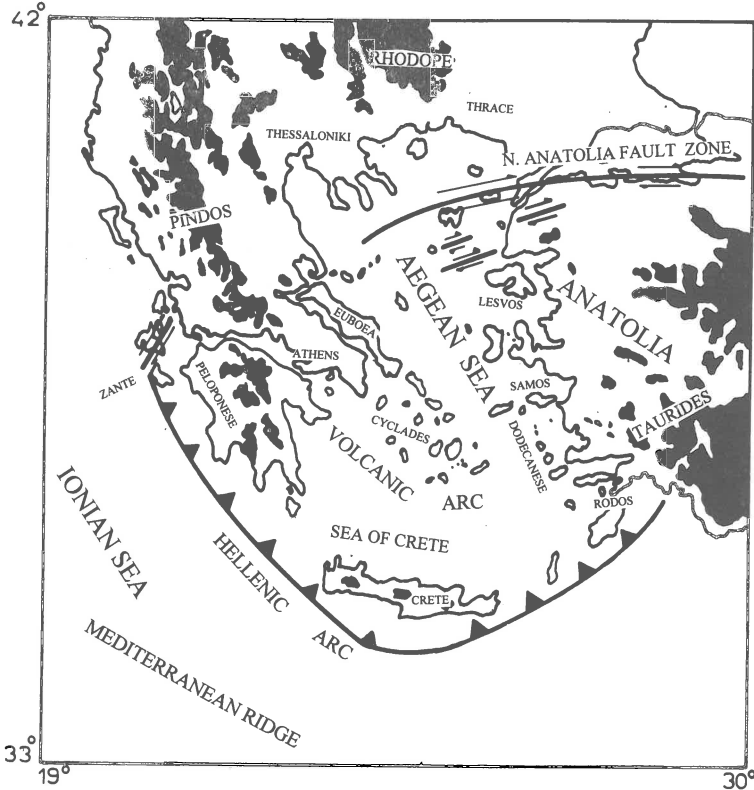
Fig.1. Schematic representation of the main tectonic features of the broader Aegean area.
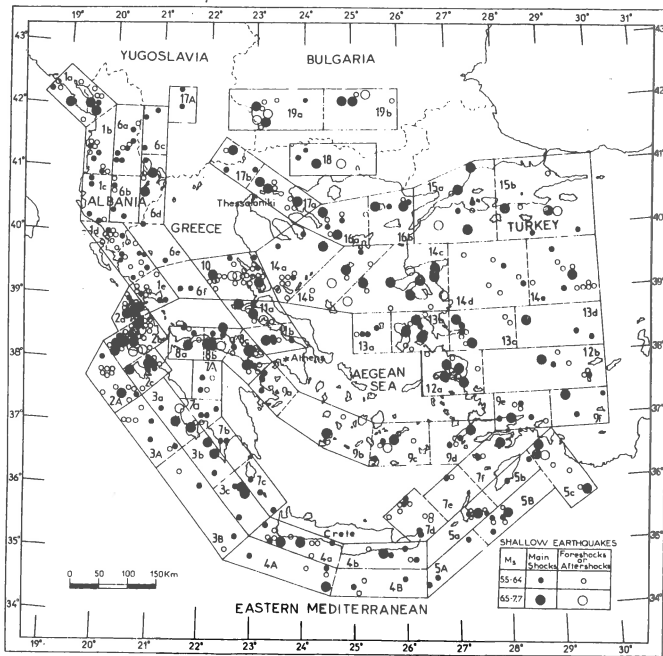
Fig.2. Map of the 67 sources and the relative seismicity determined for the Aegean area (Papazachos and Papaioannou, 1993).

together with the epicenters of the earthquakes with Ms>5.5. Papazachos and Panagiotopoulos (1994) separated Thessalia in two seismogenic regions (10a, 10b) so that the total number of these regions is 68. The rates of deformation are calculated for 63 sources, since no focal mechanisms were available for 5 seismic sources. All the information on the parameters used for each source are presented in Papazachos and Kiratzi (1994).

The fault plane solutions of the shallow events (h<40Km) with surface wave magnitude $M_S \geq 5.5$ which have occured in the studied area during the period 1963-1986 are shown in figure 3. The distribution of the focal mechanisms shows a spatial consistency of the direction of the stress field. Thus, the area was separated into 12 belts of similar focal mechanisms, within which the focal mechanism tensor, $\overline{F}$, was estimated, as well as the corresponding to this tensor fault plane solution were determined. The same $\overline{F}$ tensor was used for all the sources belonging to the same belt. However, the deformation for each of these sources varies, due to the different moment rates and to the different dimensions of each source.

TYPICAL FAULT PLANE SOLUTIONS AND CRUSTAL DEFORMATION

The fault plane solution corresponding to the tensor $\overline{F}$ for each of the twelve belts can be considered as typical one for the belt and for each of the seismogenic regions (sources) which belong to this belt. Table 1 gives information on these typical fault plane solutions. The first three columns give the code number of the corresponding belt, the name of the belt and the code numbers of the seismogenic regions (sources) as these regions are shown in figure (2). In the next columns of this table, the parameters of the two nodal planes (strike, dip, rake) and of the T and P axes (azimuth, plunge) are given. From the two nodal planes the first one is considered as the most probable nodal plane.

931

Figure (4) shows the direction of the P axis (maximum compression) and of the T axis (maximum tension) in each source of the Aegean area.

It must be noted that information given on Table 1 is also of predictive significance because it gives the expected fault parameters in each region. This information is also of practical importance because these faulting parameters can be used to define the radiation pattern of the seismic waves for the major shocks in each region.
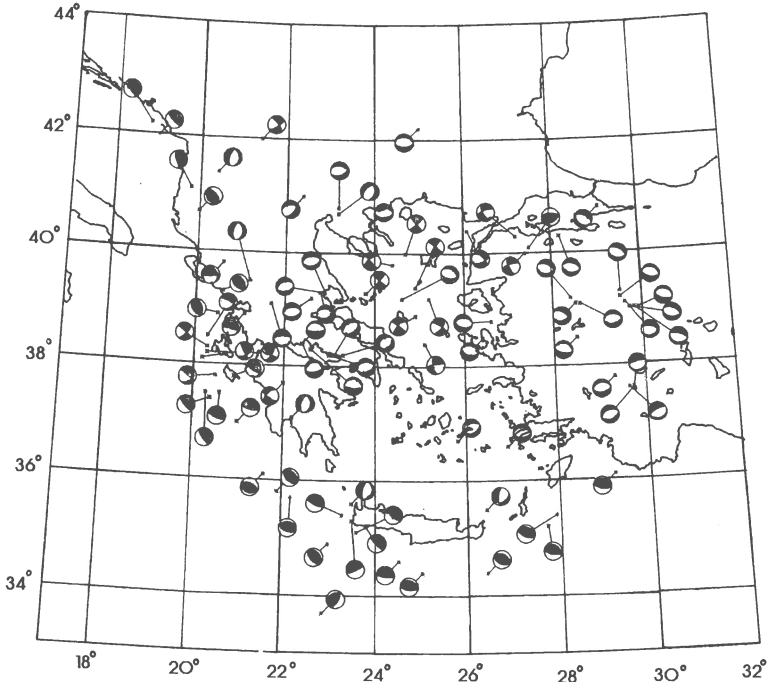
Fig.3. Equal area lower hemisphere projection for the 86 focal mechanisms used in the present study. The parameters of each fault plane solution are all listed and referenced in Papazachos and Kiratzi 1992.

Table 2 shows the eigenvectors and the eigenvalues of the crustal deformation velocity tensor for each seismogenic region of the area. The values (U_1, U_2, U_3) of these vectors are given (in cm/yr) as well as the azimuth, ξ (from north clockwise), and the plunge angle, δ (from the horizontal plane). Positive and negative values of U indicate tension and compression, respectively.

Figure (5) shows the maximum horizontal velocity (in mm/yr) for each region. Maximum compressional velocity is represented by convergent black arrow and maximum tensional velocity by divergent white arrows. In the cases of strike-slip faults only tensional velocities are given.
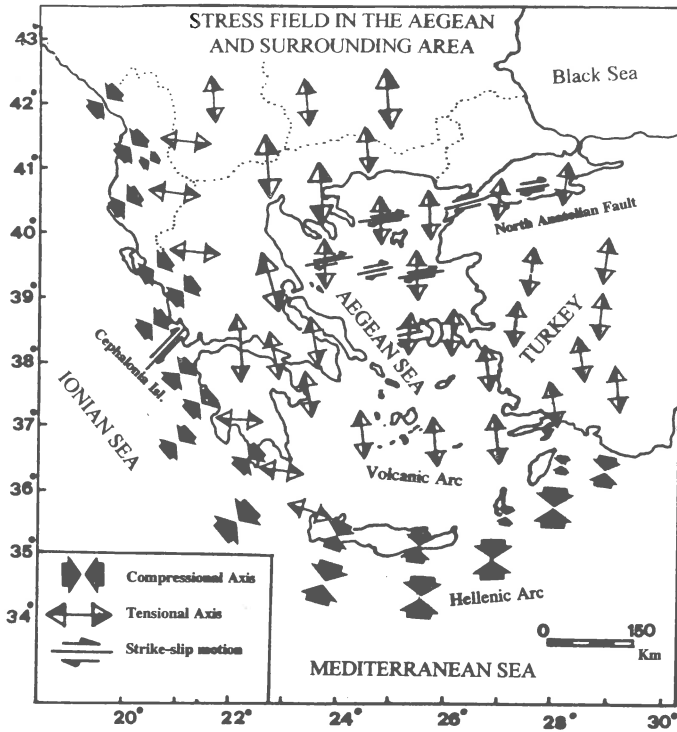
Fig.4 Direction of the typical compressional and tensional axes in the Aegean area.
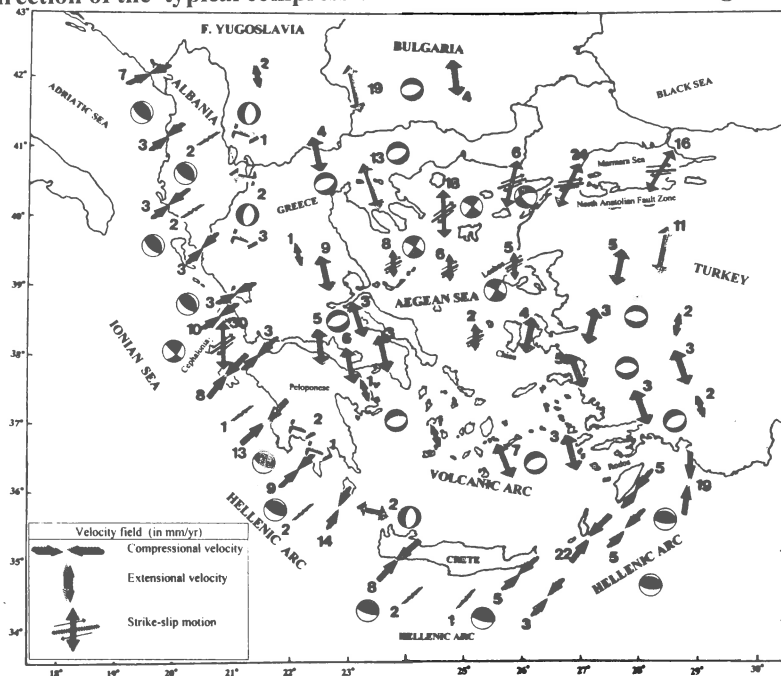
Fig.5 Distribution of the deformation velocities (in mm/yr) for the 63 sources for which data were used in the present study. The beach-balls represent the typical fault plane solutions for each source (black quadrants and white quadrants denote compression and extension, respectively).

RESULTS

Along the coastal belt in the northwest part of the investigated area (coast of Albania-northwestern coastal area of Greece), thrust faults with a dextral strike slip component trend parallel to the coast (strike=334°, dip=31°, rake=109°). In this belt, the maximum compressional deformation takes place at an average rate of 4 mm/yr in a N48°E direction.

In the convex side of the Hellenic arc, low angle thrust faults keep an almost constant northwest - southeast trend (strike=300°, dip=25°, rake=96°) all along the arc and dip to the concave part of the arc in its western part. The maximum compressional velocity is 8 mm/yr and has a N34°E direction.

The above described two thrust zones are separated by the Cephalonia strike slip dextral fault (strike=45°, dip=61°, rake=173°) where slip takes place at a rate of 3 cm/yr. This slip rate, which has been also determined by an independent method (B. Papazachos et al., 1994), is the highest one observed in the whole Aegean and surrounding area.

In the inner part of the area (Aegean sea and surroundings) crustal extension dominates. The direction of this stress field is not the same all over this area. An anticlockwise rotation of the maximum extensional deformation of about 100° from east (northwestern Turkey) to the west (Hellenides mountains) is observed and this extensional field can be separated into four domains:

1. Along the western boundary of the Aegean extensional field, a transitional zone of normal faulting with a small dextral component (belt 6 in table 1) has been identified (Papazachos et al., 1984). The typical faults in this zone strike parallel to the Hellenides mountain range (strike=7°, dip=34°, rake=-98°). The maximum horizontal deformation in this zone takes place at a rate of 2 mm/yr in a N108°E direction.

2. The second extensional domain is a curved zone of normal faulting with very weak dextral motion (strike=72°, dip=47°, rake=-98°) which includes southern Bulgaria, northern and central mainland of Greece, southern Aegean volcanic arc, southwestern Turkey (belts 7,8,9 in table 1). The extensional rate of deformation in this zone is 5 mm/yr in a N14°W direction.

3. A third extensional zone covers the central western Turkey (belt 10 in table 1) where normal faults with a very small dextral component strike in an about east-west direction (strike=93°, dip=47°, rake=-96°). Maximum tension takes place at a rate of 5 mm/yr in a N8°E direction.

4. The last domain in the Aegean area is the zone of dextral strike slip, with a considerable normal component, which includes the western part of the northern Anatolia fault (strike=79°, dip=64°, rake=-147°) and the northern Aegean strike slip faults (strike=48°, dip=86°, rake = -174°). It must be noted, however, that in northwestern Anatolia as well as in northern Aegean there are earthquakes which are produced by almost pure strike-slip dextral faults and other earthquakes which are produced by almost pure normal faults. The rate of motion is 2 cm/yr in the western part of the northern Anatolia fault and 1 cm/yr in the northern Aegean.

Table 1
Typical fault plane solutions for the 12 belts of similar stress field.

No	Belt Name	Sources	Fault pl.1 str/dip/rak	Fault pl.2 str/dip/rak	Taxis Az/Pl	Paxis Az/Pl
1	W.Albania-NW coasts of Greece	1a,1b,1c,1d,1e,2a,6a,6b	334/31/109	132/61/80	17/72	230/16
2	Cephalonia	2b	45/61/173	138/84/30	12/36	265/22
3	W.Hellenic Arc	2c,3a,3b,3c,3A,3B,8a	306/25/91	125/65/90	35/70	216/20
4	South Hellenic Arc	4a,4b,4A,4B	301/19/99	111/71/87	17/63	204/26
5	E.Hellenic Arc	5a,5b,5c,5A,5B	294/30/98	105/60/85	4/74	199/15
6	Hellenides mountain range	6c,6d,6e,7a,7b,7c	7/34/-98	197/57/-84	283/11	125/78
7	N. Greece	17a,17b,17A,19a,19b	68/46/-109	274/47/-72	351/1	258/77
8	Central Greece	8b,8c,10a,10b,11a,11b	258/41/-90	79/49/-90	168/43	50/86
9	Volcanic Arc	9a,9b,9c,9d,9e,9f,12a,12b	250/54/-94	77/37/-84	343/91	41/81
10	Central West. Turkey	13b,13c,13d,14d,14e	93/47/-96	281/44/-84	187/12	96/8
11	NW. Anatolia	15a,15b	259/64/-147	153/61/-30	25/2	117/41
12	N. Aegean	13a,14a,14b,14c,16a,16b	48/86/-174	318/84/-4	176/2	267/20

Table 2
Components of the velocity eigensystem ($U_{1,2,3}$) (in cm/yr). ξ and δ are the angles of azimuth and plunge of the eigenvector, respectively. Positive and negative values of U indicate tension and compression, respectively.

Source	U_1	ξ_1/δ_1	U_2	ξ_2/δ_2	U_3	ξ_3/δ_3
1a	.01	144/25	-.65	237/ 7	.11	341/64
1b	-.26	224/ 9	.00	132/15	.05	344/73
1c	.01	133/16	-.30	225/ 9	.06	344/72
1d	.01	138/28	-.30	231/ 7	.05	334/61
1e	.00	142/22	-.26	235/ 7	.05	342/67
2a	-.95	225/ 9	.01	132/13	.19	347/74
6a	-.22	223/ 7	.00	131/13	.03	341/75
6b	.00	134/17	-.15	226/ 9	.03	343/71
2b	2.08	2/ 8	-3.06	271/ 4	.02	154/82
2c	-.78	217/11	-.06	126/ 1	.17	33/79
3a	-1.34	212/ 9	-.13	302/ 2	.21	46/81
3b	-.88	215/11	-.07	305/ 1	.18	37/79
3c	-1.43	202/11	-.17	293/ 7	.30	56/77
3A	-.13	219/11	-.02	129/ 2	.03	28/79
3B	-.17	203/ 9	-.03	294/ 6	.03	56/79
8a	-.25	216/11	-.02	126/ 1	.05	33/79

4B	-.04	132/14		-.13	226/14		.03	359/70
5a	-2.16	213/ 4		-.07	122/13		.20	321/76
5b	-.51	211/ 7		-.02	120/12		.09	330/76
5c	-1.86	190/ 6		-.05	100/ 1		.25	2/84
5A	-.28	211/ 5		-.01	120/13		.03	322/76
5B	-.45	214/ 5		-.02	123/13		.05	323/76
6c	.00	15/ 8		.13	284/ 6		-.03	156/80
6d	.00	17/ 8		.24	286/ 8		-.07	150/79
6e	.00	19/ 5		.28	288/ 4		-.03	157/83
7a	.00	14/ 8		.24	282/ 7		-.06	151/79
7b	.00	19/ 5		.13	289/ 6		-.02	150/82
7c	.01	27/ 1		.15	297/ 6		-.03	126/83
8b	.52	168/ 2		.02	258/ 0		-.09	354/88
8c	.63	168/ 2		.03	258/ 0		-.11	355/88
10a	.89	173/ 2		.15	263/ 0		-.26	346/87
10b	.08	172/ 2		.01	262/ 0		-.01	345/88
11a	.33	162/ 2		.03	252/ 1		-.07	4/88
11b	.32	166/ 2		.03	256/ 0		-.07	358/88
9a	.10	343/ 4		.00	252/ 5		-.02	109/83
9b	.06	343/ 3		.00	252/ 5		-.01	98/84
9c	.71	343/ 5		.02	253/ 6		-.16	114/83
9d	.28	343/ 4		.01	252/ 5		-.04	106/83
9e	.29	341/ 4		.01	251/ 5		-.05	111/83
9f	.16	346/ 4		.00	255/ 6		-.03	108/82
12a	.50	342/ 3		.01	252/ 5		-.06	104/84
12b	.34	334/ 3		.02	244/ 1		-.04	127/87
13b	.38	189/ 0		.00	99/ 8		-.04	282/81
13c	.30	192/ 1		.00	102/ 8		-.04	285/82
13d	.15	187/ 0		.00	97/ 9		-.02	280/81
14d	.46	186/ 0		-.01	96/ 9		-.05	280/81
14e	1.14	186/ 1		-.02	95/ 9		-.12	279/81
17a	1.30	158/ 1		.08	67/18		-.31	250/72
17b	.40	351/ 0		.00	81/22		-.08	260/68
17A	.19	350/ 0		.00	80/19		-.06	259/71
19a	1.91	350/ 0		.00	80/24		-.35	259/66
19b	.36	355/ 1		.00	86/24		-.08	264/66
15a	2.38	26/ 0	-1.33	116/ 5		-.07	292/85
15b	1.57	26/ 0		-.88	116/ 4		-.04	291/86
13a	.19	183/ 0		-.20	273/ 2		-.01	81/88
14a	.84	184/ 0		-.53	274/ 1		-.02	85/89
14b	.58	182/ 0		-.69	272/ 1		-.02	77/89
14c	.52	182/ 0		-.74	272/ 1		-.01	72/89
16a	1.80	183/ 0	-2.40	273/ 1		-.07	76/89
16b	.64	183/ 0		-.46	273/ 1		-.02	83/89

REFERENCES

Ambraseys, N.N. and J.A Jackson, 1990. Seismicity and associated strain of central Greece between 1890 and 1988. Geophys. J.Int., 101, 663-709.

Ekstrom, G. and P. England, 1989. Seismic strain rates in regions of distributed continental deformation. J.Geophys.Res., 94, 10231-10257.

Jackson, J. and D. McKenzie, 1988a. The relationship between plate motions and seismic moment tensors, and the rates of active deformation in the Mediterranean and Middle East. Geophysical Journal, 93, 45-73.

Jackson, J. and D. McKenzie, 1988b. Rates of active deformation in the Aegean Sea and surrounding regions. Basin Res., 1, 121-128.

Kostrov,V., 1974. Seismic moment and energy of earthquakes, and seismic flow of rock. Izv.Acad.Sci. USSR Phys. Solid Earth, 1, 23-44.

Molnar,P., 1979 Earthquake reccurrence intervals and plate tectonics, Bull. Seism. Soc. Am., 69, 115-133.

Papazachos, B.C., 1990. Seismicity of the Aegean and surrounding area. Tectonophysics, 178, 287-308.

Papazachos, B.C and P.E. Comninakis, 1971. Geophysical and tectonic features of the Aegean arc. J. Geoph. Res., 76, 8517-8533.

Papazachos, B. and C. Papaioannou, 1993. Long-term earthquake prediction in the Aegean area based on a time and magnitude predictable model. Pageoph, 1404, 593-612.

Papazachos, B. and D. Panagiotopoulos, 1994. The seismicity of northern Thessalia. VII Congr. on Olymbos in the Centuries, Elasson, 26-28 August, 1994, pp 10.

Papazachos, B., A. Kiratzi, P. Hatzidimitriou, and A. Rocca, 1984. Seismic faults in the Aegean area. Tectonophysics, 106, 71-85.

Papazachos,B.C., A. Kiratzi, C. Papaioannou, and D. Panagiotopoulos, 1991a. Average regional seismic strain release rates in the Patraikos-Saronikos gulfs of central Greece based on historical and instrumental data. Bull. Geol. Soc. of Greece, 25, 225-238.

Papazachos,B.C., A. Kiratzi, and E. Papadimitriou, 1991b. Fault plane solutions for earthquakes in the Aegean area. Pageoph, 136, 405-420.

Papazachos, B.C., G. Karakaisis, and P. Hatzidimitriou, 1994. Further information on the transform fault of the Ionian sea. XXIV Gen. Ass. Europ. Seism. Commis., Athens, 19-24 September, 1994, pp. 12.

Papazachos, C. and A. Kiratzi, 1992. A formulation for reliable estimation of active crustal deformation and its application to central Greece. Geophys. J. Int., 111, 424-432.

Papazachos, C. And A. Kiratzi, 1994. A detailed study of the active crustal deformation in the Aegean and surrounding area. Publ. of the Geophysical Lab., Univ. of Thessaloniki, 15.

Papazachos, C., A. Kiratzi, and B. Papazachos, 1992. Rates of active crustal deformation in the Aegean and the surrounding area. J. of Geodynamics, 16, 147-179.

Tselentis,G. and C. Makropoulos, 1986. Rates of crustal deformation in the gulf of Corinth central Greece as determined from seismicity. Tectonophysics, 124, 55-66.

ᴐURCE PARAMETERS AND RUPTURE PROCESS STUDY FROM MACROSEISMIC AND SEISMOSYNTHETIC DATA

Del Gaudio V.[1,2], Pierri P.[2] & Calcagnile G.[1,2]

(1) Dipartimento di Geologia e Geofisica, Università di Bari, Italy.
(2) Osservatorio di Geofisica e Fisica Cosmica, Università di Bari, Italy.

ABSTRACT

Information on focal mechanism geometry and fracture process can be obtained through the synthetic reproduction of some macroseismic field characteristics such as isoseismal shape. The results of simulations show that, in some cases, the radiation pattern of extended sources (modelled as a sequence of sub-events) depends largely on the space-time characteristics of the rupture process.

The application of this methodology is rather hard-working and can be biased by subjective evaluations implied in the tracing of experimental isoseismals. In order to improve the efficiency and reduce the operator dependence of the comparison between experimental and synthetic isoseismals, a semiautomatic procedure was attempted, based on the computation of cross-correlation between experimental intensity and theoretical acceleration at each observational macroseismic site.

INTRODUCTION

Progress in instrumental seismology made possible a more and more accurate and fine modelling of seismic source and rupture process; however, for the most part of the seismological history of any country, the only available data are the macroseismic observations recorded in historical documents, so there is a noteworthy interest in the development of techniques exploiting this kind of data to obtain information on source characteristics.

Previous studies pointed out that general features of macroseismic fields often reflect mainly the geometry of seismic source and fracture mechanism (Panza & Cuscito, 1982; Panza et al., 1987), so a comparison between a macroseismic field and the theoretical ones computed for different source models gives information on some characteristics of the focal mechanism. Even though the complete reproduction of a macroseismic field generated by a theoretical earthquake is a rather complex task, the shape of the experimental isoseismals can be compared to theoretical ground motion fields obtained mapping the peak amplitude of synthetic seismograms calculated at each point of a regular grid; from this comparison it is possible to infer source characteristics such as the most probable orientation of fault, its dip angle, the direction line of the motion along the fault plane (being, however, the orientation indeterminate between the two opposite possibilities) and also a better hypocentral location.

This methodology was first applied by limiting seismosynthesis at frequency lower than 0.1 Hz (Suhadolc et al., 1988; Panza et al., 1991): at the corresponding wavelengths a point source can be assumed also for large events and this simplifies the data processing, but it should be reminded that the main effects of an earthquake are associated to higher frequencies. On the other hand, seismosynthesis at high frequencies requires a more detailed knowledge of structural characteristics which can be difficult to obtain. However method applications extended to frequencies higher than 0.1 Hz showed that the global shape of synthetic isoseismals does not seem to vary dramatically, so a compromise solution seems acceptable

which considers seismosynthesis at frequencies up to 1 Hz. The purpose of this study was to examine more thoroughly problems and possibilities resulting as a consequence of this approach.

METHODOLOGY

The procedure adopted to generate synthetic isoseismals of historical events makes use of a package developed by researchers of the University of Trieste and consists in a sequence of different stages: first a structural model of the area is defined and the corresponding spectra of some elastic and anelastic parameters are calculated; second, different source models are considered and synthetic seismograms are computed which represent the horizontal components of motion associated to P-SV and SH wave propagation: the ground motion is calculated at each point of a regular grid through the method of multimode summation (Panza, 1985; Florsch et al., 1991); third, the vectorial composition of synthetic seismograms is carried out and the peak amplitude is determined for each point of the grid; last, for each source model considered, a contour line map of these maximum amplitudes is assumed as representative of the shape of the isoseismals and the source model is searched which shows the best agreement with the experimental observations.

The structural model of the area is defined as a layered vertical distribution of phase velocity, density and phase attenuation, generally resulting from different kinds of previous studies (e.g. Deep Seismic Soundings, Rayleigh wave velocity dispersion analysis, frequency-time analysis). The source model is characterised by the hypocentre location, by the angular parameters defining the focal mechanism (strike, dip, rake), by the geometry, duration and velocity of the rupture process.

Not all these parameters have the same influence on the final result, so a limitation of the model freedom degrees can be imposed by exploiting the knowledge of some general characteristics of the earthquakes in the area examined as it is derived from instrumental observations on recent seismicity and from tectonics study. Further time saving is obtainable considering the simple relations existing between the variation of some parameters and its effect on isoseismals: changes of epicentral location and strike angle determine just a roto-translation of the macroseismic field if all the other parameters are kept constant, and a rake variation equal to 180°, causing just the inversion of ground motion direction, does not modify the isoseismal shape.

PROBLEMS IN MODELLING OF EXTENDED SOURCE

Dealing with frequencies up to 1 Hz, a point source model cannot be a priori assumed in case of large events. For the modelling of an extended source, some more parameters need to be fixed, either defining the fault length, the rupture velocity and the kind of time function describing the rupture process, or decomposing the earthquake in a time sequence of point sub-events: the latter solution gives more liberty in the source geometry modelling, but increases the variable number as well.

Previous studies showed that in many case the focal mechanism has a dominant role in determining the isoseismal shape, however, for strong events, the rupture characteristics can sometimes have a major influence on the orientation of the directions of maximum energy radiation. We ran into a similar situation when we were trying to reproduce the macroseismic field of earthquakes occurred in southern Apennines. This area was struck by several strong seismic events, whose macroseismic fields are often quite complex, but generally show an elongation of isoseismals in the direction of the Apenninic chain, i.e. NW-SE (see Fig. 1 which

refers to the earthquake of December 1456).

For the most recent events in this area, focal mechanisms are known from instrumental observations: the main shocks are associated to dip-slip fault plane solutions having an "Apenninic" strike (Ciaranfi et al., 1983a), even though data suggest sometimes that fracture modalities can be very complicated and, in a time sequence of a few tens of seconds, different and differently oriented faults are activated, some of which oriented in "anti-Apenninic" directions (i.e. normally to the Apennines chain) as well. Furthermore the main tectonical elements of the chain (faults and folds) have also a prevailing NW-SE orientation.

The modelling of a dip-slip source giving isoseismals elongated in the same direction of the fault is not a trivial question. Dealing with frequencies up to 0.1 Hz, some authors (Suhadolc et al., 1988; Suhadolc, 1989) pointed out that the fundamental modes of Rayleigh (P-SV) and Love (SH) wave influence isoseismal shape in a measure which depends on a combination of hypocentral depth and vertical distribution of velocity inside the crust; for an empirical evaluation of the dominant component an adimensional parameters R was proposed (given by the ratio between the average crustal velocities below and above the hypocentral depth) characterised by a threshold value equal to 1.7: for $R > 1.7$ the influence of SH waves becomes prevailing over that of P-SV waves. This behaviour was confirmed also at frequencies up to 1 Hz (Pierri et al., 1993): for a point source model having a dip-slip mechanism and an "Apenninic" strike, the synthetic displacement fields associated to the P-SV and SH components show an elongation axis respectively in "anti-Apenninic" and "Apenninic" direction; moving the hypocentral depth from 15 to 4 km, the R value goes from 1.25 to 1.65 and correspondently the total synthetic field changes from an anti-Apenninic elongation to a
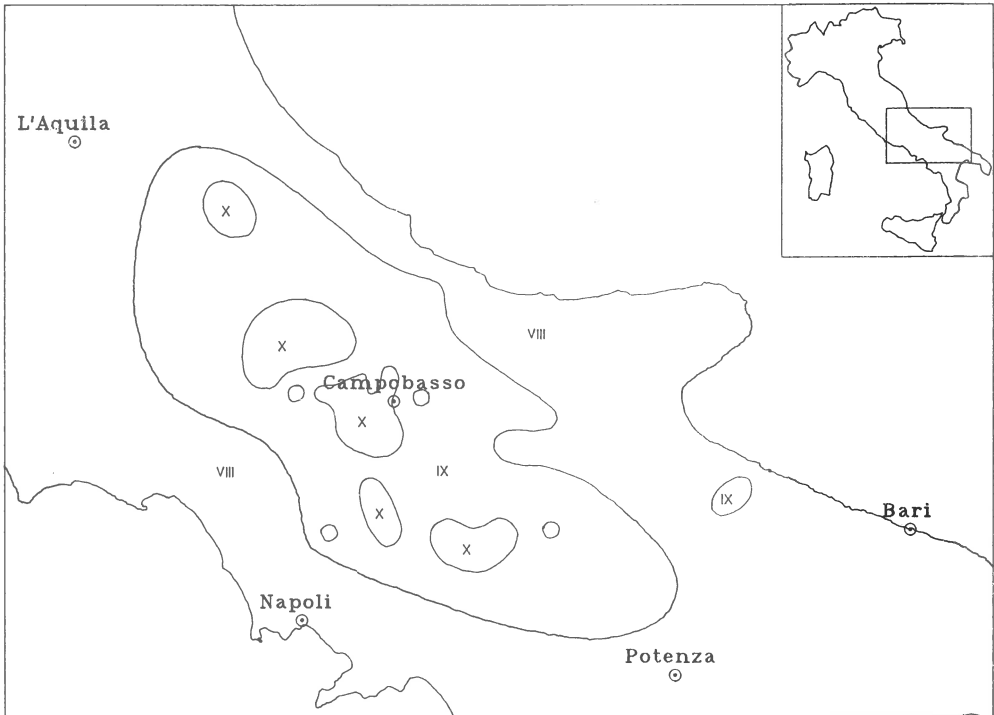
Fig. 1: *Isoseismal map of the earthquake occurred in Southern Apennines on December 1456.*

sub-circular shape. As a consequence, synthetic isoseismals elongated in the fault strike direction could be obtained only with a further reduction of the hypocentral depth or modifying the structural model to a not realistic extent.

The situation changes if an extended source model is considered. A simple model consists in defining a series of equally spaced point sub-sources aligned along the fault direction. Having attributed to each sub-source the same focal parameters previously considered for the single point source model (depth 4 or 15 km, strike 320°, dip 70°, rake 275°), the shape of total synthetic field resulted strongly influenced by the triggering time sequence of the sub-sources and by the relative weights assigned to them, particularly in the case of the hypocentral depth (4 km) for which the single point approximation had given a subcircular radiation pattern. If the sub-sources are simultaneous, the global isoseismals show a marked elongation normal to the source alignment (Fig. 2 a): this effect is apparently due to the fact that, along a symmetry axis normal to the source alignment, the similarity of shape, amplitude and arrival time of waves coming from the different sub-sources determines a strong constructive interference; at different azimuth, partial attenuation or reinforcement can take place generating an alternation of minima and secondary maxima. Attributing a different weight to the sub-sources and introducing a time shift in their triggering sequence, a significant elongation can be obtained as well, but its axis can be rotated so that it becomes parallel to the strike direction (Fig. 2 b,c). This rotation of the elongation axis seems less evident or concerns just part of the macroseismic field when the radiation pattern of single sub-source has a remarkable directionality: for instance, in the case of a hypocentral depth equal to 15 km (Fig. 2 d,e,f), rotation can be recognised in the inner part of the synthetic isoseismals, whereas the outer one maintains approximately the elongation of the single source radiation pattern.

The introduction of a time shift in the triggering sequence of sub-sources simulates the progression of a rupture process having a velocity depending on the time intervals of source triggering. Therefore, according to the rupture process velocity assumed in the model, it is possible to obtain different orientations in the isoseismal elongation, particularly if structural characteristics and focal parameters generate an approximate isotropy of the point source radiation pattern. This conclusion suggests the possibility that, under particular circumstances, the rupture process plays a more important role than focal mechanism in determining the shape of isoseismals.

SYNTHETIC INTENSITY FIELDS

Situations like that previously described make information on focal mechanism more difficult to be obtained from macroseismic data, but they do not represent a common case. Under different conditions the main characteristics of a macroseismic field can be explained with a simple point source model (Panza et al., 1991), particularly in case of structurally homogeneous areas with simple and straight tectonical characteristics which are interested by rupture processes not very complicated: for instance, the experimental isoseismals of the earthquake occurred in the Gargano promontory (Apulia, Southern Italy) in 1627 (Fig. 3) seem quite similar to the radiation pattern of a point source having a dip-slip focal mechanism characterised by an "Apenninic" strike (Fig. 4).

However, the adoption of a purely qualitative comparison criterion for the determination of a source model compatible with isoseismal map, makes this a rather laborious task liable to the bias of prejudices: since a great deal of different source models should be examined and processed, some simplifications are generally introduced which can be based on subjective evaluations. Furthermore, the same tracing of experimental isoseismals is an operation implying a certain margin of subjectivity: it should be reminded that the operator, rarely having at his

H=4 km **H=15 km**
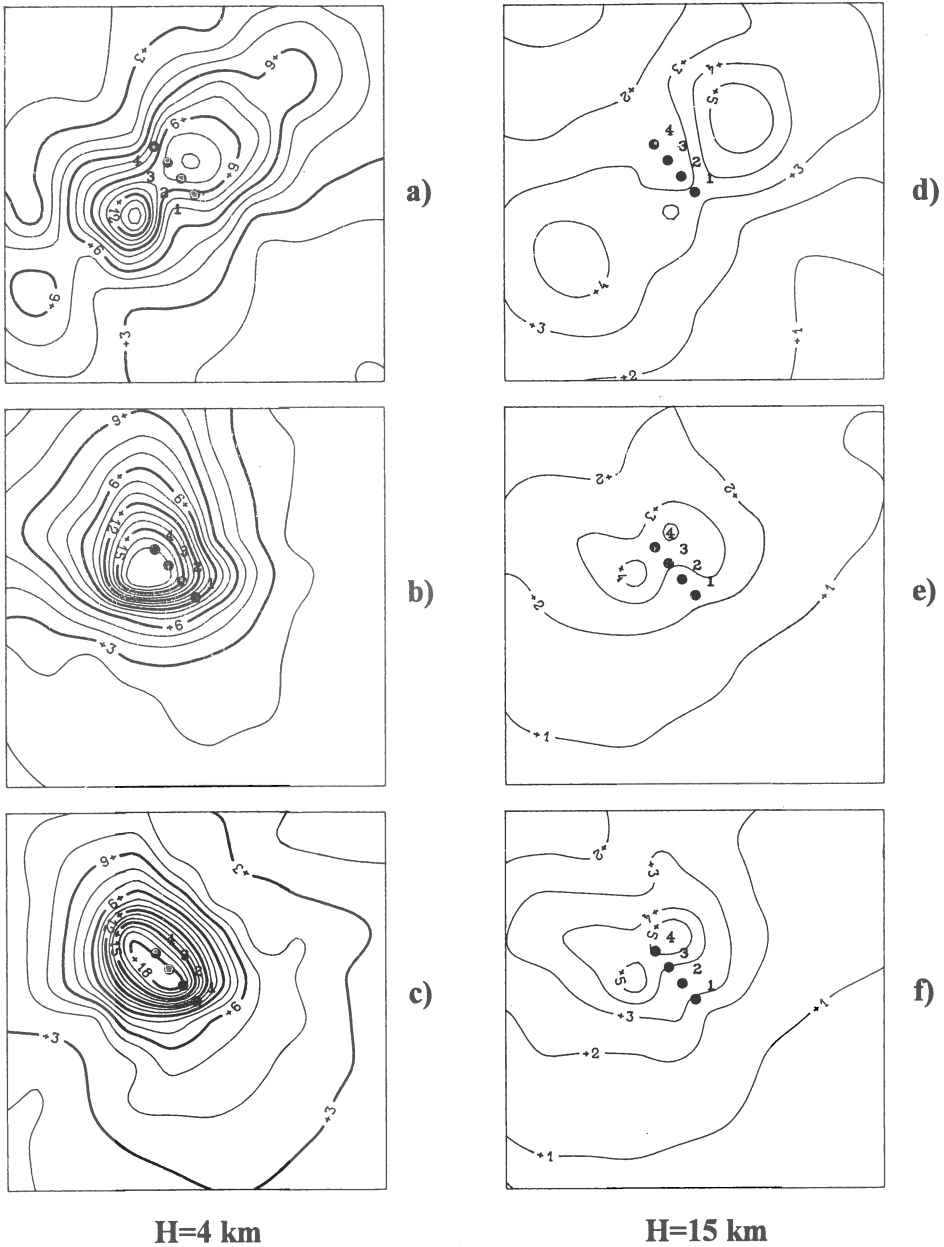
Fig. 2: *Displacement field (in cm for a seismic moment of 10^{26} dyne· cm) obtained from an extended source model consisting of four point sources at hypocentral depth H. Structural model employed: APNSUD (Costa et al., 1993); frequency interval 0.-1. Hz; strike=320°; dip=70°; rake=275°. **a)** e **d)** represent cases of four point sources simultaneously activated and having the same energy. In **b)** the sources are triggered in the time sequence 0-2-4-6 s; in **c)** **e)** and **f)** the sequence is 0-2-5-8 s but in **c)** and **f)** the four sources have relative weights respectively 1-1.2-1.4-1.6..*
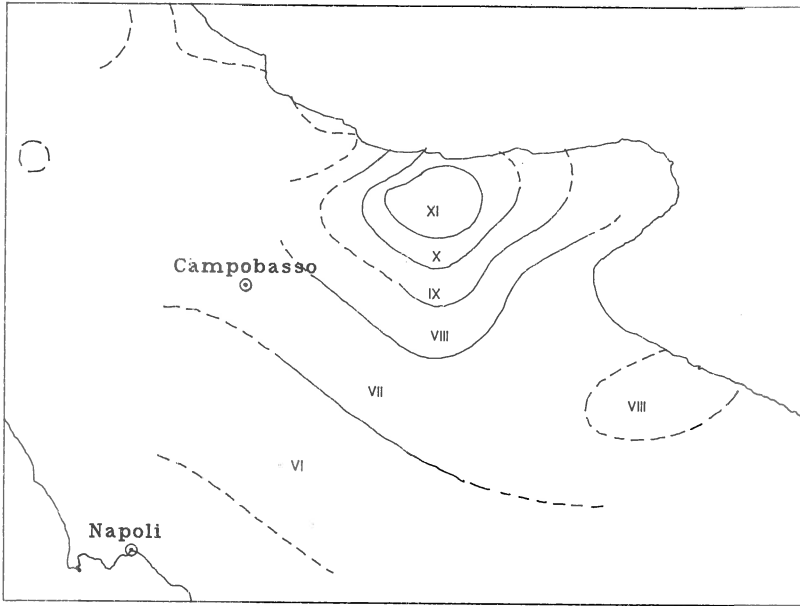
Fig. 3: *Isoseismal map of the earthquake occurred in the Gargano area on July 1627.*
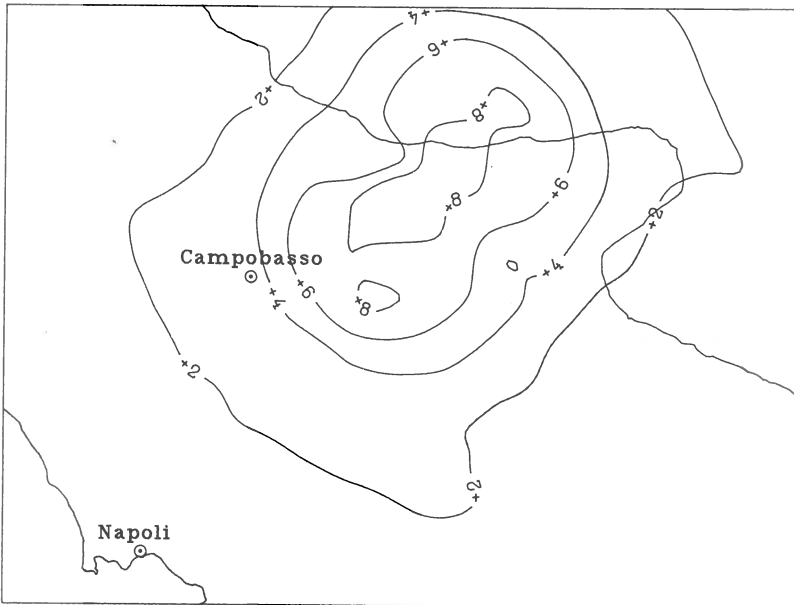
Fig. 4: *Synthetic peak horizontal acceleration field for a point source model having: seismic moment $=10^{26}$ dyne·cm; hypocentral depth=15 km; strike=310°; dip=45°; rake=90° or 270° (contour spacing 2 cm·s^{-2}). Structural model employed: PUG4A (Costa et al., 1993).*

disposal a homogeneous distribution of macroseismic observations, often fills the gaps of data by interpolating them according to criteria depending on his previous knowledge and experience.

For these reasons we planned a modification of the procedure aimed at a quicker and more objective evaluation of the agreement between experimental data and theoretical calculations. The new procedure consists in computing the peak horizontal acceleration corresponding to each source model considered at the same locations where experimental intensity values are available: in this way a numerical comparison can be carried out, based on the actually available intensity data.

The definition of an intensity-acceleration relation giving a basis for numerical comparison, presents some problems: first, the empirical formulae proposed in literature (see Trifunac & Brady, 1975; Murphy & O'Brien, 1977) generally refer to the logarithm of the observed peak horizontal ground acceleration which often corresponds to frequencies greater than 1 Hz; moreover, in order to evaluate the intensity associated to theoretical acceleration, source modelling should include a further parameter characterising the earthquake energy. Since previous studies showed that the general shape of the synthetic isoseismals does not change significantly if the considered frequency band and the seismic moment attributed to the earthquake model are modified, the aforementioned problems can be by-passed adopting a comparison criterion based on cross-correlation between intensities observed and the logarithm of synthetic peak accelerations computed at all the macroseismic observational sites.

The adoption of a numerical comparison allows an automation of the procedure. All the routines of the computational package were inserted in a single general program which computes synthetic seismograms for different source models at the sites for which geographical co-ordinates and macroseismic intensity are reported. The different source models examined are defined by combining different values of focal location and mechanism parameters whose variation range and step is defined in input, whereas rupture characteristics are kept constant. Through seismosynthesis, the peak horizontal acceleration (named AMAXA) and its logarithm (AMALOG) are determined and the cross-correlation coefficient between AMALOG and intensity values are computed. The results obtained for the different source models are finally listed in decreasing order.

Through this procedure, a global search for source models which show the best fitting with the experimental intensity fields can be carried out quite conveniently; initially the variable parameters are modified with a rough step throughout the whole possible range; then, starting from the best models that have been found, a finer exploration of solution space around them is carried out to obtain an improvement of results. The graphic representation of isoseismals can be limited just to the highest correlation solutions with a remarkable time saving. Considering a solution among the best ones found, it can be interesting to evaluate which experimental observations do not satisfactorily fit the theoretical computations; for this purpose a linear regression of intensities against AMALOG is carried out so that the coefficients for a linear transformation of acceleration logarithm in "synthetic" intensities are obtained and "residual" intensities are derived from a comparison with the experimental data. Residual distribution can point out the possible existence of systematic discrepancies related to source model defects (particularly in the case of extended source) or to site effects (if a correlation with surface geology is recognisable).

For a first experimental test of the efficiency of this procedure, the Gargano 1627 event was considered. This choice was determined by the relatively simple shape of the isoseismal map, which suggests a rupture process not too complicated (probably related to the tabular tectonic style of the area) so that the macroseismic field seems mainly controlled by the radiation pattern of the focal mechanism. For this reason a point source model was adopted and the

search for the best correspondence between experimental intensities and theoretical peak accelerations was based only on modification of hypocentre location and focal mechanism. For this event 55 intensity estimates are available from the "Atlas of isoseismal maps of Italian earthquakes" (C.N.R.- P.F.G., 1985), so the definition of the "synthetic intensity field" requires the calculation of synthetic seismograms only at 55 sites (whereas much more sites are generally necessary for a good coverage of the area when adopting a regular grid).

The point source model which gave the highest cross-correlation coefficient (0.896) between peak acceleration and experimental intensities is characterised by a hypocentral depth of 10 km and by a dip-slip mechanism having fault oriented approximately in N-S direction (strike 10°, dip 90°, rake 80° or 260°). Fig. 5 shows the intensity field obtained for this source model through the calculation of peak horizontal accelerations on a regular grid of points: the acceleration values were transformed in intensity values by means of coefficients obtained from a linear regression of peak accelerations computed at the 55 observational sites (the root mean square of the regression residuals was equal to 0.7). As a comparison, the same operation was carried out for the source model considered as the best solution on the basis of a purely qualitative comparison between seismosynthetic displacement field and experimental isoseismal (Fig. 6). The correlation of peak accelerations with experimental intensities for this model is significantly lower (0.701) and also the r.m.s. of regression residuals is worse (1.1).

A comparison between Fig. 5 and 6 shows that the "automatic" solution implies a different way of interpolating the experimental intensities (the corresponding isoseismals are elongated in direction approximately E-W instead of NE-SW). Obviously a simple list of intensities does not report all the information existing on a macroseismic field and a different picture can be justified on the basis of a more complete examination of data and their reliability; however the automatic solution suggests at least a possible alternative interpretation of the macroseismic field, which from a geological point of view is also acceptable, since important faults with a similar orientation (e.g. along the Fortore river) were recognised in the Pleistocene tectonics of the region around the epicentral zone (see Ciaranfi et al., 1983b).

CONCLUSIONS

Seismosynthetic techniques were employed for the study of historical event macroseismic fields in order to obtain information on source characteristics, with special reference to focal mechanism. The application of this technique to frequencies closer to those involved in major macroseismic effects pointed out some problems. Generally, dealing with large events, the point source approximation cannot be accepted a priori when the frequencies considered in seismosynthesis are not very low (greater than 0.1 Hz); the modelling of extended sources shows that in certain cases, particularly with focal mechanism whose radiation pattern is not strongly directional, the characteristics of the rupture process (velocity and energy), on account of interference phenomena, can influence the macroseismic field in such a measure that it does not reflects the focal mechanism.

However, if the rupture process is not very complicated, information on focal mechanism (orientation and dip of fault and direction of movement) can be obtained. An approach of inversion closer to the original data (i.e. intensity field rather than isoseismals) and a semi-automatic treatment seems preferable, since that allows the examination of a wider range of possible solutions and reduces the possible bias of subjective evaluations.
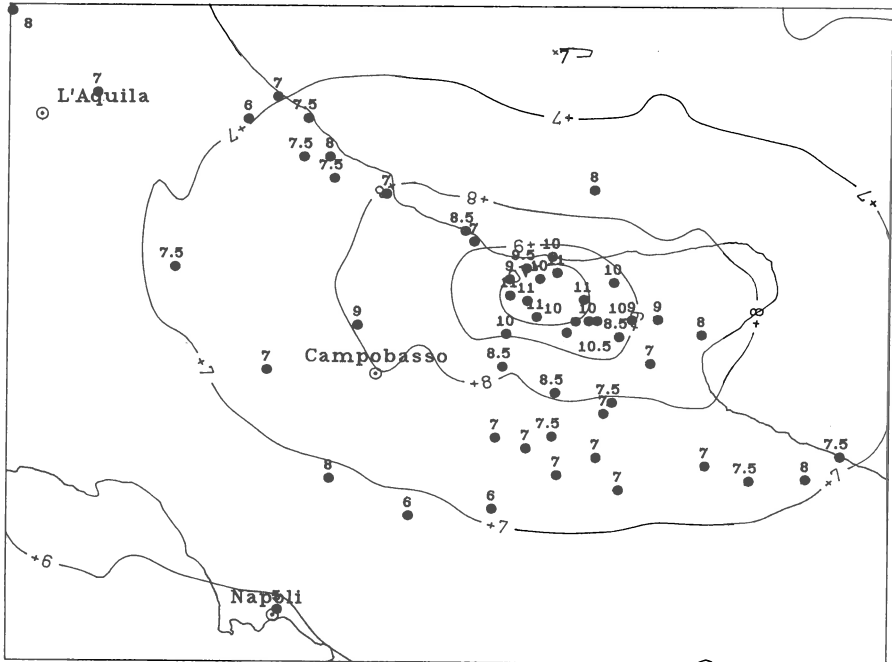
Fig. 5: *Comparison between experimental intensities and synthetic isoseismal map for a point source model having: hypocentral depth=10 km; strike=10°; dip=90°; rake=80° or 260°.*
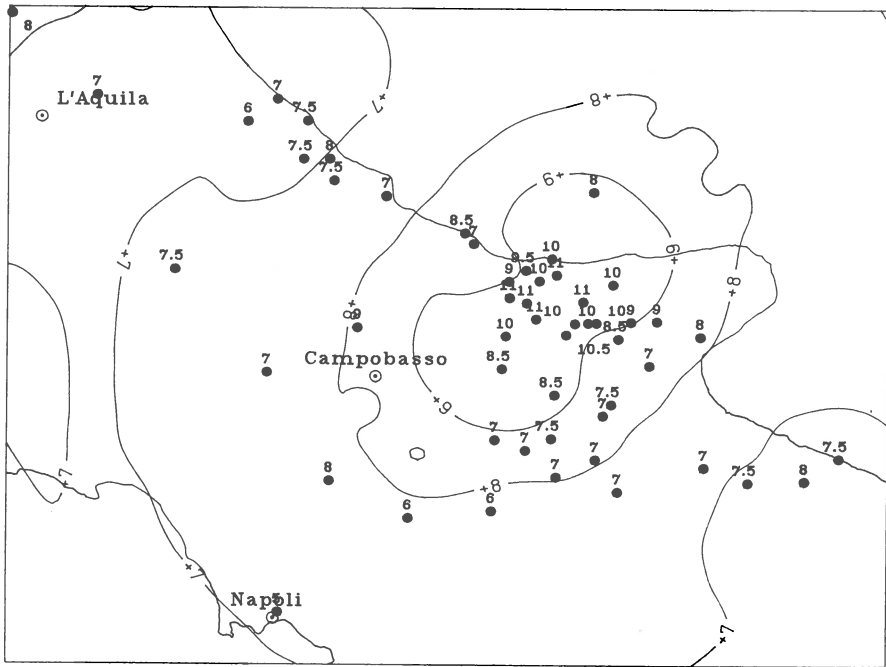
Fig. 6: *Comparison between experimental intensities and synthetic isoseismal map for a point source model having: hypocentral depth=15 km; strike=310°; dip=45°; rake=90° or 270°.*

REFERENCES

Ciaranfi, N., M. Guida, G. Iaccarino, T. Pescatore, P. Pieri, L. Rapisardi, G. Ricchetti, I. Sgrosso, M. Torre, L. Tortorici, E. Turco, R. Scarpa, M. Cuscito, I. Guerra, G. Iannaccone, G.F. Panza and P. Scandone, 1983a. Elementi sismotettonici dell'Appennino Meridionale. Boll. Soc. Geol. It., 102, 201-222.

Ciaranfi, N., F. Ghisetti, M. Guida, G. Iaccarino, S. Lambiase, P. Pieri, L. Rapisardi, G. Ricchetti, M. Torre, L. Tortorici and L. Vezzani, 1983b. Carta neotettonica dell'Italia Meridionale. C.N.R., Progetto Finalizzato Geodinamica, pubbl. n. 515.

C.N.R. - P.F.G., 1985. Atlas of isoseismal maps of Italian earthquakes. Postpischl D., Editor, Quaderni de "La ricerca scientifica", 114, 2A.

Costa, G., G.F. Panza, P. Suhadolc and F. Vaccari, 1993. Zoning of the Italian territory in terms of expected peak ground acceleration derived from complete synthetic seismograms. In: Geophysical Exploration in areas of complex geology, R. Cassinis, K. Helbig and G.F. Panza, editors, II. J. Appl. Geophys., 30, 149-160.

Florsch, N., D. Fah, P. Suhadolc and G.F. Panza, 1991. Complete synthetic seismograms for high-frequency multimode SH-waves. Pageoph, 136, 529-560.

Murphy, J.R. and L.J. O'Brien, 1977. The correlation of peak ground acceleration amplitude with seismic intensity and other physical parameters. Bull. Seism. Soc. Am., 67, 877-915.

Panza, G.F., 1985. Synthetic seismograms: the Rayleigh waves modal summation. J. Geophys., 58, 125-145.

Panza, G.F., A. Craglietto and P. Suhadolc, 1987. Influenza dei parametri di sorgente sulle caratteristiche del campo macrosismico. Atti 6° Convegno G.N.G.T.S., 255-268.

Panza, G.F., A. Craglietto and P. Suhadolc, 1991. Source geometry of historical events retrieved by synthetic isoseismals. Tectonophysics, 193, 173-184.

Panza, G.F. and M. Cuscito, 1982. Influence of focal mechanism on shape of isoseismals: Irpinia earthquake of November 23, 1980. Pageoph, 120, 577-582.

Pierri, P., V. Del Gaudio and G. Calcagnile, 1993. Influenza dei parametri di sorgente e del processo di rottura sulla forma delle isosiste. Atti 12° Convegno G.N.G.T.S., Roma, November 24-26, 1993.

Suhadolc, P., L. Cernobori, G. Pazzi and G.F. Panza, 1988. Synthetic isoseismals: applications to the Italian earthquakes. In: Seismic Hazard in Mediterranean regions, J. Bonnin, M. Cara, A. Cisternas and R. Fantechi, editors, 205-228, Kluwer, Dordrecht.

Suhadolc, P., 1989. Frequency dependence of synthetic isoseismals, First AB workshop on macroseismic methods. Poljce, Slovenija, Yugoslavia, May 9-11, 1989

Trifunac, M.D. and A.G. Brady, 1975. On the correlation of seismic intensity scales with the peaks of recorded strong ground motion. Bull. Seism. Soc. Am., 65, 139-162.

WEAK AND STRONG GROUND MOTION, SOURCE PARAMETERS AND SCALING LAWS FOR INTERMEDIATE DEPTH EARTHQUAKES FROM THE VRANCEA REGION, EASTERN CARPATHIANS

MIHNEA CORNELIU ONCESCU[1], KLAUS-PETER BONJER[1] and MIHAELA RIZESCU[2],

[1] Geophysical Institute, Hertzstraße 16, 76187 Karlsruhe, Germany
[2] National Institute for Earth Physics, P.O. Box MG-2, 76900 Bucharest-Magurele, Romania

Inversions to determine source and site spectra starting from strong motion and weak motion data were performed. The strong motion data set consists of S-wave accelerograms from 13 strong motion SMA-1 instruments which triggered on four large events: March 4, 1977 with M_w=7.4, August 30, 1986 with M_w= 7.2, May 30, 1990 with M_w= 6.9 and May 31, 1990 with M_w= 6.1. The velocity data set consists of P- and S-wave seismograms from 11 PCM5000 and PCM5800 stations which triggered on 16 small-to-moderate events with M_w= 3.9 - 5.3. All events are intermediate depth earthquakes from the Vrancea region in the Eastern Carpathians. The Joint Source-Site Determination (JSSD) method we applied uses horizontal acceleration or velocity spectra corrected for instrument, free surface and geometrical spreading as input data. The method is formulated as a linear inverse problem repeated over frequencies (Andrews, 1986; Boatwright et al., 1991), with one reference station. For this station the site amplification spectrum was calculated from known geotechnical information and from coda-Q attenuation. The inversion was performed in the 0.1 - 12 Hz frequency band for the four large events and 0.3 - 15 Hz band for the small 16 events.

Amplifications of up to six times and deamplifications of up to five times were put into evidence in the site amplification spectra, attenuation anomalies included.

We showed that the pronounced peak at 0.6 Hz at station INC, responsible for the damage of 5-7 stores buildings in Bucharest, is not site, but source related. We proved this by using the JSSD and the empirical Green function deconvolution methods. Moreover, the transfer function calculated according to the geotechnical information under the INC site does not show that peak either.

Site amplification spectra at six stations were obtained both from weak ground motion (PGA < 5 cm/sec^2) and from strong ground motion (PGA > 70 cm/sec^2) data. The analysis in the 0.3 - 12 Hz frequency band does not show evidence for non-linear behavior associated with the strong motions, as suggested by Lungu et al. (1992).

Using the source spectral models by Brune (1970) and Boatwright (1980, unbiased source parameter analyses and scaling law studies could be performed for a range of almost six orders in seismic moment. The seismic moments vary with the corner frequency to the power of minus three. The stress drop and apparent stress increase with seismic moment. The stress drops of the large events are very high, between 181 and 502 MPa, in agreement with the previous determinations of Bonjer (1983) for the 1977 event and of Oncescu (1989) for the 1986 event. The slope of the seismic energy vs. seismic moment log-log curve is 1.5 for small events and decreases to 1.2 for the large ones, in agreement with the study of Kanamori and Anderson (1975). There seems to be no correlation of the seismic efficiency and apparent stress with depth. According to the ε parameter defined by Zuniga (1993, we found a tendency for overshooting in the main shocks and for partial stress drop in the aftershocks. The scale

length of inhomogeneities on the rupture planes of the large events (Papageorgiou, 1988) is estimated at 0.9 ($\pm$ 0.2) km.

An additional inversion for the P wave vertical components was performed for the 16 small events. The comparison of the source parameters determined from P and S waves shows a robust seismic moment determination (average $M_{oP}/M_{oS}= 1$) and a consistent corner frequency determination (average $f_{cP}/f_{cS}=1.53$).

Andrews, D.J. (1986). Objective determination of source parameters and similarity of earthquakes of different size, in *Earthquake Source Mechanics*, S. Das, J. Boatwright and C.H. Scholz (Editors), American Geophysical Union, Washington, D.C., p. 259-268.

Boatwright, J. (1980). A spectral theory for circular seismic sources: simple estimates of source dimension, dynamic stress drop, and radiated seismic energy. Bull. Seism. Soc. Am., v.70, p.1-27.

Boatwright, J., Fletcher, J.B., and Fumal, T.E. (1991). A general inversion scheme for source, site, and propagation characteristics using multiply recorded sets of moderate-sized earthquakes. Bull. Seism. Soc. Am., v. 81, p. 1754-1782.

Bonjer, K.P. (1983). Seismizität als Zugang zu räumlichen und zeitlichen Anomalien der Spannungen in der Lithosphäre, in *Spannungen und Spannungsumwandlung in der Lithosphäre*, SFB 108 Report 1981-1983, Karlsruhe University, March 1983, p. 87-124.

Brune, J.N. (1970). Tectonic stress and the spectra of seismic shear waves. J. Geophys. Res., v. 75, p. 4997-5009.

Kanamori, H. and Anderson, D.L. (1975). Theoretical basis of some empirical relations in seismology. Bull. Seism. Soc. Am, v. 65, p. 1073-1095.

Lungu, D., Demetriu, S. and Cornea, T. (1992). Frequency bandwidth of Vrancea earthquakes and the 1991 edition of seismic Code of Romania, in *Proceedings of the Tenth World Conference on Earthquake Engineering*, v. 10, A.A. Balkema, Rotterdam, p. 5633-5638.

Oncescu. M.C. (1989). Investigation of a high stress drop earthquake on August 30, 1986 in the Vrancea region. Tectonophysics, v. 163, p. 35-43.

Papageorgiou, A.S. (1988). On two characteristic frequencies of acceleration spectra: patch corner frequency and f_{max}. Bull. Seism. Soc. Am., v. 78, p. 509-529.

Zuniga, F.R. (1993). Frictional overshoot and partial stress drop. Which one ? Bull. Seism. Soc. Am., v. 83, p. 939-944.

WAVEFORM·INVERSION OF VRANCEA (ROMANIA) EARTHQUAKES

M. Radulian, L. Ardeleanu

National Institute for Earth Physics, Bucharest, Romania

P. Campus

Istituto di Geodesia e Geofisica, Universita' degli Studi,
Trieste, Italy

J. Sileny

Geophysical Institute, Czech Academy of Sciences, Prague,
Czech Republic

G.F. Panza

Istituto di Geodesia e Geofisica, Universita' degli Studi,
and International Center for Theoretical Physics,
Trieste, Italy

The goal of this paper is to obtain the source moment tensor of weak Vrancea (Romania) earthquakes ($M_L < 3.5$) by waveform inversion of high - frequency seismograms, vertical component, recorded by the Romanian local network.

The method and related software are developed at the Institute of Geodesy and Geophysics of the University of Trieste and the Geophysical Institute, Czech Academy of Science, Prague (Panza, 1985, Sileny et al., 1992).

The source is described by the full moment tensor, having both volumetric and deviatoric components. The initial synthetic seismograms are constructed by convolving the time derivative of the seismic moment tensor with the so-called "base functions".

The source time function, given by the time derivative of the moment tensor, is parameterized by means of overlapping triangles delayed in time. The number and the width of the triangles are fixed parameters, while their weights are variable during the inversion.

The "base functions" are the responses of the medium to sources represented by elementary dipoles with Heaviside function time dependence. These base functions are computed by normal mode summation, for a discrete set of source depths and for two structural models, considered to represent acceptable extremes for the region under study. The algorithm allows both the source depth and the structural model to vary within an a priori chosen range, during the inversion.

The procedure is applied to two shallow earthquakes (1 May 1982, h = 22 km, M_L = 3.1; 23 June 1982, h = 19 km, M_L = 3.3) and one intermediate depth earthquake (3 April 1986, h = 60 km, M_L = 3.3) of the Vrancea region.

Six stations of the Romanian telemetered network are used in the inversion: MLR, VRI, CVO, BRD, TLB, CFR. Since their epicentral distances cover a rather wide range (from about 10 to 200 km), a specific model input structure is adopted for each source - station path. For the crust the flat layered models determined by Raileanu et al. (1994) are used. To take into account the presence of the subducting slab, which generates the Vrancea intermediate depth seismic activity, subcrustal structures with continuously increasing P and S wave velocities and high Q values are considered for the stations situated above the slab (MLR, VRI, CVO). For the other stations (TLB, CFR, BRD) an average model of continental lithosphere is adopted, with a low velocity channel within the depth interval 90 to 200 km.

The inversion is performed for time windows of 12 sec of S wave train. The retrieved source mechanisms are in good agreement with the distribution of the few P wave polarities available, that are absolutely not sufficient for the determination of a reliable source mechanism with standard methods. The fault plane solutions are quite similar to those previously obtained for moderate size earthquakes in the region.

The results of this work represent the first attempt to use multimode summation technique to study both shallow and intermediate depth earthquakes of the Vrancea region and demonstrate the possibility to reliably reconstruct the focal mechanism by using a small number of records (4 or 5 only).

References

Panza G.F., 1985. Synthetic seismograms: the Rayleigh waves modal summation. J. Geophys., 58, 125-145.

Raileanu V., C. Diaconescu, D. Mateciuc and M. Diaconescu, Velocity crustal models under the Romanian telemetered seismological network. Romanian Reports in Physics (in press).

Sileny J., G. F. Panza and P. Campus, 1992. Waveform inversion for point source moment tensor retrieval with variable hypocentral depth and structural model. Geophys. J. Int., 109, 256-274.

LARGE EARTHQUAKES, RUPTURE PROCESS AND MICROSEISMICITY IN CENTRAL GREECE

P. Papadimitriou, K. Makropoulos and J. Drakopoulos
Department of geophysics, University of Athens, Athens, Greece

ABSTRACT

Historical and instrumental data indicate that central Greece is characterised by high seismic activity which has caused important damages in the area. In this paper we study two earthquake sequences occurred along the southern part of Thessalia. The first one during the period 1954-1957 characterized by three large events and the second one during the period 1980-1985, when four large earthquakes took place. The last earthquake occurred on April 30, 1985, near Almyros. The source parameters of this event were calculated by the Gaussian Beam Summation method, using WWSSN records.

In summer 1992, a seismological network of about 70 analogue and digital seismographs was installed in the area in order to record the local seismicity. A part of the recorded microseismicity was located and fault plane solutions were computed, using P-waves first motion polarities. The results of this analysis compared with the above mentioned large events, show a similar pattern: shallow seismicity with a depth distribution between surface and 15 km and the fault plane solutions indicating normal faulting. Furthermore, strike-slip motion is observed in the region of Farsala.

The data analysis, reveals an active seismic zone, for which three parts can be distinguished: the eastern (Volos-Almyros area), is characterised by normal faulting of about 55 km length, striking E-W and dipping south. The central (Velestino area), is characterised by normal faulting of about 15km length, striking E-W and dipping south. Finally, the western part (Sofades-Farsala area), is characterised by a more complex pattern consisting of two different fault mechanisms: the Sofades normal fault, of about 30 km length, striking N300°, dipping NE and the Farsala area, where strike-slip motion is observed.

INTRODUCTION

Since 1950, Central Greece (Volos-Almyros and the surrounding area), has suffered by two strong earthquake sequences: the first started on April 30, 1954, near Sofades and was followed by the destructive earthquakes of April 19, 1955, south of Volos and March 8, 1957, near Velestino. The second, started on July 9, 1980, south of Volos (B. C. Papazachos et al., 1983), followed by the April 30, 1985, Almyros earthquake (P. Papadimitriou et al., 1993). The last one, was the first event in the area teleseismically recorded by the WWSSN network, allowing the application of modelling techniques for the source parameters determination. The analysis of the July 9, 1980, earthquake was of significant difficulty due to the waves overlapping, resulted from the almost simultaneous occurrence of the foreshock. On the contrary, the records of the April 30, 1985, earthquake were of good quality, thus allowing the calculation of synthetic seismograms. In this paper, the computed source parameters of large earthquakes supplemented with microearthquake data recorded by a temporary network installed in the area for a period of two months in 1992, as well as tectonic observations followed the Sofades, Velestino and Volos earthquakes (B. C. Papazachos et al., 1983; Papastamatiou and Mouyaris, 1986; Ambraseys and Jackson, 1990), are considered in order to resolve the stress field distribution and the rupture processes in the area.
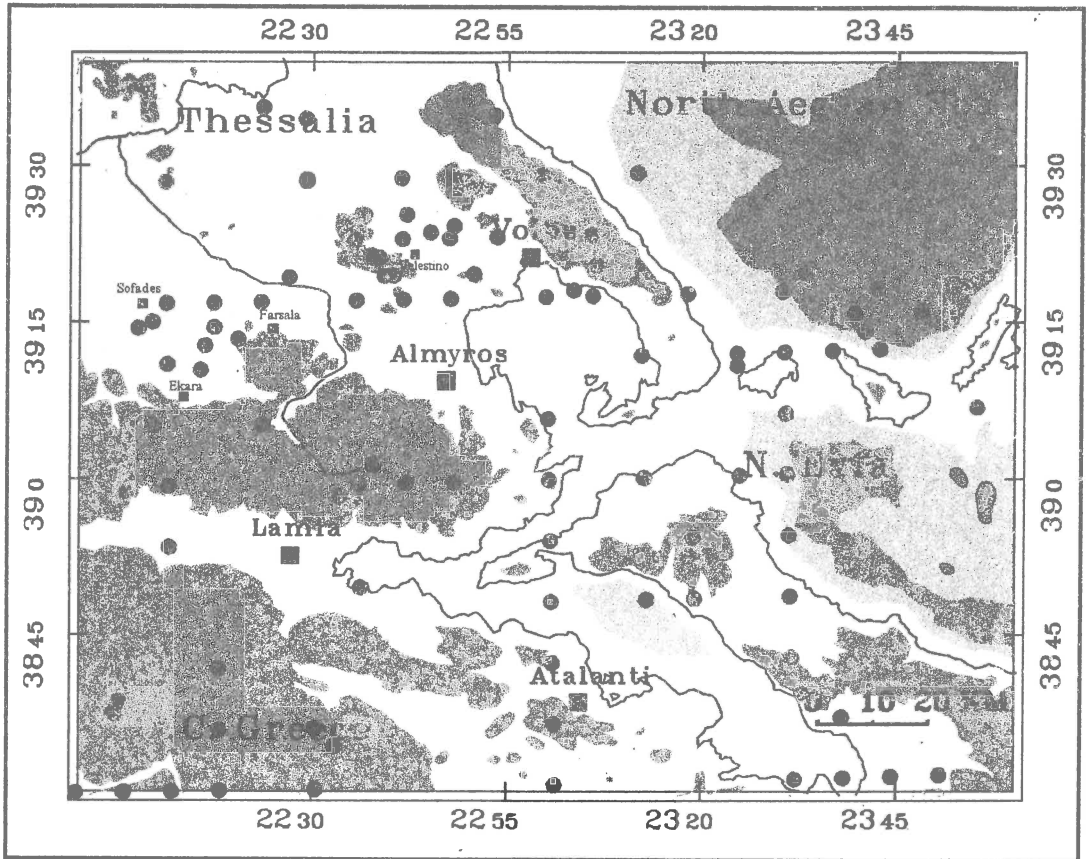
Figure 1. Seismicity map for a time period until 1962. Topography contours are at 400m and bathymetry are at 200 and 600m.

The Aegean Sea and its surrounding regions of Greece are considered to be among the most rapidly N-S extending areas. Regional considerations suggest that the rate of extension across the whole area is 40-60mm/yr (McKenzie, 1978; Le Pichon and Angelier, 1979; Jacson and McKenzie, 1988b). The seismic activity reveals that most of this extension is attributed to the motion of the large earthquakes. Jackson and McKenzie 1988a,b consider that the contribution of smaller faults and aseismic creep are probably not significant to the regional deformation of the upper crust. A large earthquake of a magnitude 6 produces a slip on a fault of about 10-15km which is similar to the dimension of the thickness of the upper seismogenic layer of the continental crust estimated 10-15km (King et al. 1985; Hatzfield et al. 1993; P. Papadimitriou et al. 1995). Since it is known that large faults take up most of the deformation, a knowledge of the geometry and kinematics of these faults is fundamental to interpret the ruture process and in general how the extension is achieved.

The seismic activity in Central Greece for the period until 1962 is presented in figure 1. The seismicity covers the whole area but it is mainly concentrated around Volos-Almyros, Velestino and Sofades-Farsala area. It is well known that the location errors for some of these events could be more than 20km, but considering that these events have caused important damages, this pattern determines relatively well the seismic active zones of the area. Figure 2 presents the seismic activity during the period 1963-1987. In this figure, the 1980-1985 earthquake sequences are also

included. The seismicity does not reveal the same pattern to that of the previous figure because only the Volos-Almyros area presents an important seismicity.

Date	Time	Lat.(N) - Long.(E)	Mag.	Depth	Az-Dip-Rake
1954 4 30	13:02:36	39.23 22.28	6.7	10	300 45 -90
1955 4 19	16:47:19	39.31 23.06	6.2	15	80 45 -90
1957 3 8	12:14:14	39.40 22.70	6.5	15	110 45 -90
1957 3 8	12:21:13	39.30 22.60	6.8	15	110 45 -90
1980 7 9	2:10:19	39.25 23.00	5.6	13	80 45 -90
1980 7 9	2:11:56	39.27 23.09	6.3	16	80 45 -90
1980 7 9	2:35:52	39.16 22.68	6.0	18	80 45 -90
1985 4 30	18:14:13	39.26 22.81	5.8	8	80 52 -115

Table 1. Source parameters determination of the large earthquakes
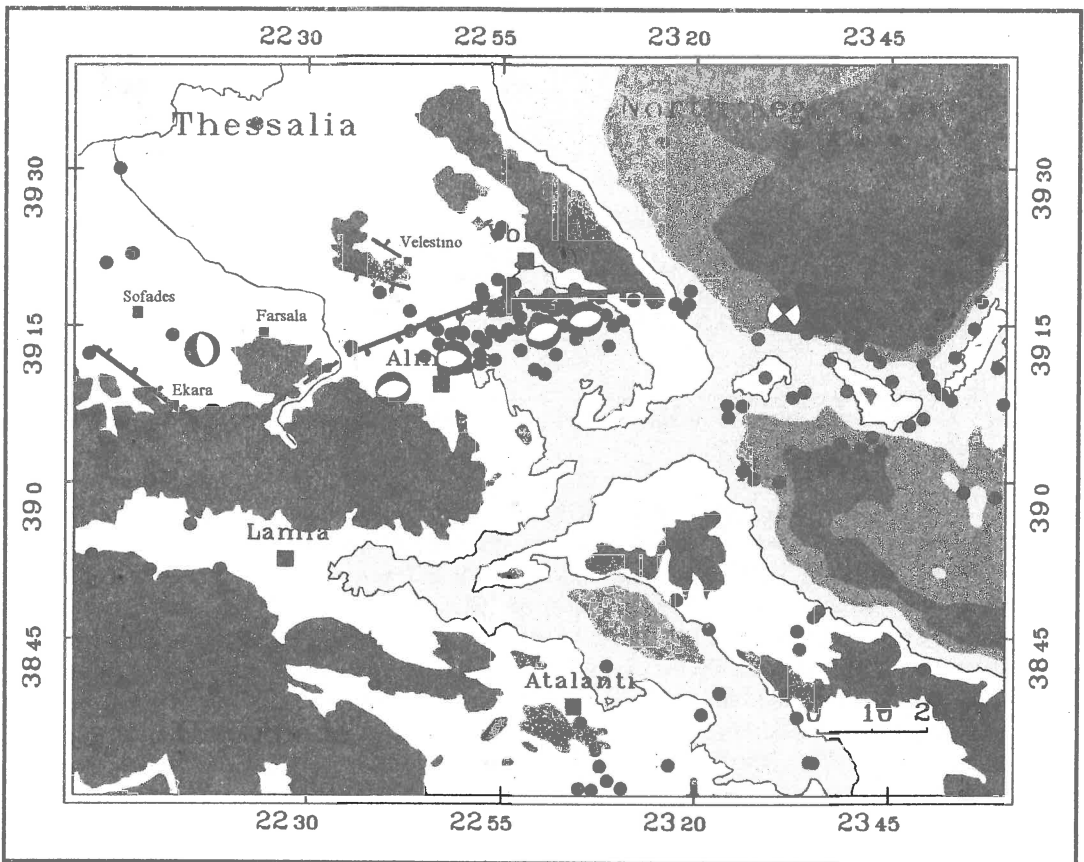
Figure 2. Seismotectonic map of Central Greece

FIRST EARTHQUAKE SEQUENCE (1954-1957)

The Sofades earthquake of April 30, 1954, was preceded by a small shock a few days earlier, that marked the beginning of the first phase of an important seismic activity in Central

Greece and caused extended distraction in the area. The earthquake was associated to a normal fault striking N300°, consisting of "an echelon" fractures dipping toward the NE which penetrated for about 5km within the limestone/periodite foothills (Papastamatiou and Mouyaris, 1986) and with an average throw of 30cm (the maximum reported was 90cm). The fractures, which cross the village Ekara, do not follow any apparent lineament of the topography. Ambraseys and Jackson, (1990), consider these fractures of a total length of about 30km. This consideration based on local cursory inspections, is more consistent with the expected fault length for such an earthquake magnitude. In addition, no clear evidence of lateral shear was observed. The focal mechanism computed by McKenzie, (1972) using P-waves' first motion polarities, indicates normal faulting in N-S direction (the fault plane solution was not very well constrained).

On April 19, 1955, an earthquake occurred south of Volos in the gulf of Pagassitikos. This earthquake, preceeded by a small shock, was associated with tsunami within the gulf. For this event there is no available focal mechanism, but while it is located in the close vicinity of the July 9, 1980, earthquake, we assume similar focal mechanisms, indicating E-W normal faulting.

The end of the first sequence is marked by the, March 8, 1957, earthquakes. Two shocks with approximately the same magnitude and a time interval of seven minutes between them took place in Velestino area. These earthquakes didn't produce clear evidence of surface faulting. Only two surface breaks of about 500m long, one NW of Velestino (striking N300° and dipping NE) and another SW of Velestino (striking E-W and dipping south). The structure and topography of the area is characterised by the Velestino fault, situated southeast of the town, striking N100° and dipping south. It is a normal fault lying at the southern foothills of the Chalkodonion mountain (≈600m relief), visible in aerial photographs and satellite images (Mountrakis et al, 1993) for a length of about 15km. We associate this earthquake with normal faulting striking N100°, similar to the July 9, 1980, earthquake.

SECOND EARTHQUAKE SEQUENCE (1980-1985)

The second earthquake sequence consists of four shocks. The first one was the foreshock occurred on July 9, 1980, just before the main shock southern of Volos. The second was the main shock occurred one minute later and 8 km eastern to the foreshock, while the third one occurred twenty five minutes later and 25 km to the west of the foreshock. This earthquake sequence produced small surface ruptures in the area (Papazachos et al. 1983). The fourth earthquake occurred on April 30, 1985, to the north-east of Almyros town.

Teleseismic body wave analysis of the April 30, 1985 Almyros earthquake is applied to determine the source parameters using WWSSN records and the GBS method (P. Papadimitriou, 1988). Synthetic seismograms of P and SH waveforms are generated for a given epicentral distance and compared to the corresponding observed ones. Figure 3, shows all the available recordings with the obtained corresponding synthetic seismograms (P. Papadimitriou et al, 1993). For each station the epicentral distance is indicated in degrees and the value of the seismic moment in 10^{24} dyne-cm. The determination of the focal depth is 8 km using a source time function of a 4 seconds duration. The calculated fault plane has a strike of 80°, a dip of 52° and a rake of -115° while the mean value of the seismic moment is 2.8×10^{24} dyne-cm.

The July 9, 1980 earthquakes occurred southern of Volos. For these events small surface breaks have been observed to the eastern part of the apparent fault indicating normal faulting striking E-W, with a downthrown block to the south (Papazachos et al., 1983). Taking an average fault length 20km, a coseismic slip 40 cm, a fault width 15 km and an elastic modulus 3×10^{11} dyne/cm^2 we obtain a seismic moment of 3.6×10^{25} dyne-cm which is approximately the expected value for an earthquake of magnitude Ms=6.3. According to these values and to the foreshock event we estimate that the length of the rupture zone is about 28 km and the length of the

aftershock rupture is about 15 km. Between the two estimated segments, a 'gap' of about 8 km is observed. The April 30, 1985 earthquake occurred in the defined 'gap' area (P. Papadimitriou et al, 1993).
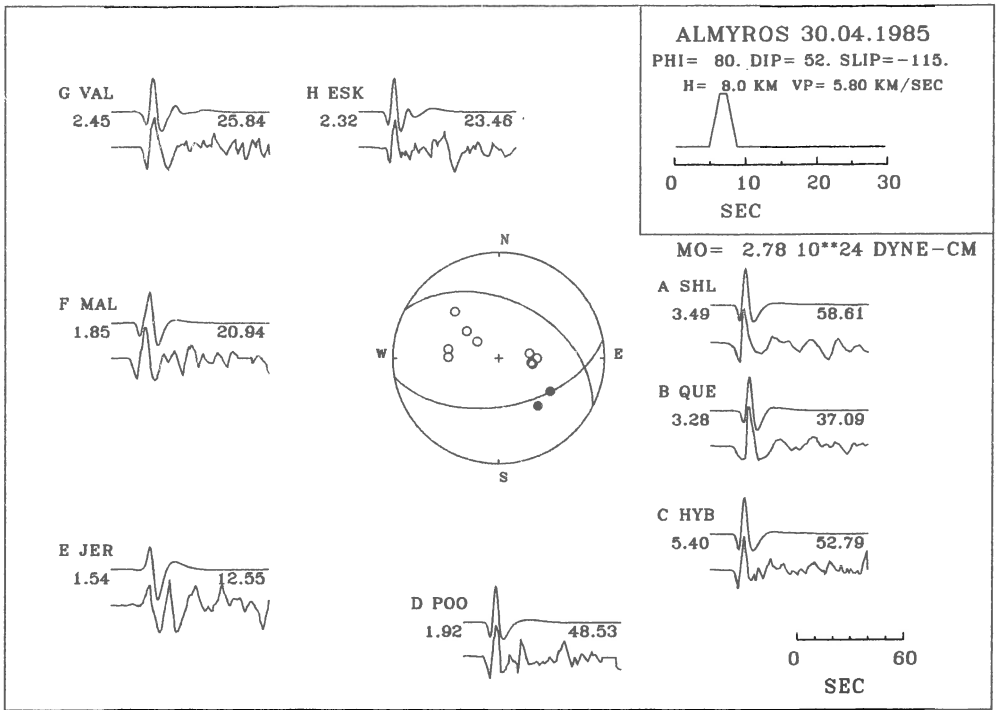
Figure 3. Teleseismic body wave modelling ussing WWSSN records.

The focal mechanisms of the July 9, 1980 earthquake sequence, using P-wave first motion polarities have been proposed by Papazachos et al. (1983). The main event and the largest aftershock show identical pure normal faulting striking N80°E. The focal mechanism of the foreshock shows normal faulting, striking N75°E, with a moderate left-lateral motion. The northward dipping nodal plane of the above solutions, is well constrained while the auxiliary plane is not. Concerning the azimuth of the fault plane of the foreshock, it is in agreement with the azimuth of Almyros fault plane but the proposed left lateral motion is not consistent with the right lateral motion proposed in this study. The fault plane solutions based only on the P-wave first motion polarities could show the type of the mechanism but in general they are not often well constrained. The focal mechanism of the Almyros earthquake is composed using waveform analysis and thus, the nodal planes are well constrained. Because of the uncertainties of the three 1980's focal mechanisms, it is conceivable to assume that the fault plane solutions are similar to those of the Almyros nodal planes (table 1). According to these remarks we propose a homogeneous normal fault system with a moderate right-lateral motion, dipping to the south with a length of about 55 km, which is in agreement with the tectonic observations (figure 2).

MICROSEISMICITY

In summer 1992, a seismological network of 70 analogue and digital portable seismographs was installed in Central Greece, for a period of two months (July, August), in order to record the local seismicity. A part of the recorded microseismicity (three weeks) and fault plane solutions computed by P-waves first motion polarities are presented.

A total amount of about 500 events were located during the experiment and more than 200 were located better than 5km both in epicenter and depth (Kementzetzidou et al, 1994; Ziazia et al, 1994). Figure 4, presents the seismic activity for a period of three weeks. The epicenters are distributed around Volos-Almyros and the surrounding area, Lamia and Evia. An important seismic activity is also observed in the North Aegean Sea. The three active seismic faults (study area), which produced the large earthquakes discussed above, continue to be active. The depth distribution of the microearthquakes varies between surface and 15km. The fault plane solutions, presented in figure 5, indicate normal faulting, in consistence with the tectonics of the area (only well constrained fault plane solutions are plotted). Concerning the area under study, normal faulting in E-W direction is
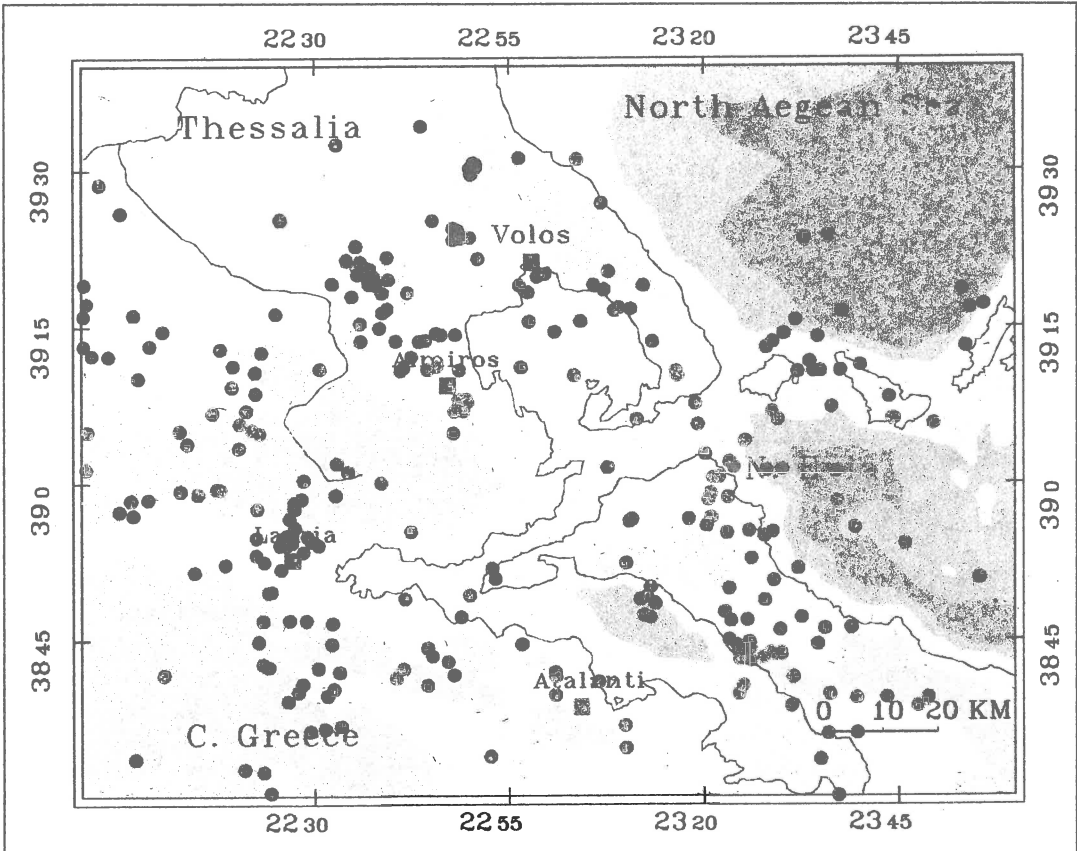
Figure 4. Seimic activity located during the microearthquake experiment in summer 1992.

revealed around Volos-Almyros area, where the focal mechanisms of large earthquakes show a similar type of faulting. Similar pattern is obtained in Velestino area, where the normal faulting is striking in N100° direction. Only one well constrained focal mechanism is available close to

Sofades, indicating N-S faulting, consistent with the focal mechanism of the 1954 Sofades earthquake. Finally, only one well constrained focal mechanism in Farsala area (between Sofades and Almyros) is available, indicating strike-slip motion.
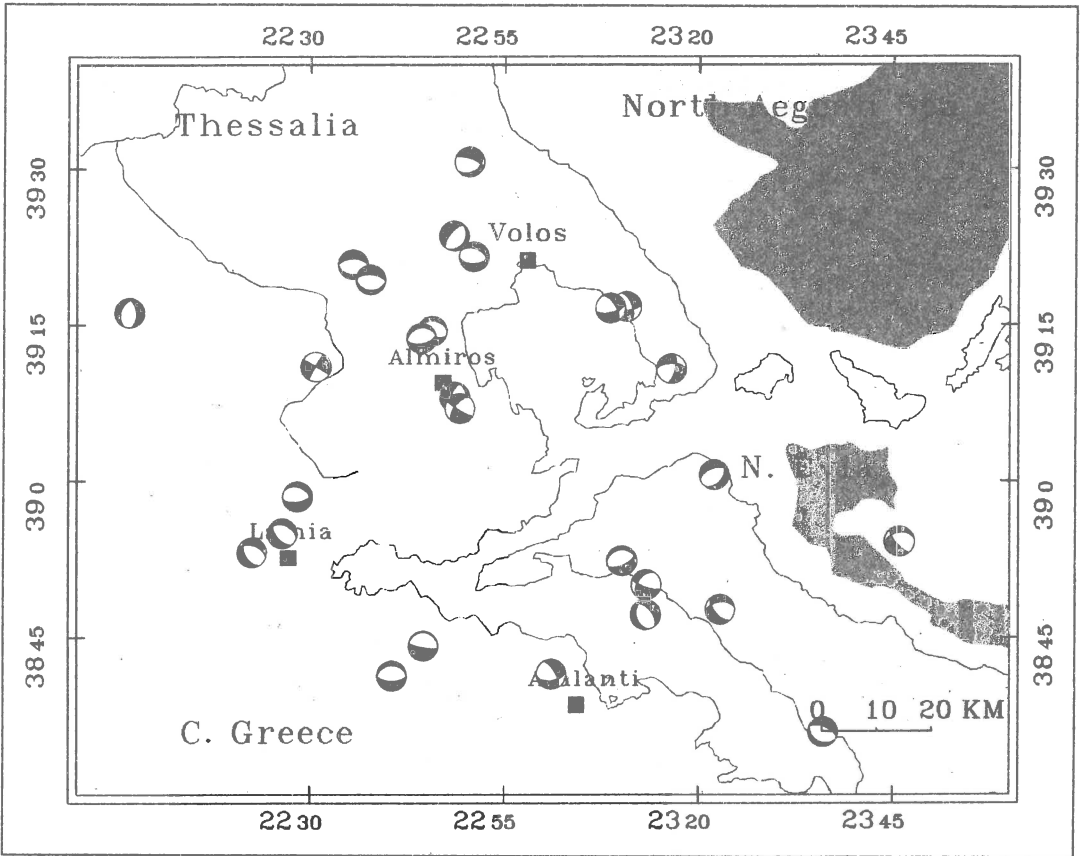
Figure 5. Fault plane solutions from the 1992 microearthquake experiment

DISCUSSION

The southern part of Thessalia area bounded by Sofades - Farsala - Velestino - Almyros and Volos regions, is characterised by a very active seismic zone, which can be divided in three parts: the eastern, characterized by the Volos-Almyros fault; the central, characterized by Velestino fault; and the western characterized by Sofades - Farsala fault zone.

The eastern part is dominated by E-W well defined by the second earthquake sequence, during 1980-1985. The combination of seismological data concerning the main four shocks and their aftershocks, determine the geometry and the rupture process of the fault (P. Papadimitriou et al., 1993). The determined normal fault, has a total length of about 55km, dipping south, while the rupture process, based on terms of barriers and asperities, indicates an irregular slip motion over the fault plane. In addition, a similar pattern is obtained recording small events by the Volnet network (V. Kouskouna, 1992).

The central part of the active zone is characterised by the Velestino normal fault. This fault has a length of about 15km striking in N100° direction and dipping south. During the Velestino earthquake sequence no clear evidence of surface breaks was observed. Only two small surface

breaks of about 500m length are observed one northwest and another southwest of Velestino (on the previously observed fault). The dipping of the two small surface breaks is in opposite direction (Ambraseys and Jackson, 1990). Unfortunately the data available do not allow the investigation of whether main shocks are located on two antithetic faults, according to the small surface breaks, or on the same fault. Nevertheless, for a shallow earthquake of a magnitude 6.8, the produced rupture is of the order of 30km. This means that if the two earthquakes had occurred on the same fault (on the observed one dipping south) this would have caused at least twice a coseimic slip. Following this assumption surface breaks should be observed. Another possibility is that the two earthquakes occurred in two antithetic faults: the observed one (dipping south) and another situated also at the foothills of the Chalkodonion mountain but at the other slope, dipping north. The last assumption could explain better the fact that no surface breaks, at least some kilometres long were observed during the earthquake sequence and the evidence of the two small scale antithetic surface breaks observed. During the 1992 seismological experiment, an important seismic activity was located in the area, which is difficult to associate with an antithetic fault system, due to the location errors, providing however a verification of the stress field revealed by the large earthquakes. As in the previous case the similar type faulting of large and small events is observed. According to the last scenario, the first shock occurred NW of Velestino on a fault plane striking about N300° and dipping north. This shock caused the main event occurred SW of Velestino on a fault plane striking in N100° direction and dipping south.

The eastern part of the active zone is characterized by the Sofades normal fault. In contradiction with the Velestino earthquakes, the Sofades main shock produced important surface breaks along 30km, dipping NE. Considering a fault length of 30km, a coseismic slip of 50 cm, a fault width of 15 km and an elastic modulus 3×10^{11} dyne/cm^2, we obtain a seismic moment of 6.7×10^{25} dyne-cm, corresponding approximately to a magnitude Ms=6.7 and not 7 which is reported. An important remark concerns the strike of the fault. The surface breaks were observed in N300° direction not following the lineament of the topography, while the eastern active zone is characterised by E-W normal faults. The microseismicity in figure 4, also shows an important activity in this area and one well constrained focal mechanism is similar to the proposed for the main shock.

In figure 4, we observe an important seismic activity in the Farsala region (between Sofades and Velestino). In this area we calculated a focal mechanism indicating strike-slip motion. Mountrakis et al, 1993 has recognised a dominant strike-slip striation in the area, corresponding to a dextral strike-slip motion. These observations could explain the transition from the eastern to the western part and the kinematics across the active seismic zone.

CONCLUSIONS

An important seismic activity occurred during the last forty years in the southern part of Thessalia (Central Greece), which is devided in two periods: the first started in 1954 with the Sofades earthquake producing normal faulting and surface breaks along 30km, striking N300° and dipping NE. After this main shock, a migration toward the east is observed with two large events one located in Pagassitikos gulf (south of Volos) and the other consisting of a double shock near Velestino. For the first one we estimate similar characteristics with the Volos-Almyros earthquake sequence: normal faulting in an E-W direction, dipping south. For the second one, the interpretation is more complex because two large events (6.5 and 6.8) with a time interval of 7min occurred near Velestino and only two small scale antithetic surface breaks of a length of 500m each were observed. Taking in account the magnitude of the earthquakes, the fact that the epicenters of the two events were in close vicinity and the total scarp length of about 15km (observed at the front

foothills of Chalkodonion mountain), we conclude that the two shocks probably occurred on an antithetic fault system located along the base of both slopes of the Chalkodonion mountain.

The second period started in 1980 with three main shocks occurred in the Volos-Almyros area and with a time interval of few minutes among them. These events produced ground ruptures in E-W direction, dipping south (Papazachos et al, 1983). On April 30, 1985 occurred the fourth event located on a well defined "gap" of the Volos-Almyros fault (P. Papadimitriou et al, 1993). The source parameters of this event were calculated using modelling techniques and thus the fault plane solution is well constrained, indicating E-W normal faulting with a right-lateral component. The fault plane solutions calculated using P-wave first motion polarities by Papazachos et al (1983) were corrected obtaining thus a pure dip-slip E-W striking, southward dipping normal faulting. By this configuration an homogeneous set of focal mechanisms was obtained, distributed over a total length of about 55km.

The above results reveal an active seismic zone with a complex pattern: the eastern part indicates normal faulting striking E-W, dipping south and a N-S extension; the western part indicates also normal faulting but in N300° direction, dipping NE and a NE-SW extension. The change of the stress field direction from N-S (in the east) to NE-SW (in the west) can be explained by the lateral strike-slip motion observed in the Farsala area.

REFERENCES

Ambraseys, N.N. & Jackson, J. A., 1990. Seismicity and associated strain in central Greece between 1890 and 1988, *Geophysical Journal International*, **101**, 663-708.

Hatzfield D., Besnard M., Makropoulos K., Hatzidimitriou P., 1993. Microearthquake seismicity and fault plane solutions in the southern Aegean and its geodynamic implications. *Geophys. J. Int.*, **115**, 799-818.

Jackson J. A. and McKenzie D., 1988a. The relationship between plate motions and seismic moment tensors, and the rates of active deformation in the Mediterranean and Middle East. *Geophysical Journal*, **93**, 45-73.

Jackson J. A. and McKenzie D., 1988b. Rates of active deformation in the Aegean Sea and surrounding regions. *Basin Research*, **1**, 121-128.

King, G.C.P., Ouyang, Z.X., Papadimitriou, P., Deshamps, A., Gagnepain, J., Houseman, G., Jackson, J.A., Soufleris, C. & Virieux, J., 1985. The evolution of the Gulf of Corinth (Greece): an aftershock study of the 1981 earthquakes, *Geophys. J. R. astr. Soc.*, **80**, 677-693.

Kementzetzidou D., Hatzfeld D., Hatzidimitriou P., Panagiotopoulos D., Karakaisis G., Ziazia M., Papadimitriou P., Makropoulos K., Saunders P., Owen T., and Deschamps A., 1994. Results of a Microearthquake experiment in Volos (C. Greece), EGS, Strasbourg.

Kouskouna V., Makropoulos K., Drakopoulos J., Ritchie M. E., 1992. The earthquake sequence in Volos, Central Greece, April 1985. Temporal and Spatial variations - focal mechanisms, Eur, Geophys. Soc. XVII Gen. Ass., Edinburgh. Annales Geophysicae, suppl. I to vol 10, p.C38.

Ziazia M., Makropoulos K., Papadimitriou P., Kementzetzidou D., Hatzfeld D., Hatzidimitriou P., Panagiotopoulos D., Karakaisis G., 1994. A microseismicity survey in central Greece (Volos): results and discussion, XXIV General Assembly of the ESC, Athens.

Le Pichon X. and Angelier J., 1979. The Hellenic Arc and trench system: a key to the neotectonic evolution of the eastern Mediterranean area. *Tectonophysics*, **60**, 1-42.

McKenzie, D., 1972. Active tectonics of the Mediterranean Region. *Geophys. J. roy. Astr. Soc.*, vol. **30**, 109-185.

McKenzie, D., 1978. Active tectonics of the Alpine-Himalayan belt: The Aegean Sea and surrounding regions (Tectonics of the Aegean Region). *Geophys. J. R. Astr. Soc.*, **55**, 217-254.

Mountrakis D., Killias A., Pavlides S., Zouros N., Spyropoulos N., Tranos M. and Soulakellis N., 1993. Field study of the southern Thessaly highly actve fault zone. proceedings of the 2nd congress of the Hellenic Geophysical Union, vol 2, 603-614.

Papadimitriou P., 1988. Etude de la structure du manteau superieur de l'Europe et modelisation des ondes de volume engendrees par les seismes egeens, *Ph. D. thesis*, Univ. of Paris.

Papadimitriou P., Makropoulos K. and Drakopoulos J., 1993. Earthquake rupture process of the Volos-Almiros area (central Greece), proceedings of the 2nd congress of the Hellenic Geophysical Union, vol 1, 509-519.

Papadimitriou P., Kassaras J., Lyon-Caen H., Makropoulos K. and Drakopoulos J., 1995. Seismic wave propagation and crustal structure in western Corinth Gulf (Greece). in press.

Papastamatiou and Mouyaris, 1986. The earthquake of April 30, 1954, in Sophades (Central Greece). *Geophys. J. R. Astr. Soc.*, **87**, 885-895.

Papazachos, B.C., Panagiotopoulos D.G., Tsapanos, T.M., Mountrakis, D.M. & Dimopoulos, G.Ch., 1983. A study of the 1980 summer seismic sequence in the Magnesia region of Central Greece. *Geophys. J. R. Astr. Soc.*, **75**, 155-168.

SEISMIC STRUCTURE AND PETROLOGICAL MODELS
OF THE UKRAINIAN AND BALTIC SHIELDS

Marek Grad[1],   Urmas Luosto[2] and Alexander Tripolsky[3]

[1]Institute of Geophysics, University of Warsaw
Pasteura 7, 02-093 Warsaw, Poland

[2]Institute of Seismology, University of Helsinki
Et.Hesperiankatu 4, 00100 Helsinki, Finland

[3]Geophysical Institute, Ukrainian Academy of Science
252142 Kiev 142, Palladina 32, Ukraine

Abstract

The results of seismic studies of the crustal structure of the Ukrainian
and Baltic shields are presented. The deep seismic sounding data along
profiles VIII and XXIV in Ukraine and profiles SVEKA and POLAR in Finland
were interpreted using the same two-dimensional modelling technique for
both P and S waves. Comparison of seismic models shows some similarities,
e.g. low velocity layers in the upper crust, high velocity plutons of
rapakivi granites, big crustal thickness. The results show a distinct
differentiation of the structure for crustal blocks of different tectonic
units. The petrological model of the Ukrainian shield is also discussed.

1. Introduction

The East European craton comprises three main crustal segments:
Fennoscandia, Volgo-Uralia and Sarmatia, marked by differences in crustal
development in the Archean and the Proterozoic (Gorbatschev and Bogdanova,
1993). The boundaries of the segments coincide very good with contours of
significant magnetic anomalies (Haines, 1985). The Baltic (Fennoscandian)
shield is a large part of Fennoscandia, while the Ukrainian shield is a
part of Sarmatia. In this paper we present the results for deep seismic
sounding profiles SVEKA and POLAR in Finland, and profiles VIII and XXIV in
Ukraine. The data were interpreted using the same two-dimensional modelling
technique for both P and S waves (Červený and Pšenčík, 1981;1983). The
results of crustal structure study of the Ukrainian shield were published
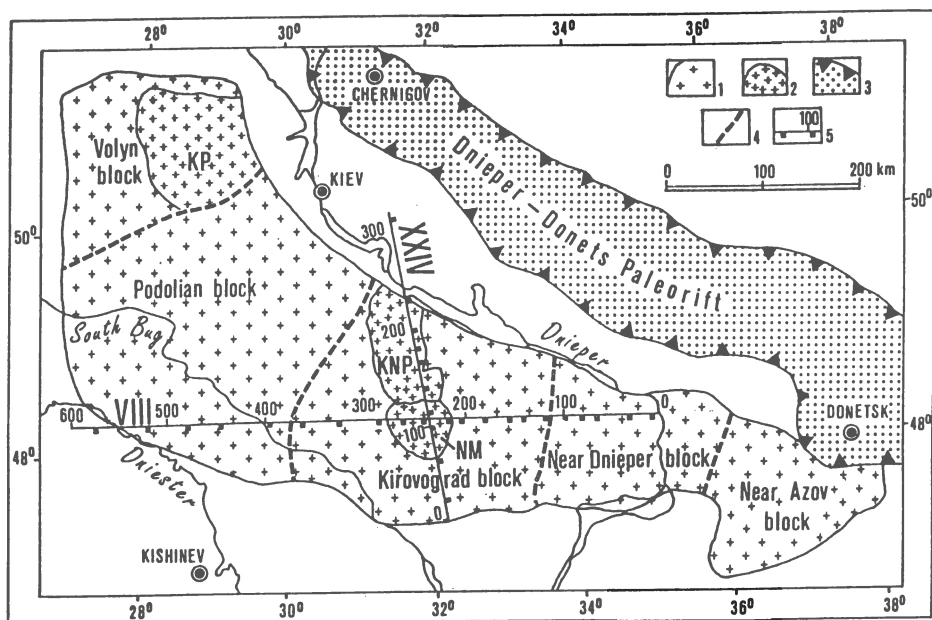
Fig.1. Location of the deep seismic sounding profiles VIII and XXIV on the background of the major tectonic units of the Ukrainian shield: 1= crystalline rocks of the Ukrainian shield; 2= massifs of the Ukrainian shield: KP - Korosten pluton; KNP - Korsun-Novomirgorod pluton; NM - Novoukrainka massif; 3= contours of Dnieper-Donets paleorift; 4= main faults of the Ukrainian shield; 5= deep seismic sounding profiles VIII and XXIV with a shot point location (black squares) and distance in km from the beginning of the profile.

mainly in Ukrainian and Russian (e.g., Aronsky and Tripolsky, 1991; Chekunov et al., 1986; Geyko et al., 1983; Sollogub 1982, 1989; Sollogub et al., 1977), so, here we present more wide results from profiles VIII and XXIV.

2. Crustal structure along profiles VIII and XXIV

The Ukrainian shield has a complicated block structure and represents large inhomogeneity of the East European platform. The contour and the general south-east strike are defined by faults separating it from the adjacent Pripiat-Dnieper-Donets, Near Black Sea, Near Dobruja, Cis Carpathian, Polessia-Volyn and Lviv depressions. The shield structure includes 3800-1700 Ma old Archean and Early Proterozoic crystalline rocks.
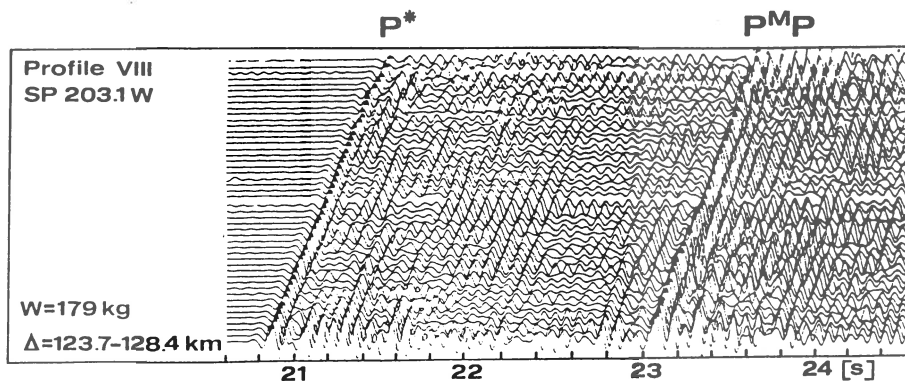
Fig.2. Example of seismogram from profile VIII.

The deep faults, of which the main are those of Teterev, Odessa-Talnov, Krivoy Rog-Kremenchung and Orekhovo-Pavlograd, subdivide the Ukrainian shield into the large Volyn, Podolian (2900-3000 Ma old), Kirovograd (1700-2000 Ma old) , Near Dnieper (2600-3800 Ma old) and Near Azov blocks (Sollogub, 1982; Chekunov et al., 1986; Tectonic map of the Ukraine and Moldavia, 1988). The deep seismic sounding profiles VIII and XXIV, discussed in this paper, are located in the central part of the Ukrainian shield. Profile XXIV runs through the Kirovograd block almost in the south-north direction. Profile VIII runs in the east-west direction through the Near Dnieper block, central part of Kirovograd block and southern margin of Podolian block. The location of profiles VIII and XXIV on the background of tectonic units of the Ukrainian shield is shown in Fig.1. Field measurements along DSS profile VIII were carried out in 1967-1972 and along profile XXIV· in 1977. The studies were made by the method of continous profiling using multichannel seismic stations with magnetic recording; the distance between the channels was 100 m. The shot points were located along profiles at a distance interval from 13 to 87 km, the mean value being about 30 km. The studies were carried out with a system of travel times of up to 320 km from the shot point. Because the magnetic tapes were re-used in field measurements, the seismograms exist only as paper records.

In the wave field one can distinguished a few groups of regular waves recorded in the interval of several tens kilometres: the P_g wave refracted in the uppermost crystalline basement; the P_{refl}^* and P_{refr}^* waves reflected and refracted from the boundary in the crystalline crust; the P^MP and P_n waves reflected and refracted from the Moho boundary. An example of

967
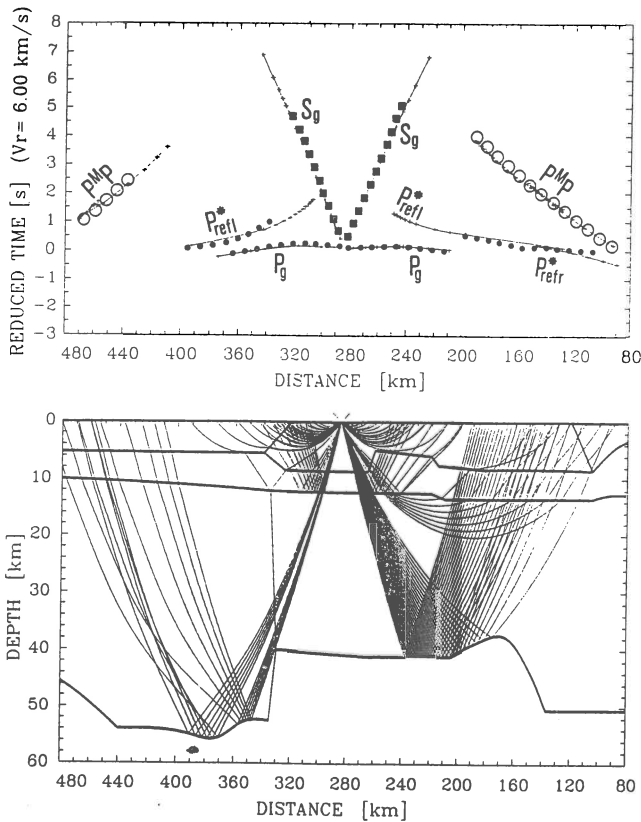
Fig.3. Example of 2-D
modelling for the crust
along profile VIII, SP
284.4. Upper diagram –
comparison of theoretical
travel times (thin lines)
with experimental travel
times of P_g, P^*_{refl}, P^*_{refr}
waves (black dots) and
P_n and P^MP waves (open
circle). Lower diagram –
chosen rays in the model.

seismogram from profile VIII is shown in Fig.2. Besides the refracted and
reflected P waves, also their S-wave analogues were recorded along profiles
VIII and XXIV.

The reinterpretation of data from deep seismic sounding profiles VIII
and XXIV were made by 1-D and 2-D modelling using refracted and reflected P
and S waves. The technique of two-dimensional modelling was used for the
first time for materials from the Ukrainian shield (Grad and Tripolsky,
1993a, 1993b and 1994). An example of the 2-D modelling of the crustal
structure for SP 284.4 from profile VIII is shown in Fig.3.

Very detailed system of measurements along profiles VIII and XXIV gave
the possibility to determine the crustal structure of the central part of
the Ukrainian shield. The final model for profile VIII is shown in Fig.4.
The main elements of the structure are the uppermost crystalline basement
with velocities 5.8-6.0 km/s at the top to 6.3-6.4 km/s at a depth of 5-8
km, and a 4-9 km thick low velocity layer with 6.0 km/s P-wave velocity.
The boundary below the low velocity layer is situated at depth 10 to 16 km,

and characterized by velocity 6.25-6.4 km/s, which increases to the lower crust up to 6.8-7.3 km/s with a gradient of 0.015-0.025 s^{-1}. The Moho depth changes in a wide range, from 30 to 56 km and the velocity below Moho is 8.0-8.35 km/s. These results show that the crustal structure is inhomogeneous and differentiated. Apart from distinct division into the upper and lower crust, the crustal blocks are observed (Podolian and Near Dnieper blocks with mean crustal thickness 50 km and Kirovograd block with mean crustal thickness 40 km) which include inhomogeneities with extraordinary properties (Novoukrainka massif and Korsun-Novomirgorod pluton). The deep fracture zones coincide with faults which are well known from surface geology. A large differentiation of the velocity ratio $k=v_P/v_S$ is observed. In the upper crust k varies usually from 1.65 to 1.71. The lower crust is characterized by low gradient and relatively low value of S-wave velocity with k reaching 1.8.
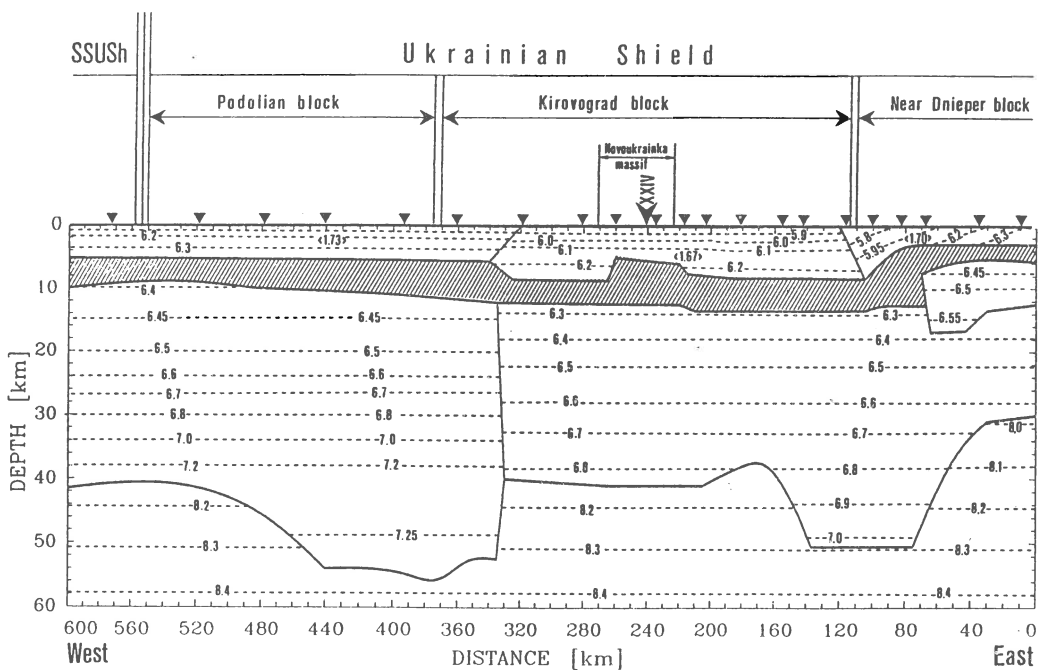
Fig.4. 2-D model of the crust along profile VIII. Solid lines — seismic boundaries; broken lines — velocity isolines and v_P velocity in km/s; dashed area — low velocity zone, v_P = 6.0 km/s, k=1.73; numbers in brackets— the value of the velocity ratio $k=v_P/v_S$; black triangles — position of shot points; the arrow shows the intersection point with profile XXIV.

3. Petrological models of the Ukrainian shield

According to the above facts, the tectonophysical models along profiles VIII and XXIV may be presented as follows. The uppermost part of the crust is represented by rocks outcropping at the surface, namely migmatites, granitoides, gneisses, granites. By analogy with the Kirovograd block, the rocks observed at the surface occur in the uppermost crust as with the rest part of the profiles. One exception is a part of the Near – Dnieper block where high v_p velocities may occur at 6-16 km depth (velocities are 0.2-0.3 km/s higher than those of the adjacent areas), and the corresponding rocks are plagiogranites and migmatites. The middle and lower parts of the crust are composed of enderbites and metamorphic rocks of granulite facies (charnockites). The rocks of the lower crust of the Podolian block with velocities of 7.2 km/s or higher are represented by a subfacies of eclogitelike rocks (Lebedev et al. 1977, 1988; Lebedev and Burtny, 1980).

4. Crustal structure along profiles SVEKA and POLAR

The results from 350 km long profile SVEKA in Central Finland based on interpretation of P, S and R waves were published by Grad and Luosto (1987, 1993 and 1994). According these investigations the crustal thickness is 55-59 km. The P-wave velocities in the upper crust are 6.0-6.35 km/s, in the middle crust 6.6-7.1 km/s and in the lower crust about 7.3 km/s. The P-wave velocity below the crust in the upper mantle is about 8.0 km/s. Ratio of P-wave velocity to S-wave velocity varies from about 1.70 in the upper crust to 1.77 in the lower crust. In the upper mantle the ratio is about 1.73. In the upper crust there is a low velocity layer between 5 and 15 km and a high velocity body was found in the northern part of profile.

The results of crustal study along 440 km long profile POLAR on the northern Baltic shield were published by Luosto et al. (1989), Behrens et al. (1989), and Von Knorring and Lund (1989). High-velocity bodies were found in the upper crust. They extend to a depth 6-13 km. In the Karelian Province a low velocity zone was found between the depths of 8 and 14 km. The thickness of the middle crust varies between 16 and 18 km. The lower crust and crust-mantle boundary (Moho) show considerable lateral variation. In the central part of profile the lower crust is characterized by rather low velocities (6.8-6.9 km/s), wheras in the southwest and northeast the velocities (6.9-7.3 km/s) resemble more typical shield structures. The Moho was found at 47 km in the Karelian Province, rises to 40 km beneath the Lapland Granulite Belt and descends to 46 km in the northeastern part of

the Kola Peninsula Province. The upper mantle velocities at the Moho range from 8.1 km/s in the region of the thin crust, to 8.5 km/s beneath the Karelian Province.
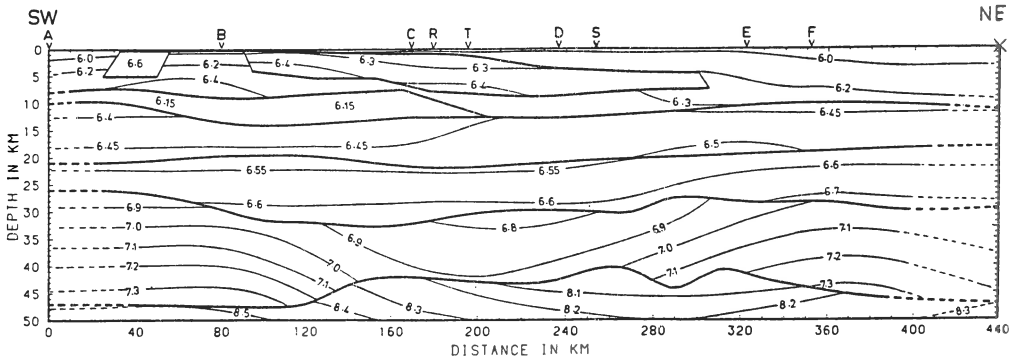
Fig.5. 2-D crustal model along the POLAR profile. Thick lines are velocity discontinuities; thin lines are velocity isolines. The location of the shot points are marked on the top.

5. Conclusions

A characteristic feature for Ukrainian and Baltic shields is the existence of a 4-10 km thick low velocity layer in the upper crust. The lower crust of the Ukrainian Shield consists of a relatively thick single layer with increasing velocity. This layer is bounded by a low velocity layer at the top and the Moho discontinuity at the bottom. The boundary below the low velocity layer is the most distinct seismic boundary observed for the Ukrainian shield. The lower crust and crust-mantle boundary beneath the Baltic shield show considerable lateral variation. The lower crust is characterized usualy by high velocities (6.9-7.3 km/s). The depth of the Moho discontinuity for both shields is changing in the wide interval from 30 to 59 km, and velocity below the Moho is 8.0-8.5 km/s.

Some similarities were found for small scale geological structures, for example, big gradient of velocity in rapakivi massifs in southern Finland and Korsun - Novomirgorod massif in Ukraine.

Good quality seismic data from Baltic and Ukrainian shields can be a base for other geophysical, petrological and geological studies.

References

Aronsky A.A. and Tripolsky A.A. 1991. Gentle fractures in the crystalline crust of the Ukrainian Shield (from data of reflection method). Dopovidi Akad. Nauk Ukrain. RSR, Ser.A, 16, 3, 89-92 (in Ukrainian).

Behrens K., Goldflam S., Heikkinen P., Hirschleber H., Lindqvist G. and Lund C.-E. 1989. Reflection seismic measurements across the Granulite Belt of the POLAR Profile in the northern Baltic Shield, Northern Finland. Tectonophysics, 162, 101-111.

Červený V. and Pšenčik I. 1981. 2-D seismic ray tracing package SEIS81, (software package). Prague, Charles University.

Červený V. and Pšenčik I. 1983. Numerical modelling of seismic wave fields in two-dimensional laterally varying layered structures by the ray method.- In: E.R. Enghdal (ed), Documentation of earthquake algorithms, WDC(A) for Solid Earth Geophysics: Boulder, Report SE-35, 36-40.

Chekunov A.V., Tripolsky A.A., Geyko V.S., Livanova L.P., Tripolskaya V.A. and Tsvetkova T.A. 1986. Seismic model of the upper lithosphere of the Ukrainian Shield. Doklady Akad. Nauk SSSR, 291, 2, 440-443 (in Russian).

Geyko V.S., Tripolsky A.A., Tsvetkova T.A., Tripolskaya V.A. and Livanova L.P. 1983. Seismic waves distribution for the Earth's crust of the Kirovograd block. Dopovidi Akad. Nauk Ukrain. RSR, Ser.B, 8, 2, 14-17 (in Ukrainian).

Gorbatschev R. and Bogdanova S. 1993. Frontiers in the Baltic Shield. Precambrian Res., 64, 3-21.

Grad M. and Luosto U. 1987. Seismic models of the crust of the Baltic Shield along the SVEKA profile in Finland. Annales Geophysicae, 5B, 6, 639-650.

Grad M. and Luosto U. 1992. Fracturing of the crystalline uppermost crust beneath the SVEKA profile in Central Finland. Geophysica, 28, 1-2, 53-66.

Grad M. and Luosto U. 1994. Seismic velocities and Q-factors in the uppermost crust beneath the SVEKA profile in Finland. Tectonophysics, 230, 1-18.

Grad M. and Tripolsky A.A. 1993. Structure of the Ukrainian Shield. Part 1: Seismic data and 1-D models. Acta Geophys. Pol., 41, 3, 177-195.

Grad M. and Tripolsky A.A. 1993. Structure of the Ukrainian Shield. Part 2: 2-D models of the uppermost crust from P- and S-waves. Acta Geophys. Pol., 41, 4, 325-336.

Grad M. and Tripolsky A.A. 1994. Structure of the Ukrainian Shield. Part 3: Seismic and petrological models of the crust. Acta Geophys. Pol., 42, 1 (in press).

Haines G.V. 1985. Magsat verticalfield anomalies above 40°N from spherical cap harmonic analysis. J.Gephys.Res., 90, B3, 2593-2598.

Lebedev T.S. and Burtny P.A. 1980. A new petrovelocity crustal model for the Ukrainian Shield. Gerlands Beitr. Geophysik, Leipzig, 89, 5, 378-382.

Lebedev T.S., Orovetskiy Yu.P. and Burtny P.A. 1977. A petrovelocity model of the Earth's crust based on the results of explosion seismology and high-pressure experiments. Gerlands Beitr. Geophysik, Leipzig, 86, 4, 303-312.

Lebedev T.S., Korchin V.A., Savenko B.Y., Shapoval V.I., Shepel S.I and Burtny P.A. 1988. Petrophysical high pT-studies and their geophysical applications. Naukova Dumka, 248 pp. (in Russian).

Luosto U., Flueh E.R., Lund C.-E. and WORKING GROUP 1989. The crustal structure along the POLAR Profile from seismic refraction investigations. Tectonophysics, 162, 51-85.

Sollogub V.B. 1982. The structure of the lithosphere of the Ukraine. Geofiz. Zh., 4, 4, 3-25 (in Russian).

Sollogub V.B. 1989. Properties of lithospheric structure of the platform part of the Ukraine: Inhomogeneities of the lithosphere from the seismic data. In: Lithosphere of the Central and Eastern Europe: East European Platform, V.B. Sollogub (ed), Naukova Dumka, 139-147 (in Russian).

Sollogub V.B., Chekunov A.V., Tripolsky A.A., Kalyuzhnaya L.T. and Gontovaya L.I. 1977. The deep structure of the Ukrainian Shield from seismic data. In: The structure of the Earth's crust and upper mantle from the data of seismic investigation, V.B. Sollogub and A.V. Chekunov (eds), Naukova Dumka, 42-52 (in Russian).

Tectonic map of the Ukraine and Moldavia, 1:500000. 1988. V.V. Glushko (ed), UkrNIGRI Mingeo., Kiev.

Von Knorring M. and Lund C.-E. 1989. Description of the POLAR Profile transect display. Tectonophysics, 162, 165-171.

CRUSTAL STRUCTURE ALONG THE SVEKA'91 PROFILE IN FINLAND

U. Luosto[1], M. Grad[2], A. Guterch[3], P. Heikkinen[1], T. Janik[3], K. Komminaho[4], C. Lund[5], H. Thybo[6] and J. Yliniemi[7]

[1] Institute of Seismology, University of Helsinki, Helsinki, Finland.
[2] Institute of Geophysics, University of Warsaw, Warsaw, Poland
[3] Institute of Geophysics, Polish Academy of Sciences, Warsaw, Poland
[4] Dept. of Geophysics, Institute of Geosciences and Astronomy, University of Oulu, Finland
[5] Dept. Geophysics & Solid Earth, Uppsala University, Uppsala, Sweden
[6] Inst. Geology, Copenhagen University, Copenhagen, Denmark.
[7] Geophysical Observatory, University of Oulu, Oulu, Finland

Abstract

In 1991 deep seismic refraction recordings were made in SW Finland. The SVEKA'91 profile is an extension to the earlier SVEKA'81, approximately along an SW-NE-oriented line from Uusikaupunki to Kannonkoski in Central Finland. It runs over the intrusive rapakivi granites of SW Finland and the Satakunta sandstone, across the Tampere Schist Belt to the large granitoid complex of Central Finland where it joins the southern end of the SVEKA'81. At five shot points, large explosions (200-1440 kg), and at two shotpoints, small explosions (80 kg), were fired, and recorded at an average station spacing of 2 km along the 350 km long profile. The high quality record sections show that the crustal structure in the area is complicated, e.g. Moho reflections are clearly seen only for the south-western and middle parts of the profile. A two-dimensional crustal model was obtained by forward modelling using ray-tracing techniques. According to this cross-section a 3-4 km thick low velocity layer was found at depths of 6 and 13 km in the upper crust. The boundary with a velocity of 6.6 km/s lies at a depth of about 17-20 km and the 7.0 km/s boundary at a depth of about 35 km in the SW but about 30 km in the NE. The Moho depth in the SW part is nearly 50 km increasing to the northeast being about 8 km thicker in the NE part of the profile. The Poisson's ratios vary from an average of 0.245 in the upper crust to about 0.265 in the lower crust with the exception of the uppermost 2 or 3 km where values up to 0.265 are found.

1. Introduction

In August 1991, seismic refraction measurements were carried out along the 350 km long line, called the SVEKA'91 Profile, in southwestern Finland. The profile is an extension to southwest of the earlier SVEKA'81 profile (Luosto & al., 1984, Grad and Luosto, 1987) in Central Finland. The aim of this investigation was to give information of the crustal structure between the SVEKA'81 profile and BABEL lines 7 and 1 in the Bothnian Sea (BABEL Working Group, 1993), especially on the strong thickness variation of the crust between the profiles, and further to improve our understanding of the composition and development of the deeply eroded 1.9 Ga old Svecofennian mountain chain (Svecofennides). The SVEKA'91 profile trends approximately northeast through Southwestern Finland from the town Uusikaupunki to Kannonkoski in Central Finland. The locations of the shotpoints are shown in Fig. 1. In the south the profile lies on the Southwest Finland rapakivi intrusion and the Satakunta Sanstone formation, crosses the Tampere schist belt and ends on the large Central Finland Granitoid complex.
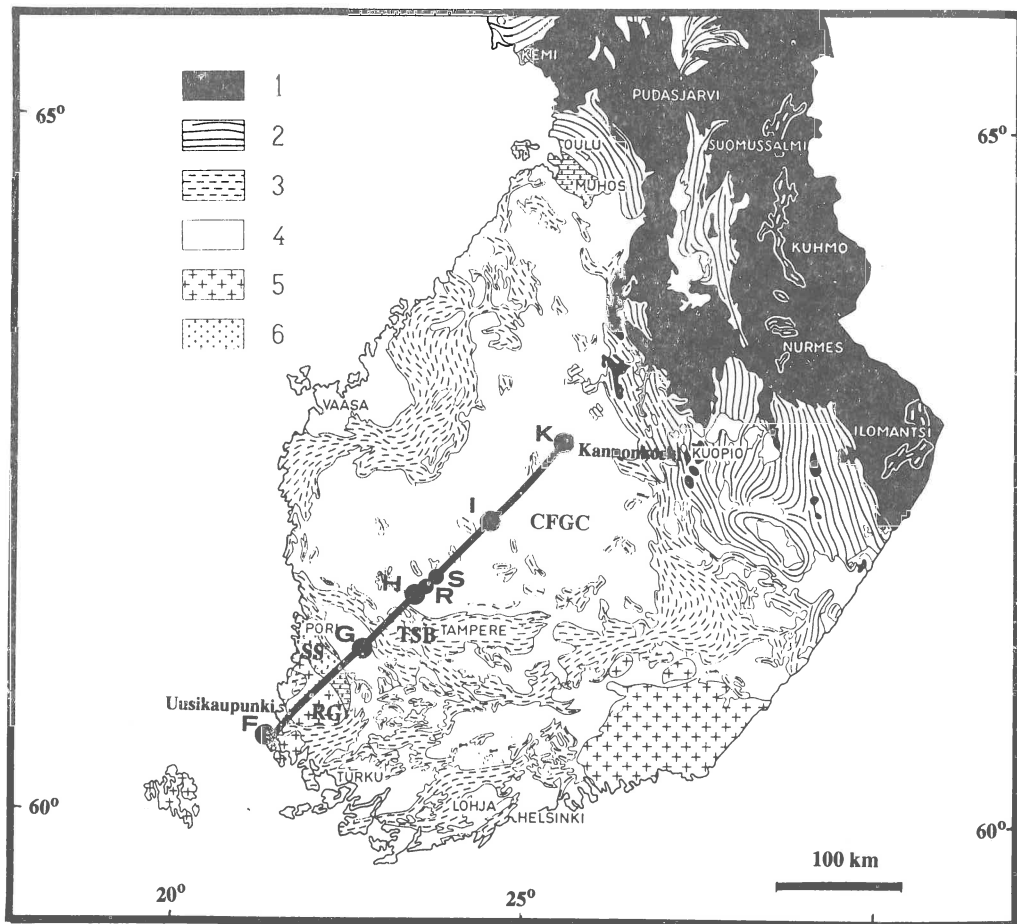
Figure 1. Location of the SVEKA'91 profile and the main structural units of the Precambrian in southern and central Finland (After Simonen, 1980). Shotpoints are marked with black dots. 1 = Archean; 2 & 3 = Proterozoic schist belts; 4 = Svecofennian granitoids; 5 = rapakivi granites; 6 = Jotnian sediments. CFGC = Central Finland Granitoid Complex; TSB = Tampere Schist Belt; RG = Rapakivi granites of SW Finland; SS = Satakunta sanstone.

The crustal structure of the Southern and Central Svecofennian Subprovinces in Finland was studied by deep seismic sounding methods along the SVEKA'81 profile (Luosto & al., 1984, Grad and Luosto, 1987). These experiments first revealed the unexpected crustal thickness of about 60 km or more in the central part of the Fennoscandian Shield. The results from the BALTIC Profile (Luosto & al., 1990) and from the BABEL line 1 (BABEL Working Group, 1993) confirmed this extraordinary thickness of the crust in the area. A deep trough of 55 km in the crust was also found in the FENNOLORA profile in Sweden almost at the same latitudes (Guggisberg & al., 1991). In Southern Finland the crust is thinner 45-50 km (Luosto, 1986, Luosto & al., 1990). This was explained by Korja & al. (1993) to be associated with the extensional tectonics there. The rapakivi intrusions of the same area are also thought to be connected with the extensional tectonics (Vaasjoki & al., 1990). A synthesis of the behaviour of the crustal thickness in Fennoscandia was made by Luosto by collecting information of

crustal thickness from refraction and wide angle reflection investigations (Luosto, 1990, 1991 and Babel Working Group, 1993). Similarly the thickness of the lowermost high velocity layer was determined and used together with the other seismic and electromagnetic data to determine the Precambrian crustal evolution of the area (Korja & al., 1993).

In this paper we describe field work, show seismic refraction data and present a two-dimensional cross-section of the crust and upper mantle, compiled by forward modelling of P- and S-wave data.

2. Field work

The field work of this profile was based on international co-operation. The measurements were carried out in August 1991 with an average station spacing of 2 km. To minimize natural and artificial seismic noise all shots were fired at night. The locations of the shotpoints are shown in Fig. 1.

The sizes of charges at shotpoints F-K vary between 200 to 1440 kg depending on the distance to the recording array. At shotpoints R and S small shots of 80 kg were fired. These shotpoints were originally planned for a reflection survey, which, however, was not included in the program. In spite of the small charges of these shots it was possible to record through the entire profile. Shot point F was in the sea, the others were in small lakes. Because of shallow depth of those lakes a special method of discharged shots was used to get enough seismic energy. The FM network of the Finnish Broadcasting Company was used to send time signals and information to the observers and the personnel at the shot points.

3. Wave field

All recordings of the 29 digital recorders were collected at the Institute of Seismology, University of Helsinki and the analog recordings of six "Mars 66" stations were digitized using a sampling rate of 80 Hz. The compiled record sections are trace-normalized and displaced with reduction velocities of 8 and 4.62 km/s. In general the signal to noise ratio of the first arrivals was excellent as can be seen in the record sections in Figs. 2a, 3a, 3b and 4a, which mainly show the P-wave arrivals for shot points F, H, S, and K, respectively. The P_n wave is, however, very weak on the record section for SP F, and these first arrivals at ca. 8 seconds in the reduced time can only be seen in the record sections plotted with a very high gain. The P_n arrivals from SP K are more intensive but diffuse in time, indicating the complex structure of the Moho boundary. P_MP reflections are usually also diffuse in time and seen only from shot points F and G to north, and from K, H, S and R to the south. The reflections most clearly seen are the strong P_MP ones from the inclined boundary in the SW in the sections of the small shot points R and S indicating that the Moho boundary in SW part of the profile is inclined to the NE, and also that the boundary there is not as complicated as in the northeast. In the NE the lower crust is very reflective and Moho reflections are difficult to see (Figs. 3a and b). As the Moho reflections at the critical distance are between 8 and 9 seconds in reduced time and the crossover distance of P_n is 240-260 km (see Figs. 2a,b and 4a,b), the thickness of the crust must be high, about 50-60 km, and dipping to the northeast. The slopes of the first arrivals correspond to velocities about 6.0-6.3 km/s in the upper crust, 6.6-6.7 km/s in the middle and more than 7 km/s in the lower crust. The velocity of the P_n is over 8.3 km/s. Clear indications of an inclined reflector to northwest in the upper crust around the area below the Satakunta sandstone formation are seen in the record sections for shotpoints G, H, R and S at 60-75 km from the SW end of the sections (only the H and S sections shown here). Similarly, but not so well pronounced, the reflected waves from another reflector of the same kind are seen 50-60

Figure 2. Comparison of observed seismograms for shot point F (a), calculated P-wave travel times for the velocity model of Fig. 6a (b), and representative ray paths in the model (c). Record sections are trace normalized, reduced with 8.0 km/s and a bandpass filter of 2-15 Hz was applied to the records.

km southwest from SP H. Indications of a reflector inclined in the opposite direction can be seen in record section of SP H, 70-80 km to NE from the shot point (Fig. 3a).

Figure 5a shows the record sections reduced by 4.62 km/s for shot point F, it contains mostly S- and surface waves. The ratio of the time axis of P- and S-wave record sections is 1.73. The same features, e.g. Moho reflections, in both sections are thus at the same level in the sections if the average ratio of the P-wave velocity to the S-wave velocity in the crust is 1.73, or the Poisson's ratio is 0.25. In broad terms the S-wave record sections resemble P-wave sections but there are certain differences. In the S-wave sections refracted waves are not

so well seen but reflections are sometimes clearer as in the case of the Moho reflections from shots at SP F to the northeast and at SP H to the southwest (not shown here). For the S-waves also the lower crust in the SE part of the profile is very reflective, and the Moho reflections are almost impossible to recognize. Well pronounced surface R-waves can be seen from shot points in the SW at distances up to 120 km but only to 60-80 km in the NE.
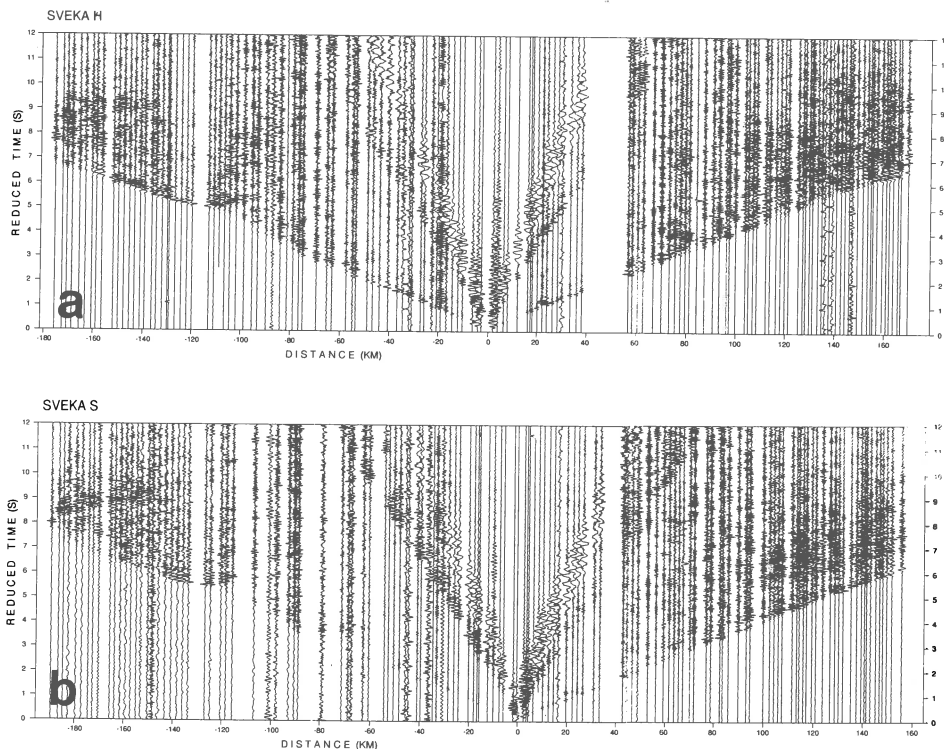
Figure 3. Trace normalized P-wave record sections for shot points H (a) and S (b), bandwith of digital filter 2-15 Hz.

4. Interpretation of P-wave record sections

The preliminary interpretation was done in a small workshop in Autumn 1992 at the Institute of Seismology of the University of Helsinki. The first step was to construct a 1-D model for each shot points. After that a starting model for the 2-D ray tracing modelling was combined by putting together the 1-D models. The ray tracing package of Červený and Pšenčik (1984) was used to obtain a model in which the calculated travel times fitted the observed ones. The locations of the inclined reflectors in the upper crust were calculated separately using a simple program with average velocity for the medium. The interpretation was later finalized in Helsinki.

The two-dimensional velocity model is seen in Fig. 6a. Examples of the calculated travel times of P-waves for shotpoints are shown in Figs. 2b and 4b, where they are plotted on the record sections. The corresponding ray diagrams are displayed in Figs. 2c and 4c. The velocity distribution in the model was calculated by linear vertical interpolation between isovelocity interfaces. This option produces cross-sections where velocity distribution in the layers and depths of the interfaces are not quite independent of each other.

978

Figure 4. Comparison of observed seismograms for shot point K (a), calculated P-wave traveltimes for the velocity model of Fig. 6a (b), and representative ray paths in the model (c). Record sections are trace normalized, reduced with 8.0 km/s and a bandpass filter of 2-15 Hz was applied to the records.

The P-wave velocity along the profile beneath the surface is about 6.0 km/s. Due to method used for the velocity distribution the depth of the velocity isoline 6.0 is inversely proportional to the actual velocity. Consequently the velocity below the surface is highest to the south from the SP I, maybe this is associated with the gabbroic and metabasaltic high velocity rocks there, and lowest at distances 70-95 km which coincides with the Satakunta sandstone. A low velocity layer, which in average is 3 km thick, is observed between depths of 6 and 14 km. The P-wave velocity above the layer is 6.2 km/s and in the low velocity layer 6.1 km/s. The bottom of the next layer lies at depths of 18-20 km. The behaviour of the upper and lower boundaries of the layer in SW means that there are higher velocities at smaller depths as in the other parts

of the profile. These velocities are probably associated with rapakivi intrusions in this area. Similar high velocities were also observed below the Viborg rapakivi batholith in the BALTIC profile (Luosto & al., 1990). The velocity contrast between the low velocity layer and this layer is, however, not large enough to produce as intensive reflections from the NE inclined boundary as those seen in the record sections of H,R and S at distances 60-75 km. Therefore it is suggested that more dense materials are concentrated in the reflector, which on the other hand could coincide with the layer interface, even if it is slightly separated in this model depending on the velocity distribution method used. The inclined reflector below shot points H, R and S, inclined to NE and the reflector south from I at distances 230-255 km, inclined to SE, are interpreted here as floating reflectors. Calculated synthetic seismograms show, that the velocity constract of these reflectors should be 0.6-0.7 km/s or the velocities between 6.7 and 6.8 km/s, which can not be layer velocities at those shallow depths but evidently again is a question of concentrated dense materials in the fault zones or to narrow intrusions.

The first arrivals with velocity about 6.6 km/s are seen on the record sections mostly at distances 160 and 200 km from shotpoints. These waves have penetrated to the layer of the middle crust. In this layer P-wave velocity varies between 6.6 and 6.75 km/s. The layer is about 15 km thick in the SW part of the profile but only 10 km in the NE part. Now, the greater thickness of the layer in the SW below the rapakivi intrusions could on the other hand be due to there being only lower velocities in this part of the layer.

The upper boundary of the lower crust is at a depth of 34-35 in the SW but of about 30 km in the NE. The lower crust is divided here into two layers. In the upper one P-wave velocity varies from 6.95 to 7.15 and in the lower from 7.35 to 7.45. This division is done mainly to make a comparison with the results of the SVEKA'81 data easier, but is not well documented by the observations. The higher velocities at about 7.5 are anyway necessary at the bottom of the crust. The velocity of about 7.0 km/s is seen as first arrivals only from SP G to NE and from I to SW only at short distance intervals at the ends of the record sections. According to the modelling they should be visible as first arrivals also at distances 210-240 km from SP K, but the records are not so good at this interval. Critical reflections from the upper boundary of the lower crust fit nicely at 190-230 km from SP F (Fig. 2c) and also in the section of SP K (Fig. 4c). There are also distinct undercritical reflections from this boundary and good fit of the calculated ones at 100-140 km from SP S to NS (Fig. 3b) and also at 140-170 km from H to SW (Fig. 3a). Therefore we conclude that this boundary really exists and that it is possible to divide the crust into three layers, i.e., the upper, middle and lower crust (see Fig.6b). The boundary between the upper and lower part of the lower crust is much more difficult to recognize. The best evidence for this can be found at the largest distances from shot points F and K, where some reflections are interpreted as overcritical ones from the boundary (Figs. 2 and 4). It is not surprising that reflections from the lower crust are difficult to find because according to the computed synthetic seismograms the velocity difference of 0.2 km/s in those depths produces such weak reflections that in practice only critically or overcritically reflected waves can be recognized.

In the SW the crust is 48 km thick and 56 km at the NE end of the profile. Thickening to NE happens rather smoothly but higher gradients are observed at the distance intervals 70-100 km and 220-250 km. P-wave velocity in the upper mantle below the crust is about 8.3 km/s.

5. Interpretation of the S-wave data

The S-wave sections were interpreted also using the 2-D ray tracing technique. In the model obtained from the analysis of the P-wave record sections only velocities were changed, the boundaries are the same as in the P-wave model (Fig. 6). The ratios of P-wave velocity to S-
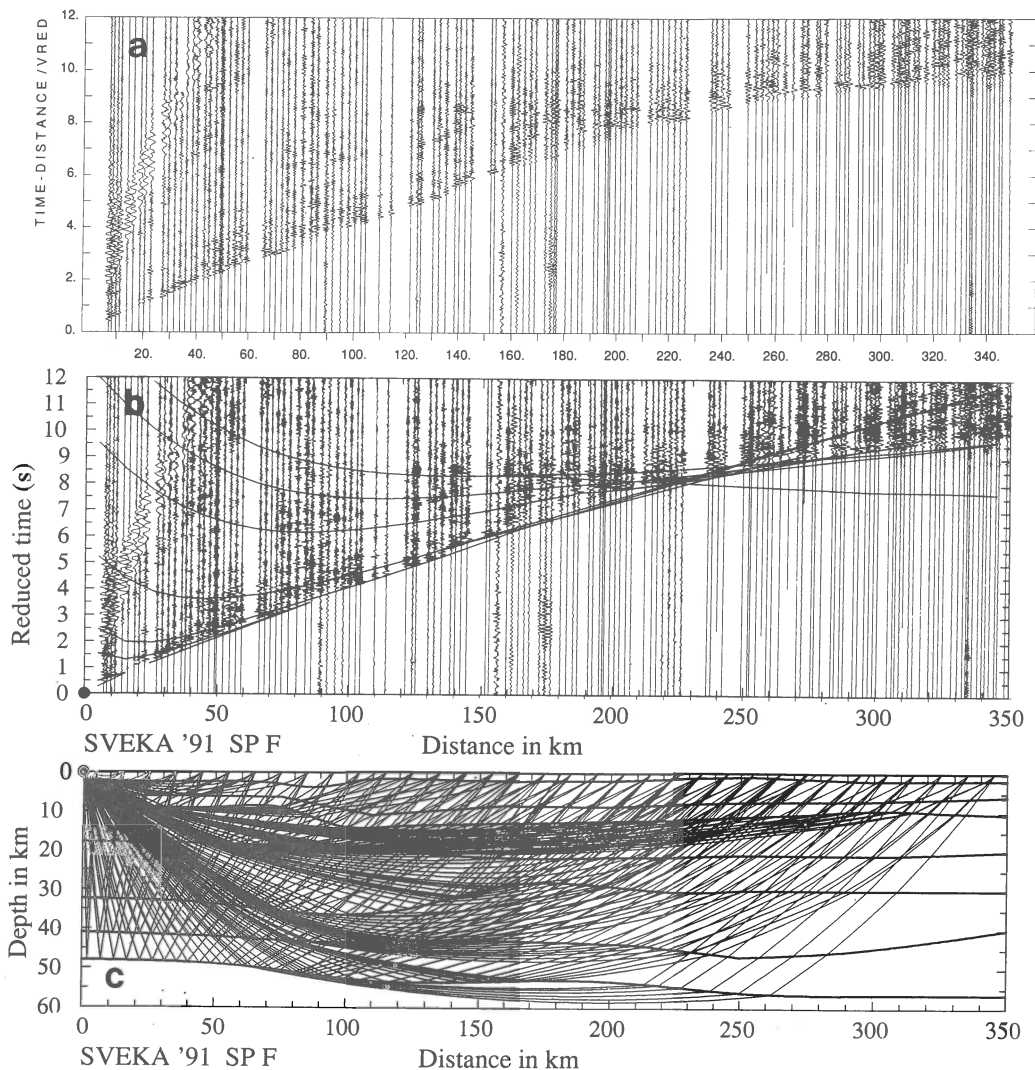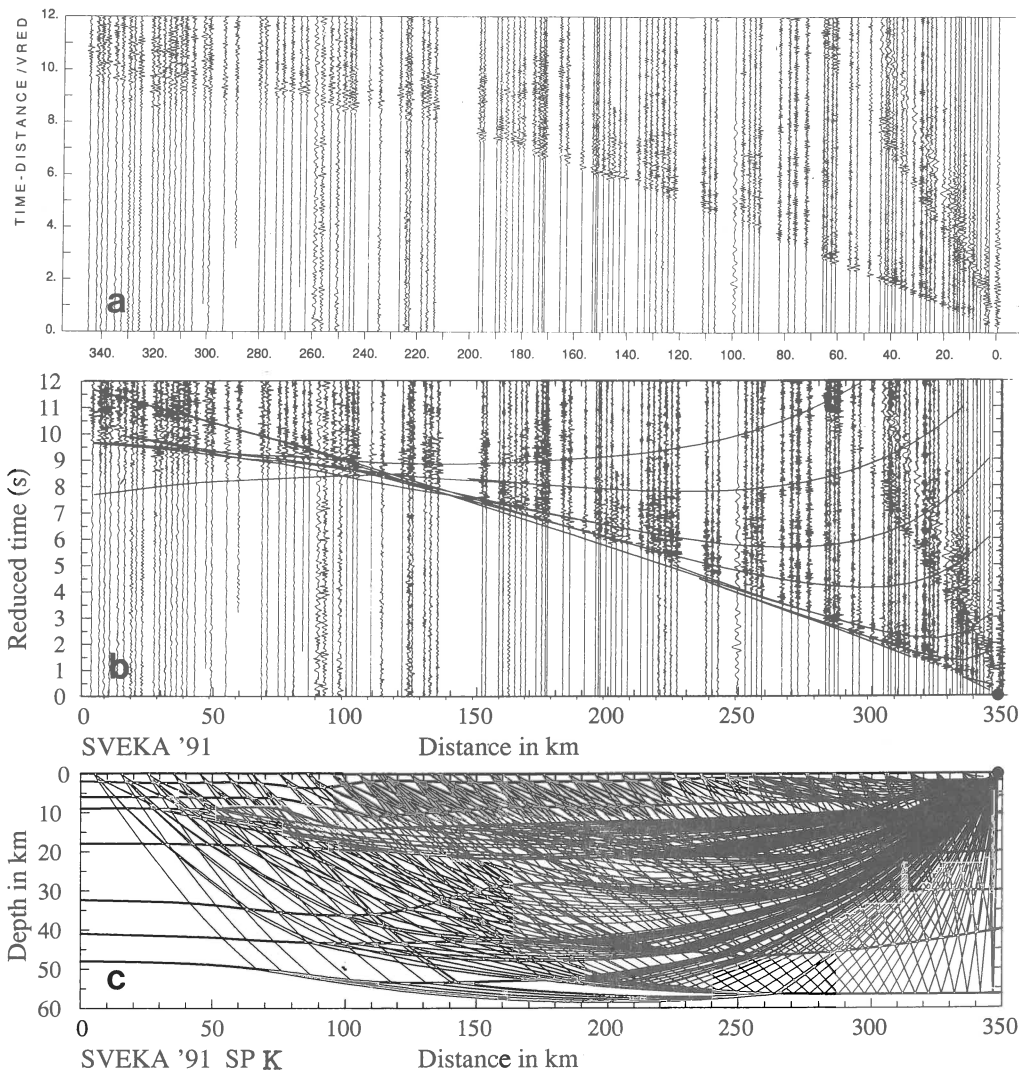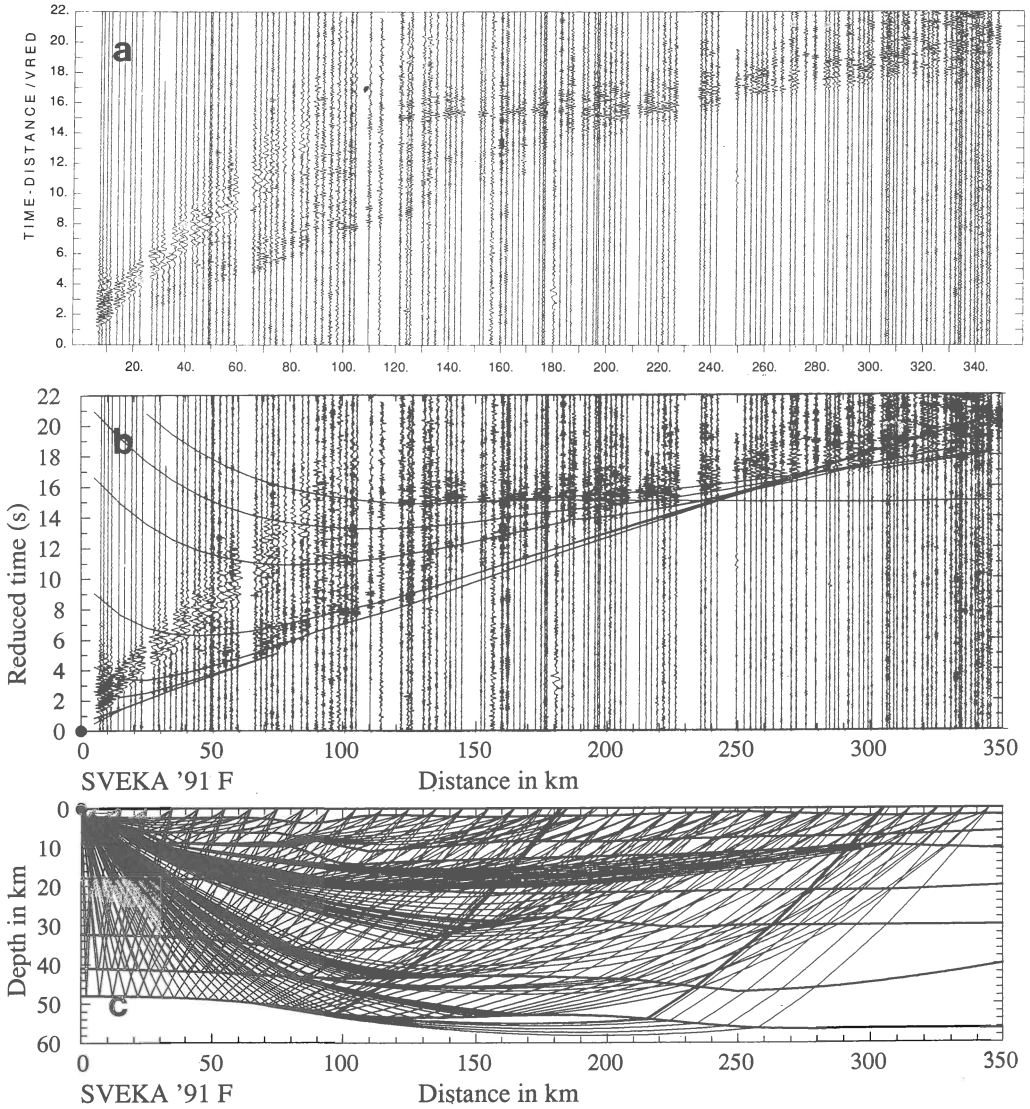
Figure 5. Comparison of observed seismograms for shot point K (a), calculated S-wave traveltimes for velocity model of Fig. 6a (b), and representative raypaths in the model (c). Record sections are trace normalized, reduced with 4.62 km/s and a bandpass filter of 2-8 Hz was applied to the records.

wave velocity (V_P/V_S) are shown in Fig. 6a. The calculated travel times and ray diagrams for the S-waves are seen only for shot point F in Fig. 5. In general the ratio V_P/V_S increases with depth being in the uppermost crust about 1.70 and in the bottom of the crust about 1.77 or Poisson's ratio increases from 0.235 to 0.266, respectively. In the uppermost 2-3 km, however, the V_P/V_S is higher than in other parts of the upper crust, being in the middle of the profile 1.73 (Poisson's ratio $\sigma = 0.25$) and at both ends of the profile 1.76 ($\sigma = 0.262$). In the upper mantle V_P/V_S is 1.78 ($\sigma = 0.269$).
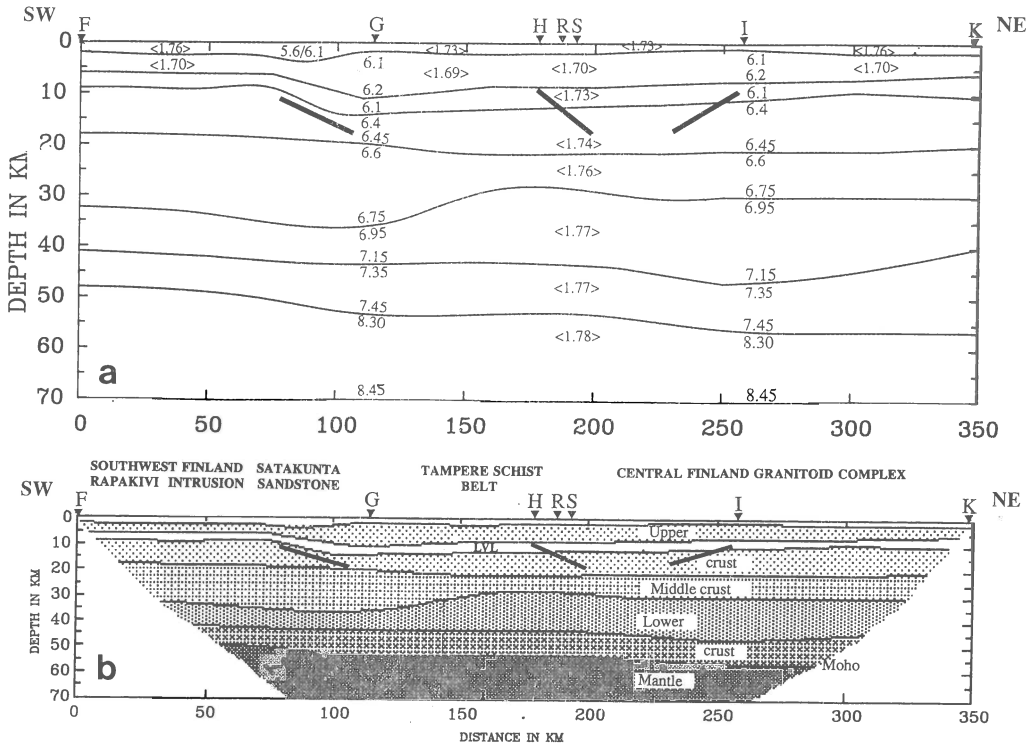
Figure 6a. Two dimensional crustal cross section along the SVEKA'91 Profile. The vertical exaggeration is 2:1. Numbers above and below the interfaces are P-wave velocities which are constants along the interfaces. Numbers in brackets indicate ratios of P-wave velocity to S-wave velocity. Inclined thick lines are floating reflectors.

6b. Generalized crustal structure along the SVEKA'91 profile derived from P- and S-wave data, with no vertical exaggeration.

6. Discussion and conclusions

Interpretation of the data resulted in a cross-section for the crust which is in good agreement with earlier DSS data in the neighbouring regions. Below the rapakivi intrusion the P-velocities are higher and the crust is thinner, as observed in the BALTIC profile (Luosto & al., 1990) and in the BABEL lines 1 and 7 (BABEL Working Group, 1993). The idea of an extensional character of the crust in the Southern Finland (Korja & al.,1993) is thus in concordance with the results of this study. The thick crust in NE is in good agreement with the earlier data of SVEKA'81, BALTIC and BABEL line 1 profiles. The thickening of the crust to the northeast in two phases is revealed in this study. The observed increase of the V_p/V_s in the crust versus depth seems to be a common feature in the shield observed also by Grad and Luosto (1987) in SVEKA'91, Stangl (1990) in the Fennolora profile and Whalter and Flueh (1993) on the Polar profile. The NE dipping reflectors coincide approximately with the southern and northern borders of the Tampere schist belt and they are evidently associated with the tectonic and lithologic features of the area.

Acknowledgements

References

BABEL Working Group, 1993. Integrated seismic studies of the Baltic shield using data in the Gulf of Bothnia region. *Geophys. J. Int.*, **112**, 305-324.

Červený, V. and Pšenčik, I., 1984. Seis83 - numerical modelling of seismic wave fields in 2-D laterally varying layered structures by the ray method. In: E.R. Engdahl (Editor), *Documentation of Earthquake Algorithms. Word Data Cent. A for Solid Earth Geophys., Boulder, Rep.* **SE-35**, 36-40.

Grad, M., and U. Luosto, 1987. Seismic models of the crust of the Baltic shield along the SVEKA Profile in Finland. *Ann. Geophysicae*, **5B:6**, 639-650.

Guggisberg, B., W. Kaminski, and C. Prodehl, 1991. Crustal structure of the Fennoscandian Shield: A travel time interpretation of the long-range FENNOLORA seismic refraction profile. *Tectonophysics*, **195**: 105-137.

Korja, A., T. Korja, U. Luosto and P. Heikkinen, 1993. Seismic and geoelectric evidence for collisional and extensional events in the Fennoscandian shield - Implications for Precambrian crustal evolution. In: A. G. Green, A. Kröner, J.-J. Götze and N. Pavlenkova (Editors), *Plate Tectonic Signatures in the Continental Lithosphere. Tectonophysics*, **219**, 129-152.

Luosto, U.,1986. Reinterpretation of Sylen-Porvoo refraction data. *Institute of Seismology, University of Helsinki, Report* S-13, 19 p.

Luosto, U., 1991. Moho depth map of the Fennoscandian Shield based on seismic refraction data. In: H. Korhonen and A. Lipponen (editors). Structure and dynamics of the Fennoscandian lithosphere. *Institute of Seismology, University of Helsinki, Report* S-25, 43 - 49.

Luosto, U., E. Lanne, H. Korhonen, A. Guterch, M. Grad, R. Materzok and E. Perchuc, 1984. Deep structure of the Earth's crust on the SVEKA profile in Central Finland, 1984. *Annls Geophys.*, **2(5)**, 559-570.

Luosto, U., T. Tiira, H. Korhonen, I. Azbel, V. Burmin, A. Buyanov, I. Kosminskaya, V. Ionkis and N. Sharov, 1990. Crust and upper mantle structure along the DSS Baltic profile in SE FINLAND. *Geophys. J. Int.*, **101**, 89-10. Simonen, A., 1980. *The Precambrian in Finland. Geol. Surv. Finland, Bull.*, **304**, 58 p.

Stangl, R., 1990. Die Structur der Lithosphere in Sweden, abgeleitet aus einer gemeinsamen Interpretation der P- und S-Wellen Registrierungen auf dem FENNOLORA-Profil. *Doctoral dissertation, Univ. of Karlsruhe, 187 p.*

Vaasjoki, M., O.T. Rämö and M. Sakko, 1991. New U-Pb ages from the Wiborg rapakivi area: constraints on the temporal evolution of the rapakivi granite-anorthosite-diabase dyke association of southeastern Finland. *Precambrian Res.*, **51**, 227-243.

Walther, Ch. and R. Flueh, 1993. The POLAR Profile revisited: combined P- and S-wave interpretation, *Precambrian Research*, **64**, 153-168.

REPROCESSING OF THE BLUE ROAD DATA

K.S.Osypov and C.-E.Lund

Department of Geophysics, Uppsala University, Sweden

ABSTRACT

The Blue Road experiment provided high quality data containing information about the velocity distribution of the lithosphere in the western part of the Baltic Shield. Previously the interpretation of the recorded data has been directed mainly towards 1-D interpretation of the single analogue shot gathers. We implemented a complex algorithm of processing digitized data including (i) semiautomatic first arrival picking, (ii) 2-D travel-time tomography and (iii) three-component analysis. This made it possible to obtain more information about the properties of the wave field and to assess the 2-D velocity structure of the crust in the region.

INTRODUCTION

The Baltic Shield forms the north-western part of the East European Platform. The westernmost rim of the Shield is covered by the remnants of the Caledonian Mountain range. The Shield represents itself the remnants of ancient orogenies of Archaean and Proterozoic age (Gaal and Gorbatschev, 1987). The Caledonides are built up of laterally compressed nappes, eastwards over-thrusted onto the Shield in an orogenic process which took place some 700 to 400 Ma ago, in late Proterozoic and Early Paleozoic time.

The present Shield uplift is thought to be caused by isostatic rebound after the last ice age about 10 000 years ago and also by other tectonic forces (Mörner, 1991; Gregersen et al., 1991). Generally there is an idea that the present-day area of the land uplift has some correspondence with the lithospheric structure. However, our present knowledge about the Moho topography in the area indicates no consistency with the present rates of mean uplift. To increase the knowledge about the tectonic evolution of the area it is important to know the lithospheric structure of the Shield.

To assess the velocity structure of the lithosphere a more than 550 km long profile was investigated in 1972, using the seismic refraction-wide-angle-reflection technique (Hirschleber et al., 1975; Vogel, 1979; Lund, 1979a, b). The profile, called the "Blue Road", runs from the Norwegian north-west coast and south-eastwards into the central part of the Shield, where it ends about 100 km into Finland (Fig.1). Along the north-westerly 100 km of the profile, the Shield is covered by the Caledonides. Further south-westwards the profile runs over the Shield proper partly covered with thin layers of loose sediments. Before the profile runs into Finland it crosses the water between the Bothnian Sea and the Bothnian Bay. In its south-easternmost part the profile crosses the area of maximum land uplift.

Five shot points spaced equally (about 100 km) over the Scandinavian peninsula were used in the experiment (Fig.1). Two series of four shots equivalent to 700 and 1400 kg TNT were recorded by 42 stations. Movement of the stations between the shot series
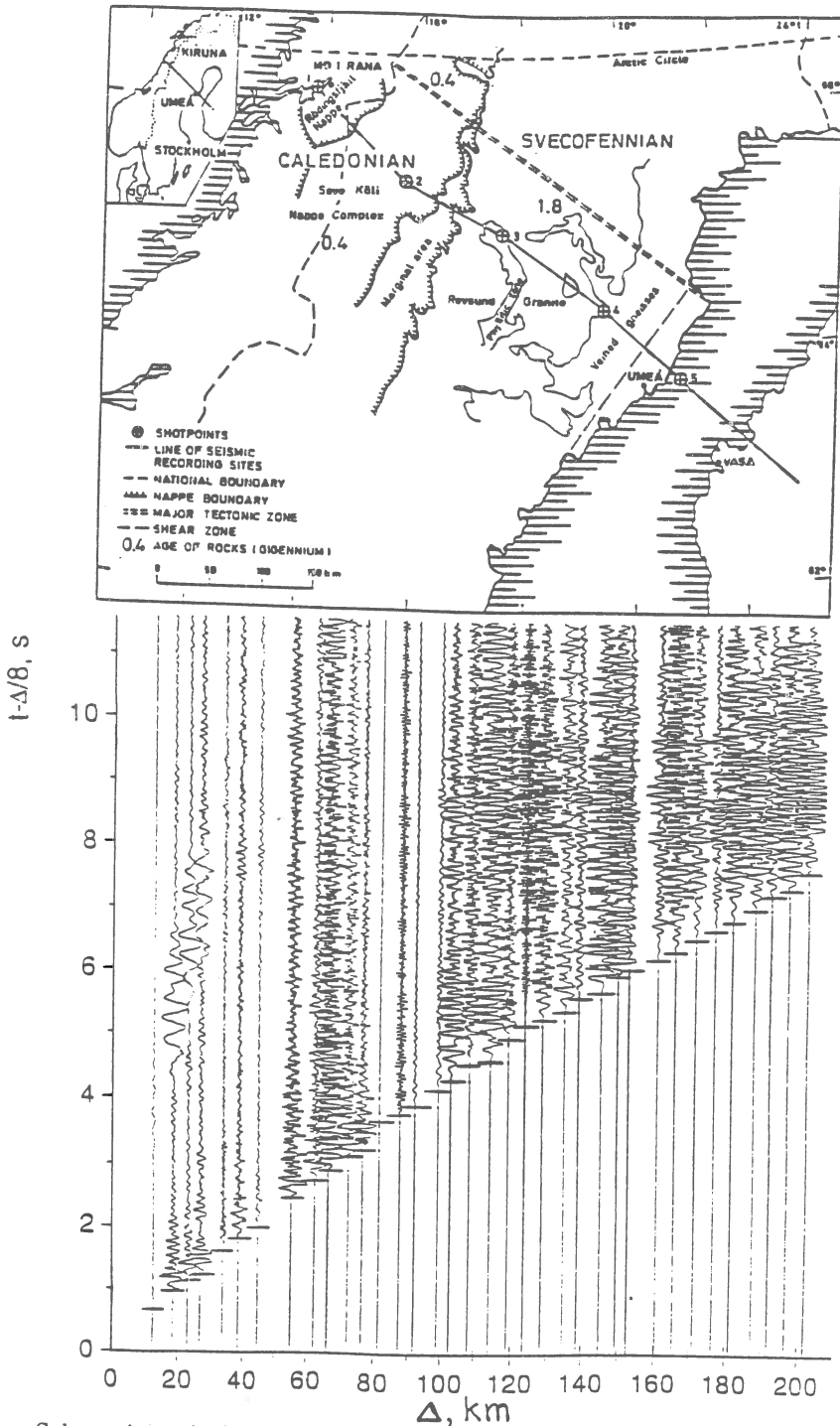
Fig.1. Top: Schematic geological map of the area of investigation, showing the position of the shot points and the line of the BLUE ROAD profile (from (Lund, 1979)). Bottom: Seismic record of shot 5A. Dashes are the onsets picked by the semi-automatic detector.

allowed to reach 4 km of average space distance between the recording sites. Every third station was set up as a three-component array. All other stations recorded only Z-component.

Previous interpretations were based mainly on the analysis of the separate analogue shot gathers. Ia a recent publication (Henkel and Lund, 1995) a 2-D BLUE ROAD velocity model, based on interpolation of the 1-D velocity models from the different shot gathers, was transformed into the density model and then adjusted to fit the corrected Bouguer gravity anomalies as obtained in the Nordkalott and Mittnorden projects.

Recently the BLUE ROAD data were digitized which made it possible to apply different modern analysis techniques to the whole data set, such as full-wave-form or diffraction tomography to reveal both smooth velocity structure and seismic discontinuities.

Inversion using full wave-form data may be divided into two separate problems, i.e., estimation of low frequency smooth variations in the velocity field by means of travel-time tomography using first arrivals, and mapping discontinuities in the medium by migration using the derived velocity model. This paper deals mainly with the first part of the inversion. To estimate onsets from the data we developed and applied an algorithm of semi-automatic first arrival picking. The migration may be improved by preliminary three-component wave-field decomposition (e.g., Roberts and Christoffersson, 1990). Therefore, we also carried out a case study of three-component analysis of the data.

SEMI-AUTOMATIC FIRST ARRIVAL PICKING

The application of tomography in its most simple form requires the estimation of the arrival time at each station of the first arrival from a number of spatially distributed sources. The performance of conventional energy detectors (e.g., Allen, 1978; Baer and Kradolfer, 1987) commonly used for picking phases from earthquakes may be improved for identification of first arrivals from explosions by using *a priori* information. Thus, knowing the coordinates of a source and a receiver and assuming a certain average velocity for the medium or using array apparent velocities, we can evaluate the time interval where the onset is expected. Moreover, we can estimate the noise variance on the basis of data before this interval. Detectors exploiting spectral, polarization or correlation characteristics (e.g., Burghardt and Savin, 1995; Christoffersson and Roberts, 1995; Lindfors et al., 1995) should be used with great care because of the unpredictable behaviour of noise and variations of signal wave-shape for different stations. Nevertheless, it is worthwhile to employ these characteristics wherever possible in the form of filtering (frequency, polarization or array). Thus, a detector only based on energy may be the most robust in our case.

Taking into account the above considerations, we developed a detection scheme including:

1. Complex demodulation using a recursive Batterworth minimum-phase filter (Osypov, 1994). This procedure increases signal/noise ratio as a frequency filter, significantly compresses data and allows direct estimation of the signal envelope used for the detection.

2. Analysis of the Fisher statistics, i.e., ratio of "signal" and "noise" variances (e.g., Hudson, 1964). The "noise" variance is estimated within the time window before the
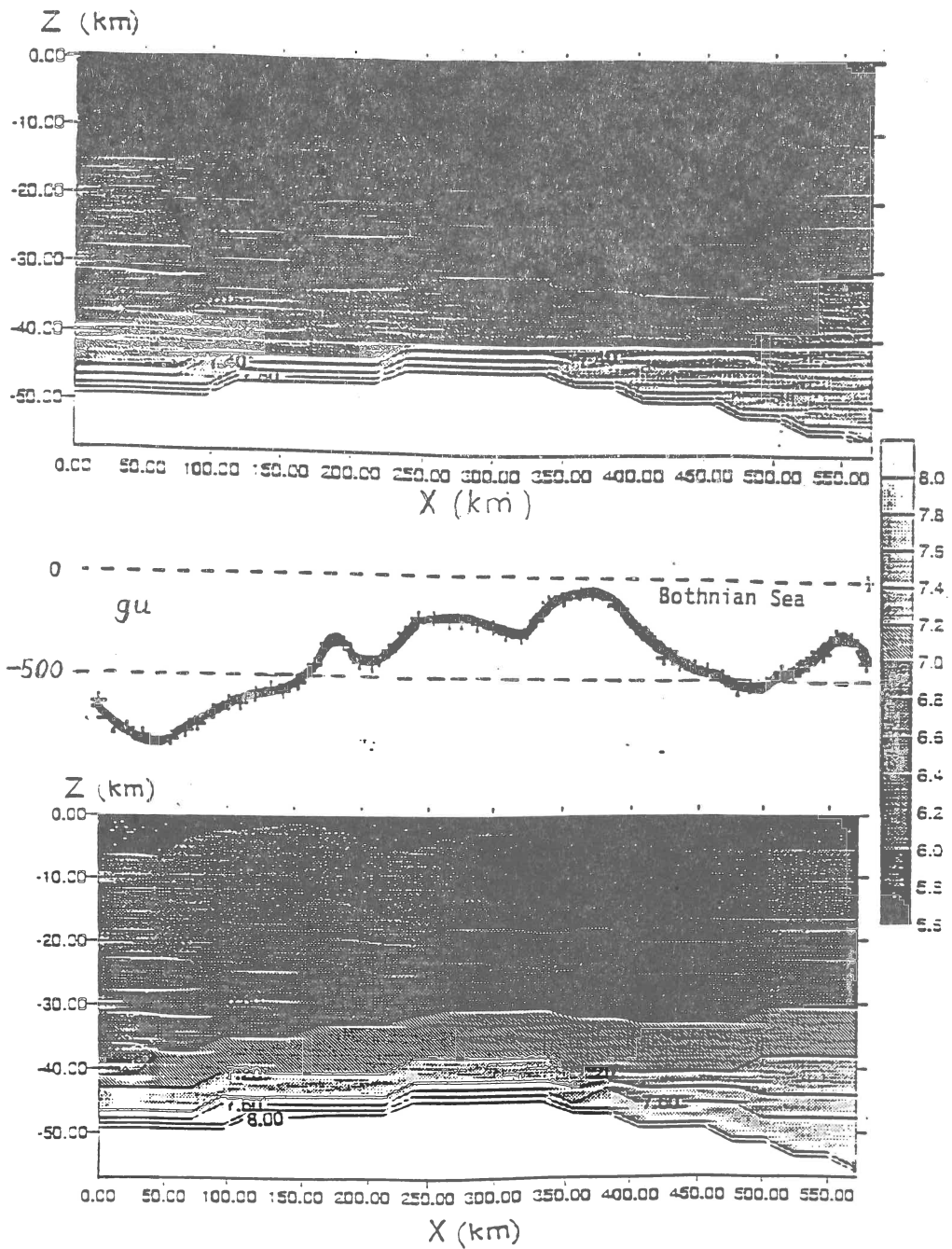
Fig.2. Top: Starting 2-D velocity model taken from (Henkel and Lund, 1995). Middle: Corrected Bouguer gravity anomalies obtained in the Nordkalott and Mittnorden projects. Bottom: Refined velocity model by the travel-time tomography of the BLUE ROAD data. Here and after the zero of the reference system corresponds to the position of the shot point 1.

signal expected interval and the signal variance is evaluated in a sliding window within this interval of interest. The threshold is chosen according to the table of Fisher statistics depending on number of degrees of freedom of "noise" and "signal" variance estimates. From the statistical point of view the choice of the threshold is more natural in this approach than in commonly used energy detectors (e.g., Allen, 1978; Baer and Kradolfer, 1987). Experience showed that for reliable detection the length of the sliding window must be of the same order as the mean signal period. In the absence of spikes we can reduce the variance analysis of a signal envelope to examine the amplitudes of its maxima, assuming that the maximum amplitude is proportional to the standard deviation. Thus, after the detection of a "signal" maximum we need more precise estimator of the arrival time, i.e., step 3.

3. The onset estimate is picked from the first maximum of the second derivative of the signal envelope back in time from the detected "signal" maximum. The maximum of the second derivative corresponds to the start of rapid growth of the energy (or discontinuity of the first derivative of the envelope) which is considered to be an onset.

The performance of the proposed detector depends on the signal/noise ratio (SNR) which varies from trace to trace. Therefore, after automatic picking, one has to check the results and adjust them if necessary. The technique may be considered as semiautomatic or interactive.

The algorithm applied to the BLUE ROAD data set successfully picked about 80% of the first breaks. Half from the remaining ones were not detected even by visual inspection. For a SNR higher than 10 the detector provides 100% success with the precision of one sample, as for example for the shot gather presented on Fig.1.

2-D TRAVEL-TIME TOMOGRAPHY

The inversion procedure deals with mapping of the estimated time delays at the different from all the shots stations into velocity perturbations within the underlying Earth. Generally, the seismic tomographic inverse problem is non-linear, ill-posed and the solution is non-unique. Thus, for the regularization *a priori* constraints on the model parameters must be included. *A priori* constraints can be included deterministically or by employing Bayesian approaches to travel-time tomography. As it was shown in (Ryzhikov and Troyan, 1993), the latter technique corresponds to a form of Tichonov's regularization accounting for *a priori* information about the "smoothness" and "smallness" of the relative values of the velocity perturbations.

We used the software package DOGSTOMO for the kinematic inversion of the first arrivals. The inversion algorithm assumes a certain smoothness of the sought function (Ditmar, 1993). In other words, mutual minimization of computed travel-time residuals and differences of velocity disturbances for all pairs of adjacent cells is performed. The functional minimum is found via the conjugate gradient method and 2-D ray tracing is performed by means of a time-field computation scheme based on graph theory (Ditmar, 1995).

We used the 2-D velocity crustal model from Henkel and Lund (1995) as a starting model for the inversion (Fig.2). Fig.3 (bottom) presents the picked travel-times plotted together with the calculated travel-time curves for the starting model. The average misfit between the observed and calculated travel-times is only about 4%. This means, that the chosen model fits well with the observed data and should therfore be a good starting
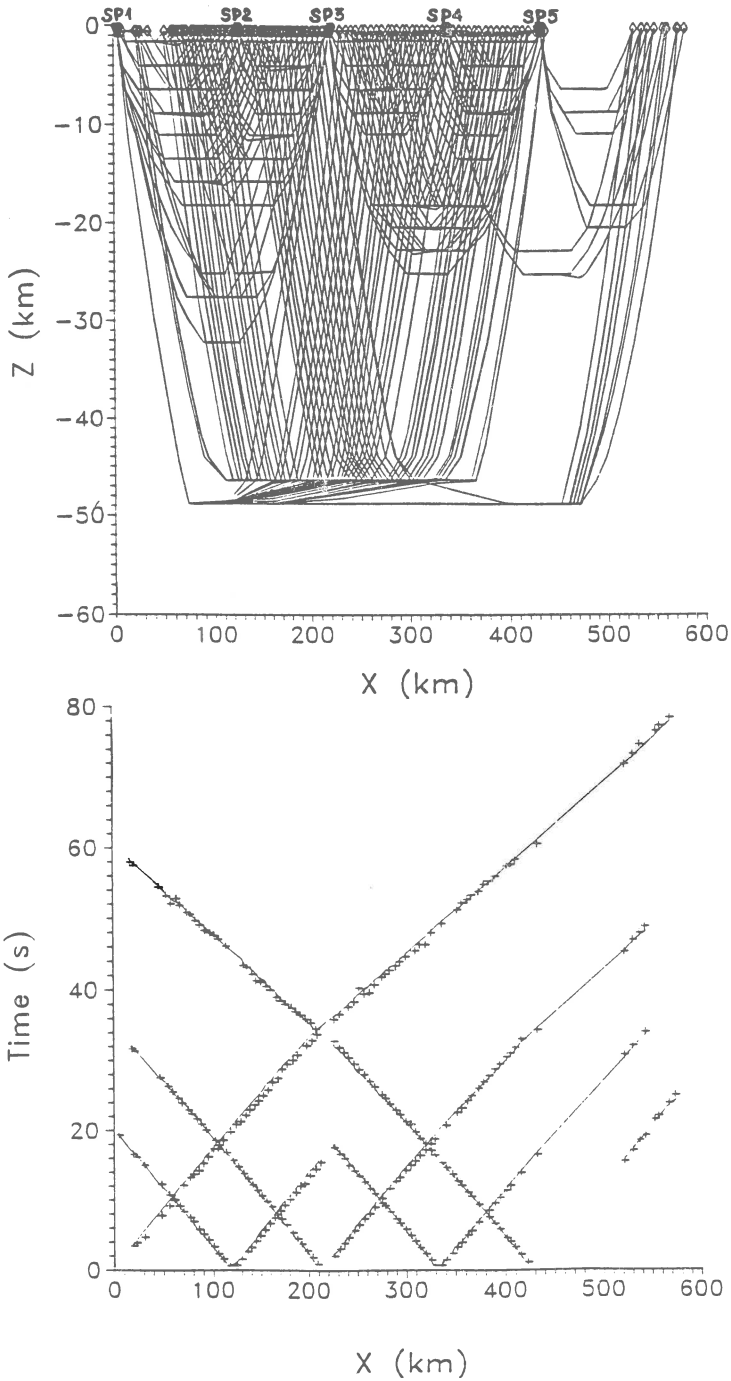
Fig.3. Top: Ray-paths in the starting velocity model. White rhombuses are the stations positions, black rhombuses are the shot points locations. Bottom: Observed travel-times (crosses) and calculated travel-time curves (solid lines).

model. Fig.3 (top) illustrates the corresponding ray pattern. As one can see, the ray coverage for the first 400 km of the profile is reasonable for the refinement of the upper crust model. Moreover, the lower crust model fits well with the low-frequency gravity field (Henkel and Lund, 1995), therefore, we decided to fix the lower crust model and other regions with the poor ray coverage, i.e., to invert only for the upper crust structure. The result of the 2-D tomographic inversion is presented in Fig.2. The travel-time misfit after the inversion was reduced to 3%. The latter level corresponds to the signal/noise ratio, i.e., the relative error of travel time estimation. It is a promising fact that the estimated 2-D velocity structure of the upper crust roughly corresponds to the density model (Henkel and Lund, 1995) estimated from the corrected Bouguer gravity anomalies (Fig.2, middle). However, the obtained model can not be considered as a final result and needs further refinement by joint inversion of the full-wave-form seismic and the gravity data.

THREE-COMPONENT ANALYSIS

In order to evaluate the reliability of the three-component BLUE ROAD data for future full-wave-form inversion, we performed a case study and examined the polarization properties of available three-component records. We implemented an approach to the decomposition of complex single-station three-component seismograms (Roberts and Christoffersson, 1990), based on covariance analysis of three-component complex demodulates and comparison with theoretical covariances for different types of waves. This technique has been successfully applied to earthquake data (Christofferson and Roberts, 1995).

Fig.4 presents an example of three-component analysis of the record from the station 77 and shot 5a (offset 72237 m). The bottom part of Fig.4 shows the pattern of the particle motion diagram in vertical-radial plane for the first arrival. The first half-period of the first break is close to linear polarization, but the particle motion after this is difficult to interpret. This complexity can be seen directly from raw data (top of Fig.4), as the transverse component contains significant energy just after the first break, and therefore, the model of pure P-wave propagating in the direction from source to receiver is not valid. This complexity means that the observed data is the superposition of different scattered waves with possible elliptical polarization and it is very difficult to identify separate phases. As it was shown in (Christofferson and Roberts, 1995), for the case of an elliptically polarized wave with variable amplitude the particle motion looks chaotic, but the phase lag between components remains constant. Therefore we analyzed the behaviour in time of the phase lag between the vertical and radial components (Fig.4, middle). The phases near 180° should correspond to P-waves. This is valid for the first arrival in our case. The large variation in the phase afterwards may indicate the interference of scattered waves of different polarizations. Phase lags about 0° within the time window 26-28 s could indicate converted P-S-arrivals.

We examined the record for the presence of different kinds of waves by the model-based approach (Roberts and Christofferson, 1990). In the upper part of Fig.5 one can see the same segment of raw data as shown in Fig.4 and in the middle part the apparent surface velocity pattern of the record for P-wave model. The vertical size of the spots approximately corresponds to the error of azimuth estimates revealed for likelihood more
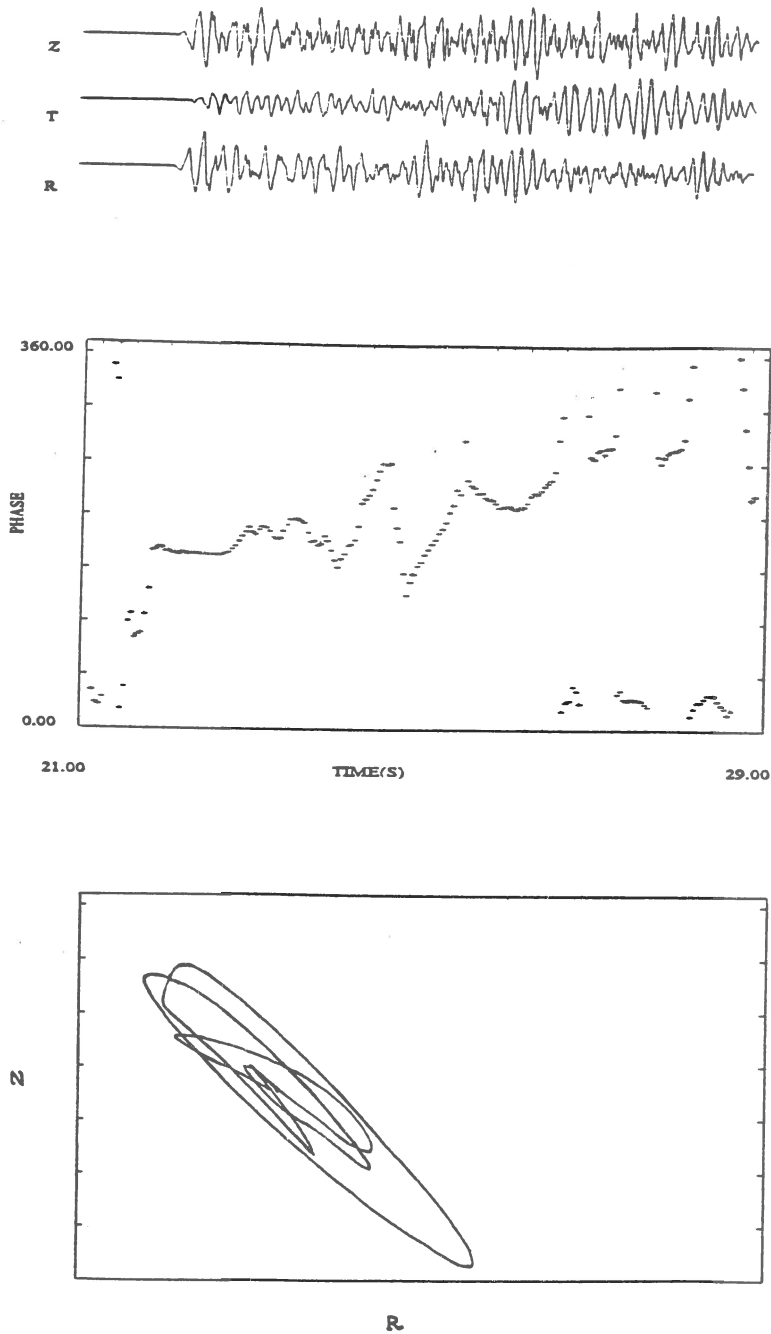
Fig.4. Top: Three-component data from the station 77 and the shot point 5a (offset 72237 m). Middle: Instantaneous phase-lag between vertical and radial components plotted against time. Bottom: Vertical-radial particle motion corresponding to the time segment 22-23 s.
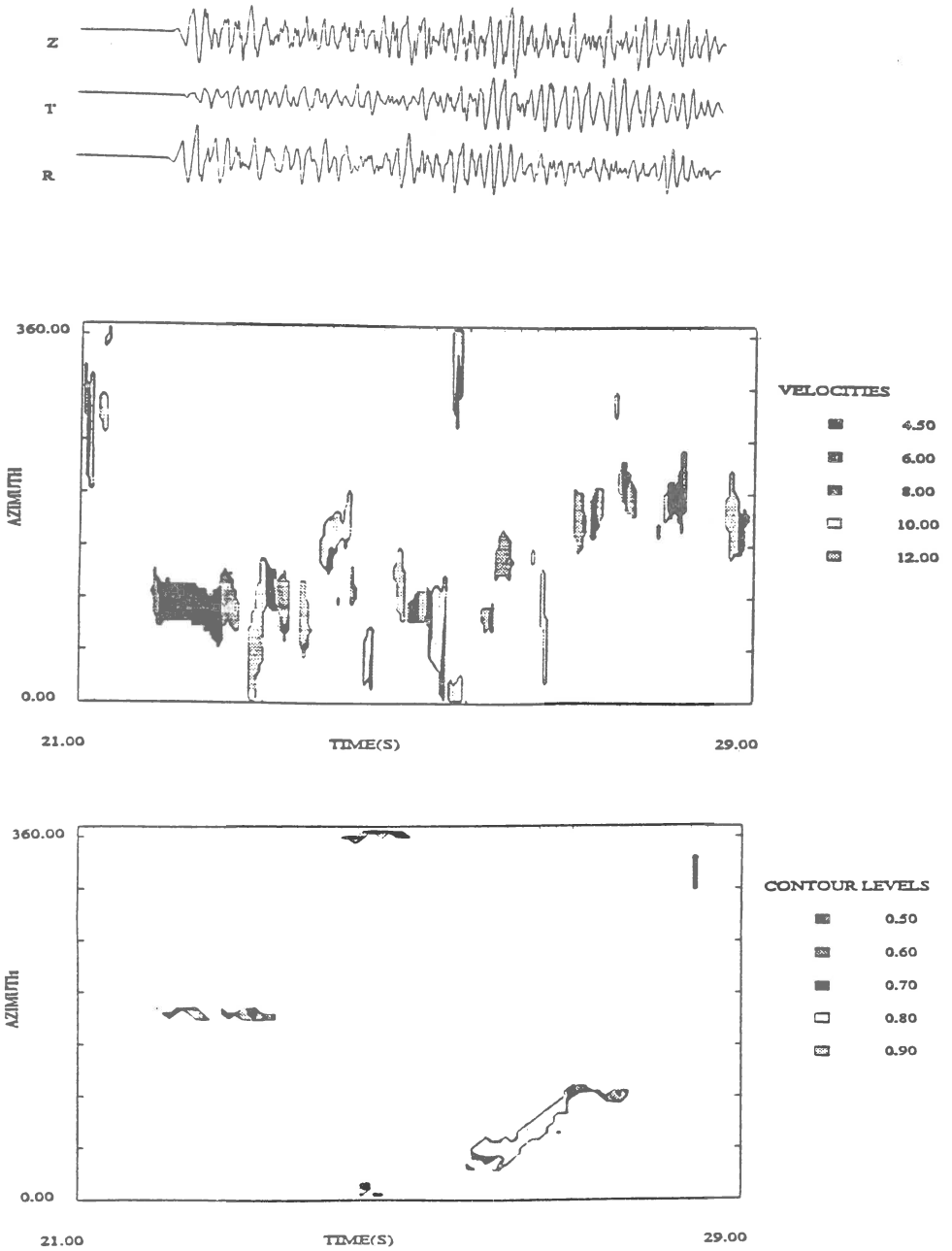
Fig.5. Top: The same data segment as on Fig.4. Apparent surface velocity for P-wave model (middle) and the maximum likelihood probability measure (below) estimated by method of Roberts and Christoffersson, 1990 and plotted as a function of time and azimuth.

than 0.5. As one can see from the figure, estimated azimuth for the first arrival is 95°, i.e., only slightly different from the expected value of 90°. Apparent velocity for the first break is similar to that revealed from the array (about 6 km/s).

These facts indicate that the three-component apparatus are relatively reliable. At the same time, the apparent velocity pattern of the signal just after the first arrival is very complicated.

We investigated the same part of the trace using an S-model and the result is presented at the bottom of Fig.5, where one can see the likelihood pattern for the hypothesis of the presence S-wave versus that of complex P-wave. Our conclusion on the existence of converted PS phase in the time window from 26 to 28 s is confirmed by the high likelihood within this window. Moreover, the existence of two clear phases with azimuth difference about 90° may point to shear-wave splitting.

The performed three-component analysis revealed an important problem of seismic phase identification in the presence of scattered P and S waves. As we can see from the presented example, the energy in that part of the seismogram considered was previously regarded as P, but we revealed some evidence of conversion to S.

CONCLUSIONS

Digitized BLUE ROAD data were processed by different techniques, such as preliminary processing and kinematic inversion. The developed semiautomatic detector made the procedure of first arrival picking more precise and more effective than the visual inspection used before. The first arrival times are the input for 2-D travel-time tomography program DOGSTOMO which we used for inversion of the crust model. Despite the general ambiguity of the inversion, the main result of this analysis is that the revealed velocity structure corresponds to the gravity field in the area and the travel-time misfit is within the error bars. This velocity model obtained may be used for migration of all the three-component wave-field data to map discontinuities in the medium. The case study of three-component analysis revealed the amount of information contained in the data and the reliability of the three-component records. At the same time the case study demonstrated the complexity of the polarization pattern caused by interference of P and S scattered waves. The latter fact figured out the problem of the wave-field decomposition and the possibility of misinterpretation of secondary phases from vertical component only. Therefore, for migration it is necessary to develop a suitable diffraction tomography scheme accounting both for P and S waves.

REFERENCES

Allen, R.V., 1978. Automatic earthquake recognition and timing from single traces. Bull. Seism. Soc. Am.,68, 1521-1532.

Baer, M. and U. Kradolfer, 1987. An automatic phase picker for local and teleseismic events. Bull. Seism. Soc. Am., 77, 1437-1445.

Burghardt, Th. and I.V. Savin, 1992. Real time detection by a statistical algorithm. Physics of the earth and planetary interiors., 69, 322.

Christoffersson,A.and R.Roberts, 1995. Trinity or verity? A Discussion of the Relative Merits of Seismological Single-Station Three-Component and Single-Component Array Data. In: Proceedings of "Nato Advanced Study Institute on Monitoring a comprehensive test ban treaty",Alvor-Algarve-Portugal 23Jan-2Feb,1995" (in press).

Ditmar, P.G., 1993. Algorithm for tomographic processing of seismic data assuming smoothness of sought-for function. Izvestiya, Earth Physics,29, 5-11.

Ditmar, P.G., 1995. An approach to 2-D ray tracing intended for non-linear seismic tomography. Subm. to Izvestiya, Earth Physics.

Henkel, H. and C.-E. Lund. 1995. Lithospheric structure in the Baltic shield from combined interpretation of refraction seismic, gravity and magnetic data. Submitted to Proceedings of IGCP-275 Symposium 94' "Precambrian Crustal Evolution in the North Atlantic Regions", Nottingham, September 13-17, 1994, Geol.Soc.London.

Hirschleber, H.B., C.-E. Lund, R. Meissner, A. Vogel, and W.Weinrebe, 1975. Seismic Investigations along the Scandinavian "Blue Road" Traverse. J.Geophys, 41,135-148.

Hudson, D.J., 1964. Statistics. Lectures on elementary statistics and probability. Geneva.

Gaal, G. and R. Gorbatschev, 1987. An outline of the Precambrian Evolution of the Baltic Shield. Precambrian Research, 35,15-52.

Korhonen, H., S.Gregersen and E.S. Husebye, 1991. Fennoscandian dynamics: Present day earthquake activity. Tectonophysics, 189, 333-344.

Lindfors, A. and R.Roberts, 1995 Array processing via phase regression. In: Proceedings of "Nato Advanced Study Institute on Monitoring a comprehensive test ban treaty", Alvor- Algarve-Portugal, 23 Jan - 2 Feb,1995" (in press).

Lund, C.-E.,1979a. Crustal structure along the Blue Road Profile in northern Scandinavia. Geologiska Föreningens i Stockholm Förhandlingar, v. 191,3, 191-204.

Lund, C.-E., 1979b. The fine structure of the lower lithosphere underneath the Blue Road profile in northern Scandinavia. Tectonophysics, 56,111-122.

Mörner, N.-A., 1991. Glacial isostasy and long-term crustal movements in Fennoscandia with respect to lithospheric and asthenospheric processes and properties. Tectonophysics. 176, 13-24.

Osypov, K.S., 1994, Algorithms and programs for statistical analysis of non-stationary geophysical processes. In: COSPAR Colloquia Series, 5, 703-706.

Roberts, R.G. and A. Christoffersson, 1990, Decomposition of complex single-station three-component seismograms, Geophys. J. Int., 103, 55-74.

Ryzhikov, G.A. and .N. Troyan, 1993, On regularization methods in 3-D tomography. In: Proc.of the 9-the International Seminar on Model Optimization in Exploration Geophysics. Berlin 1991. Edited by A.Vogel et al., Veiweg., 53-61.

Vogel, A., 1976. The Blue Road geotraverse: An interdisciplinary study on the structure and dynamics of Fennoscandian lithosphere, part 1. In: Geologiska Föreningens i Stockholm förhandlingar, 98,251-274.

NEW SEISMIC REFRACTION EXPERIMENT ACROSS THE TEISSEYRE-TORNQUIST ZONE IN NORTHWESTERN POLAND AND EASTERN GERMANY

M.Grad[1], A.Guterch[2], T.Janik[2], R.Materzok[2], U.Luosto[3],

J.Yliniemi[4], E.Lück[5], A.Schulze[6], K.Förste[6]

[1]Institute of Geophysics, University of Warsaw
Pasteura 7, 02-093 Warsaw, Poland

[2]Institute of Geophysics, Polish Academy of Science
Ks.Janusza 64, 01-452 Warsaw, Poland

[3]Institute of Seismology, University of Helsinki
Et.Hesperiankatu 4, SF-00014 Helsinki, Finland

[4]Geophysical Observatory, University of Oulu
SF-90570 Oulu, Finland

[5]Universität Potsdam, D-14473 Potsdam, Germany

[6]GeoForschungsZentrum Potsdam, D-14473 Potsdam, Germany

Abstract

The paper presents new results of seismic refraction and wide angle reflection experiment along profile LT-7, which crosses Trans European Suture Zone (TESZ) in northwestern Poland and eastern Germany. Deep crustal structure beneath this zone is very complex and highly anomalous. Thickness of the crust varies from 31 km beneath Variscides to 43 km beneath Precambrian Platform. In the Teisseyre-Tornquist Zone (TTZ) the Moho discontinuity with velocity 8.2 km/s was found at the depth 35 km, and reflected boundary at the depth 50-55 km. Depth of the consolidated basement with velocity about 5.8 km/s in the transition zone between Variscan and Precambrian Europe in this area is 8 to 11 km. Up to depth about 20 km P-wave velocity is very low, not more than 6.0 km/s. Thickness of the lower crust with velocity 6.5 and 7.1-7.2 km/s is 10-14 km only.

1. Introduction

The 560 km long refraction and wide angle reflection profile LT-7 is located in northwestern Poland and eastern Germany and crosses the Trans European Suture Zone (TESZ) perpendiculary to the main geological units in this area (Fig.1). The TESZ is a longest tectonic zone in Europe which intersects the continent in NW-SE direction between the North Sea and the
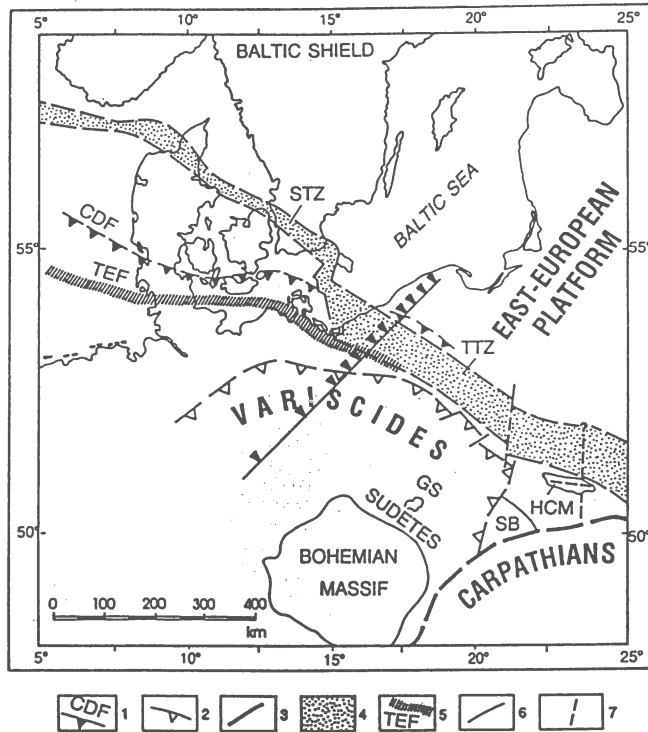
Fig.1. Simplified structural map of the investigated area and location of the LT-7 profile: 1= Caledonian Deformation Front; 2= Variscan Front; 3= Carpathians Front; 4= Tornquist Zone; (STZ)- Sorgenfrei-Tornquist Zone and (TTZ)- Teisseyre-Tornquist Zone; 5= Trans-European Fault Zone; 6= Tectonic contact zones; 7= Probable deep faults or contact zones. HCM- Holy Cross Mountains; SB- Silesian Basin; GS- Góry Sowie (Sowie Mts). Shot points along the LT-7 profile are marked by black triangles.

Black Sea. Southwestern border zone of the Precambrian Platform of Eastern Europe, between the North Sea and the Carpathians and Black Sea, named the Tornquist Zone (TZ) consists of two segments. The first one, the Sorgenfrei-Tornquist Zone (STZ) extends to Bornholm, and second segment, the Teisseyre-Tornquist Zone (TTZ) runs to the south-east (EUGENO-S Working Group, 1988). The Teisseyre-Tornquist Zone, between the Baltic coast of Poland and the Carpathians, coincidens with the Trans European Fault (Fig.1) and northwestern segment with the Avalonia-Laurussia suture (Berthelsen, 1992). In general, the TZ separates the ancient East European craton with its Palaeozoic cover from the Phanerozoic mobile belts of Western Europe. The geology of the Polish Trough is well-defined and its

relation to the TESZ is well-established (Dadlez, 1994 and its references; Kutek and Głazek, 1972; Stephenson et al, 1993). In general, it seems to be a sensitive recorder of the structural evolution within this zone.

2. Previous investigations

The crustal structure of the Teisseyre-Tornquist Zone in Central Poland (SE region from the LT-7 profile) has been studied in detail along number of seismic refraction and wide angle profiles. About 2600 km of seismic profiles have been collected in the contact zone between the Precambrian and Palaeozoic Platforms in Poland. The results of these investigations were summarized by Guterch et al. (1983; 1984; 1986). The results have shown that the crustal structure in the marginal zone of the East European Platform has highly anomalous properties. The width of the TTZ ranges from 50 km´in Central Poland to about 90 km in southeastern Poland. The crustal thickness of the Palaeozoic belt is 28-35 km, and 42-47 km for the Precambrian Platform. At the TTZ, the depth to the Moho varies from 50 to 55 km, while the velocity beneath the Moho is 8.2-8.4 km/s. In central part of the TTZ, a discontinuity with high seismic velocities of 7.5-7.7 km/s (C-M, crust-mantle transition) is also interpreted at a depth of about 40 km. Presumably it indicates the top of the crust-mantle transition layer. The nature and origin of these two seismic boundaries is unclear.

Seismic velocities and stratification of the crust vary distinctly along
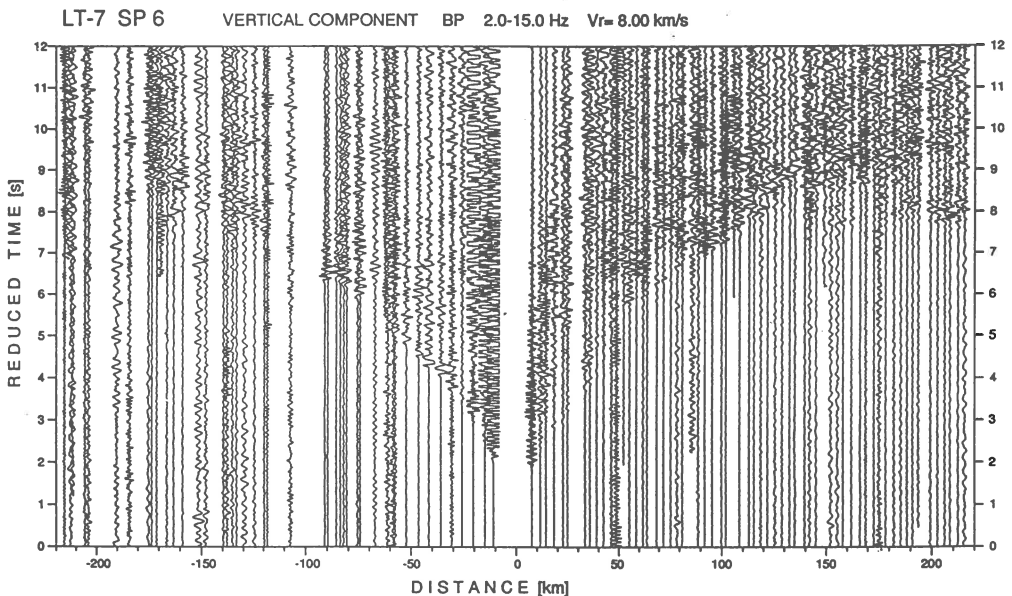
Fig.2. Example of seismic section from profile LT-7

the TTZ. The TTZ is also characterized by prominent gravity and magnetic anomalies which are compatible with the seismic structure. This is probably due to the circumstance that internal tectonic disturbances within the zone increase in size and dominance to the southeast. The TTZ determined in this manner can be interpreted as a deep Moho trough with palaeorift properties.

Along the BABEL profile A (about 170 km northwest of profile LT-7, west from Bornholm) thickness of the crust is about 40 km with velocities up to 7.4 km/s in the lower crust beneath and northwest of the Sorgenfrei-Tornquist Zone. From near-vertical reflection data below the STZ there are interpreted two seismic boundaries (M1 and M2) which may represent very complex a crust-mantle transition. Outside the STZ depth of the Moho is about 35 km and normal velocities have been observed in the lower crust (BABEL Working Group, 1993).

3. Data and interpretation

There were nine shot points in Poland with distance interval 25-40 km and two shot points in Germany, in southwestern part of profile (Fig.1). All shots were fired in boreholes. Distances between seismic stations were about 2 km. The records were performed in both directions up to distances 280 km from the shot points. Example of seismic record section is shown in Fig.2. For modelling near-surface velocity distributions (up to 4 km depth) data from 22 boreholes located near around the LT-7 profile were used (Grad, 1987; 1991). The internal structure of the sedimentary cover was interpreted from our refraction data and shalow near-vertical reflection sections.

The travel times of refracted and reflected waves determined in the correlation process provide the basis for the determination of velocity distribution and depths of seismic boundaries in the crust and upper mantle. For each shot point, the 1-D model was fitted by changing the velocity distribution until theoretical and experimental travel times were in agreement (Guterch et al., 1991). This method gives good results in the case of flat boundaries and small horizontal inhomogeneities. However, in complex media the 1-D models can be regarded only as an approximate representation of the medium. Two-dimensional model was developed using the ray tracing packages SEIS81 and SEIS83 (Červený and Pšenčík, 1981; 1983) based on ray tracing method. The calculated theoretical travel times were compared with experimental travel times. After the initial model had been altered, the travel times were recalculated many times for successive
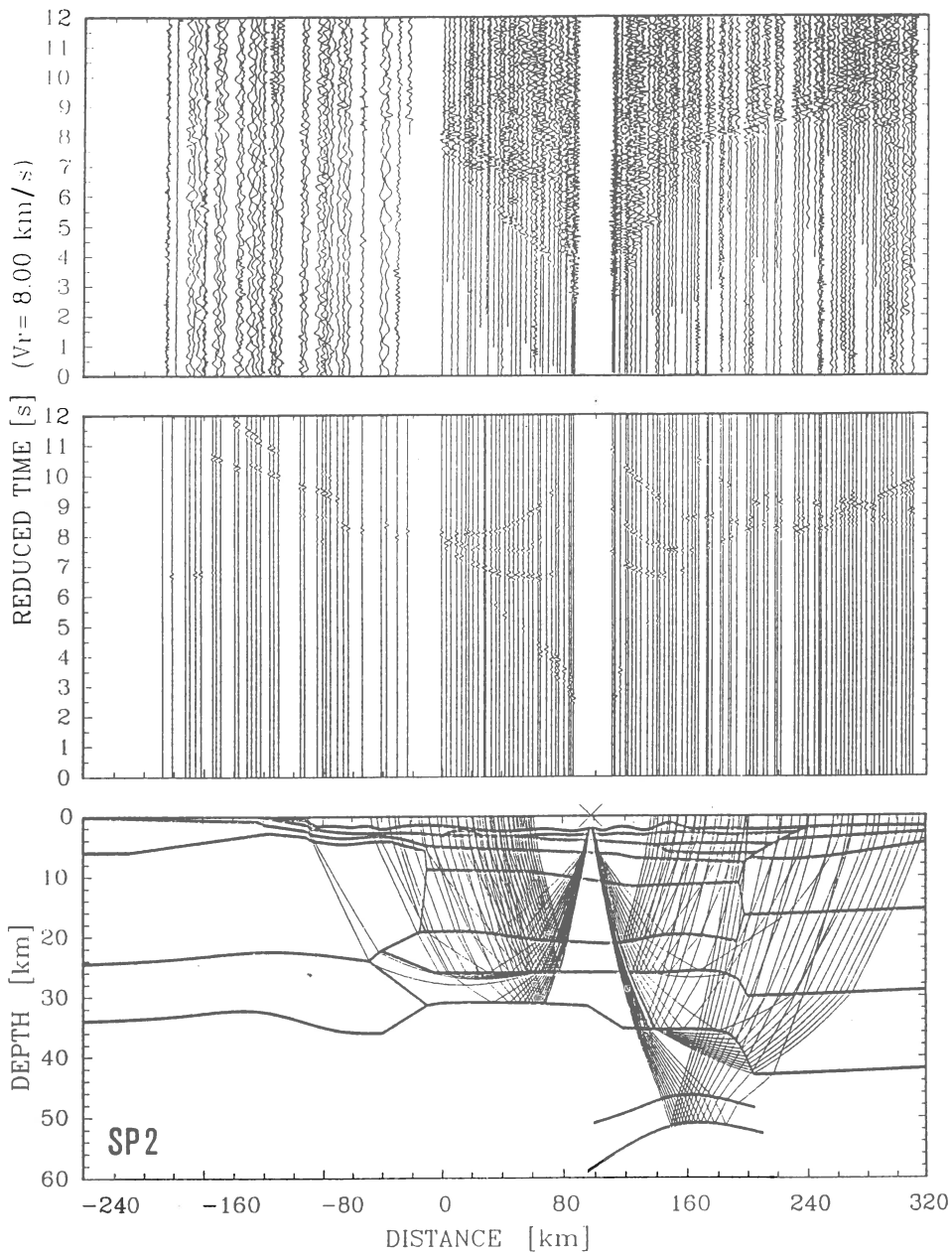
Fig.3. Example of two-dimensional modelling along profile LT-7: P-wave record section, synthetic seismograms and chosen rays for SP 2.

versions, until a very good agreement between travel times (of the order of 0.1-0.2 s) were obtained. Apart from kinematic modelling in the last step of interpretation, the synthetic seismograms were computed. Example of 2-D modelling is shown in Fig.3.

4. Model of the crust and mantle structure

The velocity structure of the crust along the LT-7 profile is shown in Fig.4. General tectonic interpretation of the seismic structure is presented in Fig.5. The thickness of the sedimentary cover varies along the profile from a few hundred meters in southwestern part of profile to about 11 km below the TTZ. Two sharp contact zone (or deep fracture) were found on the profile in the distances -20 km and 200 km. Three quite different crustal blocks are interpreted along the LT-7 profile. Southwestern part of the crustal section between -20 km and -180 km represents typical Variscan crust with very poor seismic structure. Thickness of the crust in this block varies from 31 to 35 km. Two crystalline layer were found with velocities 5.7-6.3 km/s and 6.5-6.6 km/s.
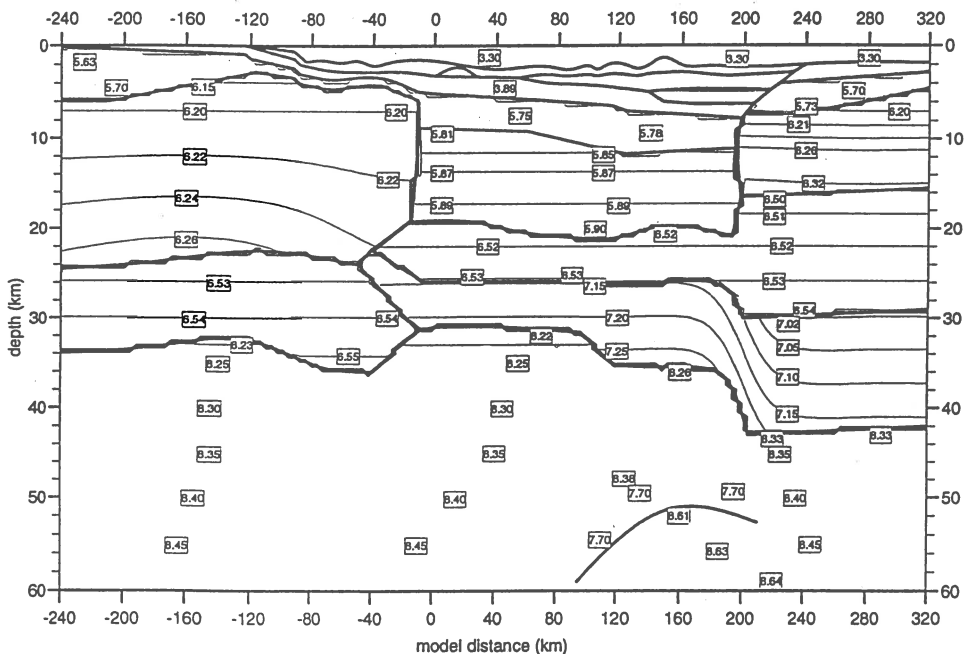
Fig.4. Seismic velocity model along the LT-7 profile. First order discontinuities are marked by thick lines and velocity contours (in km/s) by thin lines. "0" on the horizontal scale is located at the border between Poland and Germany at the Odra river.
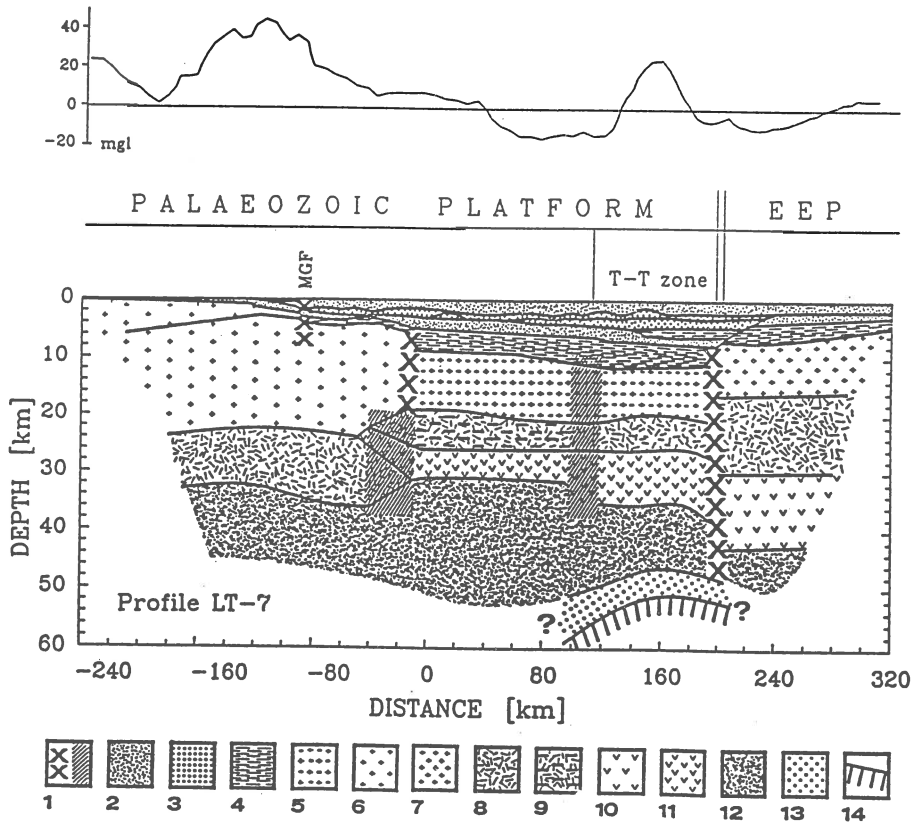
Fig.5. Interpretation of the crustal model for LT-7 profile. 1= deep fractures and contact zones between crustal blocks; 2= Cainozoic-Mesozoic cover and low velocity zone in sediments with P-wave velocity 2.0-4.0 km/s; 3= Permian and older sediments with P-wave velocity 4.0-5.0 km/s; 4= older Palaeozoic (?) with P-wave velocity 5.0-5.8 km/s; 5= low velocities of P waves in central part of profile, 5.8-6.0 km/s; 6= variscan upper crust, 5.7-6.3 km/s; 7= precambrian upper crust, 6.2-6.3 km/s; 8= variscan lower crust and middle part of the precambrian crust, 6.5-6.6 km/s; 9= distinct laminated layer, 6.5-6.6 km/s; 10= precambrian lower crust, 7.0-7.2 km/s; 11= high velocity layering lower crust of Permian Basin, 7.1-7.3 km/s; 12= upper mantle, 8.2-8.3 km/s; 13= low velocity in lower lithosphere beneath the TTZ, about 7.7 km/s; 14: reflector in lower lithosphere beneath the TTZ; MGF- Main German Fault. Upper part of the figure shows gravity anomalies along the profile.

In northeastern part of the profile (from 200 km) crystalline crust of the Precambrian Platform is formed by three layers: upper crust with velocities 6.2-6.3 km/s, middle crust with velocities 6.5-6.6 km/s, and lower crust with velocities 7.0-7.15 km/s. Such layering of the crust seems to be typical for the Precambrian Platform of Eastern Europe. The Moho is found from wide angle data at the depth about 43 km.

Structure of the Earth's crust between two described crustal blocks (from -20 to 200 km) is quite different. Thickness of the sedimentary sequences with velocities 1.8-3.8 km/s down to the top of Zechstein is about 2 km. In the middle part of sedimentary cover, below the layer with velocity about 5.0 km/s, 2 km thick low velocity layer (3.9 km/s) exists. Depth of the seismic boundary with velocity about 5.7 km/s (older Palaeozoic?) changes from 5 to 8 km. Depth of the consolidated basement characterized by velocity 5.8-5.9 km/s increases in this part of profile from 8 to 11.5 km. Below the basement crustal velocities are very low and at the depth about 20 km there are lower than 6.0 km/s only. In the lower crust, between 20 and 30-35 km depth, two layer exist. The first one with velocity 6.5 km/s and the second with velocity more than 7.0 km/s (7.15-7.25 km/s). Around 110 km there is a pronounced step in the Moho depth from 31 to 35 km. Area between 110 km and 200 km is closely connected to Teisseyre-Tornquist Zone. In the TTZ beneath the Moho discontinuity with velocity about 8.2 km/s were observed reflected waves from the depth 50-55 km. The nature and origin of this reflected boundary (M2?) is unclear. The interval between Moho and M2 (15 km) may represents a crust-mantle transition layer composed high and low velocity materials (BABEL Working Group, 1993).

5. Conclusion

Crustal structure along LT-7 profile beneath the TESZ in northwestern Poland (from -20 to 200 km) is "drastic" different in comparison to the Precambrian Platform and to the typical Variscan crust. Boundaries between the TESZ area and the surrounding crustal blocks are very pronounced. Their physical properties can be interpreted as indicators for terrane boundaries. In general, seismic crustal structure along the LT-7 profile is much more complex than along the another profiles in Central Poland.

Last seismological results of the three-dimensional study of the upper mantle structure below Europe, presented by Zielhuis and Nolet (1994), show that the TTZ is not only discernible at crustal depths but that it also

forms very effective boundary at upper mantle. Another new results from monitoring the regional seismicity in Central Europe, reported by Schweitzer et al. (1992), show that the tectonic feature of the TTZ reaches down to about 200 km in the upper mantle.

References

BABEL Working Group, 1993. Deep seismic reflection/refraction interpretation of crustal structure along BABEL profiles A and B in the Southern Baltic Sea. Geophys. J. Int., 112, 325-343.

Berthelsen A. 1992. Mobile Europe. In: A continent revealed: The European Geotraverse. D.J. Blundell, St. Mueller and R. Freeman (eds). Cambridge University Press, 11-32.

Červený V. and Pšenčík I. 1981. 2-D seismic ray tracing package SEIS81, (software package). Prague, Charles University.

Červený V. and Pšenčík I. 1983. Numerical modelling of seismic wave fields in two-dimensional laterally varying layered structures by the ray method.- In: E.R. Enghdal (ed), Documentation of earthquake algorithms, WDC(A) for Solid Earth Geophysics: Boulder, Report SE-35, 36-40.

Dadlez R. 1994. Strike-slip movements in the Polish Lowlands. Geological Quarterly, 38, 2, 307-318.

EUGENO-S Working Group, 1988. Crustal structure and tectonic evolution of the transition between the Baltic Shield and the North German Caledonides (the EUGENO-S Project). Tectonophysics, 150, 253-348.

Grad M. 1987. Velocities of seismic waves in sedimentary cover of the East European platform. Kwart. Geol., 31, 97-114 (in Polish).

Grad M. 1991. Seismic wave velocities in the sedimentary cover of the Palaeozoic platform in Poland. Bull. Pol. Ac., Earth Sci., 39, 13-22.

Guterch A., Grad M., Materzok R. and Toporkiewicz S. 1983. Structure of the Earth's crust of the Permian basin in Poland. Acta Geophys. Pol., 31, 121-138.

Guterch A., Grad M., Materzok R., Pajchel J., Perchuć E. and Toporkiewicz S. 1984. Deep structure of the Earth's crust in the contact zone of the Palaeozoic and Precambrian Platform and the Carpathian Mts. in Poland. Acta Geophys. Pol., 32, 25-41.

Guterch A., Grad M., Materzok R. and Perchuć E. 1986. Deep structure of the Earth's crust in the contact zone of the Palaeozoic and Precambrian Platforms in Poland (Teisseyre-Tornquist zone). Tectonophysics, 128, 251-279.

Guterch A., Luosto U., Grad M., Yliniemi J., Gaczyński E., Korhonen H., Janik T., Lindblom P., Materzok R. and Perchuć E. 1991. Seismic studies of crustal structure in the Teisseyre-Tornquist zone in northwestern Poland (preliminary report). Publs. Inst. Geophys. Pol. Acad. Sc., A-19 (236), 147-156.

Kutek J. and Głazek J. 1972. The Holy Cross area, Central Poland in the Alpine cycle. Acta Geol. Pol., 22, 603-653.

Schweitzer J., Jost M.L. and Gestermann N. 1992. GERESS - A new array for on-line monitoring the regional seismicity in Central Europe. Tire a part des Cahiers du Centre Europeen de Geodynamique et de Seismologie. Ruhr University, Bochum, Germany, 5, 1-10.

Stephenson R.A. and the EUROPROBE Intraplate Tectonics and Basin Dynamics Dnieper-Donets and Polish Trough working groups, 1993. Continental rift development in Precambrian and Phanerozoic Europe: EUROPROBE and the Dnieper-Donets Rift and Polish Trough basins. Sedimentary Geology, 86, 159-175.

Zielhuis A. and Nolet G. 1994. Deep Seismic Expression of an ancient plate boundary in Europe. Science, 265, 79-81.

Dispersion of Rayleigh Waves along the Prague-Warsaw Profile

O. Novotný[*]), T.A. Proskuryakova[**]), A.V. Shilov[**])

[*]) Department of Geophysics, Faculty of Mathematics and
Physics, Charles University, Prague
V Holešovičkách 2, 180 00 Praha 8, Czech Republic
[**]) Department of Physics of the Earth, Faculty of Physics,
Moscow State University, Moscow
117 234 Moscow, Russian Federation

Extended abstract

Phase velocities of Rayleigh waves propagating along the Prague-Warsaw profile were determined using records of 11 earthquakes at these stations. Although much attention was paid to selecting the seismograms and to their processing, the experimental values of phase velocities displayed rather a large scatter (Novotný et al., 1995). This can be explained by Warsaw being close to the Teisseyre-Tornquist fault zone.

The Prague-Warsaw profile is crossed by international profile VII of deep seismic soundings (DSS); see Novotný et al. (1980, 1995). Consequently, we used the DSS results along profile VII to determine an initial crustal model for the Prague-Warsaw profile. We projected the Prague-Warsaw profile on profile VII and averaged the corresponding DSS crustal models. In the mantle we adopted the Canadian Shield model CANSD (Brune and Dorman, 1963). In this manner we obtained the initial model, the cross-section of which is shown in Fig. 1 by curve O.

The initial model was then changed by a gradient method to satisfy the observed dispersion. In the 20th iteration we arrived at the model, denoted as F (the final model); see Fig. 1. The characteristic features of this resulting model of the crust and upper mantle structure are as follows: nearly constant velocities at depths of about 10-20 km, presence of certain discontinuities at depths of 21 and 28 km, a less prominent discontinuity at a depth of 36 km (Moho) and relatively low velocities in the upper mantle.

The full text of this contribution will be published in the paper by Novotný et al. (1995).

References

Brune, J. and J. Dorman (1963). Seismic waves and Earth structure in the Canadian Shield. *Bull. Seism. Soc. Am.* 53, 167-210.

Novotný, O., T.A. Proskuryakova and E.V. Voronina (1980). Com-
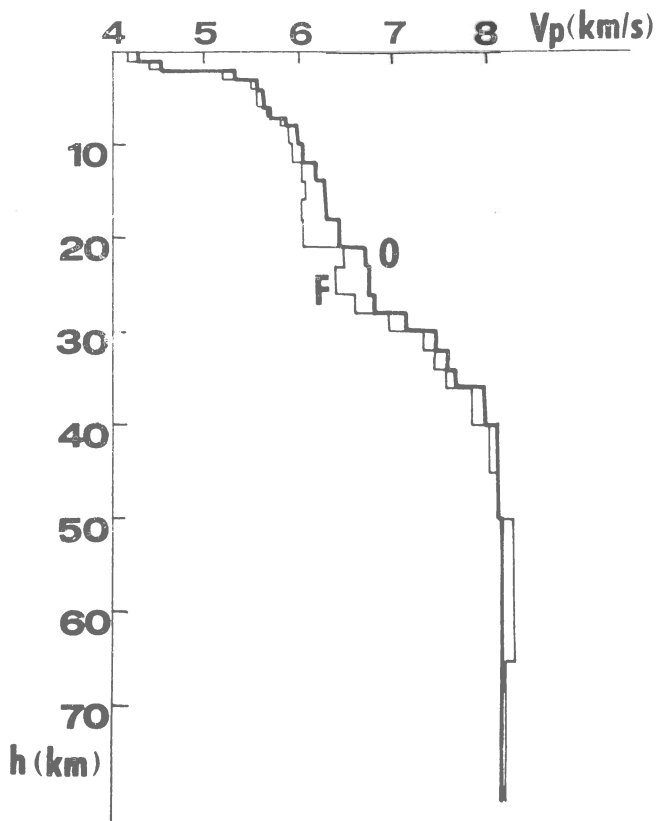
Fig. 1. Cross-sections of compressional velocities: the bold line corresponds to initial model O, the thin line to final model F.

parison of the results of surface wave investigations and deep seismic soundings along the International Profile VII, in *Proceedings of the 17th Assembly of the ESC, Akadémiai Kiadó*, Budapest, 325-328.

Novotný, O., T.A. Proskuryakova and A.V. Shilov (1995). Dispersion of Rayleigh waves along the Prague-Warsaw profile. *Studia geoph. et geod.* 31, (in press).

2-D SEISMIC MODELS OF THE LITHOSPHERE IN THE YOUNG RIFT ZONE - THE BRANSFIELD STRAIT, WEST ANTARCTICA

Tomasz JANIK

Institute of Geophysics, Polish Academy of Sciences,
Ks.Janusza 64, 01-452 Warsaw, POLAND

Abstract

Four Polish Antarctic Geodynamical Expeditions in 1979/80, 1984/85, 1987/88 and 1991 undertook seismic investigations in West Antarctica. Seismic measurements, including multichannel seismic reflection and deep seismic refraction, were carried out in the region of the west coast of the Antarctic Peninsula, between Antarctic Sound and Adelaide Island, Bransfield Strait, South Shetland Islands and South Shetland Trench, along several lines with a total length of about 5000 km. Selected sections and two-dimensional models of the crust for this area are presented. In detail the paper presents new results of two-dimensional modeling of DSS-1 profile, which crosses Bransfield Strait between King George Island and Antarctic Peninsula. A common model for two land stations and two OBSs is shown.

Introduction

During four Polish Antarctic Geodynamical Expeditions in 1979-91, deep seismic sounding measurements were performed in the transition zone between the Drake and South Shetland microplates and the Antarctic plate in West Antarctica. The Bransfield Rift together with the Bransfield Platform represent a back-arc basin with respect to the South Shetland Islands volcanic arc. For the Bransfield Strait area, the seismic records of five land stations in South Shetland Islands, three stations at Antarctic Peninsula, and nine OBSs were used (Fig.1). The network of deep seismic profiles with lengths from 150 to 320 km covered all the Bransfield Strait area. Most of them crossed the Bransfield Rift. One profile, of 320 km length, obtained with the use of six OBSs was located along the Bransfield Rift.
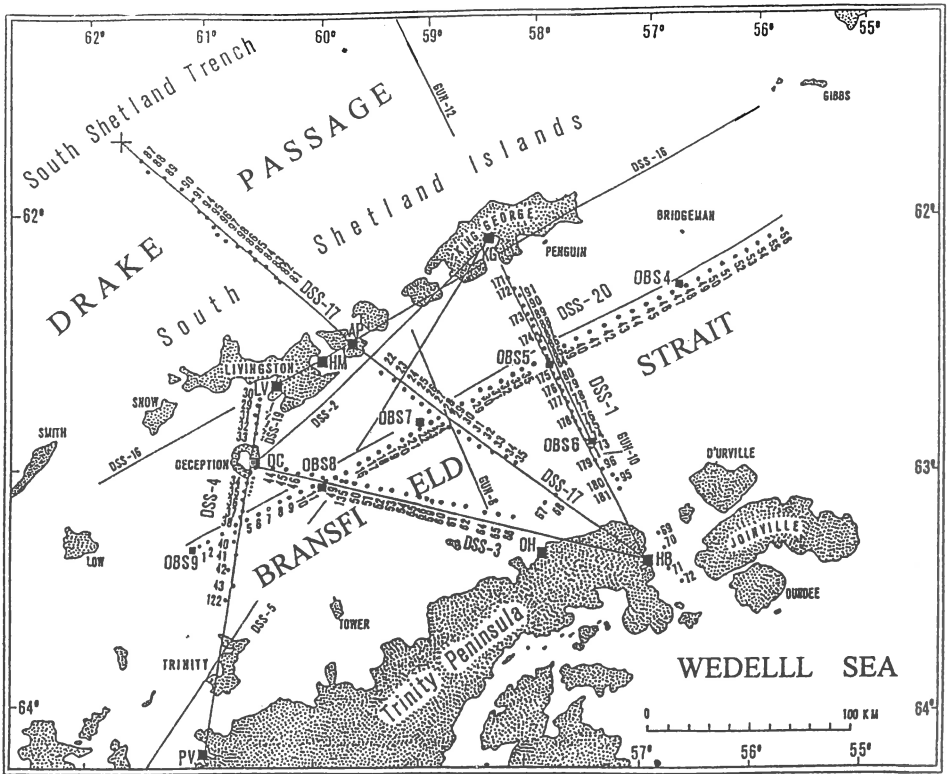
Fig. 1   Location of selected deep seismic profiles (DSS) in West Antarctica. Dots - shot points and their .
consecutive numbers; black squares - seismic stations: AP - Arturo Prat,   HM - Half Moon,
OH - O'Higgins,   HB - Hope Bay,   PV - Primavera.   GUN - selected reflection seissmic profiles.

Data and interpretation

Interpretation of the material is still under way. Following one-dimensional
models, presented earlier at few papers by Guterch et al. (1985,1990,1991)
and Grad et al.(1992), two-dimensional models of some profiles were prepared.
2-D model of DSS-17 was presented by Grad et al.(1993). 2-D model of DSS-1
was presented at papers Guterch et al.(1985), and Grad et al.(1993); it was
based on data from the expedition in 1979/80. During the expedition in 1991
we made 11 new shots on DSS1 . Same land stations on King George I. and at
Hope Bay, and additionally two ocean bottom seismometers, OBS-5 and OBS-6
(Fig.1) recorded those shots. New model, common for stations King George I.
(Fig.2), OBS-5 (Fig.3), OBS-6 (Fig.4) and Hope Bay (Fig.5) is presented in
 Fig.6 . A comparison of theoretical travel times, synthetic seismograms and
the observed wave field together with ray diagrams provide good coincidences.
New data made it possible to approximate more accurately the sedimentary
layers with velocities of 1.9-3.3 km/s, 4.0-4.5 km/s, 5.2-5.9 km/s and an
anomalously high velocity body, with $v_p > 7$ km/s, at a depth grater then

1008
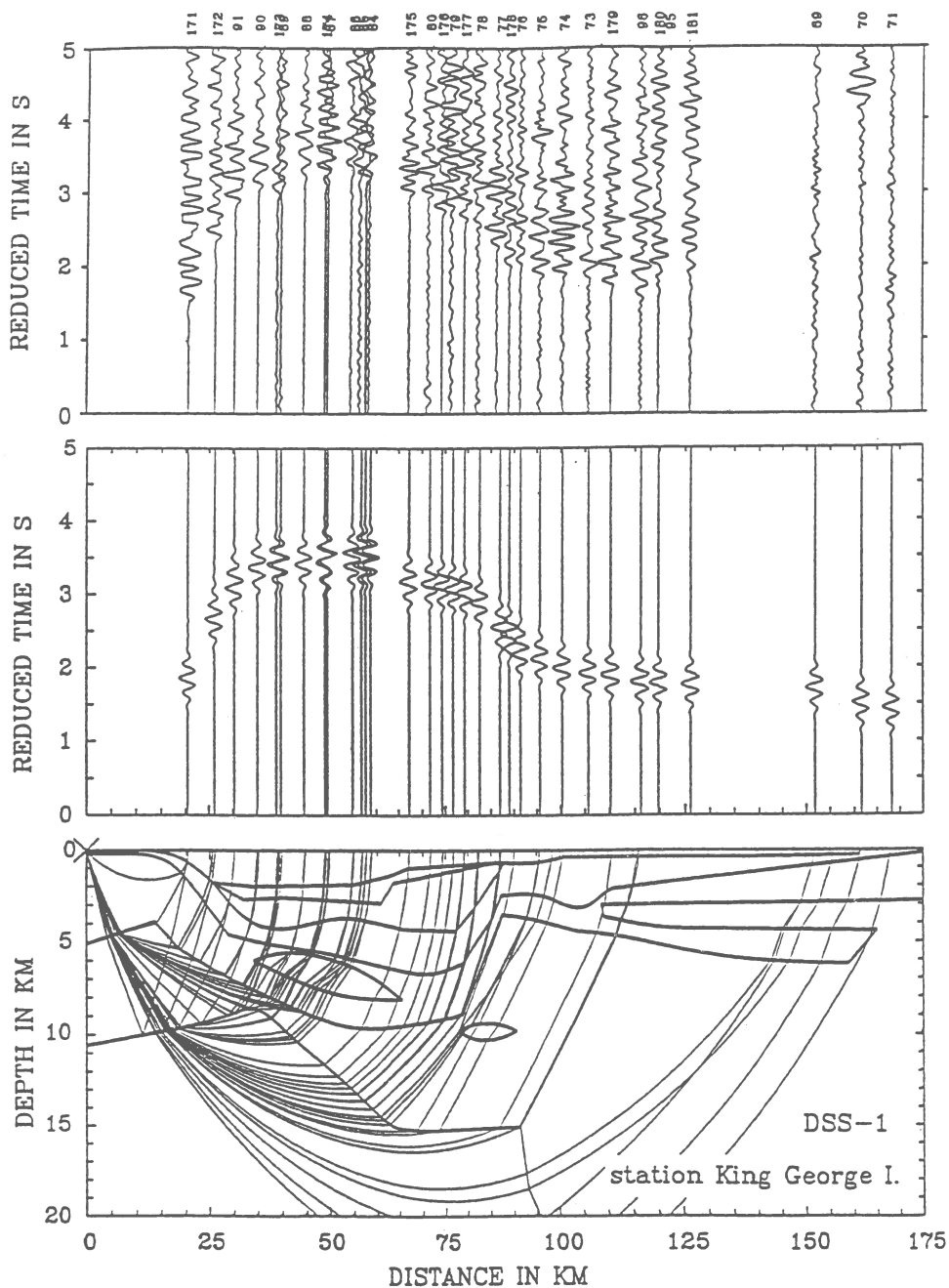
Fig.2 An example of the results of crustal structure modelling along profile DSS-1. Seismic record section with theoretical tevel time of the first arrivals (upper diagram), synthetic seismograms (middle) and model of the structure with seismic rays (bottom) for the station at King George Island, Reduction velocity 7.0 km/s.
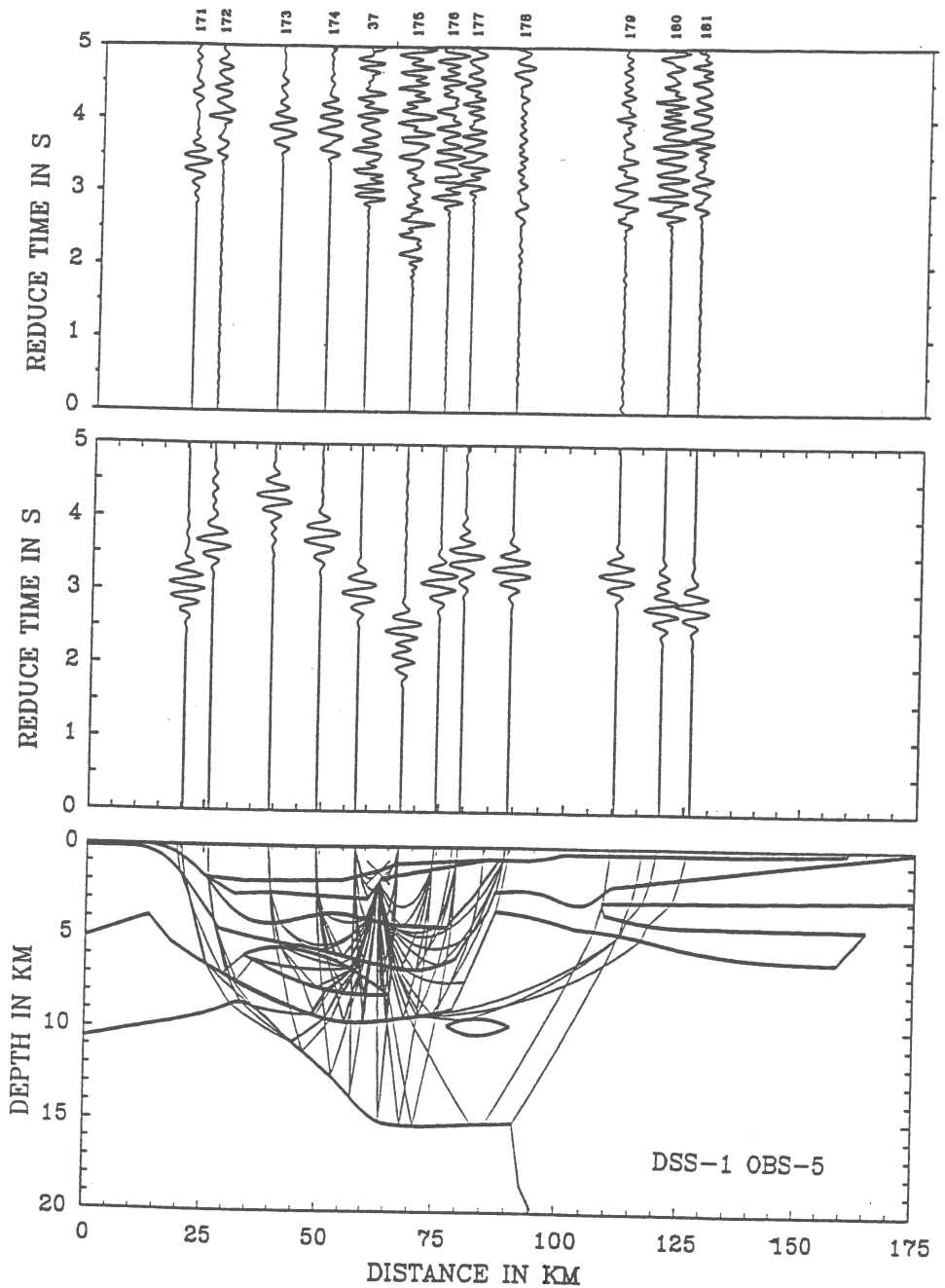
Fig.3   An example of the results of crustal structure modelling along profile DSS-1. Seismic record section with theoretical travel time of the first arrivals (upper diagram), synthetic seismograms (middle) and model of the structure with seismic rays (bottom) for the OBS-5. Reduction velocity 7.0 km/s.
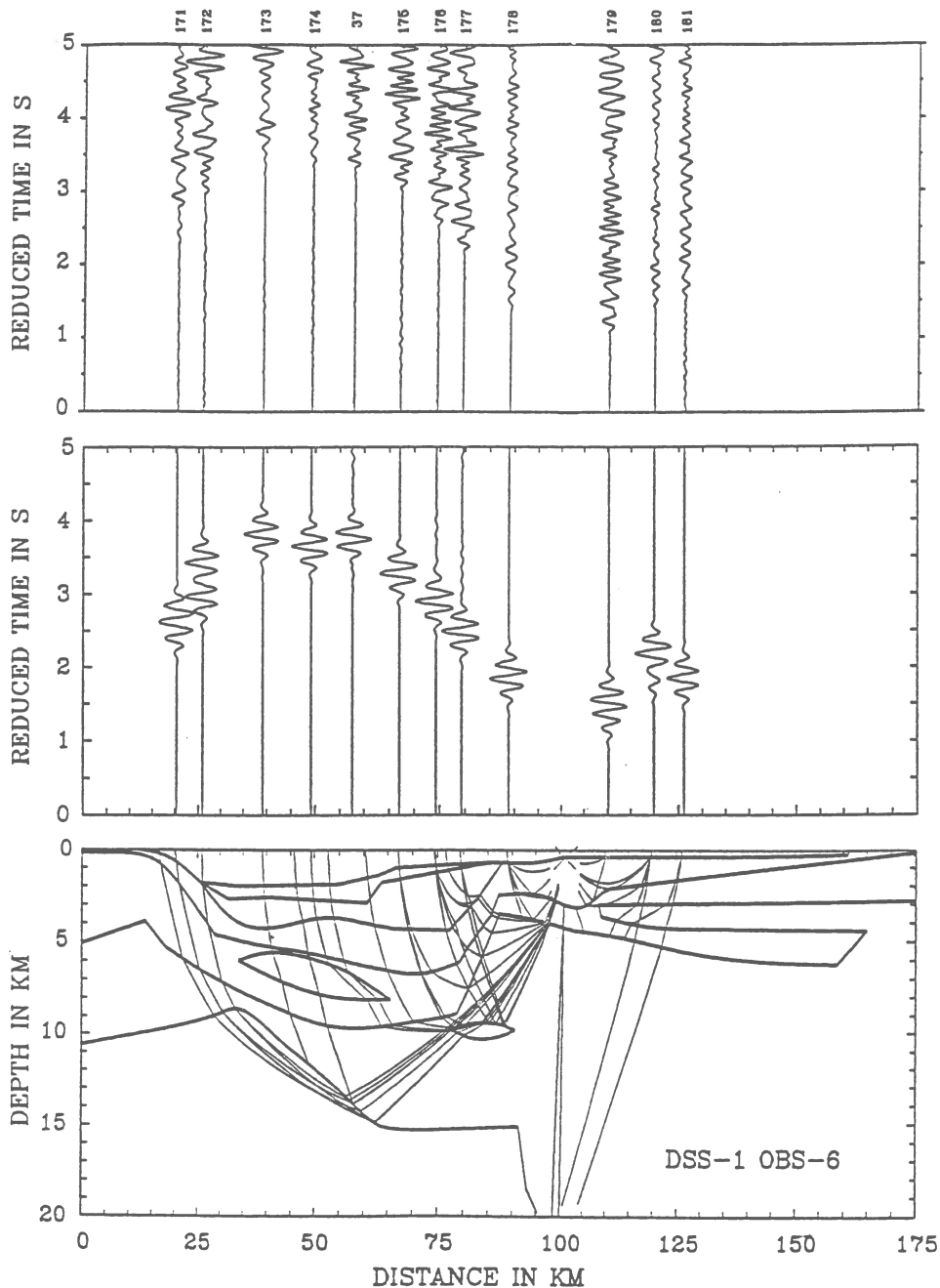
Fig.4 An example of the results of crustal structure modelling along profile DSS-1. Seismic record section with theoretical travel time of the first arrivals (upper diagram), synthetic seismograms (middle) and model of the structure with seismic rays (bottom) for the OBS-6. Reduction velocity 7.0 km/s.
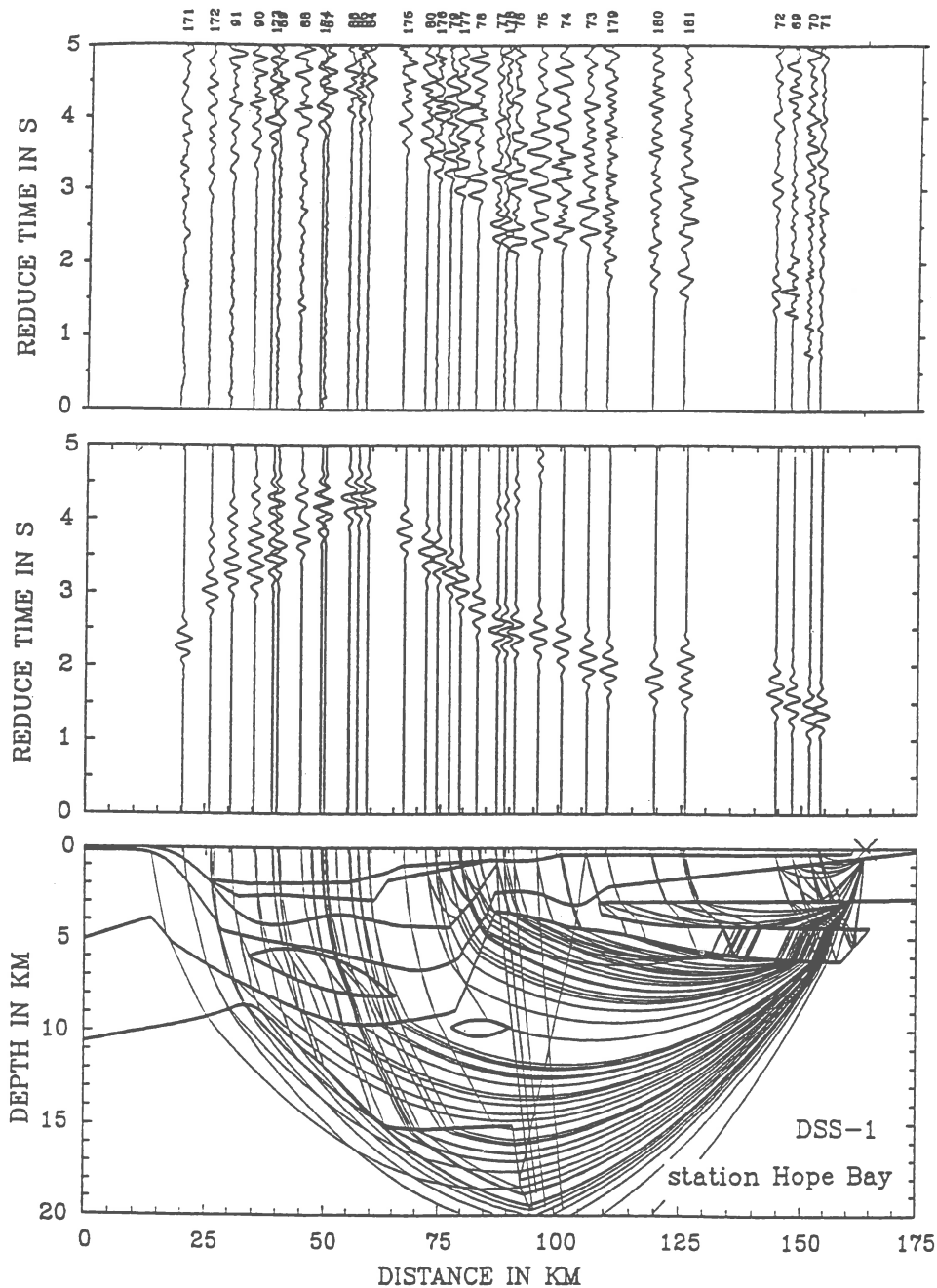
Fig.5 An example of the results of crustal structure modelling along profile DSS-1. Seismic record section with theoretical travel time of the first arrivals (upper diagram), synthetic seismograms (middle) and model of the structure with seismic rays (bottom) for the station at Hope Bay. Reduction velocitiy 7.0 km/s.
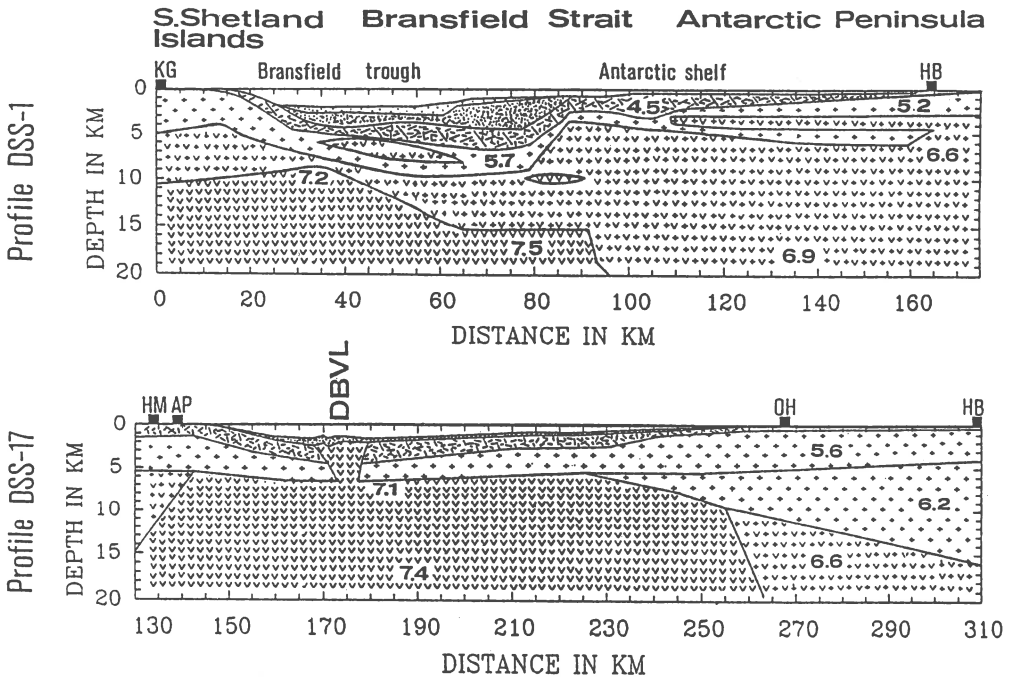
Fig. 6   Crustal models of the Bransfield Strait between the South Shetland Islands and Antarctic Peninsula
for profiles DSS - 1 and DSS - 17. DBVL = Deception - Bridgeman volcanic line; numbers are Vp
velocities in km/s. KG - the station on the Keller Peninsula at King George Island, AP - the Arturo
Prat station at Greenwich Island, HM - the station at Half Moon Island, HB - station at the Hope Bay,
OH - station O'Higgins.

10-15 km under the Bransfield Strait. A low-velocity zone, with $v_p > 5.7$ km/s,
was found under the crust layer with $v_p > 6.4$ km/s at the 5 km depth, near
Hope Bay station. Also two small "high-velocity bodies" was found in central
part of the profile. A comparison of crustal models of the Bransfield Strait
on profile DSS-1 and DSS-17 is presented in Fig.6.

The interpretation yielded two-dimensional models of the crust and litho-
sphere, down to 80 km depth, on profile DSS-17 (Fig.7). In the uppermost
crust, the unconsolidated and poorly consolidated young sediments with
velocities of 1.9-2.9 km/s cover the 4.0-4.2 and 5.6-5.9 km/s layers .The
crustal structure beneath the trough of Bransfield Strait is highly
anomalous. The presence of a high velocity body, with longitudinal seismic
wave velocities $v_p > 7.0$ km/s, was detected in the 6-30 km depth range. This
inhomogeneity was interpreted as an intrusion, coinciding· with the
Deception-Penguin-Bridgeman volcanic line. In the study area the Moho
boundary depth ranges from 10 km beneath the South Shetland Trench to 40 km
under the Antarctic Peninsula. In the transition zone from the Drake Passage
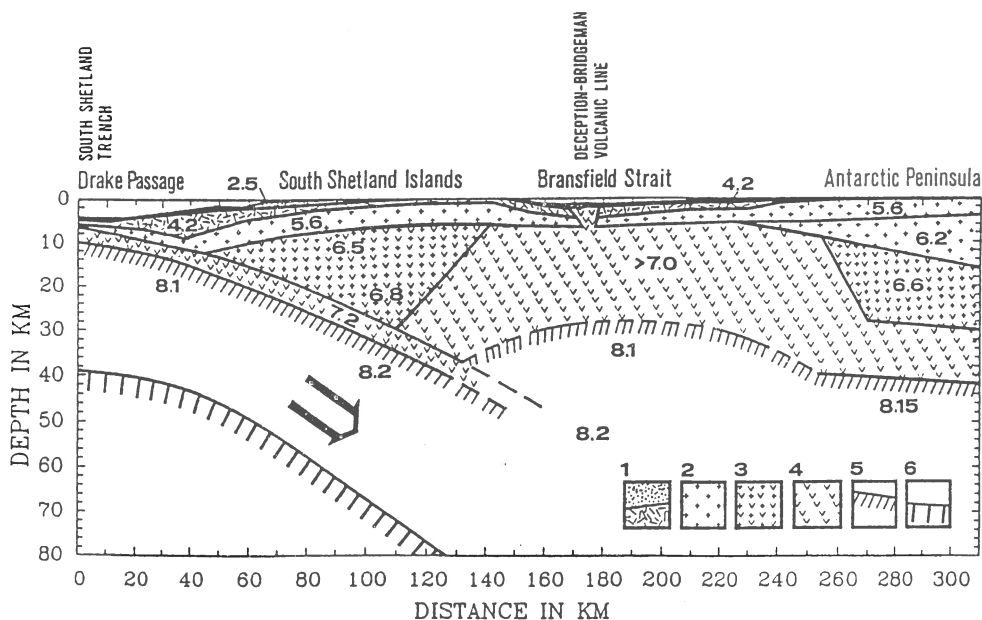
Fig. 7   Seismic model of the lithosphere along profile DSS-17 between Drake Passage and Antarctic Peninsula. (1) sediments, Vp=2.5-4.2 km/s; (2) upper crust, Vp= 5.4-6.3 km/s; (3) middle crust, Vp=6.4-6.8 km/s; (4) lower crust and high-velocity body in Bransfield Strait, Vp>7.0 km/s; (5) Moho boundary, Vp>8.0 km/s; (6) reflection boundary in the lower lithosphere.

to the South Shetland Islands, a seismic boundary in the lower lithosphere occurs at a depth ranging from 35 to 80 km.

Conclusions

The modeling of the crustal structure of the transition zone between the South Shetland Islands and Bransfield Strait indicates that the tectonic underplating has played a major role in the process of accretion and formation of the crustal blocks. The seismic wave fields change along the profile. Physical properties of the upper, middle and lower crust are different from block to block. Recent geophysical and geological investigations in the West Antarctica confirm the view that the Bransfield Strait is an active rift. The details of velocity structure in the lower crust in Bransfield Strait, which we have tested, are uncertain, because a high-velocity layer in the upper crust (v_p>7 km/s at a depth of 6-15 km) masks observations of the lower crust. The recent detailed deep refraction study

in Bransfield Strait by the use of sensitive ocean bottom seismographs and two-dimensional modeling will shed more light on the interpretation of the transition from the lower crust to the upper mantle in the Bransfield Trough. Two-dimensional models for DSS-3, DSS-4 and DSS-20 profiles will be calculated in the next step.

REFERENCES

Ashcroft, W.A., 1972. Crustal structure of the South Shetland Islands and Bransfield Strait, *British Antarctic Survey Scientific Report*, **66**, 43 p.

Barker, P.F. & Daniel, I.W.D., 1983. Progress in geodynamics in the Scotia Arc region, in *Geodynamics of the Eastern Pacific Region, Caribbean and Scotia Arcs, Geodynamics,* ed. R. Cabrw. American Geophysical Union Series 9, 137-170, Washington, DC.

Birkenmajer, K., Guterch, A., Grad, M., Janik, T. & Perchuć, E., 1990. Lithospheric transect Antarctic Peninsula - South Shetland Islands, West Antarctica, *Polish Polar Research*, **11**, 241-258.

Červený, V. & Pšenčík, I., 1983. 2-D seismic ray tracing package SEIS83, (software package). Prague, Charles University.

Gambõa, L.A.P. & Maldonado, P.R., 1990. Geophysical investigation in the Bransfield Strait and Bellinghausen Sea - Antarctica, in *Antarctica as an Exploration Frontier - Hydrocarbon Potential, Geology and Hazarde, AAPG Studies in Geology*, **31**, pp. 127-141, ed. St. John B., American Association of Petroleum Geologists, Tulsa, Oklahoma.

Garrett, S.W., 1990. Interpretation of reconnaissance gravity and aeromagnetic surveys of the Antarctic Peninsula, *J. geophys. Res.*, **95**, No. B5, 6759-6777.

González-Ferrán, C., 1985. Volcanic and tectonic evolution of the northern Antarctic Peninsula - Late Cenozoic to Recent, in *Geophysics of the Polar Regions, Tectonophysics,* **114**, 389-409, eds E.S. Husebye, G.L. Johnson & Y. Kristoffersen. ·

González-Ferrán, C., 1991. The Bransfield rift and its active volcanism, in *Geological Evolution of Antarctica*, 505-509, eds M.R.A. Thomson, J.A. Crame & J.W. Thomson, Cambridge Univ. Press.

Grad M., Guterch A., Janik T., 1993, *Seismic structure of the lithosphere across the zone of subducted Drake plate under the Antarctic plate, West Antarctica,* Geophysical Journal International, **115**, 586-600.

Grad M., Guterch A., Janik T., Šroda P., 1993, *2-D seismic models of the lithosphere in the area of the Bransfield Strait,West Antarctica,* Polish Polar Research, v.14,no.2,123-151.

Grad, M., Guterch, A. & Šroda, P., 1992. Upper crustal structure of Deception Island area, Bransfield Strait, West Antarctica. *Antarctic Science*, **4**, 469-476.

Guterch, A., Grad, M., Janik, T., Perchuć, E. & Pajchel, J., 1985. Seismic studies of the crustal structure in West Antarctica 1979-1980 - preliminary results, in *Geophysics of the Polar Regions, Tectonophysics*, **114**, 411-429, eds E.S. Husebye, G.L. Johnson & Y. Kristoffersen.

Guterch, A., Grad, M., Janik, T. & Perchuć, E., 1990. Deep crustal structure in the region of the Antarctic Peninsula from seismic refraction modeling (next step of data discussion), *Polish Polar Research*, **11**, 215-239.

Guterch, A., Grad, M., Janik, T. & Perchuć, E., 1991. Tectonophysical models of the crust between the Antarctic Peninsula and the South Shetland trench, in *Geological Evolution of Antarctica*, 499-504, eds M.R.A. Thomson, J.A. Crame & J.W. Thomson, Cambridge Univ. Press.

Guterch A. & Shimamura H., 1991. An OBS-Land refraction seismological experiment in the Bransfield trough, West Antarctica, 1990-91, in *Sixth International Symposium on Antarctic Earth Sciences, 9-13 September 1991*, pp. 201-202, Tokyo.

Henriet, J.P., Meissner, R., Miller, H. & the GRAPE Team, 1992. Active margin along the Antarctic Peninsula, in *Detailed Structure and Processes of Active Margins, Tectonophysics*, **201**, 229-253, eds H. Shimamura, A. Hirn & J. Makris.

Jeffers, J.D. & Anderson, J.B., 1990. Sequence Stratigraphy of the Bransfield Basin, Antarctica: Implications for tectonic history and hydrocarbon potential, in *Antarctica as an Exploration Frontier - Hydrocarbon Potential, Geology and Hazarde, AAPG Studies in Geology*, **31**, pp. 13-29, ed. St. John B., American Association of Petroleum Geologists, Tulsa, Oklahoma.

Para, J.C., Yanez, G. & Grupo de Trabajo USAC, 1988. Aeromagnetic Survey on the Antarctic Peninsula and surrounding seas: Integration of the data obtained at different altitudes, *Ser. Cient. INACH*, **38**, 117-131.

ZAKINTHOS-NW PELOPONESSUS AREA REVISITED. 2-D CRUSTAL STRUCTURE INVESTIGATIONS

N. Voulgaris[1], G. Karantonis[1], N. Delibasis[1], E. Baier[2] and J. Drakopoulos[1]

[1]Geophysics-Geothermy Division, Geology Department, University of Athens, Panepistimioupolis, Ilissia 15784.
[2]Institute fur Meteorologie und Geophysik, Johann Wolfgang Goethe Universitat, Feldbergstrasse 47, 6 Frankfurt a.M.

Abstract

The crustal structure of the western part of the Hellenic margin has been investigated using seismic refraction and wide angle reflection techniques. Data acquisition was carried out along an E-W trending 120 km long profile in the area of Zakinthos-NW Peloponessus, during September 1987. The acquired data set includes 15 shots combined with 4 profile segments. Interpretation of the recorded data was originally accomplished by iterative 2-D forward modeling, based on the Gaussian beam theory. The result of this procedure is a well determined velocity model including 9 seismic units from the surface down to a maximum depth of 36 km, which is in good agreement with the surface geology information and the general tectonic framework of the area.

However, the interpretation technique used is unable to provide quantitative estimates of model non-uniqueness in terms of parameter uncertainty and resolution. Thus, an attempt is made to use 2-D inversion interpretation procedures for the simultaneous determination of velocity and interface structure. First order asymptotic ray theory with numerical solution of ray tracing equations is used for the forward modeling while a damped least-squares iterative approach for inversion.

Results and efficiency of methods are discussed.

Data Description

In the fall of 1987 a deep refraction and wide angle reflection profile was carried out in the western part of the Hellenic margin in the area of Zakinthos - W. Peloponessus (figure 1). This experiment was a joint venture of the Geophysics Geothermy Department of the University of Athens and the Institute for Meteorology and Geophysics of the Johann Wolfgang Goethe University in Frankfurt. The aim of this study was to investigate the complex geological and tectonic structure of the area characterised by a relatively high seismicity and active salt tectonics associated with the Triassic evaporites, the later possibly being the key for the assessment of its hydrocarbon potential.

Field work operations were carried out using 12 MLR-II analog magnetic tape stations, located 2 km apart. Additional MEQ-800 smoked paper analog stations were placed in between to be used in case of data loss or to provide additional information. In order to cover the total 120 km length of the profile, shot perpendicular to the main geological and tectonic structures of the area (Monopolis and Bruneton, 1982, Nikolaou, 1986), with the available instrument resources, deployment and operations were successively repeated along four subsections (DRO, SKO, KIL and ZAK). For each
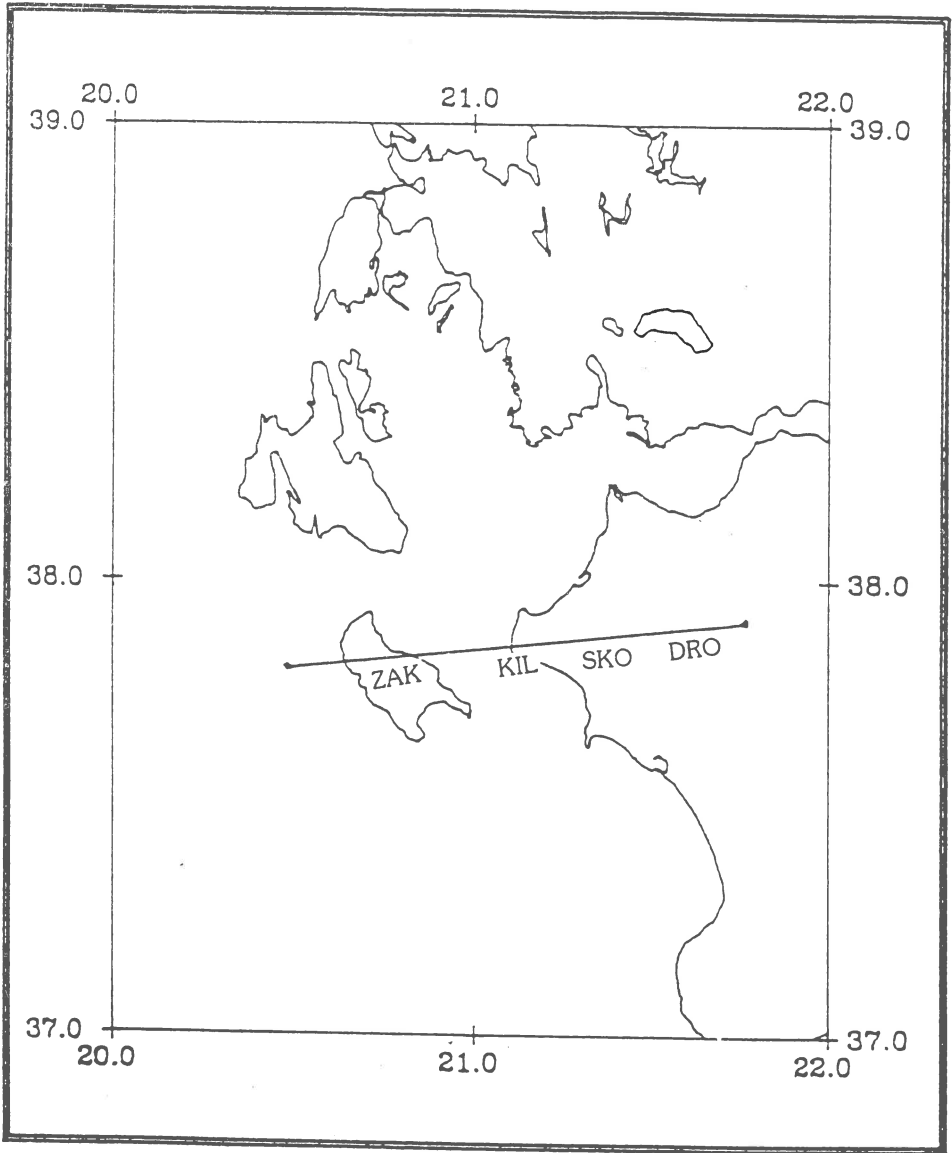
Figure 1. Location map of the seismic profile in NW Greece.

subsection, three underwater explosions and one shot in five borehole configuration were detonated. In the present reevaluation study the westernmost subsection (ZAK) was used, since the very good data quality allows for comparison of different interpretation procedures.

Following the completion of field operations the MLR-II recorded signals were decoded, using the DCF time signal. and subsequently digitised and filtered in order to obtain the desired reduced travel time sections.

Original Interpretation: Gaussian Beam Method

For the original interpretation of the 2D seismic profile, Gaussian beam (Cerveny et al, 1982) forward modeling ray tracing techniques were used by implementing the algorithms developed by Weber (1988), which allows for both travel time and synthetic seismogram calculations. According to the requirements of the method an initial 2D model was constructed by combining all the available geological and geophysical information from the area with the preliminary results from the velocity analysis. This model was then parametrised by defining a number of first order discontinuities i.e. surfaces where refraction or reflection of seismic rays can be observed. This is achieved by using a number of points with fully defined coordinates and physical properties to describe these interfaces. As a result, second order discontinuities are automatically defined by combining points between the initial first order interfaces. In that way the medium is described by subdividing the model into a set of triangles within which ray propagation is controlled by linear density and velocity laws. This technique allows for flexible modeling of complicated structures as well as faster computations during ray tracing.

Kinematic ray tracing is the first stage of the computational procedure, in which observed and calculated travel times of different phases are repeatedly compared and the model is adjusted until a satisfactory agreement is reached. By repeating this computational sequence for every shot of the given profile segment a final model of the medium can be obtained. This can be further refined in the second stage using dynamic ray tracing and comparing the recorded seismic signals with synthetic seismograms. However, it should be noted that due to inherent problems in refraction data (Weber, 1988), such as environmental noise which can reach 50% of the maximum signal amplitudes, reverberations after the arrival of strong seismic signals due to the bad coupling of the seismometers to the ground, multiples and diffractions from small inhomogeneities and problems associated with the attenuation of the seismic signal of the explosive source, a direct comparison between observed and computed seismic signals is not possible since the above mentioned problems allow only relative comparisons.

In figure 2 a reduced traveltime section for the ZAK segment of the profile as well as the final 2-D model are presented (Voulgaris et al, 1994). It should be noted that these results were obtained using both first and later seismic arrivals.

Reinterpretation: ART Ray Method and LSQR Inversion

The method used for the reinterpretation of the data was developed by C. A. Zelt and R. B. Smith (1992). It is an automated damped least squares inversion routine which uses ray tracing for the calculation of the partial derivatives of traveltime with respect to velocity and boundary depth. The method allows for simultaneous determination of velocity distribution and boundary geometry.

An important initial stage of the reinterpretation was the conversion of the 2D velocity model produced with the Gaussian Beam method to the parametrisation required for the application of this technique. This parametrisation is a layered, variable block size representation of a 2D isotropic velocity structure. The layer boundaries must cross the model from left to right and are specified by an arbitrary number and spacing of nodes. The velocity distribution within each layer is determined by means of upper and lower velocity nodes using linear interpolation between them. It is obvious, that even though the model geometry determined by the original interpretation can be represented very accurately in terms of the described parametrisation, there are problems in the representation of the
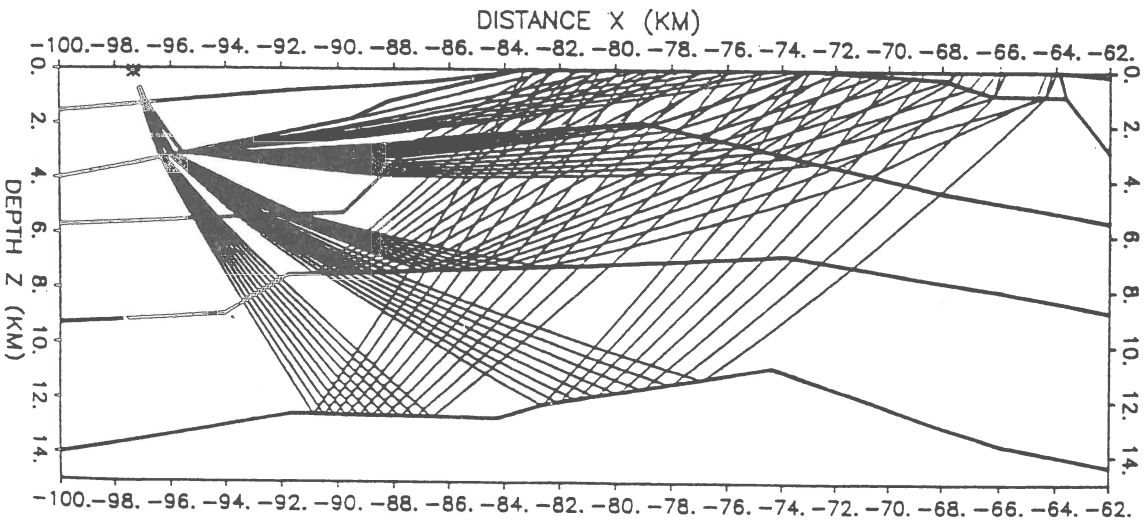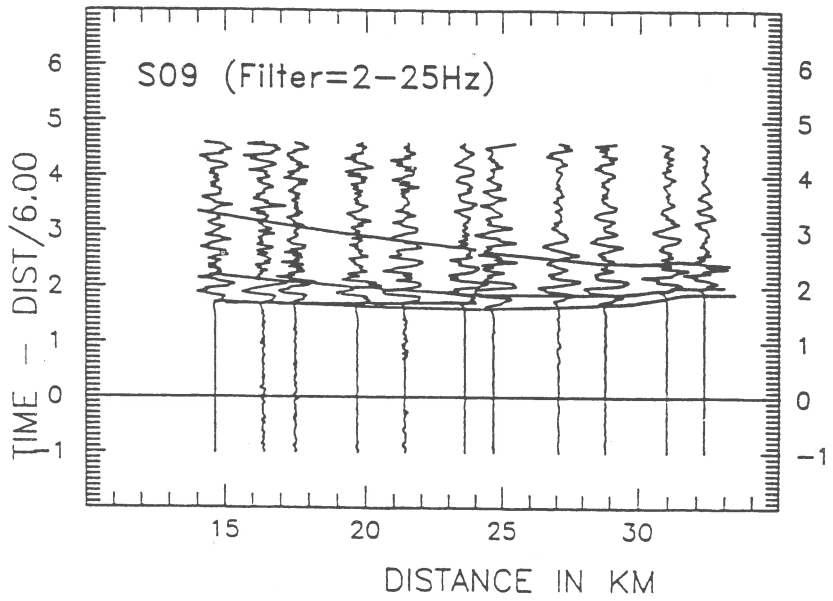
Figure 2. Reduced traveltime section for the ZAK segment and corresponding 2-D model (Voulgaris et al, 1994)
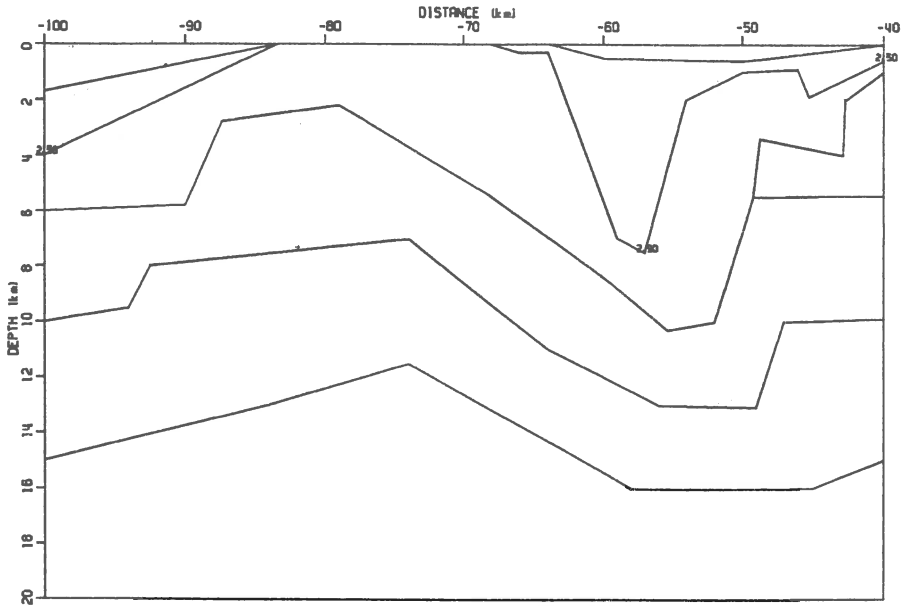
Figure 3. Original 2-D model

velocity field, which was originally expressed by means of triangles. However, it is believed that due to the scale of the problem small inaccuracies caused by the model translation are not crucial for this study.

The first step of the application of the method includes ray tracing through the velocity model using zero order asymptotic ray theory by solving the ray tracing equations numerically. For the effective application of the method an iterative shooting/bisection technique is used for the determination of the ray take-off angles. In addition, a smooth layer simulation can be applied in order to improve the distribution of rays and avoid effects caused by the block type model parametrisation. The final product of the ray tracing stage was the calculation of the required partial derivatives, which will be inverted in the second stage.

Iterative damped least squares techniques are then used for the inversion of the calculated partial derivatives. This procedure leads to the minimisation of the difference between calculated and observed traveltimes through successive alteration of the 2D model. A very important factor for the successful application of the method is the positive identification of the various seismic phases and the comparison of their traveltimes. For this reason it is suggested that in the initial steps of the interpretation only first phases are used while later phases are examined when they can be reliably modeled.

In this study several tests were carried out and various velocity and boundary nodes were inverted at each test. Special attention was paid to keep the number of inverted model parameters low in comparison to the number of data, in order to obtain stable solutions. It should be noted that only first arrivals were used, at this study.

Finally, after careful evaluation of the results of each test an interpretation sequence of three steps was adopted. Thirty nine observations were used and the original RMS traveltime residual was 0.210 s (chi squared: 106.256). At the first step 7 boundary nodes were updated and after 6 iterations the RMS traveltime residual was reduced to 0.193 s (chi squared: 48.733). At the second step 9 velocity nodes were updated leading to an RMS

1021
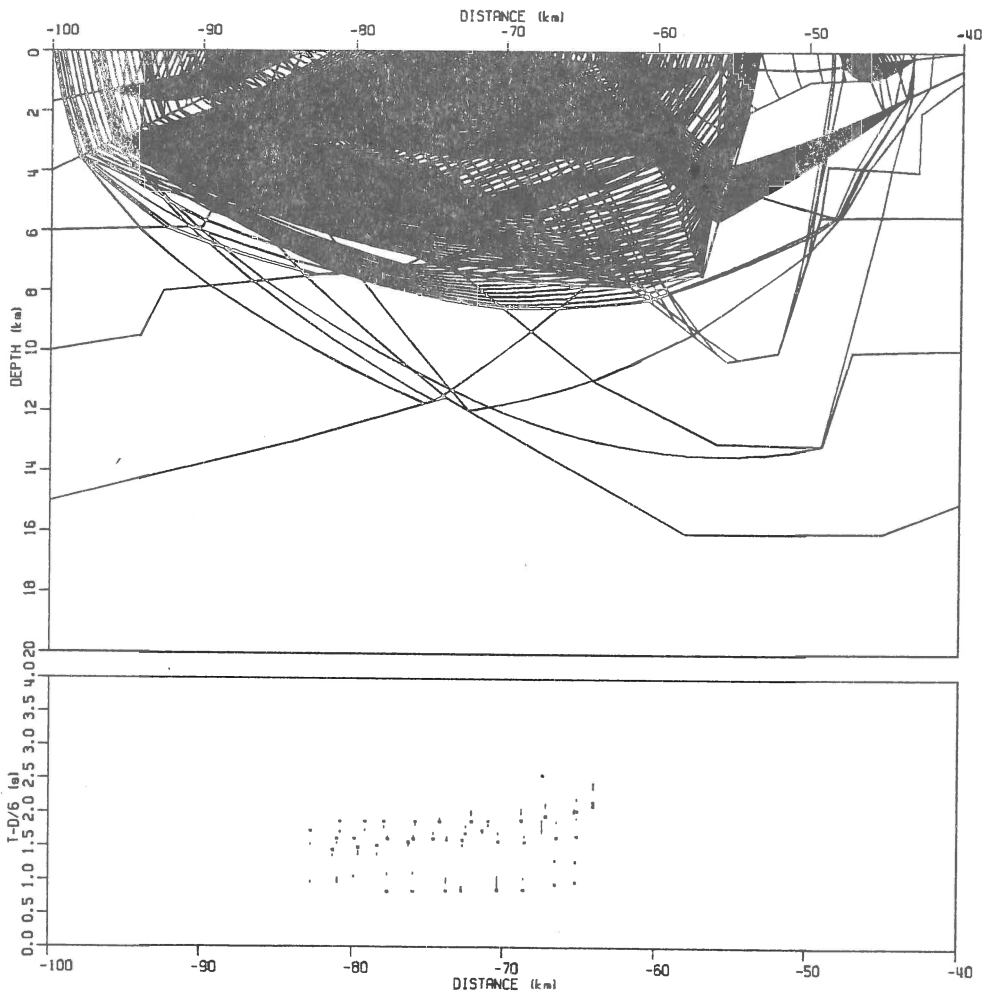
Figure 4. First reintepretation step with 7 boundary nodes updated. After 6 iterations RMS = 0.193 s, chi squared = 48.733

traveltime residual of 0.132 s (chi squared 36.242), after 2 iterations. At the final step 5 boundary nodes were updated and after 2 iterations the RMS traveltime residual was further reduced to 0.131 s (chi squared 34.021). The final 2D velocity model is presented in figure 7.

Conclusions

During the course of the original interpretation using the Gaussian Beam forward modeling it has become apparent that the implementation of the method does not allow for an overall quantitative estimate of the goodness of fit and respective errors. Furthermore,

interpretation must be carried out on one shot at a time basis a fact that demands reevaluation of interrelated shots when even a minor change is introduced to the velocity model.
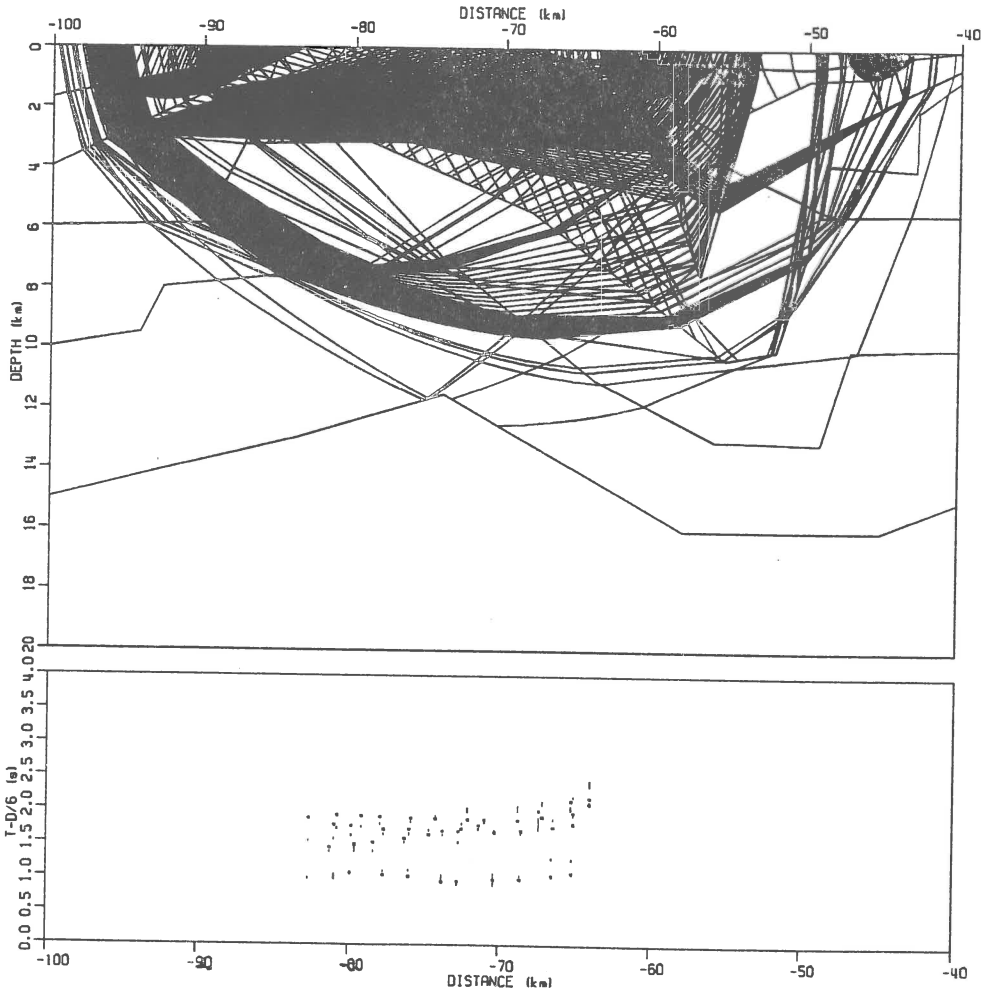
Figure 5. Second reintepretation step with 9 velocity nodes updated. After 2 iterations RMS = 0.132 s, chi squared = 36.242

The implementation of the second methodology was a useful tool in order to overcome the above mentioned drawbacks since, all shots were processed and evaluated simultaneously and quantitative measures of fit improvement were available at the end of each step. However, it should be emphasized that the key to the successful application of

the method lies with the initial forward modeling approach which provided a reliable initial 2-D model and positive seismic phase identification.

Hence, it is suggested that forward modeling and inversion techniques should be applied successively, as presented in this study. Forward modeling can provide a realistic structure incorporating the available geological information, while inversion techniques can refine the interpretation following well defined mathematical norms.
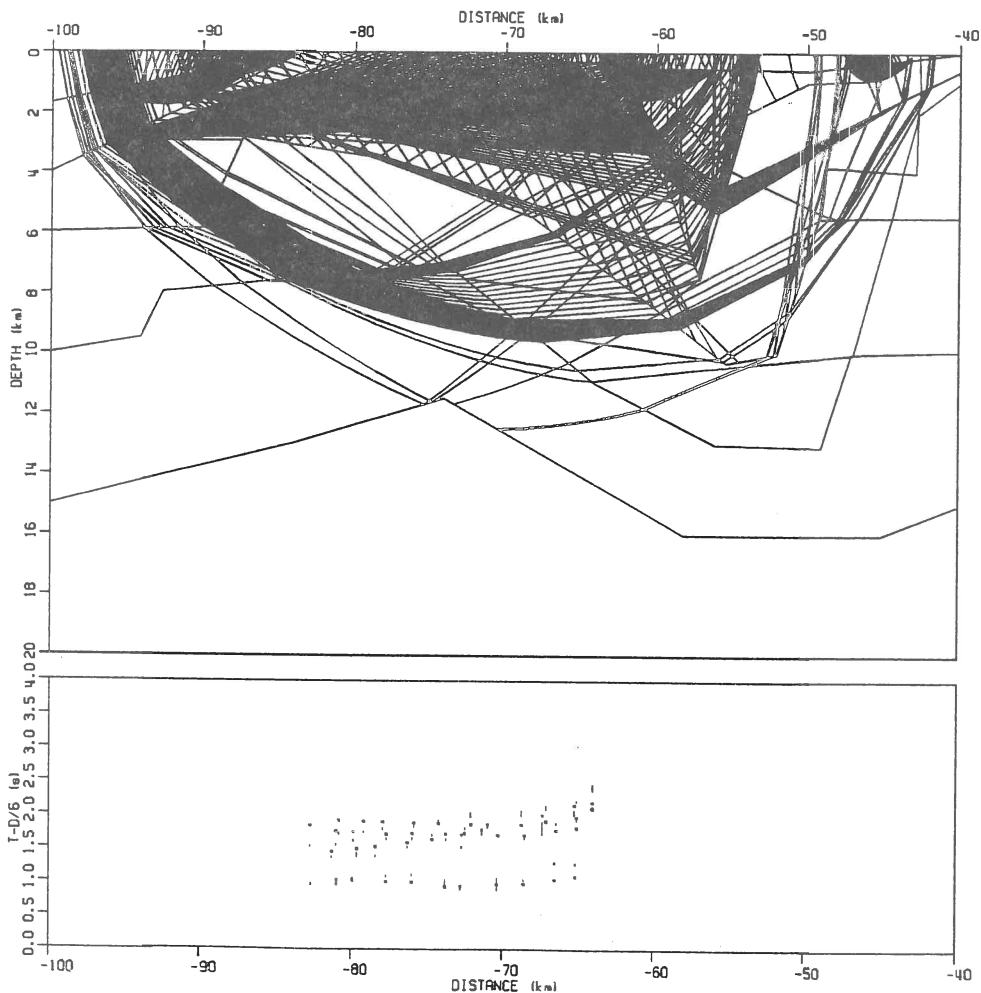
Figure 6. Third reintepretation step with 5 boundary nodes updated. After 2 iterations RMS = 0.131 s, chi squared = 34.021
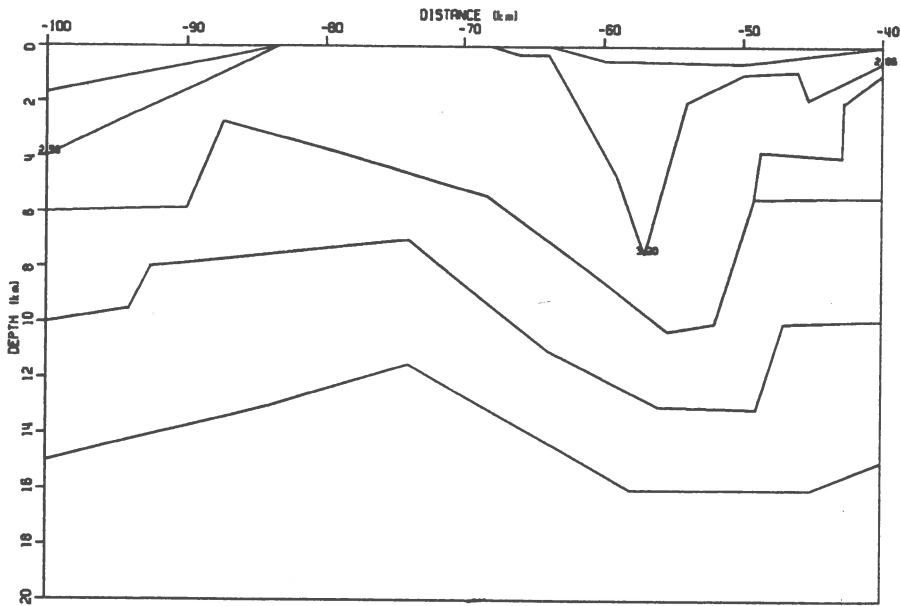
Figure 7. Final 2-D model

References

Cerveny, V., Popov, M., M. and Psensik, I., 1982. Computation of wave fields in inhomogeneous media - Gaussian beam approach, Geoph. J. R. astr. Soc., 70, p 109-128.

Monopolis, D. and Bruneton, A., 1982. Ionian sea (Western Greece): Its structural outline deduced from drilling and geophysical data, Tectonophysics, 83, p 227-242.

Nikolaou, K., 1986. Contribution to the knowledge of the Neogene, the geology and the position of the Ionian and Preapoulian zones in relation to petroleum geology observations mainly on the islands of Strophades, Zakinthos and Cephalonia, Phd Thesis, University of Athens.

Voulgaris, N., Delibasis, N., Makropoulos, K., Drakopoulos, J., Baier, B. and Schulze-Frerichs, K., 1993. Crustal investigations in Zakinthos - NW Peloponessus area (W. Greece), Proceedings of the 2nd Geophysical Congress, Florina, Macedonia, Greece, 2, p. 505-515.

Weber, M., 1988. Computation of body-wave seismograms in absorbing 2-D media using the Gaussian beam method: comparison with exact methods, Geophys. J., Vol. 92, p 9-24.

Zelt, C., A. and Smith, R., B., 1992. Seismic traveltime inversion for 2-D crustal velocity structure., Geophys. J. Int., 108, p 16-34.

EARTHQUAKE PREDICTION PROBLEM
AND THE WAYS OF ITS SOLUTION

S. BALASSANIAN

National Survey of Seismic Protection
under the Government of the Republic of Armenia

ABSTRACT

1. Earthquake prediction is one of the necessary components of seismic risk reduction in Armenia. This is associated with the fact that owing to the subjectively underestimated seismic hazard in the territory of Armenia earthquake resistance level of buildings and structures had appeared to be significantly lower than the seismic hazard level. **2.** Earthquake prediction should be considered as a stage-by-stage seismic hazard assessment which consequently passes from a long term to current one when strong seismic event is under preparation. **3.** Notion of strong seismic event preparation and realization processes as repeated, quantized (leap-type) transitions of a deformed geological medium from one energy allowed state to another with these transitions accompanied by different effects in geosphere, biosphere and atmosphere can be one of the important elements of seismic hazard correct assessment in the zone of Arabian and Eurasian plates collision.

SUMMARY

It is intimated in the work that earthquake is a phenomenon which may be considered as an electroseismic effect prepared by the specific structure of geological medium as well as by the internal and external impacts.

INTRODUCTION

The experience accumulated over a period of 20 years' earthquake research particularly with respect to prediction suggests that many of experimental points could hardly be explained in the context of existing earthquake origination mechanical model, namely: deep focus earthquakes with hypocenters located within the plastic astenospheric material; earthquake triggers of different physical nature from chromospheric flashes at the Sun to sharp change of atmospheric electricity; appearance of precursors at the distances several times exceeding the size of earthquake preparation zone in all of matter states (solid, liquid and gaseous) and any of media accessible to observation (lithosphere, lower layers of atmosphere, ionosphere, biosphere); etc.

Considering that mechanical forces play an important role in earthquake origination an attempt was made in the present work to show that other forces capable to contribute to earthquake preparation and realization act concurrent with the mechanical ones in nature.

EARTHQUAKE AS AN ELECTROSEISMIC EFFECT

The preparation and realization of strong earthquakes within the collision zone of Arabian and Eurasian plates (where the territory of Armenia is situated) is related to the process of rocks compression spread over large area and causing their long-term deformation followed by rupturing.

The earthquake preparation process displayed from the energy standpoint it appears that certain local area of earthquake preparation zone changes from the W_0^P quasi-equilibrium energy state over the W_{CR}^P critical energy level during Δt time period. This is followed by rocks rupturing, i.e. potential-to-kinetic energy conversion.

Assumed that potential energy being accumulated in an earthquake preparation zone must reach the value of 10^6j order, it is not difficult to imagine that this should be attendant with severe changes of physical, physical-and-chemical and chemical properties of the medium, especially in the specific energy active points.

The changes of medium properties might be expected in all of the three phases-liquid, solid and gaseous. It is known that they are registered by special geophysical, hydrogeodynamic and geochemical methods the more accurately the closer these changes to the surface of observation.

If $W_0^P \rightarrow W_{CR}^P$ medium state transition is supposed to be smooth then continuously increasing anomalies of registered parameters would be observed starting from the moment when the intensity of changes exceeds the metering instrument sensitivity.

The retrospective analysis of earthquake precursors in the territory of Armenia as well as in the other seismically active zones of the world evidences that the above character of anomalies is observed practically nowhere.

All of the recorded amplitude anomalies preceding seismic events are of little duration - life time (Δt_{AN}) and often repeat several times up to the moment of seismic event.

The above character of anomalies implies their association with short living processes excited in the medium during earthquake preparation.

The investigation we have performed shows that multiple quantized (leap-type) transitions of the medium from one energy level to another under continuously increasing elastic stress forces may be attributed to such processes.

How much is this model real physically? How does it correlate with practice?

Let us conceive how the seismically active zone appears in a W_0 quasi-equilibrium state.

According to [1] it is a multiphase (solid, liquid, gaseous) geological medium with the zones of separated charges (SCZ) formed at the phase interfaces.

As it is known in the chemistry of colloids the SCZs are noted for unique features: charges separated both along and across of the phase interface [2]; multiplicity of layers, which are in general up to $1\,\mu$m thick [2]; huge electric

capacitance with $\varepsilon*$ complex dielectric permittivity, ranging up to 10^5 at the cost of gigantic low frequency dielectric dispersion effect [2]; electrostatic field strength featuring values of 10^5-10^8 V/cm (breaking for dielectrics) within the SCZ both along and across of the phase interface [2,1].

Seismically active zone as one of the most weakened lithosphere zones is characterized by anomalous polydispersivity, heterogeneity, multiplicity of phases and components [1], i.e. presents high concentration area of elementary SCZs or huge electric energy (W) accumulation area.

Let us give some numerical evaluations of the W.

The electric energy concentrated in the medium including the seismically active zone is estimated by the following well-known expression:

$$W = \frac{\varepsilon\varepsilon_0 \left|\vec{E}\right|^2}{2} V \, , \qquad (1)$$

where V is the volume of considered medium, E is the electric field strength, ε is the dielectric permittivity, ε_0 is the electric constant.

Let's suppose, that the linear size of earthquake energy emission zone is equal to 20 km (this, for instance, is possible for the realization of M7,0 earthquake); the zone is 1 km in width; distribution in depth is 10 km, i.e. $V=200\ km^3$. If E is assumed to be 10^6 V/cm in the SCZ formed at phase interface and $\varepsilon=1$ then substituting these values in expression (1) we have $W=10^{16}j$ (joule).

This amount of energy accumulated in the rock massif corresponds to the energy of a earthquake (M8).

The $\varepsilon*$ complex magnitude may reach 10^5 and up in an anomalously polydispersive, multiphase and multicomponent, heterogeneous media such as the active fault zones if only due to the gigantic low frequency dielectric dispersion effect [2]. The effective area of double electric layers and consequently the $V*$ effective volume is much larger than V is. It hence becomes clear that the geoelectric energy reserve accumulated in rock massif even within single active fault can exceed the annual emission of seismic energy on the Earth.

Thus, considering driving forces of earthquake preparation and realization, geoelectric energy deserves attention in energy respect.

Let us consider the state of geological medium of seismically active zone under mechanical stress forces exerted on it, the latters associated with the start of earthquake preparation, i.e. its first stage.

Subjected to the gradually increasing deformations the diversely orientated movable SCZ-s will start to re-arrange themselves, changing the size and shape and gaining certain orientation conforming to the direction of acting external stress forces [Fig.1].

The state-to-state SCZ transition will thus go on not smoothly, but in a leap-type manner.

The physics of leap-type transitions can be explained as follows.

- orientated SCZ direction

- disorientated SCZ direction

- SCZ transition from the disorientated to the orientated state

- acting stress forces
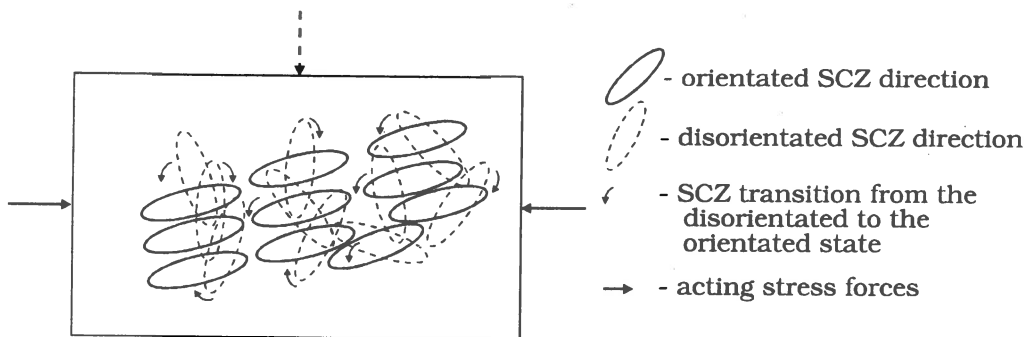
Fig. 1. Formation of SCZ domains

There are defects, impurities, dislocations in each element of a geological medium. A specific or electromagnetic interaction arises between the elementary SCZ and any of these formations. As a result, when the SCZ rotates or grows it can not be changed over another state till the external impact reaches the value exceeding the restraining force. The leap of SCZ to a new state occurs at this particular moment.

Accounting for the "collectivity"of this effect in a medium the rotation of SCZ appears to reside in a leap type transition between two energy allowed states separated by V potential barrier,which is of different size for the different elements of geological medium.Each transition is noted for its own τ. So,

$$\tau = \frac{\pi}{\omega_0} exp\left(\frac{V}{KT}\right), \qquad (2)$$

where ω_0 is the angular frequency of the SCZ dipole components oscillations around the equilibrium position under the T temperature.

The leap-type transition of diversely orientated SCZ-s from one energy allowed state to another at the first stage of external stress force impact is attendant with the organization of arranged SCZ groups orientated in a same manner. The latters remind of naturally induced domains known in ferromagnetism and ferroelectricity.

The process of leap-type SCZ transitions will thus take place simultaneously after a lapse of some Δt_1 time required for each of SCZ-s to overcome its $V_1, V_2,......V_N$ potential barrier. As a consequence, collective SCZ constructions (domains) are formed.

The zone of seismic event preparation featuring W_1^P level of accumulated potential energy which is other than W_0^P is formed at this stage.

The second stage resides in the formation of specific energy active points in the earthquake preparation zone. Due to the higher concentration and mobility of the SCZ-z as well as the direction of resultant acting forces vector the process of SCZ-s formation and their $W_1^P \rightarrow W_0^P$ energy state transition at these points will proceed faster than in a background medium.

The third stage is characterised by leap-type state-to-state transitions of SCZ domains up to the critical level at the energy active points.

At this stage which immediately preceds rupturing of rocks, a specific energy active point, where SCZ leader-domain is formed at the cost of rapidly proceeding process of critical potential energy accumulation, stands out.

Exposed to the increasing elastic strain forces there comes a point of SCZ-s mutual overlapping within the SCZ leader-domain. This causes an effect of SCZ mutual polarization and, correspondingly, non-linear growth of electric field strength inside the domain up to the level of SCZ substance break-down.

If the field strength in a medium volume unit involving N quantity of SCZ is noted by E, then

$$E = E_0 + E_{NIP} , \qquad (3)$$

where E_0 is the strength of homogeneous medium field; E_{NIP} is the field strength of naturally induced SCZ polarization under the action of increasing elastic strain forces

$$E_{NIP} = -4\pi \overline{P}_{NIP}, \qquad (4)$$

$\overline{P} = P_{NIP} / 3$ - the mean dipole moment of medium volume unit

$$P_{NIP} = N \mu E_0 , \qquad (5)$$

N - is the SCZ dipole elements number in the medium volume unit, μ- is the sensitivity of each medium element with respect to naturally induced polarization process.

Substituting expression (4) into (3), allowing for $\overline{P} = P_{NIP} / 3$ and substituting value E_0 (5) into (3) we have:

$$P_{NIP} = [\frac{N\mu}{1 - (4\pi / 3)N\mu}] , \qquad (6)$$

It follows herefrom that in accordance with (5) the sensitivity of the medium volume unit to the naturally induced polarization process is

$$M = N\mu , \qquad (7)$$

and can be expressed as

$$M \cong \frac{N\mu}{1 - (4\pi / 3)N\mu} , \qquad (8)$$

If the concentration of dipole components (N) and, consequently, the SCZ concentration is small regardless of the seismic event preparation stage, then $(4\pi / 3)N\mu \ll 1$ and this term can be discounted in the denominator of expression (6). In this case the medium is characterised by the linear relationship (5) between E and P_{NIP} that is typical of E_{NIP} weak quazi-linear field obeying to Ohm's law. This field is spread over the seismic event preparation zone including areas of energy active points at the first and second stages of earthquake preparation. The N concentration is initially high in the region of energy active point (which may be more than one). As the stress forces grow the N concentration in a volume unit increases up to the level when the term $(4\pi / 3)N\mu \rightarrow 1$, while $M \rightarrow \infty$.

The latter implies polarization catastrophe characterized by the disruption of E_{NIP} and E linear relationship (expression 6) and formation of strong non-liner electric field subject to Poul's law.

The non-linear growth of electric energy (W) in the energy active point emerges from expression (1) since $\varepsilon = \varepsilon*$ ranges up to values of order 10^5 and greater under the mutual SCZ polarization effect. This results in the 5 orders change of W^P relative to W^P of $\varepsilon = 1$.

The strong electric field of the SCZ mutual polarization non-linear effect arises first in the SCZ leader-domain of the specific energy active point. The first break-down of SCZ substance occurs just here creating strong displacement current (J_{dp}),

$$J_{dp} = \frac{dP(t)_{NIP}}{dt},\qquad (9)$$

which is able to serve as a trigger for the SCZ substance electric break-down process spreading all over the zone containing strongly polarized SCZ-s.

The electric break-down of some region in the seismic event preparation zone results in the medium elastic stress discharge as an earthquake.

The phenomenon during which rock rupture takes place because of the SCZ substance electric break-down may be called an electroseismic effect [1]. The process of electroseismic effect preparation spreads light over the nature of many phenomena registered practically in the seismic event preparation zone as well as over the regularity of their occurrence.

If we follow the general course of electroseismic effect preparation process on the basis of the above model then all the stages of seismic event preparation are realized in a special energy active point from which the rock rupture starts.

If we assume that transition from one energy level to another is quantized by one and the same constant value $\Delta W = const$ then during the earthquake preparation sequential increase of transition frequency is expected [Fig. 2]

$\mdwnarrow$ - seismic event

$\blacktriangle$ - anomalies of different parameters measured in field
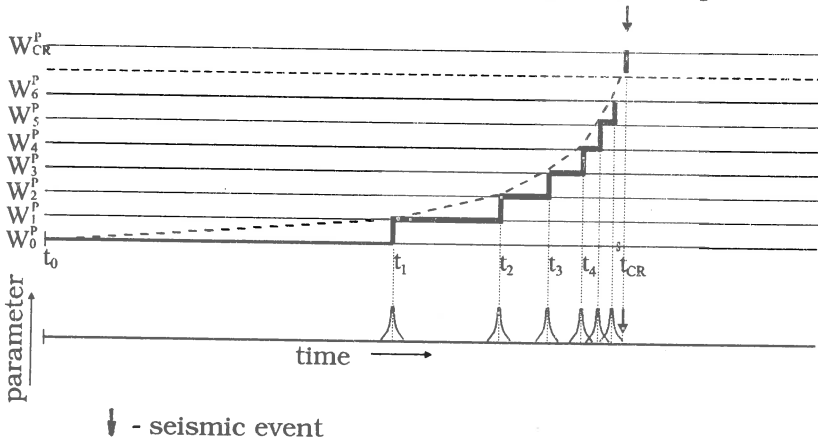
Fig. 2. SCZ quantized trabsitions from one W energy level to another during strong seismic event preparation

As this takes place the process is expressed most severely in the energy active point area.

We shall take into consideration that each transition taking place momentary is accompanied with sharp changes of medium physical parameters. That's why occurrence of different anomalous geophysical, geochemical, hydrogeodeformation and biological events registered on the observation surface should be expected just at the moment of transitions.

Along with this frequency of anomalies may change over total "quiescence" in registered characteristic changes just before the event since the transition velocity exceeds relaxation time of the induced process.

In order to analyse all peculiarities of earthquake preparation process we may compare the energy active point and the whole of earthquake preparation zone with harmonic oscillator, movable SCZ-s in which execute forced oscillations under the action of periodically acting external forces of a planetary scale (gravity influence of the Moon and the Sun, etc.). Powerful pulses of quantized (leap-type) transitions of the medium from one energy state to another superpose over these oscillations sporadically. Under all the acting forces beatings, resonance and other effects, peculiar to the systems executing forced oscillations will be observed in the area of energy active point.

Here we shall mention that any external force which is able to additionally influence the energy active point at the stage close to rock rupture, i.e. either to increase its electrical potential or reduce the electric break-down threshold, is able to serve as a trigger which will faster the seismic event. The electric potential may increase owing to the sharp additional inflow of charges to the energy active point, and the electric break-down threshold may reduce because of rapidly increasing pressure or temperature in the energy active point area.

The external forces capable to play the role of a trigger are: periodical, daily gravitation effects of the Sun and the Moon; daily variations of atmospheric electricity and pressure; nutation and precession of the Clobe; such sporadic forces as chromospheric flashes on the Sun; sharp change of the solar wind plasma flow bombardiring the Earth as a target (as a result the Earth in charged extremely unevenly because of its inhomogeneity); substorms in the ionosphere; circular currents in magnerosphere; thunderstorm discharges in atmosphere.

Before describing some phenomena which may accompany the W^P transitions in the seismic event preparation process, as its precursors, we should specially emphasize that the very evidence of an earthquake realization in the form of electroseismic effect is the vegetation along the seismogenic rupture on the Earth's surface burned at the moment of strong earthquake. This case is particularly fixed for the catastrophic December 7, 1988 Spitak earthquake (M7.1) in Armenia [Fig. 3].

During the strong earthquake in Erznka (M6.8, Turkey, March 13, 1992) an analogous effect of burned vegetation referred to the presence of methane in marshy area while this factor was not available in Armenia.
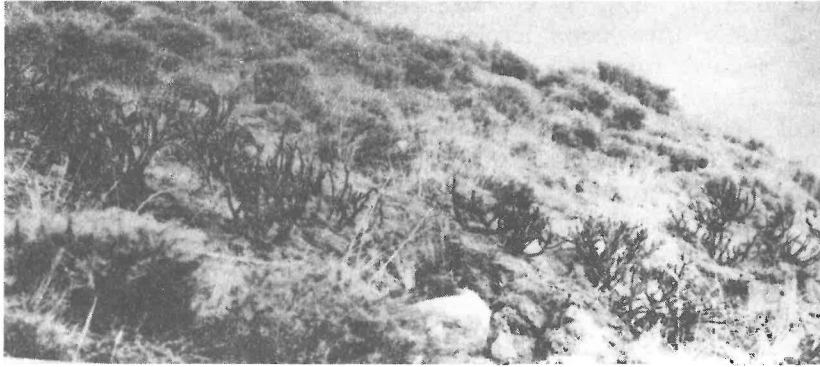
Fig. 3. The vegetation burned along the seismogenic rupture of Earth surface at the moment of Spitak earthquake (M7.1, 7 December, 1988) (photograph by A. Karakhanian)

Affected by the external sequentially increasing stress forces the effect of the medium mutual polarization in the energy active point area will lead to a strong local polarization of the medium as a result of which all its electromagnetic characteristics, namely-specific resistance, polarizability, dielectric permeability, electrochemical activity, etc. are changed.

By this is meant that anomalous changes of earth currents (tellurium currents), natural electric potentials, specific effective electric resistance and specific electric effective polarization etc. are expected in the energy active point area.

The strong electric field which occurs during the SCZ mutual polarization effect causes geomagnetic field anomalies, hysteresis of induced polarization process, mechanical panderomotor forces manifestation. The latters also exert pulsed pressure P upon rocks owing to the pulsed character of electric forces initiating them.

This, in its turn, initiates rock deformation which is called electrostriction in dielectric physics.

Substituting the possible values $E \geq 10^6$ $V/cm, \varepsilon^* \geq 10^5$ into the known expression

$$P = \frac{\varepsilon_0 \varepsilon^* E^2}{8 \cdot 10^3 \pi},\qquad (10)$$

(where E is the strong electric field intensity within the SCZ construction) it is easy to verify that the pressure upon rocks in the energy active point area may reach rather high values-from unities to hundreds of bars.

This means that in the energy active point sharp changes of rock deformation up to a critical level (10^4) [3], deformation variations, surface anomalous slopes and vertical and horizontal motions, changes in ground water level, radon gas concentration changes in ground waters and soil gases, anomalous electrokinetic effect, electromagnetic radiation, piezomagnetic effect, etc. may be expected.

The strong electric field of energy active point apart from the above phenomena causes anomalous migration of chemical elements, variation of their isotope composition and concentration.

The same effect is caused by strong currents of displacement according to (9).

We shall emphasise that the strong electric field may act in the energy active point during the whole of pre-seismic stage.

A series of well-known effects in the energy active point accompany the process of SCZ domain transition from one allowed state into another: quick change of electromagnetic field which in its turn creates vortex currents in a unit volume of polarized medium. The vortex currents spend the energy to heat the medium.

The leap-type growth and deformation of the naturally caused domain is accompanied with a small acoustic wave. Accounting for the collectivity of this effect it may be perceived as an underground noise or hum depending on its intensity.

The sharp change of energy active points potential means local change of the Earth surface potential. This inevitably results in local change of the atmosphere electric field stress which can cause a series of atmospheric phenomena, including formation of clouds, thunders, precipitation.

The changes of atmosphere parameters over the energy active region of the earthquake preparation zone area are able to disturb radiowave propagation.

The electric phenomena in energy active point, i.e. electromagnetic radiation, noise and other effects, can become the sources of biosphere excitation (i.e. to increase the activity of animals, fish, etc. that can often be observed before strong seismic events).

All the above phenomena refer to the class of strong earthquake precursors and can be used for their prediction.

Besides, the above model of the electroseiemic effect explains well foreshocks and aftershocks attendant with the process of preparation and realization of a strong seismic event.

CONCLUSION

1. The notion of strong seismic event preparation and realization process as of repeated quaintized (leap-type) tranzitions of a geological medium from one energy allowed state to another accompanied by different effects in geosphere, biosphere and atmosphere at the transition moment might be one of the most important elements of correct seismic hazard assessment in the zone of collision of the Arabian and Eurasian plates.

2. The process of medium transition from one energy allowed state to another attendant with potential energy accumulation reaches its critical level which corresponds to the rock rupturing not all over the earthquake preparation zone but only in its particular areas- the energy active points.

3. The rupturing of rock in an energy active point presents an electroseismic effect connected with substance break-down in the

zones of separated charges (SCZ) formed at the interfaces of multiphase, polydispersive, heterogeneous and multicomponent geological medium experiencing continuous action of increasing elastic strain forces in the zone of seismic event preparation.

4. When the earthquake is assumed as a phenomenon induced by the action of not only mechanical but at least electrical forces as well, in a medium consisting not only of solid but at least of a liquid phase, too, the wide range of phenomena and regularities known in the seismic events research experience could be explained.

5. The current seismic hazard assessment developed to the earthquake prediction level should account for the non-uniformity of earthquake preparation evolution in different points of the seismic event preparation zone.

6. The earthquake prediction should be treated as a stage-by-stage seismic hazard assessment consequently passing from long-term to a current one under strong seismic event preparation. This will allow for making decisions which are adequate to the hazard data and reduce the seismic risk.

REFERENCES:

Balassanian S.Y.,1990, - Dynamic geoelectrics, Novosibirsk, Nauka,   232.

Doukhin S.S., 1972, - Dielectric phenomena and coupled layer in dispersive systems and polyelectrics Kiev, Naukova dumka, 206.

Tsuboi C., 1956 - Earthquake energy. earthquake volume, aftershock area and strength of the Earth's crust. T.Phys. Earthq., 4, 63-6.

APPLICATION OF MEE (MAP OF EXPECTED EARTHQUAKES) PROGNOSIS ALGORITHM IN GREECE.

Zavyalov A.D.

Seismological Institute of United Schmidt Institute of Physics of the Earth Russian Academy of Sciences, B.Gruzinskaya, 10, 123810, Moscow, Russia

ABSTRACT
Results of application of MEE (Map of Expected Earthquakes) prognosis algorithm in Greece are discussing in this paper. Data about MEE algorithm effectiveness received for Greece is comparing with similar data for other seismoactive regions.

INTRODUCTION
In this report we have analyzed an application of Map of Expected Earthquakes algorithm in Greece (Sobolev et al., 1991). We persecuted two goals: 1). to study how is working MEE algorithm in Greece and define seismically dangerous zones for the nearest future; 2). accumulate the experience in application of MEE algorithm in different seismoactive regions.

DATA SET
The regional catalog of Greece from 1964 up to September 1993 was used for the study. The catalog includes about 39 thousands earthquakes with magnitude $M_l \geq 1.5$. In the beginning the catalog was studded for selection of low magnitude cutoff and evaluation for representative area for it. For this purpose the technique described in Sadovsky, Pisarenko, 1991 and software developed by V.B.Smirnov was applied. The low magnitude $M_l = 3.5$ was taken for further studies because this magnitude level is representative for the most part of area under study (Fig.1,2).

We choose earthquakes with $M_l \geq 5.5$ as target events for prediction. There were 44 earthquakes with $M_l \geq 5.5$ in the catalog (Table 1).

SELECTED PRECURSORS AND TECHNIQUE OF MEE CONSTRUCTING
Statistical characteristics of precursors were retrospectively estimated on the second step. We used six seismological precursors (Table 2):

1. B-value (ξ_b parameter);
2. Quiescence in number of weak earthquakes (ξ_{nq});
3. Activation in number of weak events (ξ_{na});
4. Quiescence in seismic energy release of weak events (ξ_{eq});
5. Activation in seismic energy release of weak events (ξ_{ea});
6. Density of seismogenic faults K_{sf}.

Each of them has a clear physical sense. A dimensionless parameter ξ has been chosen as a measure of statistical significance. The full definition of the ξ-parameter has been done in Sobolev et al., 1991.
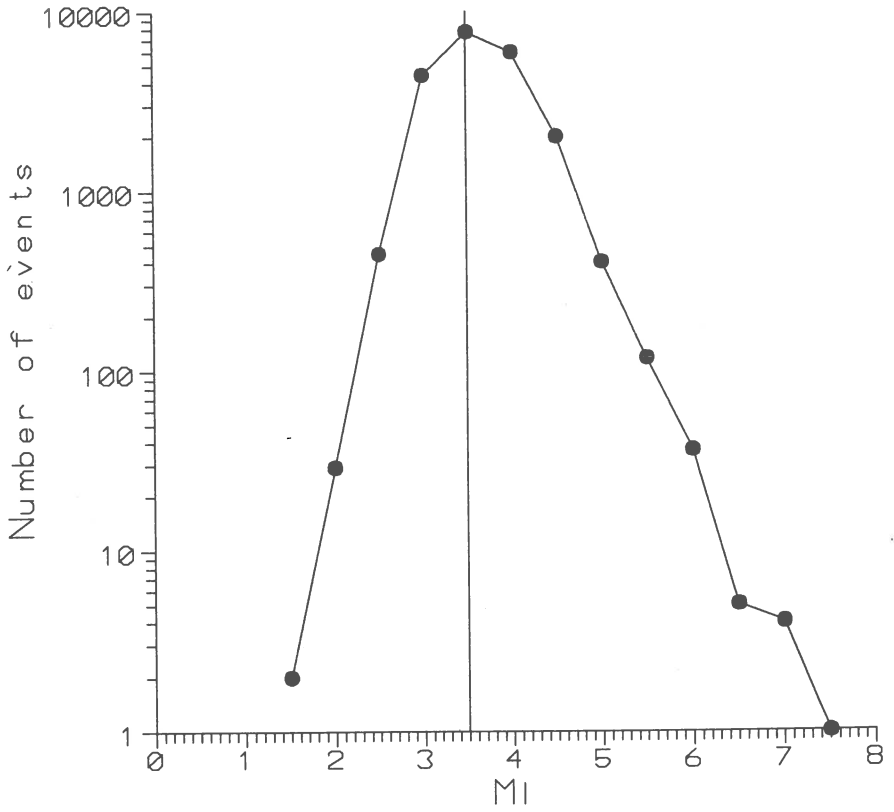
Fig.1. Magnitude—frequency relation graph for Greece
during the period 1964—Sept.,1993
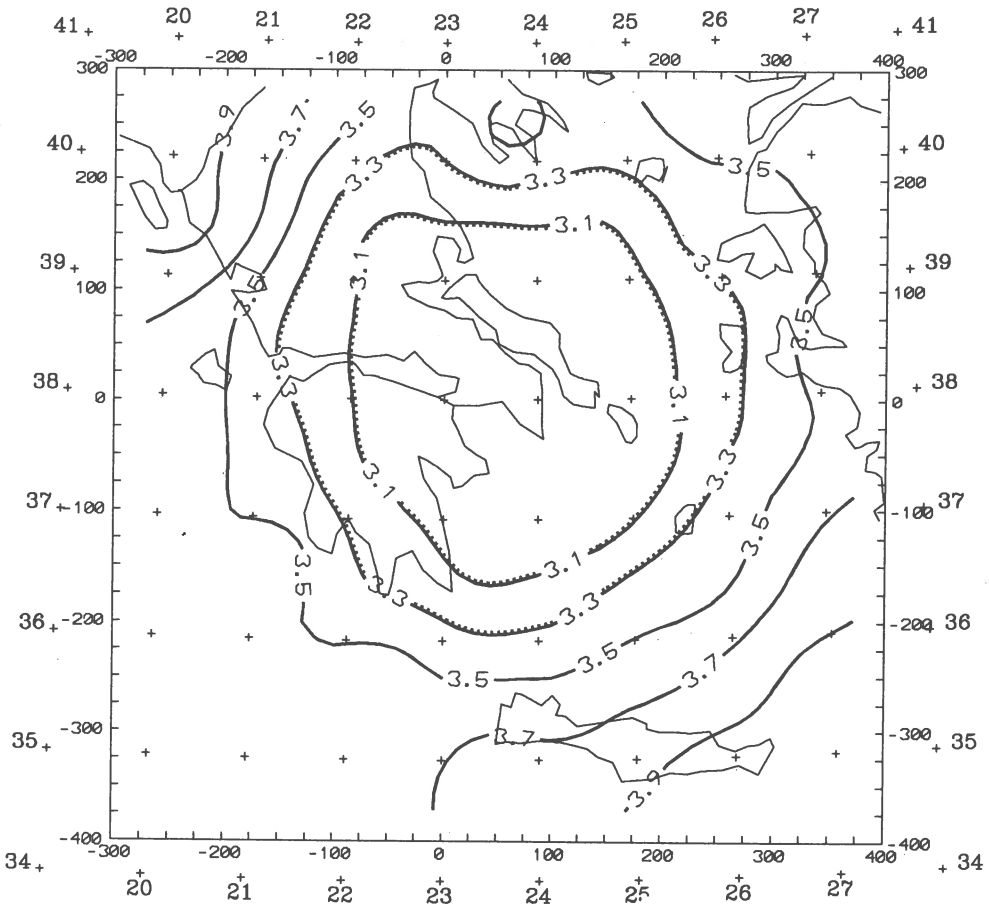
Fig.2. Map of representative magnitude Mmin for Greece during the period 1964-Sept.1993. The distances along X and Y are shown in kilomiters. Geographical coordinate net is notated by "+" (by V.B.Smirnov).

TABLE 1. LIST OF PREDICTED EARTHQUAKES IN GREECE

N	Date	φ^0	λ^0	H, km	M_1	B	NQ	NA	EQ	EA	KSF	70%	90%
1	1964.04.11	39.75	25.25	0	5.7								
2	1964.04.29	39.25	23.75	0	5.8								
3	1964.10.06	39.75	28.00	0	7.0								
4	1964.10.17	35.00	25.50	0	5.9								
5	1965.12.20	40.10	24.80	0	5.9								
6	1966.02.05	39.10	21.60	0	5.9								
	1966.05.04	39.30	21.30	0	5.5								
7	1966.09.01	37.50	22.30	0	6.0								
8	1966.10.29	38.80	21.00	0	6.0								
9	1967.11.30	41.40	20.50	0	6.6					★			
10	1968.02.19	39.50	24.80	0	7.1		★				★		
11	1968.03.28	37.80	20.90	0	5.6		★				★		
12	1968.10.31	36.70	27.10	0	5.6		★						
	1968.12.05	36.60	27.10	0	6.1								
13	1969.01.14	36.20	28.90	0	6.0								
14	1969.03.23	39.00	28.50	0	5.8								
	1969.03.25	39.00	28.50	0	5.7								
	1969.03.28	38.60	28.50	0	6.6								
15	1969.04.03	40.50	19.90	0	5.5					★			
16	1969.04.06	38.40	26.80	0	5.5	★	★			★			
17	1969.06.12	34.50	25.00	0	5.6		★			★			
18	1969.07.08	37.60	20.10	0	5.7		★				★		
19	1969.10.13	39.60	20.70	0	5.6			★	★	★	★		
20	1972.05.04	35.30	23.60	50	6.1	★	★			★			
21	1972.09.17	38.20	20.40	0	5.8		★				★		
22	1973.11.29	35.20	23.60	0	5.5		★			★			
23	1975.03.27	40.40	26.10	0	5.7	★							
24	1976.06.12	37.30	20.40	7	5.6	★	★			★		★	
25	1977.09.11	35.00	23.10	0	5.9	★	★			★		★	
26	1978.06.20	40.80	23.30	33	6.0								
27	1979.06.14	38.70	26.60	0	5.5	★				★	★		
28	1980.05.16	35.70	27.40	0	5.6					★		★	
29	1980.07.09	39.20	23.90	0	6.0	★					★		
30	1980.07.09	39.20	22.70	0	5.6								
31	1981.02.24	38.14	23.00	0	6.3		★				★	★	
	1981.02.25	38.20	23.00	0	5.9								
	1981.03.04	38.30	23.20	0	5.8						★		
	1981.03.05	38.30	23.20	0	5.6								
32	1981.06.28	37.90	20.10	0	5.5	★	★				★	★	★
33	1981.12.19	39.20	25.30	0	6.3	★			★	★		★	★
	1981.12.27	38.90	24.90	0	6.0			★					
	1982.01.18	39.74	24.54	1	6.9	★	★						
34	1982.06.22	36.88	20.93	40	5.8	★		★	★	★	★	★	★
35	1983.01.17	37.97	20.25	9	6.2		★	★			★	★	★
	1983.01.19	38.05	20.41	6	5.5						★		
	1983.03.23	38.19	20.40	10	5.7								
36	1983.07.05	40.27	27.13	35	5.9			★		★	★		
37	1983.08.06	40.08	24.81	22	6.6	★	★	★			★	★	
38	1984.06.21	35.36	23.31	46	5.9	★		★		★	★	★	★
39	1986.09.13	37.10	22.19	1	5.5	★							
40	1986.10.11	37.99	29.01	3	5.5								
41	1988.10.16	37.90	20.96	4	5.5	★	★	★		★	★	★	★
42	1990.06.16	39.13	20.38	38	5.5	★		★	★	★	★	★	★
43	1992.04.30	35.22	26.75	1	5.6	★		★	★	★	★		
44	1992.11.06	38.02	27.16	39	5.7	★				★	★		

1042

TABLE 2. STATISTICAL CHARACTERISTICS OF PRECURSORS IN GREECE

Background period: 19640101-19921231
Target earthquakes: $M_l \geqslant 5.5$

Para-meter	Alarm level	Probability of detection $P(K_i \mid D_1)$	false alarm $P(K_i \mid D_2)$	Average expectation time, years $T_{ex} \pm \delta_t$	square, km^2 $S_{ex} \pm \delta_s$	Prediction effectivity on time J_t	square J_s
ξ_b	+1.06	0.2986	0.1387	3.7±3.8	16053±4512	2.04	1.97
	+1.56	0.2847	0.1131	3.3±3.7	16111±3950	2.37	2.27
	+2.06	0.2569	0.0927	3.3±3.9	15000±4456	2.60	2.47**
	+2.56	0.2361	0.0762	3.4±3.9	14167±4537	2.84	2.70
	+3.06	0.2014	0.0657	3.3±3.9	14063±4171	2.82	2.68
ξ_{nq}	-1.06	0.5208	0.1572	6.6±6.0	16750±4695	2.61	2.50
	-1.56	0.3819	0.0912	7.0±6.6	15938±4824	3.00	2.84
	-2.06	0.2708	0.0562	6.3±5.9	15417±4794	3.44	3.20**
	-2.56	0.1667	0.0106	5.5±5.4	15455±5101	6.48	5.79
	-3.06	0.0833	0.0074	3.5±2.6	16500±4873	7.23	6.45
ξ_{na}	+1.06	0.1944	0.0501	7.1±5.3	15385±4660	2.73	2.71
	+1.56	0.1597	0.0359	7.0±5.6	17222±3411	3.05	2.94**
	+2.06	0.1111	0.0311	7.0±6.1	14688±3882	2.72	2.59
	+2.56	0.0972	0.0172	5.1±4.4	14643±4190	4.05	3.77
	+3.06	0.0833	0.0134	5.5±4.6	13214±4725	4.16	3.88
ξ_{eq}	-1.06	0.2222	0.1611	6.9±6.0	14265±3930	1.34	1.31
	-1.16	0.1597	0.1214	6.8±6.1	12188±3146	1.29	1.26
	-1.26	0.1181	0.0840	7.1±6.6	11071±2129	1.36	1.32**
	-1.36	0.0764	0.0704	8.4±6.6	11111±2205	1.09	1.07
ξ_{ea}	+1.06	0.3056	0.3229	8.3±5.5	17647±3900	0.96	0.96
	+1.56	0.2222	0.2006	8.8±5.1	15500±4247	1.09	1.09
	+2.06	0.1458	0.1396	8.7±4.8	15250±4480	1.04	1.04
	+2.56	0.1111	0.0714	9.1±4.6	14688±3882	1.40	1.41**
	+3.06	0.0417	0.0263	8.9±5.0	11000±2236	1.43	1.43
K_{sf}	3.8	0.1304	0.0060	3.4±3.2	4375±1127	15.45	15.45
	5.3	0.3152	0.0844	4.3±3.7	4212±1267	3.50	3.50**
	6.8	0.4348	0.1773	5.1±4.0	4554±1213	2.35	2.35

Notes: 1. Selected alarm levels marked "**".
       2. Average expectation time on the all precursors
          with selected alarm leves Tex=6.2±2.1 years.

Space-time distributions of these parameters were calculated in the sliding space-time window. At the same time we calculated the main statistical characteristics of all precursors for different alarm levels. Then few experts choose the optimal one for each precursor. These levels marked by two stars in the Table 2.

Average expectation time for strong earthquakes for the all precursors with selected alarm levels $T_{ex}=6.2\pm2.1$ years. Average expectation square is equal $S_{ex}=12942\pm4718km^2$ consequently. For future calculations we choose $T_{ex}=6.2+2.1=8.3\cong8$ years and $S_{ex}=13000km^2$.

The result of analysis of prediction for each precursor is shown in the right part of Table 1. One can see that the most part of strong events, essentially with M≥6.0 was predicted at least by one precursor.

Assuming seismic process as Poisonian the unconditional probability of target event occurrence during average expectation time on the average expectation square $P(D_1)$ was calculated. It was equal $P(D_1)=0.1642$.

In this study we used non-seismological precursor as well. It was the presence of faults in the seismoactive subcell under study. We have gotten data need from the Seismotectonic Map of Greece issued in 1989. It was found that in subcells where are tectonic faults the probability of target events occurrence was equal $P(K_t|D_1)=0.8857$ and false alarm $P(K_t|D_2)=0.7288$.

Using the Bayesian approach and selected precursors with choosen alarm levels maps of conditional probability distribution of strong earthquakes occurrence $P(D_1|K)$ (Map of Expected Earthquakes) were calculated. In general we calculated the series of MEE with the one year shift.

RESULTS

Fig.3, 4 and 5 are shown maps of expected earthquakes for the different time periods. There are shown strong events occurred during the next 8 years. One can see the changing in the configuration of 70% unconditional probability isolines.

On Fig.6 are shown the resulting strong earthquakes epicenters map after all MEE series analysis. As can be seen all events with $6.0\leq M_l<7.0$ were occurred inside zones with 70% level of unconditional probability. Only 4 (29%) events with $5.5\leq M_l<6.0$ were not occurred in that zone. Moreover 3 of them took place out of representative contour.

Table 3 shows the summary of study of MEE series for Greece in compare with other seismoactive regions. The prediction effectiveness means here the ratio of density of target events in alarm square to density of total number of target events on the observation area $J_{MEE}=(N_p/S_{al})/(N_\Sigma/S_{obs})$. The effectiveness value for Greece is equal $J_{MEE}=2.6$. Comparison of this value with similar values for other seismoactive regions shows the usefulness MEE prognosis algorithm application for medium-term earthquake prediction. MEE algorithm allows to distinguish dangerous zones for the nearest 5-10 years and to intensify observations of short-term precursors in alarm zones.

ACKNOWLEDGMENTS

GREECE. MAP OF EXPECTED EARTHQUAKES, 1981-1988.
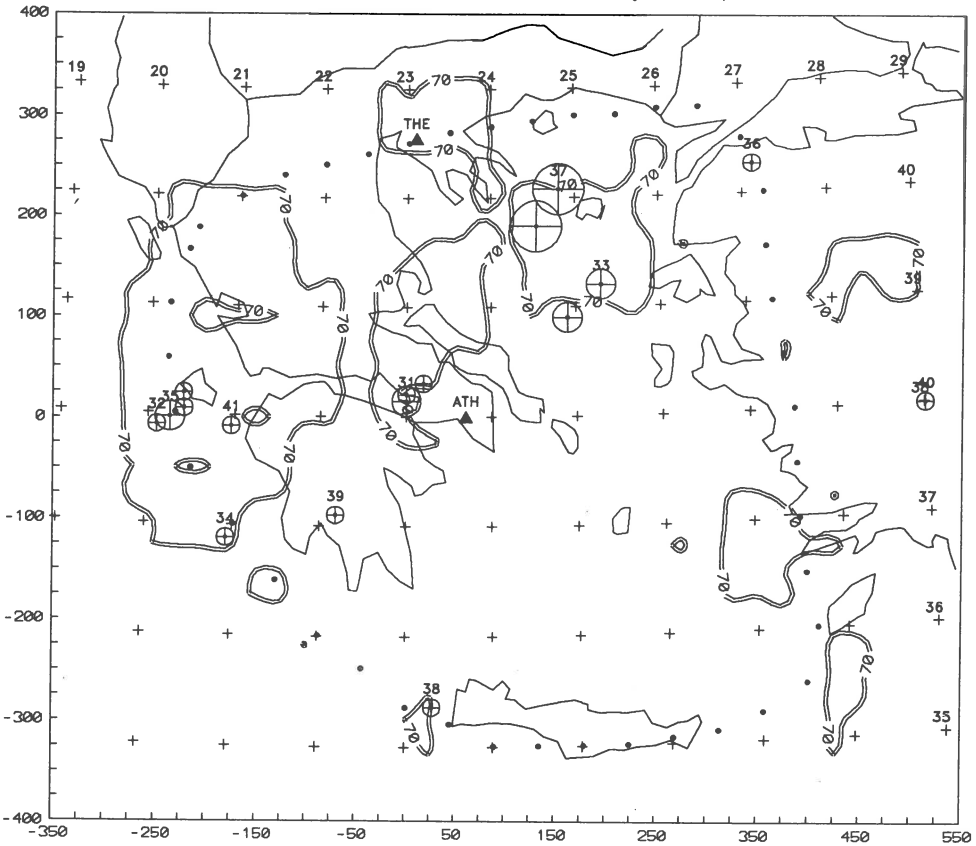
Fig.3. Map of expected earthquakes in Greece for the period
1981-1988 compiled from a combination of seismological
precursors based on the 1964-1980 earthquake catalog.
The 1981-1988 target earthquakes are plotted. Thick iso-
line outline the zones with conditional probability
$P(D_1|K) \geqslant 0.7$. Numbers above epicenter circles are the
earthquake number in the Table 1. Other notations are
the same as in Fig.2.
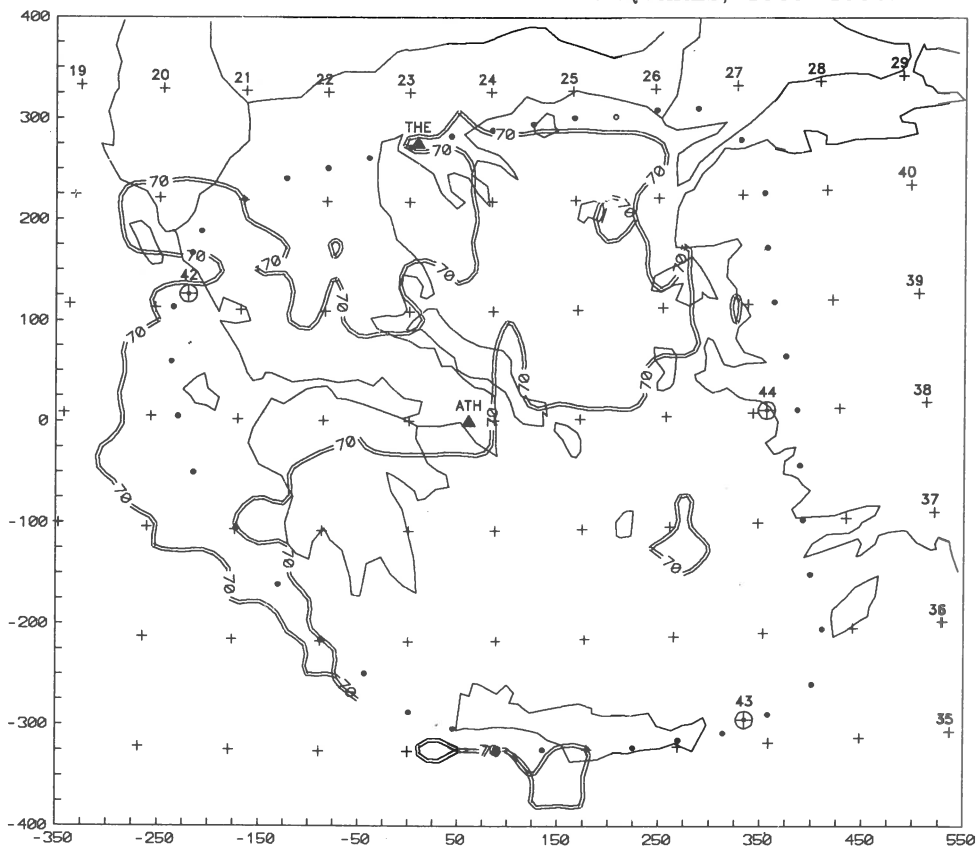
Fig.4. Map of expected earthquakes in Greece for the period
1989-1996 compiled from a combination of seismological
precursors based on the 1964-1988 earthquake catalog.
The 1989-Sept.1993 target earthquakes are plotted. Other
notations are the same as in Fig.2,3.

GREECE. MAP OF EXPECTED EARTHQUAKES, 1992–1999.
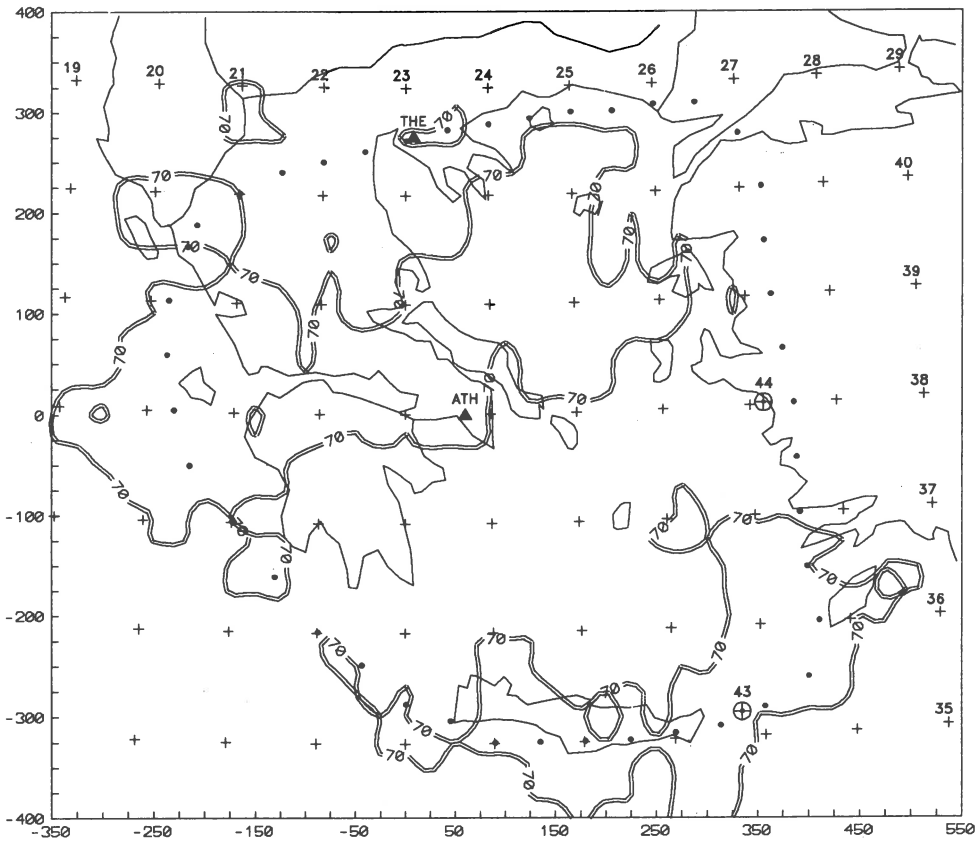
Fig.5. Map of expected earthquakes in Greece for the period
1992-1999 compiled from a combination of seismological
precursors based on the 1964-1991 earthquake catalog.
The 1992-Sept.1993 target earthquakes are plotted. Other
notations are the same as in Fig.2,3.

Fig.6. Map of earthquake epicenters for the period 1981–Sept.
1993. Black circles are epicenters of earthquakes which
were occurred outside zones with $P(D_1 |K) \geqslant 0.7$. Other no-
tations are the same as in Fig.2,3.

TABLE 3. RESULTS OF ANALYSIS OF MAPS OF EXPECTED EARTHQUAKES

Region	Cauca-sus	Kopet-Dag	S.Cali-fornia	Kirgiz-stan	Kam-chatka	N-E China	S-W China	Greece
Periods for MEE series	1976-1988	1973-1989	1954-1989	1979-1992	1977-1990	1981-1990	1982-1993	1981-1992
Zones with $P(D_1|K)$								
70%	23-38	15-30	8-18	20-31	24-25	12-22	32-39	21-34
90%	12-25	10-26	2-5	13-26	13-14	6-13	23-27	10-17
in % to the whole observation area								
Number of predicted earthquakes at zones with $P(D_1|K)$ levels								
70%	72	59	56	76	80	60	80	71
90%	40	54	15	44	57	20	64	50
in % to the total number of target earthquakes								
Total number of target earthquakes	25	39	27	25	26	5	25	14
Prediction effectivness for zones $P(D_1|K)$								
70%	2.4	2.6	4.3	3.0	3.3	3.9	2.3	2.6
90%	2.2	3.0	4.3	2.3	4.2	2.1	2.6	3.7

REFERENCES

Sadovsky M.A., Pisarenko V.F., 1991. Seismic process in block media. Nauka, Moscow, 96p. (in Russian)

Seismotectonic Map of Greece with seismological data, 1989. Institute of geology and mineral exploration. Athens.

Sobolev G.A., Chelidze T.L., Zavyalov A.D. et al., 1991. Maps of expected earthquakes based on a combination of parameters. Tectonophysics, v.193, 255-265.

AN EARTHQUAKE EARLY WARNING SYSTEM

Walid A. moh'd

Jordan Seismological Obs.

Introduction

Earthquakes have been the most frightening enemy of humanity, because it is not possible to forecast the time of occurrence precisely, and because they kill and destroy very quickly and effectively.

One of the earliest earthquakes on which there is detailed information was in Lisbon in ·1755 when almost 70,000 people lost their lives within six minutes. That earthquake was felt in the continent of Europe and the north of Africa.

Japan and China have a long record of disastrous earthquakes. In Japan there have been a few earthquakes on the magnitude of the one that happened in 1923 when almost 100,000 persons lost their lives.

Recently, there have been major shocks in china, Algeria, Yemen, Iran, Mexico, Armenia and Egypt.

Chinese and Japanese were the earliest to notice that reptiles became nervous shortly before the earthquake, and later on some other creatures such as pigeons, rabbits and rats acted strangely as though they were forecasting an earthquake.

In Dhamar, Yemen 1982, students at elementary school were frightened by some snakes coming out of the brick walls into the classroom, they rushed out to the yard and were calmed down and pass overed by the teachers who decided to send them home for the day. As soon as students re-entered the classroom to pick up their books, the building collapsed on them and they never knew what happened. Also, dogs and cows went crazy just before that shock. (A. Jaber and J. Shaalan, 1992)

Estimation:

This evidence and many other evidences indicate that there is some kind of activity shortly before an earthquake, which is not felt or noticed by human beings, simply because man does not hear or feel vibrations with the same range of frequencies other creatures do. Also, man is not as sensitive, and even if he has some premonition, he would probably relate that to other environmental activities.

The Seismograph does not record this hypothesized activity because it is tuned to the seismic frequency range (0.01-30)Hz and all other frequencies are filtered out.

Elastic rebound theory:

Reid theory which was based on the San Francisco 1906 earthquake says:

.Fracture that causes the shock, is a result of ELASTIC STRESS. .The energy released by the earthquake is an energy of ELASTIC STRESS just before the fracture. (Richter, C 1958).

Proposal:

I hypothesize therefore, that there must be some kind of activity shortly before the fracture as a result of pressure and stress, and it could well appear as vibrations. But those vibrations are not detected by seismographs or humans, and I propose that what is needed is a new instrument to be designed and tuned to those estimated activity frequencies.

But what range of frequencies will that be...?

Seismic exploration:

In seismic exploration for oil, vibrators are designed to generate vibrations from 8 to 70 Hz. Field engineers usually start the vibrator at 70 Hz and sweep down to 8 Hz or whatever seems to them to be best. One shock of the vibrator is of a few second duration. But as soon as the vibrator gets started, all reptiles in the area become agitated and come to the surface.

In the case of vibrations 70 Hz could be close to the low corner of that range. It is also possible there are Ultra Sonic frequencies because that is audible to dogs and cats {In Yugoslavia in 1960, cats left the area three days before the earthquake .(EDDEESY, A. Orally, 1993)}.

So, if we are able to discover the frequency range of that hypothesized activity, we may be able to locate and forecast earthquakes more precisely.

A quick research, in the anatomy of the reptilian ear, however, shows evidence that snakes are certainly sensitive to ground borne vibrations as well as to air borne sounds and are quite sensitive to a limited range of frequencies (100Hz - 500Hz). It is not known which part -if any - causes them to deviate from of there normal behaviour.(Bellairs & Carington 1969).

A sensitivity curve for the small Burrowing snake is shown in Fig.1. Gratest sensitivity is at 100Hz, decreasing for higher tones and for the two lower tones used in the test.(Bellairs & Attridge, 1975)

In the case of Ultra Sonic frequencies, cats and dogs can hear up to 40k HZ While a healthy man can hear up to 20k Hz only. (Weaver, 1902).

Cracks:

Craks in rock range in size from falts measuring hundreds of thousands of feet in length to intra-granular cracks with lengths of a thousandth of a foot. In this sense, cracks must be defined as confined regions within a body of rock across which the displace-ments usually shear but some times normal, can be discontinuous under certain stress conditions.

In all discussions of brittle fracture the nature and description of the fractured surface is of greatest importance. The types which occur may be illustrated from the behavior of solenhofen limestone at various confining pressures as described below. in unconfined

Figure 1

　a　　　　　　b·　　　　　　c　　　　　　d　　　　　　e
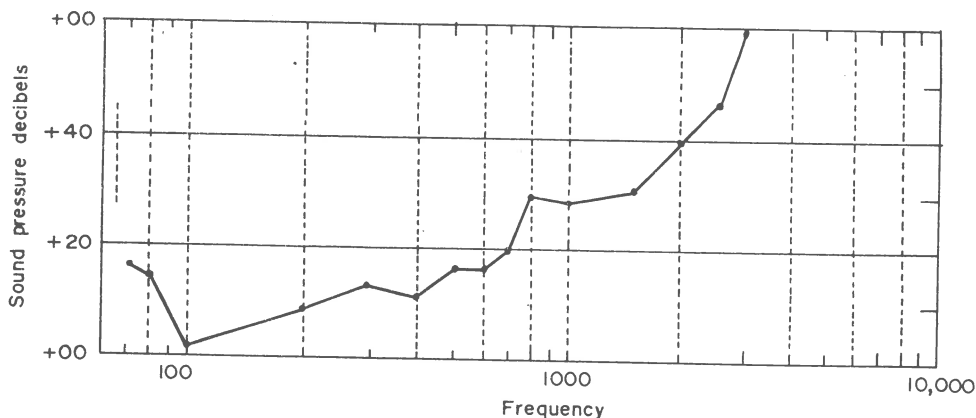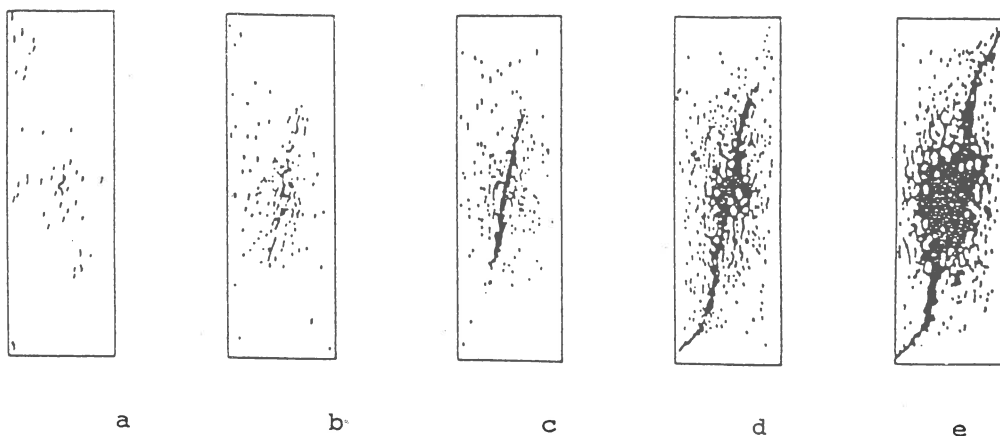
Figure 2

compression, Fig. (2.a), irregular longitudinal splitting is observed. With quite a moderate amount of confining pressure, a single plane of fracture appears, Fig. (2.b) and it is described as a Shear Fracture. Griggs and Handen (1960), who introduced a classification of fractures, call it a FALT because of its correspondence with geological falting. If the confining pressure is increased so that the material becomes fully ductile, a network of shear fractures appears. Fig. (2.c).

To approach the practical situation more closely, Hallbaure (1973) used a suite of specimens made from one piece of quartzite and the compression of different specimens was stopped at predetermined points along the complete stress-strain curve. Careful macroscopic and microscopic studies of longitudinal sections through the axes of the

specimens enabled the development of microcracks and the growth of fractures to be studied in relation to the complete stress-strain curve.

Some of the results are illustrated in Fig. (2). The first structural damage appears as elongated microcracks distributed at random but concentratedining of microcracks and initially there is a little or no movement across this fracture plane Fig. (2.d, 2.e). Finally, the fracture plane extends towards the ends of the specimen where its direction changes so as to allow relative movement to take place across its surface between the two halfs of the specimen, and a rapid drop in the resistance of the specimen to the applied load occurs.

The applicability of this concept of failure, based on grain-sized cracks, to a heterogeneous aggregate such as rock is questionable however, the body of theory which has grown up around this concept is very useful for studying the effect of these cracks on the elastic properties of rock, and there seems to be no reason why it should not be applied to the behavior of much larger cracks using a scale on which rock can be regarded as homogeneous, thereby providing an approach to the growth of fracture in rock. (Jaeger & Cook, 1979)

Summary:

If we wish to forecast earthquakes precisely, thereby reducing their disastrous consequences, we must start looking for so-called- Ultra Seismic precursory frequencies, preceding an earthquake. Therefore, I'm convenced that the present day technological realm must design and test an earthquake early - warning device that simulates the sensitivity of those creatures.

References

Bellairs, A & Attridge, J. 1975, Reptiles.
Bellairs, A & Carington, R. 1969, The world of reptiles.
Jaeger, J. C. & Cook, N. G. W. 1979, Fundamentals of rock mechanics.
Richter, Charles F. 1958, Elementary Seismology.
Wever, E.Glen, 1902, The Reptile ear,
Wever, E.Glen, 1902, The amphibian ear.

Long Term Earthquake Prediction in Mid-Ocean Ridges Based on the Time and the Magnitude Predictable Model

THEODOROS M. TSAPANOS
Aristotle University of Thessaloniki, Geophysical Laboratory, Thessaloniki 54006, Macedonia, Greece.

ABSTRACT

Instrumental information, since 1898, on strong mainshocks in 32 seismogenic sources of the Mid-Oceanic Ridges have been used to show that the interevent time, T_t (in years), between two strong shallow earthquakes and the magnitude, M_f, of the following mainshock are given by the relations:

$$\log T_t = 0.21 M_{min} + 0.30 M_p - 0.42 \log M_o + 8.38$$

$$M_f = 0.78 M_{min} - 0.34 M_p + 0.54 \log M_o - 9.92$$

where T_t is the interevent time, measured in years, M_{min} the surface wave magnitude of the smallest mainshock considered, M_p the magnitude of the preceding maishock, M_f the magnitude of the following mainshock, M_o the moment rate in each source per year. A multiple correlation coefficient equal to 0.73 and a standard deviation equal to 0.18 for the first of the above relations were computed. The corresponding quantities for the second of these relations are 0.81 and 0.29. Time-dependent conditional probabilities for the occurrence of the next large ($M_s \geq 6.5$) and very large ($M_s \geq 7.0$) shallow mainshocks in each one of the 32 seismogenic sources during the next 10 years (1993-2002) are estimated, by the use of the first of these relations. The magnitudes of the expected mainshocks are also determined, by the second of the above relations. Currently, 11 seismogenic sources exhibit the relatively higher ($P_{10} \geq 0.60$) probabilities to experience the occurrence of a very large ($M_s \geq 7.0$) mainshock during the next decade.

METHOD APLLIED

Papazachos and Papaioannou (1993) used interevent times of strong mainshocks in seismogenic sources of the Aegean area to propose two relations of the form:

$$\log T_t = b\, M_{min} + c\, M_p + d\, \log M_o + t \qquad (1)$$

$$M_f = B\, M_{min} + C\, M_p + D\, \log M_o + m \qquad (2)$$

where T_t is the interevent time, measured in years, M_{min} the surface wave magnitude of the smallest mainshock considered, M_p the magnitude of the preceding mainshock, M_f the magnitude of the following mainshock, M_o the moment rate in each source per year. The model expressed by the relations (1) and (2) has the advantage that all parameters (b, c, d, t, B, C, D, m) of these relations are calculated by all available data for all sources.

The moment rate, M_o, that is, the moment released per year in

each seismogenic source is a measure of the seismicity level and varies from source to source, but it can be reliably calculated if enough data are available for the source. These data concern not only the magnitudes of the few mainshocks but all the complete data of strong and small shocks available for each sources. The values of M_o have been determined by applying a method suggested by Molnar (1979). This method makes use of the maximum magnitude, M_{max}, and of the parameters a and b of the relation of Gutenberg and Richter (1944):

$$logN = a - bM \qquad (3)$$

normalized for one year, as well as, of the parameters r, k of the moment-magnitude relation:

$$logM_o = rM + k \qquad (4)$$

which are 1.5 and 16.1, respectively, according to Kanamori (1977).

By the use of the observational data (M_{min}, M_p, T) for all (32) seismogenic sources and the moment rates M_o, the parameters, b, c, d, and t of the relation (1) were determined by the application of a common multi-linear analysis. However, one can use the well-known technique (Draper and Smith, 1966; Weisberg, 1980) which has been widely used, especially in strong-motion attenuation studies (McGuire, 1978; Joyner and Boore, 1981; Dahle et al., 1990). This technique has been applied in the present case by the use of a computer program written by C. Papazachos.

THE SEISMOGENIC SOURCES AND DATA USED

The mid-oceanic ridges as well as the continental rifts (e.g. the east African rifts) were divided, for the purpose of the present study, in 32 seismogenic sources. The criteria for this division were based on the seismicity level, the spatial distribution of the epicenters of the earthquakes, the seismotectonic structure and maximum earthquake observed. The fit of the data of each source to the tiime-predictable model has been used as an additional criterion for this division. Figure (1) depicts the 32 seismogenic sources of the Atlantic, Indian and Pacific oceans. Earthquakes with magnitudes $M_s \geq 5.5$ are considered for the purpose of the present study, which occurred in the three mid-ocean ridges and in the east African rift system from 1898 to 1993. Figure (2) through (4) depict the subregions of the three seismic zones in which the mid-oceanic ridges system was divided. In each figure the seismogenic sources in which each zone was divided are shown along with epicenters of the mainshocks (black circles) and fore- or aftershocks (open circles) in a broad sense.

The data sources used for this work are the catalogues of Pacheco and Sykes (1992), Lomnitz (1974), Kanamori and Abe (1979), Abe (1981), Abe and Noguchi (1983) and Tsapanos et al. (1990). For the most recent events the bulletins of I.S.C. and N.E.I.C. were used.

Foreshocks and aftershocks are used in a broad sense, that is, earthquakes, within the complete sample of data, which may occur up to several years before or after the main shocks,

respectively. We used the terms "aftershock" and "foreshock" in their broad sense because in the present paper we seek for a model which can predict the mainshocks in each seismogenic source, that is, the large earthquakes which occurred at the beginning and the end of each seismic cycle and not smaller earthquakes that occur during the preseismic and post seismic activation. This concept of foreshocks is in accord with the suggestion of Mogi (1985), that seismic activity over a wide area would increase through a rise in crustal stress and that these shocks are foreshocks in the broad sense. The foreshock activity period is taken equal to 3 years for all the mainshocks, in accordance with Karakaisis et al. (1991) who found that the last phase of the seismic cycle is characterised by an accelerated activity period with duration of 2.7 years, which culminates before the second mainshock and does not depend on the magnitudes of the first or the second mainshock. In the present study, we considered as aftershocks the earthquakes that follow a mainshock in a time interval of t-years, which depends on the magnitude of the mainshock according to the formula (Papazachos 1993, personal communication) :

$$logt = 0.06 + 0.13M \qquad (5)$$

Table (1) lists the values of the parameters b, a, M_{max} and the $logM_0$ for each seismologenic source. The number and the code name of each source, corresponding to the seismogenic sources of Figure (1), are written in the first two columns of this Table. One common value for the parameter b (1.25) was computed for all the seismogenic sources. The M_{max} was estimated by considering all the available data (historical and instrumental) for each source.

RELATIONS FOR THE REPEAT TIME AND THE MAGNITUDE
We have now the mainshocks and the year of their occurrence, for each seismogenic source. We need the interevent times between the mainshocks having magnitudes larger or equal to a certain value, taking into consideration the completeness of the data for the certain time period. The estimation of these interevent times, needed in the application of the present methodology, is described in detail by Papazachos (1992). According to this methodology better results are obtained if the less reliable observations (about 10% of the total observations) are omitted (Papazachos and Papaioannou 1993).

For the mid-oceanic ridges we applied the same technique and omitted the 9.5% of the total (327) avalaible observations. Finally, the remained data (296 observations) were used to determine the relation:

$$logT_t = 0.21M_{min} + 0.30M_p - 0.42logM_0 + 8.38 \qquad (6)$$

with a correlation coefficient and a standard deviation equal to 0.73 and 0.18, respectively. The positive correlation between the repeat time and the magnitude of the preceding mainshock indicates that the time predictable model holds. In Figure (5) the frequency distribution of $log(T/T_t)$ is shown (where T is the observed and T_t the calculated repeat times), which is fitted by a normal distribution with $\mu=0$ and $\sigma=0.18$.

Following a similar procedure, the values of the parameters of the relation (2) were determined and the following empirical formula was obtained: ·

$$M_f = 0.78M_{min} - 0.34M_p + 0.54logM_o - 9.92 \qquad (7)$$

with a correlation coefficient equal to 0.81 and a standard deviation equal to 0.29. The negative value of C (-0.34) means that large mainshocks are followed by small ones an vice versa. In Figure (6) the frequency distribution of the difference, M_f-M_f, between the observed magnitude, M_f, and the calculated magnitude, M_f, by the relation (7) is illustrated. This is fitted by a normal distribution with $\mu=0$ and a standard deviation equal to $\sigma=0.29$.

LONG TERM PREDICTION OF THE NEXT SHALLOW MAINSHOCKS
    The validity of the model tested in this study, provides a useful tool to calculate the time of occurrence of the next large shallow mainshock in each one seismogenic source, by equation (6). It is, however, preferable to estimate the probability of occurrence of the next mainshock greater than a certain magnitude and in a given time span because differences exist between the observed repeat times, T, and the calculated ones T_t (see Figure 5).
    Methods for probabilistic approach of the forecasting of future earthquakes, by using either Gaussian (Lindh, 1983; Sykes and Nishenko, 1984) or Weibull distribution (Rikitake, 1976; Nishenko, 1985), have been applied. Nishenko and Buland (1987) investigated the utility of the simple function T/T_{ave}, to help define the overall distribution properties of earthquake recurrence, where T_{ave} is the average recurrence interval observed for a specific fault or plate boundary segment and T is an individual recurrence interval. They suggested that the lognormal distribution provides better fit to the T/T_{ave} data than the previously used Gaussian or Weibull distributions. Papazachos (1988, 1991, 1993) and Papazachos and Papaioannou (1993) have also found the lognormal distribution of T/T_t as more appropriate for data concerning the occurrence of earthquakes in the area of Greece. This distribution was also assumed in the present study to calculate the probability for the occurrence of a mainshock during the next decade.
    Given the date and the magnitude of the last event in a seismogenic source, the expected magnitude and the probability of occurrence of the next shallow mainshocks with $M_s \geq 6.5$ and $M_s \geq 7.0$, during the next ten years were computed. Table (2) gives information on the expected large ($M_s \geq 6.5$) and very large ($M_s \geq 7.0$) shallow mainshocks based on the time and magnitude predictable model expressed by the relations (6) and (7). The first column gives the code number and the name of the seismogenic source. The other four columns give the magnitudes, M_f, of the expected earthquakes, as these magnitudes were calculated by the relation (7), and the corresponding highest probabilities, P, for the occurrence of large ($M_{min} \geq 6.5$) and very large ($M_s \geq 7.0$) shocks, in the next decade (1993-2002). The values of P_{10} varry considerably among the seismogenic sources, suggesting that the seismic history in each one of them plays an

importand role in this estimation.

At present, a number of 11 seismogenic sources out of 32, exhibit high ($P_{10} \geq 0.60$) probabilities for the occurrence of very large ($M_s \geq 7.0$) shallow mainshocks, while a number of 5 seismogenic sources exhibit very high ($P_{10} \geq 0.70$) probabilities for the occurrence of great mainshocks in the mid-ocean seismic zones. Black and white rectangles in Figure (1) show seismogenic sources for which the probability is very high ($P_{10} \geq 0.70$) and high ($P_{10} \geq 0.60$), respectively, for the occurrence of such mainshocks during the decade 1993-2002.

As it is obvious from Table (4), we estimated the probabilities for 30 seismogenic sources, because two of them (ATLADIS and BALLENY) have no earthquakes with magnitude greater or equal to 6.5. An effort is made to compute the probabilities for these seismogenic sources for magnitudes $M_s \geq 6.0$ and $M_s \geq 5.5$ respectively (since BALLENY have no earthquakes with magnitude greater or equal to 6.0). For ATLADIS the expected magnitude M_f, is equal to 6.1 with probability $P_{10}=0.61$, while for BALLENY the corresponding quantities are $M_f=5.7$ and $P_{10}=0.75$.

REFERENCES

Abe, K., Magnitudes of large shallow earthquakes from 1904 to 1980, Phys. Earth Planet. Inter., 27, 72-92, 1981.

Abe, K. and S. Noguchi, Revision of magnitudes of large shallow earthquakes 1897-1912, Phys. Earth Planet Inter., 33, 1-11, 1983.

Dahle, A., H. Bungum and L. Kramme, Attenuation models inferred from intraplate earthquake recordings, Earthq. Eng. Struct. Dynam., 19, 1125-1141, 1990.

Draper, N.R. and H. Smith, Applied regression analysis, John Wiley, New York, 407pp., 1966.

Gutenberg, B. and C. F. Richter, Frequency of earthquakes in California, Bull. Seismol. Soc. Am., 34, 185-188, 1944.

Joyner, W.B. and D. M. Boore, Peak horizontal acceleration and velocity from strong-motion records including records from the 1979 Imperial valley, California earthquake, Bull. Seismol. Soc. Am., 71, 2011-2038, 1981.

Kanamori, H., The energy released in great earthquakes, J. Geophys. Res., 82, 2981-2987, 1977.

Kanamori, A. and K. Abe, Reevaluation of the Turn-of-the-Century seismicity peak, J. Geophys. Res., 84, 6131-6139, 1979.

Karakaisis, G.F., M. C. Kourouzidis and B. C. Papazachos, Behaviour of seismic activity during a single seismic cycle, Int. conf. earthq. prediction, Strasbourg 15-18 Oct. 1991, 1, 47-54, 1991.

TABLE 1. Information on the basic parameters used for every source. The first column gives the source number and the code name of every source. The constants a and b for Gutenberg and Richter (1944) relation are given in the next two columns. In the last two columns, the maximum magnitude and the logarithm of the moment rate are given.

Seismogenic Source	a	b	M_{max}	$\log M_o$
Source 1 - YANMAYEN	6.29	1.25	6.3	24.743
Source 2 - ICELAND	6.53	1.25	7.0	25.158
Source 3 - REYKJANES	6.34	1.25	6.5	24.843
Source 4 - AZORES	7.27	1.25	8.0	26.148
Source 5 - ATLANT1	6.87	1.25	7.0	25.498
Source 6 - ATLANT2	7.17	1.25	7.1	25.823
Source 7 - ATLANT3	7.19	1.25	7.1	25.843
Source 8 - ATLADIS	6.24	1.25	6.2	24.668
Source 9 - ATLANT4	6.78	1.25	6.5	25.283
Source 10 - SANDWICH	7.67	1.25	7.5	26.423
Source 11 - SHETLAND	7.02	1.25	7.1	25.673
Source 12 - ATLANT5	6.81	1.25	6.8	25.388
Source 13 - INDIAN3	6.76	1.25	7.7	25.563
Source 14 - INDIAN2	6.51	1.25	6.5	25.013
Source 15 - INDIAN1	7.15	1.25	7.4	25.878
Source 16 - CARLSBERG	7.06	1.25	7.6	25.838
Source 17 - OWEN	6.82	1.25	7.1	25.473
Source 18 - AFRICA	7.13	1.25	7.5	25.883
Source 19 - REDSEA	6.80	1.25	6.6	25.328
Source 20 - AMSTERDAM	6.95	1.25	6.7	25.503
Source 21 - NINETY	6.98	1.25	7.5	25.733
Source 22 - BROKEN	6.62	1.25	6.8	25.198
Source 23 - KANGAROO	6.80	1.25	6.7	25.353
Source 24 - TASMAN	7.11	1.25	7.0	25.738
Source 25 - MAC	6.95	1.25	7.5	25.703
Source 26 - BALLENY	6.26	1.25	5.8	24.588
Source 27 - PACIF	7.03	1.25	6.8	25.608
Source 28 - NAZCA4	6.42	1.25	6.6	24.948
Source 29 - NAZCA3	8.80	1.25	6.6	25.328
Source 30 - NAZCA2	7.20	1.25	7.0	25.828
Source 31 - NAZCA1	6.88	1.25	6.3	25.333
Source 32 - COCOS	6.78	1.25	7.0	25.408

TABLE 2. Information on the expected magnitudes. M_t and the corresponding probabilities, P_{tu} for the occurrence of large ($M_{min} \geq 6.5$) and very large ($M_{min} \geq 7.0$) shallow mainshocks during the period 1993-2002. in the mid-ocean ridges.

Seismogenic Source	$M_{min} \geq 6.5$		$M_{min} \geq 7.0$	
	M_t	P_{tu}	M_t	P_{10}
Source 1 - YANMAYEN	6.8	0.53	---	---
Source 2 - ICELAND	6.8	0.62	7.2	0.49
Source 3 - REYKJANES	6.6	0.60	---	---
Source 4 - AZORES	7.0	0.98	7.4	0.56
Source 5 - ATLANT1	6.7	0.40	7.2	0.72
Source 6 - ATLANT2	6.8	0.74	7.2	0.55
Source 7 - ATLANT3	6.8	0.31	7.3	0.14
Source 8 - ATLADIS	---	---	---	---
Source 9 - ATLANT4	6.7	0.55	---	---
Source 10 - SANDWICH	7.0	0.75	7.6	0.55
Source 11 - SHETLAND	7.1	0.76	7.5	0.58
Source 12 - ATLANT5	6.9	0.75	7.4	0.62
Source 13 - INDIAN3	6.8	0.65	7.3	0.51
Source 14 - INDIAN2	6.8	0.51	7.2	0.52
Source 15 - INDIAN1	7.3	0.85	7.7	0.72
Source 16 - CARLSBERG	6.6	0.51	7.1	0.30
Source 17 - OWEN	7.1	0.84	7.5	0.63
Source 18 - AFRICA	6.7	0.31	7.2	0.14
Source 19 - REDSEA	6.5	0.22	7.0	0.09
Source 20 - AMSTERDAM	6.7	0.69	7.2	0.72
Source 21 - NINETY	7.0	0.92	7.5	0.77
Source 22 - BROKEN	6.7	0.47	7.2	0.62
Source 23 - KANGAROO	6.7	0.28	---	---
Source 24 - TASMAN	6.9	0.60	7.4	0.74
Source 25 - MAC	6.6	0.34	7.1	0.16
Source 26 - BALLENY	---	---	---	---
Source 27 - PACIF	7.0	0.74	7.4	0.55
Source 28 - NAZCA4	6.7	0.64	---	---
Source 29 - NAZCA3	6.9	0.71	7.3	0.65
Source 30 - NAZCA2	6.9	0.79	7.3	0.60
Source 31 - NAZCA1	6.7	0.69	7.2	0.59
Source 32 - COCOS	6.7	0.82	7.2	0.66
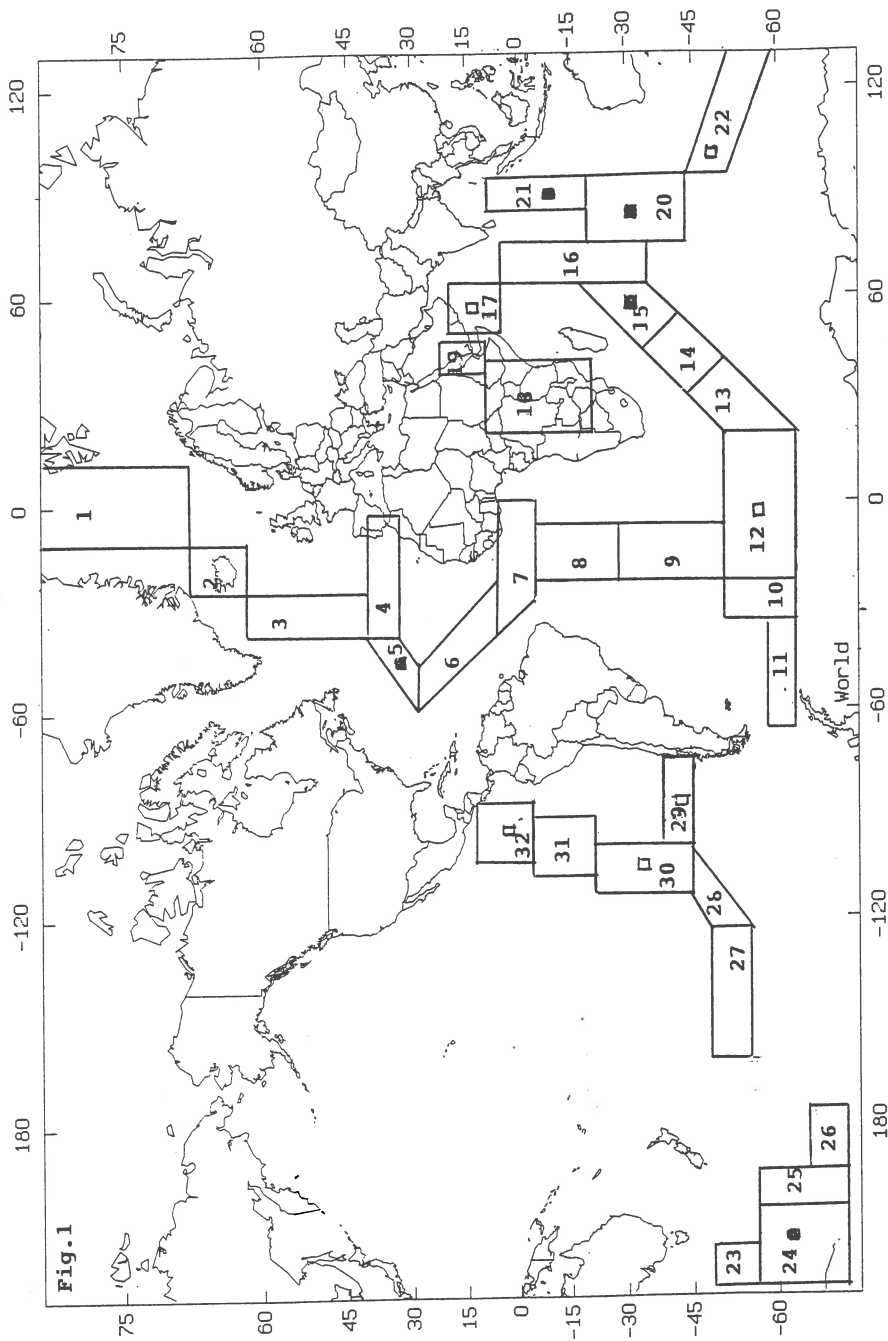
Fig. 1. The three examined seismic zones (Atlantic, Indian and Pacific oceans) with their seismogenic sources. Black and open rectangles denote the sites of very high (P≥0.70 and high (P≥0.60) probabilities for the occurrence of very large (M≥7.0) shallow mainshocks during the next decade.
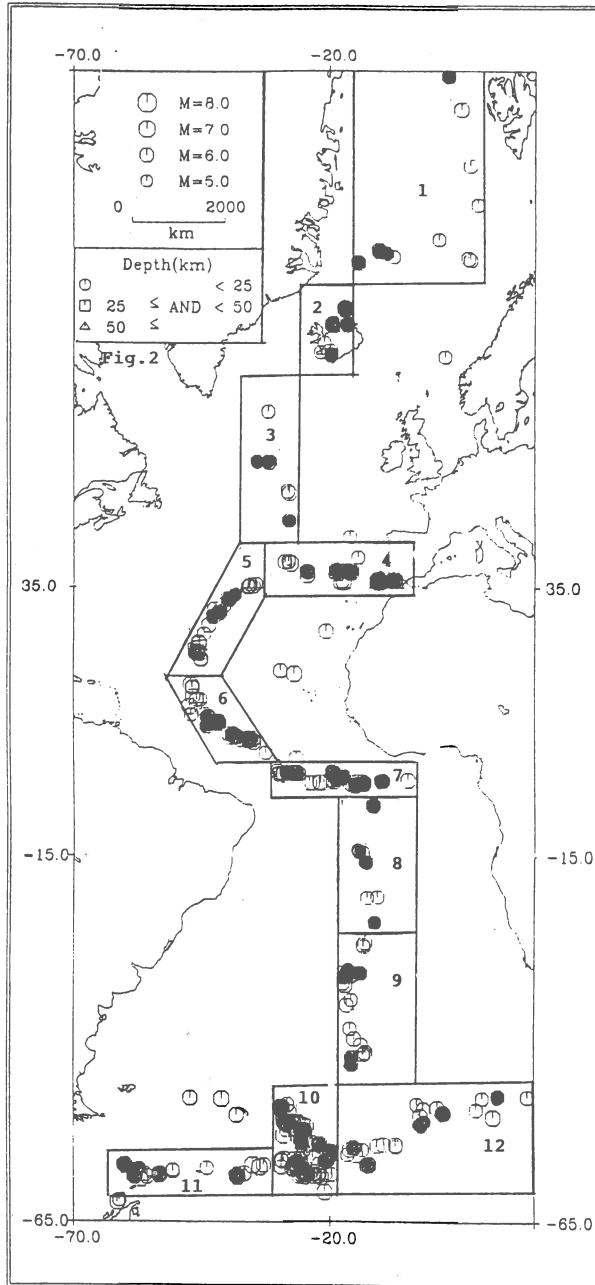
Fig. 2. Spatial distribution of the epicenters of shallow mainshocks (black circles) and foreshocks or aftershocks (open circles) occurred in the Mid_Atlantic ridge during the time period 1898-1993.
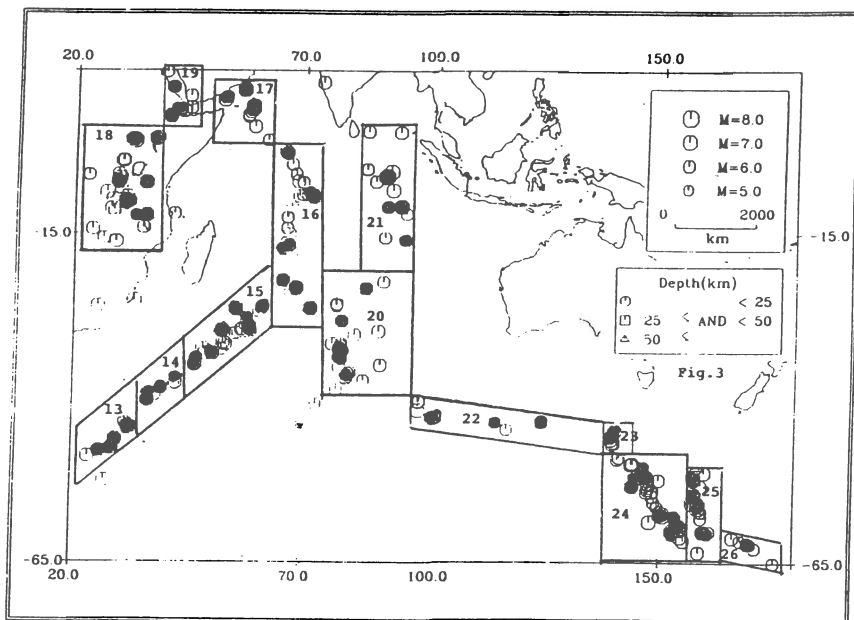
Fig. 3. Spatial distribution of the epicenters of shallow mainshocks (black circles) and foreshocks or aftershocks (open circles) occurred in the Indian ocean, as well as in the south Pacific during the time period 1898-1993.
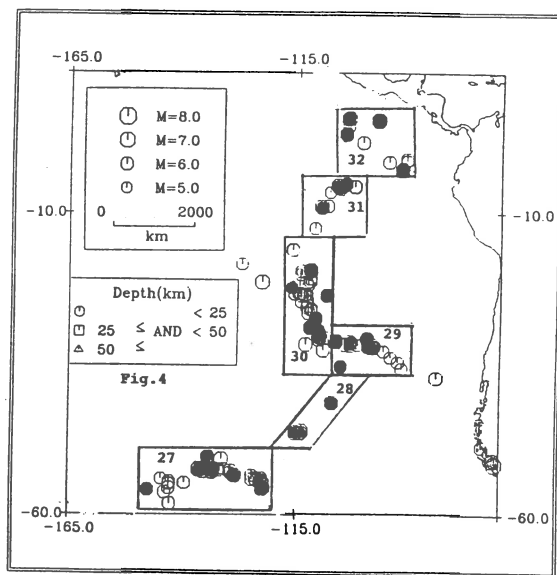
Fig. 4. Spatial distribution of the epicenters of shallow mainshocks (black circles) and foreshocks or aftershocks (open circles) occurred in the Pacific ocean during the time period 1898-1993.

1062
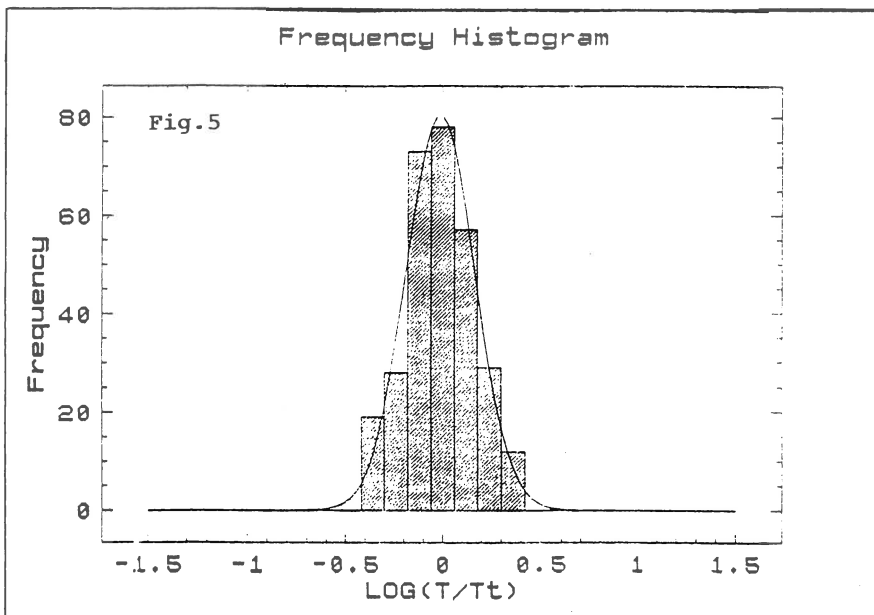
Fig. 5. The frequency distribution of the observed repeat times, T, compared to the theoretical ones, T_t.
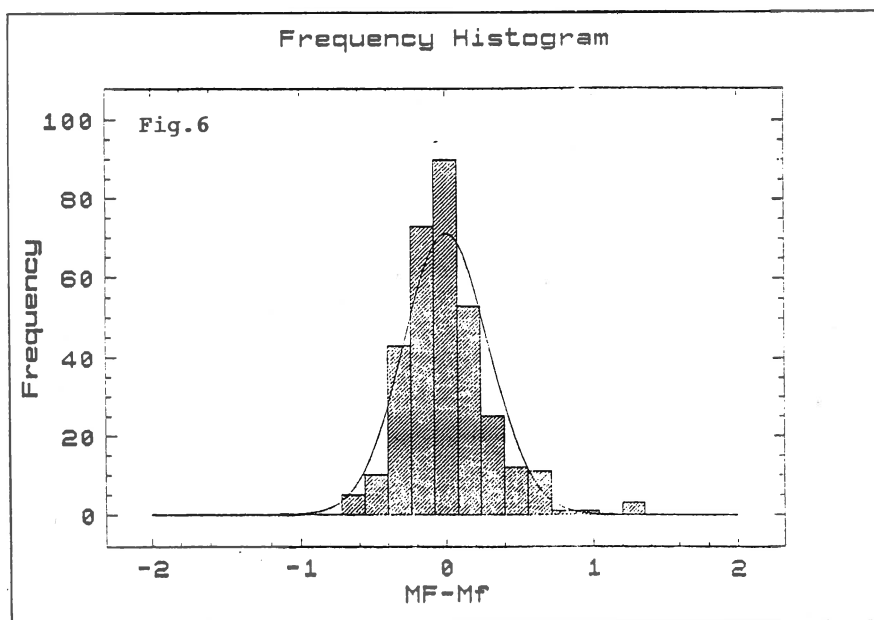
Fig. 6. The frequency distribution of the difference between the observed magnitudes of the following mainshocks, M_F, and the calculated ones, M_f.

TEMPORAL CHANGE IN CODA WAVE
PARAMETERS FOR VRANCEA EARTHQUAKES

Victoria Oancea and Olivia Bazacliu

National Institute for Earth Physics
P.O. Box MG-2, Bucharest, Romania

Abstract
The temporal variation of some parameters based on coda waves is studied for intermediate depth earthquakes in Vrancea (Romania) seismic region. The analysed parameters are: coda duration for events of the same magnitude, the coda amplitude decay rate, the relation between maximum S wave amplitude and coda duration.
The results are discussed in terms of changes in the attenuation properties of the propagation medium, asssociated with the occurrence of large earthquakes in the region. They are also correlated with the anomalous behaviour previously evidenced for other parameters.

INTRODUCTION
Studies performed in different areas of the world evidence temporal variations of the attenuation determined from coda waves, associated with the occurrence of large earthquakes. They are based on the possibility offered by coda analysis to define the stress accumulation before a large event occurrence, which leads to changes in the scattering properties of the propagation medium in the zone sampled by coda waves.
Sato (1988) synthetized the results obtained in the world in the domain of the temporal variation of coda waves parameters, correlated with large earthquake occurrence. Results on: relation between coda duration and magnitude, the coda decay gradient, ratio of coda duration on horizontal component to that on vertical component, are critically reviewed.

PREVIOUS RESULTS ON TEMPORAL VARIATION OF CODA WAVE
PARAMETERS IN VRANCEA REGION
The dominant seismic activity on the Romanian territory occurs at depths between 60 and 200 km in Vrancea region, a small area located at the Carpathian Arc Bend (hachured rectangle in Figure 1).
Previous studies performed for intermediate depth events in Vrancea region evidenced temporal variations of coda waves parameters. Oancea and Bazacliu (1988, 1991) studied the time evolution of the coda envelope decay gradient, expressed by the α parameter defined by Gusev and Lemzikov (1980, 1984, 1985), during 1974-1990, using the records obtained at MLR station located in the epicentral area. The obtained results

show that the coda decay gradient is higher in the time intervals when large earthquakes occur than in the rest of the time. This observation was correlated with the increase of the attenuation defined by Q_c^{-1} (Q_c= the quality factor determined using coda waves) during the preparation period of a strong event in the area.
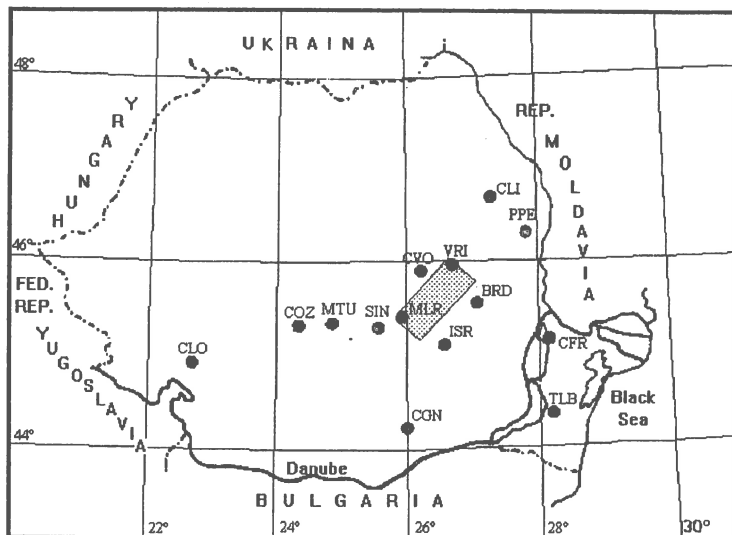
Figure 1 - Occurrence zone of Vrancea intermediate depth earthquakes (hachured rectangle) and the Romanian seismic telemetered network.

The similarity of the results obtained using band-pass filtered seismograms confirmed the existence of the anomalies and the change in medium properties as their cause (Oancea et al., 1989).
A temporal variation of the predominant frequency of coda waves was noticed in correlation with the anomalies evidenced in the temporal variation of the coda decay gradient (Oancea et al., 1989). The predominant coda frequencies (dependent on the time in coda measured from the origin time) are lower in the intervals with anomalous large decay gradient.
In this paper the analysis is continued for the coda decay and is extended to the temporal variation of coda duration, as well as to the relation between maximum amplitude and coda duration.

TEMPORAL VARIATION OF CODA DURATION
The analysis is performed for the period 1986-1991, when three large intermediate depth earthquakes occurred in Vrancea region: 1986 August 30 (M_w=7.2), 1990 May 30 and 31 (M_w=6.9 and 6.3, respectively).
The coda duration τ_c was determined using the analog

records obtained at MLR station on short period S-13 instruments. τ_c was defined starting from the origin time and ending when the signal amplitude equals the noise one.

The temporal variation of coda duration was analysed for earthquakes with the same average magnitude M_D (determined from signal duration and S-P time).

Separately, the τ_c values for all the earthquakes with M_D in three different small domains: 2.5-2.8, 2.9-3.2, 3.3-3.6 (events with constant magnitude, considering the error of determination) were plotted versus time. Events with depths around the one of the major earthquake which occurred in the studied time interval are used, in order to take into consideration the same Earth volume where the seismic wave attenuation takes place, for all the set of events.

Figure 2 presents the temporal behaviour of the τ_c values determined for the earthquakes which occurred during 1986-1987, at depth $100 \le h \le 160$ km (the major event in August 30, 1986 had $h=130$ km), for $M_D=2.5-2.8$ (a), and 2.9-3.2 (b). Figure 3 shows similar plots for the time interval January 1989-August 1991, obtained using the earthquakes with $60 \le h \le 120$ km (the major events on 30 and 31 May 1990 had depth around 90 km).

The visual analysis of Figures 2 and 3 leads to the following observations:
- time intervals can be defined, with different mean values $\overline{\tau_c}$ and different scattering of τ_c;
- the intervals before the major events have smaller $\overline{\tau_c}$ and smaller scattering of τ_c than the rest of the time;
- $\overline{\tau_c}$ increases, as well as the scattering of the τ_c values, during a short interval (3-6 months) preceding the major events;
- $\overline{\tau_c}$ values and the τ_c scattering remain large for the aftershocks, generally;
- in the time interval following the aftershocks, $\overline{\tau_c}$ decreases, but the scattering remains rather large.

In order to check the significance degree of the observed differences in the τ_c time behaviour, Fisher and Student's t tests are applied for comparing the dispersions and average values, respectively, for the periods separated on the time variation of τ_c (see Figure 2a).

The statistical analysis leads to the following conclusions:
- the scattering of the τ_c values differs significantly between the periods I-IV and I-V, at a confidence level of 95%;
- the scattering of the τ_c values of the aftershocks differs significantly from all the other time intervals, at a confidence level of 99%;
- the average $\overline{\tau_c}$ values differ significantly for the pairs of time intervals I-II, I-IV, II-V, III-II and III-IV, at confidence levels greater than 95%.

These results, evidencing a temporal variation of coda duration for earthquakes with the same magnitude, can be correlated with the intensification of the process of seismic wave scattering on the heterogeneities in the hypocentral
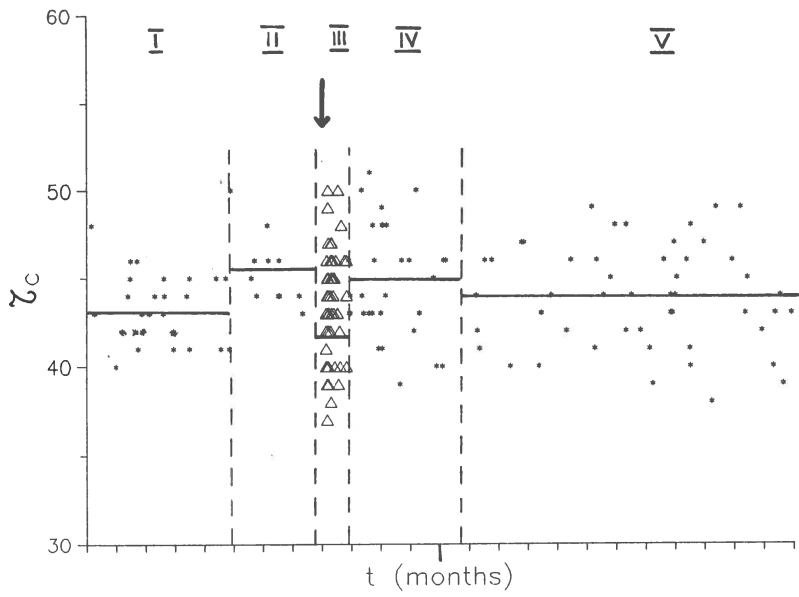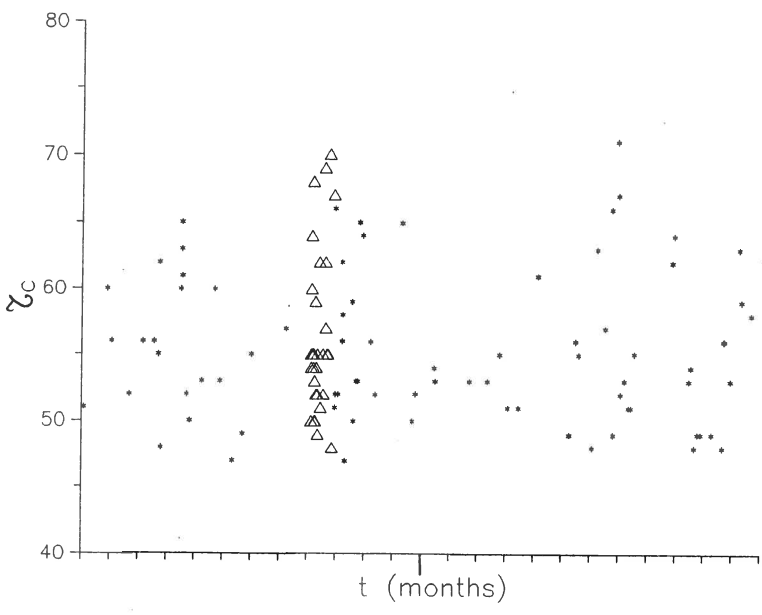
Figure 2 - Coda duration for earthquakes with M_D=2.5-2.8 (a) and 2.9-3.2 (b) which occurred in 1986-1987, at depth $100 \le h \le 160$ km.
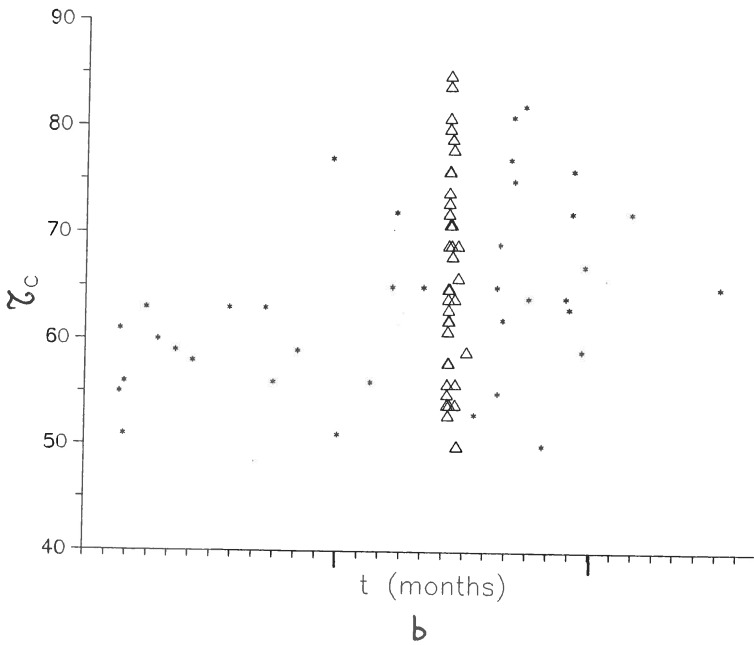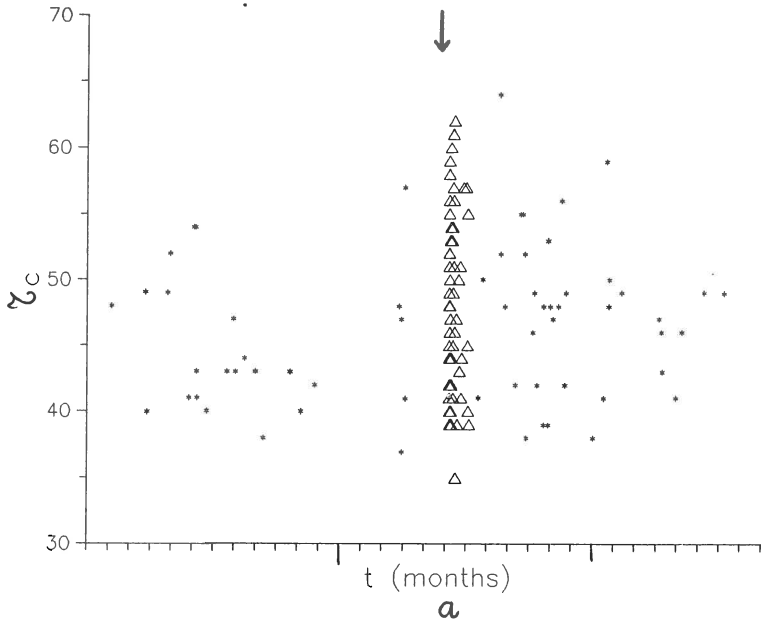
Figure 3 - Coda duration for earthquakes with M_D=2.5-2.8 (a) and 2.9-3.2 (b) which occurred in 1989-1991, at depth 60≤h≤120 km.

area, which leads to generation of late coda waves (arriving at the station after longer time) and so to large τ_c values.

CODA AMPLITUDE DECAY

A simple measure of the coda amplitude decay was analysed. It is the parameter A expressed by the ratio between the values of the coda envelope amplitude A_c corresponding to two time moments t_1 and t_2 (measured from the earthquake origin time): $A=A_c(t_1)/A_c(t_2)$.

The pairs of time moments $t_1=40$ s and $t_2=60$ s, as well as $t_1=45$ s and $t_2=60$ s are used to define A_1 and A_2, respectively.

Figure 4 presents the time behaviour of A_1 and A_2 parameters, for the earthquakes which occurred in Vrancea zone during 1989-1990, in the depth range 60-120 km.

The plots evidence that A_1 and A_2 and the scattering of their values increase in the period around the main shock occurence; the aftershocks have similar A values as in the period preceding the main shock.

This result confirms the increase of the coda decay gradient in the intervals when large earthquakes occur, as obtained in previous studies (Oancea and Bazacliu, 1988, 1991) and correlated with the increase of the attenuation defined by Q_c^{-1}.

THE RELATION BETWEEN MAXIMUM AMPLITUDE AND CODA DURATION

Starting from the conclusions obtained from the temporal variation of coda duration, we test if the relation between $\log(A_{max}^S/T)$ and τ_c changes, in connection with a large earthquake occurence.

The intermediate depth Vrancea earthquakes which occurred during 1986-1987 at depths in the range 100-160 km, are used. Figure 5 presents this dependence, using different symbols for the earthquakes preceding the major event in August 30, 1986 (*), its aftershocks (Δ) and the events which followed (□). No separation of different dependences, for these time intervals, can be evidenced on the plot in Figure 5.

CONCLUSIONS

The increase of the coda duration and of the scattering of its values in the time interval before large earthquake occurrence is noticed together with the increase of the coda decay gradient. Both results (confirming previous ones obtained for Vrancea intermediate earthquakes) support the hypothesis of the intensification of seismic wave attenuation in the Earth volume, in the occurrence area of the future strong event, followed by a slow return to the initial attenuative properties of the medium.

Similar results were obtained in other seismic regions and they were correlated with variations in the propagation medium properties, especially in the distribution of the lateral heterogeneities in the lithosphere (Jin, 1981; Jin and Aki,
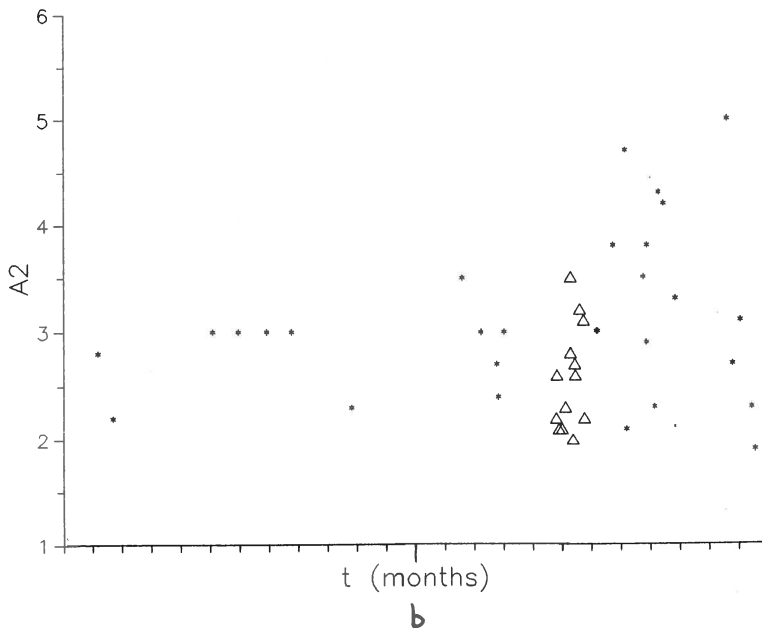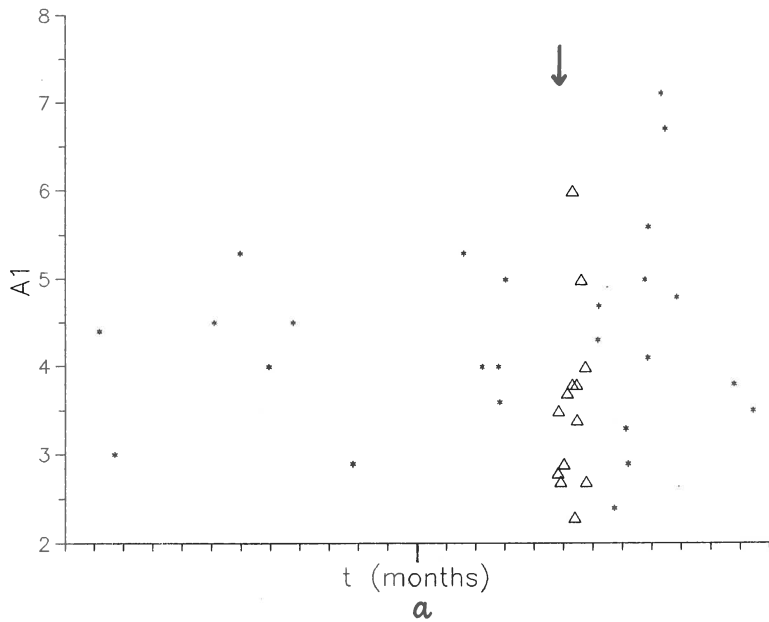
Figure 4 - Coda amplitude decay described by A_1 (a) and A_2 (b) parameters, for the earthquakes which occurred during 1989-1990 at $60 \leq h \leq 120$ km.
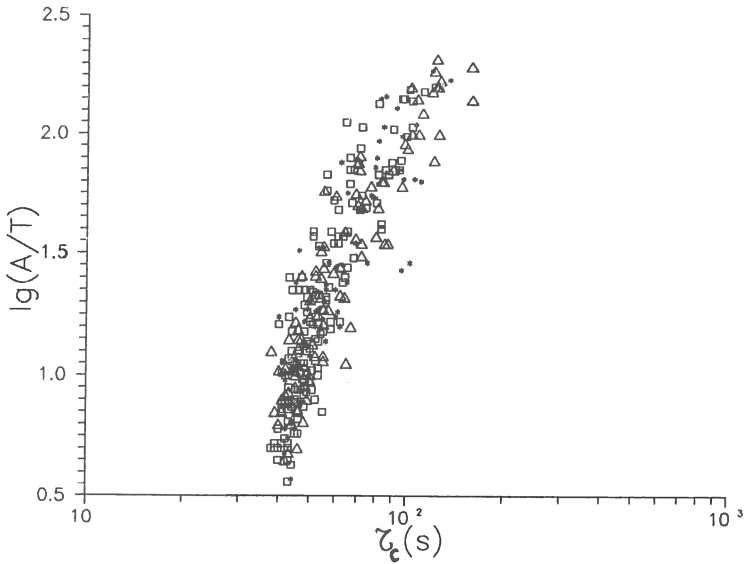
Figure 5 - Relation between $\log(A_{max}^S/T)$ and coda duration, for the earthquakes preceding the major event in August 30, 1986 (*), its aftershocks (Δ) and during the following period (□).

REFERENCES

Gusev, A.A. and V.K. Lemzikov, 1980. Preliminary results of studying the coda-wave envelope shape variations of the near earthquakes before the 1971 Ust-Kamchatka earthquake (in Russian). Vulkanol. Seismol., 6, 82-93.

Gusev, A.A. and V.K. Lemzikov, 1984. Anomalies of coda wave characteristics of small earthquakes before three large earthquakes in Kurile-Kamchatka zone (in Russian). Vulcanol. Seismol., 4, 76-90.

Gusev, A.A. and V.K. Lemzikov, 1985. Properties of scattered elastic waves in the lithosphere of Kamchatka: Parameters and temporal variation. Tectonophysics, 112, 137-153.

Jin, A., 1981. Duration of coda waves and the back-scattering coefficient. Paper presented at the Symposium on Seismology in China, State Seismol. Bur., Shanghai, China.

Jin, A. and K. Aki, 1986. Temporal change in coda Q before the Tangshan earthquake of 1976 and the Haicheng earthquake of 1975. J. Geophys. Res., 91, 665-673.

Oancea, V. and O. Bazacliu, 1988. The temporal variation of the coda envelope shape for Vrancea intermediate earthquakes. Gerlands Beitr. Geophys., 91, 354-357.

Oancea, V., O. Bazacliu, G. Mihalache and A. Dumitrascu, 1989.

Anomalies of coda wave parameters correlated with large Vrancea intermediate earthquake occurrence. Proc. of the XXI General Assembly of the ESC, Sofia, 404-409.

Oancea, V. and O. Bazacliu, 1991. The temporal variation of the coda envelope shape for Vrancea intermediate earthquakes occurred during May 1974 - May 1990. Report CFP/IFA 30.91.9, II, 74-83.

Sato,H., 1986. Temporal change in attenuation intensity before and after the eastern Yamanashi earthquake of 1983, in central Japan. J. Geophys. Res., 91, 2049-2061.

Sato, H., 1987. Precursor-like change in coda excitation before the western Nagano earthquake (M_s = 6.8) of 1984 in central Japan. J. Geophys. Res., 1356-1360.

Sato, H., 1988. Temporal change in scattering and attenuation associated with the earthquake occurrence - A reviev of recent studies on coda waves. Pure Appl. Geophys., 126, 465-497.

THE RELATIONSHIP BETWEEN PRECIPITATION AND SHALLOW EARTHQUAKES (M>5.5) REVISITED

Ioannis Liritzis and Basil Petropoulos

Academy of Athens, Research Center for Astronomy and Applied Mathematics, 14 Anagnostopoulou str., Athens 106 73, Greece

ABSTRACT

Preliminary results have indicated a possible relationship between precipitation changes before the onset of a large earthquake in the region of Athens (a radius of 100 km); the larger the rainfall peak the longer the period for an expected major earthquake to occur. According to the obtained empirical relationship a possible major earthquake event was expected till 1993 (M=5.5,Jan. 2, 1990). Further data and reconsideration has strengthen this empirical relationship. The relationship refers to the height of a premonitory rainfall peak (A2) above the average of 397 mm (1871-1993), but within the range of 397-460 mm, which occur prior the onset of a large shallow earthquake, against the time-lapse between earthquake to premonitory peak. Updated data foresee a large earthquake between 1996-98.

The problem we dealt with has both statistical and physical aspects. This indicative causal connection for the region of Athens is explained by a) the apparent underground waters and limestone environment. b) the many fault systems, c) the role of water in controlling seismic stress release. d) from recent fracture mechanics models, the effect of water-saturated rock specimens on temporal changes in seismic b-values (onset of b-value increase precedes earthquake occurrence).

INTRODUCTION: A Review on dilatation models

The rainfall has been considered as a possible triggering parameter, causing seismic energy release in the region of Athens. The role of pore water in controlling seismic stress release is now a subject of intensive study and it has been recognised as an important triggering factor in earthquake prediction. (Stacey,1977; Main et al. 1989; Sammonds et al. 1992). The general physical processes (dilatation model) has been described by Frank (1965) and Nur (1972).

The essential feature of the dilatancy hypothesis is that many (perhaps all) shallow earthquakes are preceded by progressive opening of cracks and pores in critically strained rock, as a consequence of which the rock dilates. But, so long as the pores are dry, frictional contact between grains or blocks suffices to prevent the occurrence of an earthquake: the dilatation is accrued by dilatation hardening.

The earthquake occurs only after the pores have been filled with water, which reduces the friction across a fault and allows it to move. Although some observations appear to contradict this hypothesis it does explain well others and provides a valuable focus for current ideas on earthquake prediction. The occurrence of deep earthquakes remains a problem to which dilatation effect appear to be irrelevant. Other hypotheses have been offered to explain them.

A recent systematic study of temporal changes in seismic b-values (defined as the log-linear slope of the earthquake frequency-magnitude distribution) has shown that large earthquakes are often precede by an intermediate-term increase in b-value, followed by a decrease in the months to weeks before the earthquake. The onset of the b-value increase can precede earthquake occurrence by as much as 7-years. (Smith, 1981).

A recently proposed fracture mechanics model of the earthquake source (Main et al. 1989) explains these temporal fluctuations in b-value in terms of the underlying physical processes of time-varying applied stress and crack growth. Further controlled laboratory experiments, done in simulated upper-crustal conditions on both air-dried and water -saturated rock specimens, have reinforced earlier observations regarding fracture mechanics models.

In particular, in water-saturated specimens, when pore-fluid volume is kept constant, a second intermediate-term b-value minimum is produced. The b-value variation as a function of time follows the dynamic stress-time behaviour of rock deformation, that is; for an air-dried specimen, first appears the elastic loading zone, followed by strain hardening, peak stress, stress softening, dynamic stress drop and finally, sliding on shear fault.

For a saturated specimen under conditions of constant pore-fluid pressure, first appears the compaction or built -up of stress zone, then the onset of cracking (peak stress), followed by dilatancy and ending with the power-law fall off in dynamic stress release zone (Sammonds et al., 1992).

The double b-value minimum is related to foreshocks and aftershocks, and in our empirical model may correspond to M>5.5 earthquake of deep/intermediate depth, occurring around the time of a M>5.5 shallow earthquake event. (years of 1962 in Corinthos ánd 1964 in Elevsis, in Table 1).

Noteworthy is, also, the lower b-values in continental south America, middle America and Mexico and higher b-values in oceanic regions of island arcs of the circum-pacific belt (starting from Alaska and the Aleutian islands and proceeding south-eastwards) (Tsapanos, 1990).

The specific region of Athens (longitude=22.5° - 24.5° E, latitude=37°-39° N) was chosen which corresponds to a radius of about 100 km around Athens. Within this region earthquakes of M>5.5 are highly perceptible in the city.

On the territory of Greece, which has experienced a complicated history of tectonic development during Alpine cycle, several zones of tectonic regions are distinguished (Bath,1983; Mackenzie, 1978; Le Pichon and Angelier, 1979).

A similar study has been carried out in California for shallow earthquakes (Li-Shang Huang et al, 1979) . The present work is an extension of an earlier attempt (Liritzis and Petropoulos, 1992).

The rainfall data (1871-1993) were obtained from the climatological Bulletin of the National Observatory of Athens (1871-1986) and from the Institute of Meteorology of the National Observatory of Athens (1986-1993). Earthquake data (M>5.5) were obtained from catalogues of Galanopoulos (1977), Bath (1983), Comninakis and Papazachos (1982) and Makropoulos and Burton (1981).

REASSESSMENT OF EARTHQUAKE - RAINFALL RELATIONSHIP

Table 1 presents all earthquake data used in this study, as well as the initially empirically considered three rainfall premonitory peaks (A1, A2, A3) characteristics. This is an updated catalogue of the earlier one (Liritzis and Petropoulos,1992) and includes only twelve shallow earthquakes (focal depth < 60 km) .

Fig.1 shows the variation of total annual precipitation (in mm) in Athens (1871-1993). Comparing precipitation between local rain gauge stations, it has been noted that the annual distribution of precipitation in Athens is similar, at least, to that of Corinth and Elevsis, while some differences occur in the distant areas of 100 km from Athens. Years of high and low precipitation are immediately distinguishable. Once rainfall patterns were devised from the tabular data it was possible to compare patterns for years preceding large earthquakes, in order to search for any valid correlation between the earthquake occurrence and rainfall distribution.

Annual rainfall peaks were arbitrarily grouped to three ranges above average (397 mm), namely; low (397-460 mm), medium (460-530 mm) and high wet (>530 mm) periods.

The increased rainfall signals before a major earthquake are represented by the three peaks labelled (A1, A2, A3) which fall within the above three rainfall levels. The rainfall peak which precedes or coincides with an earthquake event, called premonitory, could be of A1, A2 or A3 type. The time-lag between an earthquake and the three rainfall peaks A1, A2 and A3 is shown in Table 1.

In order to examine the precipitation- earthquake relationship the following were considered : a) the time interval when rainfall was below average (drought), b) the time interval between the earthquake event and a preceding rainfall peak above average of A1, A2 or A3 type, and c) the duration of this premonitory peak.

These criteria along with earthquake data are given in Table 1 compared with the results of Li-Sheng Huang et al. (1979).

DISCUSSION

The drought period varied between 3-6 years, the time interval between earthquake and premonitory peak varies between 0-9 years, and that the duration of the premonitory peak varies between 0.5-2 years. Li-Sheng Huang et al. (1979) reported a 4-6 years drought followed by an increase in seasonal precipitation of above average for one and occasionally 2-3 years before a major earthquake.

Following the above observations during the last decade and after the last earthquake (1981) a dry period of 6 years occurred followed by a 2-years duration premonitory peak of A2 type in 1987-1988, and a severe drought in 1989, the worse since 1897.

According to our earlier observations an earthquake was envisaged to occur within 6 years following 1987. This, we believe, has occurred in 1990 (Table 1).

Confirmation of the above tentative relationship by Liritzis and Petropoulos (1992) was made by applying a correlation test between the height of the premonitory precipitation peak (A1, A2, A3) and the time-lag between either of them and the onset of the great earthquake.

An interesting linear relationship was noted then, especially for the A2 peak, less for the A3 peak, but very poor for A1. Depending upon which peak (A2 or A3) is present, the appropriate linear regression was employed, that is:

for A2: $P = 1.41 (\pm 0.28) T + 11.9 (\pm 1.12)$ (1)
(r=0.927, R-squared=85.97%)
for A3: $P = 1.26 (\pm 0.26) T + 28.9 (\pm 1.75)$ (2)
(r=0.94, R-squared=88.49%)

where, T is the time-lag between earthquake occurrence and A2 or A3 peak, and P the height of the respective rainfall peak (scale: 13 mm = 100 mm of precipitation)

For the year 1991 and the A2 rainfall peak - peak height of 121 mm above average- the time-lag is 4-6 years, that is a large earthquake is expected between 1996-1998 (Fig.2). If this peak is included in our statistics, then the derived linear regression for A2 becomes:

$P = 1.35(\pm 0.29)T + 12.2(\pm 1.12)$ (3)

(R=0.90, SD=1.66, Prob. = 0.0063), which is similar, within the errors of their coefficients, to eq. (1), and provides a probable time for the event of 6 ± 1.7 years post-1991.

This proposed relationship of earthquake occurrence seems to roughly .follow earthquake statistics; for example, the mean recurrence period of earthquakes ("shakeability") of intensity M=7 for Athens is 9 years (Riznichenko et al. 1973).

CONCLUSION

Our reassessment indicates the apparent relationship between precipitation changes before the onset of a large (M>5.5) earthquake , at least for the region of Athens. The larger the rainfall peak the longer the period for an expected major earthquake to occur. In summary, the following conclusions have been drawn : 1) the revised linear relationship between large shallow (M>5.5) earthquakes (excluding deep and intermediate ones) and precipitation has not altered compared to our earlier work (Liritzis and Petropoulos, 1992); 2) the expected shallow earthquake within 6-years since 1987 has occurred in 1990 (Corinthian gulf); and 3) the recent rainfall data indicate a probable occurrence of another shallow earthquake 100 km around Athens during 1996-98.

The relationship between seismic energy release due to water fluids applied stress is regaining the interest. Surely, a full quantitative description of this relationship (model) is awaiting an understanding of crack development, porosity and permeability changes for the complete deformation cycle in shallow depths.

REFERENCES

Bath,M., 1983. Earthquake frequency and energy in Greece. Tectonophysics, 95, 233-252.

Comninakis, P.E and B. C. Papazachos, 1982. A catalogue of historical earthquakes in Greece and surrounding area. Univ. of Thessaloniki, Geophysics Lab., Publ. No 5, pp.24.

Frank, F. C., 1965. On dilatancy to seismic sources. Revs. Geophys., 3, 485.

Galanopoulos, A. G., 1977. On the difference in the seismic risk for normal and tall structures at the same site. Univ. of Athens, Seismol. Lab. and National Observatory of Athens, pp.33.

Le Pichon, X and J. Angelier, 1979. The Hellenic arc and trench system: A key to the neotectonic evolution of the eastern mediterranean area. Tectonophysics, 60, 1-42.

Liritzis, I and Petropoulos, B., 1989. A preliminary study of the relationship between large earthquakes and precipitation for the region of Athens, Greece. Earth, Moon, Planets, 57, 13-21.

Li-Sheng Huang, McRaney, J., Ta-Liang Teng and M. Prebish, 1979. A preliminary study for the relationship between precipitation and large earthquakes in southern California. PAGEOPH, 117, 1286-1300.

Makropoulos, K. C and Burton, P. W., 1981. A catalogue of seismicity in Greece and adjacent areas. Geophys. J. R. astr. Soc., 65, 741-762.

Main, I. G, Meredith, P. G and C. Jones, 1989. Geophys. J, 96, 131-138.

McKenzie, D., 1978. Active tectonics of the Alpine-Himalayan belt: the Aegean sea and surrounding region. Geophys. J. R. astr. Soc., 55, 217-254.

Nur, A., 1972. Dilatancy, pore fluids and premonitory variations of ts/tp travel times. Bull. Seism. Soc. America, 62, 1217-1221.

Riznichenko, Yu. V, Drumya, A V, Stepanonko, N. Ya, Gromowaga, T. P and N. I. Onofrasa., 1973. Seismicity and shakeability of the Carpathian- Balkan region. Izv. Akad. Nauka USSR, or in Phys. Solid Earth, 1973, 10, 639-649 (English translation).

Sammonds, P. R, Meredith, P. G and Main, I. G, 1992. Role of pore fluids in the generation of seismic precursors to shear fracture. Nature, 359, 228-230.

Smith, W. D., 1981. Nature, 289, 136-139.

Stacey, F. D., 1977. Physics of the Earth. 2nd edition, J. Wiley & Sons, New York, pp. 414.

Tsapanos, T. M., 1990. b-values of two tectonic parts in the Circum-Pacific belt. PAGEOPH. 134, 2, 229-242.

TABLE 1
Earthquake and rainfall data for the region of Athens, compared with that of California by Li-Sheng Huang (1979) (Updated table 1 of Liritzis and Petropoulos, 1992)

1	2	3	4	5	6	7	8	9
Kern county	35°	119°	7.7	21.7.1952	5	0.5	2	Li-Sheng et al
Imperial valley	32°45	115°	6.25	23.6.1915	4	0.5	2	>>
Carrizo mountain	32°59	116°	6.5	21.10.1942	5	2	4	>>
San Bernardino	34°	117°	6.25	23.7.1923	5	0.33	2	>>
Borrego mountain	33°11	23°71	6.4	9.4.1968	6	1.3	2	>>
Atalanti	38°25	23°71	7.0(<70)	27.4.1894	6 (1887-92)	1,-,9	1	This work
Egion	38°25	22°20	6.0(20)	30.5.1909	4 (1901-04)	-,3,-	1	>>
Thebes	38°20	23°5	6.0(8)	17.10.1914	3(1907-09)	0.5,2,4	1	>>
Loutraki	38°08	23°12	6.5(8)	22.4.1928	6(1921-27)	0,7,7	1	>>
Atalanti	38°25	23°71	6.0(7)	20.7.1938	4(1931-35)	-,-,2	1.5	>>
Corinthos	35°50	22°40	5.5(48)	19.1.1962	5(1955-61)	-,0,7	2	>>
	37°90	22°30	5.5(43)	4.10.1962	>>	>>	>>	>>
Elevsis	39°20	23°70	53/4(10)	23.2.1964	5(1955-61)	-,2,8.5	2	>>
	39°20	23°70	53/4(20)	29.4.1964	>>	>>	>>	>>
Alkyonides-Kapandriti	38°23	22°97	(6.7, 6.3 6.4)	24, 25.2.1981 4.3.1981	2-3(1978-81)	3,5,-	0.5	>>
Corinthos	38°58	24°16	5.5(14)	2.1.1990	3(1988-90)	-,3,-	2	>>

(1) Region; (2) Latitude; (3) Longitude; (4) magnitude in Richter. The numbers in parenthesis is depth in km; (5) Date; (6) Drought in years; (7) Period between earthquake-to-premonitory peak (A1,A2,A3) in years; (8) Duration of premonitory peak in years; (9) References.

PS. Following the year 1990 two earthquakes occurred; one in Galaxidi (18/11/92, M=5.7, 23 km), and the other in the Corinthian gulf (4/2/1993, M=5.1 , 5 km). The former was considered beyond the 100 km radius from Athens, and the latter of lower than the hitherto considered M=5.5 magnitude.

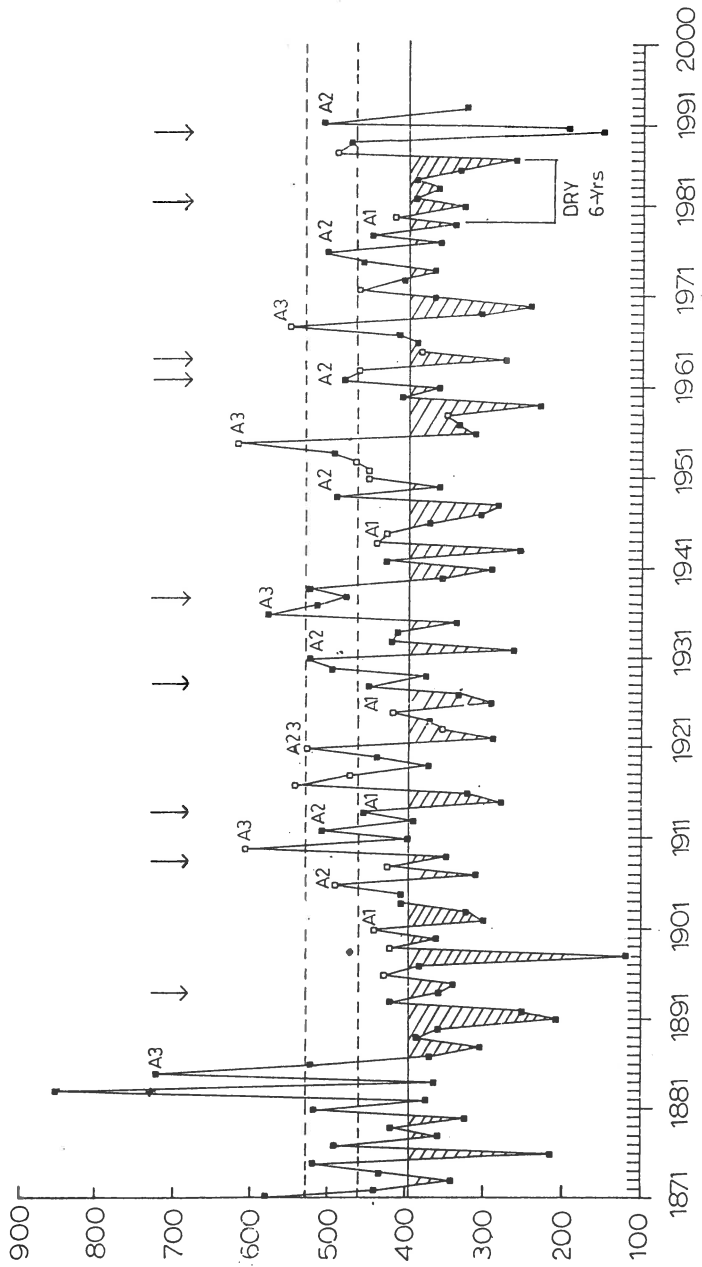Fig.1 Annual variation of precipitation in Athens, 1871-1993. Sample size = 122, average = 397, standard deviation = 105, standard error = 9.6. Designatory peaks A1, A2 and A3 correspond to three rainfall ranges. Arrows indicate earthquake events, M > 5.5.
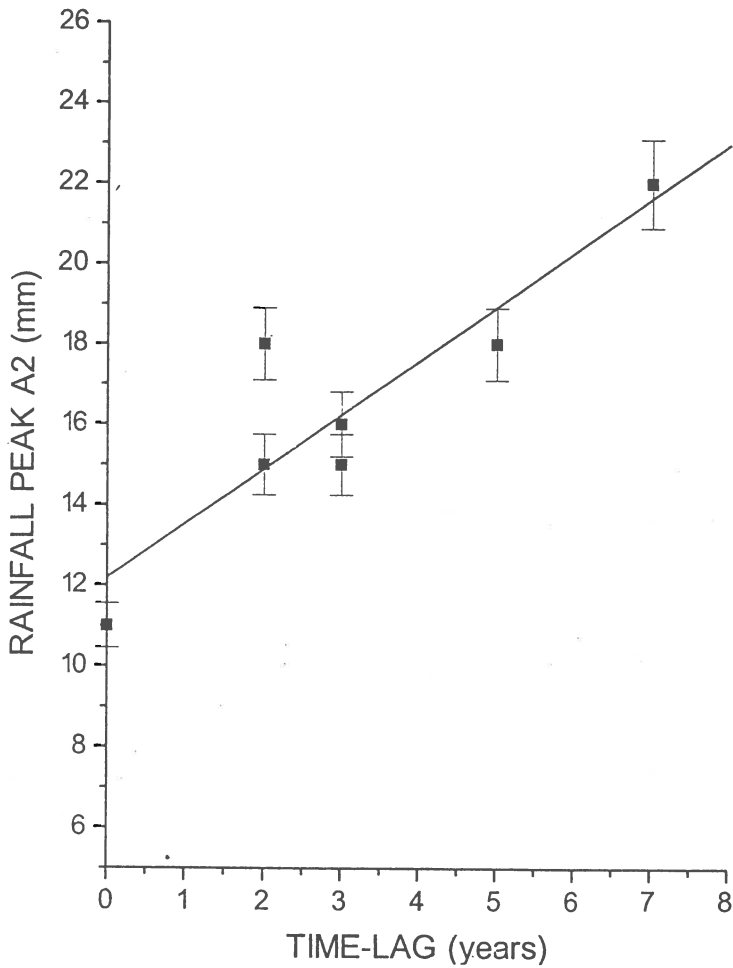
Fig.2 Height above the average of rainfall peak A2 , against, the time-lag between this peak and the forthcoming earthquake. Rainfall measurements are associated with a 5% error.

G.F. Karakaisis

Geophysical Laboratory, University of Thessaloniki, Thessaloniki 54006, Greece.

Abstract

The Italian peninsula has been separated in six seismogenic (regions) sources where shallow earthquakes occur, on the basis of certain seismological criteria. Another seismogenic region, where intermediate-depth and deep earthquakes occur at the southern Tyrrhenian sea, has also been defined. In each of these sources, the interevent times between successive main shocks with magnitudes equal to or larger than a certain magnitude threshold were considered.

By the use of the relations:

$$LogT_t = 0.19M_{min} + 0.33M_p - 0.39Logm_o + 7.81$$
$$M_f = 0.73M_{min} - 0.28M_p + 0.40Logm_o - 6.07$$

which relate the expected interevent time, T_t, and the magnitude of the following main shock, M_f, with the magnitude of the smallest main shock considered, M_{min}, the magnitude of the preceding main shock, M_p, and the yearly released seismic moment, m_o, conditional probabilities for the occurrence of strong earthquakes ($M_s \geq 6.0$) in each seismogenic source were calculated for the next ten years (1993-2002).

Introduction

The area of Italy, being part of the zone of deformation between the African and Eurasian lithospheric plates, ranks among the European countries with the higher seismic activity. During the last two decades two strong earthquakes occurred in Italy causing heavy damage at the northern and at the southern parts of the country (Friuli 1976, M_s=6.5; Campania-Basilicata 1980, M_s=6.9).

The Adriatic region, which includes the peninsula of Italy, Sicily and the Adriatic Sea, has long been the subject of many seismotectonic studies. These studies were mainly focused on the question whether the Adriatic Sea behaves as an independent rigid block or acts as a promontory of Africa (Argand, 1924; Celet, 1977; Hsu, 1982; Morelli, 1984).

In a recent work on active tectonics of the Adriatic region, Anderson and Jackson(1987a) showed that the Adriatic Sea is behaving as a rigid block, which is rotated counterclockwise with respect to both Africa and Eurasia (Mantovani et al., 1985). Very recently Mantovani et al. (1990) proposed a driving mechanism for this rotation. Along the peninsular Italy, which is the W-SW boundary of this block, NE-SW extension on normal faults is the dominant style of deformation, but changes to N-S compression in Sicily and in northern Italy (McKenzie 1972; Gasparini et al., 1982,1985; Mantovani and Boschi, 1983; Anderson and Jackson, 1987a,b; Westaway and Jackson, 1987; Jackson and McKenzie, 1988; Gentile and Slejko, 1990). Jackson and Mckenzie(1988) determined seismic convergence rates of 8 mmyr^{-1} in Sicily and 2.1 mmyr^{-1} in central Italy. Similar values were determined by Kiratzi (1992).

The shallow seismic activity is concentrated along the Apennines mountain chain and in the eastern Alps, while the deep and intermediate-depth earthquakes of the Tyrrhenian Sea are concentrated within the Tyrrhenian Benioff zone which dips to NW and reaches a maximum depth of about 500 Km (Gasparini et al., 1982; Anderson and Jackson, 1987b).

Since most of the strong earthquakes in Italy occur at the vicinity of urban areas, it is worth attempting to search for any seismicity pattern and, if such pattern does exist, to determine probabilities for the generation of strong earthquakes during the next years.

Considerable progress has been made in estimating long-term probabilities for the generation of strong earthquakes. This progress is based on a primary feature of the earthquake process, that is, the repetition of the seismic cycle (Scholz, 1990). Recent studies show that time-dependent models seem to be more plausible in comparison to the

slip-predictable models (Bufe *et al.*, 1977; Shimazaki and Nakata, 1980; Sykes and Quittmeyer, 1981; Wesnousky *et al.*, 1984; Nishenko and Buland, 1987; Nishenko, 1991). As it is known, according to the time-predictable model, the time of occurrence of a future earthquake in a certain seismic source depends on the size and the time of occurrence of the last earthquake in this source, while according to the slip-predictable model the size of a future earthquake depends on the time elapsed since the last earthquake.

During the last several years Papazachos (1988a,b; 1989; 1992; 1993) an investigation has been carrying out to identify time-dependent relations between main shocks in the Aegean area. He proposed a model in which the interevent time and the magnitude of the expecting main shock were quantitatively expressed in terms of the magnitude of the preceding main shock in each seismogenic source. This model was subsequently improved by taking into account the yearly released seismic moment in each source (Papazachos and Papaioannou, 1993). The regional time and magnitude predictable model has already been applied in several areas of the world (New Guinea, Iran, Turkey, South America, North Pacific, Indonesia, Japan, Solomon islands etc.) (Karakaisis, 1993; 1994a, b; Papadimitriou, 1993, 1994; Papadimitriou and Papazachos, 1994; Papazachos *et al.*, 1994a; Panagiotopoulos, 1994).

It is the aim of the present work to test the applicability of this model in the seismogenic sources of Italy and to determine probabilities for the generation of strong earthquakes for the next years in these sources.

Seismogenic sources and data used

Since the seismic activity in the studied area seems to be concentrated in a belt that runs through the backbone of Italy following the Appennines trend (Anderson and Jackson, 1987a), the separation of Italy into discrete seismogenic sources was based mainly on seismological criteria, such as the spatial clustering of epicenters, the seismicity level and the maximum earthquake that occurred during the period in which the data are assumed to be complete. Especially, the contour mapping of the seismic activity concerning events with $M \geq 4.0$ that occurred in Italy during 1900-1986 (Mulargia *et al.*, 1987), as it is depicted in a more recent work (Gasperini and Mulargia, 1992, p. 423) formed the cornerstone of this separation. The spatial distribution of the IX intensity (M.C.S.) felt effects in Italy (Vinci *et.al.*, 1992) was also taken into account.

In an attempt to ensure completeness of the data set, i.e. that there are neither earthquakes missing nor mislocated, only earthquakes with $M \geq 5.5$ which occurred after 1900 have been considered along with some large historical earthquakes($M \geq 6.5$), although there is strong evidence that completeness for earthquakes with $M \geq 5.5$ starts at 1820 (Mulargia *et al.*, 1987). Information on the data used in the present study concerning earthquakes with $M \geq 5.5$, comes from various sources. Since the methodology applied throughout this work depends substantially on the magnitudes of the main shocks, special attention has been paid on these magnitudes. The magnitudes of the earthquakes which occurred during 1783-1930 have been taken from the catalogue of Italian earthquakes during 1000-1980 (C.N.R. 1985). In this catalogue the magnitudes quoted are based on Karnik's (1969) intensity-magnitude relations. The magnitudes of the earthquakes that occurred during 1931-1968 have been taken from the catalogue of earthquakes of Mediterranean (1900-1975) of Comninakis and Papazachos (1978). Finally, the magnitudes of the earthquakes that occurred from 1969 onwards were taken from the ISC and USGS bulletins. Data concerning other focal parameters (epicenter coordinates, depth) have also been taken from a literature concerning seismic sequences and several large earthquakes of shallow and deep origin (Cagnetti and Pasquale, 1979; Cipar, 1980; Gasparini *et al.*, 1982; Martini and Scarpa, 1983; Mulargia and Boschi, 1983; Console and Favali, 1988; Margottini *et al.*, 1991; Ambraseys and Bommer, 1991). It has to be noted, however, that the discrepancies which have been observed between the magnitudes assigned by different authors on the same earthquakes are small and, in any case, do not affect substantially the results.
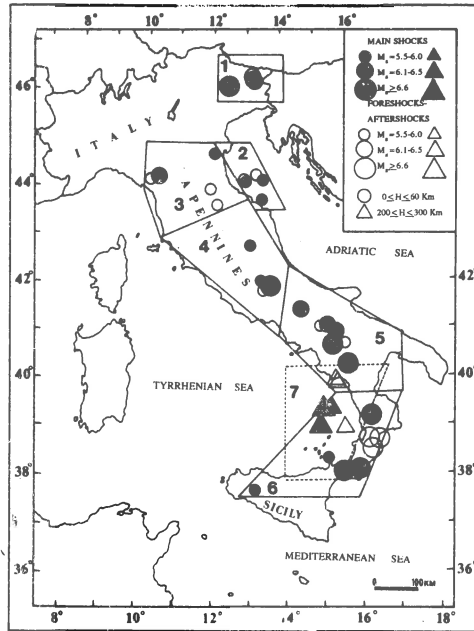
Fig. 1. The seven seismogenic sources in which the area of Italy is separated. The dashed line defines the source (7), where deep and intermediate depth earthquakes occur. Black circles and triangles denote epicenters of main shocks with $M_s \geq 5.5$, while open circles and triangles denote epicenters of their larger foreshocks and aftershocks.

These seismogenic sources are shown in Figure 1 along with the epicenters of the earthquakes considered in the present study. Solid circles and triangles denote epicenters of main shocks (shallow and intermediate depth or deep earthquakes, respectively), while open circles and triangles denote epicenters of their larger foreshocks and aftershocks in the broad sense, i.e. earthquakes which may occur up to several years before or after the main shock, respectively.

The seismogenic sources, from north to south, are:(1) eastern Alps; (2) northern Adriatic coasts; (3) northern Apennines; (4) central Apennines; (5) southern Apennines; (6) Calabrian arc. The intermediate-depth and deep earthquakes define the last source, (7), in the southern Tyrrhenian Sea.

Method and results

The regional time- and magnitude predictable model aims at predicting the main shocks in a certain seismogenic source, that is, the strong earthquakes which occur at the beginning and the end of each seismic cycle and not the smaller ones that occur during the preseismic and postseismic activations. Mogi (1985) suggested that the seismic activity over a wide area would increase through a rise in crustal stress and that these earthquakes are foreshocks in the broad sense, while according to the time predictable model, the duration of the preseismic activity is constant. Regarding this topic, recent studies on the seismic cycle showed that its last phase is characterized by an accelerated activity period with a fairly constant duration equal to 2.7±0.6 years, thus confirming Mogi's idea, which culminates before the second main shock of the seismic cycle and does not depend neither on the first nor on the second main shock magnitudes (Karakaisis *et al.*, 1991). This duration of the foreshock activity has been taken into account in the present study. Mogi (1985) also suggested that according to the time predictable model the duration of the postseismic activity depends on the magnitude of the preceding main shock. Recently

1082

Papazachos *et al.* (1994b), based on data from the Alpine-Himalayan and circum-Pacific belts, proposed the following relation between the duration, t (in years), of the aftershock activity and the magnitude, M, of the main shock, which has been used in this study:

$$logt = 0.06 + 0.13M$$

The first column in Table 1 gives the code number and the name of the seismogenic sources depicted in Fig. 1, while the second column gives the year since the data are complete, in the sense given before, above a certain minimum magnitude, which is written next to it. For example, in the first source, i.e the eastern Alps, the data are complete for earthquakes with $M_s \geq 6.8$ during 1873-1991 and for $M_s \geq 6.5$ during 1900-1991. The completeness has been determined for each source separately. The third, fourth and fifth columns correspond to the date, epicenter coordinates(north latitude, east longitude) and the surface-wave magnitude of the main shocks considered. The sixth column gives the cumulative magnitude, M, of each sequence, that is, the magnitude that corresponds to the total moment, M_o, released by the major shocks (main shock and large foreshocks and aftershocks) of each sequence according to the relation between magnitude and seismic moment proposed by Kanamori (1977):

$$LogM_o = rM + k \quad (3)$$

where r and k are equal to 1.5 and 16.1, respectively. Relation (3) gives similar results with the one suggested by Giardini *et al.* (1984).

Table 1. Earthquakes considered in every source

Source	Completeness	Date			lat.	long.	M_s	M
1. Eastern	1873 6.8	29	6	1873	46.2	12.4	6.8	6.8
Alps	1900 5.8	27	3	1928	46.4	13.0	5.8	5.8
		6	5	1976	46.4	13.3	6.5	6.6
		15	9	1976	46.3	13.2	6.1	a*
		15	9	1976	46.3	13.2	6.0	a
2. Northern	1900 5.6	17	5	1916	44.2	12.9	5.8	5.9
Adriatic		16	8	1916	44.2	12.9	5.6	a
Sea		30	10	1930	43.7	13.3	5.9	6.0
		30	11	1934	44.3	13.5	5.6	a
		23	1	1962	44.3	13.4	5.9	5.9
3. Northern	1910 5.5	27	10	1914	44.1	10.5	5.7	5.8
Apennines		26	4	1917	43.5	12.1	5.5	a*
		10	11	1918	44.0	11.9	5.7	f*
		7	9	1920	44.3	10.3	6.3	6.3
		30	12	1967	44.8	12.1	5.8	5.8
4. Central	1900 5.5	24	2	1904	42.1	13.3	5.7	5.7
Apennines		13	1	1915	42.0	13.6	6.8	6.8
		29	12	1922	41.8	13.6	5.5	a
		19	9	1979	42.8	13.0	5.8	5.8
5. Southern	1805 6.5	26	7	1805	41.5	14.5	6.5	6.5
Apennines	1900 5.5	16	12	1857	40.3	15.9	7.0	7.0
		23	7	1930	41.1	15.4	6.5	6.5
		26	9	1933	42.1	14.2	5.5	a
		21	8	1962	41.1	15.1	5.6	a
		21	8	1962	41.1	15.1	6.1	6.3
		21	8	1962	41.2	15.0	6.0	a
		23	11	1980	40.8	15.3	6.9	6.9
6. Calabrian	1783 6.6	5	2	1783	38.2	16.0	7.1	7.2
Arc	1900 5.5	7	2	1783	38.6	16.3	6.7	a
		28	3	1783	38.8	16.5	6.7	a

4	10	1870	39.3	16.3	6.6	6.6
8	9	1905	38.8	16.1	7.0	f
23	10	1907	38.0	16.1	5.9	f
28	12	1908	38.2	15.6	7.1	7.3
15	1	1968	37.7	13.1	5.8	6.0
16	1	1968	37.9	13.0	5.5	a
25	1	1968	37.7	13.1	5.5	a
15	4	1978	38.4	15.1	5.8	5.9
28	5	1980	38.4	14.3	5.6	a

7. South Tyrrhenia Sea	1900 6.3 1915 5.9 1937 5.8					
1	8	1910	39.0	15.0	6.8	6.9
5	4	1911	40.0	15.5	6.3	a
7	7	1915	39.0	15.0	5.9	a
17	10	1937	39.3	15.2	5.8	f
13	4	1938	39.4	15.0	7.0	7.0
26	12	1952	40.0	15.5	6.2	6.4
23	11	1954	38.5	14.9	5.8	a
1	2	1956	39.1	15.7	6.2	a
3	1	1960	39.3	15.3	6.3	6.3

(*) a: aftershock, f:foreshock

Table 2 gives information on the magnitude, M_{min}, of the smallest main shock considered, the magnitudes M_p and M_F of the preceding and following main shocks and the observed interevent time, T, which is the difference of the year of occurrence of the preceding main shock, t_p from the year of occurrence of the following main shock, t_f.

Table 2. Data used for the determination of the parameters of the relations (1) and (2)

Source	M_{min}	M_p	M_F	T(yrs)	t_p	t_f
1. Eastern	5.8	5.8	6.6	48.11	1928	1976
Alps	6.6	6.8	6.6	102.86	1873	1976
2. Northern	5.9	5.9	6.0	14.45	1916	1930
Adriatic Sea	5.9	6.0	5.9	31.23	1930	1962
3. Northern	5.8	5.8	6.3	5.86	1914	1920
Apennines	5.8	6.3	5.8	47.31	1920	1967
4. Central	5.7	5.7	6.8	10.89	1904	1915
Apennines	5.7	6.8	5.8	64.68	1915	1979
	5.8	6.8	5.8	64.68	1915	1979
5. Southern	6.3	6.5	6.3	32.08	1930	1962
Apennines	6.3	6.3	6.9	18.26	1962	1980
	6.5	6.5	7.0	52.39	1805	1857
	6.5	7.0	6.5	72.60	1857	1930
	6.5	6.5	6.9	50.34	1930	1980
	6.9	7.0	6.9	122.94	1857	1980
6. Calabrian	5.9	7.3	6.0	59.05	1908	1968
Arc	5.9	6.0	5.9	10.25	1968	1975
	6.0	7.3	6.0	59.05	1908	1968
	6.6	7.2	6.6	87.67	1783	1870
	6.6	6.6	7.3	38.23	1870	1908
	7.2	7.2	7.3	125.90	1783	1908
7. Southern	6.3	6.9	7.0	27.70	1910	1938
Tyrrhenian	6.3	7.0	6.4	14.70	1938	1952
Sea	6.3	6.4	6.3	7.02	1952	1960
	6.4	6.9	7.0	27.70	1910	1938
	6.4	7.0	6.4	14.70	1938	1952
	6.9	6.9	7.0	27.70	1910	1938

In every seismogenic source after considering the first minimum magnitude, M_{min}, of all main shocks, the interevent times, T, between successive main shocks with magnitudes equal to or larger than M_{min} are calculated. Then, the second minimum magnitude, M_{min}, is considered and new interevent times between successive main shocks with magnitudes equal to or larger than the second M_{min} are calculated. This procedure is continued until the last M_{min} is considered.

The yearly released seismic moment in each seismogenic source is a measure of the seismicity level and can be reliably determined if adequate data for the source are available. The values of m_o have been determined by applying a method suggested by Molnar (1979), which makes use of the parameters a, b' of the Gutenberg-Richter relation and of the magnitude, M_{max}, of the maximum observed magnitude in each source.

Table 3 lists information which was used for the calculation of the yearly seismic moment rate, i.e the values of a and b', the M_{max} and the logarithm of the yearly seismic moment rate. The values of the parameters a and b' have been determined by using earthquakes occurred after 1900, with magnitudes greater than or equal to 5.5.

Table 3. Information on the basic parameters of every source, on the magnitude of the expecting earthquake and its probability of occurrence

Source	a	b	M_{max}	$LogM_o$	M_f	P
1 Eastern Alps	4.01	0.90	6.8	24.59	6.2	0.28
2 N. Adriatic Sea	3.76	0.90	5.9	23.56	6.0	0.28
3 N. Apennines	3.37	0.90	6.3	23.71	6.1	0.25
4 Central Apennines	3.72	0.90	6.8	24.30	6.4	0.41
5 S. Apennines	3.93	0.90	7.0	24.63	6.2	0.17
6 Calabrian arc	4.13	0.90	7.1	25.01	6.6	0.60
7 S. Tyrrhenian Sea	3.35	0.75	7.1	24.94	6.6	0.52

The regional time- and magnitude predictable model (Papazachos and Papaioannou, 1993) which is applied in this study, is expressed by the following relations:

$$LogT_t = bM_{min} + cM_p + dLogm_o + q \quad (1)$$

$$M_f = BM_{min} + CM_p + DLogm_o + m \quad (2)$$

where T_t is the calculated interevent time, M_{min} is the smallest main shock considered, M_p and M_f are the magnitudes of the preceded and the expecting main shock and m_o is the yearly moment rate in each source, while b, c, d, q, B, C, D and m are parameters to be determined by using all the available data from all sources. The method to calculate these parameters is a multilinear regression techinque and is described by Papazachos and Papaioannou (1993). Very recently, the parameters of the relations (1) and (2) have been determined by using a very large data set consisting of 1811 observations (T, M_p, M_f, m_o) which concern 274 seismogenic sources from the Alpine-Himalayan and circum Pacific seismic zones (Papazachos et al, 1994b). Experience gained from the above mentioned work shows that it is better to calculate the last term of these relations (q and m) by using the data of the region, keeping the other parameters (b, c, d, B, C, D) as they have been determined from the large data set. In the present case, these two relations take the form:

$$LogT_t = 0.19M_{min} + 0.33M_p - 0.39Logm_o + 7.81 \quad (3)$$
$$M_f = 0.73M_{min} - 0.28M_p + 0.40Logm_o - 6.07 \quad (4)$$

with standard deviation equal to 0.30 for relation (3) and 0.29 for relation (4).

The essence of the regional time- and the magnitude predictable model is that, given the time of occurrence and the magnitude of the last main shock in a certain seismic source, one can calculate the time of occurrence of the next main shock by the use of the relation (1), as well as its magnitude through the relation (2).

Previous efforts to apply probabilistic methods in long-term earthquake prediction have used either Gaussian distribution (Lindh, 1983; Sykes and Nishenko, 1984) or Weibull distribution (Rikitake, 1976; Nishenko, 1985). Recently, Nishenko and Buland (1987) and Nishenko(1991) investigated the use of the quantity T/T_{ave} in order to define the distribution properties of characteristic earthquake recurrence, where T_{ave} is the average repeat time observed for a specific fault and T is an individual repeat time. They found that the log-normal distribution provides better fit to the variations of the quantity T/T_{ave} than the Gaussian and Weibull ones.

It has been shown that the ratio T/T_t follows the log-normal distribution (Papazachos et al., 1994b). On the basis of this fact and taking also into account the time of occurrence and the magnitude of the last main shock that has occurred in every one of the seismogenic sources of Italy, the probability of occurrence of the next main shock with $M_s \geq 6.0$ during the next ten years is calculated. The last two columns of Table 3 give, for every region, information on the magnitudes of the expecting main shocks as they have been calculated by the relation (2) and the highest probability of occurrence during the next ten years.

Discussion and Conclusion

During the last decade several studies that concern long- and intermediate-term earthquake prediction in Italy have been conducted.

Purcaru and Berckhemer (1982) had identified two regions as candidate for the generation of large ($M \geq 7.0$) earthquakes. In one of them (southern Apennines) the 1980($M_s = 6.9$) earthquake occurred. The second is located in southern Sicily, where a very strong earthquake($I_o = X$) occurred on January 11, 1693.

Caputo (1987) using pattern recognition techniques identified several areas in Italy where strong earthquakes are expected.

Basili et al. (1990) studying central and southern Italy, have computed the mean interevent times of earthquakes with intensities $I_o \geq IX$ (M.C.S.) and found a value equal to 20 ± 12 years, while Vinci et al. (1992) defined several seismic hazardous zones on the basis of macro- and microseismic data.

In the present study it was found, first, that the results support the basic concept of the regional time-predictable model that the larger the magnitude of the preceding main shock, the longer the time interval till the next one (see Table 2). Second, it was found that the probabilities for the generation of strong earthquakes, which have been calculated on the basis of this model, are high for the next ten years in several seismogenic sources of Italy. The seismic source (6), i.e. the Calabrian arc, is assigned with a high probability (=0.50), since the last large earthquakes occurred there in 1905 and 1908. The magnitude of the expected earthquake is estimated to be 6.6. In the source (7) where deep and intermediate-depth earrhquakes occur the probability is equal to 0.52.

Undoubtedly, there are some inherent uncertainties which inevitably introduce errors in this model, apart from the uncertainties of the magnitudes of the historical earthquakes. These uncertainties concern dynamical interaction between adjacent regions during the stress accumulation and release processes and the temporal clustering of seismicity.

There is evidence that the first source of uncertainties exists in the present case, since it has been observed that most of the large earthquakes in the southern Apennines have followed a major seismic crisis in the southern Dinarides and northern Aegean (Mantovani et al., 1986, 1987a, b, 1992; Mucciareli et al., 1988; Albarello et al., 1989). Nevertheless, until the earthquake generation process will be better understood, studies on long-term forecasting will be a prerequisite for the expensive monitoring of short-term precursors in areas assigned with high probabilities.

REFERENCES

Albarello, D., M. Mucciarelli, and E. Mantovani, 1989. Use of non parametric correlation test for the study of seismic interrelations, Geophys. Journal, 96, 185-188.

Anderson, H. and J. Jackson, 1987a. Active tectonics of the Adriatic region, Geophys. J. R. astr. Soc., 91, 937-983.

Anderson, H. and J. Jackson, 1987b. The deep seismicity of the Tyrrhenian Sea, Geophys. J. R. astr. Soc., 91, 613-637.

Ambraseys, N.N. and J.J Bommer, 1991. Database of European strong ground-motion records, European Earthquake Engineering, 2, 18-37.

Argand, E., 1924. La tectonique de l' Asie, in Proceedings of International Geological Congress, XIII, pp. 171-372.

Basili, A., P. Favali, G. Scalera and G. Smriglio, 1990. An attempt to evaluate seismic hazard in central-southern Italy, Natural Hazards, 3, 31-47.

Bufe, C.G., P.W. Harsh and R.D. Burford, 1977. Steady-state seismic slip: a precise recurrence model, Geophys. Res. Letts., 4, 91-94.

Cagnetti, V. and V. Pasquale, 1979. The earthquake sequence in Friuli, Italy, 1976, Bull. Seism. Soc. Am., 69, 1797-1818.

Caputo, M. (1987) : Pattern recognition delle aree con vocazione a forti terremoti in Italia: una rassegna, in Aree sismogenetiche e rischio sismico in Italia, edited by E. Boschi et al., pp. 177-222.

Celet, P., 1977. The Dinaric and Aegean arcs: the geology of the Adriatic, in The Ocean Basins and Margins, edited by A.E.M. Nairn, W.H. Kanes and F.G. STehli, Vol. 4A, pp. 215-261.

Cipar, J., 1980. Teleseismic observations of the Friuli, Italy earthquake sequence, Bull. Seism. Soc. Am., 70, 963-983.

Comninakis, P.E. and B.C. Papazachos, 1978. A catalogue of earthquakes in the Mediterranean and the surrounding area for the period 1900-1975, Publication of Geophys. Lab., No. 5, University of Thessaloniki, pp. 96.

Consiglio Nazionale delle Ricerche, 1985. Catalogo di Terremoti Italiani dall' Anno 1000 al 1980, edited by D. Postpischl, Bologna, pp. 239.

Console, R. and P. Favali, 1988. Historical seismograms in Italy, in Historical Seismograms and Earthquakes of the World, edited by W. Lee, H. Meyers and K. Shimazaki (Academic Press, San Diego, California), pp. 447-450.

Gasparini, C., G.Iannaccone, P. Scandonne and R. Scarpa, 1982. Seismotectonics of the Calabrian arc, Tectonophysics, 84, 267-286.

Gasparini, C., G. Iannaccone and R. Scarpa, 1985. Fault plane solutions and seismicity of the Italian peninsula, Tectonophysics, 117, 59-78.

Gasperini, P. and F. Mulargia, 1992. Statistical analysis of Italian seismicity at regional scale, in Earthquake Prediction, 5th Course, edited by M. Dragoni and E. Boschi (Instituto Nazionale di Geofisica, Roma), pp. 417-430.

Gentile, G.F. and D. Slejko, 1990. A 3-D study of the faut pattern in Friuli(northeastern Italy) from local mechanism characteristics, Boll. Geof. Teor. ed Appl., XXXII(127-128), 199-214.

Giardini, D., A. Dziewonski, J. Woodhouse and E. Boschi, 1984. Systematic analysis of the seismicity of the Mediterranean region using the centroid-moment tensor method, Boll. Geof. Teor. ed Appl., XXVI(103), 121-142.

Jackson, J. and D. McKenzie, 1988. The relationship between plate motions and seismic moment tensors, and the rates of active deformation in the Mediterranean and Middle East, Geophys. J. Int., 93, 45-73.

Hsu, K.J., 1982. Alpine Mediterranean geodynamics: past, present and future, in Alpine Mediterranean Geodynamics, edited by H. Berckhemer and K.J. Hsu (Am. Geophys. Union Geodynamic series), Vol. 7, pp. 7-14.

Kanamori, H., 1977. The energy released in great earthquakes, J. Geophys. Res., 82, 2981-2987.

Karakaisis, G.F., 1993. Long-term earthquake prediction in the New Guinea-Bismarck Sea region based on the time and magnitude predictable model, J. Phys. Earth, 41, 365-389.

Karakaisis, G.F., 1994a. Long-term earthquake prediction in Iran based on the time and magnitude predictable model, Physics Earth Planet. Inter., 83, 129-145.

Karakaisis, G.F., 1994b. Long-term earthquake prediction along the North and East Anatolian Fault Zones based on a time predictable model, Geophys. J. Int., 116, 198-204.

Karakaisis, G.F., M.C. Kourouzidis and B.C. Papazachos, 1991. Behaviour of the seismic activity during a single seismic cycle, in Proceedings of the International Conference on Earthquake Prediction: State-of-the-Art, Strasbourg, France, 15-18 October 1991, pp. 47-54.

Karnik, V., 1969. Seismicity of the European area: Part I, (D. Reidel, Dordrecht, Holland).

Kiratzi, A.A., 1992. Active deformation of the Italian peninsula and Sicily based on seismicity data, Publication of Geophys. Lab., No. 14, University of Thessaloniki, pp. 1-25.

Lindh, A.G., 1983. Preliminary assessment of long-term probabilities for large earthquakes along selected fault segments of the San Andreas fault system in California, U.S.G.S. Open-File Report, 83-63, 1-15.

Mantovani, E. and E. Boschi, 1983. Tectonics and seismicity in the Italian region, in Earthquakes: Observation, Theory and Interpretation, LXXXV Corso, edited by H. Kanamori and E. Boschi, Soc. Italiana di Fisica, (North Holland Publishing Co., Amsterdam), 519-529.

Mantovani, E., D. Babbucci and F. Farsi, 1985. Tertiary evolution of the Mediterranean region: Major outstanding problems, Boll. Geof. Teor. ed Appl., 27, 67-90.

Mantovani, E., D. Albarello and M. Mucciarelli, 1986. Seismic activity in North Aegean region as middle term precursor of Calabrian earthquakes, Phys. Earth Planet. Inter., 44, 264-273.

Mantovani, E., D. Albarello and M. Mucciarelli, 1987a. Evidence of the interrelation between the seismicity of the southern Apennines and southern Dinarides, Phys. Earth Planet. Inter., 49, 259-263.

Mantovani, E., D. Albarello and M. Mucciarelli, 1987b. Interrelation between the seismicity of Calabria and Balkan areas, Annales Geophysicae, 5, 143-148.

Mantovani, E., D. Babbucci, D. Albarello and M. Mucciarelli, 1990. Deformation pattern in central Mediterranean and behaviour of the Africa-Adriatic promontory, Tectonophysics, 179, 63-79.

Mantovani, E., E. Boschi, D. Albarello, D. Babbucci and M. Mucciarelli, 1992. Medium term earthquake prediction in Italy, in Earthquake Prediction, 5th Course, edited by M. Dragoni and E. Boschi (Instituto Nazionale di Geofisica, Roma), pp. 181-198.

Margottini, C., G. Martini and D. Slejko, 1991. An instrumental earthquake catalogue for northeastern Italy since 1900, Publ. of ENEA, RT/AMB/90/38.

Martini, M. and R. Scarpa, 1983. Earthquakes in Italy in the last century, in Earthquakes: Observation, Theory and Interpretation, LXXXV Corso, edited by H. Kanamori and E. Boschi, Soc. Italiana di Fisica, (North Holland Publishing Co., Amsterdam), 479-487.

McKenzie, D.P., 1972. Active tectonics of the Mediterranean region, Geophys. J. R. astr. Soc., 30, 109-185.

Mogi, K., 1985. Earthquake Prediction (Academic Press Japan).

Molnar, P., 1979. Earthquake recurrence intervals and plate tectonics, Bull. Seism. Soc. Am., 69, 115-133.

Morelli, C., 1984. Promontorio Africano o microplacca Adriatica, Boll. Ocean. Teor. Appl., II(2), 151-168.

Mucciarelli, M., D. Albarello and E. Mantovani, 1988. Earthquake forecasting in southern Italy on the basis of logistic models, Tectonophysics, 152, 153-155.

Mulargia, F. and E. Boschi, 1983. The 1908 Messina earthquake and related seismicity, in Earthquakes: Observation, Theory and Interpretation, LXXXV Corso, edited by H. Kanamori and E. Boschi, Soc. Italiana di Fisica, (North Holland Publishing Co., Amsterdam), 493-518.

Mulargia, F., P. Gasperini and S. Tinti, 1987. Contour mapping of Italian seismicity, Tectonophysics, 142, 203-216.

Nishenko, S.P., 1985. Seismic potential for large and great interplates earthquakes along the Chilean and southern Peruvian margins of South America: a quantitative reappraisal, J. Geophys. Res., 90, 3589-3615.

Nishenko, S.P., 1991. Circum-Pacific seismic potential: 1989-1999, Pure Appl. Geophys., 135, 169-257.

Nishenko, S.P. and R. Buland, 1987. A generic recurrence interval distribution for earthquake forecasting, Bull. Seism. Soc. Am., 77, 1382-1399.

Panagiotopoulos, D.G., 1994. Long-term earthquake prediction along the seismic zone of Solomon islands and New Hebrides based on the time- and magnitude predictable model, Natural Hazards, (in press).

Papadimitriou, E.E., 1993. Long-term earthquake prediction along the western coast of south and central America based on a time predictable model, Pure Appl. Geophys., 140, 301-316.

Papadimitriou, E.E., 1994. Long-term earthquake prediction in the North Pacific seismic zone based on a time-predictable model, Natural Hazards, 9, 303-321.

Papadimitriou, E.E. and Papazachos, B.C., 1994. Time dependent seismicity in the Indonesian region, J. Geophys. Res., J. Geophys. Res., 99, 15387-15398.

Papazachos, B.C., 1988a. Seismic hazard and long-term earthquake prediction in Greece, European School of Earthquake Sciences, Course on Earthquake Hazard Assessment, Athens, 9-16 May 1988, pp. 1-10.

Papazachos, B.C., 1988b. Long-term earthquake prediction of earthquakes in seismogenic sources of Greece, United Nations Seminar on the Prediction of Earthquakes, Lisbon, Portugal, 14-18 November 1988, pp. 1-10.

Papazachos, B.C., 1989. A time-predictable model for earthquake generation in Greece, Bull. Seism. Soc. Am., 79, 77-84.

Papazachos, B.C., 1992. A time- and magnitude predictable model for generation of shallow earthquakes in the Aegean area, Pure Appl. Geophys., 138, 2, 287-308.

Papazachos, B.C., 1993. Long-term prediction of intermediate depth earthquakes in southern Aegean region based on a time-predictable model, Natural Hazards, 7, 211-218.

Papazachos, B.C. and Ch. A. Papaioannou, 1993. Long-term earthquake prediction in the Aegean area based on a time- and magnitude predictable model, Pure Appl. Geophys., 140, 593-612.

Papazachos, B.C., Papadimitriou, E.E., Karakaisis, E.E. and Tsapanos, T.M., 1994a. An application of the time- and magnitude predictable model for the long-term earthquake prediction of strong shallow earthquakes in Japan area, Bull. Seism. Soc. Am., 84, 426-437.

Papazachos, B.C., Papadimitriou, E.E., Karakaisis, G.F. and Panagiotopoulos, D.G., 1994b. Long-term earthquake prediction in the circum-Pacific convergent belt, Pure and Applied Geophysics (in press).

Purcaru G. and H. Berckhemer, 1982. Regularity patterns and zones of seismic potential for future large earthquakes in the Mediterranean region, Tectonophysics, 85, 1-30.

Rikitake, T., 1976. Recurrence of great earthquakes at subduction zones, Tectonophysics, 35, 335-362.

Scholz, C.H., 1990. The mechanics of earthquakes and faulting, (Cambridge University Press.

Shimazaki, K. and T. Nakata, 1980. Time-predictable recurrence of large earthquakes, Geophys. Res. Letts., 7, 279-282.

Sykes, L.R. and R.C. Quittmeyer, 1981. Repeat times of great earthquakes along simple plate boundaries, in Earthquake Prediction, An International Review, edited by D.W. Simpson and P.G. Richards, Maurice Ewing Series, A.G.U., Vol. 4, 297-332.

Sykes, L.R. and S.P. Nishenko, 1984. Probabilities of occurrence of large plate rupturing earthquakes for the San Adreas, San Jacinto and Imperial faults, California, 1983-2003, J. Geophys. Res., 89, 5905-5927.

Vinci, L., F. Frugoni, A. Basili, P. Favali, G. Scalera and G. Smriglio, 1992. Target areas for prediction and prevention studies in Italy, in Earthquake Prediction, 5th Course, edited by M. DRAGONI and E. BOSCHI (Instituto Nazionale di Geofisica, Roma), pp. 431-443.

Wesnousky, S. G., C. H. Scholz, K. Shimazaki and T. Matsuda, 1984. Integration of geological and seismological data for analysis of seismic hazard: A case study of Japan, Bull. Seism. Soc. Am., 74, 687-708.

Westaway, R. and J. Jackson, 1987. The earthquake of 23 November 1980 in Campania-Basilicata (S. Italy), Geophys. J. R. astr. Soc., 90, 375-443.

ON SEISMIC-GRAVITATIONAL PULSATIONS AND SEISMIC ACTIVITY OF THE EARTH

L.N.Petrova and K.S.Osypov[1]

Department of Earth Physics, St.Petersburg University, Russia

ABSTRACT

Seismic-gravitational pulsations (SGP) are a new phenomenon discovered in St.Petersburg. SGP are detected mainly before powerful earthquakes. Evidence of the correspondence between SGP and strong seismicity is presented. Energy and spectral characteristics of SGP are analyzed for prognostics aims.

INTRODUCTION

Seismic-gravitational oscillations (SGO) are such oscillations of the Earth which inertial and gravitational accelerations in the normal direction to its surface are of the same order. It is a well-known fact, that inertial acceleration is greater than gravitational one for ordinary seismic signals with periods up to 1000 s. Vice versa, gravitational acceleration dominates for the Earth's tides with the main periods equal to 12 and 24 hours. These accelerations are almost the same for the oscillations with 1 hour period. Thus, we consider that the period band of seismic-gravitational oscillations is in the limits from 0.5 to 5 hours.

Until recently special seismic studies in this period band were not performed elsewhere in the world. Systematic special observations of seismic oscillations in the band 0.5-5 h were started in St.Petersburg 20 years ago. Statistical analysis of the data have revealed non-identified oscillations with periods up to 300 min (Lin'kov et al., 1982; Savina et al., 1988). The remarkable feature of these oscillations is that they are observed as before, as after strong earthquakes. Systematic long-term observations in the period band 0.5-5 hour showed that the detected oscillations are the real planetary geophysical phenomenon (Petrova, 1992).

A new phenomenon -- seismic-gravitational pulsations (SGP), was discovered in the data obtained by super-long-period (0.5 - 5 hour) seismograph in St.Petersburg (Lin'kov et al., 1990). SGP are perturbations on the background of SGO and have sign-changing shape, duration equal to 5-17 h and amplitudes several times greater than the mean level of SGO. We note that the SGP phenomenon differs from the

---

[1] Now at the Department of Geophysics, Uppsala University, Sweden

SGO phenomenon. SGP were observed many times before strong earthquakes (e.g., Spitak 1988, Loma-Prieta 1989, Rachen 1990, Indonesia 1991). Therefore we tried to reveal the correspondence between SGP and seismic activity (Lin'kov et al., 1990). We showed that the sampling distribution of the time residuals between the SGP and earthquakes with M>5 is uniform. This means that there is no correlation between SGP occurrence and low seismicity. On the other side, we revealed that the occurrence of SGP before strong earthquakes (M > 6.5) is not a random fact with a probability of 95 %.

Such a high statistical value indicates the necessity of investigation of SGP as a possible earthquake precursor. For the practical purposes of earthquake prediction it is important to reveal the prognostic features of SGP and their connection with the processes in an earthquake source.

The aim of this paper is the study of SGP statistical features as prognostic parameters for the problem of short-term earthquake prediction.

APPARATUS

The apparatus for measurements is based on Kirnos pendulum with free period equal to 15 sec. Vertical pendulum is inserted in a special chamber which protects it from the direct influence of pressure-variations (Lin'kov et al., 1982). Horizontal pendulum is installed on a special anti-tilt platform to avoid tilts (Lin'kov et. al., 1990). Pendulum displacement is converted into electrical current by a photo-element sensor. Analogue active filters provide the frequency characteristics of the system in the band 0.5-5 hour with amplification approximately 10 for the period 1 hour.

METHOD

For the analysis of time-variant characteristics of SGP we applied a complex technique (Osypov, 1994) based on advanced methods of adaptive signal processing (Proakis et al., 1988). The processing scheme includes (1) complex demodulation; (2) variance analysis of complex demodulates; and (3) frequency-time analysis. On the first step of the analysis we apply complex demodulation using a recursive Batterworth filter (Osypov, 1994). This procedure performs a frequency filtering and therefore increases signal/noise ratio (SNR). Moreover, complex demodulation significantly compresses data and improves the efficiency of the following processing. On the second step we analyze the value and the first derivative of the instantaneous variance in dependence with time. As it will be shown below, the latter parameter characterize the sharpness of the pulsation fronts. On the third step we apply two techniques of frequency-time analysis: one

17.04.1982

08.02.1987
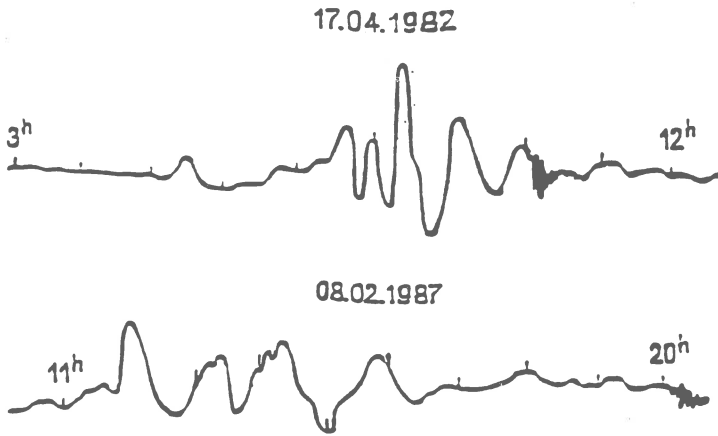
Fig.1. Observations of SGP obtained by vertical pendulums registering seismic oscillations in the period band 0.3-2.0 hour in St.Petersburg (top) and Tbilisy (bottom) before the first arrivals from earthquakes in Philippine (17.04.82, MPV=6.8) and New Land (8.02.87, MLV=7.2) correspondingly.

Fig.2. Records of long-period horizontal seismograph on anti-tilt platform in St.Petersburg; top -- SGP before the earthquake in Spitak (7.12.88, M=7.0), bottom -- SGP before the earthquake in Sudan (9.07.90, M=6.6).

is Fourie spectral estimation in a running window (see e.g., Bendat and Piersol, 1990) and another is adaptive maximum entropy method based on autoregression modeling using lattice filtering (Osypov, 1994). We revealed that the both techniques applied to the SGP data provide similar results.

DATA ANALYSIS

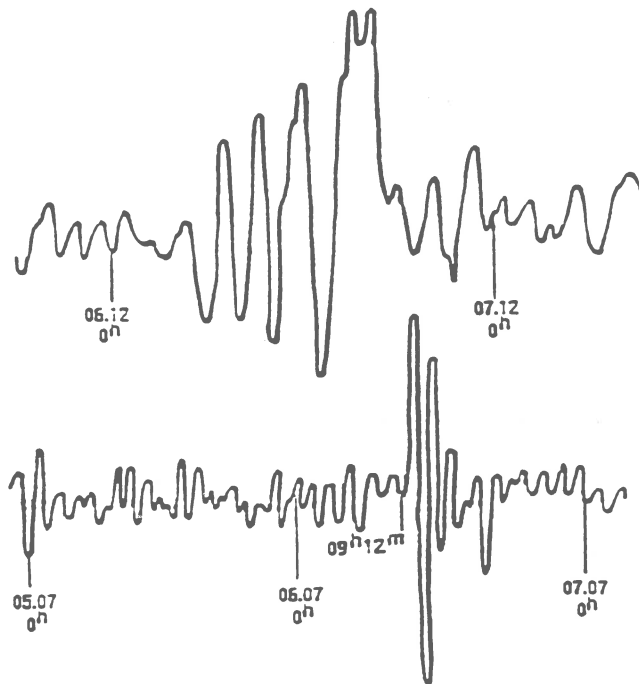More than 60 pulsations were registered since 1989. Here we present only several examples. Fig.1 presents observations of SGP obtained by vertical pendulums registering seismic oscillations in the period band 0.3-2.0 hour in St.Petersburg (a) and Tbilisy (b). The data presented in Fig.1 show the existence of the lond-period phenomenon just before the high-frequency first arrivals from the earthquakes in Philippine (17.04.82, MPV=6.8) and New Land (8.02.87, MLV=7.2). Fig.2 presents records of the long-period horizontal seismograph on the anti-tilt platform in St.Petersburg; a -- SGP before the earthquake in Spitak (7.12.88, M=7.0), b -- SGP before the earthquake in Sudan (9.07.90, M=6.6). This is an illustration of the two types of SGP, i.e., relatively short-term pulse (Fig.2 a) and oscillation package with frequency variations similar to surface wave dispersion (Fig.2b).

We revealed that the frequency of SGP appearance correlates with the seismic activity level. For example, there were no powerful earthquakes in June-July 1989 and no pulsation was detected this time. With increasing of the seismic activity the SGP number becomes higher. The characteristic example is April 1989 when 7 earthquakes with M>6.6 happened. It is an extraordinary fact that the total seismic energy of 1.13×10^{22} erg was released only within an area of 20° x 20° in the Pacific Ocean. Corresponding onsets of SGP, their duration and earthquakes times and magnitudes for this period are presented on Fig.3. Horizontal size of black rectangular corresponds to SGP duration which varies from 6-7 to 15-17 hour. Most SGP advance moments of earthquakes with M > 6.5 (vertical arrows) by period varying from several hours to four days. We note that in March 1989 SGP were observed only on 1.03.89 and on 2.03.89 and powerful earthquakes occurred only on 10.03.89 and 11.03.89. Therefore we can conclude that the pulsation on 3.04.89 really advances the earthquake on 6.04.89 and does not follow any previous event. One can see from the figure that in some cases more than one pulsation are observed before an earthquake. Such effect is observed quite often, but still the correspondence between number or duration of SGP and some source characteristics is not clear.

Following our processing scheme we firstly performed complex demodulation in the band 0.05 - 0.7 1/hour. As it was stated above, there are the two types of SGP, i.e., relatively short-term pulse (Fig.2 a) and oscillation package with
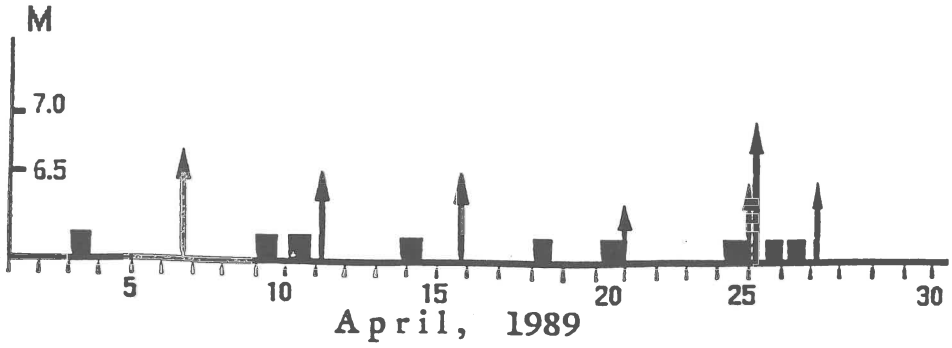
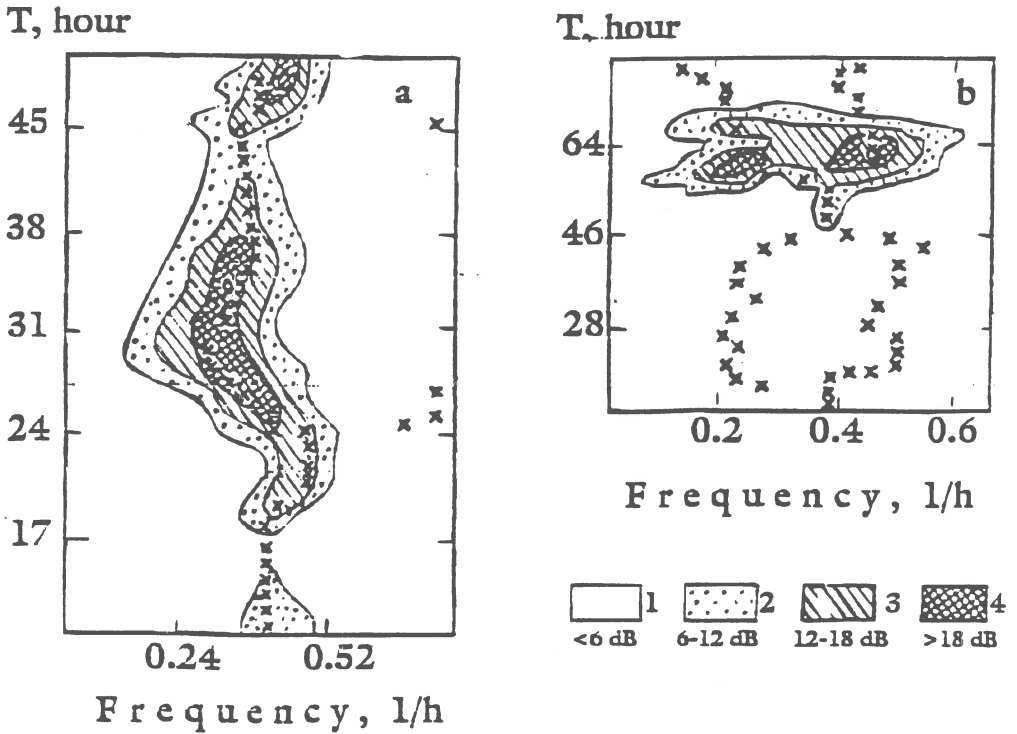Fig.3. Illustration of SGP (black rectangulars) and times of earthquakes with M > 6.5 (vertical arrows).

Fig.4. Frequency-time maps of SGP shown on Fig.2, a -- SGP before the earthquake in Spitak (7.12.88, M=7.0), b -- SGP before the earthquake in Sudan (9.08.90, M=6.6). Crosses correspond to reliable maxima of instantaneous maximum entropy spectra.

frequency variations (Fig.2b). To analyze the spectral dynamics of SGP we applied frequency-time analysis by adaptive maximum entropy method. Fig.4 presents the frequency-time maps of SGP. The effective time window of the analysis is 10 hours, AR-order is equal 2. Crosses correspond to reliable maxima of instantaneous maximum entropy spectra or principal frequencies. Pulsation (a) is characterized by one main component with frequency variation from 0.4 to 0.2 1/hour for the first half of the pulsation and from 0.2 to 0.3 1/hour for the second one. Pulsation (b) consists of two components with almost constant frequencies equal to 0.2 and 0.5 1/hour.

We could not reveal any correspondence between the frequency-time characteristics of SGP and earthquake parameters. Therefore we consider the energy of SGP as the most informative parameter correlated with earthquake energy release. This statement is illustrated in Fig.5 showing instantaneous variance of seismic data (a) and its derivative (b), estimated in a sliding window (12 hours) for the record window from 28.11.88 to 21.12.88. Pulsation 3 corresponds to Fig.1a and precedes the earthquake in Spitak (7.12.88, M=7.0). Arrows indicate the moments of the earthquakes. The most intensive sharp increases of the variance correspond to SGP (numerated). One can clearly see that they precede the powerful earthquakes. We revealed that the variance derivative containes additional useful information about SGP, i.e. the sharpness of their front. For example, the pulsation 1 in Fig.5a is more intensive than pulsation 3, but the front of the latter is sharper (Fig.5b). As one can see from the figure, the ratio of the variance derivatives for the pulsations 1 and 3 (Fig.5b) is more consistent with the corresponding ratio of the earthquakes magnitudes (M=7.0 after the pulsation 1 and M=6.4 after the pulsation 3) than the ratio of the variances (Fig.5a).

CONCLUSIONS

1. The phenomenon SGP is observed only during the periods of high seismic activity of the Earth and is not registered within seismic silent time.

2. SGP are characterized by different complicated patterns in the frequency-time domain.

3. Results presented in Fig.5 allow us to suggest instantaneous variance of seismic signals and its derivative to use as informative (possibly prognostic) parameters. This is consistent with the physical idea that value and speed of the acceleration (gravity and/or inertial) correspond to the stress in a source zone of an earthquake. Thus we assume that SGP may be considered as a trigger for an earthquake.
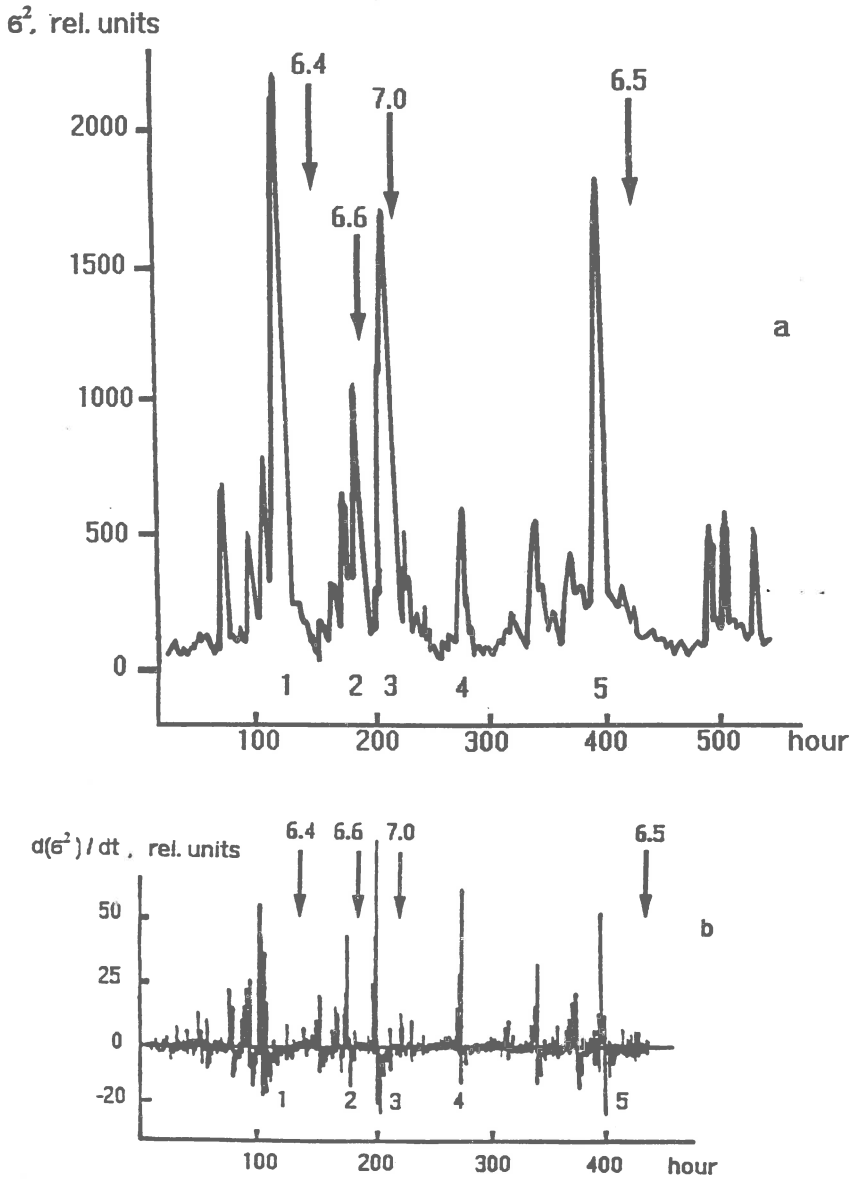
Fig.5. Instantaneous variance of seismic data (a) and its derivative (b), estimated in a sliding window (12 hours) for the record from 28.11.88 to 21.12.88. Pulsation 3 corresponds to Fig.1a and precedes the earthquake in Spitak (7.12.88, M=7.0). Arrows show the moments of earthquakes.

REFERENCES

Bendat, J.S. and Piersol, A.G., 1988. Random data: analysis and measurement procedures. John Wiley & Sons, New York, 540.

Lin'kov, Ye.M., Petrova, L.N., Savina N.G. and Yanovskaya, T.B., 1982. Superlong-period oscillations of the Earth. Doklady of the USSR Academy of Sciences, 262, 2, 321 - 324.

Lin'kov Ye.M., L.N.Petrova and K.S.Osypov, 1990. Seismic-gravitational pulsations of the Earth and atmospheric perturbations as possible precursors to strong earthquakes, Dokl. of the USSR Akad. Sci., v.313, 4, 76-79.

Osypov, K.S., 1994. Algorithm and programs for statistical analysis of non-stationary geophysical processes. COSPAR Coloquia Series, v.5, 703-706.

Proakis, J.G., Rader, C.M., Ling, F. and Nikias, C.L., 1992. Advanced digital signal processing. Macmillan Pub. Comp., New York, 610.

Petrova, L.N., 1992. Seismic-gravitational fluctuations of the Earth and the possible mechanism of their formation. Biophysics (Proceedings of "Fluctuations in bio and physical-chemical systems", Pushino, 1990), v.37, 3, 418-423.

Savina, N.G., Makarov, E.S., Lin'kov, E.M. and Chernobay, I.P., 1988. Synchronized observations of long-period Earth oscillations. Izvestiya Acad. Sci., USSR, Physics of the Solid Earth, v. 24, 8, 654-658.

Time Dependent Seismicity in the Zones of the Continental Fracture System

Papazachos, B.C., Papadimitriou, E.E. and Karakaisis, G.F.

Laboratory of Geophysics, University of Thessaloniki, Thessaloniki, GR54006, Greece.

Abstract
A very large sample of 1811 observations concerning 274 seismogenic regions in the continental fracture system (Alpine-Himalayan belt, Circum-Pacific convergent belt) are used to determine the following relations of the time and magnitude predictable model:

$$\log T_t = 0.19\, M_{min} + 0.33\, M_p - 0.39 \log m_o + 7.72$$

$$M_f = 0.73\, M_{min} - 0.28\, M_p + 0.40 \log m_o - 6.23$$

where T_t is the interevent time, M_p and M_f are the surface wave magnitudes of the preceding and the following mainshocks, M_{min} is the magnitude of the smaller mainshock considered and m_o is the yearly seismic moment release in each seismogenic source. The model described by the first of these relations and the lognormal distribution, is testing against the classical non time dependent model, described by the Gutenberg-Richter empirical law and the Poisson time distribution, for earthquakes in Greece. The results show the superiority of the time dependent model for large earthquakes. Some other features of the time and magnitude dependent model, especially those concerning the definition of foreshocks and aftershocks are also discussed.

Introduction
Most of the work on seismicity studies and seismic hazard assessment is based on the assumption that seismicity does not change with time but only with space. Such time independent models are usually based on the Gutenberg and Richter (1944) formula for the distribution of magnitudes and the Poisson distribution for the time. During the last two decades, however, several attempts have been made to test time dependent seismicity models. This research led to the conclusion that repeat times for earthquakes which occur in single faults or in simple plate boundaries favor the time predictable model (Bufe et al., 1977; Shimazaki and Nakata, 1980; Sykes and Quittmeyer, 1981; Thatcher, 1984) although some other opinions also exist on this problem (Davis et al., 1989; Kagan and Jackson, 1991). This model suggests that the time of occurrence of a future earthquake in a fault depends on the size and on the time of occurrence of the last earthquake in this fault. In addition to repeat times, observations on the time variation of the foreshocks and aftershocks (in the broad

sense) strongly support this model (Mogi, 1985). According to Scholz (1982), several basic tenets of the model are implicit in the elastic rebound theory.

During the last decade (Papazachos, 1988a,b, 1989, 1992), repeat times of strong earthquakes in the Aegean area have been used to show that the time predictable model holds also for seismogenic sources which include, in addition to the fault of the characteristic earthquake, other faults where other smaller main shocks occur. This idea was also strongly supported by observations concerning "foreshocks" and "aftershocks" (Karakaisis et al., 1991). This research led to what is called "regional time and magnitude predictable model" (Papazachos, 1992) and its latest version (Papazachos and Papaioannou, 1993) includes two relations. The first one relates the repeat time, T_t, with the magnitude, M_{min}, of the minimum earthquake considered, with the magnitude, M_p, of the preceded mainshock and with the moment rate, m_o (per year), released in the seismogenic source. The second relation gives the magnitude, M_f, of the following mainshock in the source as a function of M_{min}, M_p and m_o.

The regional time and magnitude predictable model has been tested in almost all zones of shallow earthquakes of the continental fracture system (Alpine - Himalayan belt and Circum-Pacific convergent belt) by seismologists of the Laboratory of Geophysics of the University of Thessaloniki (Papazachos, 1992; Papazachos et al., 1994a, b; Karakaisis, 1993a, 1994, b; Papadimitriou, 1993, 1994a, b; Papadimitriou and Papazachos, 1994; Panagiotopoulos, 1993, 1994a, b). This collective work, in addition to its scientific contribution (improvement of the relations, determination of seismicity parameters, etc), led to the creation of a very large sample of complete and homogeneous data, which is in digital form and can be used for further seismicity studies.

The purpose of the present paper is to use this data sample to make a better determination of the parameters for the two relations which describe the regional time and magnitude predictable model and to test it against a time independent model. Furthermore, some properties of this model (foreshocks, aftershocks, etc) are also discussed.

Method and Data

Papazachos and Papaioannou (1993) based on the observed interevent times of strong mainshocks in 74 seismogenic sources of the Aegean area, proposed relations of the following forms:

$$\log T_t \;=\; b\,M_{min} \;+\; c\,M_p \;+\; d\,\log m_o \;+\; q \tag{1}$$

$$M_f \;=\; B\,M_{min} \;+\; C\,M_p \;+\; D\,\log m_o \;+\; m \tag{2}$$

where T_t is the interevent time measured in years, M_{min} the surface wave magnitude of the smallest mainshock considered, M_p the magnitude of the preceding mainshock, and m_o is the moment rate per year, calculated for each source by the application of

a method suggested by Molnar (1979) which makes use of the parameters a,b of the Gutenberg and Richter relation and of the magnitude, M_{max}, of the maximum observed magnitude in each source.

The method for calculating the parameters (b, c, d, q, B, C, D, m) of these relations is described by Papazachos and Papaioannou (1993). Furthermore, relation (1) in combination with the assumption for a lognormal distribution of the observed repeat time, T, to the calculated one, T_t, has been used to estimate the probability of occurrence of the next mainshock and relation (2) has been applied to estimate the magnitude of the expected earthquake in each seismogenic source.

The variation of the values of the parameters of the relations (1) and (2) do not seem to be correlated with the seismotectonic regime of the seismogenic sources. This is strongly supported by the fact that application of this method on 93 seismogenic sources of deep focus earthquakes (h > 60 km) in several subduction zones gave values for these parameters in the same range as for the shallow earthquakes. It is the sample size used in each case which mainly affects the results.

Before any attempt to calculate the parameters of the relations (1) and (2) by the use of the data of a catalogue, a procedure of declustering of this catalogue must be applied, that is, to accurately define the foreshocks and aftershocks which are responsible for the clustering and must be omitted. Such a definition of foreshocks and aftershocks must be based on independent information and not on the data of the catalogue and the return periods of the earthquakes for which relations (1) and (2) are valid must be clearly larger than the cluster durations.

The terms "preshocks" and "postshocks" are used here for this intermediate term cluster. The preshock duration, t_p, and the postshock duration, t_a, are given by relations of the form:

$$t_p = c_p \tag{3}$$

$$\log t_a = a_a + b_a M_p \tag{4}$$

where c_p, a_a, b_a are constants and c_p and b_a are positive.

A constant preshock time as well as an increase of the postshock time with the magnitude of the preceding mainshock is expected by the time predictable model (Mogi, 1985) and has been checked by independent observations in Japan (Mogi, 1985) and in Greece (Karakaisis et al., 1991). The form of the relation (4) has been originally defined by a very large number of observations in Greece (Karakaisis et al., 1991) but was later checked by data in other regions of the continental fracture system.

The frequency, n, of foreshocks and aftershocks in the broad sense is large just before and after the mainshock, respectively, but it decreases rapidly with time, t (measured from the origin time of the mainshock) (Karakaisis et al., 1991). Data show that both relations, for foreshocks and aftershocks, have the form:

$$n = n_o t^{-p}$$

where n_o, p are parameters with positive values. From data concerning earthquakes in the continental fracture system, the value of the parameter p is 0.7 for preshocks and 0.9 for postshocks.

Relations (3), (4) and (5) have their own predictive significance because describe the way in which clustering occurs.

The magnitude used in relations (1) and (2) are the cumulative magnitude, M, which is coming from the transformation of the sum of the seismic moment of all major shocks of the sequence (preshocks, mainshocks, postshocks) by a formula suggested by Kanamori (1977). It is this magnitude which represents better the whole sequence than the magnitude of the mainshock, although the difference between these two magnitudes is usually small. In other words, the time and magnitude predictable model predicts the occurrence of a seismic sequence rather than a certain shock of the sequence.

The regional time and magnitude predictable model, expressed by relations (1) and (2) and the lognormal distribution of T/T_t has been tested in many parts of the world and the results are very satisfactory. However, the very accurate determination of the parameters of the relations (1) and (2) is still a problem because a very large number of observations are needed for this purpose.

For this reason, all available data for 16 seismic areas of the continental fracture system have been used in the present paper to calculate one value for each of the parameters of the relations (1) and (2). This is a very large sample of 1811 sets (T_t, M_{min}, M_p, M_f) with a wide range of magnitudes (5.5 - 8.6). This comes from 274 seismogenic sources for which the corresponding values of the moment rate m_o have also been calculated. The data are available in the data bank of the Laboratory of Geophysics of the University of Thessaloniki and are described in detail in the corresponding papers mentioned above.

Results

On the basis of the above mentioned sample of observations, the following two relations have been determined:

$$\log T_t = 0.19 M_{min} + 0.33 M_p - 0.39 \log m_o + 7.72 \qquad (6)$$

$$M_f = 0.73 M_{min} - 0.28 M_p + 0.40 \log m_o - 6.23 \qquad (7)$$

with a standard deviation equal to 0.28 and a correlation coefficient equal to 0.60 for relation (6) and corresponding values equal to 0.34 and 0.87 for relation (7). Relation (6) in combination with the normal distribution of $\log(T/T_t)$ can be used to calculate the probability for the occurrence of mainshocks larger than a certain value.

The relations (6) and (7) can be applied to any region of the continental fracture system or probably to any other region. Our experience is that the best way to make this application is to use the data of the region (if these data are enough) to recalculate

the last term of these relations (q and m parameters in 1 and 2) and the standard deviations, but keeping the other parameters as in (6) and (7).

If in relation (1) we omit the term cM_p and make the calculations with the same data for the continental fracture system, we find the relation:

$$\log T_t = 0.39\, M_{min} - 0.29\, \log m_o + 6.19 \tag{8}$$

with a standard deviation equal to 0.31 and a correlation coefficient equal to 0.48. This is equivalent to the empirical Gutenberg-Richter law for mainshocks and in combination with the Poisson distribution in time form the classical model for time independent seismicity.

Values of the parameters of the relations (3), (4) have been originally determined by the use of a very large sample of mainly small as well as large earthquakes (magnitude range 4.5-7.0) in the Aegean area (Karakaisis et al., 1991). These values have been checked in other seismic regions of the continental fracture system and were slightly improved. The following two relations have been finally adopted and are used in the present study:

$$t_p = 3\ yrs \tag{9}$$

$$t_a = 0.06 + 0.13\, M_p \tag{10}$$

We had a very good chance to check the validity of these two formulas for the very small preshocks and the very small postshocks of the December 20, 1990 ($M_s=5.9$) and July 20, 1978 ($M_s=6.5$) earthquakes respectivelly, which occurred in Northern Greece. The epicenters of these earthquakes are within the network of the Laboratory of Geophysics of the University of Thessaloniki which is in continuous operation since January 1, 1980 and recorded shocks of these sequences with M_L magnitude down to 2.0. The duration of the foreshock sequence of the 1990 earthquake was found equal to 2.6 years (Karakaisis, 1993b) in agreement with the relation (9). The activity in the seismogenic volume of the 1978 earthquake reached the background activity several years after the generation of the mainshock, which is in good agreement with what is expected by the relation (10).

It must be noted that relations (9) and (10) give the duration for the total cluster time of small and large earthquakes. Usually, however, this duration for the large earthquakes is much smaller, of the order of a few years and in many cases of the order of some months. Thus, the cluster time is relatively small in comparison with the mean return period for the mainshocks in the Aegean area with $M_s \geq 6.0$, for which the time and magnitude predictable model is better valid in this area.

A Statistical Test

It is of much interest to check how well the time predictable model, expressed

by relation (5) and the lognormal distribution, fits the reliable instrumental observations, in comparison with the time independent model, expressed by the Gutenberg-Richter formula and Poisson distribution. For this reason, instrumental data in the Aegean area (1901-1992) for mainshocks with $M_s \geq 5.5$ have been used. For this reason, the last term of relation (6) was recalculated by the use of these data and a value equal to 7.78 was obtained with a standard deviation equal to 0.30. For this test the following procedure was applied.

For each of the seismogenic regions of the Aegean area and for each possible decade just after the occurrence of the first mainshock and up to the occurrence of the last mainshock (e.g. 1901-1910, 1902-1911, ..., 1983-1992) the probability for the occurrence of a mainshock with magnitude $M_s \geq 5.5$ was calculated by the time predictable model and a corresponding "yes" or "no" was assigned to each decade if such mainshock had occurred or not in this decade. Then, the total range of the calculated probabilities were separated in equal intervals with a step of 0.1 (0.0-0.9, 0.1-0.19, ...) and all decades were groupped in these intervals according to their probabilities. Finally, the ratio, λ, of the number of "yes" to the total number (yes + no) of decades was calculated for each group. The same procedure was repeated by calculating probabilities for the occurrence of the mainshock on the basis of the time independent model (Gutenberg and Richter law for distribution in mangitude, Poisson law for the distribution in time).
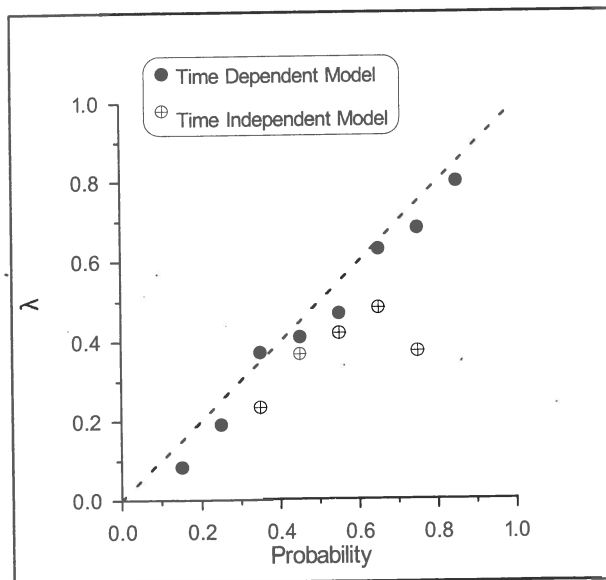

Fig. 1. Success ratio, λ, versus calculated probability for time dependent (dots) and time independent (open circles with crosses) model.

The results of this test are shown in Figure (1), where success ratios, λ, are plotted against probabilities, P, for both the time dependent model (dots) and the time independent models (open circles). The line $\lambda = P$, which means full success, is also shown. The superiority of the time predictable model for mainshocks of this range of magnitude ($M_s \geq 5.5$) in the Aegean area is clear.

References

Bufe, C.G., P.W. Harsh, and R.D. Burford, 1977. Steady state seismic slip: A precise recurrence model. Geophys. Res. Lett., 4, 91-94.

Davis, P.M., D.D. Jackson, and Y.Y. Kagan, 1989. The longer it has been since the last earthquake the longer the expected time till the next? Bull. Seism. Soc. Am., 79, 1439-1456.

Gutenberg, B., and C.F. Richter, 1944. Frequency of earthquakes in California. Bull. Seism. Soc. Am., 34, 185-188.

Kagan, Y.Y., and D.D. Jackson, 1991. Long term earthquake clustering. Geophys. J. Intern., 104, 117-133.

Kanamori, H. 1977. The energy released in great earthquakes. J. Geophys. Res., 82, 2981-2987.

Karakaisis, G.F., 1993a. Long term earthquake prediction in the New Guinea - Bismarck sea region based on the time and magnitude predictable model. J. Phys. Earth, 41, 365-389.

Karakaisis, G.F., 1993b. A microseismicity precursor before the December 21, 1990 earthquake ($M_s = 5.9$, Northern Greece). Proc. 2nd. Congr. Hellenic Geophys. Union, Florina, May 5-7, 1993.

Karakaisis, G.F., 1994a. Long term earthquake prediction along the north and east Anatolian fault zones based on the time and magnitude predictable model. Geophys. J. Int., 116, 198-204.

Karakaisis, G.F., 1994b. Long term earthquake prediction in Iran based on the time and magnitude predictable model. Phys. Earth Planet. Inter., 83, 129-145.

Karakaisis, G.F., E.M. Kourouzidis, and B.C. Papazachos, 1991. Behaviour of seismic activity during a single seismic cycle. In: Earthquake Prediction: State of the Art, Council of Europe, Strasbourg, France, October 15-18, 1991, 47-54.

Molnar, P., 1979. Earthquake recurrence intervals and plate tectonics. Bull. Seism. Soc. Am., 69, 115-133.

Mogi, K., 1985. Earthquake Prediction. Academic Press, San Diego, Calif., 355pp.

Panagiotopoulos, D.G., 1993. Long term earthquake prediction in the Philippines region based on the time and magnitude predictable model. Proc. of the 2nd

Congr. of the Hellenic Geophys. Union, Florina 5-7 May 1993, 472-481.

Panagiotopoulos, D.G., 1994a. Long term earthquake prediction along the seismic zone of Solomon islands and New Hebrides based on the time and magnitude predictable model. Natural Hazards (in press).

Panagiotopoulos, D.G., 1994a. Long term earthquake prediction in central America and Carribean Sea based on the time and magnitude predictable model. Proc. of the 7th Congr. Geol. Soc. Greece, Thessaloniki 25-27 May, 1994 (in press).

Papadimitriou, E.E., 1993. Long term earthquake prediction along the western coast of south and central America based on a time predictable model. Pure Appl. Geophys., 140, 301-316.

Papadimitriou, E.E., 1994a. Long term earthquake prediction of large shallow mainshocks along the Tonga-Kermadec-New Zealand seismic zone based on a time- and magnitude predictable model. Tectonophysics, 235, 347-360.

Papadimitriou, E.E., 1994b. Long term earthquake prediction in the north Pacific seismic zone based on the time and magnitude predictable model. Natural Hazards, 9, 303-321.

Papadimitriou, E.E. and B.C. Papazachos, 1994. Time dependent seismicity in the Indonesian region. J. Geophys. Res., 99, 15387-15398.

Papazachos, B.C., 1988a. Seismic hazard and long term earthquake prediction in Greece. European School of Earthquake Sciences, Course on Earthquake Hazard Assessment, Athens, 9-16 May 1988, 1-10.

Papazachos, B.C., 1988b. Long term prediction of earthquakes in seismotectonic sources of Greece. United Nations Seminar on the prediction of earthquakes, Lisbon, portugal, 14-18 November 1988, 1-10.

Papazachos, B.C., 1989. A time predictable model for earthquake generation in Greece. Bull. Seism. Soc. Am., 79, 77-84.

Papazachos, B.C., 1992. A time and magnitude predictable model for generation of shallow earthquakes in the Aegean area. Pure Appl. Geophys., 138, 287-308.

Papazachos, B.C. and Ch.A. Papaioannou, 1993. Long-term earthquake prediction in the Aegean area based on a time and magnitude predictable model. Pure Appl. Geophys., 140, 593-612.

Papazachos, B.C., E.E. Papadimitriou, G.F. Karakaisis and Th.M. Tsapanos, 1994a. An application of the time and magnitude predictable model for the long term prediction of strong shallow earthquakes in the Japan area. Bull. Seism. Soc. Am., 84, 426-437.

Papazachos, B.C., G.F. Karakaisis, E.E. Papadimitriou, Th.M. Tsapanos and Ch.A. Papaioannou, 1994b. Time dependent seismicity in the Alpine-Himalayan belt. Proc. of the 7th Congr. Geol. Soc. Greece, Thessaloniki 25-27 May, 1994 (in press).

Shimazaki, K. and T. Nakata, 1980. Time predictable recurrence of large earthquakes. Geophys. Res. Lett., 7, 279-282.

Scholz, C.H., 1982. Earthquake prediction without precursors (abstract), Eos Trans AGU, 63, 583.

Sykes, L.R., and R.C. Quittmeyer, 1981. Repeat times of great earthquakes along

simple plate boundaries. In: Earthquake Prediction, An international Review, D.W. Simpson, and P.G. Richards, Editors, Maurice-Ewing Series, Amer. Geophys. Union 1981, 4, 297-332.

Thatcher, W., 1984. The earthquake deformation cycle, recurrence, and the time predictable model. J. Geophys. Res., 89, 5674-5680.

THE DETECTION
OF ULTRASONIC PRECURSORS OF AN EARTHQUAKE
USING MULTIPLE-BEAM INTERFEROMETRY

A.Suladze and V.Sukholinin

Institute of Structural Mechanics & Earthquake Engineering
Georgian Academy of Sciences, Tbilisi, Georgia

Abstract

There are many sources of acoustic waves which interfere with the detection of faint vibrations initiated in the crust long before an earthquake.The paper presents a method which allows us to isolate the useful signal from the interference.

Introduction

Mogi [1962] has demonstrated that it is possible to predict the occurrence of a major rupture, when stress is applied to heterogeneous materials such as rocks and concrete. Heterogeneous materials contain many weak places. Local fractures occur at these places even at low-stress levels, and gradually increase as the stress level rises. Accordingly, acoustic emission due to microfractures gradually begins to increase, accelerating sharply just prior to the break.

The occurrence of local fractures in the crust is accompanied by acoustic emission. At the same time there are many extraneous sources of acoustic waves which interfere with the detection of faint vibrations initiated in the crust long before an earthquake.

We have found out a method which allows us to isolate the useful signal from the interference.

General Principles

1. We detect a SIGNAL of Acoustic Emission which occurs when the stress level in the earth's crust rises. All other vibrations we consider as a NOISE.

2. The spectral distribution curve of energy of acoustic emission has a maximum and this shifts towards the region of higher frequencies as the stress level rises.

At high-stress levels before earthquakes ultrasonic vibrations at frequencies of 50 kHz and above become significant enough to be isolated from the interference.

3. In this frequency range the Sensitivity Improvement is not only possible because of a low level of interference, but it is also necessary as high-frequency vibrations, which are weak even near the source, attenuate rapidly on passage through a medium.

4. It is possible to detect ultrasonic vibrations Far From The Epicentre, because the stress level rises not only in the hypocentre of the coming earthquake, but in a big area around it. Local fractures occur in this strained area. So there are sources of acoustic emission far from the future epicentre.

Instrument Description

In our observations we use a Fabry-Perot interferometer. It is mounted on a steel plate fastened to the rock. The He-Ne laser with wavelength $\lambda = 630$ nm is used as a light beam source. A beam intensity I on the outlet of the Fabry-Perot interferometer depends on the distance d between mirrors, and is at its maximum when $d = m(\lambda/2)$, m =1,2,3,...

The plot of $I=f(d)$ has a form of narrow peaks, and their width depends on the mirrors' reflectivity R. At R = 0.99 the half-width of lines δ (width at half of maximum) is approximately 300 times smaller than the distance between the nearest peaks.

If the interferometer is adjusted for one of the peaks, it allows us to detect vibrations with amplitude $A \ll \delta$. The detection limit is determined by an optical noise of a laser beam.

Signal is analysed by an electronic device.

Observations and Results

We detected precursors even of small earthquakes at epicentral distances of about 100 km.

The most important are signals detected after relatively long period of quiescence when it is absolutely clear that these are precursors, not phenomena due to previous events.

A period of time from the first changes in the signal level till the moment of the occurrence of an earthquake depends on the energy of an expected earthquake. The higher the energy the longer this time interval.

| Events	Precursors
July 4, 1991, M = 5.8 epic.dist. = 95 km	Changes in the 60 kHz acoustic vibrations level were noticed from June 27. The signal level rose rapidly to about 10 times the normal value 1 hour before the main shock, and dropped gradually to the normal value over a period of 3 hours after the main shock.
May 4, 1993, M = 4.8 epic.dist. = 85 km	First changes in the signal level were observed 40 hours before the earthquake.
July 1, 1994, M = 4.1 epic.dist.=90 km	Ultrasonic precursors were recorded 3 hours before the earthquake.
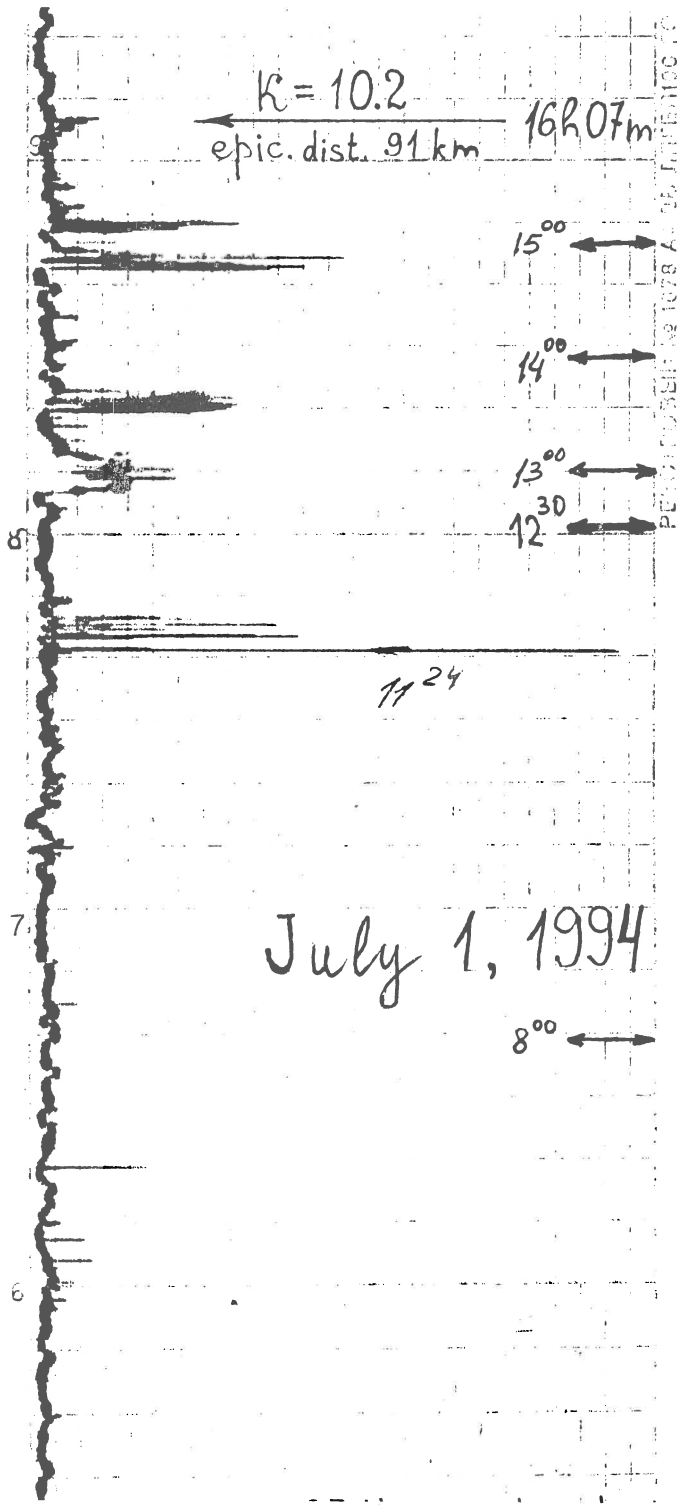
Figure 1: Changes in the 25 kHz acoustic vibrations level before a small earthquake. M=4.1, Δ=90 km.

Conclusions

Observations show that it is possible to detect ultrasonic precursors of an earthquake.

In order to pass from investigations to practical earthquake prediction it is necessary to have a set of stations.

References

Born, M. and E. Wolf, 1968. Principles of optics. Pergamon Press, Oxford.

Fabry, C. and A. Perot, 1899. Ann.Chim.Phys., 16, 115.

Mogi, K., 1962. Study of elastic shocks caused by the fracture of heterogeneous materials and their relation to earthquake phenomena. Bull.Earthquake Res.Inst., Univ.Tokyo, 40, 125-173.

Mogi, K., 1985. Earthquake Prediction. Academic Press, Tokyo.

Suladze, A.S. and V.L. Sukholinin, 1991. The registration of acoustic emssion before an earthquake. Bull.of Georgian Academy of Sciences, 14, #3, 377-379.

Alexander Suladze and Vladimir Sukholinin, Institute of Structural Mechanics and Earthquake Engineering, Georgian Academy of Sciences
1 Rukhadze St., Tbilisi, 380093, Republic of Georgia

DEVELOPMENT OF A TELEMETRIC SYSTEM FOR OBSERVATION OF RADIOEMISSION ASSOCIATED WITH EARTQUAKES IN CRETE ISLAND.

K. Nomikos[1], M. Bakatsakis[2], D. Paterakis[2], T. Kogionis[2], S. Sideris[2], B. Zaxaropoulos[2], C. Cristou[2], I. Kaliakatsos[2] and F. Vallianatos[3].

[1] Technological Educational Institute,Piraeus, Greece.
[2] Technological Educational Institute of Crete,Crete,Greece
[3] Technical University of Crete,Chania 73110,Crete, Greece.

Abstract

A description of the telemetric system which is working unattended and records the electric field variations of the Earth, in four field stations in Crete island, is presented. In each station we measure, using tuned antennas, the two horizontal components of the electric variation in low (i.e. 3 and 10 kHz) and high (i.e. 41 and 53 MHz) frequencies.

Recordings for a two year period observation and a possible association of anomalous variation of the electric field, with local earthquakes, are presented. The results suggest radioemission prior to earthquake in the vicinity of Crete island and this phenomenon is important for the study of earthquake process and earthquake prediction.

Introduction

In geophysical literature much attention has been given into the problem of electromagnetic (RF) emission prior to earthquakes (Gokhberg et al, 1982; Takahashi and Takahashi, 1989; Fujinawa and Takahashi, 1990; Fraser-Smith et al, 1990). In the present paper a telemetric system which is installed in Crete Island, in order to observe radioemission prior to earthquakes, is described. The system records the earth's electric field variations in four field stations installed along Crete island (see Fig.1). The Central station is installed in Chania.

In each field station we measure, using tuned loop antennas, the two horizontal components of the electric field variations in low –LF- (3 and 10 kHz) and high –HF- (41 and 53 MHz) frequencies. The system is based in a data-loger installed in the field station, which digitizes the information and stores them in its memory. The central station uses a computer which communicates with the data-logger and collects the data via a standard telephone line and finally plots the recordings. The telemetric system has been designed to work unattendedly. Data from the telemetric system for a time period of almost two years are given.

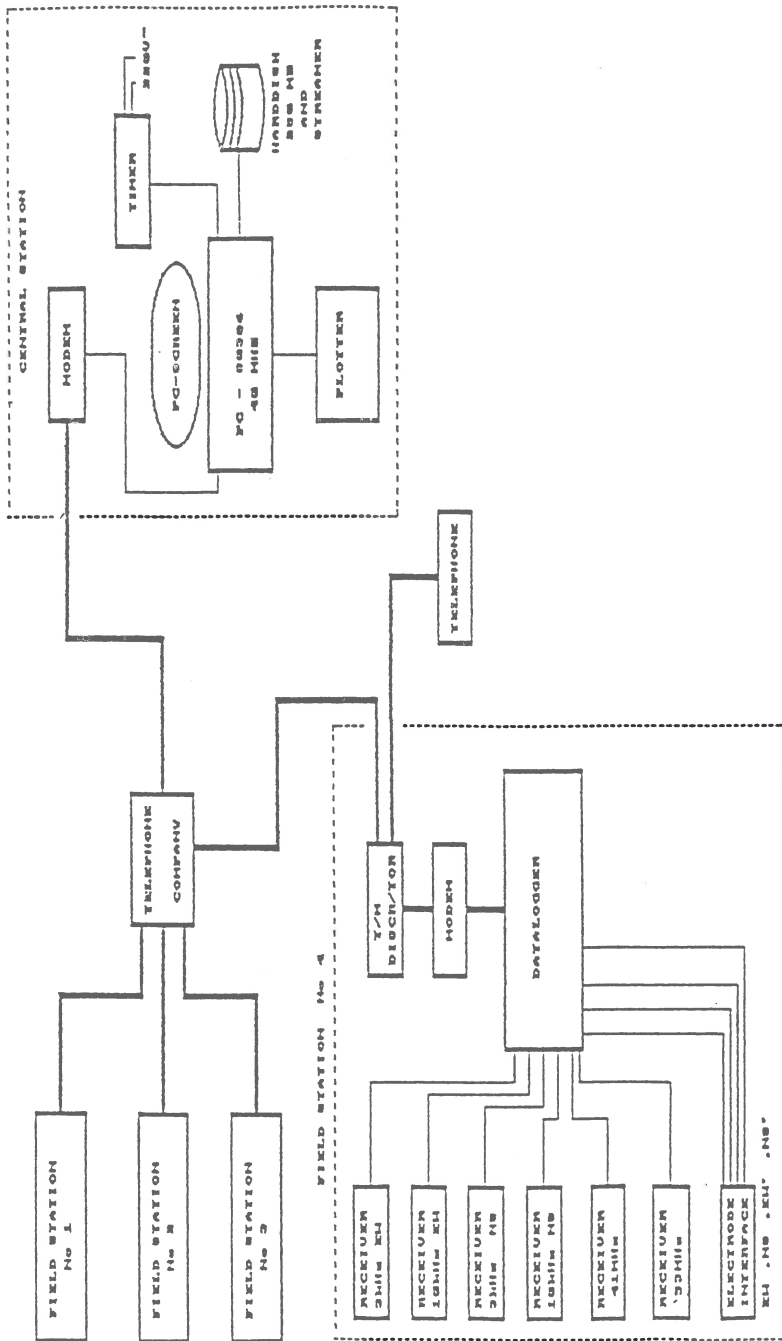Mailing address:111 Homirou St.,Moschato 18345,Athens,Greece.

Figure 1 Configuration of the Telemetric network.

Field Station arrangement.

In each field station the following instruments are used (fig. 1):

1) four receivers appropriate for measuring the electric field variations at 3 and 10 KHz into EW and NS directions. These receivers are constructed using wide band and low noise amplifiers and switching band-pass filters which are tuned via crystal oscillators. The final stage of the receiver is an RMS to DC converter. Thus, the output of the receiver is a DC voltage which is proportional to the input amplitude of the electric field which excites the antenna (fig.2b).
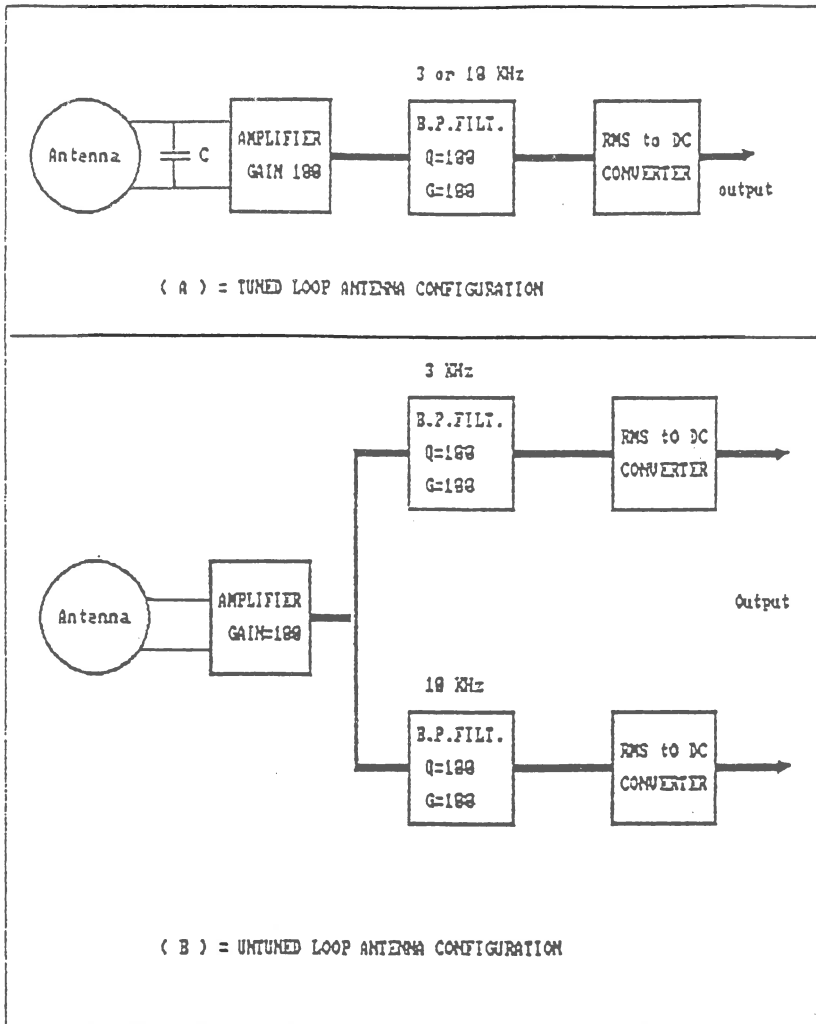

Figure 2 Configuration of the low frequencies receivers.

For observations in the low frequency region (i.e. 3 and 10 kHz) tuned antennas are constructed. The voltage across the tuned antenna is given by (Radio Amateur Handbook, 1991):

$$V= k\,E, \qquad k =2\pi ANQ/\lambda \tag{1}$$

where A is the area of the antenna, N the wire revolutions, Q the quality factor, λ the wavelength and E the electric field.

The signal to noise ratio (SNR) in the output of the tuned antenna is:

$$SNR= 66.3\ N\ A\ E\ \sqrt{(Q\ f/L)}\ /\ \sqrt{W_b} \tag{2}$$

where W_b is the frequency bandwidth of the receiver and L the inductance of the antenna.

In order to maximize the requirements, concerning gain and signal to noise ratio, we choose a wire diameter of 0.3mm and an antenna diameter of 1m, giving us N=165 revolutions for the 3 kHz tuned antenna and N=56 revolutions for 10 kHz, and thus k=0.1; Q and SNR for both frequencies were 12 and 10 respectively.

At the first stage of the experiment untuned antennas were used. The configuration of them is shown in fig.2a. Formulas (1) and (2) are still valid, but with the factor Q=1.

For untuned antennas, the coefficient $k=2\pi AN/\lambda$ is proportional to the tuned receiver frequency. The latter implies that if the recording voltage outputs have the same amplitude for all the measured frequencies, then the variation of the electric field is inversely proportional to the measured frequency.

2) Two receivers for measuring the electric field variations at 41 MHz and 53 MHz. The receivers are constructed using double supper heterodyne technology and the output in each of them is a DC voltage which is proportional to the input amplitude of the electric field which appears on the antenna. The antennas used for these very high frequencies are horizontal $\lambda/2$ dipoles tuned at the above frequencies.

3) a data-logger which is the main instrument for reading the analog information from the RF receivers. The data-logger used in the field station, is that of Campbell Scientific (model 21X). The sampling rate was taken on a channel basis every second, and the average value of 60 samples for each channel saved in the final memory (see Nomikos and Chatzidiakos, 1993; Vallianatos and Nomikos, this issue).

Instrumentation of the Central Station.

The Central station equipped with a personal computer PC, a fast plotter, a switched telephone line, a digital timer which switches on the computer every night for a time period of 30 minutes in order to communicate with the field stations and a standard CCITT smart modem V21/V22. In fig.1 we see the instrumentation arrangement of the telemetric system. Using telecommunication software we communicate with the data-logger in the field station, unattended in order to collect the data from the field stations data-logger's memory in a similar way as described by Nomikos and Chatzidiakos (1993).

Experimental results

The measurements obtained from the telemetric network for a period of almost two years are separated into three main stages, according to the development of the network.

1) First stage :from 15 March 91 to 15 April 91

During this period there was only one field station at Nipos Apokoronou (Chania). The station was working on an experimental basis in order to study the

communication problems between central and field stations and to learn about the noise level at low frequencies ranging from 1 to 20 KHz. The frequencies chosen during this period were 1.25, 2.5, 10 and 20 KHz. On March 18, 1991 and with duration of the order of 1.5 day, disturbances of the same amplitude were observed, at all the frequencies (fig.3 is such a typical 4 hour recording). On March 19, 1991 near Ierapetra (Koufonisi island) three earthquakes recorded - 5.8 (12:0), 4.7 (20:06) and 5.2 (21:29)-which may be related with the observed electromagnetic variations. The fact that the variations were of the same order of magnitude leads to the conclusion that the change in the electric field follows the law ΔE 1/f. Therefore we establish a criterion that for untuned antennas the recorded electromagnetic disturbances are related to earthquake events if they obey the latter law.
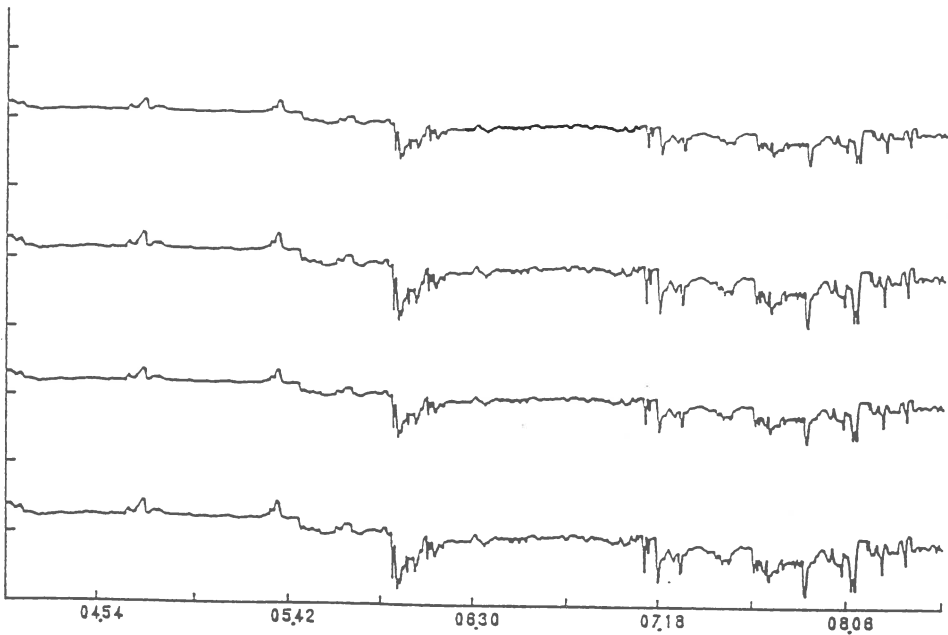

Figure 3 A typical 4h recording of Nipos station on March 18, 1991 of low frequencies during 1.5 day signals.

2) Second stage : From 1 November 91 to 30 May 92.

During this period two field stations were installed one at Nipos Apokoronou (Chania) and the other at Anatoli (Ierapetra). For low frequencies an untuned loop antenna was used. These measurements were carried out at two frequencies, 5 and 10 KHz. Furthermore, two tuned $\lambda/2$ antennas in 41 and 53 MHz were installed. We proceed now to the discussion of the results obtained during the second stage. Table 1 shows all the earthquakes with magnitude greater than 4.9^R in the area of

1116

Crete (latitude 34–37, longitude 22–28) during the time window November 1, 1991–August 31, 1993, which covers all the stages of the experiment. Fig.4 shows the earthquakes during this period and the numbering of the position refers to the same numbering of table 1. On the same figure we can see that the positions of the field stations are inticating with their initial (N=Nipos, I=Ierapetra, H=Heraklio and D=Drapania; H and D Stations are installed latter on the third stage).

TABLE 1

| a/a	Y	M	D	T	Lat.	Long.	Mag	Dep.
1	92	01	9	13:45:26.4	36.34N	22.85E	4.9	17
2	92	01	29	13:39:51.2	35.00N	27.16E	5.3	98
3	92	03	20	05:37:24.5	36.66N	24.58E	5.3	4
4	92	03	21	11:47:28.0	35.33N	27.29E	4.9	10
5	92	04	21	17:42:39.4	34.43N	26.63E	5.1	1
6	92	04	30	11:44:28.6	34.26N	27.33E	6.4	21
7	92	05	3	08:35:36.6	35.04N	26.83E	5.1	7
8	92	07	31	23:13:13.1	34.41N	26.93E	4.9	39
9	92	08	11	08:21:39.5	34.41N	27.06E	5.1	1
10	92	11	21	05:07:19.4	35.58N	22.39E	6.0	70
11	93	01	27	23:41: 1.0	36.02N	22.36E	5.4	120
12	93	06	1	09:45:25.2	34.07N	26.25E	5.2	1
13	93	06	29	04:37:12.5	35.39N	27.07E	5.5	1
14	93	08	18	12:09:26.1	35.15N	26.11E	5.2	72
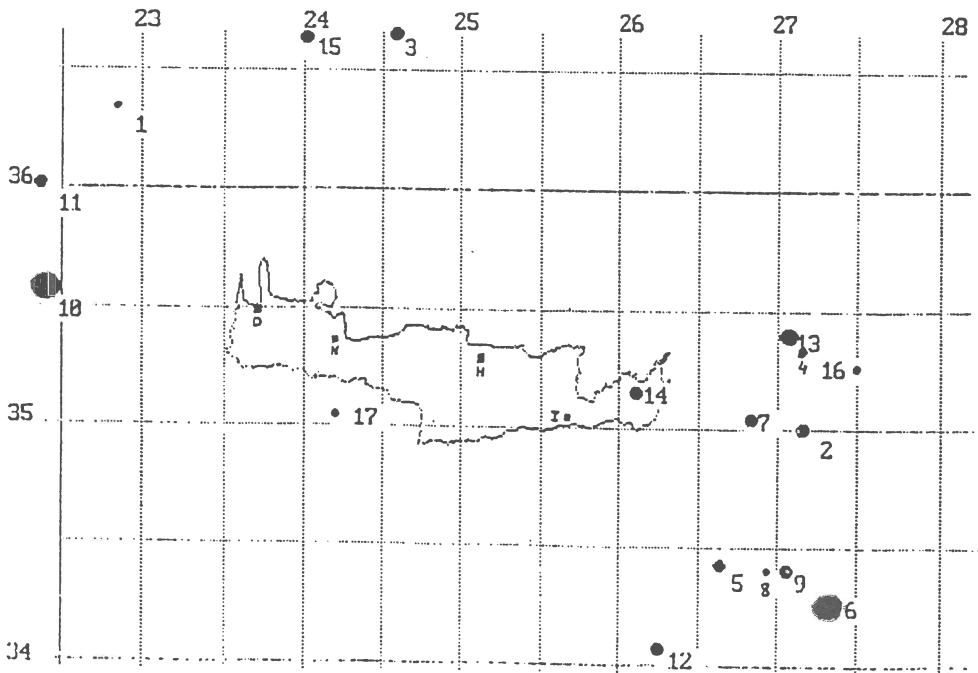
Figure 4 Distribution of the epicentre of earthquakes with Ms›4.9 which occured near Crete, from November 1st, 1991 to August 31st, 1993.

The criterion for the recognition of signals during the second stage, with the setup of untuned antenna, was that the low frequency signals of 5 and 10 KHz should both be of the same amplitude. For the high frequencies, 41 and 53 MHz, the only criterion should be the existence of signals in both components simultaneously, otherwise they could be man-made interference (e.g. from radio stations) even though these frequencies were checked with radio receivers for long periods of time, to make sure that they were silent. Any interference from mobile transmitters at these two frequencies obviously will produce spikes on the recordings for a period of at most a few minutes and in the specific frequency of the transmitter and not simultaneously in both of them.

The most important signals during this period are shown in Table 2. The values presented in this table, for low frequencies LF (5 and 10 KHz) correspond to maximum signal in the antenna. Beside the values, the initial letter of the recording station is written.

During the time period from June 1992 to the end of September 1992 the structure of the telemetric system changed by adding two new field stations in the area of Heraklion and Drapania-Kisamou (Chania). In all the field stations the instrumentations of low frequencies (antennas and receivers) replaced by new tuned loop antennas at 3 and 10 KHz and new receivers, having higher sensitivities. During the period of these changes and trials the telemetric network was not operating and therefore no signals were recorded for earthquakes 8 and 9 of Table 1.

3), Third stage: from 1 October 92 to 31 August 93.

During this stage we collect data from all field stations at low frequencies (3 and 10 KHz), in the directions EW and NS using tuned loop antennas. Therefore during this period the recordings of the signals between 3 and 10 Khz should follow if possible the

TABLE 2

LF	HF	a/a EQ
50μV-N ,100μV-I 1-1-92 00:00-12:00 GMT	4 db(μV)-N, 1 db(μV)-I 00:00-16:00 GMT	1
No signals	3 db(μV)-N, 1 db(μV)-I From 7:00 on 28-1-92 to 16:00 of 29-1-92	2
10μV-N, 20μV-I from 11:00 (17-3-92) to 16:00 (18-3-92)	2 db(μV)-N, 1 db(μV)-I from 4:00 (17-3-92) to 17:00 (18-3-92)	3,4
~2μV-N ,50μV-I from 22:00 (19-4-92) to 14:00 (20-4-92)	HF signals appeared from 8:30 (19-4-92) to several days with diferent amplitudes	5,6,7

TABLE 3

3KHz	10KHz	41MHz	53MHz	EQ
120μV-EW-N	20μV-EW-N	6 db(μV)-D	6 db(μV)-D	
160μV-EW-H	30μV-EW-H	8 db(μV)-H	8 db(μV)-H	
40μV-EW-D	15μV-EW-D	2 db(μV)-N	3 db(μV)-N	10
80μV-NS-N	70μV-NS-N	Signals from 1:00 GMT of		
80μV-NS-H	50μV-NS-H	19-11-92 to 22:00 GMT of		
20μV-NS-D	20μV-NS-D	20-11-92 .		
From 13:15 to 13:25 GMT on 17-11-92				

ratio 3:1. In Table 3 the signals are shown which are recorded prior to the isolated in time earthquake with magnitude 6.3^R (No. 10 of table 1).

In order to compare the noise level between tuned and untuned antennas, from January 18,1993 to August 27,1993 the tuned antennas in EW direction replaced with untuned ones in the same direction. On August 28, 1993 the tuned antennas in the direction EW at all stations were reinstalled, except Ierapetra's because in this station the noise level was low. Table 4 shows the signals observed from January 18, 1993 to August 31, 1993.

By inspecting tables 1,2,3 and 4 we see that the most important earthquakes which take place in the area of Crete during the time period October 1,1992 -August 31,1993, where the four stations were operated, were:

1) The earthquake West of Crete (Nov. 21, 1992) with magnitude 6.3^R (No. 10 of table 1), which was quite strong and "isolated in time".

2) The earthquake on August 18, 1993 with magnitude 5.2^R (No 14 of table 1), near Sitia town, which was quite close to stations Heraklion and Ierapetra.

TABLE 4

3KHz	10KHz	41MHz	53MHz	EQ
100μV-NS-N 30μV-NS-N 19:30-19:45 GMT 27-1-93 HF Signals start at 3:30 GMT on 27-1-93 to 2:00 GMT of 28-1-93		6 db(μV)-D 3 db(μV)-D ----- 2 db(μV)-N		11
No signals up to 10 days before				12
140μV-EW-I 140μV-EW-I (ratio 1:1) 100μV-NS-I 30μV-NS-I (ratio 3:1) 8:45 έως 10:00 GMT της 28-6-93		2 db(μV)-D 4 db(μV)-D 1 db(μ)V-N 3 db(μV)-N Signals from 8:00 to 14:00 to 28-6-93		13
200μV-EW-N 80μV-EW-N 180μV-EW-I 160μV-EW-I (ratio 1:1) 120μV-EW-D 40μV-EW-D 160μV-NS-N 50μV-NS-N 100μV-NS-I 30μV-NS-I 50μV-NS-D NS-D: out of order HRA LF: out of order Signals from 15:30 to 15:45 GMT on 9-8-93		Signals different amplitudes from 2:00 GMT to 19:00 of 15-8-93 at stations HRA, NIP ,DRAP Stonger signals at HRA		14

We proceed now to discuss the electromagnetic variations which precede the aforementioned earthquakes.

1) Electromagnetic variations prior to the November 21, 1993 earthquake .

The electromagnetic variations recorded prior to the Nov. 21, 1993 earthquake:

(i) At the low frequencies, 3 and 10 KHz, on Nov.17, 1992 and at 13:15 GMT time, for a time period of 15 minutes a simultaneous electromagnetic variation were recorded, at the three stations (i.e. Drapania, Nipos and Heraklion) and at both directions EW (the stronger one) and NS. The ratio of these variations at the two frequencies deviates from 3:1 only in the NS direction. The strongest signal appeared in Heraklion station and the weakest in Drapania station. Ierapetra station being the furthest away from the epicenter of the earthquake, did not record any signal.

(ii) At high frequencies the electromagnetic variations started mainly from 1:00 GMT of Nov. 19, 1992 and continued until 22:00 GMT of the same day, even though slight variations did continue over the next day. From the recordings it can be seen that the strongest signals were recorded at the nearest (to the epicenter) station of Drapania.

2) Electromagnetic variations prior of Sitia earthquake on August 18,1993.

This earthquake presents a great interest because it is the nearest to the stations of Ierapetra and Heraklion. The signals recorded prior to this earthquake were the following:

(i) On August 9, (15:30 GMT) at low frequencies of 3 and 10 KHz, electromagnetic variations of duration of about 10 to 15 minutes were recorded simultaneously by the stations of Drapania, Nipos and Ierapetra. The latter were recorded at both EW and NS components, strongest being the EW component. At Ierapetra in EW direction as mentioned already, we had an untuned antenna and it is just as well that the ratio of the signals at the two frequencies is approximately 1:1, but at NS with tuned antennas the ratio was 3:1.

(ii) At high frequencies 41 and 53 MHz electromagnetic variations observed on August 15,1993 (from 2:00 GMT to 19:00 GMT) at the stations of Drapania, Heraklion and Nipos. The strongest variations were recorded at Heraklion station. We mention that the Ierapetra station did not picked up any high frequency signals.

Conclusions

Summarizing the results of the present paper we can state that :

(1) a telemetric system appropriate for the measurement of electromagnetic emission prior to earthquakes designed.

(2) the experimental data indicates the existence of radioemission in the frequencies of 3 and 10 kHz and 41 and 53 MHz, prior to earthquakes in the vicinity of Crete island.

Acknowledgments

REFERENCES

Fraser-Smith, A.C., P.R. Bernardi, P.R. McGill, M.E. Ladd, B.A. Halliwell and O.G. Villard, 1990. Low -frequency magnetic field measurements near the epicenter of the 7.1 Loma Prieta earthquake. Geophys. Res. Lett., 17, 1465- 1467.

Fujinawa, Y. and K. Takahashi, 1990. Emission of electro-magnetic radiation preceding the Ito seismic swarm of 1989. Nature 347, 376–378.

Gokhberg, M.B.,V.A.Morgounov, T.Yoshino and I. Tomozawa.1982. Experimental measurement of electromagnetic emissions possibly related to earthquakes in Japan. Journal of Geophysical Research 87, B9 ,7824–7828.

Loop antennas, Chap.5 of Radio Amateur Handbook (Ed.), 1991.

Nomikos, K. and P. Chatzidiakos, 1993. A telemetric system for measuring electrotelluric variations in Greece and its application to earthquake prediction. Tectonophysics 224, 39-46.

Takahashi, H. and K. Takahashi, 1989. Tomography of seismo–radio wave source regions for predicting imminent earthquakes. Phys. Earth Planet. Inter.,57,40-44.

Description of a real-time system appropriate for the
subtraction of the inductive component from electrotelluric
recordings. An application to earthquake prediction.

F. Vallianatos[1] and K. Nomikos[2]

(1) Technical University of Crete,Chania 73110,Crete,Greece.
(2) Technological Educational Institute, Piraeus, Greece.

ABSTRACT
    A system for the real time subtraction of the inductive
component from the total variation of the electric field of
the Earth is described. The system is working unattended and
is based on communicating between a datalogger and a PC. An
application of the above system for a better identification
of the electric signal which is preceded by an earthquake in
West Greece is presented. Furthermore, a qualitative approach
on the form of the preseismic electric variations, based on
the charge dislocation model is given.

Introduction
    Over the past few years intensive efforts have been made
to study the use of electrotelluric field variations in the
short-term prediction of strong shallow earthquakes mainly in
North-North Western Greece (Varotsos et al., 1993 and
references therein).
    The instrumentation used, on the most of the monitoring
electrotelluric stations, based on a datalogger technique
(Nomikos and Chatzidiakos, 1993). The latter has been
developed over the last years to a large extent, especialy
for communications and data storage in personal computers.
Using dataloggers for the storage of magnetotelluric
measurements we determine the impedance tensor between
electric and magnetic field variations, for different
stations located in Greece (Vallianatos,1989; Hadjioannou et
al.,1993).Using the impedance tensor elements' the telluric
inductive component could be subtracted from the
electrotelluric recordings.
    The resulting real-time recording of the residual
electric field allows a better indentification of any
preseismic electric variation. Furthermore, the precise
determination of the form of preseismic electric variation
generally could be an index of the evolution of deformation
during the preparation stage of an earthquake (see Appendix).
    It is the scope of the present paper to describe a system
that measures and stores the magnetotelluric variations with
the help of dataloggers which is installed in the field
station.At the Central station, a personal computer
communicates with the field station via a leased telephone

Mailing Address:111 Homirou St.,Moschato 18345,Athens,Greece.

line, collects the data from the memory of the datalogger and stores them into the hard disk of the computer. A special software written for this purpose restore the data file from the hard disk and then creates a new file with the data of the non-inductive component of the Earth's electrotelluric field.Both the initial and after processing files are plotted using a fast plotter for visual display. Furthermore, the data are stored on a back-up tape streamer in compressed mode for further processing. The system works unattended.

Instrumentation of the field station

The instrumentation used in the field station for data collection consisted of a datalogger - Campbell Sc., Inc., model 21X - (with an 14 bit A/D convertor), a modem for the communication with the central station, and one set of magnetotelluric equipment. The sampling rate was set at one sample per second. To reduce the noise in our recordings a passive RC filter was used to cut off all the electromagnetic variations with period less than 1 sec . The filter was used in both electric and magnetic channels. The electric field was measured with an electrode spacing of the order of one hundred meters. The dipoles were deployed in north-south (NS) and east-west (EW) directions and made use of $Pb-PbCl_2$ electrodes. The time derivative of the magnetic field was measured in NS and EW directions by using two induction coil magnetometers. The datalogger is programmed for full scale range ± 50mV for the channel of electric recordings and ±500 mV for the magnetic one, with resolutions ±3.3μV and ±33 μV, respectively. The samples for each of the four channels are saved in the final memory of the datalogger which is able to store data without overlapping for a time period approximately of about 40 minutes. Within this time period the central station has to communicate with the datalogger in order to fetch the collected data file to the central station. We point out that the consumption of the data-logger for the above sampling rate is 5mA at 12Vdc. The supply is held from an internal rechargable battery 12V , 2.5 Ah. A small "pack charger" charges the internal battery if the station has access to 220v ac, otherwise a small solar panel is fitted directly eliminating the 220 V mains.

A modem (model DC112 of Campbell Sci.,) is mounted to the serial port of the datalogger and communicates with a V22 mode (1200 bits/sec) in full-duplex mode. This modem has a special construction and does not follow the standard RS232 protocol concerning the digital data voltage level in order to reduce power consumption. For the aforementioned reason the modem circuit is switched off, except for the ring sensor. In this way the current consumption reduced from 30 mA to a few μA when the modem is in the hook-off condition.

In the case of leased telephone network the smartmodem DC112 modified by an external circuit which triggers the ring circuit of the modem when a 1300 Hz signal appears at the input of the circuit. The aforementioned signal normally is send from central's station modem when communication begins. The external circuit has a threshold sensitivity of -30 dbm

which is reasonable for leased networks.

Instrumentation of the Central Station.

The Central station has only commercial instrumentation consisting of a personal computer with high resolution color monitor and a mathematical coprocessor, a fast plotter (Grathtec FR6302R), a switched or leased telephone line, and a standard CCITT smartmodem V22. Using telecommunication software (Telecom), the computer communicates with the datalogger in the field station and all the stored (since the last call) data, into the datalogger's memory, are transfered into the hard disk of the PC, creating a file which usually has the name of the field station. Another file is used to save the communication parameters of the station (e.g the baud rate). The communication protocol of the above software gives reliability 99.998 % for the transfered data. The data are transmited in blocks of 512 bytes followed by the security communication protocol. If the central station receives the data with errors (e.g due to noise in telephone line), it requires from the datalogger to retransmit the block of data. Each time that the Central Station communicates with the datalogger the collected data are stored into the hard disk, in an append file.

The system has designed to be automatic and is unattended A software (written in Turbo-Basic), uses the file of the stored data and divides it into files of 4096 samples. These files are stored temporally on a different subdirectory of the hard disk and permanently on a tape streamer every day, upon request. When the first file of 4096 samples is formed, an approptiate software (written in FORTRAN) proceeds to the subtraction of the telluric inductive component from the original ellectrotelluric recordings, reading both the stored file of the 4096 recording and the file of those already estimated, for the particular station, impedance tensor elements. Since the values of e_x, e_y, h_x and h_y in time domain are read, the program proceeds to obtain a Fast Fourier Transform (FFT) of them in order to convert the time domain values to the frequency domain. In frequency domain the program makes the calculation of the quantities :

$$\Delta_x(\omega) = E_x(\omega) - [\; Z_{xx}(\omega) \; H_x(\omega) \; + \; Z_{xy}(\omega) \; H_y(\omega)]$$
$$\Delta_y(\omega) = E_y(\omega) - [\; Z_{yx}(\omega) \; H_x(\omega) \; + \; Z_{yy}(\omega) \; H_y(\omega)]$$

or briefly : $\Delta(\omega) = E(\omega) - Z(\omega) \; H(\omega)$ where x and y refer to the directions EW and NS, respectively. If the quantities $\Delta_x(\omega)$ and $\Delta_y(\omega)$ are considerable different from zero, then the remaining field indicates the existence of a source with no-magnetotelluric origin. Converting the quantities $\Delta_x(\omega)$, $\Delta_y(\omega)$ from the frequency domain to $\delta_x(t)$, $\delta_y(t)$ in the time domain, using inverse fast Fourier transform (IFFT), 4096 points of $\delta_x(t)$ and $\delta_y(t)$ are stored in a temporary file in the hard disk of the computer. Both the files, before and after the subtraction of the inductive component are ploted using an appropriate created software (in Pascal).The latter program communicates with the plotter in parralel mode

(Centronics output) in order to be faster, and use is made of
special GP ploter commands.The aforementioned executable
programs form a batch file, which uses a proper loop that
runs unattended.

We proceed now to give an application of the already
described procedure. Fig.(1) refers to the period during
which a preseismic electric variation was detected, in the
station of Ioannina (Epirous, North-West Greece) and precedes
a 5.5^R magnitude earthquake in W. Greece (Dologlou, 1993).
In fig.(1) we see that the simultaneous recordings of the
total electric field, the output of the coil magnetometers
and the results $-\delta_x(t)$ and $\delta_y(t)$ -of the subtraction of the
inductive component from the total electrotellouric
variation.
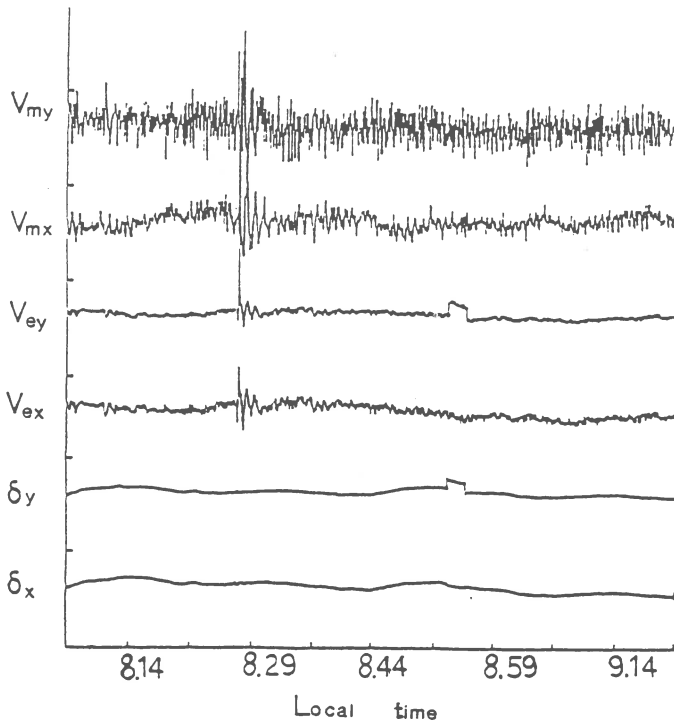
Fig.1 Simultaneous recordings. From top to bottom: the output
       of the coil magnetometers, telluric field variations
       and the corresponding residual electric field ($\delta x, \delta y$)
       in Ioannina station.

We discuss now the form of the preseismic electric variation
shown in fig.(1). According to the charge dislocation model
the deformation has the form depicted in fig.2 (see Appendix)
Thus a preseismic electric variation could be an index of the
evolution of deformation in earthquake focus during its
preparation stage.

Conclusions

Summarizing the results of the present paper we can state that :

(1) a procedure based on communication between a datalogger and PC applied for the collection of magneto-telluric variations is described.

(2) A developed software enables the subtraction of the inductive telluric component from that of the total ellectro-telluric variations.

(3) The designed system works unattended.

(4) We successfully apply the aforementioned procedure for the improved indentification of a preseismic electric variation. The precise determination of the form of the latter variation, qualitatively expresses the evolution of deformation in the preparation stage of an earthquake.

Appendix: Comment on the form of the transient preseismic electric variations.

We shall attempt now a qualitative analysis of the form of the observed variations based on the charge dislocation model (Slifkin, 1993).

According to the latter model all the crustal and upper mantle rocks contain crystalline materials which already bear linear defects (i.e., charge edge dislocations) due to a deformation they were previously subjected to. On the other hand, an earthquake zone is represented by cracks or, equivalently, by dislocation arrays i.e., by a concentration of charge dislocations (Teisseyre, 1987). Thus, the earthquake preparation (i.e., the non-linear evolution of stress) and energy release processes are determined by the propagation of these defects and changes in their density also.

The aforementioned representation of the earthquake source leads to the conclusion that electric current is generated whose intensity is proportional to the velocity of the propagation of the charge dislocation and to their density. The current density vector at the source is parallel to the velocity vector. Then, the electric field horizontal component, measured at a given point, in a horizontal distance x from the source and at time t_x , can be qualitatively presented by (Ernst et al., 1993) :

$$E(x, t_x) \propto \sum_i (\alpha_i V_i) \frac{x - x_i(t_x)}{R_i^n (t_x)} \qquad (1)$$

where R_i is the distance of the observation point from the moving charge dislocation element located at x_i, n=2 for a linear source ; α_i is the (charged) dislocation density at point x_i ; V_i is the dislocation velocity at x_i , which is determined by the applied shear stress σ and other thermochemical variables (temperature, fugacity of water, etc.). We clarify that expression (1) is based on the assumption that the time sequence of stress evolution is the same at each point on the source plane, only shifted by the time delay needed for crack propagation and thus on the

evolution of stress. However, when a dislocation motion occurs on a macroscopic scale, a macroscopic deformation will result; thus the macroscopic deformation rate, $\dot{\varepsilon}$, is related to the mobile charged dislocation density and velocity via Orowan's law $\dot{\varepsilon}(t_x) \propto \alpha_i \cdot V_i$ (Nabarro, 1987) and thus equation (1) becomes :

$$E\ (x,\ t_x\ ) \propto \Sigma\ \dot{\varepsilon}(t_x) . (\ \Delta x_i(t_x)\ /\ R_i^n(t_x))\qquad (2).$$

Equation (2) reveals that the observed transient electric variation is related to the non-stationary accumulation of deformation. Thus, with the help of a preseismic electric variation, recorded in a particular site, the deformation rate during the preperation stage of an earthquake, qualitatively could be observed.
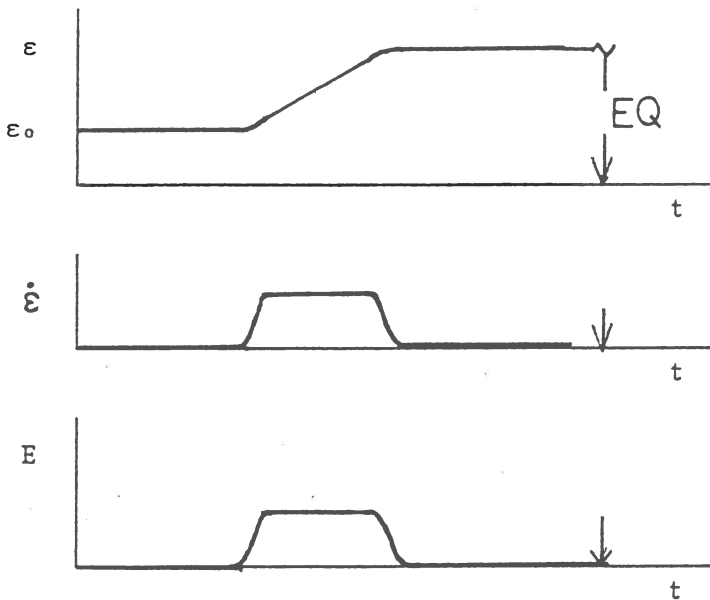
Fig. 2:Diagrame depicting the deformation (upper), the deformation rate (midle) and the corresponding electric field variation (lower).

Specifically, when the deformation rate increases with respect to a variable rate (i.e., $\dot{\varepsilon} > 0$ and $\ddot{\varepsilon} \neq 0$) then two cases are distinguisted:if $\ddot{\varepsilon} > 0$ ($\ddot{\varepsilon} < 0$) then $\dot{E} > 0$ ($\dot{E} < 0$); the latter means an increase (decrease) of the observed electric field variation. If $\dot{\varepsilon} > 0$ and $\ddot{\varepsilon} = 0$ (i.e., $\dot{\varepsilon}$ is constant with time) then E is also a constant (see Fig.2). Thus, the charge dislocation model could explain the form of a preseismic electric signal and lead to the conclusion that the preseismic electric variation controlled by the evolution of the deformation rate, during the preperation stage of an earthquake.

REFERENCES

Dologlou, E., 1993. A three year continuous sample of officially docmented predictions issued in Greece using the VAN method:1987-1989.Tectonophysics, 224, 189-202.

Ernsst, T., J. Jankowski, C. Rozluski and R. Teisseyre, 1993. Analysis of the electromagnetic field recorded in the Friuli seismic zone, norheast Italy. Tectonophysics, 224, 141-148.

Hadjioannou, D., F. Vallianatos, K. Eftaxias, V. Hadjicontis, and K. Nomikos, 1993. Subtraction of the telluric inductive component from VAN measurement. Tectonophysics, 224, 113-124.

Nabarro, F.R.N.,1987.Theory of crystal Dislocations,Dover.

Nomicos, K. and P. Chatzidiakos, 1993. A telemetric system for measuring electrotelluric variations in Greece and its application to earthquake prediction. Tectonophysics, 224, 39-46.

Slifkin, L., 1993. Seismic electric signals from displacement of charged dislocations. Tectonophysics, 224, 149-152.

Teisseyre, R., 1987. Earthquake generation in different stress states. Phys. Earth Planet. Inter., 49,24-29.

Vallianatos, F., 1989. Magnetotelluric investigation of the electrical conductivity in the areas of Thivaand Ioannina (Greece).Univ. of Athens, Athens, Greece.

Varotsos, P., K. Alexopoulos, and M. Lazaridou, 1993. Latest aspects of earthquake prediction in Greece based on seismic electric signals,II. Tectonophysics,224,1-37.

LONG-TERM ELECTROTELLURIC PRECURSORS OF EARTHQUAKES

Ponomarev A.V., Khromov A.A.

Seismological Institute of United Institute of Physics of the Earth, Russian Academy of Science, B.Gruzinskaya 10, 123810, Moscow, Russia

SUMMARY.

The changes of electrotelluric field during tens of months on the base of long-term observations in Kamchatka and the Middle Asia were investigated. Field works conducted on the base of the same technique, using the following analysis of mean monthly values of the field. Field level changes coincided with alteration of seismic situation in explored region, and also long-lived anomalies, connected with local seismity activization are determined. It is considered that electrical anomalies are caused by various mechanical-electrical transformations in the rock, which are the result of stress changes in the environment massif.

INTRODUCTION.

During the last years for the purpose of a search for the earthquakes precursors the variations of natural electrical field (self potential) are studied in many countries. A broad set of such investigations took place in China, the former USSR, Greece (Znang Zhaocheng et al., 1993; G.A. Sobolev, 1975; P.Varotsos, K. Alexopoulos, 1984). Numerous anomalies of electotelluric field have been determined. They were interpreted as medium and short-term precursors of the earthquakes. Different mechanism of electrical disturbances have been suggested. However it should be considered that the nature of electrotelluric forerunners is not quit clear.

By now, long-term self potential time series are accumulated. This data may be used as a basis for the search of ETF(SP) anomalies of hundreds days duration, not observed earlier. This paper containes the results of researches, which goal is to discover such anomalies.

TECHNIQUE AND RESULTS OF OBSERVATION.

The systematic observation for variations of electrotellutic field (ETF) were conducted by Institute Seismology RAS (Institute of Physics of the Earth) on the east coast of Kamchatka and in Garm test area in the Middle Asia for more than 25 years. These regions are considerably distinguish on natural-climatic and seismotectonic conditions. The most of the earthquakes epicenters in Kamchatka are located in subduction zones of Pacific plate, whereas the earthquakes sources in the Middle Asia are confined to the area of continental plates collision.

In both regions a uniform technique of observation was used. At the first stage, spatial structure of a natural electrical

field and apparent resistivity at the stations areas was researched and the sites, exemplified by relatively high gradients of geoelectric parameters were determined. Within these sites on depth of 2 meters sensors were grounded for measurement of a difference of potentials ETF with space about 200 meters. Copper nonpolarized ($Cu|CuSO_4$) and lead ($Pb|PbOHCl$) electrodes, characterized by stable and easy reproduced own potential were used as sensors. Analog and digital registration (in the recent years) was conducted in automatic mode with sampling rate 1 hour. The accuracy of individual measurement was determined by an instrument error (about 1 mV).

Observations on Kamchatka. The station "Shipunskyi" is located on the same cape, at 40 kms from focal zone, where main sources of the earthquakes of Kamchatka are located. Numerous tectonic dislocations are mapped in the region of the station. The measuring lines are developed directly in the zone of such dislocations, characterizing by relatively high gradient of SP - up to 100 mV/200 m.

Comparison of seasonal changes of ETF potentials and minimum temperatures of soil surface on c.Shipunskyi shows good correlation between these parameters, which have extremum: for potential - minimum in April and maximum in September, for temperature - minimum in February and maximum in July. At bi-monthly shift factor correlation of these parameters is about 0.75. Assuming, that the difference of temperatures in the places of electrode pairs grounding does not exceed $5-6^0$ C (amplitude of a annual temperature wave on the depth 2m) and accepting temperature factor of electrode potential about 0.4 mV/^{0} C, we evaluate annual ETF temperature variations due to own electrode processes by size about 2 mV. At the same time the observed amplitudes of a seasonal ETF course make 30-40 mV and, probably, are defined by filtration-diffusion processes in the ground, which are connected with temperature variations.

For the further analysis daily and monthly mean values of ETF were used. For revealing of secular changes of the field, time series of average ETF values in winter were constructed, when variations stipulated by meteorological and technogenic factors, are minimum. Such approach permits us to suppress influence of regular seasonal patterns considerably.

The average values on chosen intervals (January - March) were evaluated with the help of equivalent samples. According to our calculations the deviations varied in the range of 4-6 mV for 95 % confidence range.

Fig. 1 illustrates changes of mean ETF values on the north - south 200 m lines for winter season for 22-year period of observations. The graph of mean ETF values during November - February (1972-1981) for parallel measuring line located at 40 meters off is also presented. The moments of all earthquakes with theoretical estimation of precursor deformation more than 10^{-6} near the station are marked [Dobrovolsky I. et al.,1979].

The decrease of field level, exceeding probable error of measurements, began in 1983 and reached till 1987 the value 20-25 mV, comparable with amplitude of seasonal variations. During subsequent 4 years the signal level is gradually restored, though it remains lower than the values of a previous decade. Since 1993 the tendency to a new decrease of a signal
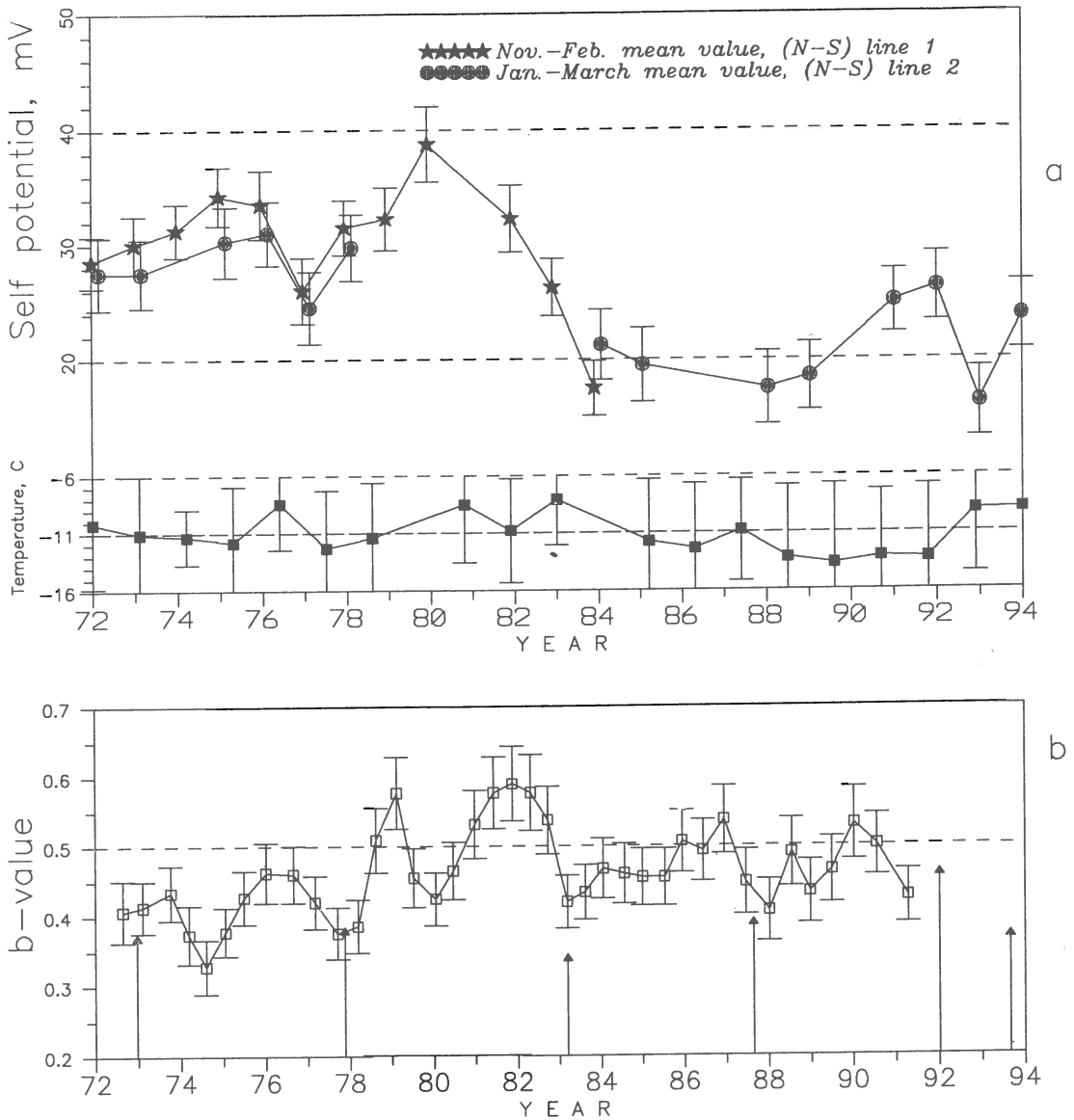
Fig.1. Changes of ETF and soil temperature mean values
in st."Shipunsky", Kamchatka (a) and b-value (b).
Moments of local close EQs (M>5.5) are marked with arrows.

is noted.

At the same 1983 long-term decrease of average temperature of soil surface in a winter-grade period, which was lowered till 1989 almost on 6^0 C, with being restored up to the previous values till 1992-1993. (Not numerous air and soil surface temperature observations are described in literature. The duration of them reaches the first years [Mei Shirong, 1985]).

For illustration of seismic regime features during researched period, the Gutenberg-Richter b-value changes for the earthquakes within the area of 300 km radius from observation station is presented. (Aftershocks were excluded from accounts. b-value was calculated in the moving windows of 150 events volume with shift on 75 events). Since 1972 to 1982 b-value gradually grows, reaches maximum value for submitted by 20-years period, then it gradually decreases down to 1992.

Thus, it is possible to ascertain, that after 1982-83 appreciable change of a ETF level and long-term trend of b-value has taken place.

For submitted period of ETF observation two earthquakes with close hypocenters (M_L = 6.6 (06.10.87) and M_L = 7.1(02.03.92) are registered on epicentral distance about 40 kms from the observation point. Both of seismic event have taken place after decrease of ETF level, and only for them the theoretical precursor deformations is about 10^{-5}, i.e on the order higher, than at another earthquakes. It is possible to give the cautious assumption, that general change of electrical field level is connected to development of mechanic-electrical phenomena on the area of observation at preparation of close strong earthquakes.

<u>Observation in Garm test area.</u> The "Chusal" station is located in zone of Pamir - Tian-Shan conjugation, on northern side of Gissar-Kokshaal fault. The self potential prospecting has found out a marked linear anomaly on the territory of station by intensity up to 800 mV. A gradient of SP intensity is about 100 mV/200 m in the region of the electrodes grounding. The results of SP prospecting and resistivity survey across the anomaly (N-S direction) are submitted on Fig 2. Comparison of these data to a geological structure of a region shows that SP anomaly is connected to a subvertical contact of large granodiorite intrusion and containing metamorphic rocks. The zone of contact is composed by a layer low resistance coalificated shales, their thickness is up to 0.5 m.

The graphs of monthly average ETF values for two independent parallel lines N-S and also E-W line are presented on Fig.3. At the and of 1981-82 long-term variation of the field, fixed by lines of meridian extension begins. This disturbance seizes rather significant area, as far as is synchronously registered by two lines, distance between which makes 200 m. On line of a perpendicular direction of such expressive changes is not found out. Arisen anomaly is developed until 1984, then begins to decrease, and is recovered to the former level of the field. The duration of anomaly is not less than 25-30 months, an it's value reaches 40 mV. Second long-lived anomaly of electrical field by amplitude more 50 mV is noted in 1987-1988.

For a period of under examination 3 earthquakes with $M_L \geqslant 5.5$ took place in Garm test area. On October 26,1984 Dzirgatal
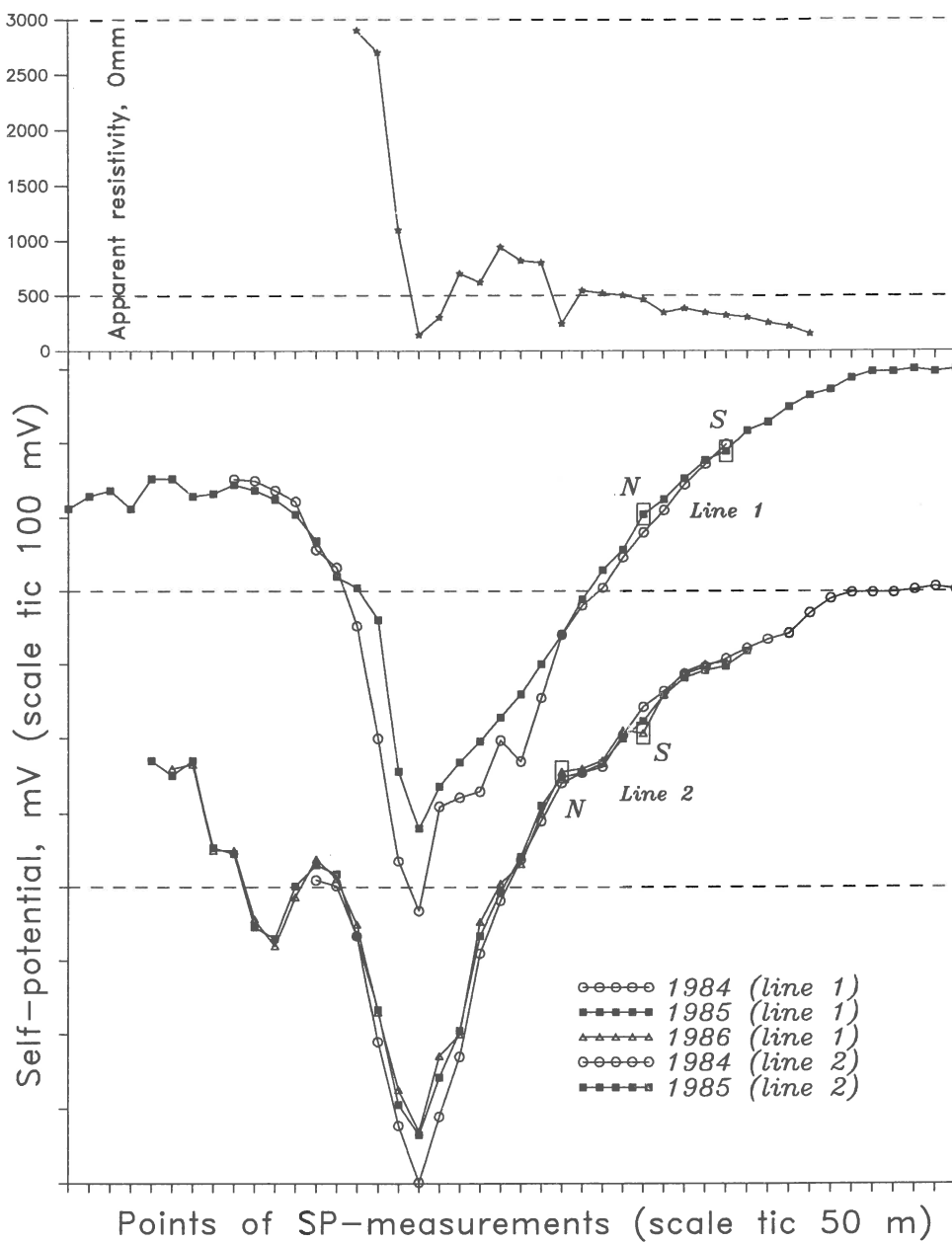
Fig.2. Results of geoelectrical prospecting in st."Chusal"
Garm site.
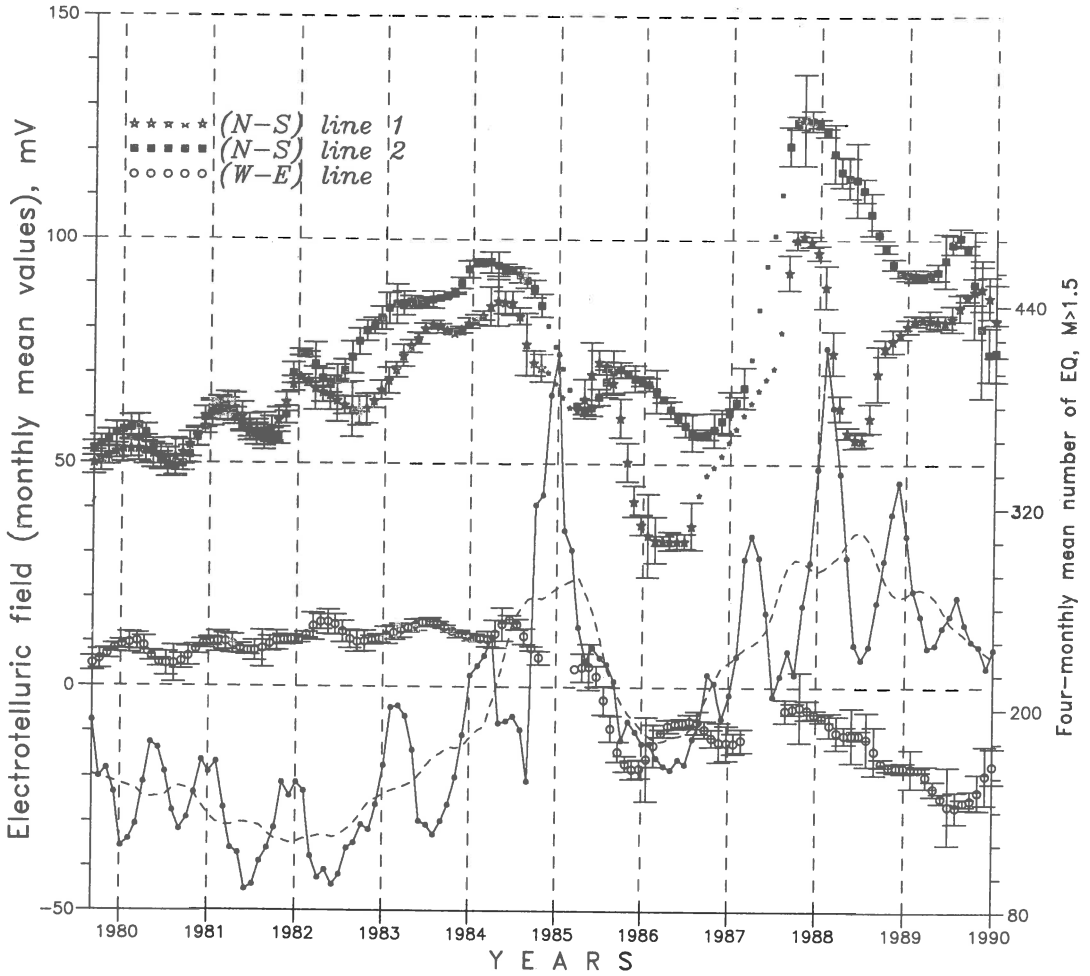N and S positions - the places of stationary electrodes.

Fig.3. Changes of ETF mean-month values in st."Chusal".
Dashed line is the low-frequency component of the variations
in the number of EQs (Garm region).

earthquake have taken place with M = 6.4 on epicentral distance of 45 km. It was the strongest one in the region since disastrous Khait earthquake on July 10, 1949 with M_L = 7.4. The assessment of precursor deformation is $\approx 10^{-5}$, that is on 1-2 order more, than for other events of a region. Two other earthquakes with M_L = 5.5 took place on December 12, 1987 and January 9, 1988 on epicentral distances about 30 km and 60 km, respectively. It is obvious, that all events have taken place during the periods of extreme values of ETF.

One more interesting feature connected to infringement of a seasonal course of potential difference. Good developed during 1980-1982 annual variations of the field are appreciably deformed till 1984 and almost completely disappear after Dzirgatal earthquake.

The self potential prospecting was repeated on the same positions in July - August 1984, 1985 and 1986. If we consider variability of SP anomaly on contact of intrusion and containing rocks directly, it is easy to notice, that observations in 1985 and 1986 give good concurrence of the values of potential almost on all points of the profile. The deviations do not exceed first mV. At the same time prospecting of 1984 shows a divergence up to 80 mV in the central part of SP anomaly. The similar situation is observed on the parallel profile. Comparing these data with ETF variations on lines N-S, we can conclude, that long-lived variation of ETF found out by stationary measuring dipoles is stipulated by local change of SP. This change is displayed in the zone of geological contact much more intensively, than on the "wings" of anomaly, where stationary electrodes were located.

RESULTS AND DISCUSSION.

We consider, that found out long-lived ETF anomalies are caused by slow variations of stress-strain condition of the rock massif in the area of observation. These variations give rise to mechanical-electrical phenomena, which are distinctively displayed in the zones of structural hetergeneities, where localization and an increase of deformations are possible. As appear, the particular gears of anomaly generation could be various: electrical-kinetic, diffusion, electrochemical and another. For example, the form of SP anomaly on "Chusal" station indicates on vertically polarized object. Obviously, this is a contact zone, which polarization is caused by development electrochemical (red-ox) processes frequently observed in coalified rocks. The intensity of such processes may be also stimulated by fluid filtration in permeable rocks of geological contact under the influence of tectonic stress.

There is a basis to consider, that such long-lived precursors and long-term trend changes are not connected to separate earthquake, but more probable they reflect general activization of seismic regime in the extensive region. As a result time concurrence of ETF anomaly and concrete earthquake may have place. This hypothesis is supported by such facts, as observation of forerunners in the area essentially exceeding aftershock zone, weak dependence of anomaly amplitudes from

distance, slow change of anomaly course after separate seismic event..

In this context we note, that for Garm test area fluctuating character of seismic process is established, and the periods of increased activity correspond to the end of 1984 and beginning of 1985, the end of 1987 and beginning of 1988, i.e. to those periods, when intensive ETF anomalies are observed [A.Lukk et al., 1992].

CONCLUSIONS

1. ETF variations are determined by a duration of hundred of days and also by the amplitude of first tens of mV. The development of these long-lived anomalies connected with mechanical-electrical processes, which will be realized in zones of dislocations and other geological contacts.

2. ETF anomalies are dated to periods of seismic activity and may be considered as intermediate precursors of strong local earthquakes.

REFERENCES

Dobrovolsky I.P., Zubkov S.I., Miachkin V.I.,1979. Estimation of the size of earthquake preparation zones. PAGEOPH, 117, 1025-1044.

Lukk A.A., Zhuravlev V.I. and Galaganov O.N., 1992. Oscillatory structure of the geophyisical fields recorded at the Garm site. J. of Earthquake Prediction Research, 1, N 2, 147-163.

Mei Shirong, 1985. On the variety and complexity of the shortterm and urgent precursors of the Tangshan earthquake. Norhtwest.Seismol.J.,7, N.3, 72-89.

Sobolev G.A., 1975. Application of electric method to the tentative short-term forecast of Kamchatka Earthquakes. PAGEOPH, 113, 231-235.

Varotsos P. and Alexopoulos K., 1984. Physical properties of the variations of the electric field of the earth preceeding earthquakes.I,II. Tectonophysics, 110, 73-125.

Zhang Zhaocheng, Zheng Dalin, Luo Yongsheng and Jia Qing, 1993. Studies on earhquake precursors and the comprehensive criteria for earthquake prediction. Seismological Press, Beijing,215-218.

WELL LEVEL ANOMALIES FOLLOWING THE
M5.9 ROERMOND EARTHQUAKE :   DATA
(extended abstract)

H.-J. Kümpel and J. Endom,
Geological Institute, Section Applied Geophysics, University of Bonn
Nussallee 8, D-53115 Bonn, F.R.Germany

On April 13, 1992, a Magnitude 5.9 Earthquake hit the Dutch-German border area near Roermond-Heinsberg. The Earthquake was one of the strongest events during the past 500 years in Mid-Europe. Various continuously monitoring well level sensors at Bonn, 95km SE of the epicentre, recorded a small coseismic step that persisted for at least a few days.

In order to collect a large set of well level rocords we have mailed questionnaires to about 180 institutions, authorities and individuals - mostly in The Netherlands, Belgium and Germany. In that way we got notice of 191 continuously operating sensors located within 150km distance of the epicentre.

Nearly all data are from shallow wells drilled into the quarternary deposits of the Lower Rhine Embayment. Generally, the corresponding aquifers are unconfined and have a high hydraulic conductivity. The wells are clustered around the cities of Bonn, Cologne, Düsseldorf, Duisburg and Mönchengladbach. The results from a first inspection are: Levels in 107 wells showed no reaction to the quake, 28 responded dynamically to the passage of the seismic waves; 56 wells revealed a persistent drop or rise in the level curve, partly superimposed by a dynamic response. Amplitudes of the persistent changes were of cm magnitude at most. In no case a precursory anomaly is evident.

Fig. 1 shows the distribution of wells in the Lower Rhine Embayment that are known to us and were operating on April 13, 1992. Figs. 2 and 3 are sample plots of digitized recordings from two cities. Fig. 4 displays the variation of barometric pressure and precipitation some hours before and after the Earthquake. Note that overall barometric pressure change is small and that only about 1mm of rain fell here a few hours before the event.

We will focus our future investigations (a) on the identification of instrumental effects from the agitation of well level sensors during the passage of seismic waves (like mechanical triggering), (b) on the spatial coherence of well level anomalies, especially in areas of dense coverage, (c) on the study of possible relationships between amplitudes of well level anomalies and known

geological, hydrological, and tectonic features. The latter will include field testing of wells for recognition of hydrologic parameters. We finally plan to apply numerical modelling in order to interprete the anomalies with respect to crustal stress redistribution caused by the Earthquake.

Unfortunately, for our purpose, the quality of the raw data is far from being splendid. In particular we wish to have more signals from deeper, unconfined aquifers which are generally more sensitive to changes in pore pressure and confining stress (Roeloffs, 1988; Kümpel, 1992). Nevertheless, the now available data set is probably the most extensive one of hydrological signals ever collected for a single Earthquake.

REFERENCES:

Ahorner, L., 1992: Das Erdbeben von Roermond am 13. April 1992 und die daraus zu ziehenden Lehren für das Erdbebengefährdungspotential im Rheinland.- Open lecture, University of Cologne, June 24, 1992.

Kümpel, H.-J., 1992: About the potential of wells to reflect stress variations within inhomogeneous crust.- Tectonophysics, **211**, 317-336.

Pelzing, R., 1992: Das Erdbeben von Roermond, 13. April 1992.- Report of the Geologisches Landesamt Northrhine-Westfalia, Krefeld.

Roeloffs, E., 1988: Hydrological precursors to earthquakes: a review.- Pure Appl. Geophys., **126**, 177-209.
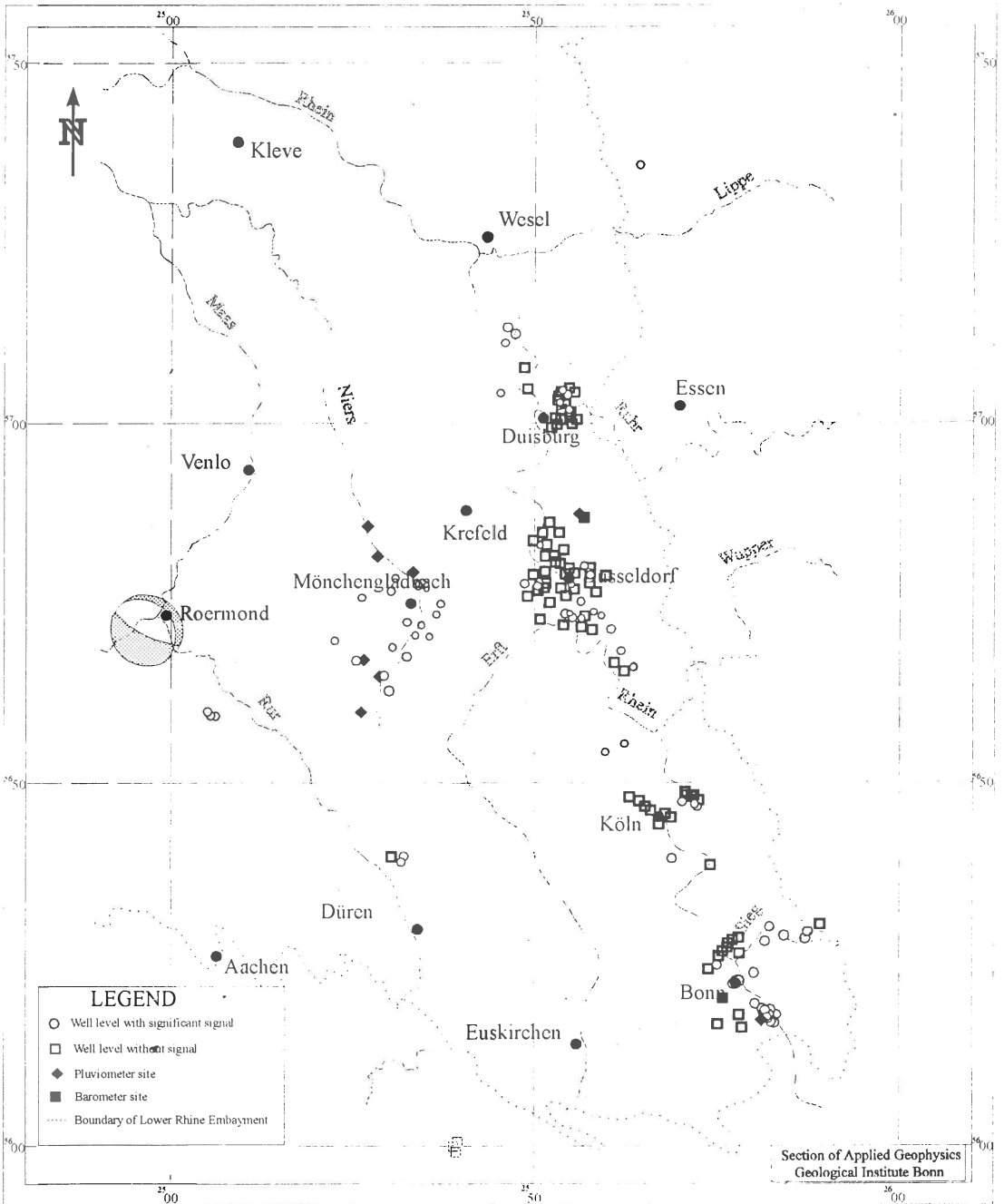
Fig. 1: Distribution of wells showing either a significant or no level anomaly in the Lower Rhine Embayment. Fault plane solution of the Roermond Earthquake after Ahorner (1992) and Pelzing (1992), respectively.
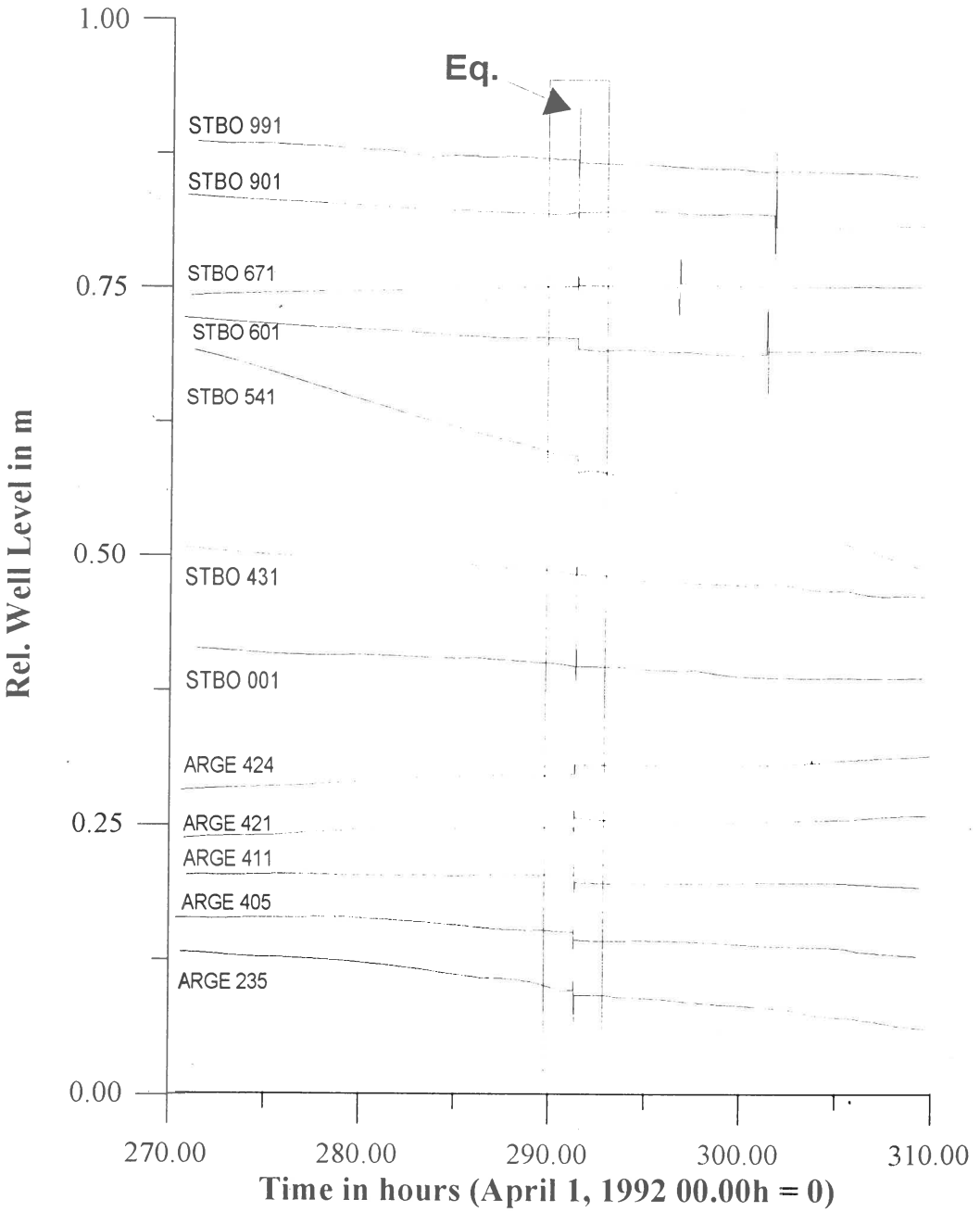
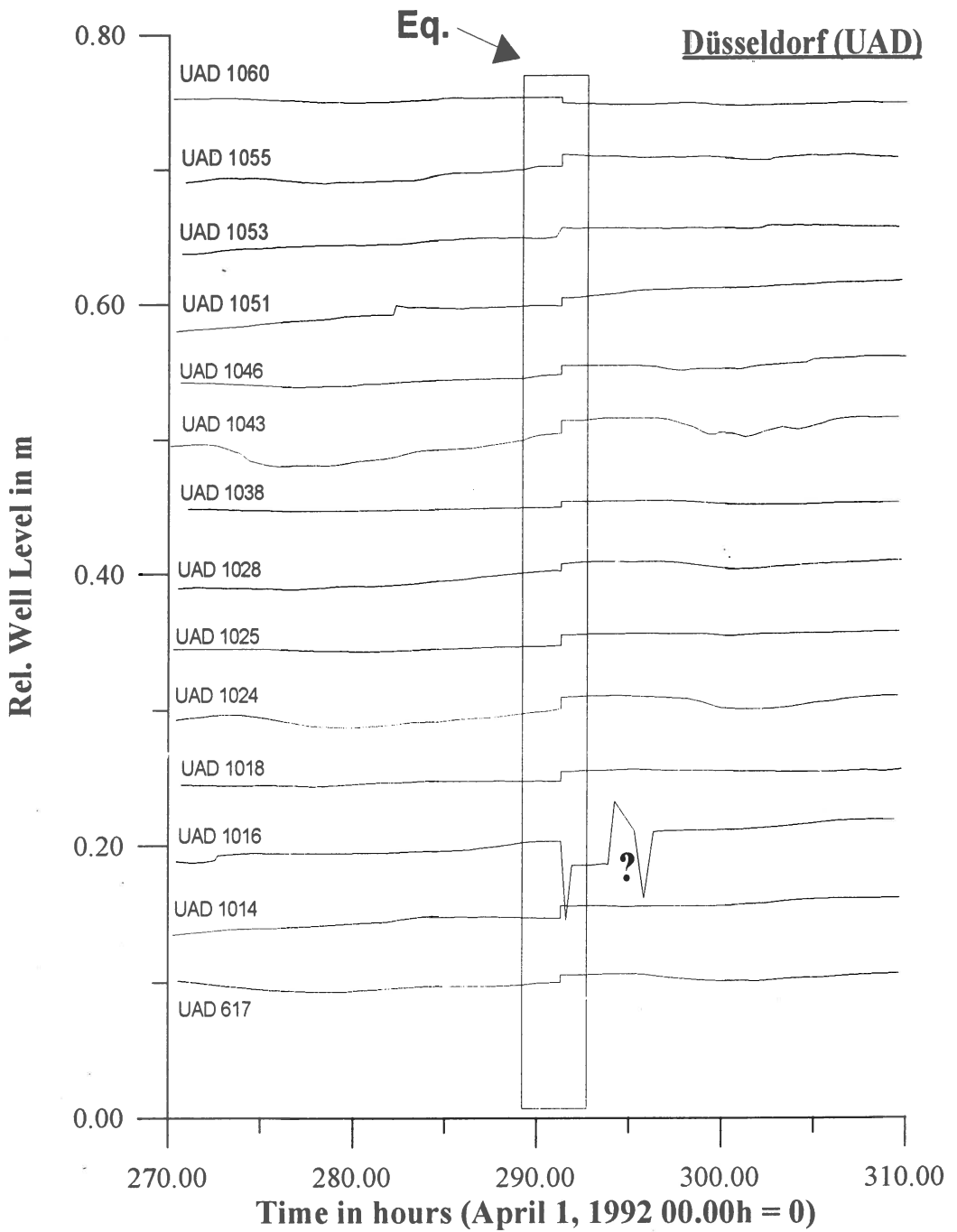**Fig. 2:** Digitized well level recordings of various locations from Bonn.

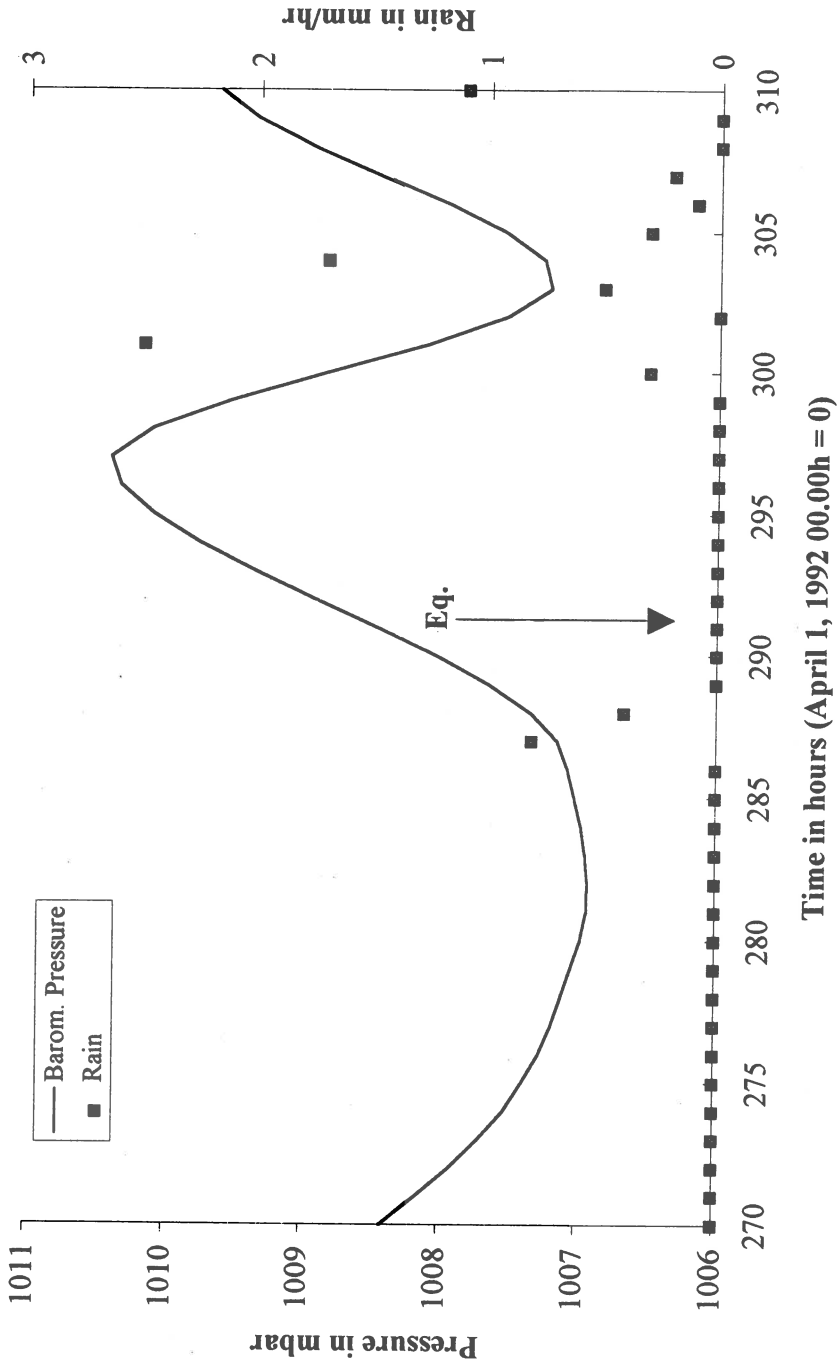**Fig. 3:** Digitized well level recordings of various locations from Düsseldorf.

Fig. 4: Precipitation and barometric pressure fluctuation 20 hours before and after the Earthquake at Düsseldorf.

A DECADE OF RESEARCH OF THE SHALLOW UNDERGROUND WATER LEVEL AND TEMPERATURE IN THE AREA OF MYGDONIAN BASIN,NORTHERN GREECE FOR PRECURSORY PHENOMENA

G. Asteriadis and M.E. Contadakis,*Department of Geodesy and Surveying, Univ. of Thessaloniki,540 06, Thessaloniki, Greece*

ABSTRACT

A shallow underground water level and temperature monitoring network was installed in the area of the lakes Langada and Volvi,in Northern Greece by the end of 1983 and was followed since then for a decade. The results so far shows that: (a) The atmospheric pressure and earth tides do not affect the observations of the shallow underground water level in accordance with the results of other investigators while the rainfall does, and (b) although there is not a unique response pattern for all the stations of the network, sharp changes in the underground water level and temperature can be related to earthquakes occured in this area as pre- and post - seismic phenomena.

INTRODUCTION

In Northern Greece close to Thessaloniki there is a seismic zone which is associated with the Servomacedonian geological massif. In this zone there is a basin which includes the lakes Lagada and Volvi. This is a very active seismic area in which many large earthquakes have occured in the past.

In order to verify if the well known (Rikitake 1976,1981,Wakita 1982) pre- and post-seismic response of the underground water level and temperature manifest itself in the case of the shallow underground water,a shallow underground water level and temperature monitoring network was installed (Asteriadis and Contadakis 1991) in December of 1983 in this seismic active area and has been followed up ever since.The reason is obvious and has to do with the cheap instrumentation and the low running cost of such a monitoring network.Our expectation was justified (Contadakis and Asteriadis 1993) in accordance with the results of other of similar researches of other investigators (Oki and Hiraga 1988).

In this paper we present the results of this ten year investigation.

THE NETWORK AND THE MEASUREMENT

Four KLT-OTT type electric contact gauges were installed in 1983 by the Department of Geodesy and Surveying, University of Thessaloniki, at selected wells in the seismically active area of Northern Greece, between the latitudes $40^{0}.35$ and 41^{0} N and longitudes $22^{0}.7$ and $23^{0}.85$ E. Figure 1 shows the position of the four villages, Liti, Assiros, Melissourgos and Nymfopetra, where the six selected wells belong. Table 1 displays the position and the depth of the well stations of the network as well as the respective number of measurements which were performed in the time interval between 1983,December 20 and 1993 ,December 10.

The continuous daily sampling at the stations of Liti,Assiros 1&2,Melissourgos 1 and Nymfopetra have started on 1983 December 20 and at the station of Melissourgos 2 on 1984 April 16.However it happened that some stations were out of work for some periods of time, mostly because the respective well have became dried due to the drought, as it is happened during the extremely dry year of 1990, where all the wells exept that of the Assiros 1 and 2

stations have became dried by the end of May.It should be noted that the well of Liti remain dry until today and we were forced to replace the well in the network.The continuous measurements at the two wells of Melissourgos were terminated on the second of April 1993.
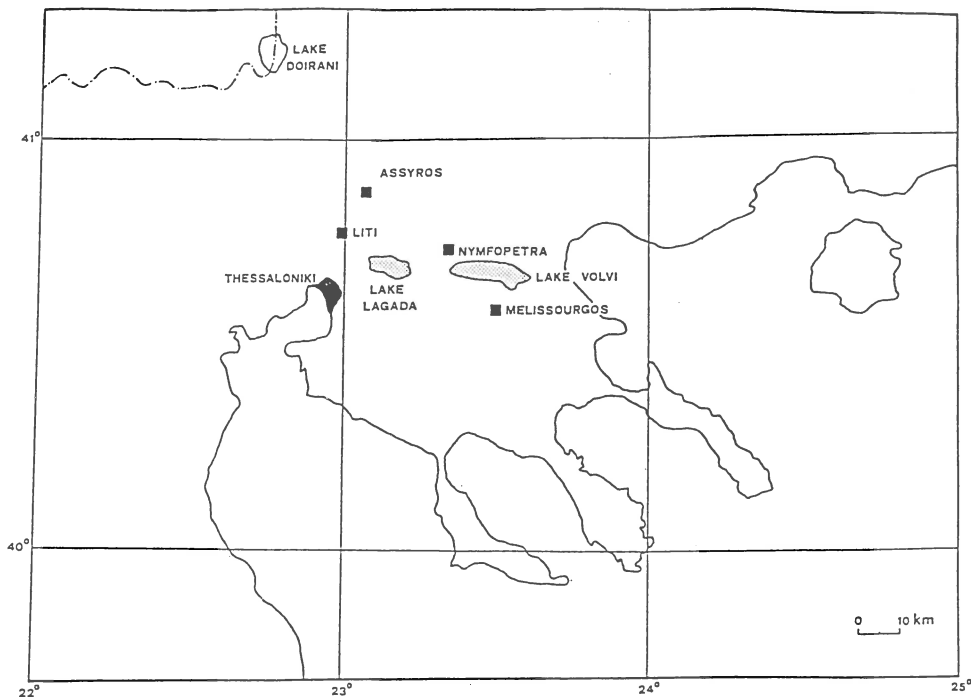

Figure 1. The location of the network stations

Two HELLMAN-type rain-gauges for the rainfall measurements were installed in the area in order to study for the influence of the rain in the changes of the underground water level. The seismic data have been selected from the monthly bulletin of the Seismological Institute of the National Observatory of Athens (SINOA) . These data are for earthquakes with epicentres extending from $\varphi=40^0.3$ N to $\varphi=41^0.0$ N and from $\lambda=22^0.7$ to $\lambda=23^0.8$.

Table 1. Position and depth of the wells of the network stations and the total number of the performed measurement.

	Monitoring wells				
well	$\varphi[^0]N$	$\lambda[^0]E$	height (m)	depth (m)	numb/meas
LITI	40.75	22.98	170	11.0	2065
ASS1	40.82	23.03	200	4.2	3772
ASS2	40.82	23.03	200	2.2	3772
MEL1	40.60	23.42	110	4.1	3342
MEL2	40.60	23.42	110	5.1	3227
NYMF	40.69	23.34	90	10.0	3376

During the time period between December 20,1983 and December 31,1993 , 433 earthquakes with epicentres in this area occured, 100 from them had magnitudes M≥ 3.0. The monthly bulletin of SINOA does not provide information about the magnitudes if this is less than about 2.5 ,and for these cases we assign the value 1.0 to facilitate the computerized graphic work.

THE INFLUENCE OF NON TECTONIC FACTORS IN THE WATER LEVEL MEASUREMENTS

Since it is generally accepted that changes in the tectonic stresses are the main cause for the underground water variations which are connected with the earthquakes, it is expected that non tectonic stress sources ,such as Earth tides and Barometric pressure will also produce similar variations in the wells water level and a great deal work has been done in this field (see for example Melchior ,1982; Reoloffs, 1988; Roeloffs et. al. 1989; Rojstaczer, 1988).

In order to test the response of our network to these non tectonic stresses and to the precipitation as well ,we have performed statistical test on the observational samples of the involved quantities for the time periods of 1988-89 (Contadakis 1993) and 1991-92 (Contadakis and Asteriadis 1994). Before we proceed to the analysis of the cross correlations between the involved variables we note that all of them present a well (earth tides) or weakly (water level) expressed periodicity of one year . This fact we have to have in mind in the interpretation of the cross correlation functions.In particular the results of those test are as follows.

a) Rainfall

The cross correlation function between the rainfall heights collected by our rainfall -gauges and the water level variations shows no correlation. This result may be explained by the fact that a threshold amount of rainfall is required in order to initiate the recharge of the aquifer and this was not surpassed by the weak rainfalls as they are spreaded in a relatively long
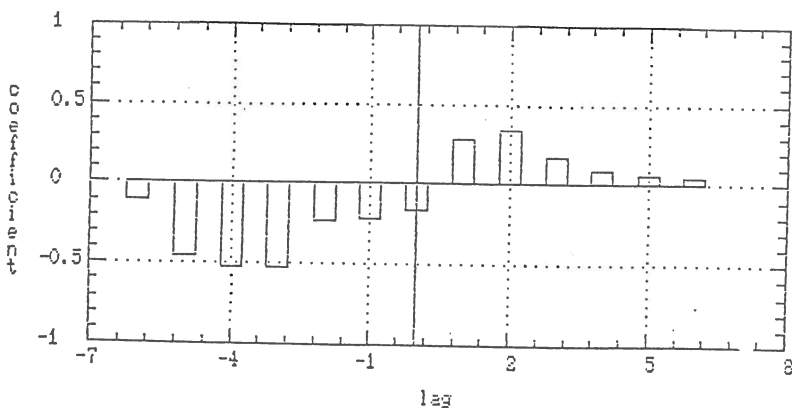

Figure 2 . Cross-correlation functions between monthly rainfall heights and mean monthly moving averages of the water level at the well of Nymfopetra in 1988. Lags are in months.

period of time. However the monthly heights of precipitation show a weak correlation with the moving average of the water level in all the wells, except for that of the well of Liti in the year 1988,with a phase lag of two or one month . Figure 2 displays an example for the well of

Nymfopetra in 1988. This result is fully understood since rainfall water needs some time to reach the water table moving in the aerization zone.The behavior of the well of Liti is abnormal with respect of rainfall. It should be noted that during the extremely drought year 1990 the well of Liti became dry and remain dry until today. Therefore it maybe concluded that a permanent change occured on the water table of the well of Liti.

b) Earth tides

The sampling interval of our measurements is too large for a proper investigation of the influence of earth tides on the wells water level. However the existence of such an influence may be detected from our sample using statistical tests.The cross-correlation function between the tidal perturbation on the earth gravity field (Arabelos 1991) in the region of the network (the quantity which has to be subtracted from the total gravity field in order to correct for the tidal effect) and the wells level variations shows a weak correlation with a varying phase lag between 25 days for Melissourgos 2 months for Assiro1 and 3 months Liti, Assiro2 and Nymphopetra . Spectra power analysis shows the 13.6 days component in the
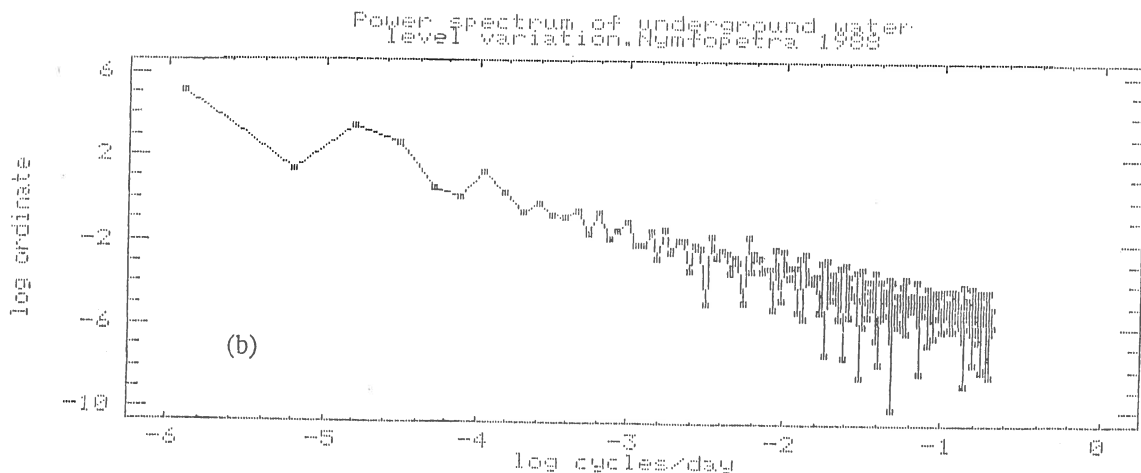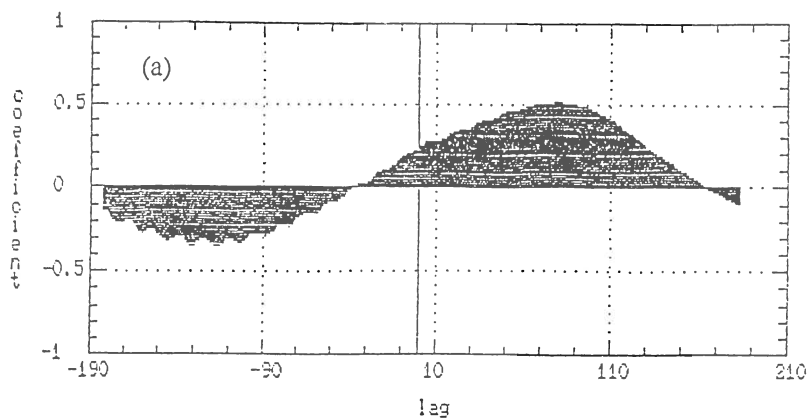

Figure 3 . (a) Cross-correlation functions between the tidal gravity variation and the water level (lags are in days) and (b) the power spectrum of the water level at the well of Nymfopetra in 1988.

spectra of the well water level which found in the limit of the noise. Figure 3a,b displays an example for the well of Nymfopetra in 1988.The Nyquist limit ,which is 2 days for our sample,does not allow us to detect any correlation of the well water level with the diurnal and semidiurnal components of earth tides.

c) Barometric pressure

The cross correlation function between the barometric pressure and the well water level shows very weak or no correlation, with phase lag varying to.Figure 4 displays an example for the well of Nymfopetra in 1988.It should be noted that the power spectrum of the barometric pressure shows the 13.6 and the 27.5 days tidal component.
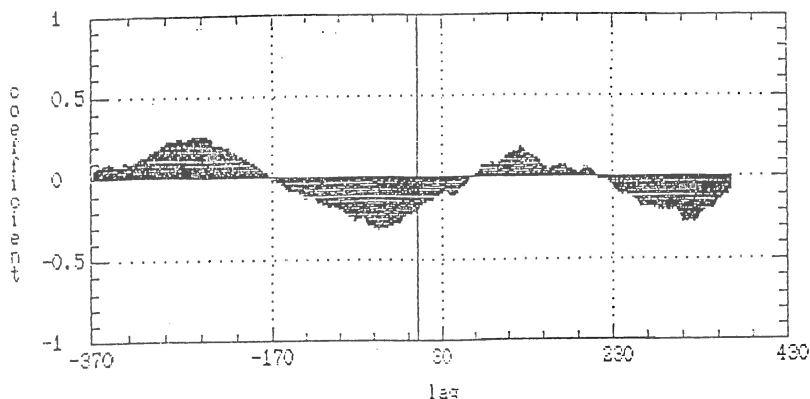

Figure 4 . Cross-correlation functions between the barometric pressure and the water level at the well of Nymfopetra in 1988. Lags are in days

The above mentioned statistical tests show that earth tides and barometric pressure have a small influence on the water level measurement of the shallow wells of our network. This result is in accordance with the results of the theoretical and observational research in the field, since a network of shallow wells is connected with unconfined aquifers and horizontal ,as well as vertical ,flow from the wells to the water table and vice versa occur. This fact ,together with the high porosity of the surface ground, will produce attenuation of the water level variations due to earth tides as well as to barometric pressure (Melchior 1982, Rojstaczer 1988 Roeloffs,1988). In addition a phase lag greater of about a month is suggested by these tests. Specific investigation of the influence of earth tides require sampling interval of the order of at least an hour for the observations and of course more sophisticate instrumentation than of this investigation.The precipitation effect also is small and has a phase lag of one month. It is obvious that the recorded sharp changes on the underground water level can not be attributed to the above mentioned sources if their period is of the order of 7 days or less as it is observed in our case.

RESULTS AND DISCUSSION

During the seismic periods of quiescence, the overall behavior of the underground water level shows a gradual long term variation in water level caused by the rainfalls .This variation has a period of a year in accordance to the rainfall annual periodicity .The underground water temperature shows the well known seasonal, one year periodic variation with amplitudes ranging between 0.6 ^{O}C in the deepest well, NYMF (10.0m), up to 8 ^{O}C in the shallowest well,

ASS2 (2.20m), and a phase lag with respect to the atmospheric temperature which depend on the depth of the well. These long term variations do not bother the detection of any sharp change caused by other reasons.
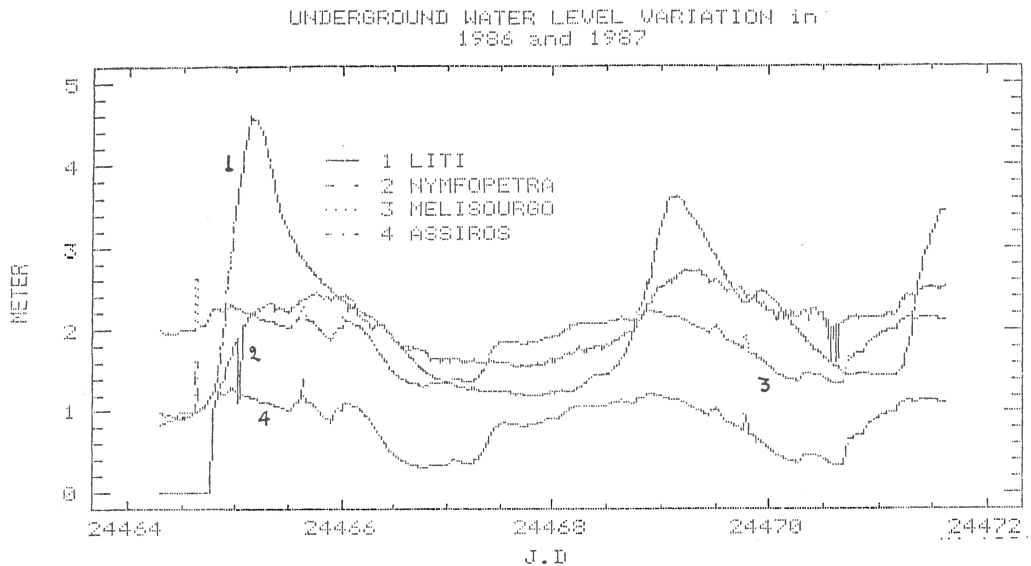

Figure 5 . Underground water level variations at the wells of the network during the years 1986 and 1987 .

Sharp changes in the underground water level and temperature can be related to earthquakes with epicenters in this area as pre- and post- seismic phenomena (Asteriadis and Livieratos 1989 a,b , Asteriadis and Contadakis 1991). There is not a unique response pattern of these changes for all the wells, a fact which is also reported by others investigators (Wakita 1982,Ma Zongjin et.al. 1990).The magnitudes of these changes vary between a few centimeter to 90 centimeter in the water level changes and from a few tenths up to one degree centigrade in the temperature changes. Figure 5 and 6 displays some examples of the underground water level and temperature variations .Our results indicate that there is a correlation between the magnitude of the change in underground water level and temperature and the magnitude of the shock as well as the epicentral distance of the respective station. Finally the water level and the temperature changes occur in a time interval up to seven days before or after the associated shock (see also Asteriadis and Zioutas 1990),except the disturbances in underground water level and temperature which correspond to the strongest shock observed during this investigation .This earthquake occured in 1990 December 21 , has . a magnitude of 5.4 and the corresponding disturbances in underground water level and temperature started 20 days before .This fact is found in accordance with the suggestion of Zongjin et. al. (1990) that the precursory disturbances in underground water precede the event by 10 to 20 days,if the magnitude of it is 5. In general we may say that the observed time lag of the precursory disturbances in underground water level and temperature are in favor of the

suggestion of Zongjin et. al. (1990) that they are correlated with the magnitude of the associated event.

Table 2. The observed sudden changes in underground water level and temperature and the associated earthquakes which have occured in the above mentioned area within the time interval 1983,January 1 and 1993,December 10 .

Period		Assiros1		Liti		Meliss/gos		Nym/petra		Shock	sud.	Ch
		A	B	A	B	A	B	A	B	Tot	%	%
1983-85	W/L	6	17	6	11	5	8	4	6	84	60	92
1986-87	W/L	7	57	14	42	0	39	1	8	76	86	100
	Temp	12	46	6	24	2	28	3	13	"	76	92
1988- 89	W/L	26	3	40	5	30	4	16	1	143	72	98
	Temp	19	5	38	8	21	6	11	6	"	64	100
1991-92	W/L	10	0	-	-	7	0	5	0	17	89	67
	Temp	11	0	-	-	6	0	1	0	"	94	60
1993	W/L	4	3	-	-	0	0	1	3	7	100	52
	Temp	1	3	-	-	0	0	3	3	"	100	53

Table 2 displays a brief statistics of the network response on the seismic activity of the region in the time interval between 1983 ,,December 20 and 1993, December 10 (Contadakis and Asteriadis 1993,1994, Asteriadis and Zioutas 1990). The Whole decade has been devided in five periods of two months duration except the last one. The year 1990 has been ommited because during that year most of the wells had become dry, as we have already mentioned. In this table the number of the sudden changes in underground water level (row named "W/L") as well as in underground water temperature (row named "Temp.") for each period.Those changes which can be attributed to a particular shock are given in the columns under the heading A while those changes which occur within an earthquake swarm or sequence are given in the columns under the heading B. The total number as well as the percentage of the total number of the shocks which can be correlated with a sudden change in the water level or in the temperature are displayed in the two respective columns. Finally the percentage of the sudden changes in unterground water level or temperature which are associated with earthquake are given .

From this table we realize that in the decade 1983-93 the necessary condition of an earthquake to follow an observed sudden change in the underground water level or in temperature in a well of the network is fulfilled with a mean probability of 81% and 83% respectively,while the sufficient condition of a sudden change in underground water level or temperature to be followed by an earthquake is fulfilled with a mean probability of 82% and 76% respectively.

Table 3. The number of earthquakes with epicenters within the broader area of Volvi for the respective time periods.

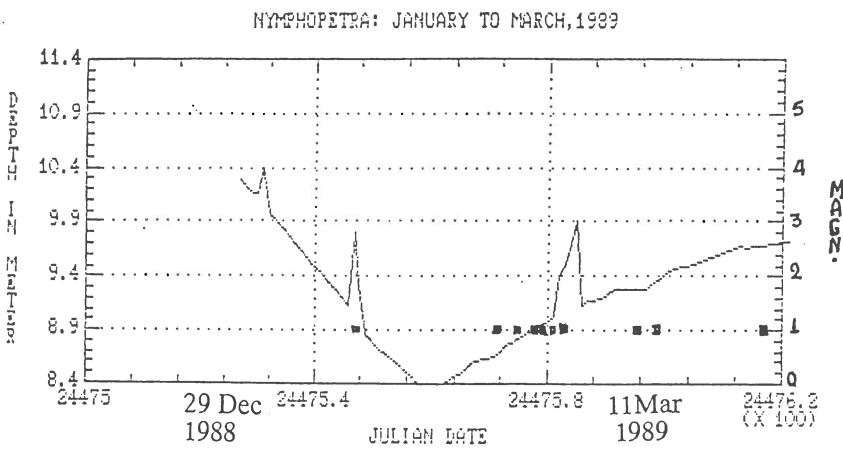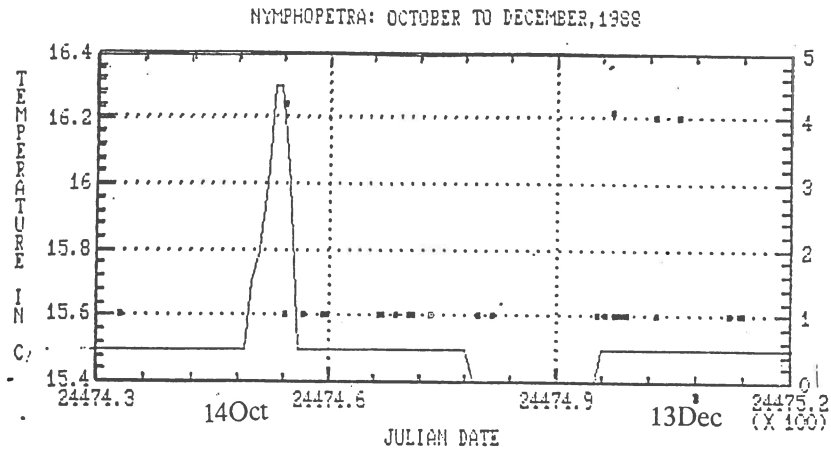| Shock\Period	1984-85	1986-87	1988-89	1991-92	1993
Total Number	94	76	143	17	7
M ≥ 3.0	19	7	27	10	5
%	20	9	19	59	71

Figure 6 . Underground water temperature and level variations at the well of Nymfopetra around the end of 1988. Dots indicate the earthquake which occured at the respective time intervals.The magnitude of the earthquakes are given at right hand scales.

The probability for the verification of the necessary condition increases within the decade while the probability of the sufficient condition decreases within the decade . This is to be expected if the seismological results for the last years of the decade are free of weak shocks. This trend is indicated from the Table 3.From this table we realise that the number of the

earthquake at the late years of the decade 1983-93 is decreased while the percentage of the shocks with magnitude greater than 3.0 is drastically increased.

CONCLUDING REMARKS

The results of this investigation indicate that there is a correlation between the underground water level and temperature variation and the microseismic activity in the broader area of the network manifested by sharp changes of these quantities within 7 days before the shock.However the time interval between the 5.4R shock of 1990 December 21 and its associated disturbance in underground water level and temperature,which is 20 days, indicates that a correlation between the event magnitude and the time lag of the associated disturbance may exist.

Crustal movements,expansion or contraction of the ground cause changes in the pore pressure of the underground rocks and deformation of the underground water system Therefore the seismogenic process is expected to cause such a deformation.The exact way that this deformation manifest itself depend on many factors e.g. the epicentral distance the magnitude of the shock and the tectonic environments of the well network .The last factor presumably is responsible for the different response pattern of the different wells of the network.

REFERENCES

ARABELOS, D., 1991: *Improvement of the accuracy of the Lacoste Romberg model G Gravity meter with an electronic feedback.* FESTSCHRIFT, Prof.Dr.Wolfgang Torge, zum 60. Geburtstag. Wissenschaftliche Arbeiten der Fachrichttung Vermessungwesen der Universität Hannover, Nr. 172, S. 7-13, Hannover.

ASTERIADIS, G., LIVIERATOS, E. , (1989a) Pre- and post-seismic response of underground water level and temperature: A first experience in Greece, *Acta Geoph. Polonica XXXVII*, no. 3-4 , p. 233- 245.

ASTERIADIS, G., LIVIERATOS, E. (1989b). Pre- seismic responses of underground water level and temperature concerning a 4.8 magnitude earthquake in Greece , *Tectonophysics*, 170, 165 .

ASTERIADIS, G., ZIOUTAS, G. (1990). Application of an outlier detecting method for identifying changes in the underground water level caused by crustal movements, *Geophys. J. Int.* , 103, 415-424

ASTERIADIS, G., CONTADAKIS, M. E. (1991). *Current research on the underground water and temperature in the area of Volvi, for pre- and post- seismic response*, Proceedings of the 1st General Conference of the Balkan Physical Union,Thessaloniki Greece ,September 26-28 1991,1,511-513.

CONTADAKIS,M.E. and ASTERIADIS, G.,1993: *Variations on the underground water level and temperature related to the seismic activity.*Proceedings of the XVIII General Assembly of European Seismological Commission,Prague 1992, 2,333-336.

CONTADAKIS,M.E. (1993),*On the influence of non tectonic factors upon the shallow underground water level variations,*European Seismological Commission 2nd Work shop on Statistical Models and Methods in Seismology,Applications on Prevention and Forecasting of Earthquakes,Cephalonia 2-5 June 1993,(Proceedings in preparation)

CONTADAKIS,M.E. and ASTERIADIS, G.,1994: *Variations on the underground water level and temperature related to the seismic activity.* in the *Area of Volvi,Northern Greece during the years 1991-92,* XIX General Assembly of the European Geophysical Society, Grenoble 1994, Abstracts in Annales Geophys. Vol.12,Suppl. I ,C144 .

MA ZONGJIN, FU ZHENGXIANG, ZHANG YINGZHEN, WANG CHENGMIN, ZHANG GUOMIN, LIU DEFU (1990). *Earthquake Prediction (Nine major earthquakes in China 1966-1976)*, 149, Seismological Press Springer Verlag, Heidelberg.

MELCHIOR, P. 1982: *The Tides of the Planet Earth*, 2nd Edition, Pergamon Press.

OKI, Y. and HIRAGA, S.,1988: Groundwater monitoring for earthquake by an amateur network in Japan. *Pageoph,*Vol.**126**,Nos.2-4,p.211-240.

RIKITAKE,T. (1976). *Earthquake Prediction,* p. 23, Elsevier , Amsterdam.

RIKITAKE,T. (1981). *Current Research in Earthquake Prediction I* , 35, Reidel,Dotrecht.

ROELOFFS, E. A.,1988:Hydrologic precursors to earthquake. *Pageoph.* Vol.**126**,Nos.2-4,p177-209.

ROELOFFS, E. A. ,BARFORD, S. S.,RILEY, F.S.,RECORDS, A.W.,1989:Hydrologic effects on water level changes associated with episodic fault creep near Parkfield,California.*J. Geophys. Res.,*Vol **94,** B9,p. 12.387-12.402.

ROJSTACZER, S.,1988: Intermediate period response of water levels in wells to crustal strain:Sensitivity and noise level. *J. Geophys. Res.,*Vol **93**,B 11,p. 13.619-13.634.

Seismological Institute of the National Observatory of Athens. Monthly Bulletins of Earthquakes 1988 January 31 - 1989 December 12.

WAKITA,H. (1982). *Earthquake Prediction Techniques*, 175, University of Tokyo Press.

SITING OPERATIONS IN TEST AREAS OF SAXONIA (GERMANY) AND BASILICATA (SOUTHERN ITALY) FOR EARTHQUAKES PRECURSORY PHENOMENA RESEARCHES

W. Balderer [1], V. Cuomo [2], J. Heinicke [3], U. Koch[3],
V. Lapenna [4], M. Leggeri [5] and G. Martinelli [6]

1 ETH Ingenieurgeologie Honggerberg, Zurich, Switzerland
2 DIFA Università della Basilicata, Potenza, Italy
3 Saxon Academy of Sciences at Leipzig, Freiberg, Germany
4 IMAAA/CNR, Area della Ricerca del CNR, Potenza, Italy
5 CGIAM, Potenza, Italy
6 Regione Emilia-Romagna, Servizio Cartografico, Bologna, Italy

Abstract

Saxonia and Basilicata areas are affected by peculiar seismicity patterns. In particular Vogtland (Saxonia) host frequent earthquakes of medium magnitude (< 4) while Irpinian Apenninic belt (Basilicata) is recognized as one of the most seismically active areas of the Mediterranean Region. Geophysical and geochemical parameters changed macroscopically in Vogtland and in Basilicata areas in the past and in the recent age. The strong degassing activity from deep layers as marked by CO_2 and He_3/He_4 anomaly occurrences has been identified as responsible of the observed geochemical phenomena. Geophysical (i.e. self potential) anomalies can be strictly linked to geochemical phenomena through electrokinetic phenomena. A strategy able to identify the most promising sites for earthquakes prediction researches has been developed both for geophysical and geochemical parameters.

Introduction

In selected sites of Saxonia and Basilicata Regions recently started a geochemical and geophysical monitoring activity with the purpose to detect possible earthquake's precursory phenomena (see also Balderer et Al., this volume) Both in Vogtland and in Basilicata the observed parameters are compared with local seismicity.

The Basilicata area is presently monitored by the seismic network of the National Institute of Geophysics (ING), by the seismic network of the Vesuvium Observatory (OV) and by a local

accelerometric network of the Centre for the Integrated Geomorphology of the Mediterranean Area (CGIAM), now in implementation.

The seismicity of the Vogtland Region is monitored by 6 local networks equipped by 34 stations. An in depth geochemical prospection has allowed to recognize strong similarities among Vogtland and Basilicata areas : deep gases mantle originated make possible the occurrences of similar anomalous surface phenomena in both places.

Geological and seismotectonic setting of Basilicata

The studied sector of Southern Apennines consists of a pile of thrust sheets forming a complex system orogenically transported over the flexured South-Western margin of the Apulia foreland. The deepest tectonic units underlying in the roof-thrust are represented by Mesozoic-Tertiary shallow-water carbonates stratigraphically overlained by upper Messinian and Pliocene terrygenous marine deposit (Ortolani et Al., 1981). Quaternary volcanitic rocks of the Mt. Vulture volcanic complex separate the Apulia platform from the Campania-Basilicata segment. An extensive distribution of intrasedimentary tertiary and Quaternary volcanitic bodies at dephts ranging from 9.5 to 12 kms. are also recognizable (Cassano et Al., 1986) clearly responsible of localized magnetic anomalies. Two geothermal anomalies characterizes the Irpinia area and the Mt. Vulture area with temperatures exceeding 80 °C at 2,000 meters depht with respect to ground level (Panichi and Squarci, 1982).

The historical seismicity pattern (Alessio et Al., 1993) confirms intense regional seismic activity and related complexity in crustal faulting (Pantosti and Valensise, 1990). The November 23, 1980 earthquake, one of the most violent events of Southern Italy (I= X,   MCS), occurred in this area. Furthermore the highest number of disastrous events with I > /= X, MCS took place in this area at historical times. The most historically relevant events are clustered in the same zone (1694, 1930) while a strong event, the December 16, 1857 earthquake, occurred in Val D'Agri, located in the southern sector of the studied area (Mallet, 1862). The seismic activity occurred after the 1980 event consisted of medium-intensity events (>/= VII) located near the border between the Basilicata and the Campania regions. The main events occurred in the last ten years have been located in the south-east border of the seismogenic belt (Alessio et Al., 1993).

The May 5, 1990 (M = 5.2) earthquake (Tertulliani et Al., 1992; Azzara et Al., 1993) , the May 26,1991 (M = 4.9) earthquake and the May 8, 1992 (M = 3.7) earthquake can be considered the

strongest events after the Irpinia, 1980 earthquake. The events occurred in the studied zone have been followed by aftershocks sequences which identify a fault structure, strictly linked with the South Apenninic fault, located near the Potenza town (Valensise et Al., 1994).

The South Apenninic fault structure and the connected complex rupture events of the surface are strictly linked with deep originated fluid occurrences, such as geothermal manifestations, mofettes etc. strongly affected by preseismic phenomena reported in the historical seismicity studies (Battista, 1858; Mallet, 1862).

Saxonia geological and seismotectonic setting

The Saxonia geological situation is strongly affected by the Central Saxonian Lineament (NE-SW) which lies between the Fichtelgebirge granitic complex (S) and the mica slate (N). This great tectonic structure is subdivided into different blocks by fault zones in NW-SE direction (block juncture zones). The S Vogtland area is limited by the Tachov-As-Hainichen fault zone to the SW and by the Marianske Lazne fault zone to the NE. Old tectonic elements in N-S direction lead to a segmentation of the Marianske Lazne fault zone. According to Bormann (1989) only intersections of the disturbed Marianske Lazne fault zone are seismically active. Quaternary volcanism (Eger basin), mofettes, mineral and geothermal springs as well as strong gas emissions (CO_2, N_2) are the main evidence of subrecent volcanism (Polyak et Al., 1985; D'Amore et Al., 1989; Weinlich et Al., 1993). These emissions were strongly affected by preseismic phenomena in 1985 (Kaempf et Al., 1989).

Recent neotectonic processes are observable in regional seismicity and dislocations due to the regional stress field with main component in NW-SE direction. This region is characterized by a low magnitude seismicity (M < 4). Historical seismicity studies report about intensive swarms occurred in 1897, 1903 and 1908/09 with less intensive swarm sequences in between (1900, 1901, 1904, 1906, 1908). Swarms also occurred in 1914, 1929, 1936, 1962 and 1973 (Gruenthal,1989). A distinction has to be made between the Vogtland swarm quakes (shallow hypocenters located at 3-12 kms. depht and characterized by a typical frequency of occurrence) and single earthquakes with hypocenters in the depth range of 8-20 kms (Neunhofer and Guth, 1988). The seismicity of the Vogtland/West Bohemia region has been monitored by 6 local networks with 34 stations since 1962 (Neunhofer, 1993).

How to choose "sensitive" fluids localities

As a general rule Irwin and Barnes (1980) showed the correlation between active seismic regions and CO_2 degassing from deep sources. O'Nions and Oxburgh (1988) showed furthermore the peculiarities of He3/He4 ratio as a pathfinder for deep originated fluids when related to other geochemical and isotopic parameters. The assessment of the above mentioned pathfinders linked with the check of all the available historical literature on geophysical and geochemical precursory phenomena may strongly help in site locations when respected the following proposed and experimented procedures.

1) The first step to do is to compile the full list of all the spring sources and gas emissions of the investigated area.

2) The second step is characterized by a contemporary historical, geochemical and field survey (see also Dall'Aglio et Al., 1992), in particular:

   -the historical survey is devoted to check all the possible informations on macroscopic precursory phenomena occurred in the past, such as: light phenomena, flow rate variations, small changes, mud and gas emissions etc.

   -the geochemical field survey is devoted to the characterization of the natural fluids in order to eliminate all the sites possibly affected by meteorological or man induced disturbances. Temperature, flow rate, electric conductivity and pH are in the main parameters to observe in this phase.

3) In the selected sites are to carry out laboratory geochemical and isotopic analysis. Geochemical pathfinders of deep originated fluids and isotopic patterns allow a further selection for promising localities.

4) Final sites evaluations consider further possible source of artificial noise in order to avoid, f.i., disturbances in self-potential monitoring (see also Cuomo et Al., 1990), flow rate monitoring etc. Finally it must be considered the effective accessibility to the site in order to reduce logistic troubles.

It is useful to remind that the investigated Basilicata area is characterized by a 10,000 sq. kms surface, where 20 emergencies were identified at step 1), 13 localities survived at step 2), and 10

localities survived after step 3); finally, the most suitable sites are 6 after step 4) (Balderer and Martinelli, 1993).

Two sites out six are now equipped with automatic multiparametric stations (Di Bello et Al., 1994 ; Balderer et Al., this volume). The investigated area of Vogtland is characterized by a 6,000 sq. kms. surface, where 41 emergencies where identified at step 1), 17 localities survived at step 2) and 13 localities survived after step 3) (Weinlich et Al., 1993); finally, the most suitable sites are 7 after step 4) (Kaempf et Al., 1992).

Two sites out seven are now equipped with automatic multiparametric stations (Heinicke et Al., 1994).

Conclusions

The most promising test sites areas of Vogtland and Basilicata Regions have been identify following an iterative historical, geophysical, geochemical and geological strategy. We conclude that the preliminary reported results can be considered as a possible confirmation of the proposed and experimented site-selection procedure within the framework of a research project oriented on precursory phenomena. The followed strategy revealed as a practical tool also for the economic optimization in research project planning.

Acknowledgments

Thanks are due to R. Console (ING) for seismic data supply and kind suggests.

REFERENCES

Alessio, G., Esposito, E., Gorini, A., Luongo, G., Porfido, S., Identification of seismogenic areas in the Southern Apennines, Italy, Annali di Geofisica, 36 (1993), n.1 : 227-235

Azzara, R., Basili, A., Beranzoli, L., Chiarabba, C., Di Giovambattista R., Selvaggi, G., The seismic sequence of Potenza (May, 1990), Annali di Geofisica, 36 (1993) : 237- 243

Balderer W., Cuomo V., Di Bello G., Heinicke J. Lapenna V., Martinelli G. Tramutoli V., Geochemical and Geophysical precursory phenomena jointly monitored in a selected area of Southern Italy : preliminary results, IASPEI 27th General Assembly, (Poster session), Wellington (New Zealand)1994

Balderer W., Martinelli G., Geochemistry of Groundwaters and gases occurring in the November 23, 1980 earthquake area (South Italy), in " Proceedings of the 2nd International Colloquium on Gas Geochemistry", Besançon 1993, Environmental Geochemistry and Health, in press

Battista, R., Il terremoto di Basilicata, (technical report), Potenza, 1858, 55 pp.

Bormann P., (ed.), Monitoring and analysis of the earthquake swarm 1985/86 in the Region Vogtland/Western Bohemia, Potsdam, 1989, 282 pp.

Cassano, E., Fichera, R., Arisi Rota, F., Aeromagnetic survey of Italy : a few interpretative results, A.G.I.P.- D.E.S. - M.E.S.G., 1986, 13 pp.

Cuomo, V., Lapenna, V., Macchiato, M., Patella, D., Satriano, C., Serio, C., Statistical analysis of noisy voltage recording in geoelectrical prospecting, Boll. Geof. Teor. Appl., 32 (1990) : 127-138

Dall'Aglio, M., Quattrocchi, F., Bencini, A., Duchi, V., Brondi, M., Selecting proper sites for the automatic monitoring of geochemical premonitory events of earthquakes : case histories from Italy, in "Water-Rock Interaction WRI-7", Proceedings of the 7th International Symposium on Water-Rock Interaction / Park City/ 13-18 July 1992, Rotterdam, 1992, pp. 371- 375

D'Amore, F., Fancelli, R., Nuti, S., Michard, G., Paces, T., Origin of gases in Variscan massifs of Europe, in "Water-Rock Interaction WRI-6", Proceedings of the 6th International Symposium on Water-Rock interaction / Malvern/3-8 August 1989, Rotterdam, 1989, pp. 177-180

Di Bello, G., Lapenna, V., Satriano, C., Tramutoli, V., Self potential time series analysis in a seismic area of Southern Italy: first results, Annali di Geofisica, Vol.37, N°6,1994.

Gruenthal,G., About the history of seismic activity in the focal region Vogtland/Western Bohemia, Bormann P. (ed.) " Monitoring and analysis of the earthquake swarm 1985/86 in the region Vogtland/Western Bohemia", Potsdam, 1989, pp. 30-34

Heinicke, J., Koch U., Martinelli G., CO2 and Radon measurements in the Vogtland area (Germany) - A contribution to earthquake prediction research, Geophys. Res. Lett., (1994), in press

Irwin, W.P. and Barnes, I., Tectonic relations of carbon dioxide discharges and earthquakes, J. Geophys. Res., 85 (1980) : 3115-3121

Kaempf, H., Strauch, G., Vogler, P., Michler, W., Hydrologic and hydrochemic changes associated with the December 1985/January 1986 earthquake swarm activity in the Vogland/NW Bohemia seismic area, Z. geol. Wiss., Berlin, 17 (1989) : 685-698

Kaempf, H., Strauch, G.,Weinlich, H., Fluidaregime, Entgasungsungsverhalten Kruste/Mantel Entlang des NNW-SSE-Profils: Ronneburg-Bad Brambach-Marianske Lazne, (technical report), 1992

Mallet, R., The first principle of observational seismology as developed in the report to the Royal Society of London of the expedition made by command of the Society into the interior of the Kingdom of Naples to investigate the circumstances of the great earthquake of December 1857, London, 1862 (Reprint Istituto Nazionale di Geofisica, Roma, 1987)

Neunhofer, H. and Guth, D., Mikrobeben seit 1962 im Vogtland, Seismologische Aspekte una Beziehungen zur lokalen Geologie, Z. Geol. Wiss., 16 (1988) : 135-146

O'Nions, R.K., Oxburg, E.R., Helium, Volatile fluxes and the development of continental crust, Earth Plan. Sci. Lett., 90 (1988) : 331-347

Ortolani, F., de Gennaro, M., Ferreri, M., Ghiara, R.M., Stanzione, D., Zenone, F., Prospettive geotermiche dell'Irpinia centrale (Appennino Meridionale) Studio geologico-strutturale e geochimico, Boll. Soc. Geol. It., 100 (1981) : 139-159

Panichi, C., Squarci, P., Carta delle temperature sotterranee in Italia, C.N.R. - P.F.E. - S.P.E.G., 1982

Pantosti, D., Valensise, G., Faulting mechanisn and complexity of the November 23, 1980 Campania-Lucania earthquake, inferred from surface observations, J. Geophys. Res., 95 (1990) : 15319 - 15341

Polyak, B.G., Prasolov, E.M., Cermak, V., Verkhovskiy, A.B., Isotopic composition on noble gases in geothermal fluids of the Krusne Hory Mts., Czechoslovakia, and the nature of the local geothermal anomaly, Geochim. Cosmochim. Acta, 49 (1985) : 695-699

Tertulliani, A., Anzidei, M., Maramai, A., Murru, M. Riguzzi, F., Macroseismic Study of the Potenza (Southern Italy) Earthquake of 5 May, 1990, Natural Hazards, 6 (1992) : 25-38

Valensise, G., Pantosti, D., Boschi, E., Matching History with Geology : a novel approach to Italian seismic hazard, submitted to Nature (1994)

Weinlich, F.H., Brauer, K., Kampf, H., Strauch, G., Weise, S., Mantel-Kruste-Wechselwirkung im Bereich der Marienbader Storungszone, Teil 2, Z. Geol. Wiss., 21 (1993), 1/2 : 135-142

The joint monitoring of geochemical and geophysical parameters in a selected test site of Southern Italy: preliminary results.

by

P. Balderer°, V. Cuomo°°, G. Di Bello°°°, J. Heinicke',
V. Lapenna°° , G. Martinelli", V. Tramutoli"'.

ABSTRACT.

Southern Italy is one of the most seismically active area of the Mediterranean region. In the area damaged by the November 23, 1980 earthquake (M=6.9) geochemical fluids reach the ground surface bringing physical and chemical informations on deep environments potentially affected by geodynamic phenomena. A preliminary screening of spatial and temporal patterns of geochemical and geophysical precursors is carried out in the Southern Appeninnes chain. An automatic station, able to detect possible precursory phenomena, has been set up close to an anomalous fluid emission on the studied area. The station is equipped with sensors suitable for CO_2, Rn 222, electrical conductivity in water, temperature and self-potential probes to detect the electrotelluric currents. The countinously collected data are stored on magnetic support and statistically checked in order to distinguish geodynamically induced anomalies with respect to the background. Stochastic models are applied to describe the dynamics of precursory time series and to evaluate the occurrence probability of anomalies. Technological features of the device are discussed together with preliminary results.

° ETH Ingenieurgeologie Hongerberg, Zurich, Switzerland,Italy.
°°Istituto di Metodologie Avanzate di Analisi Ambientale, CNR, Tito(PZ), Italy.
°°° Dipartimento di Ingegneria e Fisica dell'Ambiente, Università della Basilicata, Potenza, Italy.
' Saxon Academi of Sciences, Freiberg, Germany.
" Servizio Cartografico Regione Emilia Romagna, Bologna, Italy.
"' Università della Basilicata, Facoltà di Scienze, Potenza, Italy.

1. Introduction

On November 23, 1980 a (Ms=6.9) earthquake happened in the Irpinia and Basilicata Apenninic regions (Fig.1). It was the largest and most destructive earthquake that occurred in Southern Italy for over 100 years (Westaway and Jackson, 1984) and, also, among the biggest earthquakes reported in the Italian seismic catalogue (Pantosti and Valensise, 1990). From historical records it is recognizible that in this region periodically very strong earthquakes happened throughout the centuries (Westaway and Jackson, 1984). In the same Irpinia-Basilicata area a lot of precursors and coseismic phenomena are also documented by historical reports. Robert Mallet (1862) collected systematically testimonies on precursor fluid changes, which occurred before, during or immediately after the Neapolitan Earthquakes of 1857 whose epicentre has been recognized very close to the epicentre of the earthquake of November 23, 1980. Changes in many geochemical and geophysical parameters have been observed before and during an earthquake and many models have been proposed to describe, in the time domain, the anomalies in the precursory phenomena measured near the epicentral areas (Wood R.M. and King G.C.P., 1993).

A scientific approach to the problem can be based on the analysis of the space and time patterns of seismic precursors, around the focal region, continuosly monitored by a network of multiparametric stations and on the application of advanced statistical methods to pick out the anomalies related to the seismic events.

On the basis of these considerations a preliminary screening of spatial and temporal patterns of geochemical and geophysical precursors was carried out in Southern Italy. Furthermore a first automatic station, able to detect the geochemical and geophysical parameters, has been set up close to an anomalous fluid emission on the studied area (Tramutola station). (Fig.1)

The goal of this work is the monitoring of both geochemical and geophysical parameters in order to build up advanced statistical methods to study the correlation beetween different precursory phenomena and seismic sequences.

Fig.1 Satellite image of selected area.
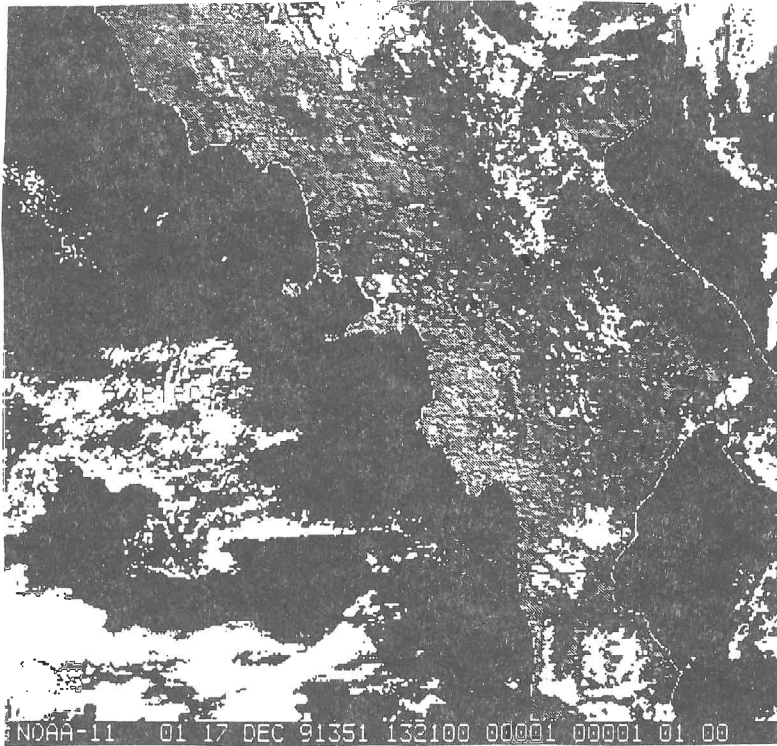
2. Searching for geochemical and geophysical precursory phenomena.

The historical seismicity pattern (Pantosti and Valensise,1990) confirm intense regional seismic activity and related complexity in crustal faulting. Deep faults can be responsable of anomalous fluids occurrence, while rock porosity is suitable for hydrothermal phenomena (De Gennaro et al., 1981). Short circulation spring waters widely occurs in the entire area. The locations of the sampled springs coincides with the epicentral area of the Irpinia-Basilicata, 1980 earthquake. The investigated area is located in a tectonically active region where great amounts of rocks and gases interact as recognized by recent investigations (Balderer and Martinelli, 1994). In this region there are favourable conditions for studies of interactions and correlations between tectonic activity and variations of the chemical and isotopic compositions in fluids and gases (Balderer et al.,1994) . Finally we have a *natural laboratory* where it is possible to study the electrokinetic processes possibly induced by geochemical/electrochemical anomalies.

3. Tramutola station

An automatic station, able to detect precursory phenomena, has been set up close to an anomalous fluid emission on the studied area. The station is equipped with sensors suitable for CO2, Radon 222, electrical conductivity in water, temperature and self-potential probes to detect the electrotelluric currents (Fig.2). The sampling interval is 15 min.

Fig.2 The scheme of the station.
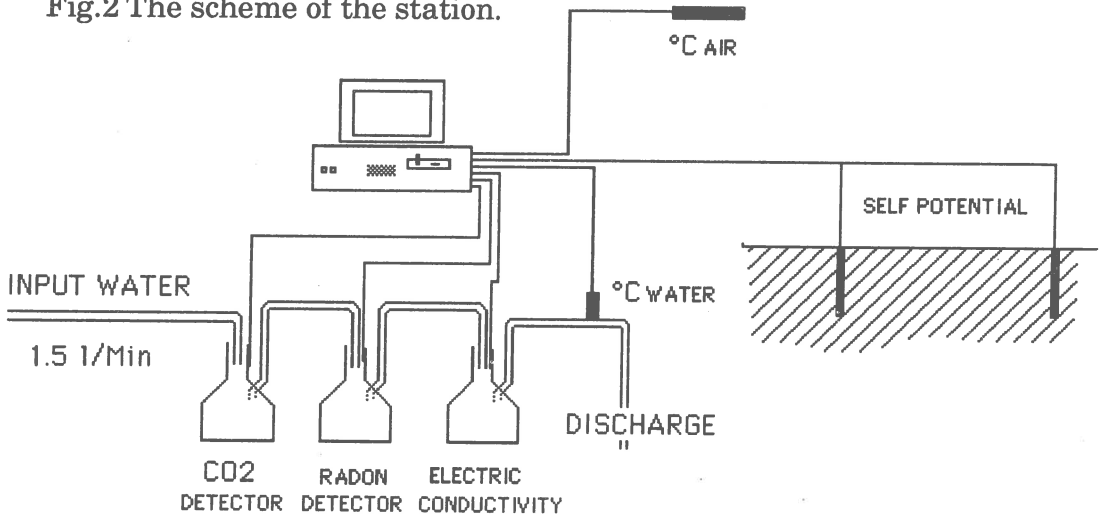
4. Statistical analysis of precursory phenomena.

Changes in many geochemical and geophysical parameters measured near the epicentral area are observed before and during an earthquake The correlation between the observed anomalies and the seismic sequences very often is performed only with a qualitative approach and without robust statistical tests. In this way we have always the reasonable doubt: *are the anomalies random fluctuations intrinsic to the processes or are extreme events related to the earthquake?* (Burton, 1985).

It is necessary to evaluate the occurrence probability of the anomalies (successive values above/below a prefixed threshold) and to select only the anomalies with a very low occurrence probability. Only in this way we will be able to reject the events that are just random fluctuations around the mean values: this could be

considered an objective methodology (Lapenna et al., 1994).

The time series are realizations of a stocastic process: it is necessary to know the statistical law to describe the time dynamic of the variable. The occurrence probability of anomalies is strongly related to the stocastic model that describes the data.
We suggest a statistical analysis of precursory phenomena that can be subdivided in the following steps for each precursor:
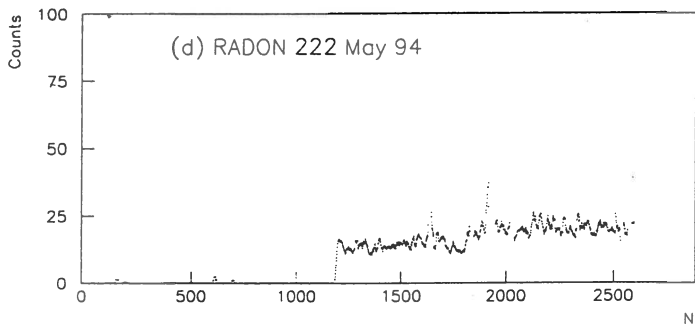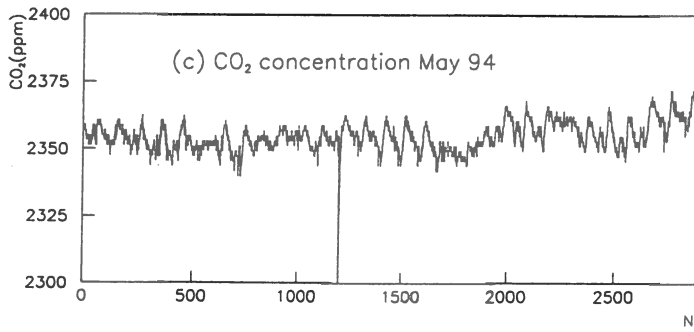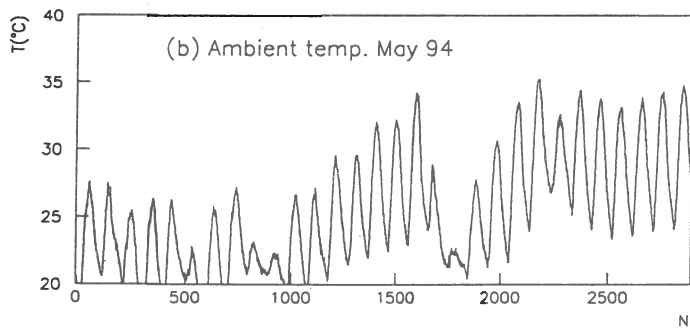a) to analyze the spectral features of the time series and to study the correlation with meteo-climatic parameters;
b) to remove the periodic components for precursory record in order to obtain residual time series;
c) to define a threshold and localize in the time series the value above/below the threshold;
d) to use stochastic models to describe experimental data in order to evaluate the occurrence probability of the extreme events;
e) to study the correlation with seismic sequence.

5. Preliminary results.

In the following graphs (Fig.3) we show some preliminary results regarding the parameters continuously monitored at Tramutola station. The observed variables are: a) water temperature; (b) ambient temperature; (c) $CO2$; (d) radon 222; (e) self-potential (N-S); (f) self-potential (E-W); (g) electrical conductivity in water. The results ragarding the spectral analysis of the recorded time series we obtain using the maximum entropy method are shown in the Fig.4.

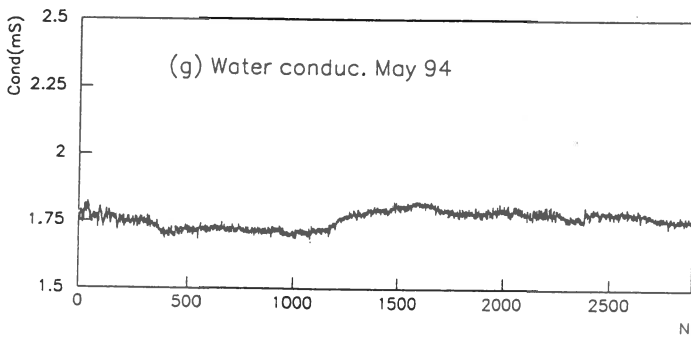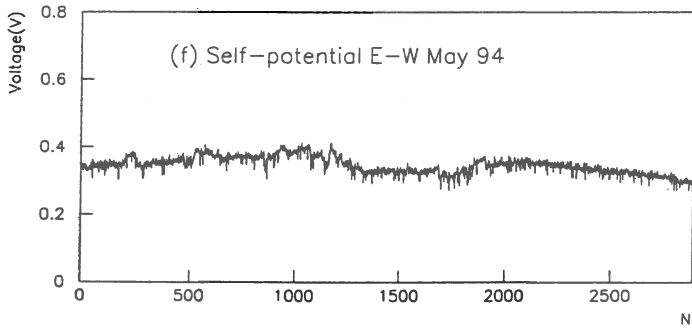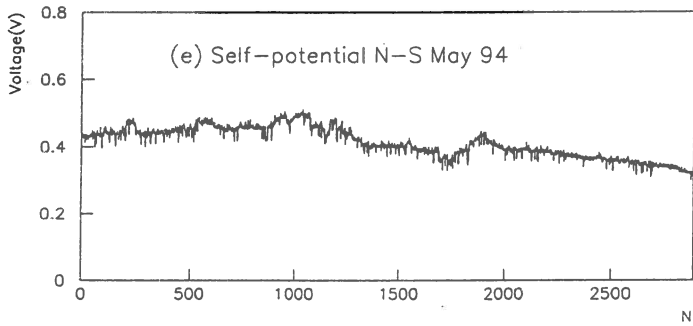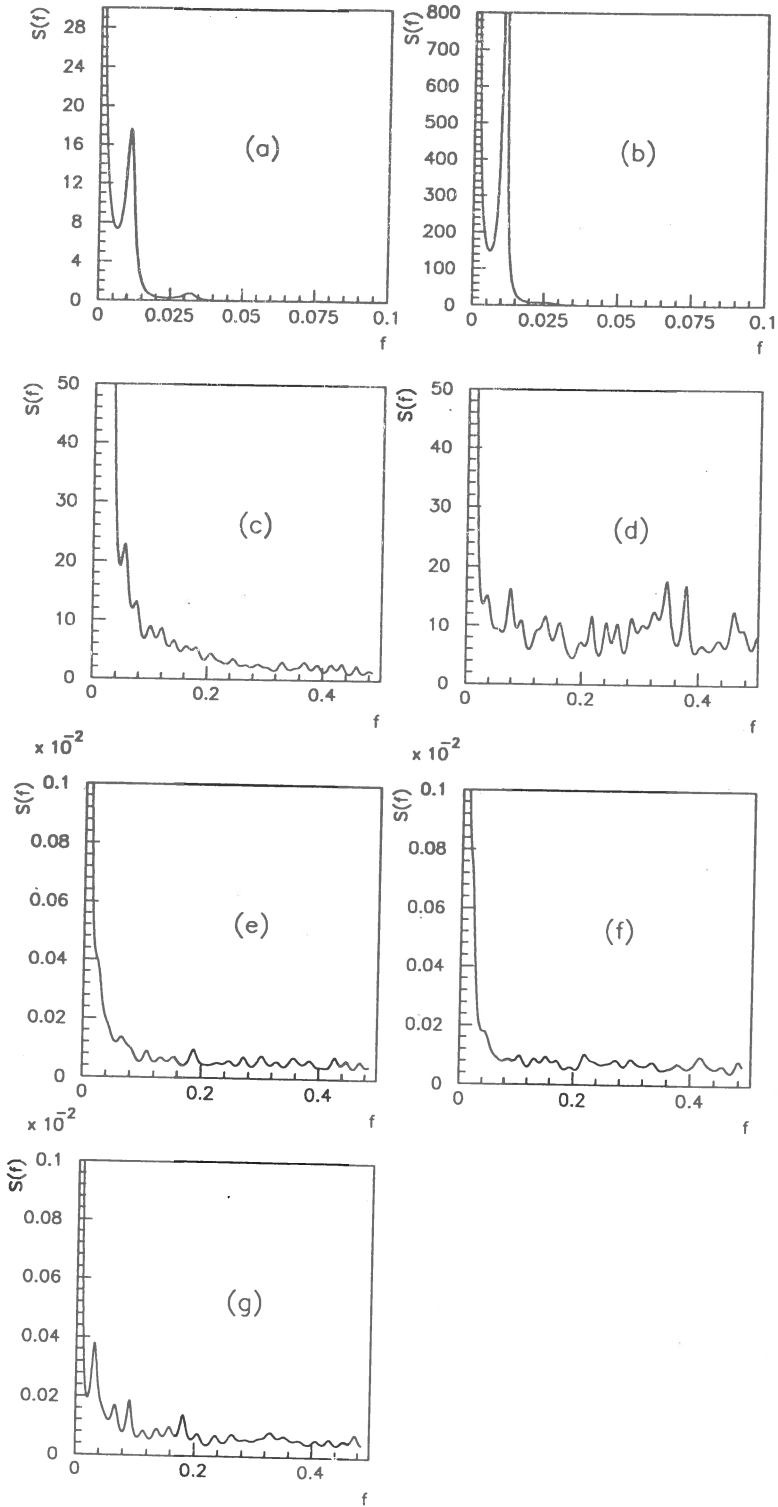Fig.3 First data recorded by Tramutola station during May '94.

1164

(b) Ambient temp. May 94

(c) CO$_2$ concentration May 94

(d) RADON 222 May 94

(e) Self-potential N-S May 94

(f) Self-potential E-W May 94

(g) Water conduc. May 94
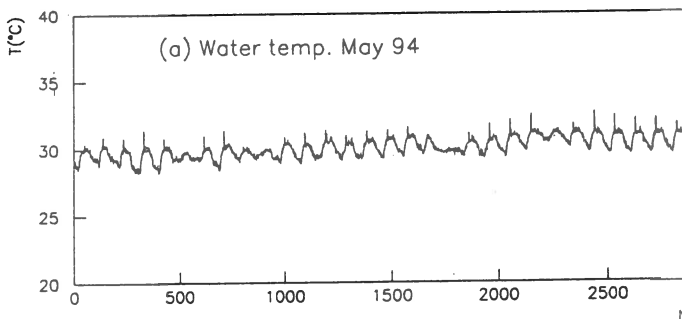
Fig.3 Power spectra of first data in the same order of Fig.2.

6. Conclusions

After a preliminary screening of geochemical and geophysical precursory phenomena observed in historic and in recent years, we selected a set of sites. In the Tramutola area a multiparametric station able to jointly monitor anomalies in deep fluids and electrical field has been set up. In Tito a self-potential automatic station was also set up. In S. Cataldo test site a multiparametric station is now starting the monitoring activity. Furthermore a complete and objective statistical analysis is applied to all parameters. In the next future we plan to have very long time sequences for each parameter in order to check the possible correlations with tectonic activity by mean of stochastic models.

References

Balderer and Martinelli:*Geochemistry of groudwaters and gases occurring in the November 23, 1980 earthquake area.* Environmental Geochemistry and Health (1994)
Balderer et al.: *Siting operation in test areas of Saxonia (Germany) and Basilicata (Southern Italy) for earthquakes precursory phenomena reseaches.* ESC Athens (1994)
Burton P.W. : *Electrical earthquake prediction,* Nature, Vol. 315 (1985)
Di Bello G., Lapenna V., Satriano C. and V. Tramutoli (1993) *Self-potential time series analysis in a seismic area of Southern Italy: first results.* Annali di Geofisica (in press)
Jenkins and Watts (1968), *Spectral Analysis and Its Applications*, Holden-Day, San Francisco.
Lapenna V., Macchiato M., Patella D., Serio C., Satriano C. and Tramutoli: *Statistical Analysis of non stationary voltage recording in geoelectrical prospecting.* Geophysical Prospecting 42 (1994)
La Volpe L., Patella D., Rapisardi L. and A. Tramacere (1984): *The evolution of the Monte Volture Volcano (Southern Italy): inferences from volcanological, geological and deep electrical sounding data.* Journ. of Volcanology and Geothermal Res. 147-162.
Mallet R. (1862): *Great Napolitan Earthquake of 1857.* The first principles of observational seismology, 2nd Vol. London 862pp. ING-SGA Bologna(1987).
Nur A., (1972) *Dilatancy, pore fluids and premonitory variations of tp / ts travel times,* Bull. Seismol. Soc. Am., 62, 1217-1222.
Pantosti D. and G. Valensise (1990): *Faulting mechanism and complexity of the November 23 1980, Campania -Lucania Earthquake, inferred from surface observations,* Journ. Geophys. Res., 95, 15,319-15,341.
Westaway R., and J. Jackson (1984): *Surface faulting in the Southern Italian Campania Basilicata earthquake of November 23, 1980.* Nature, 312, 436-438.
Wood R.M. and King G.C.P. (1993):*Hydrological signatures of earthquake strain,* Journal of Geophysical Research.

STUDY OF DEFORMATION PARAMETERS IN THE GRUIU-CALDARUSANI GEODYNAMIC POLYGON (ROMANIA)

by Mateciuc D., Nacu V., Radulescu Fl., Stiopol D.

NATIONAL INSTITUTE FOR EARTH PHYSICS
P.O.Box MG-2, Bucharest-Magurele, ROMANIA.

ABSTRACT

Repeated trilateration-triangulation measurements of local or regional networks are frequently the basis of geodetic strain analyses. As a rule, the strain field is considered homogeneous for the whole area under investigation or at least for parts of it. However, the treatment of strain as homogeneous over a large area means averaging strains and is often not desired. Therefore, the area under investigation can be dissected into finite elements, i.e. triangles. The individual analyses of these elements lead to meaningful results which can serve as a basis for refined models of interpretation. Using finite element method for Gruiu-Caldarusani geodynamic polygon (consisting of 12 deep benchmarks which covered an area of about 1.5 * 1.0 Km) the strain parameters for the period 1982-1984-1986-1989 were calculated. For each finite element of the network, maximum principal strain (ε_1) and minimum principal strain (ε_2) are represented.

1. INTRODUCTION

Strain analyses are frequently performed on the basis of repeated measured local or regional geodetic networks. Doing so, strain is usually considered homogeneous for the whole polygon or, at least, for parts of it. However, this approach does not always work in reality. This can be done by dissecting the area concerned into finite elements. The triangle was the finite element used for computations of the deformation parameters in *Gruiu-Caldarusani* geodynamic polygon.

Taking into account tectonic and geodynamic considerations, the *Gruiu-Caldarusani* polygon is situated in the Northern part of the *Moesian   Platform* on the   transition zone with the *Pericarpathian Depression*.

The crystalline basement is divided into different sectors, the *Dobrudjan* and *Vallachian*, separated by an important tectonic accident called the *Intramoesian Fault* which extends quite some distance, especially in the Southern part of the *Black Sea* area.

This one seems to be a tectonic line of major importance which divided the Platform into different domains with various sedimentary conditions, depending on the petrologic constitution of the basement and the geothermal regime.

Geodetic measurements of distance were performed in the polygon in the years 1982, 1984, 1986, 1989 (Ghitau et al, 1989).

For the periods mentioned above, the compensating coordinates were resulted after processing the initial data. The base data of the calculation for the deformation parameters are the displacement vectors **x**. The paper presents the deformation parameters for each finite element of the networks.

2. MATHEMATICAL TREATMENT

2.1 *Deduced displacement vectors and their error ellipses.*
Displacement vectors **x** are deduced from the new and old position vectors **X'**, **X''**(see Tab.1)

$$X = X' - X''$$ (1)

Variance – covariance matrix Σ of the displacement vectors can be obtained from variance-covariance matrix Σ and Σ of new and old position vectors as follow :

$$\Sigma_\mathbf{x} = \Sigma_{\mathbf{x'}} + \Sigma_{\mathbf{x''}}$$ (2)

where:

$$\Sigma_{\mathbf{x''}} = \begin{vmatrix} \sigma^2_{x''} & \sigma_{x''y''} \\ \sigma^2_{x''y''} & \sigma^2_{y''} \end{vmatrix}$$ (3)

σ^2_x, σ^2_y is variance of x, y components of the determined displacement vectors respectively, and σ_{xy} is the covariance. Similarly, $\sigma^2_{x'}$ σ^2_y , $\sigma_{x'y'}$, and $\sigma^2_{x''}$, $\sigma^2_{y''}$, $\sigma_{x''y''}$ are variances and covariances of new and old positions. Usually in geodesy x is taken as the N – S and y as E-W directions.
Major axis a, its orientation ϕ, and minor axis b of error distribution with respect to azimuth for the obtained displacement vector are given by the formulae:

$$a^2 = 1/2 * (\sigma^2_x + \sigma^2_y + \omega)$$ (4)

$$b^2 = 1/2 * (\sigma^2 + \sigma^2 + \omega)$$

$$\omega = \{(\sigma^2_x - \sigma^2_y)^2 + 4 * \sigma^2_{xy}\}^{1/2}$$

$$\phi = 1/2 \tan^{-1} 2\sigma / (\sigma^2 - \sigma^2)$$

DISPLACEMENT VECTORS (mm)			
No	1982/1984	1984/1986	1986/1989	1982/1989
1	4.46	2.28	2.69	4.04
2	9.41	3.54	4.30	6.71
3	2.77	9.01	10.82	2.21
4	2.45	2.92	4.30	3.19
5	2.84	3.07	7.21	6.80
6	7.92	3.50	6.07	5.10
7	2.52	1.71	1.49	3.27
8	2.62	2.60	0.85	0.82
9	6.20	1.00	6.07	13.00
10	2.18	1.92	0.41	2.38
11	1.66	3.44	2.86	1.99
12	3.88	4.24	2.77	3.07

ANGLES OF DISPLACEMENT VECTORS TO N DIRECTION			
No	1982/1984	1984/1986	1986/1989	1982/1989
1	146.97	132.01	334.81	146.65
2	13.64	147.45	298.52	2.85
3	354.89	266.69	72.06	5.77
4	213.07	42.27	334.15	345.76
5	188.75	378.86	151.25	153.97
6	70.84	301.82	190.52	131.19
7	107.60	77.16	346.97	73.97
8	244.85	17.38	77.16	384.40
9	0.00	340.97	290.52	298.53
10	217.72	342.95	184.40	263.30
11	236.37	160.51	359.48	219.47
12	286.79	90.97	71.51	78.86

Tab. 1   Displacement vectors and their angles

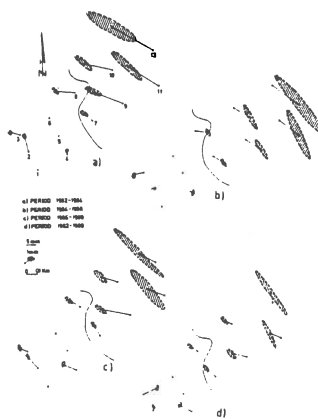Displacement vectors and their error determination ellipses are shown in Fig. 1 and Tab. 2 for Gruiu-Caldarusani network.

Fig. 1   Displacement vector in the Gruiu-Caldarusani geodynamic polygon and the distribution of their error ellipses

No	Major axis	Minor axis	Angle to N	a\b	
1	0.52602026	0.14529973	189.4860	53/15	1982–1984
2	0.27265013	0.21758987	152.8481	27/22	
3	0.44544862	0.16762138	21.9207	45/17	
4	0.33951704	0.16767295	25.3068	32/17	
5	0.25032290	0.12149711	359.9041	25/12	
6	0.36113902	0.12557099	175.5704	36/13	
7	0.85937266	0.13155736	352.7504	86/13	
8	0.62589677	0.12586323	350.2343	63/13	
9	0.58179972	0.16902028	355.0380	58/17	
10	0.47696307	0.22605693	360.4366	48/23	
11	0.61917954	0.25607044	10.2985	62/26	
12	1.15472206	0.35330793	177.0722	115/35	
No	Major axis	Minor axis	Angle to N	a\b	
1	0.64713876	0.14475122	190.7160	65/14	1984–1986
2	0.31173351	0.22450649	352.4913	31/22	
3	0.60731925	0.18018076	26.3272	61/18	
4	0.41411368	0.18748632	22.5883	41/19	
5	0.30567529	0.12210471	359.5913	31/12	
6	0.47859947	0.13368054	179.7183	48/13	
7	0.96576776	0.14332224	351.9135	97/14	
8	0.72155862	0.13453138	351.6063	72/13	
9	0.60606844	0.21426157	350.6703	61/21	
10	0.47112790	0.24736211	359.7643	47/25	
11	0.68055639	0.24978361	9.4116	68/25	
12	1.23561001	0.36774998	175.3133	124/37	
No	Major axis	Minor axis	Angle to N	a\b	
1	0.63748771	0.14256228	191.2515	64/14	1986–1989
2	0.30592795	0.20554205	153.4407	31/21	
3	0.59550576	0.17901425	26.8439	60/18	
4	0.41146915	0.18694085	22.7958	41/19	
5	0.30357456	0.12140544	359.8250	30/12	
6	0.47517659	0.13129342	179.3114	48/13	
7	0.95423474	0.14318525	351.8228	95/14	
8	0.71115189	0.12662811	351.3477	71/13	
9	0.58245001	0.21357000	350.0069	58/21	
10	0.44778045	0.21445955	367.2685	45/21	
11	0.67742373	0.24281625	9.0708	68/24	
12	1.00899630	0.29292368	164.8530	101/29	
No	Major axis	Minor axis	Angle to N	a\b	
1	0.51621940	0.14326061	190.1713	52/14	1982–1989
2	0.26840707	0.19706293	160.2459	27/20	
3	0.43321807	0.16687192	22.5443	43/17	
4	0.31694089	0.16705911	25.6548	32/17	
5	0.24822989	0.12079011	360.2416	25/12	
6	0.35801367	0.12288634	174.9617	36/12	
7	0.84781102	0.13144900	352.6612	85/13	
8	0.61559571	0.11785429	150.0761	62/12	
9	0.55773644	0.16877356	354.6724	56/17	
10	0.45383320	0.19293680	367.1253	45/19	
11	0.61598432	0.24916565	9.8857	62/25	
12	0.92232250	0.28426748	165.8536	92/28	

Tab.2 Error ellipses

2.2 Strain analysis

Strain parameters (Tab.3) are deduced from displacement vectors by the following method expressed in a matrix form.

Let X be the displacement vector, U the strain matrix, and A the coefficient matrix:

$$X = A * U \tag{5}$$

where:

$$X = \begin{vmatrix} x_i \\ y \end{vmatrix} \qquad i = 1, 2, 3 \tag{6}$$

$$U = \begin{vmatrix} u_1 \\ u_2 \\ u_3 \\ u_4 \\ u_5 \\ u_6 \end{vmatrix} = \begin{vmatrix} x_0 \\ \varepsilon_{xx} \\ 5 * (\gamma_{xy}) - \omega \\ y_0 \\ 5 * (\gamma_{xy}) + \omega \\ \varepsilon_{xy} \end{vmatrix} \tag{7}$$

(x_0, y_0) represents a shift, ε_{xx}, ε_{yy}, γ are the strain components and ω is the rotation. We represent the coordinates of three terminal stations of a triangle with respect to its centre:

$$dX = \begin{vmatrix} dx_i \\ dy_i \end{vmatrix} \qquad , i = 1, 2, 3 \tag{8}$$

then :

$$A = \begin{vmatrix} 1 & dx_1 & dy_1 & 0 & 0 & 0 \\ 1 & dx_2 & dy_2 & 0 & 0 & 0 \\ 1 & dx_3 & dy_3 & 0 & 0 & 0 \\ 0 & 0 & 0 & 1 & dx_1 & dy_1 \\ 0 & 0 & 0 & 1 & dx_2 & dy_2 \\ 0 & 0 & 0 & 1 & dx & dy \end{vmatrix} \tag{9}$$

Solving eq. 5 we obtain:

$$U = A^{-1} X \tag{10}$$

Dilatation Δ, maximum shear strain γ_{max}, pure shear γ_1, engineering shear γ, principal strain ε_1 and ε_2 are :

$$\Delta = u_2 + u_6 = \varepsilon_{xx} + \varepsilon_{yy} \tag{11}$$

$$\gamma_{max} = \{(u_2-u_6)^2+(u_3+u_5)^2\}^{1/2} = \{(\varepsilon_{xx}-\varepsilon_{yy})^2+\gamma_{xy}^2\}^{1/2}$$

$$\gamma_1 = \varepsilon_{xx}-\varepsilon_{yy} \quad ; \quad \gamma_2 = 2\varepsilon_{xy} \tag{11}$$

$$\epsilon_1 = (\Delta + \gamma_{max})/2 \quad ; \quad \epsilon_2 = (\Delta - \gamma_{max})/2$$

STRAIN PARAMETERS							
Finite element	*Dilatation*		*Maximum shear strain*		*Maximum principal strain*		*Minimum principal strain*	
(triangle)	Δ		γmax		ε1		ε2	
No	84/82	86/84	84/82	86/84	84/82	86/84	84/82	86/84
1	0.45	-0.02	0.60	1.03	0.52	0.50	-0.07	-0.52
2	0.26	-0.82	2.77	0.95	1.51	0.06	-1.26	-0.89
3	0.53	0.14	2.95	1.54	1.74	0.84	-1.21	-0.70
4	1.89	1.90	1.04	2.93	1.47	2.42	0.42	-0.52
5	-2.28	1.00	2.00	0.81	-0.14	0.90	-2.14	0.10
6	0.03	-0.48	0.48	0.54	0.25	0.03	-0.23	-0.51
7	-0.29	0.85	0.16	0.55	-0.06	0.70	-0.23	0.15
8	-0.43	0.74	1.76	0.67	0.67	0.71	-1.10	0.04
9	2.10	-0.82	2.37	0.69	2.24	-0.07	-0.14	-0.75
10	-1.09	0.40	1.16	0.68	0.03	0.54	-1.13	-0.14
11	-1.20	0.23	1.19	1.77	0.00	1.00	-1.20	-0.77
No	89/86	89/82	89/86	89/82	89/86	89/82	89/86	89/82
1	0.92	0.35	2.37	2.29	1.64	1.82	-0.73	-0.47
2	1.73	1.16	0.94	2.77	1.34	1.97	0.39	-0.80
3	-1.95	-1.28	1.01	1.86	-0.47	0.29	-0.48	-1.57
4	-2.42	1.38	4.61	0.75	1.10	1.06	-3.52	0.31
5	0.24	-1.04	1.48	0.28	0.86	-0.38	-0.62	-0.66
6	1.46	1.00	1.41	1.28	1.44	1.14	0.02	-0.14
7	-1.83	-1.27	2.63	1.93	0.40	0.33	-2.23	-1.60
8	-0.14	0.17	2.41	3.87	1.13	2.02	-1.28	-1.85
9	1.02	2.31	3.17	6.00	2.10	4.15	-1.08	-1.85
10	-1.08	-1.77	0.92	1.65	-0.08	-0.06	-1.00	-1.71
11	1.44	0.48	0.75	2.68	1.10	1.58	0.34	-1.10

Tab.3 Strain parameters

The Earth's strains in the Gruiu-Caldarusani geodynamic polygon and the distribution of their error ellipses are shown in Fig.2, where the full-line shows the extension and the dotted-line the contraction.

The authors made up a program which is able to compute all the above mentioned strain parameters.

The program is structured in three sections, as follows:

1. The computation of strain parameters as described in the [11] relations.
2. The computation of displacement vectors.

3. the computation of error ellipses.
4. Graphic representation of the triangular network.
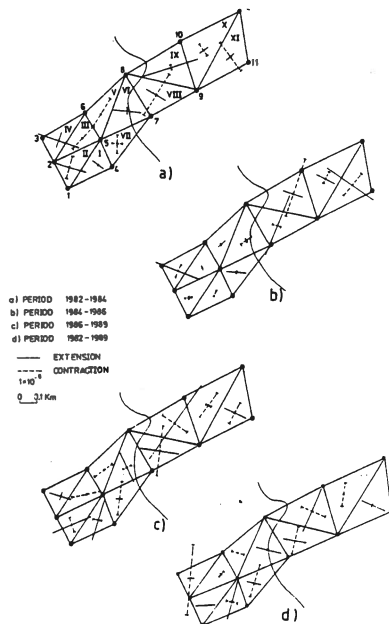
Fig. 2 Earth's strains in the Gruiu-Caldarusani
geodynamic polygon

3. Conclusions and Results
covering the period 1982-1984-1986-1989

Compensation by indirect observation method has been used for the computation of the network benchmarks coordinates. After the compensation, the x, y coordinates, denoted with **X** vector in the strain analysis are at the measurement time.

By the application of the above working method, we have calculated the deformation parameters for each finite element of the polygon in both periods of measurements.

The μ – strain $* 10^{-5}$ is the measure unit of the maximum main strain ε_1, and the minimum main strain ε_2. One can observe that, the maximum main strain values cover a limited domain , between $-0.14 * 10^{-5}$ and $+ 1.74 * 10^{-5}$, for the first period. Moreover, only four values from the eleven, which correspond to the finite elements are negative, being close to zero.

For the second period (1984 – 1986), only one value is negative, namely $- 0.07 * 10^{-5}$ in the IV triangle.

The other values are grouped in the $[+ 0.06 * 10^{-5}, + 2.42 * 10^{-5}]$ interval.

For the third period (1986 – 1989) one may notice only two negative values of the maximum strain, very close to zero

On the contrary, the positive values are increasing, as we compare them to the other two periods, reaching up to $4.15 * 10^{-15}$ with the finite element 9.

When we refer to the minimum strain ε, one may notice that for each of the three above mentioned periods, there are very few positive values, while the negative values reach up to -3.52 with the finite element 4, in the third period. Considering the alternative chance of the main parameters, from one sign to the other, we can not draw a relevant final conclusion.

And yet, one should mentioned the high accuracy of the working measurements in respect of the error ellipse axis values for the determination of the displacements. These values are generally with more than one degree smaller than the resulted movements, and this situation occurs in the case when there are movements of first degree.

REFERENCES

Airinei St.,1976. *Anomalies gravimetriques regionales pouvant refleter des segments de plaque ou de microplaques de la lithosphere sur le territoire de Roumanie*, XXV Congrès Comité de géologie et de géophysique marine, Split.

Constantinescu L., Cornea I. and Lazarescu V., 1975. *Seismotectonic Map of the Romanian Territory*, St. tehn. ec., seria D, 10: 291-298.

Cornea I. and Polonic Gabriela, 1979. *Data on the seismicity and seismo-tectonics of eastern part of the Moesian Platform.* St. cerc. geol. geofiz. geogr., seria geofiz., 17(2): 167-176, (in Romanian).

Cornea I., Zugravescu D., Ghitau D., Popescu M, and Radulescu F., 1980. *The Caldarusani-Gruiu Geodynamic Polygon.* Rév. Roum. Géol. Géophys. Géogr., Sér. Géophys., 24(2): 171-191.

Cornea I. and Lazarescu V., 1980. *Tectonics and geodynamic evolution of the Romanian territory.* Prepr. Centr. Inst. Physics, 100 pp. (in Romanian).

Fuji Y., and Nakane K., 1983. *Horizontal crustal movements in the Kanto-Tokai District, Japan, as deduced from geodetic data,* Tectonophysics, 97 115-140.

Ghitau D., 1991. *Geodatische Erfassung lokaler und regionaler Mikroplatten Bewegungen in Rumanien fur die Erdbeden - Vorhersage, Mitteilungen,* 57: 25-30.

Popescu M.N, 1986. *A possible interpretation of the preliminary results obtained in the Gruiu - Caldarusani Geodynamic Polygon,* Rév. Roum. Phys., 31: 89-93.

Radulescu F., Nacu V., and Mocanu V., 1991. *Study of Recent Crustal Movements,* Prepr. Inst. for Atomic Physics, 103 pp.

Radulescu F.,Ghitau D.,Nacu V.,Stiopol D., 1992. *Study of Recent Crustal Movements in Romania (Gruiu - Caldarusani Polygon),* Tectonophysics, 202: 141-144.

Rikitake T., 1986. *Crustal Movements as revealed by Geodetic Surveys,* Earthquake Prediction Research, 4: 280-301.

Sandulescu M., 1984. *Geotectonics of Romania,* Technical Publishing House, 336 pp., (in Romanian).

Welsch W., 1983. *Finite element analysis of strain patterns from geodetic observations across a plate margin.* Tectonophysics, 97, 57-71.

VERTICAL CRUSTAL MOVEMENTS IN THE VRANCEA AREA (ROMANIA) GENERATED BEFORE AND AFTER A SEISMIC EVENT

by   Stiopol D., Radulescu Fl., Nacu V., Mateciuc D.

NATIONAL INSTITUTE FOR EARTH PHYSICS
P.O.Box MG-2, Bucharest-Magurele, ROMANIA

ABSTRACT

The results derived from integrated investigations on the present-day vertical earth movements over high seismic Eastern Carpathian Arc Bend area (Vrancea region) using geodetic procedures, morphostructural appearance, as well as geophysical fields are presented in this paper. There, have been given two profiles which have been measured at short periods of time, before and after some high intensity seismic earthquakes had taken place.

1. GENERAL

It is worth mentioning the importance of certain sequence of earth crustal movements accompanying a seismic cycle. Among these, the anomalous vertical movements produced at short period of time before a seismic event are important for studying the earthquake prediction.

In this paper, the results of geodetic observations are analyzed in order to make clear the detailed process of the crustal movements in the Vrancea area, and some discussions on tectonic implications, based on the idea of fluctuating fault movements associated with the subduction phenomenon are presented.

The *Eastern Carpathian Arc Bend* area - the so-called Vrancea region showing special structure features, is obviously, of great interest of the kind; it could improve knowledge on the surface effects during the subcrustal tension intensifications, earthquake generation mechanism over Vrancea region, and the earth crust behaviour after a seismic event specific to this area had taken place.

In April and May 1990 surveys along *Focsani - Valea Sarii* line (59 Km.) were made. On May 30th, 1990 an earthquake featured by $\phi = 45°82'$ and $\lambda = 26°90'$ coordinate epicenter, a 91 Km. focus depth and VII degrees intensity, on Mercalli scale, took place, in the area.

Just the second day, on May 31st, 1990 an aftershock event having a $\phi = 45°83'$ and $\lambda = 26°89'$ coordinate epicenter, a 77 Km. focus depth and a VII degree intensity took place.

During Oct.- Nov. 1990 this segment was re-surveyed, giving the possibility to know the vertical crustal surface behaviour over that segment.

On 1st September 1991 another earthquake of less intensity, but also an important one (degree V) featured by 32 Km. focus depth and $\phi = 45°51'$, $\lambda = 26°91'$ took place on the *Ciorasti - Ramnicu Sarat* line, an other case on which geodetic measurements were made.

In August 1991 surveys prior to that earthquake offered the possibility to re-survey and compare the results with repeated surveys over *Ciorasti - Ramnicu Sarat* line performed after this earthquake (in September 1991) on the whole line. These two lines are located in the Vrancea region (Fig.1)
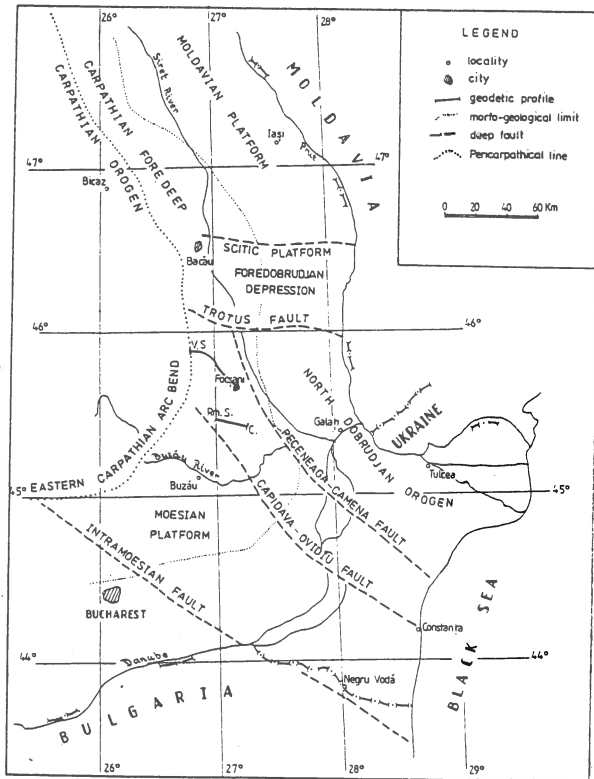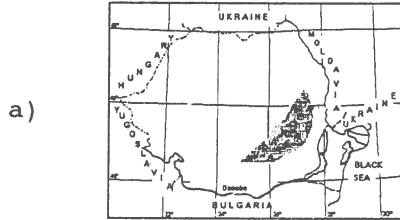
a)

b)

Fig. 1 a) Position of the Vrancea region
        b) Sketch with the discussed lines
           emplacement and the tectonic
           background of the region

2. THE GEOSTRUCTURAL CONFIGURATION
OF THE INVESTIGATED AREA

The Romanian territory which includes the *Romanian Carpathian Foredeep Arc Bend* is situated in the eastern part of the country, consisting of a major *Moldavian Platform* (its S-W extremity) and other tectonic units as *North Dobrudjan Orogen* and the eastern, north-eastern part of the *Moesian Platform*. These structural units have a different geotectonic evolution.

The whole region has been studied by various geophysical methods, by seismic refraction and reflection with DSS inclusively (Radulescu 1988); earthquake seismology (Radu and Polonic 1982); 3-D seismic tomography, (Oncescu 1984, Spakman 1990, 1993); high precision levelling (Popescu and Dragoescu 1986).

However, both the quality and the geographic distribution of the available data are heterogeneous and not sufficient to study the detailed deep structure of this complex region.

Recent crustal movements characterize the area of intense uplift (the Carpathians up to 5 mm/year) and active subsidence (up to 3 mm/year in the Carpathian Foredeep).

High precision levelling cover the entire area satisfactorily; DSS are only of regional scale. Geodetic measurements are now being undertaken in a few test-areas overlapping the *Intra-Moesian* fault, in the Vrancea region.

The subduction zone was recognized in the Eastern Carpathian, in a SE-NW direction, subsequently a paleosubduction zone in a NE-SW direction, with its south-eastern end branched (Fuchs et al 1979).

The subduction phenomenon, giving rise to some crustal fractures, entails a surface crust intensity, whose values could be measured at the ground surface. It is the Vrancea area where strong recent earthquakes (depth between 70-180 Km.) occured. Here is the only place in the entire Carpathians where folding and thrusting occured during the early Pleistocene in the outermost zone, between two deep faults in the *Moesian Platform* NW-SE oriented : *Peceneaga - Camena* and *Intra-Moesian* .

Recent horizontal and vertical motions are accompanied by moderate crustal seismic activity (M_{max} = 5.5), which associated to intermediate depth activity, produce a high seismic risk in a densely populated area.

3. REPEATED PRECISE LEVELLING
ON THE FOCSANI - VALEA SARII LINE

Considering its structure, this repeated levelling line shows an orthogonal direction as to the Carpathian one. Starting from *Odobesti Depression* - a *Neogene Pericarpathian Depression*, it passes over *Miocene* area, within *Pericarpathian Unit*, intercepts the *External Line* (*Pericarpathian*) and goes through the Unit with the same name (Fig.2).
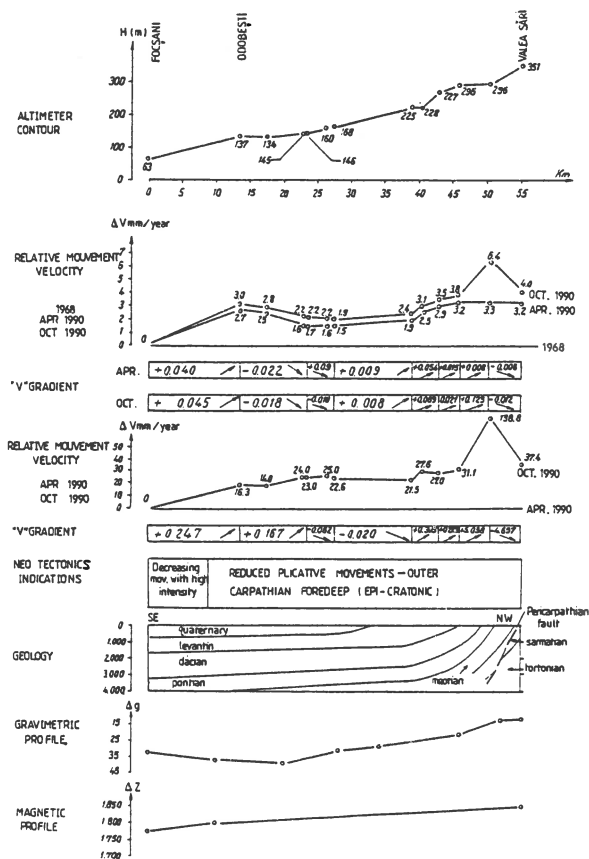
Fig. 2   Vertical movement profiles on the
FOCSANI - VALEA SARII line

The two surveys cycles carried out in 1990 (during April -
May and October - November) show the features listed in Tab.1.

Surv date	Length (Km.)	No of seg- ments	Type Eq. Staff	Method	Precission (mm/Km.)		No of compa- red pcts.	Movement network precission (M)
					(η)	(σ)		
Apr. May	59.08	53	Zeiss Ni002 rod	Coinci- dence	0.43	0.06	53	$\pm$ 0.59
Oct. Nov.	58.49	53	Zeiss Ni002 rod	Coinci- dence	0.41	0.08	53	$\pm$ 0.59

Tab. 1   Geodetic measurements characteristics
of levelling performed along
FOCSANI - VALEA SARII line

The relative movement and gradient velocity calculations have the origin point (*Focsani* railway station) considered as having zero velocity (V=0) and have been calculated for the existing cycles April 1990, October-November 1990.
The following conclusions could be drawn:
   • The height segment profile is positive (from H = 63 m to H = 351 m) showing a crustal surface rising in 1990 as compared to the 1968's one, a + 4.0 mm/year relative velocity of the final point (*Valea Sarii*), a + 6.4 mm/year maximum in *Colacu* point located at 4.5 Km distance from *Valea Sarii*. The velocity gradients for the various line segments are ranging from - 0.112 to + 0.06 mm/year/km values.
   • The positive profile between *Odobesti* and *Vidra* has a smaller value (3.0 to 3.5 mm/year), then it shows an important rising up to 6.4 mm (*Colacu*) and a 4.0 mm/year sinking in the final point (*Valea Sarii*).
   • The comparison of the two profiles having movement velocity over 22 years (1968 - 1990) and six months (Apr. - Oct., 1990) respectively, points out, both a continuous earth crustal surface rising along line and a much higher rising value after the earthquake has taken place. The superior stratum balance is to become stable in the course of time.

4. REPEATED PRECISE LEVELLING
ON THE CIORASTI - RAMNICU SARAT LINE
Considering its structure, the profile also belongs to the *Odobesti Neogene Pericarpathian Depression* where *Neogene* formations are located. The general sediment thinning trend is on a N - E direction, parallel to the crustal thinning, resulting from the Moho discontinuity rise; gravimetric profile also points it out. So, starting from *Ciorasti* to *Ramnicu Sarat* settlements, we notice the Δg value, which decreases with a minimum gravimetric background after an almost uniform gradient (Fig.3).
The strong minimum gravimetric background shows a larger surface width over *Odobesti Depression*.
Although magnetometry is physically limited to *Curie* surface, considering the magnetic sediment sensitiveness as

against the crystalline basement, undoubtedly, Δz value decreases from N-E to S-W evidencing a N-E crustal thinning.

The repeated geodetic surveys to compute the vertical movement velocity and their gradients have the following features, as given in Tab. 2.

Surv date	Length (Km.)	No of seg-ments	Type Eq. Staff	Method	Precission (mm/Km.)		No of compa-red pcts.	Movement network precission (M)
					(η)	(σ)		
1984	26.31	22	Zeiss Ni002 rod	Coinci-dence	0.27	-0.0	19	0.12
1991 Aug.	26.50	19	Zeiss Ni002 rod	Coinci-dence	0.35	0.04	19	0.12
1991 Sept	26.53	19	Zeiss Ni002 rod	Coinci-dence	0.39	0.04	19	0.14

Tab. 2   Geodetic measurements characteristics
         of levelling performed
         along CIORASTI - RM.SARAT line
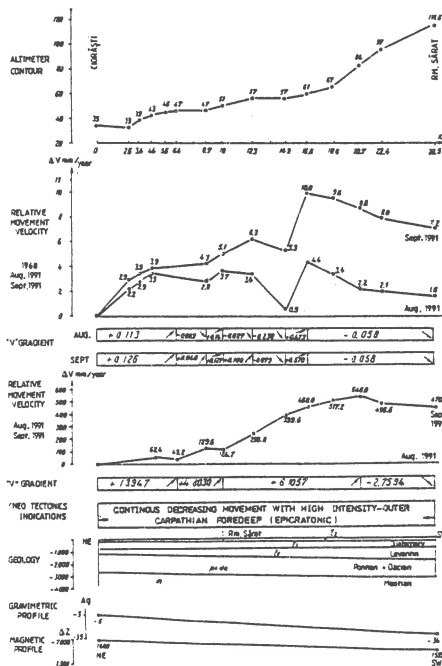
Fig. 3   Vertical movement profiles
          on the CIORASTI - RM.SARAT line

This line was divided into 19 segments between 0.1 and 2.4 Km. and on each segment there are presented their vertical movements. The most important is that in 13th segments, the direction of the vertical movements after the seismic event is modified (Fig.4).
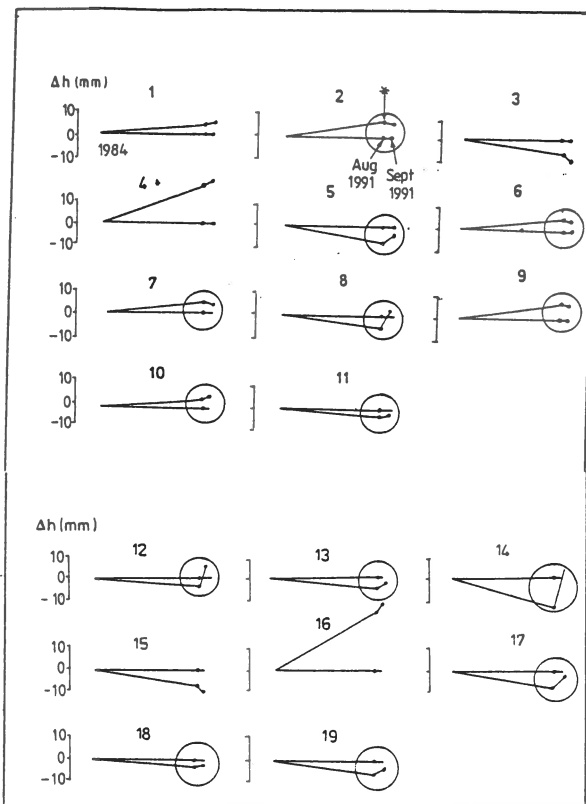
Fig. 4   Vertical movements on the 19th segments
of the CIORASTI - RM. SARAT line.

5. ANALYSIS OF GEODETIC AND GEOPHYSIC DATA

Movement velocities and their gradients computation consisted in :

- establishing each repeated survey accuracy based on the (m) mean measuring error calculation, (η) random mean square error , and (σ) mean systematic error, as well;
- identifying common central points for both surveys;
- computing the (ΔV) relative movement velocities among successive common points cumulated as function of the initial point (*Focsani*) and (M) accuracy giving the relative

velocities;
- establishing the line segments for gradient value calculations (level "V");
- making up full geological-geophysic interpretation diagrams, showing the various movement values and velocities using the geodetic procedure.

6. GENERAL CONCLUSIONS ON THE ANALYZED LINES

A comprehensive interdisciplinary study on the *Carpathian Arc Bend* showing a high seismicity, gives us the possibility to draw some conclusions related to the recent earth crust mobility.

From a structural point of view, one can easily see that *Ciorasti - Rm. Sarat* line intercepts an *Hercinic* age basement, while *Focsani - Valea Sarii* intercepts different types of basement.

A *Caledonian* age basement is intercepted between *Focsani - Odobesti* (green schists) and a *Hercinic* age basement occurs between *Odobesti -Valea Sarii* (as well as *Ciorasti - Rm. Sarat* line).

All these basement types are marked by important tectonic alignments.

Because *Focsani - Valea Sarii* line is passing over an area affected by various tectonic accidents, its passage explains the possibility to be an alternative as direction and orientation.

The relief of energy accumulated into the focus could result in possible leaps of the transverse faults profiles, evidencing local changes of the movement trend, without affecting the general earth crust rising trend.

The subduction phenomenon of *The Black Sea* subplate within the contact area with the other plates (*Vrancea Area*) once more proved to be true, justifying thus the various seismic events in the respective zone.

The repeated surveys should be further carried on, both to point out the height changes values of the earth crustal surface, caused by tensions accumulated in the subcrustal mass, and to define the active fault dynamics

So, micro test fields for detailed geodetic and geophysic surveys using highly sensitive equipment (*Geodimeters, Strainmeters, Tiltmeters*), could be established.

The continuous geophysic surveys and the geodetic ones, carried out at shorter time intervals before and after the seismic event, could bring forth the accurate knowledge on the structure element behaviour, of the various types existing within this important seismic area.

Dr.eng. I. Dragoescu for its critical comments and
suggestions, which led to great improvements in the original
manuscript.

REFERENCES

Airinei, St., 1977, *Geophysics for geologists.* Technical
  Publishing House, Buch. 336 pp. (in romanian).
Airinei, St., 1979, *Romanian terrytory and plate tectonics,*
  Scient. and Enciclop. Publish. House, no 48, Buch,
  (in romanian).
Bancila, I., 1958, *Eastern Carpathian geology,* Scient.
  Publish. House, Buch., (in romanian).
Botezatu, R., 1982, *Geophysical modellings of the
  geological Units of Romania,* Academy Publish. House,
  Buch, no 56 - 66, (in romania).
Calota, C., Lazarescu, V., Moldoveanu., and Zugravescu D.,
  1988, *Time variation of gravity on the geodynamic polygons
  of Romania,* St. Cerc. Geol. Geof. Geogr. Ser. Geof. 26:
  3 - 16, Buch.
Ciocardel, R., and Popescu, M., 1965, *Tendences actuelles de
  mouvement de l'écorce terrestre en Roumanie,* Rév. Roum.
  Géol. Géoph. Géogr., Sér. Géoph.,no 10: 5-32, Buch.
Ciocardel, R., and Esca, A., 1966, *Essay de sinthése des
  données actuelles concernant les mouvements verticaux
  récents de l'écorce terrestre en Roumanie,* Rév. Roum.
  Géol. Géoph. Géogr., Sér. Géoph. no 9 (2), 141-147, Buch.
Ciocardel, R., Socolescu, M., Esca, A., and Teodorescu C.,
  1968, *Mouvements verticaux actuelles de l'êcorse terrestre
  dans le bassin de la Mer Noire et les aires
  avoisinantes,* Rév. Roum. Géol. Géoph. Géogr., Sér. Géoph.,
  no 12 (1), 17-21. Buch.
Constantinescu, L., Cornea, I., and Lazarescu, V., 1973,
  *An approach to the seismotectonics of the Romanian
  Eastern Carpathian,* Rév. Roum. Géol. Géoph. Géogr., Sér.
  Géoph., no 17 (2) 133 - 143, Buch.
Dragoescu, I., 1980, *Researches for determination of recent
  vertical crustal movements in Vrancea area,* Analae
  I.G.Ph.C.L.M., Buch.
Dragoescu, I., Radulescu, Fl., Nacu, V., and Stiopol, D.,
  1989, *Publication of horizontal gradients for the vertical
  displacements of the Earth crust in the Carpatho-Balkanian
  and East-European regions,* Analae I.G.Ph.C.L.M., vol.X,
  Buch.
Joo, I., and Dragoescu, I., 1975, *An investigate of the recent
  vertical Earth'movements of the Carpathian Balkanian
  region,* R.C.M. Symposium, no 5, Grenoble, Budapest.
Joo, I., 1979, *Map of recent vertical crustal movements in
  the Carpatho - Balkan region,* Scale 1:1,000,000,
  Budapest.
Popescu, M., and Dragoescu, I., 1986, *Maps of recent vertical
  crustal movements in Romania. Similarities and differences,*
  Geodynamics, no 8; 123 - 136.
Sandulescu, M., 1984, *Geotectonics of Romania,* Technical
  Publishing House 336 pp. Buch.

Geomagnetic Field Changes at Grocka Observatory at the Time of the 1991 Timisoara (Romania) Earthquakes: A Search for Possible Seismomagnetic Effect

Mirjana Popeskov

Geomagnetic Institute, 11306 Grocka, Belgrade, Yugoslavia

Abstract

On July 12, 1991, an earthquake with M5.7 occurred near Timisoara, at about 90 km from Grocka (GCK) geomagnetic observatory. Considering the location of other adjacent standard geomagnetic observatories with respect to the epicentral region, GCK happened to be the nearest continuously recording magnetic station at the time of the earthquake. After taking into account the reasons pro and con based on so far established facts which define the possibility of a seismomagnetic effect detection, an analysis has been carried out using GCK data referenced to four other European observatories - Panagyurishte, L'Aquila, Niemeg and Dourbes. Results show that the geomagnetic field at Grocka exhibited somewhat characteristic variations around the middle of 1991 in comparison with other observatories, i.e. it seems to have been depressed in a period before the earthquake. It is particularly noticeable in declination, especially in the monthly means of the differences in instantaneous values at 02:00 UT and in daily mean differences between Grocka and observatories PAG and AQU. However, relying only on time coincidence between anomalous geomagnetic field changes and seismic activity, the actual relation between these two phenomena cannot be ascertained. Yet, over the areas where there are no specially planned networks of stations for continuous monitoring of the geomagnetic field changes for the purpose of seismomagnetic effect detection, the analysis of any available data is worthwhile and may contribute to the general understanding of the subject.

Introduction

Data on the Earth's magnetic field provided by standard geomagnetic observatories are basically not appropriate for tectonomagnetic effect study and detection. The reason lies partly in the nature of the studied phenomena itself, e.g. its small magnitude (up to few nanoteslas) and spatially localized appearance (see for example Johnston, 1978; Rikitake, 1988; Sasai, 1991). Furthermore, it is well known that geomagnetic observatories have to be located in a magnetically homogeneous area. This is again not favorable from the point of view of a tectonomagnetic effect detection (Zlotnicki and Cornet, 1986). However, in spite of numerous facts that have been established from intensive experimental and theoretical studies in the last few decades, it is still an open question under what conditions an anomalous tectonomagnetic field change can be generated or detected. There are notable discrepancies between the results reported by different authors regarding each of the three main prognostic

parameters - time, epicentral location and the magnitude of a forthcoming event. For instance, contrary to the above quoted authors, concerning the spatial limitations of the effect, Shapiro *et* al. (1978) report on a large total field intensity changes at the distance of 180-250 km from the epicenter of M=7.5 Gazly (Middle Asia) earthquake. Similarly, Dobrovolsky *et al*. (1979) assume that a precursory change can be detected at the distance of about 380 km for M=6.0 and strain value of 10^{-8}. Slavina and Myachkin (1994) also plead for the idea that earthquake preparation process occupies large territory beginning actually at its border zone. Considering the criterion of magnetic homogeneity, it can be found in Shapiro and Abdullabekov (1982) that anomalous geomagnetic field change of +23 nT (which led to the successful prediction of M=7.0 Alay earthquake) was detected, although there were no static magnetic anomalies greater than 10 nT in a radius of 25-30 km around the epicenter.

Taking into account above discussed points, it seemed justified to examine this particular earthquake and its accompanying effects, even if the possibility of the detection of local geomagnetic field anomaly is very small.

Presentation and Discussion of Results

The results presented below are based on the analysis of the data from five European observatories shown in Fig. 1. Data include the instantaneous values of the geomagnetic field components - declination (D), horizontal (H) and vertical intensity (Z) - hourly, daily and monthly mean values and values of the daily range in D, H and Z.

The choice of time interval in which the geomagnetic field data were analyzed has been done on the basis of relation logT=0.6M-1.01 (Rikitake, 1975; 1979), where T denotes the so-called precursor time in days and M is the earthquake magnitude. For the main shock magnitude M=5.7 of Timisoara earthquakes, T=257 days or approximately 8.5 months is obtained. It means that eventual local disturbances in the variation of the geomagnetic field at Grocka observatory could have already appeared before the end of 1990. We took into consideration the interval from the beginning of 1990 in order to be able to define more easily what could be assumed to be "normal" geomagnetic field beahviour at GCK and then, with respect to that, to isolate possible anomaly.

Whenever it is a matter of detection of local geomagnetic field changes, i.e. changes which are characteristic for a limited region around particular observation site, a comparison must be made with a simultaneous magnetic field observations at location which is presumably beyond the influence of the source of disturbance that is to be investigated. Several European observatories were selected for that purpose. The choice was made so as to include observatories closer to GCK as well as those further away, but a final decisive factor was the

availability of data from certain observatory at the time when this work was initiated.
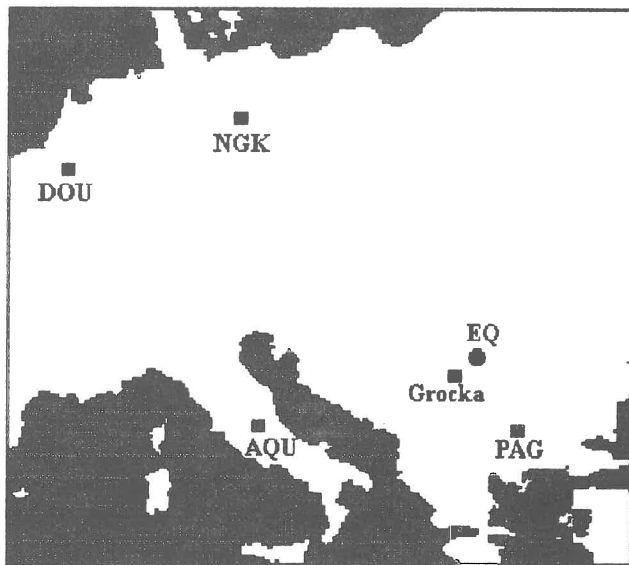
Fig. 1 The location of Grocka (GCK) observatory with respect to the epicenter (EQ) of the July 12,1991, Timisoara (Romania) earthquake and the distribution of other European observatories whose data were used in the study.

It is nowadays widely acknowledged that the best correction for secular change and other external disturbances is achieved with Wiener filtering techniques (Davis *et al.*, 1981). However, in this work a simple difference method was applied as commonly used procedure for the elimination of non-local variations of the geomagnetic field i.e., variations that have their origin in the ionosphere and magnetosphere, in order to detect eventually local field disturbances of crustal origin that are characteristic for particular area.

Instantaneous geomagnetic field values at 0200 UT

Changes in each geomagnetic field component (D, H, Z) are examined separately. General features of the obtained results will be discussed but only the most interesting points will be presented in details. Firstly, monthly mean values of declination for 1990 and 1991 have been considered, taking the

differences GCK-PAG, GCK-NGK, GCK-DOU and DOU-NGK in order to examine general trend and long-period variations in this two-year interval. Two characteristic features can be noticed. As it was to be expected, because of less efficient elimination of external source variations in ΔD values, the amplitudes of ΔD differences as well as corresponding standard deviations are larger when more distant observatories are included (NGK, DOU). Secondly, there is an obvious trend in ΔD differences (mostly linear) which reflects the difference in the rate of magnetic field secular change between distant observatories. Differences between Grocka and Panagyurishte might be particularly indicative since they are the two closest observatories, meaning that external field variations can be assumed to be rather homogeneous over the area that encompasses both observatories and, therefore, more successfully eliminated in formed differences. On the other hand, local features of the geomagnetic field behaviour in the vicinity of either of them should be emphasized.

Differences ΔD(GCK-PAG) presented in Fig. 2 are practically constant from June 1990 with noticeable decrease starting at June 1991. Similarly, another decrease appears in October 1991. It should be noticed that in both cases one and a half month later released seismic energy shows remarkable increase. Unfortunately, the cause of such a behaviour cannot be unambiguously ascribed to increased seismic activity since the geomagnetic activity, indicated by Ap index, also increased in June and October thus certainly influencing the differences ΔD(GCK-PAG). However, the decrease of ΔD(GCK-PAG) around the time of the main shock with respect to the level that is almost constant from the middle of 1990 is about 0.'5-0.'6, while corresponding change in standard deviation is only 0.'1. Moreover, the increase of geomagnetic activity might increase the standard deviation of ΔD of differences but not necessarily decrease their mean value.

Some common features of the changes in the differences of horizontal and vertical intensities can be summarized as follows. Seasonal variation with minimum in summer months and maximum in winter for H component. The above mentioned form of variation seems to be disturbed (the broadening of minimum beginning about 3-4 months before the main shock) towards the end of 1991 in the differences including GCK observatory. This may lead to assumption that some local geomagnetic field changes peculiar to GCK are superposed on already existing regular variation. Also, there is clearly expressed linear trend in the case of more distant observatories due to the difference of the rate of the geomagnetic field secular change.

Monthly mean values of the differences of vertical intensity Z between observatories GCK, PAG, NGK and DOU exhibit the following characteristics. Differences ΔZ(GCK-PAG) show slow increasing liner trend with no particular changes that could be related to seismic activity. Linear increasing trend in

ΔZ(GCK-DOU)·is easily noticeable untill the middle of 1991 and then the differences slowly decrease towards the end of the year. The turning point of the secular change trend is around the time of the main shock. The inspection of the curve ΔZ(GCK-NGK) shows that on the background of almost constant trend which is being maintained from the middle of 1990, there is a noticeable deviation (increase) immediately before and at the time of Timisoara earthquakes. Differences ΔZ(DOU-NGK) do not exhibit any particular form of variation except slowly decreasing linear trend.
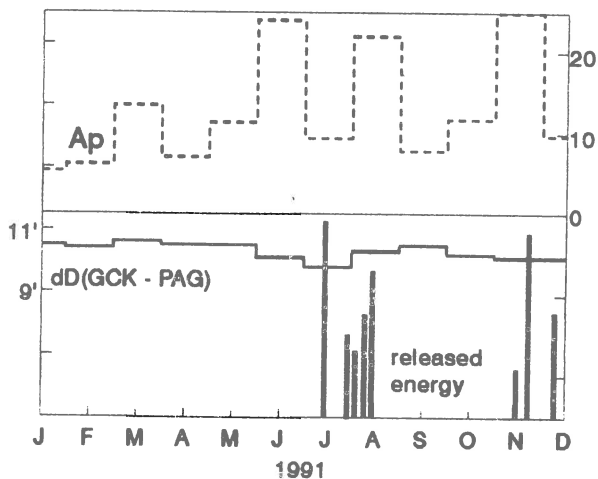
Fig. 2 Monthly mean values of the differences in declination at 0200 UT between Grocka and Panagyurishte, Ap mean values for ten selected days in a month, and released seismic energy.

In general, it may be concluded that differences involving Grocka observatory show more expressed variation in the middle of 1991, but increased geomagnetic activity characterizes the same time period and therefore imposes necessary precaution in drawing any definite conclusions concerning connection between geomagnetic field changes and seismic activity.

Differences of the range of daily variations

Quiet daily solar variation Sq has clearly expressed maximum and minimum for each component of the geomagnetic field. Forming the range of daily variations i.e., the differences between the maximum and minimum value of particular component during the day, the main field is eliminated. Comparison
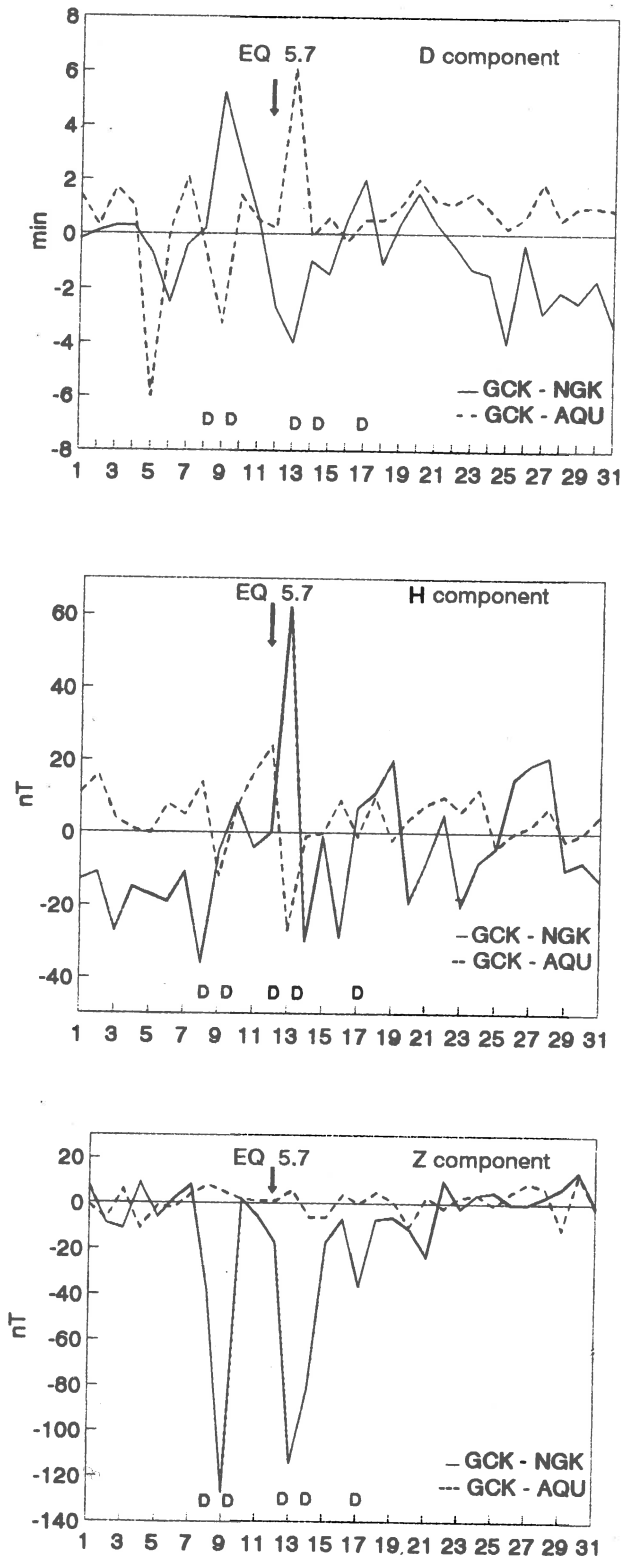
Fig. 3 Differences in the range of daily
variations for July, 1991.

1192

of the range of daily variations between two relatively close stations also eliminates the influence of solar activity to a great extent (Fanselau, 1976). Therefore, differences of the range reflect the contribution of internal field component and it is reasonable to expect that seismic activity in the vicinity of one of the stations might influence the local geomagnetic field behaviour. Because of the lack of identical data sets, the only differences in the range of daily variations which were considered are those between observatories Grocka, Niemegk and L'Aquila.

Differences of the range in D, H and Z for both GCK-AQU and GCK-NGK (see Fig. 3) show disturbances around the middle of July, which are rather difficult to interpret because of temporal coincidence between increased seismic and geomagnetic activity. Nevertheless, some common features can be observed. The amplitudes of ΔR variations are larger for GCK-NGK than for GCK-AQU (which are closer to each other) and mostly in the opposite sense. Although the largest deviations coincide with magnetically disturbed days within the period 8-17 July, 1991, they do not very in the same sense with respect to Ap values before and after the main shock. Otherwise, no peculiar change can be noticed.

Differences of the hourly mean values

The analysis of the differences of the hourly mean values of declination, horizontal and vertical intensity between observatories Grocka, L'Aquila and Niemegk, has been done with the data covering 9-13 July, 1991, i.e. the period of a few days before and at the time of the main shock. Two days, July 9 and 13, 1991, were magnetically disturbed with respective Ap values 117 and 134. The range of variations of differences between distant observatories (GCK-NGK, AQU-NGK) for these two days is up to 15' in D, about 200 nT in H and 150 nT in Z component. Otherwise, on other days they do not exceed about 5', 40 nT and 30 nT, respectively. From the point of view of possible short-term precursory change (up to several hours), close examination of the geomagnetic field behaviour on the day of the main shock occurrence has not revealed any variation that would be significant with respect to the standard deviation of the differences of the hourly mean values. Of course, nothing can be said about possible anomalous variations with duration shorter than one hour, since, if there are any, they are averaged out in the hourly mean values.

Differences of the daily mean values

Differences of the daily mean values of the geomagnetic field components D, H and Z were analyzed for observatories GCK, AQU and NGK for July 1991. Generally, the differences between more distant observatories show larger deviations on magnetically disturbed days. Accordingly, differences between Niemegk and L'Aquila, i.e., those involving Grocka observatory, clearly exhibit
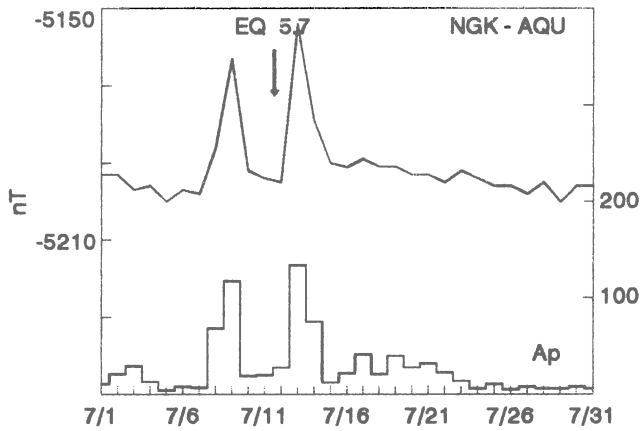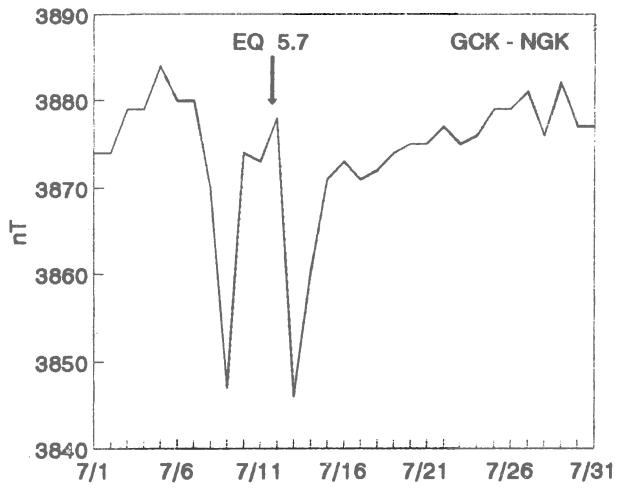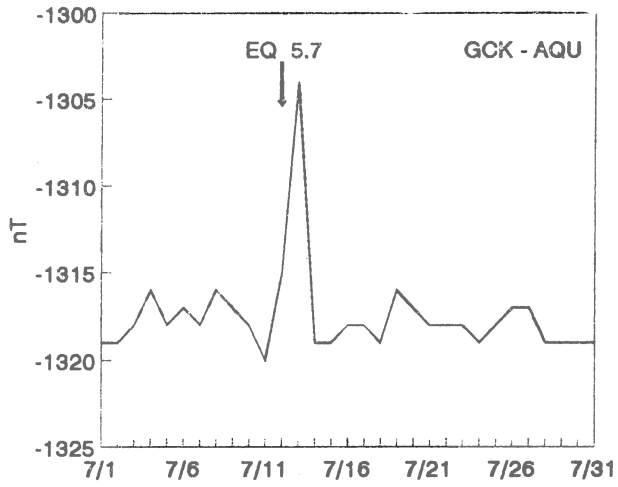
Fig. 4 Differences of daily mean values in horizontal intensity for July 1991.

two peaks at the time of pronounced geomagnetic activity on the 9th and 13th of July, 1991 with respective Ap values 117 and 134, due to the poor elimination of external field components between distant observatories. The same thing is true for the differences GCK-NGK. However, in the case of differences GCK-AQU the behaviour is somewhat peculiar. Namely, on the background of random fluctuations around a certain constant level, the second peak value, being one day delayed with respect to the time of the main shock, is much more expressed. It is particularly evident in $\Delta H(GCK-AQU)$, in Fig. 4. These differences vary within 2 nT throughout the whole month except around the time of the main shock when they reach the value of 8 nT. There are no doubts that a great deal of this peak variation originates from the disturbed geomagnetic conditions on the 13th of July 1991, but it is not understandable how the same kind of disturbance has been more successfully eliminated on the 9th of July. The analysis shows that the standard deviations of the differences of hourly mean values of D and H are larger on the 9th than on the 13th of July, and yet the differences of daily mean values between GCK and AQU on the 9th of July are much smaller. This may lead to assumption that the geomagnetic field was somewhat depressed at GCK immediately before the main shock and, possibly, in connection with it. In the $\Delta D(GCK-AQU)$ and $\Delta Z(GCK-AQU)$, the second peak value is again dominant, although the situation is not so illustrative as in the case of the horizontal intensity H.

Conclusion

No reliable conclusion can be made about possible relation between the geomagnetic field changes and tectonic forces or more precisely seismic activity in a given area, based only upon the coincidence in time between these two phenomena. Bearing this in mind, it should be still emphasized that the field differences including Grocka observatory exhibit more pronounced variations around the middle of July 1991. It is, for instance, seen in the case of peculiar change in differences of monthly means of instantaneous values of declination and horizontal intensity at 02:00 UT, or in the case of well expressed peak value at the time of the main shock, when the differences of the daily mean values in the horizontal intensity between Grocka and L'Aquila are considered. For the reasons already discussed, the real nature of these changes cannot be asserted, but the possibility of a seismomagnetic effect existence cannot be ruled out.

REFERENCES

Davis, P. M., D. D. Jackson, C. A. Searls, and R. L. McPherron, 1981. Detection of Tectonomagnetic Events Using Multichannel Predictive Filtering. J. Geophys. Res., **86**, 1731-1737.

Dobrovolsky, I. P., S. I. Zubkov, and V. I. Myachkin, 1979. Estimation of the Size of Earthquake Preparation Zone. Pageoph, **117**

Fanselau, G., 1976. Splitting of Magnetic Fields Into External and Internal Parts (Sq Anomaly in GDR). In: Geoelectric and Geothermal Studies, A. Adam, Editor, KAPG Geophysical Monograph, Akademiai Kiado, Budapest.

Johnston, M. J. S, 1978. Local Magnetic Field Variations and Stress Change Near Slip Discontinuity on the San Andreas Fault. J. Geomag. Geoelectr., **30**, 511-522.

Rikitake, T., 1975. Earthquake Precursors. Bull. Seismol. Soc. Am., **65**, 1133-1162.

Rikitake, T., 1979. Classification of Erthquake Precursors. Tectonophysics, **54**, 293-309.

Rikitake, T., 1988. Earthquake Prediction: An Empirical Approach. Tectonophysics, **148**, 195-210.

Sasai, Y., 1991. Tectonomagnetic Modeling on the Basis of Linear Piezomagnetic Effect. Bull. Earthq. Res. Inst., **66**, 585-722.

Shapiro, V. A. , A. N. Pushkov, K. N. Abdullabekov, E. B. Berdaliev and M. Yu. Muminov, 1978. Geomagnetic Investigations in the Seismoactive Regions of Middle Asia. J. Geomag. Geoelectr., **30**, No. 5, 503-509.

Shapiro, V. A. and K. N. Abdullabekov, 1982. Anomalous Variations of the Geomagnetic Field in East Fergana - Magnetic precursor of the Alay Earthquake With M7.0 (1978 November 21). Geophys. J. R. astr. Soc., **68**, 1-5.

Slavina, L. and V. Myachkin, 1994. Regularities of Occurrence of Kinematic Earthquake Precursors in Time and Space. Book of Abstracts, p. 82, XXIV ESC General Assembly, 19-24 September 1994, Athens.

Zlotnicki, J. and Cornet F. H, 1986. A Numerical Model of Earthquake-induced Piezomagnetic Anomalies. J. Geophys. Res., **91**, 709-718.

MAGNETOTELLURIC STRIKES AND THEIR CORRELATION TO THE REGIONAL SEISMOTECTONICS OF GREECE

G. CHOULIARAS, G. DRAKATOS and J. DRAKOPOULOS

National Observatory of Athens - Seismological Institute, P.O. Box 20048 GR 118-10
Athens GREECE

ABSTRACT

Magnetotelluric (MT) regional strikes for eight sites in Greece have been determined in this study. In order to investigate their correlation with the regional seismotectonics, they are compared with the strikes of major active regional faults as determined from geological maps as well as earthquake focal mechanisms, macroseismic intensity data and aftershock distributions. The results show a very good agreement for most of the investigated sites. This can be attributed to the presence of conductive fluids in fault zones which can act as major conduits for fluid flow through the crust. The implications of these results to earthquake prediction research by means of precursory electromagnetic phenomena, can be considered of great importance.

INTRODUCTION

In earthquake prediction research, the monitoring of precursory geoelectric phenomena has provided several similar observations regarding an anisotropic behaviour that is exhibited by different types of geoelectric precursors. In particular, it is reported that a monitoring station's ability to detect precursory phenomena, such as anomalous changes in ground resistivity or earth potentials, is dependant on the azimuthal orientation of the measuring electrode system with respect to the epicentral area (Sobolev and Morozov, 1970; Fuye et al., 1983; Varotsos and Alexopoulos, 1984, 1987; Kayal and Banerjee, 1988). Further on, major regional structures and lineaments have been observed to cause the channeling of geoelectrical currents (Beamish 1986; Adam et al., 1986; Adam, 1987) and this phenomenon can be attributed to the presence of conductive fluids in fault zones (McCaig, 1989; Shankland, 1989; Bailey et al., 1989). For these reasons, it is believed that the orientation of local and regional structures can be of great importance in the detection of precursory geoelectric currents.

Magnetotelluric (MT) measurements have been performed at several sites in Greece (Chouliaras and Rasmussen, 1986, 1988) during periods of seismic activity local to these sites. It is well known that the MT sounding method is capable to determine the strike of the local or regional conductive structure with great accuracy (Zhang et al., 1987). In this study, based on the MT data (Chouliaras and Rasmussen, 1986, 1988) from eight stations in Greece the MT strikes are determined for each site according to the methods described in Zhang et al., (1987) and Vozoff (1972). It has been postulated by many researchers that the upper crust is pervated by fluid filled crack system of rocks under stress and also that fault zones act as major conduits for fluid flow through the crust (Shankland 1989; McCaig 1989; Adam 1987; Bailey et al., 1989; Evans et al., 1987). For this reason, further on in this study we proceed to compare the MT regional strikes with the direction of major faulting near stations as obtained from published earthquake focal mechanisms, macroseismic intensity maps and also from aftershock distributions for earthquakes which have occured in the past, close to each station.

METHOD AND DATA ANALYSIS

Digital magnetotelluric (MT) measurements in the frequency range 10 - 1/3600 Hz have been performed in many sites in Greece and these have provided an accurate description of the underlain resistivity structure at each station (Chouliaras and Rasmussen 1986, 1988). For the purpose of this study we employ the MT data in order to determine the MT regional strike of the conductive geoelectric structure for eight stations. The MT data were collected in two field campaigns in Greece. For the stations PIR and AMF during April - May 1983 and for the rest of the stations during October - November 1984. By examining the seismic activity for these time intervals from the Bulletin of the National Observatory of Athens it was found that the regions surrounding the MT stations were seismically active.

Assessment of the regional magnetotelluric strike (θs) is based on the horizontal rotation properties of the impedance tensor and in this study the conventional method proposed by Sims and Bostick (1969) and later adjusted for a 2-D structure by Zhang et al., (1987) is used. However, the MT data from three stations namely AMF, PIR and GOR indicate the presence of a static or DC-like distortion in the data. This observation is made when one looks at the apparent resistivity curves from the two measured directions and sees that they are nearly parallel and do not join in the high frequency end as one would expect (Chouliaras and Rasmussen, 1986). This static shift of the curves is most likely the result of the distortion due to a near surface laterally inhomogeneous layer.

In this case we use the method of Zhang et al., (1987) in order to determine a local 2-D strike (θL) underlay by a regional 2-D strike (θR). This is because the conventional method of 2-D strike estimation would give a result biased towards the local or near-surface and not the true regional strike. The MT strike angles determined by the above two methods, are inherently ambiguous by 90°. This is because 2-D structures provide symmetrical properties for the rotated tensor in increments of 90°. Thus, for measurements of the horizontal MT components alone, one finds a strike direction or a direction perpendicular to it, without being able to tell which is which. To resolve the ambiguity, this study also employs the vertical magnetic field transfer function (A, B) in order to determine the tipper angle ΦT, according to the method of Vozoff (1972). The tipper angle is in general relatively free from near-surface distortion and according to the MT theory, ΦT will be perpendicular to the strike of a 2-D structure while in the case of a 3-D structure ΦT will point away from the region of high conductivity. It is therefore apparent that when combined with geological information, the tipper can provide an unambiguous assessment of the regional strike angle.

The magnetotelluric strikes as determined by the above mentioned methods are inturn compared to the strikes of major regional faults near the MT stations determined from a combination of the following data sets: i) the Seismotectonic Map of Greece (I.G.M.E., 1989) ii) earthquake focal mechanism data (Drakopoulos and Delibassis, 1982) iii) macroseismic intensity data (UNESCO, 1974) and iv) aftershock epicentral distribution data published in the Bulletin of the Seismological Institute of the National Observatory of Athens. To determine the strike of the regional fault for every investigated area we use a combination of the above geological and seismological data. In this respect it should be kept in mind that focal mechanism provides a result that is ambiguous by 90°. There are two strike directions which are perpendicular and we are not able to distinguish the true strike. To solve this problem we use macroseismic or aftershock data in combination with geologic data to establish the strike of the fault in question. Since it was not possible to obtain all four sets of data for every one of the eight investigated areas we make sure that for every area we have at least geologic data to be combined with either one of macroseismic, focal mechanism or aftershock data.

RESULTS AND DISCUSSION

Figure 1 shows the orientation of the major active seismotectonic structures near the sites where magnetotelluric measurements were performed (from the seismotectonic map of I.G.M.E, 1989). The results from the magnetotelluric (MT) strike analysis for the eight investigated sites in Greece are presented in Figure 2. From these results it is observed that in most of the sites the tipper angle is nearly perpendicular to the MT regional strikes. This observation indicates that the employed 2-D model in determining the MT strikes is the appropriate. The seismological data for the eight sites are presented in Figures 3 - 9, so that we can determine the regional fault orientation to each case.

For the sites VOL and IOA we observe that the seismological data (Figs 3 and 4) show a fault plane orientation similar to that obtained from the MT results (Fig. 2) and the seismotectonic map (Fig. 1). In both sites we also observe that the focal mechanism data show a slightly different fault plane strike than that which is obtained from the other seismological data for the same seismic events.

The orientation of the regional faults for the sites PIR, ASS and AMF, (Fig. 1), agrees quite well with that determined from the MT strike analysis. The seismological data for these sites are shown in Figures 5, 6 and 7, respectively and these indicate an overall agreement with respect to the fault orientation and the MT regional strike.

Nevertheless we note that the macroseismic data for PIR (Fig. 5) and the focal mechanism for ASS (Fig. 6) indicate a different fault plane orientation when compared to the other seismological and geological data. In the case of PIR this may be explained by the fact that the macroseismic data are for a different seismic event. The macroseismic data for the site THI (Fig. 8) show a trend which is in agreement with the fault orientation and the MT strike. For the sites REN and GOR we observe that the MT strikes are in good agreement with the orientation of the regional faults. However, in both sites the available seismological data are limited and we can only indicate that the macroseismic data for a strong earthquake near REN (Fig. 9) show a trend which agrees with the orientation of the strikes (Figs 1 and 2).

The above comparison between the MT strikes and the strikes of the regional faults determined from geological and seismological data for the eight sites in Greece results in a good qualitative agreement. The physical mechanism that can be responsible for this result may be the presence of conductive fluids in the active fault zones as suggested by many researchers (McCaig, 1989; Shankland, 1989; Evans et al., 1987). This mechanism of course implies that the conductive faults can cause the channeling of geoelectrical currents as suggested by Adam et al., (1986) and by Adam (1987). For these reasons, the anisotropic behaviour of geoelectric anomalies that have been observed to precede earthquakes (Sobolev and Morozov, 1970; Fuye et al., 1983; Varotsos and Alexopoulos, 1984, 1987; Kayal and Banerjee, 1988) can be attributed to the effect of current channeling by fluids in the active fault zones.

CONCLUSIONS

Magnetotelluric (MT) strikes for eight sites in Greece have been determined following the methods of Zhang et al., (1987) and Vozoff (1972) employing the MT measured data of Chouliaras and Rasmussen (1986, 1988). In addition to this, a comparison between the MT strikes and the major regional faults obtained from seismotectonic data has been performed. The results show a very good agreement for most of the investigated sites. The application of these results to the on going earthquake prediction research by means of precursory electromagnetic phenomena can be considered to be of great value. Thus, the orientation of major regional and local structures must be investigated by multidisciplinary methods prior to any future earthquake prediction research by means of electromagnetic methods.
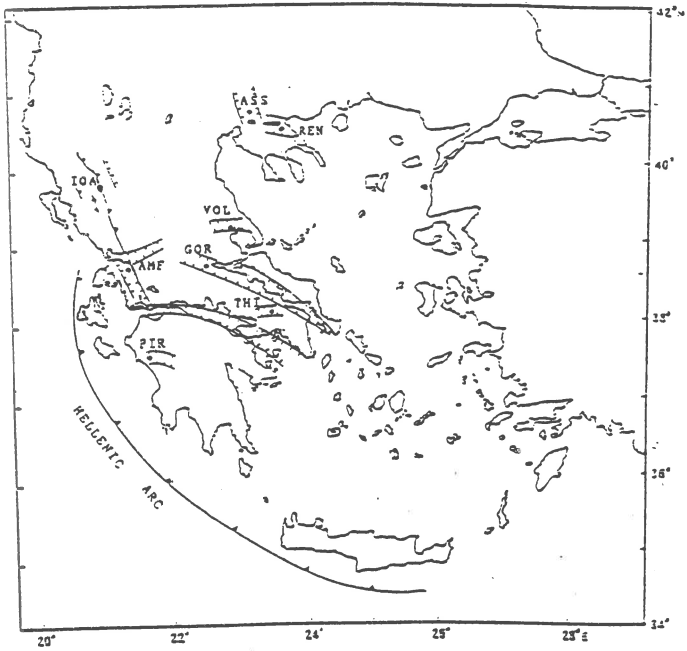
Figure 1. Sites where MT measurements have been performed, as well as the local seismotectonic regime are shown.
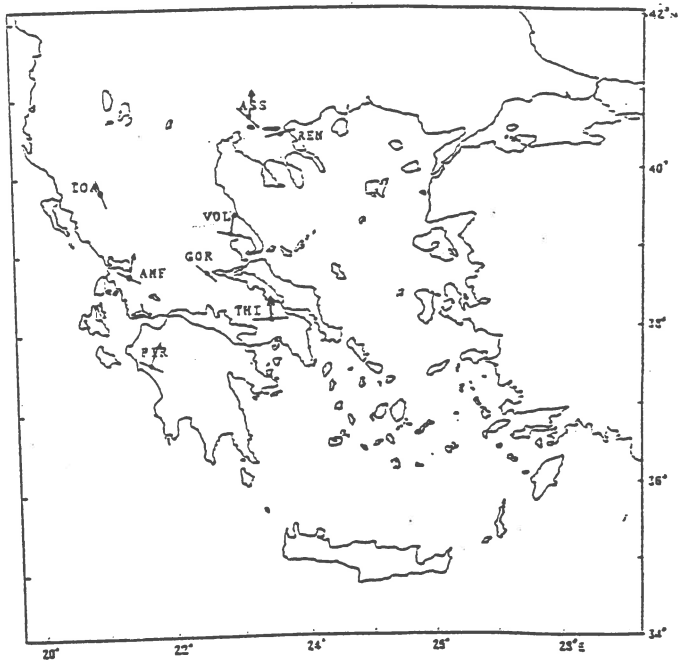

Figure 2. The results of the MT strike analysis are shown. The solid line indicates the orientation of the magnetotelluric strike and the vector indicates the tipper orientation.
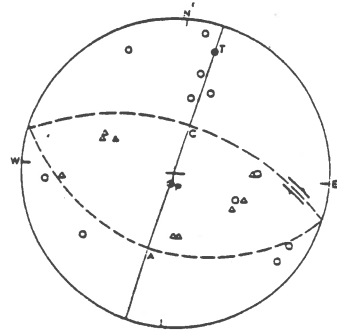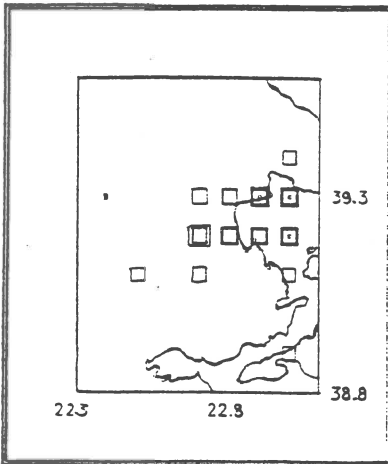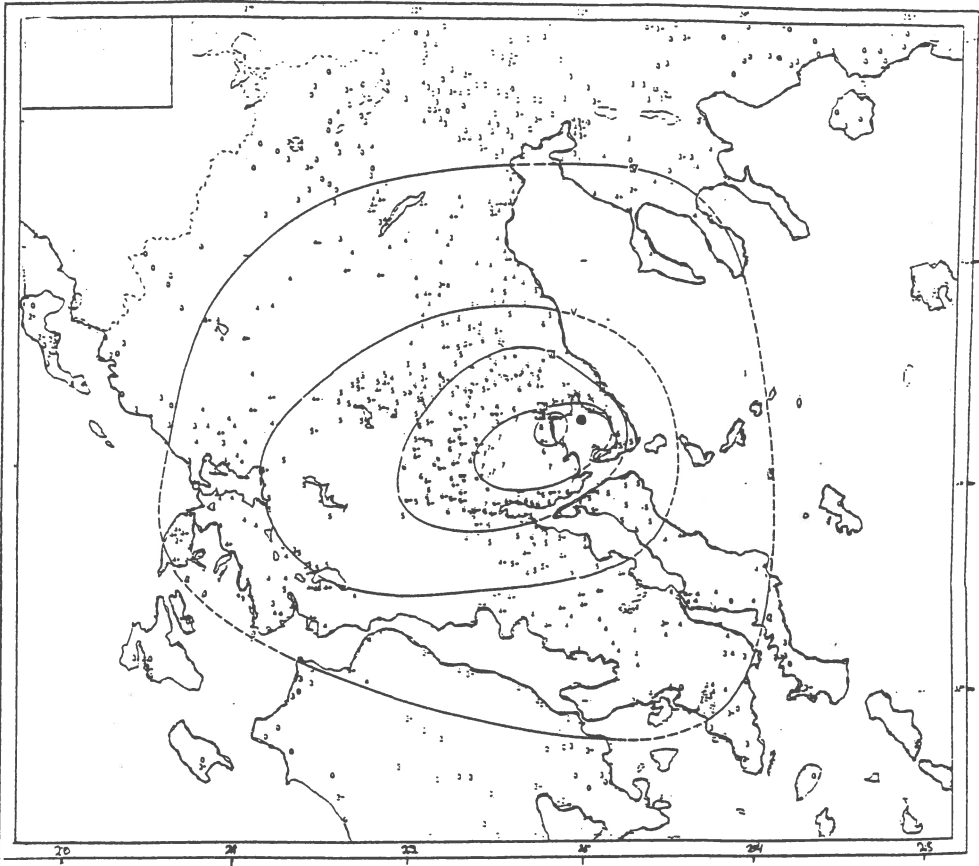
Figure 3. Isoseismal map , aftershock distribution and focal mechanism are shown, for the Almyros (VOL) earthquake (1980-7-9).
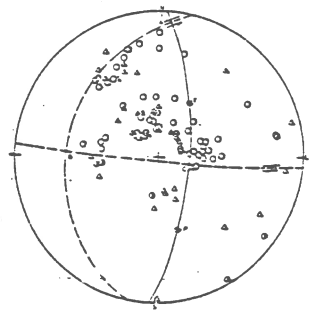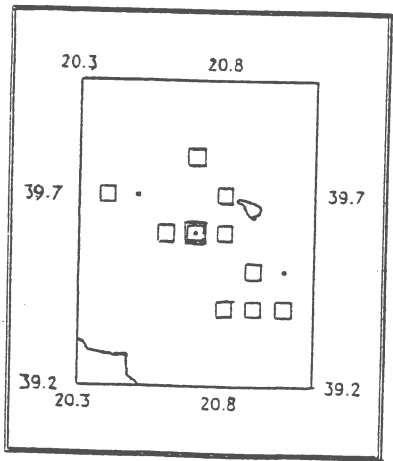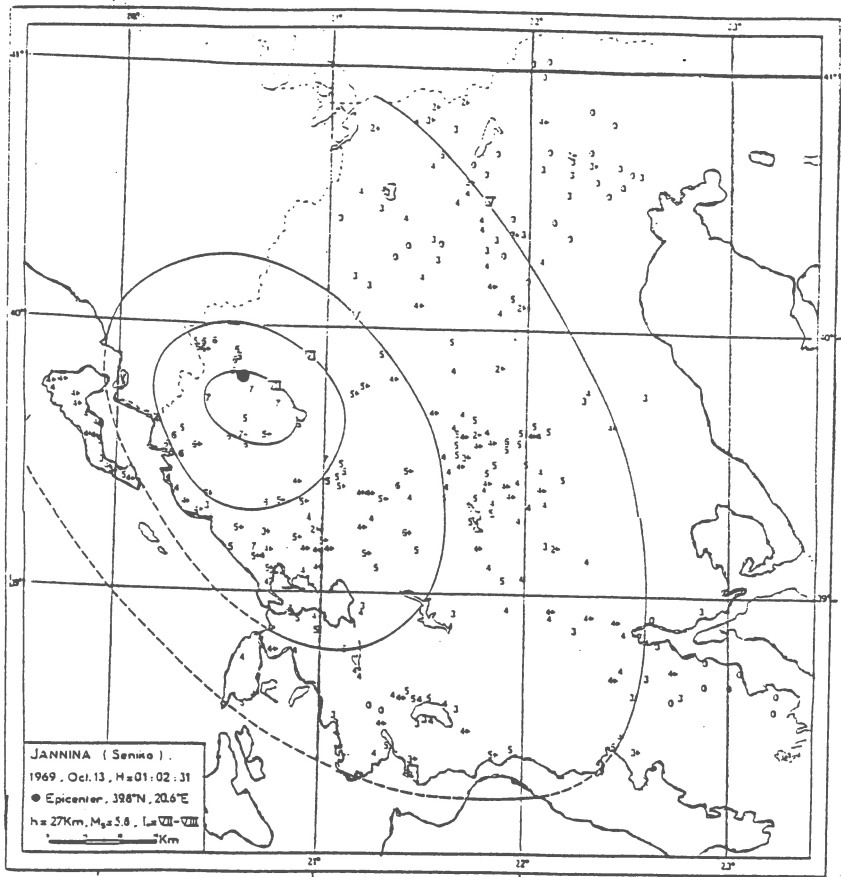
Figure 4. Isoseismal map, aftershock distribution and focal mechanism are shown, for the Ioannina (IOA) earthquake (1969-10-13).
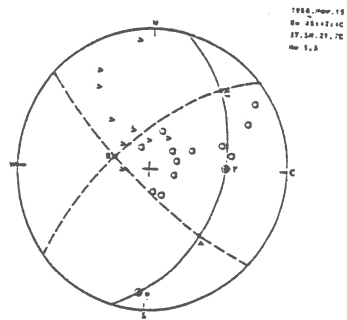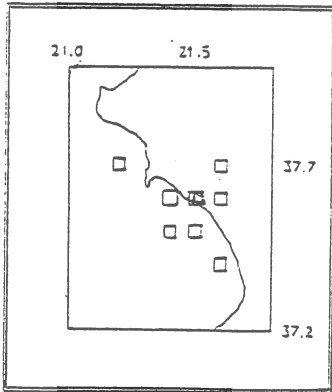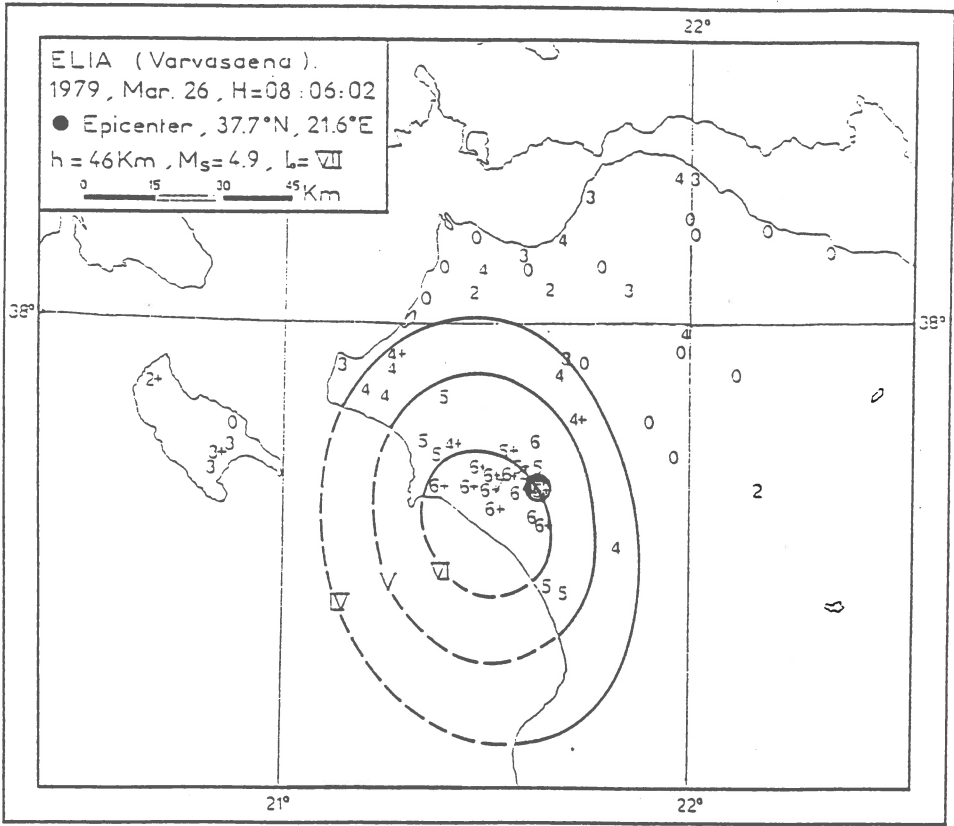
Figure 5. Isoseismal map of 1979-3-6 earthquake is shown. Aftershock distribution and focal mechanism for 1958-11-15 Elia (PIR) earthquake are also shown.
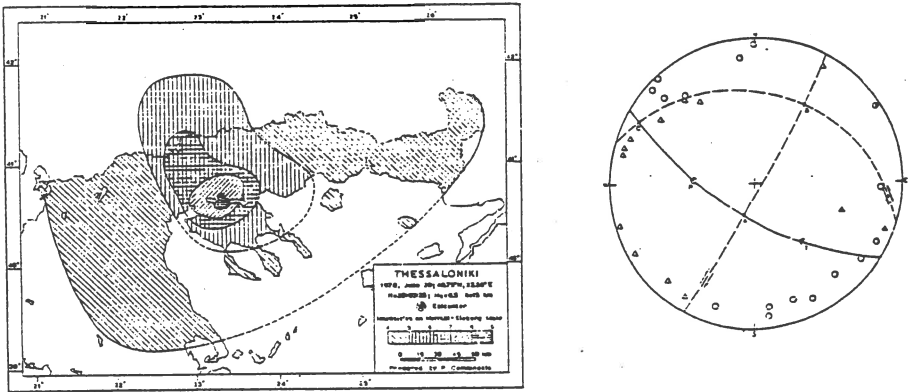
Figure 6. Isoseismal map and focal mechanism for Thessaloniki (ASS) earthquake (1978-6-20) are shown.
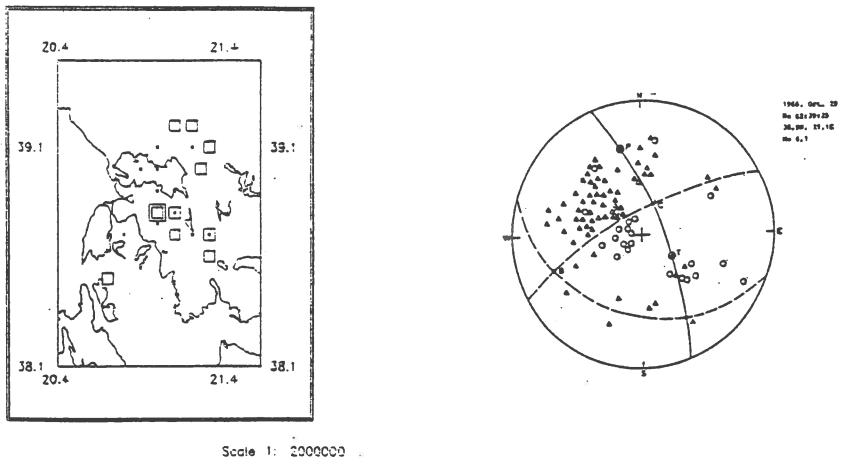
Figure 7. Isoseismal map and focal mechanism are shown, for the 1966-10-29 Amfilochia (AMF) earthquake.
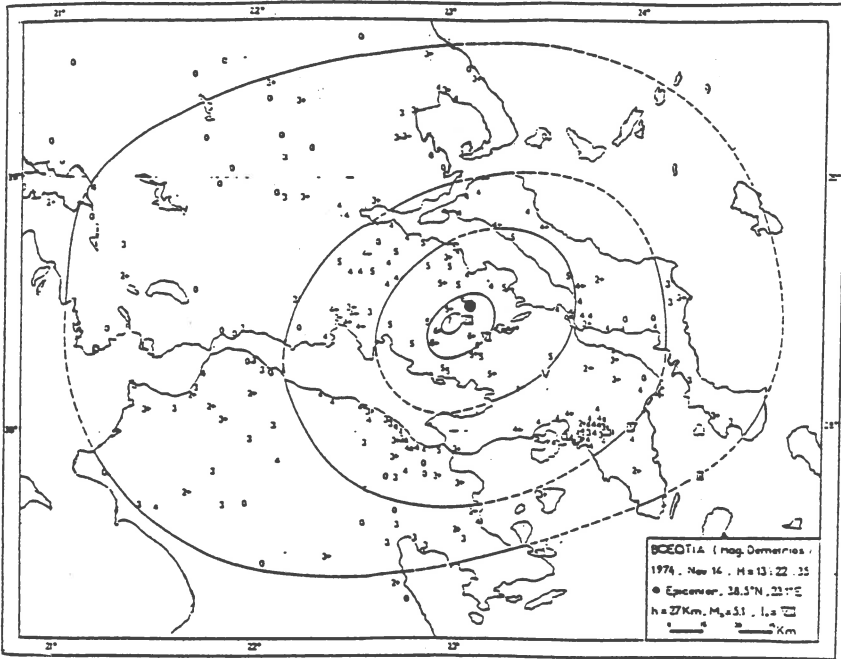
Figure 8. Isoseismal map is shown, for Boeotia (THI) earthquake (74-11-14).
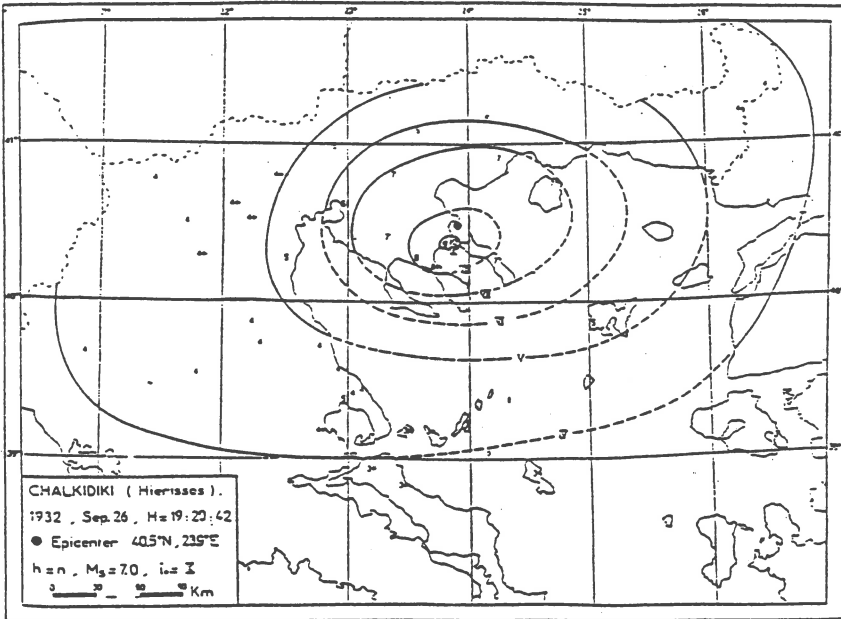
Figure 9. Isoseismal map of Chalkidiki (REN) earthquake is shown

REFERENCES

Adam, A., 1987. Magnetotelluric response functions determined from normal and long dipoles at the Greek V.A.N., earthquake prediction network. Technical report, Seismological Department, Uppsala University, 4 - 89.

Adam, A., Szarka, L., Varo, J. and Wallner, A., 1986. Magnetotellurics in mountains-noise, topographic and crustal inhomogeneity effects. Phys. Earth Plan. Int.,42: 165 - 177.

Bailey, R.C., Cravent, J.A., Macnae, J.C. and B.D. Polzer, 1989. Imaging of deep fluids in Archaean crust. Nature,Vol. 340, 136 - 138.

Beamish, D., 1986. The correlation between geoelectricvariations and LANSAT in aged lineaments in the North umberland trough. Geophys. J.R. Astr. Soc., 85(1):250.

Chouliaras, G., and Rasmussen, T.M., 1986. Magnetotellurics at the V.A.N earthquake prediction research network in Greece. Seismological Department, Uppsala Univ., Report12-86, 51pp.

Chouliaras, G., and Rasmussen, T.M., 1988. The application of the magnetotelluric impedance tensor to earthquake prediction research in Greece. Tectonophysics, 152:119-143.

Drakopoulos, J. and N. Delibassis, 1982. The focal mechanism of earthquakes in the major area of Greece for the period 1947 - 1981. University of Athens, Seismological Laboratory, Publ. N 2.

Evans, R., Beamish, D., Crampin, S. and Ucer, B.S., 1987. The Turkish Dilatancy Project (TDP3): Multidisciplinary studies of a potential earthquake source region. Geophys. J. R. Astr. Soc., 91: 265-286.

Fuye, Q., Yulin, Z., Mouming, Y., Zhixian, W., Xiaowei, L. and Simin, C., 1983. Geoelectric resistivity anomaliesbefore earthquakes. Scientia Sinica (Series B), 26:326-336.

Institute of Geology and Mineral Exploration of Greece (I.G.M.E), 1989. Seismotectonic Map of Greece with Seismological data.

Kayal, J.R. and B. Banerjee, 1988. Anomalous behaviour of precursor resistivity in Shillong area, NE India. Geophysical Journal, 94, 97-103.

McCaig, A., 1989. Fluid flow through fault zones. Nature, 340:600.

Shankland, T., 1989. A case of two conductors. Nature, 340:102.

Sims, W.E., and Bostick, F.X, 1969. Method of magnetotelluric analysis, Res. Lab. Tech. Rep., 58, Univ. of Texas-Austin.

Sobolev, G.A. and Morozov, V.N., 1970. Local disturbances of the electrical field in Kamchatka and their relation to earthquakes. In M.A. Sadovsky (Editor), Physical basis of earthquake prediction prospecting. Nauka, Moskow, pp.110 - 121.

Atlas of Isoseismal Maps. UNDP-UNESCO survey of the seismicity of the Balkan Region. Unesco, Skopje.

Varotsos, P. and Alexopoulos, K., 1984. Physical properties of the variations of the electric field of the earth preceding earthquakes, I, II. Tectonophysics, 110:73-88, 99-125.

Varotsos, P. and Alexopoulos, K., 1987. Physical properties of the variations in the electric field of the earth preceding earthquakes, III. Tectonophysics, 136: 98-141.

Vozoff, K., 1972. The magnetotelluric method in the exploration of sedimentary basins. Geophysics, 37:98-141.

Zhang, P., Roberts, R.G. and Pedersen, L.B., 1987. Magnetotelluric strike rules. Geophysics, 52:267-278.

Analysis of the Secular Strain Field Variations in NE-Italy.

G.Rossi[1,2] and M.Zadro[1]

1. Istituto di Geodesia e Geofisica-Università di Trieste (Italy)
2. Istituto Nazionale di Geofisica (Italy)

Abstract.

The Friuli (NE-Italy) seismic area has been monitored by a tilt-strainmeter network since 1977, whereas a tiltmeter station, installed in the Grotta Gigante near Trieste as Earth tide station in 1958, gave continuous information on the deformation field since 1967. The array covers therefore a time interval of about 15 years, and for the single Grotta Gigante station, of about 25 years. More then a decade of deformation rate variations has been analyzed, to evidence time-space variations of the deformation field. The results of the correlation between tilt records of different sites suggest that the region is subject to slow deformations, that cause a tilting normal to the Alpine and Dinaric structures respectively. The results of the deformation field analysis have been compared with the times of the seismic activity in the region, showing a certain correlation.

Introduction

The analysis of the secular terms of the strain field allows to follow the evolution of the seismogenic processes in a region. The area here considered is located in NE-Italy, at the NE border of the Adria microplate.Here two important structural systems merge and interact with eachother, both bound to the collision of the Adria microplate with the Eurasiatic block: the Alpine and the Dinaric system.The intense seismicity that characterizes the region proves the ongoing of the activity of the collision process (Anderson and Jackson, 1987). The most recent strong earthquake occurred in 1976, on May 6th. After it the seismic activity gradually decreased and recently it shows an almost regular pattern, with an event of M>4 which occurs about each 3-4 years.

One year after the earthquake the Istituto di Geodesia e Geofisica (IGG) of the University of Trieste (Italy) installed a strain-tiltmeter network for the monitoring of the deformations in the seismic area,

whereas the same year the Osservatorio Geofisico Sperimentale (OGS) of Trieste installed a local seismometric network.

The IGG network is constituted by five tiltmeter stations (VI, CE, IN, BA and GE on the map of Fig.1), equipped with a pair of Marussi horizontal pendulums with Zöllner suspension, housed in caves or in man made old underground buildings. A strainmeter station is also housed in one of the caves (VI), equipped with three Cambridge wire longitudinal strainmeters in addition to the two tiltmeters.
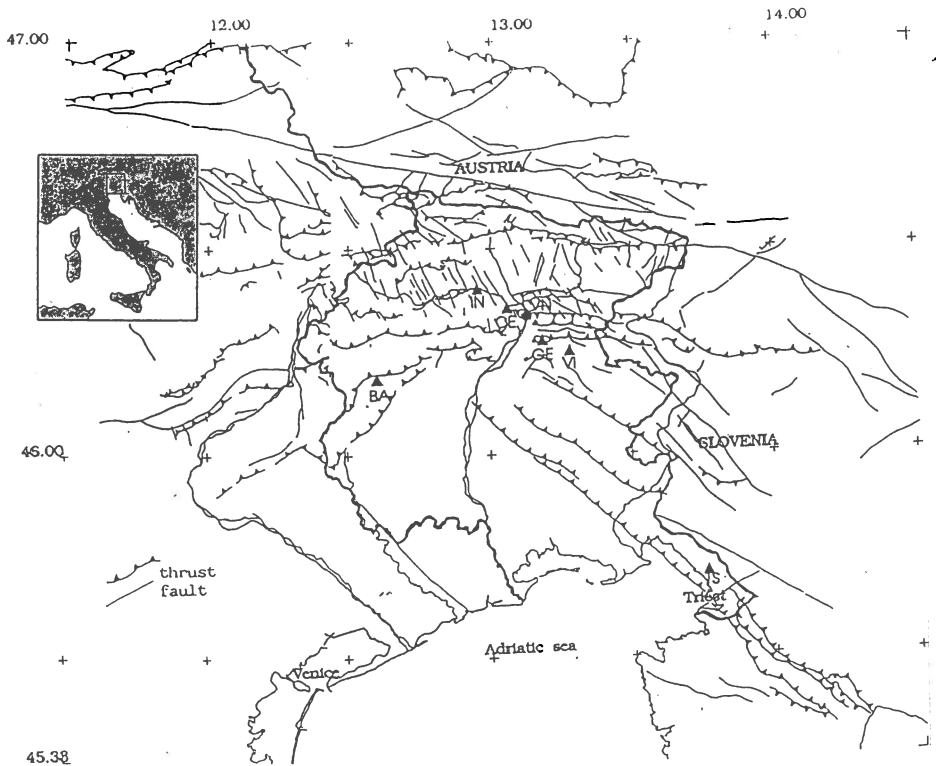

Fig. 1. Schematic map of the region under study. Δ indicate the tiltmeter stations and the tilt-strainmeter station of VI; • indicate the well level recording station.

About 70 km south from the seismic zone, another cave, the Grotta Gigante cave on the Karst, hosts an horizontal pendulum station since 1958 (TS in Fig. 1). The two instruments are again horizontal pendulums with Zöllner suspension, but the huge dimensions of the cave allowed a distance between the upper and lower attachments of about 100 meters, masses of 15 kg, and a free period of 6 minutes.

The array covers therefore a time interval of about 16 years, and for the single Grotta Gigante station, of 27 years: the data constitute therefore a rare and precious database for the monitoring of the slow movements in a collision area (Marussi, 1959; Zadro, 1978; Mao et al., 1989; 1990).
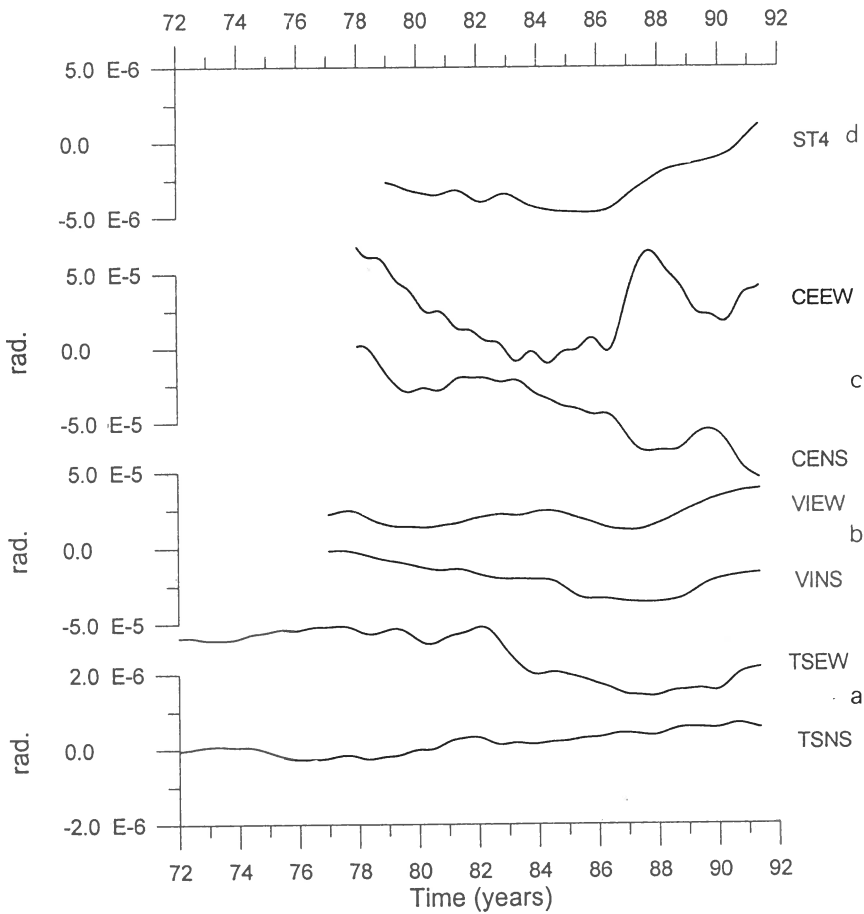

Fig. 2 a,b,c Long term trends for the EW and NS components of TS, VI and CE tiltmeters stations.Eastwards and Northwards tilting are positive.d)The same for the longidudinal strainmeter along N68E direction. Elongation positive.

Data

The hourly data, decimated to a daily sampling, have been low-pass filtered by a convolution in the time domain with a filter charaterized by a 300 days lag and a cut-off of 1/3 c/y, to evidence the long term variations.Fig. 2 shows the filtered data relative to TS, VI and CE tilt EW

and NS components and to the longitudinal strainmeter ST4, N68E oriented.
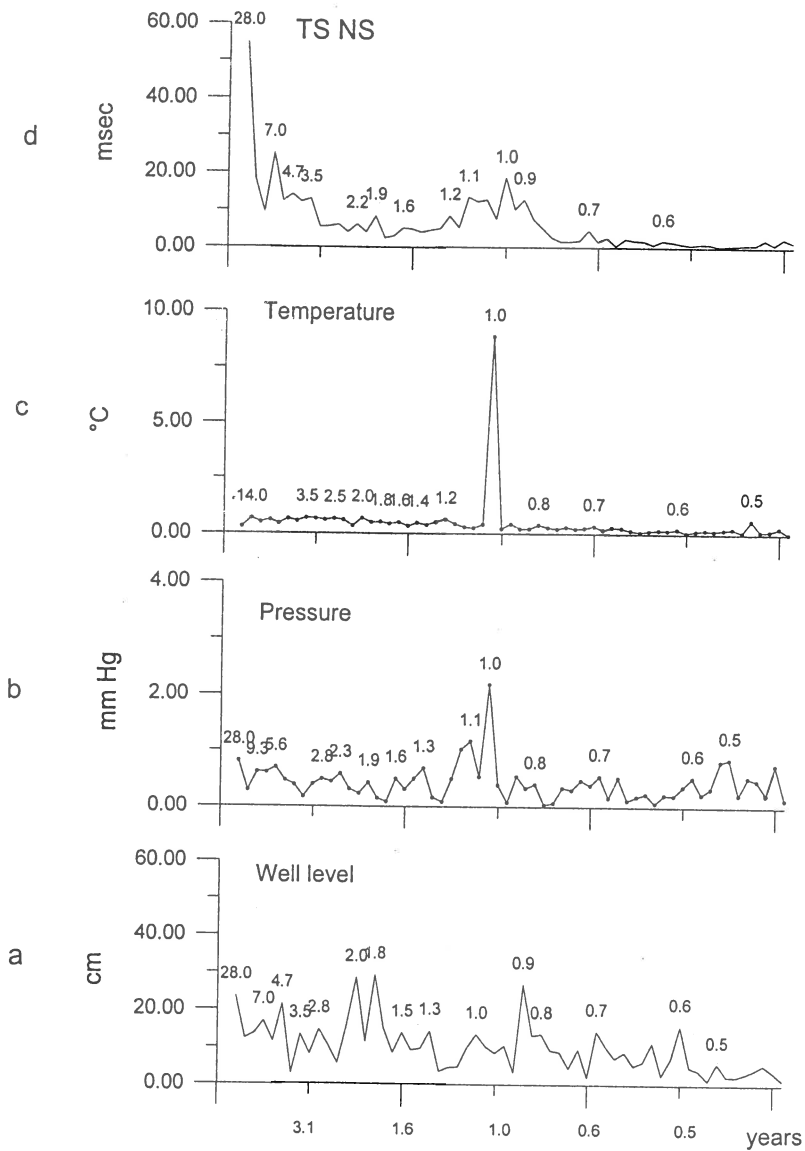
Fig. 3. a) Spectrum of the well level recorded in the VN station (see Fig. 1).b) Spectrum of pressure recorded in Trieste; c) Spectrum of the temperature recorded in Trieste; d) Spectrum of NS component of TS tilt signal.

The geographical position, local structure, topography and depth of the station act as filters, affecting the signal amplitude. The strain rates here observed (10^{-6} per year) are in the range of the strain rates per year inferred in the Alpine area from geological data (Pfiffner and Ramsay, 1982) and in the Friuli area from geodetic measurements (Talamo et al., 1978), and often observed in other seismic zones (Mortensen and Johnston, 1975; Rikitake, 1976; Kasahara, 1979; Savage et al. ,1979; Meertens et al., 1989).

Even if to a first glance the strain field appears heterogeneous, there are some common features, that confirm preceding observations (Zadro and Rossi, 1991). The NS components show a very long period term, that appears southwards directed in VI and CE signals, whereas in the same period TS signal is tilting northwards. The EW components appear interested by undulations of period of few years, out of phase between VI and CE, whereas appear in phase for TS and VI signals after 1985. It is noteworthy, that the long term undulations are not related to meteorological effects: the four spectra of Fig. 3 are relative to temperature, pressure, well level, and the NS component of TS tiltmeter station. In this last case, the spectrum has been calculated on the original data, in order to compare also the entity of the annual signal. It is interesting to look at the different characteristics: the temperature is dominated by the annual term, whereas the well, pressure and tilt spectra show a more articulated frequency content, but high energy at the lowest frequencies is a characteristic of the single tilt signal, therefore independent from meteorological effects. The other tilt and strain spectra are comparable.

Data analysis

It is important, in the study of the strain field, to reconstruct not only its time variations, but also its space variations, since it has been recognized that there may exist a spatial migration both in the strain field variations (Kasahara, 1979) and in the earthquake hypocentres (Mogi, 1968).

TS, VI and CE are located in different geological conditions: VI and CE are both located in the hearth of the seismically active area, whereas TS is about 70 km south of it. Nevertheless the three stations, defining an ideal N45W profile, belong all to the northern boundary of the Adria microplate, and it may be assumed that deformations at regional scale, originated at depth, can be recognized in all the three stations, through a

cross-correlation analysis of the signals. Moreover, both NS and EW signals are recorded in each tilt station, so that we can obtain the tilt signal for whatever azimuth, through a vectorial composition of the two ones. On this basis, the cross-correlations between the two couples TS-VI and VI-CE have been computed for six common azimuths from N to N150E, ranging 30 by 30 degrees.
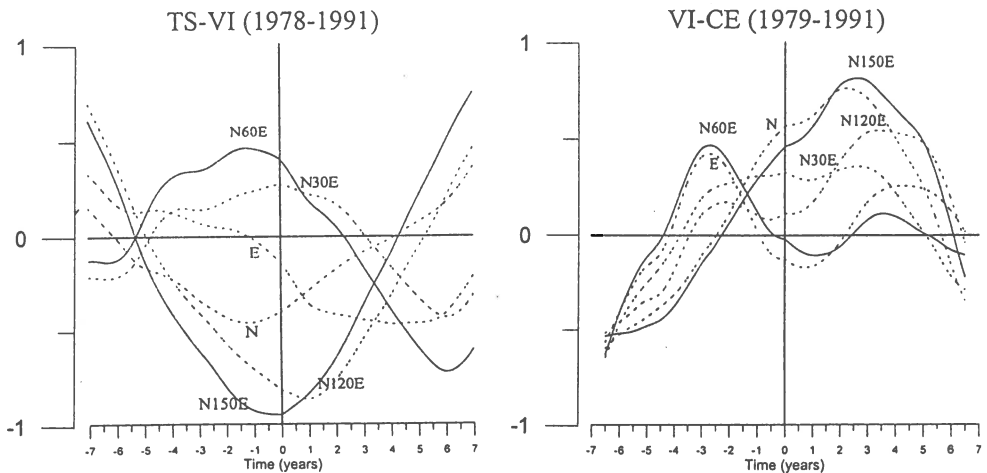

Fig. 4. a) Cross-correlation computed along various directions between the tilt signals in TS and VI. b) Cross-correlation computed along various directions between the tilt signals in VI and CE. On x-axis the time lag (years).

In Fig. 4a the results for the first pair of stations, TS-VI are shown. In Fig. 4b the results for VI-CE. The time interval is of 16 years, and the maximum lag is the 40% of it.

The curves show the superposition of terms of different frequencies. In both cases the cross-correlation reaches high absolute values both for N150E direction and for N60E direction.

For the TS-VI case, for the N150E direction, the minimum occurs almost in correspondence of the 0 lag, that means that the two sites are tilting in opposite sense in this direction in the same time. The second direction shows a positive maximum about one year before in VI than in TS.

For the VI-CE case the N60E direction shows an evident periodicity of 7 years,with a phase lag between the two signals of about 3 years.

Discussion and Conclusions

The strain field at the NE border of the Adria plate appears to be subject to the action of some transient deformations, that act along N150E and along a direction close N60E direction respectively. The first direction is coincident with the direction of the maximum compression acting in the region, which may be inferred from the fault plane solutions of the seismic events. The second one is close to the normal to the Dinaric structures. Not very far from this area, on the Dalmatian coast, the compression is oriented along this direction, and some of the fault plane solutions of the seismic events occurred in the area show a slight rotation of the compression axis eastwards (Slejko et al., 1989; Anderson and Jackson, 1987).
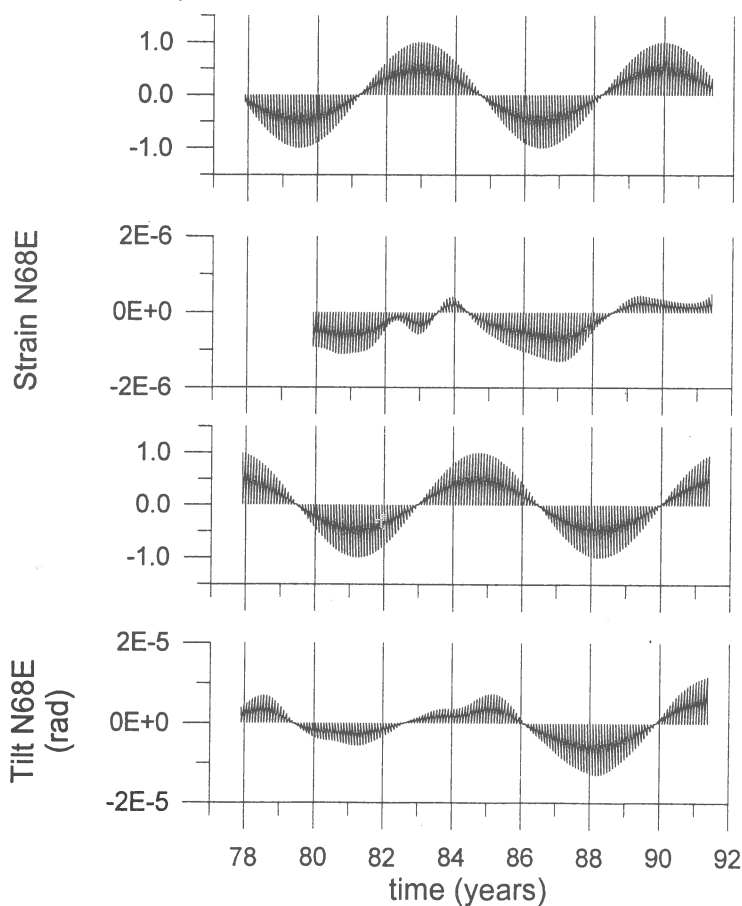
Fig. 5 a)VI tilt signal along the N68E direction; c) strainmeter signal along N68E direction. b) sin(ωt) with T=7 years; d) cos(ωt+kx)

The second direction shows a periodicity of about 7 years, evident in the VI-CE cross-correlations. This period is about the double of the time occurrence of the M>4 events occurred in the area in the last 15 years (OGS, 1977-1993). We could then suppose that there is a sort of deformation-stress wave, which propagates along a direction comprised between E-W and N60E, and in some way related with the medium energy events. If such a wave would exist, in the same point the horizontal and the vertical earth movements would show a phase delay of $\pi/2$. Fig. 5a shows the VI tilt signal along the N68E direction (which may be assimilated to a vertical movement) and (Fig. 5c) the correspondent strainmeter signal (horizontal movement). The curves of Fig.5b and Fig.5d are $\sin(\omega t+kx)$ with T=7 years and $\cos(\omega t+kx)$ respectively. The agreement between the observed data and the sinthetic curves is amazing.

Earthquake and strain propagation have been reported also in the past by Mogi (1978) and Kasahara (1979), and it has been suggested that the earthquake on the Italian side of the Adriatic see would be induced by the ones occurred on the Dalmatian coast (Mantovani et al., 1991). Moreover, recently (Albarello and Martinelli, 1994) the analysis of well levels in the Appennic piedmont area evidenced the propagation of variations with a period of 8 years in an approximately EW direction: what appears to confirm our results. It is on study a rheologic model that may help to understand what is really undergoing in this region, that may be considered a sort of natural laboratory for the study of the collision process in a continental zone.

References
Albarello, D. e G.Martinelli, 1994,Piezometric levels as possible geodynamic indicators: analysis of the data from a regional deep waters monitoring network in Northern Italy, Geoph.Res. Lett., **21**, 1955-1958.

Anderson, H. and J. Jackson, 1987. Active tectonics of the Adriatic region. Geophys. J. R. astron. Soc., **91**, 937-983.

Gutdeutsch, R., P. Steinhauser, K: Aric, W. Seiberl, G. Duma and J. Drimmel, 1981. Geophysical contribution to the Geodynamics of the Eastern Alps. In: Bundesministerium für Wissenshaft und Forschung ;- Forschung (Ed.),Results of

the Austrian Investigations in the International Geodynamic Project 1972-1979,Wien, 1981, 7-33.

Kasahara, K., 1979. Migration of crustal deformation, Tectonophysics, **52**, 311-329.

Mantovani,E.,E.Boschi,D.Albarello,D.Babbucci and Mucciarelli,1991. Regularities of time -space distribution of seismicity in the periadriatic regions:tectonic implications, Tectonophysics, **188**, 349-356.

Mao, W.J., C. Ebblin and M. Zadro, 1989. Evidence for variations of mechanical properties in the Friuli area.Tectonophysics, **170**, 231-242.

Mao, W. J., P. Santero and M. Zadro, 1990. Long- and middle-term behaviour of the tilt and strain variations in the decade following the 1976 earthquake in NE-Italy. Pageoph., **132**, 653-677.

Marussi, A., 1959. The University of Trieste station for the study of the tides in the vertical in the Grotta Gigante. In: Proceedings of the Third International Symposium on Earth Tides, Pubbl. 49, Ist. di Topog. e Geodesia, Univ.Trieste, Trieste, 45-52.

Meertens, C., J. Levine and R. Busby, 1989. Tilt observations using borehole tiltmeters. 2. Analysis of data from Yellowstone National Park. J.Geophys. Res., **94**, 587-601.

Mogi,K,1968.Sequential occurrences of recent great earthquakes, J. Phys. Earth, **16**, 30-36.

Mortensen,C.E. and M.J.S. Johnston,1975.The nature of surface tilt along 85 km of the San Andreas fault.Preliminary results from a 14 instruments array. Pageoph., **113**, 237-249.

OGS, 1977-1981. Bulletin of the Friuli Venezia Giulia seismological network, OGS, Trieste, (Italy).

OGS, 1982-1993. Bulletin of the North-Eastern Italy seismometric network, OGS, Trieste, (Italy).

Pfiffner,O.A. and J.G. Ramsay,1982.Constraints on Geological strain rates:arguments from finite strain rates of naturallly deformed rocks. J.Geophys.Res.,**87**,B1,311-321.

Rikitake, T., 1976. Earthquake prediction. Dev. in Sol. Earth Geophysics, 9, Elsevier Scient. Pub. Company, Amsterdam, 1976, 357pp.

Savage, J.C., W.H: Prescott, M. Lisowski, N: King, 1979. Deformation across the Salton Trough, California, 1973-1977. J. Geophys. Res., **84**, 3069-3079.

Slejko, D., G.B. Carulli, R. Nicolich, A. Rebez, A. Zanferrari, A. Cavallin, C. Doglioni, F. Castaldini, V. Iliceto, E. Semenza and C. Zanolla, 1989. Seismotectonic of the Eastern Southern Alps: a review. Boll. Geof. Teor. Appl., XXXI, **122**, 109-136.

Talamo, R., M. Pampaloni and S. Grassi, 1978.Results of the high precision leveling performed by the Istituto Geografico Militare in the areas of Friuli object of the recent seismic activitiy (in Italian).Boll.Geod. Sc.Aff., **1**, 61-71.

Zadro, M. 1978. Use of tiltmeters for the detection of forerunning events in seismic areas. Boll.Geod.Sci. Aff., **37**, 597-618.

Strains, Seismicity and Rain

Braitenberg C. & Zadro M.

Institute of Geodesy and Geophysics, University of Trieste, Trieste, Italy

Abstract

The region under study is the seismic Friuli region of NE-Italy, the most seismic region of the Alpine arc. In '77 the Friuli high-resolution clinometric/extensometric network was set up, with the aim of observing crustal deformation related to the local seismicity and to serve as a seismic precursors monitoring facility. It is a well known problem that atmospheric agents as rain, watertable variation, temperature and atmospheric pressure, emerge as a deformational signal in the records. This signal is in danger of being confused with a seismically induced deformation, if not correctly recognized. In the present work, the hydrologic influence on clinometric and strain records is studied, as well as it's relation to seismicity. The rain-induced deformational signal is quantified for two different stations of the network before and after the occurrence time of a seismic event (M=3.9) with the aim of retrieveing the tectonic deformation.

Introduction

The detection of a seismic precursor by instrumental observation is tied to the ability of identifying an anomalous signal which emerges with statistically significant amplitude above the background recordings. The amplitude limit, above which the signal may be regarded as significant, depends on the noise level. What is to be considered as noise depends on the extent of our knowledge on all agents which may produce a deformational signal. Among these, as well known (e.g. Langbein et al., (1990), Wyatt (1982,1989), Wood and King (1977), Edge et al., (1981), Schüller (1985), Gerstenecker (1985), Kümpel (1985), Wolfe et al. (1981), Zschau (1979)), atmospheric agents as rain, watertable variations, temperature and atmospheric pressure must be included.

The order of magnitude of the deformational signal associated to a medium local earthquake may be estimated as modelling the event as a dislocation (Okada, 1985), bearing in mind though, that the value obtained may underestimate the real value, as was observed for the 1976 Friuli earthquake (Tokuyama, 1976). Assuming an event of M=4.5 with thrust fault mechanism (20° inclination), hypocentral depth equal to 5 km, we obtain as maximum values e.g. of tilt 190 msec. At an epicentral distance of 10 km the expected tilt and strain signals are at the level of the tidal deformational amplitudes. Regarding the small amplitudes of the signals to be detected, it may be concluded that all signals independent from seismic activity must be predicted as accurately as possible in order to reduce the noise level to a minimum.

At the present state of our study we completed a preliminary analysis of the rain induced signal for two stations of our network. The modelling of the deformational signal given the rainfall and watertable variation is extremely difficult, (Edge et al., 1981) and has been attempted in the past by various authors (for example Kümpel, 1989, Yamauchi, 1987).

Modelling of the physical process involved is the most direct method and surely the more satisfactory as well. It requires however, exact knowledge of the local structure such as mechanical properties with depth (porosity, elastic moduli, permeability), which in general cannot be assumed to be homogeneous. In our case only an oversimplified model may be set up, due to the lacking knowledge on details on structure and the aquifer system, with consequent unreliable calculated induced deformation signals. For this reason we prefer the approach from a statistical point of view, regarding the problem of determining that filter which represents the system adequately.

Instrumentation

In '77 the Friuli high-resolution clinometric/ extensometric network was set up (Fig.1 of Rossi & Zadro, present volume), with the aim of observing crustal deformation related to the local seismicity and to serve as a seismic precursors monitoring facility (Zadro, 1978, 1980, 1992). The network includes 5 clinometric stations (2 components, NS,EW) and one extensometric station (3 components: ST2, ST3, ST4, oriented respectively: 128°, 27°, 68° from N eastwards). In the present study we have considered the tilt station Gemona (GE) and the tilt/strain station Villanova (VI). The horizontal pendulums, built at the University of Trieste, are kept at an eigenperiod of about 90 sec. The extensometers are Cambridge Invar wire strainmeters. The sampling rate is fixed to one sample per hour. The station GE is located in an artificial gallery excavated 80 years ago and has a rock overburden of about 30m. The station VI is located in a cave at 60m depth. The annual temperature variation at the two stations is of 1.5°C in VI, and 2.5° C in GE. The rainfall data pertain to a station (Venzone) located in a 20 km distance range from the two tilt-strain stations and are provided by the Ufficio

Idrografico e Mareografico di Venezia at a daily sampling rate. At the same site, the watertable level is measured every three days and provided by the Regione Friuli Venezia Giulia. The barometric pressure is recorded by our own Institute (Climatology Laboratory) at an hourly sampling rate in a station situated in Trieste. Monitoring of micro-seismicity has been accomplished since 1977 by the OGS (Osservatorio Geofisico Sperimentale, Trieste) Seismological network.

Rain and strain

We will treat the problem of modelling of the hydrologically induced deformational signal for the tilt stations VI and GE, and the strainmeter station VI, for the year 1991. The year 1991 is of particular interest, as two seismic events of magnitude near 4 have occurred, the first on June 11 (M=3.8, Lat=46.26, Lon=12.90, depth=14km), and the second on October 5 (M=3.9, Lat=46.24, Lon=13.31, depth=19.5km) of which though only the October, 5 event generated an aftershock sequence (Fig. 1). In our studying area an event of magnitude M=4 occurs in the mean once every 3-4 years. In Fig. 1 the VI-NS tilt, the VI-strainmeter ST2, ST3, ST4 and GE-NS tilt recordings, the rainfall in mm/day and the well level depth in cm from the surface are graphed. In the graph the original hourly deformational recordings have been resampled to daily sampling, applying in precedence an antialiasing filter. The seismicity of Friuli in number of events/day during 1991 has been added to the graph as well, except for the months from January to May, when no data from OGS are available. All instruments show the annual thermoelastic deformation, which is regularly observed on all stations of the network. The extreme values are found February/March (tilt VI towards NW, tilt GE towards SW, strainmeter S2 in extension, S3 and S4 in compression) and, in the opposite senses, September/October.
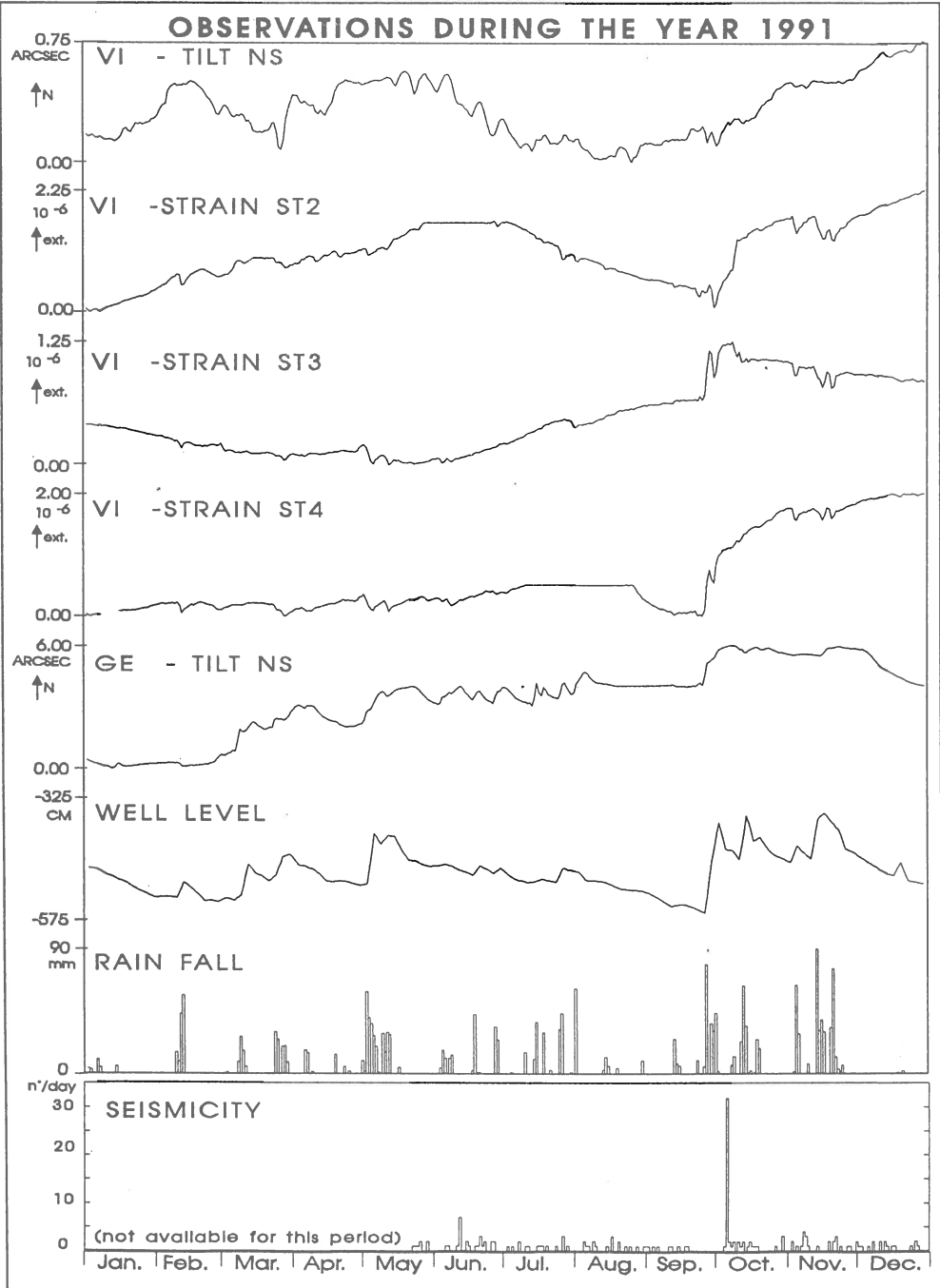
Fig.1- Tilt and Strainmeter recordings, atmospheric agents and seismicity during 1991: Tilt NS (in arcsec) at VI, strain (in μstrain) ST2,ST3 ST4 (azimuths from N towards E:128°, 27°, 68°, respectively) at VI. Tilt NS (in arcsec) at GE. Rainfall in mm/day, well level in cm, local seismicity in events/day.

Superposed to the annual cycle some aperiodic events are evident in the strainmeter records characterised by a compression observed on all three instruments, followed by a nearly exponential recovering over a time interval of about 10 days.

In the tiltmeter records of VI and GE, these signals appear as a Southward and Northward movement, respectively, and are examples of the hydrologically induced deformation we intend to model.

The statistical analysis

Experimental tilt observations (Kümpel, 1989) made in a test field where water was pumped into and extracted from wells at a constant flow rate, have shown that the induced deformation is proportional to the local gradient of the watertable level. In the case of the aquifer in Friuli, the recharge is given by the total rainfall in the proper hydrological basin. The azimuth of the induced tilt signal is greatly constant in mountainous areas, as ours, and is determined by the topography of the impermeable substratum. The time variation of the level $H(t)$ of the waterhead in a single point (e.g. Davies and De Wiest, 1966) may be expressed in linear approximation by the equation:

$$\frac{dH(t)}{dt} = a_0 P(t) + a_1 + a_2 H(t)$$

where $P(t)$ is the rainfall, and a_0, a_1, and a_2 are the parameters describing the recharge (a_0), and the outlet (a_1, a_2) of the system. As we are dealing with sampled time series, the above equation is evaluated at discrete times t_n, $n=0,N$ and the time derivative is replaced by a finite difference scheme. In terms of digital signal analysis the above system is an auto-regressive process of first or second order, depending on how the time derivative is estimated. The parameters $a_0 \dots a_2$ of the process describe the dynamics of the system,

whereas the rainfall $P(t)$ is the random input. The absolute value of the gradient being calculated from the difference between two points of the waterhead, it itself is also described by an autoregressive process. It is thus plausible to reduce the determination of the rain induced deformation to the problem of finding the appropriate parameters of the above difference equation. In developing this approach, the above model may be expanded, introducing a non-linear term in the input variable or in the autoregressive terms. This leads to a formulation of the problem which is a generalization of the concatenated tanks in the approach of Yamauchi (1987).

An example - the October 1991 event

We consider as an example, where the determination of the rain-induced signal is of particular interest, one month preceding and following the October,5, 1991 event. In Fig.2 the deformational recordings, the barometric pressure, rainfall and seismicity are given for the months September and October, 1991. As we study the rain-induced signal for short periodic variations, the data were high-pass filtered, at cut off frequency of 1/90 days. A short-period deformational signal is observed on the instruments of the test sites GE and VI a few days previous the event. We observe though also that strong rainfall (75 mm in one day. Yearly percentage of a rainy day with 75 mm/day rain or more is equal to 1.3%) has occurred in the days preceding the event, and that the well level has increased 2 m. Therefor the observed signal is the sum of the rain-induced deformation and the pre-, co- and postseismic deformation. Following the method presented in the previous paragraph, we have estimated the rain induced deformational signal for the year 1991 for the instruments shown in Fig.2. The daily sampling rate of rainfall furnishes the prediction of the rain-induced deformation at the resolution of 1 day.
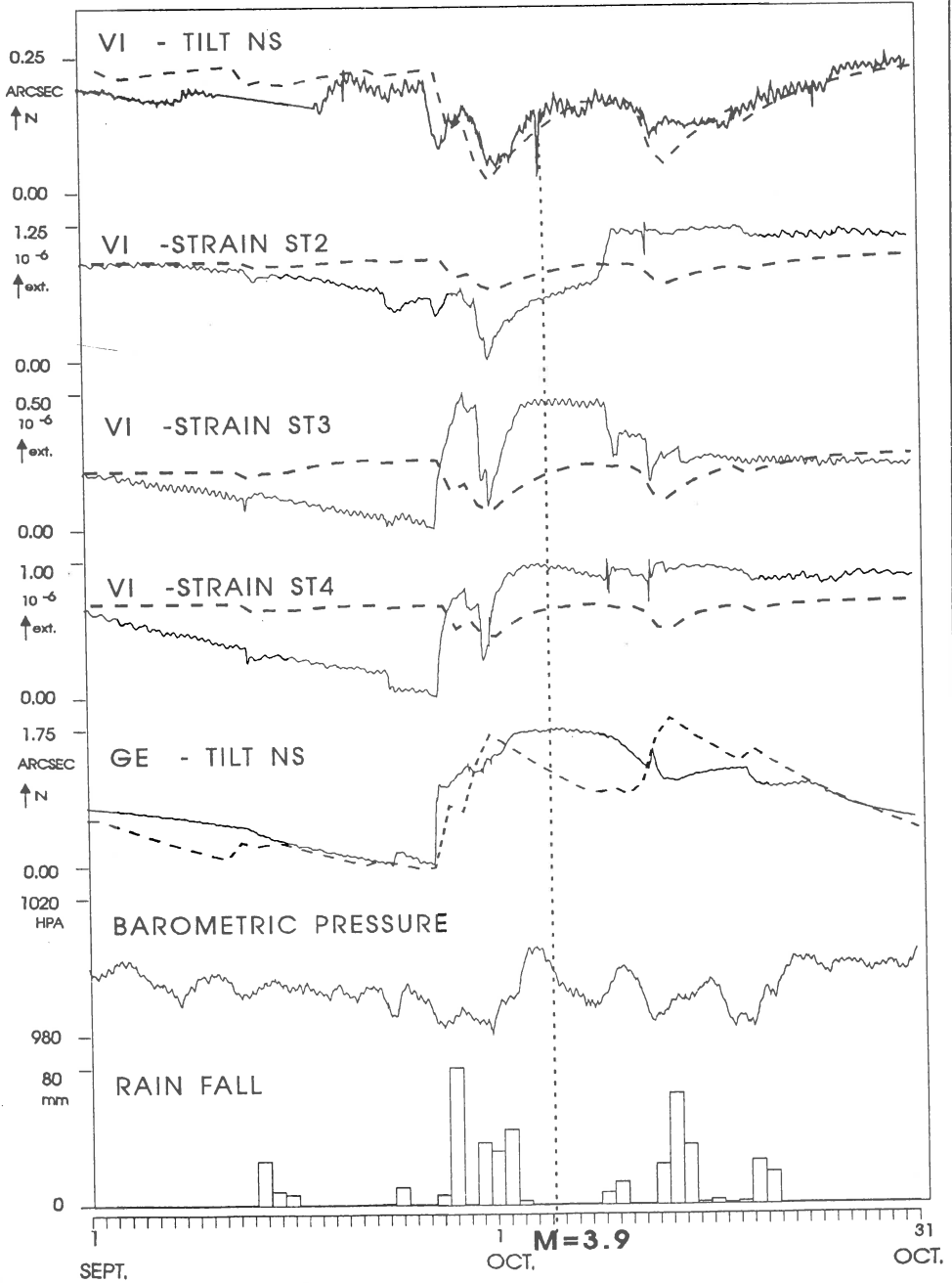
Fig.2- Seismic event October, 5, 1991: Tilt and Strainmeter recordings, Rainfall in mm/day and barometric pressure (Trieste station) in hPa during September and October, 1991. Abbreviations as in Fig.1. Broken line shows predicted rain-induced deformation.

In Fig.2 the predicted rain-induced deformation (broken line) is superimposed on the observed deformation. For both sites qualitatively the time evolution of the rain induced signal is correctly predicted, whereas the amplitudes reveal that the algorithm works well for the tilt in VI, satisfactory for the tilt in GE, and only poorly for the strainmeters. A considerable percentage of the deformation recorded previously to the October event is revealed to be rain-induced.

Interesting though is a short-period deformation observed on the tiltmeter NS of Villanova, which is surely not rain-induced. It started 12 hours before the event, reaching a peak value 5 hours later, recovering up to the time and beyond the event.

Discussion and Conclusion

We have shown our first results in identifying and quantifying the tiltmeter and strainmeter signal induced by strong rainfall. This is crucial in the monitoring of seismic deformational signals, as the rain induced signals may now be predicted and separated from the tectonic signals in the deformational records. We have applied our methodology to determine the tectonic deformation related to a M=3.9 event which occurred in the range of 14 km of the stations. 10 days before the event a strong deformational signal is recorded, which is partly rain-induced. The tilt signal observed 12 hours before the event in station VI, located at only 3km from the epicentre, is shown to be not rain-induced, and could be the evidence of the observation of a precursory tectonic deformation.

Apart from determining the hydrologic effects on deformational measurements, the study of the rain-induced deformation has application to the possible existence of hydrologic triggering of seismicity.

The hydrologic agents have been shown in different regions of the world to be correlated to seismicity. In fact a vast literature reports on watertable, lake-level or artificial basin level variations causing the

triggering of seismic events, including dedicated symposia (for example O'Reilly and Rastogi, 1986; present ECS assembly). This phenomenon, termed "Hydroseismicity" in the review article of Costain et al., (1987), has been reported in a number of cases in connection with the draining or filling of artificial reservoirs (for example Evans (1966)), with water levels in lakes (for example Kafri & Shapira, 1990) and also due to water table level variations (Roth et al., 1992). In the Friuli region the hydrological agents take up a relevant position, as the area is characterised by high annual rainfall, the total annual precipitation, averaged over a time interval of 60 years (1922-1982) being 1880 mm (Ferla, 1983). The high rainfall values are accompanied by large annual watertable variations, with values which range from 3m to 25m, according to the geographical location of the observation well. The first evidence of the hydrologic influence on seismicity was given by Brussa Toi et al.,(1989), who found strong resemblance for the years 1978-1982 between the local microseismicity variation, defined as the detrended cumulative number of local earthquakes (25 km radius centred on the rainfall station, magnitude M< 2.5) and the detrended cumulative rainfall. We have extended the analysis computing auto- and crosscorrelation functions of rainfall and seismicity, taking the years 1979-1991. The geographical window was [45.5°-46.5°N,12.0°-14.0°E], with epicentral depths less than 10 km and magnitudes with 2.5 < M < 3.5. The detrended cumulative quantities were calculated with a time resolution of 3 days. Both rainfall and seismicity functions were high pass filtered, with cut off period at 1 year, in order to eliminate long term trends. The normalized autocorrelation and cross correlation functions are shown in Fig.3. The dotted lines indicate ± one standard error of the correlation values. The first maximum of the auto correlation functions (lag about 165 days) gives evidence of a semiannual variation in both rainfall and seismicity. As

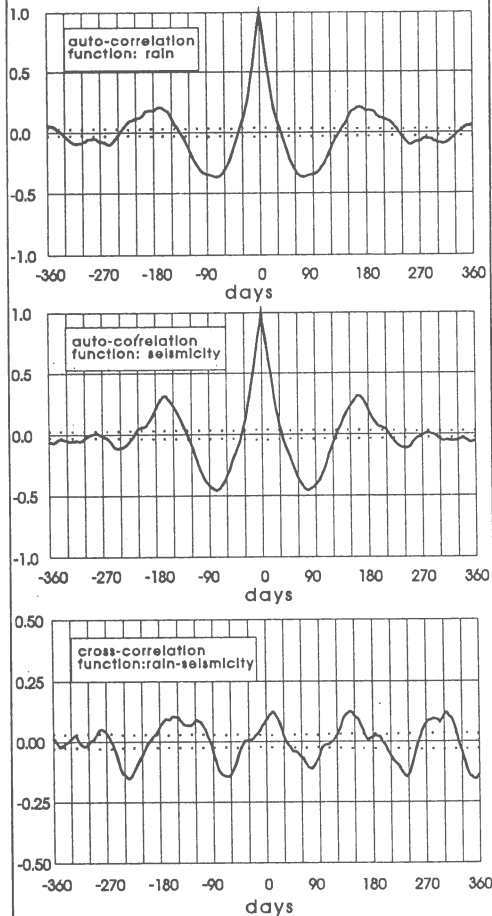AUTO- AND CROSSCORRELATION FUNCTIONS.
RAINFALL AND SEISMICITY.

Fig.3- Auto and cross correlation functions of detrended cumulative curves of rainfall and seismicity calculated for the years 1979-1991. Sampling=3 days. $2.5 < M < 3.5$. $0\,km < d < 10\,km$.

although the result is not clear due to the presence of maxima also at lag=144, 300 and -150 days. At this stage the causal dependence of the two quantities cannot be stated, and is a topic of further investigations.

We conclude that the study of the rain-induced tilt signal is thus important as it stands alone, i.e. not only in order to eliminate noise from the deformational records (Evans and Wyatt, 1984), but also with the aim of achieving a better understanding of the frequently discussed rain-induced seismicity.

References

Brussa Toi B. and Zadro M., 1989. Weil fluctuations, rain and seismic activity in Friuli, NE-Italy (Abstract). Special Issue Annales Geophysicae. XXII Assembly EGS, March 1989, Barcellona.

Costain J.K., Bollinger G.A. e Speer J.A., 1987; Hydroseismicity: a hypothesis for the role of water in the generation of intraplate seismicity, Seism. Res. Let., **58**, 41-64.

Davies S.N. and De Wiest R.J.M., 1966. Hydrogeology. 1-463. J.Wiley, New York.

Edge R.J., Baker T.F. and Jeffries G., 1981. Borehole tilt measurements: aperiodic crustal tilt in an aseismic area, Tectonophysics, **71**, 97-109.

Evans D.M., 1966. The Denver area

this observation was to be expected for rain, the cause of the semiannual variation of seismicity is unknown. We find a maximum of the cross correlation function for lag=15 days, which could indicate that statistically seismicity lags rainfall by this quantity,

earthquakes and the Rocky Mountain Arsenal Disposal well, Mountain Geol., **3**, 23-26.

Evans K. and Wyatt F. 1984 . Water table effects on the measurement of earth strain. Tectonophysics, **108**, 323-337.

Ferla 1983 , Annali Idrologici, parte II, Ufficio Idrografico e Mareografico di Venezia.

Gerstenecker L., 1985 . The investigation of the air pressure and temperature effects on the Hughes borehole tiltmeter by finite element analysis. Proceedings of the 10th International Symposium on Earth Tides, (ed. Vieira R.), 923-931.

Kafri U. and Shapira A., 1990 . A correlation between earthquake occurrence, rainfall and waterlevel in Lake Kinnereth, Israel. P.E.P.I., **62,** 277-283.

Kümpel H.J., 1985 . Model calculations for rainfall induced tilt and strain anomalies. Proceedings of the 10th International Symposium on Earth Tides, (ed. Vieira R.), 889-904.

Kümpel H.-J., 1989 . Verformungen in der Umgebung von Brunnen. Habilitationsschrift an der Math.-Naturwiss. Fakultät, Christian-Albrechts Universität, Kiel.

Langbein J.O., Burford R.O. and Slater L.E., 1990 Variations in fault slip and strain accumulation at Parkfield, California: Initial results using two-color geodimeter measurements, 1984-1988., Journ. Geoph. Res., **95**, 2533-2552.

Okada Y. 1985 . Surface deformation due to shear and tensile faults in a half space. BSSA, **75,** 1135-1154.

O'Reilly e Rastogi B.K., (Ed.), 1986; Induced seismicity. Papers presented at the IASPEI Symposium, Hyderabad, India, 1984. Special Issue of Phys.Earth Planet.Int., **44,** 73-199.

Rossi and Zadro, 1995 . Analysis of the secular strain field variations in NE-Italy. Proceedings of the XXIV Genera' Assembly of the Europear Seismological Commission, 1994 September, 19-24, Athens. (in press).

Roth. Ph., Pavoni N., Deichmann N., 1992 . Seismotectonics of the eastern Swiss Alps and evidence for precipitation-induced variation in seismic activity. Tectonophysics, **207**, 183-197.

Schüller K. 1985 , Simultaneous tidal and multichannel input analysis as implemented in the HYCON method, Proceedings of the 10th International Symposium on Earth Tides, (ed. Vieira R.), 889-904.

Tokuyama A., 1976 . Crustal deformation after the Friuli earthquake, 1976. Proceedings of the International meeting on the Friuli earthquake, Udine, December 4-5, 1976. Boll.Geof.Teor.Appl., **XVIII**, 945-952.

Wood M.D. and King N.E., 1977 . Relation between earthquakes, weather and soil tilt. Science, **197,** 154-156.

Wyatt F., 1982 . Displacements od surface monuments-horizontal motion, Journ. Geoph. Res., **87**, 979-989.

Wyatt F., 1989 . Displacements od surface monuments-vertical motion, Journ. Geoph. Res., **94**, 1655-1664.

Wolfe J.E., Berg E. and Sutton G.H., 1981 . The change in strain comes mainly from the rain: Kipapa, Oahu, Bull.Seism.Soc.Am., **71**, 1625-1635.

Yamauchi,T. 1987 . Anomalous strain response to rainfall in relation to earthquake occurrence in the Tokai area, Japan. J.Phys.Earth., **35**, 19-36.

Zadro, M. 1978 . Use of tiltmeters for the detection of forerunning events in seismic areas. Boll. di Geod. e Sc. Affini. XXXVII, pp.597-618.

Zadro, M., 1980 . Point crust deformations: tiltmeter and strainmeter measurements. Quaterniones Geodesiae, 3, pp.103-115.

Zadro M., 1992 .Tilt and Strain Variations in Friuli,NE Italy, after the 1976 Earthquake. Proceedings of the V Course of the International School of Solid Earth Geophysics:Earthquake Prediction, Erice, July 16-23,1989. Edited by Dragoni M. and Boschi, (Il Cigno Galileo Galilei Edizioni, Roma),

pp.295-313.

Zschau J. 1979 . Air pressure induced tilt in porous media, Proceedings of the 8th International Symposium on Earth Tides, (ed. Bonatz M. and Melchior P.), 418-433.

LARGE SCALE MODELING OF EARTHQUAKES

G.A.Sobolev

Institute of Physics of the Earth,
B.Gruzinskaya 10, Moscow, Russia.

ABSTRACT.

Deformation of large blocks of marble and limestone in condition of gradual moistening revealed precursors of macrodestruction in the field of local strains, rate of acoustic emission, travel time, amplitude and spectra of elastic waves passing through the blocks. Precursors in the amplitude of elastic waves were more pronounced as compared to travel time variations. The regular shift of the peak of acoustic emission in successive cycles of loading appeared as universal feature of dynamic instability of rocks. The origin of the anomalies may be explained by joint application of dilatancy-diffusion and avalanche unstable fracturing models of earthquake preparation.

INTRODUCTION

In spite of the great effort made by scientists of different countries to solve the problem of earthquake prediction, reliability of the predictions is far inferior to what it should be to permit regular use in practice. This is mainly due to the fact that both the processes of earthquake preparation and the nature of precursors are poorly known. Most methods of prediction are based on empirical patterns that relate anomalous changes of weak seismicity, geophysical, hydrogeodynamical, and geochemical fields to the location, time and magnitude of a future earthquake. These patterns are based on limited data and do not permit a precise determination of main characteristics of the predicted earthquake. New data on precursors are slow to accumulate due to rare occurrence of large earthquakes in the areas provided with the modern systems of prognostic observations.

Therefore, considerable attention is being paid to laboratory earthquake modeling that permits, in principle, obtaining reproducible results within relatively short time periods. It should be noted that the available models of earthquake preparation, dilatancy-diffusion model DD and avalanche-unstable fracturing AUF [Myachkin V.I. et al.,], are largely based on laboratory research.

Inhomogenity of structure and of the state of stress and strain in the crust and the associated mosaic character of the occurrence of precursors need a simultaneous study of the latter at many sites. In the laboratory this may be realized by using the deformation of large blocks. Previous large-scale earthquake modeling [Sobolev G.A and A.V.Kolzov,1988] used dry blocks, while pore fluid plays a significant part in the process of failure and affects the characteristics of precursors.

The present paper aims at finding the stages of development of instability inside large deformed rock blocks occurring in the field of water filtration. In this case a set of physical parameters whose changes may be interpreted as macrorupture precursors was recorded.

THE METHOD

Two types of rocks have been studied under the conditions of uniaxial compression: marble and limestone (lumachelle) which have the same strength, grain size and filtration properties. The marble had the following mineral composition: 85-90% of calcite, 5-10% of pyroxene and diopside, 5% of epidote. It has the following properties: Young's modulus is 25 GPa, density is 2,69 g/cm, average P-wave velocity Vp = 5,3 km/s and average S-wave velocity Vs = 3,1 km/s, porosity 0,2%, permeability 0,4 mkdarcy. The limestone had the following mineral composition and properties: calcite 50%, dolomite 30%, clay additions up to 20%, Young's modulus 8.3 GPa, density 2.3 g/cm, Vp=3.8 km/s, Vs=2.5 km/s, porosity 6-7%, permeability 140 mkdarcy. Separate small pores and rather large cavities up to 3 mm across were typical of the limestone.

These rocks were employed to out blocks in the form of rectangular 1000x500x500 mm prisms. In center of each block a series of through holes along a line at an angle of 30 to the long axis of the block was drilled. These holes served as concentrators of stress, the loading producing a region of interval failure transforming into a shear macrorupture. Figure 1 presents the block sides with assigned numbers, the adopted system of coordinates and the locations of the sensors. A hole of 250 mm depth and 13 mm diameter was drilled at the center of the upper side to supply water. The water pressure was about 0,5 bars in the hole and was maintained constant during the whole experiment.

The blocks were loaded along the long axis using the 50,000-ton press. The changes in block length (total longitudinal strain L) were recorded by means of bar strainmeters installed at three sides of the block. Ten strain sensor sockets with 20 mm base were glued onto side 1. Each socket included three independent strain sensors oriented in the directions Z, X and at an angle of 45 to them.

Signals of acoustic emission (AE) due to rupture formations were received and located by two independent systems. The effective sensitivities of the systems were chosen to be different, so that the 1st system recorded a large number of relatively weak acoustic signals, while the 2nd the largest ones that had waveform records on all channels. Event location in both systems was based on ideologically similar algorithms minimizing a functional involving the times of first arrivals and compressional velocities [Sobolev G.A. and A.V.Koltsov,1988].

The ultrasound surveying (US) was made before the experiments and in the process of deformation along 15 horizontal and dipping paths (Figure 1). The variations of arrival times for compressional and shear waves, their amplitudes and spectra were determined. The measurement accuracy for arrival times amounted to 0,5% and for their amplitudes to 1%.
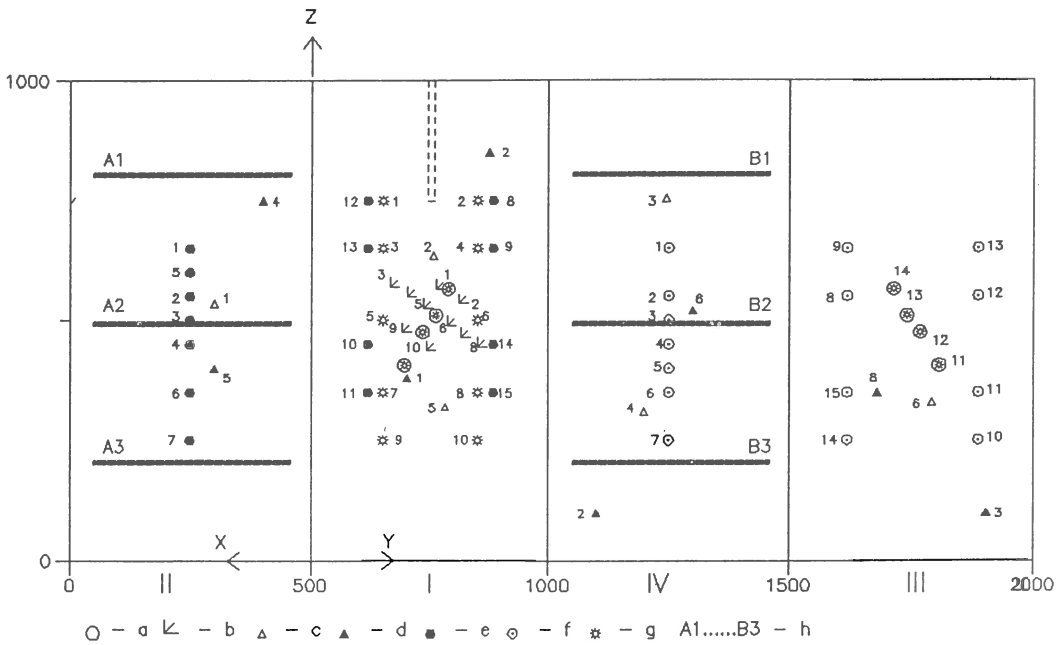
Fig.1. Sides of the block and location of the sensors. a-
holes (stress concentrators), b - sockets of strain sensors, c
- AE sensors of the PTI system, d - AE sensors of the IPE
system, e - radiators of ultrasound waves, f - receivers of
ultrasound waves, g - surface and internal (11-14) measuring
electrodes, h - current electrodes.

RESULTS

In this paper we consider thouse results on marble block which repeate itself qualitatively on the limestone. In all, 12 loading cycles were made involving three periods divided by intervals of partial unloading (Figure 2). Each cycle lasted 1 hour and was divided into two subcycles of equal duration: loading at a constant rate and maintenance of the loading level achieved.

It follows from Figure 2 that the AE distribution within cycles changed during the experiment. During cycles 3-7 the AE reached a maximum in the middle of a cycle and then decreased in spite of continued loading. However, beginning from cycle 8, these maxima were observed at the end of the loading subcycle or during the subsequent constant-load subcycle.

Among thousands of acoustic signals only several, largest ones were shown by acoustic location to be emitted from the center of the block near the set of holes which served as stress concentrators. A series of such acoustic events was recorded 23 min after the beginning of loading in cycle 9. Their times are shown by arrows in Figure 2 and the coordinates in the insertion of Figure 2.

A great number of acoustic events of large amplitude concentrated in time and in the region of the set of holes were then recorded during first 5 minutes of cycle 12. Immediately after that a fracture shown in Figure 2 was visually seen on side 1 of the block. It consisted of elements of shear type which connected the holes and of "whiskers" projecting up and down from the end holes. Complete failure followed by a loading decrease occurred during cycle 12. A series of macrofractures passed diagonally from the upper and lower holes up to the upper right and lower left angles of the block, thus lengthening the central macrorupture.

Taking into account the results of observations of visible cracks and the distribution of sources of acoustic signals (Figure 2), we can conclude that the central part of the block failed at the beginning of cycle 12, a substantial stage of preparation occurring during cycles 9-11.

Changes of P- and S-wave velocities for the dipping path 5-5 (Figure 1) that crosses the central part of the block are shown in Figure 3a. Increasing velocity of both wave types (Vp and Vs) in the earlier cycles indicates a closing of initially existing defects as a result of loading. The reversal of Vp variation, i.e., the beginning of decreasing P-wave velocity was observed after cycle 8 (9 hours). Obviously, by this time the effect of new defects exceeded the initially dominating effect of closure of the older ones. At the same time the Vs values continued to increase up to cycle 10 (10 hours). Sharp changes in Vp and Vs were observed in the final part of cycle 10.

The amplitude of compressional wave Ap reached the maximum in cycle 8 and then decreased towards the end of the experiment (Figure 4b).Substantially different behavior was observed for the amplitude of S-waves compared to Ap. After a small - decrease in the first two cycles, As gradually
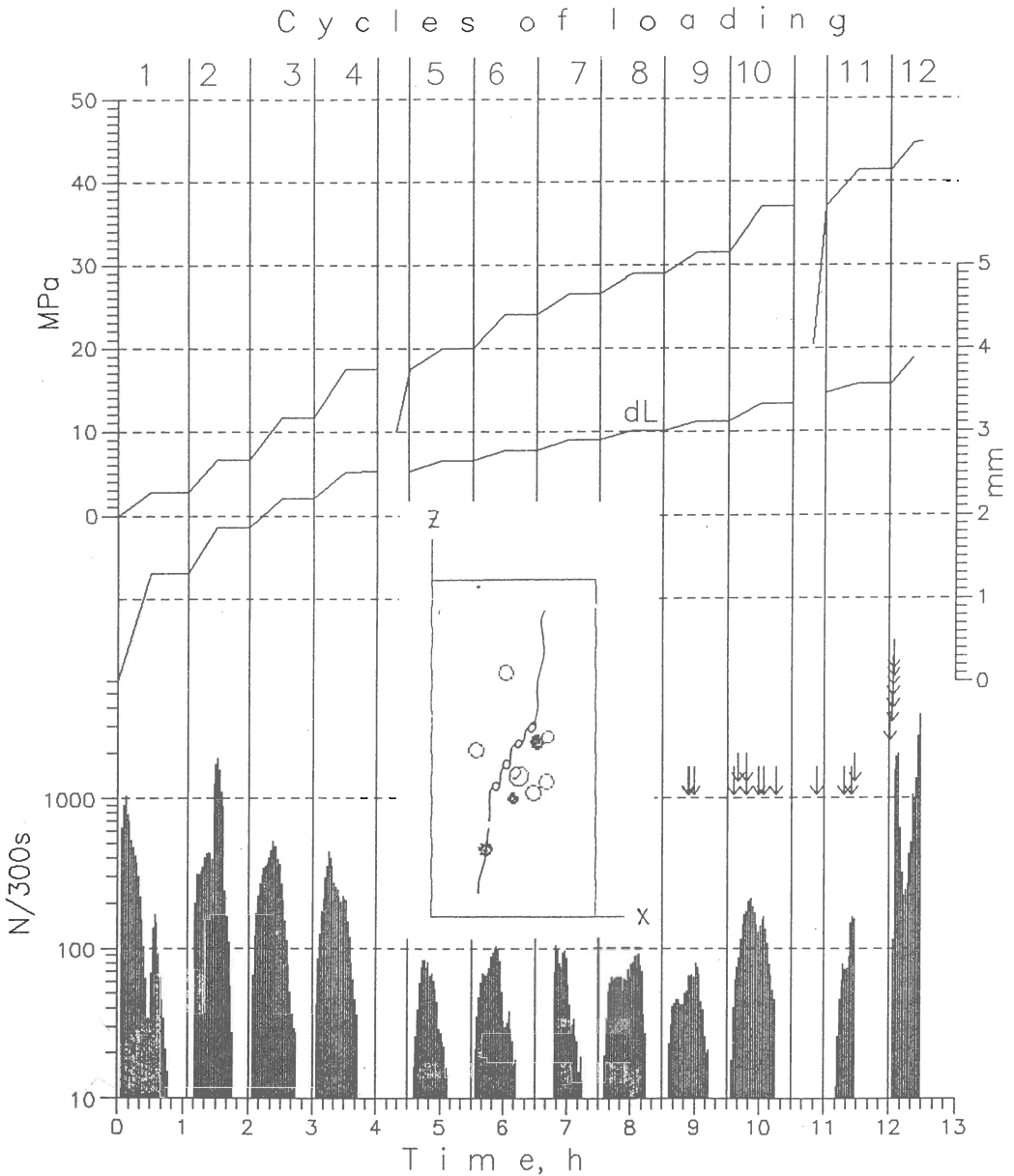
Fig.2. Variations in stress, block height L, and intensity of acoustic emission during the marble block test. Arrows indicate the times of acoustic signals whose sources were situated in the central part of the block. The location of the sources of the acoustic pulses (cycles 9-10) and macrofracture (after cycle 11) are shown in the insertion. The sources of first three pulses are shown in black.
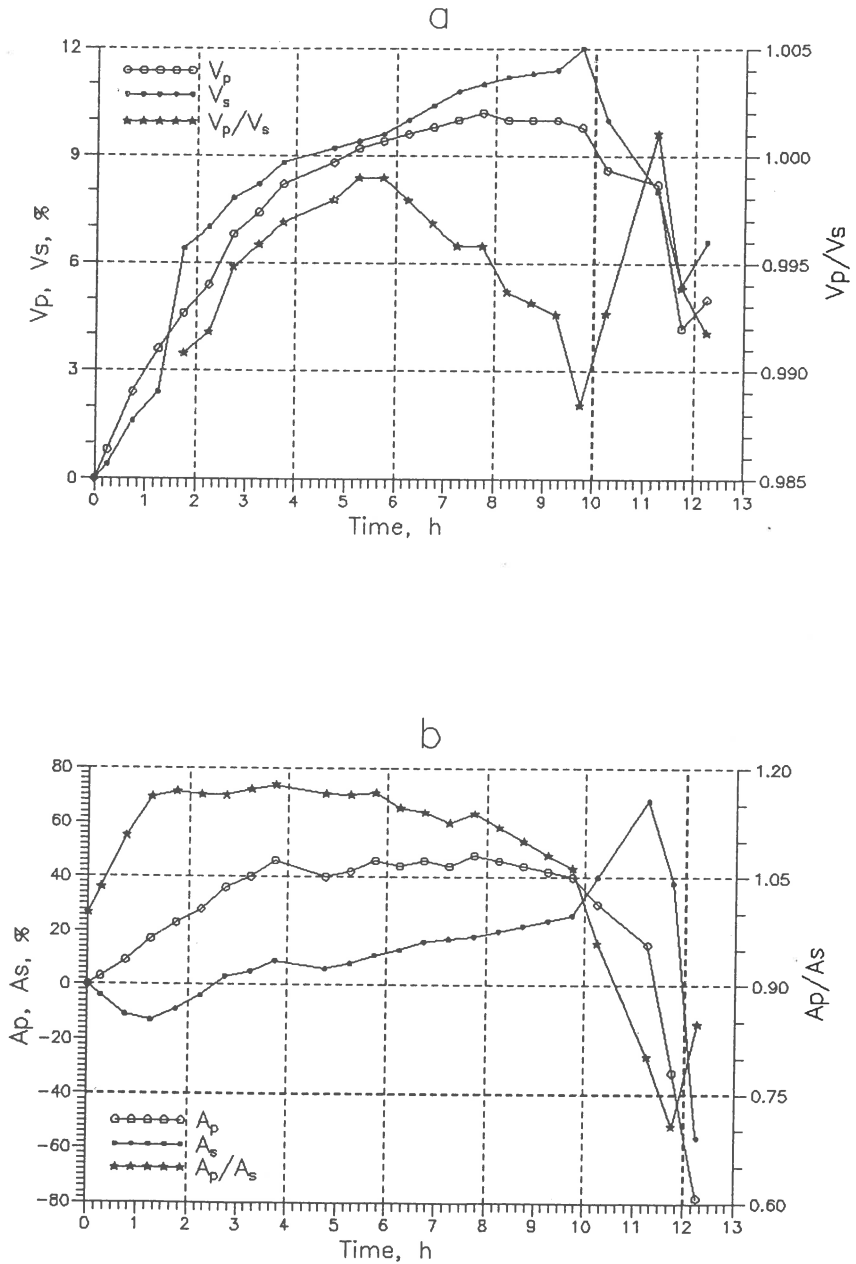
Fig.3. Variations in the velocities (a) and amplitude (b) of compressional and shear elastic waves and in the velocity ratio in the experiment with the marble block.

increased up to cycle 11. A sharp increase in As began during cycle 10, in spite of the decreasing velocity.

To reconstruct the strain field in the central part of the block the records of 30 strain meters mounted in 10 sockets were used (Figure 1). An example of variation for vertical, horizontal and inclined components of local strain in one of the sockets glued onto side 1 of the marble block is given in Figure 4a. The parameter of interest, as found in earlier experiments [Sobolev G.A. and A.V.Koltzov, 1988], is the first invariant of the tensor of planar strain, which is the sum of vertical and horizontal strain for a socket, S = v+ h. Increasing S means in our case a decreasing area of the respective element of the block surface. Some of the sockets showed increasing S during the whole experiment, while others experienced dilatancy at some stages of the experiment. Figure 4b presents a map of strain for side 1 accumulated by the time of the first acoustic signal in cycle 9 whose source was located in the central part of the block. One can see a distinct separation of the strain field into zones of compression and tension in the lower part of the set of holes. The boundary between the zones passes along the holes. This means that the system acts as a single defect inclined with respect to the axis of external compression.

DISCUSSION

The development of dilatancy and cracking in the region of future macrorupture (earthquake) is a general symptom of dynamic macroinstability obtained as a result of many laboratory experiments and considered both by the DD and AUF models. However, we encountered a more complex manifestation of this effect during the experiments. Before the macrofailure during cycles 9-10 and in the period when acoustic signals came from the center of the block, an anomaly in the records of some components (Figure 4a) and in the parameter S = v + h was recorded. Importantly enough, it appeared in all 10 sockets, which indicates its reliability and at the same time enables one to plot area distribution of the anomalous region. The map of strain during the anomaly is presented in Figure 4c. It shows the variation in S during a 30 min interval of constant external stress (maintenance in the second half of cycle 9). On can see that the anomaly is represented by a zone of compression in the area of two central holes inside a surrounding region of relative tension. We may regard it as a precursor of macrorupture in the central part of the block (Figure 2). One cause may be the formation of a strong barrier between the central holes which hampered the dilatancy. At any rate, the simple scheme of the development of dilatancy in the region of future macrorupture (the DD model and to some degree the AUF model) is not suitable in this case.

We shall analyze the recorded precursors of failure in large rock blocks with a view to revealing their properties in comparison with theoretical models of earthquake preparation. Since solid blocks were deformed, the results are mainly relevant to the dilatant-diffusive DD model and the model of avalanche-unstable fracturing AUF [Myachkin V.I.et al.,1975]
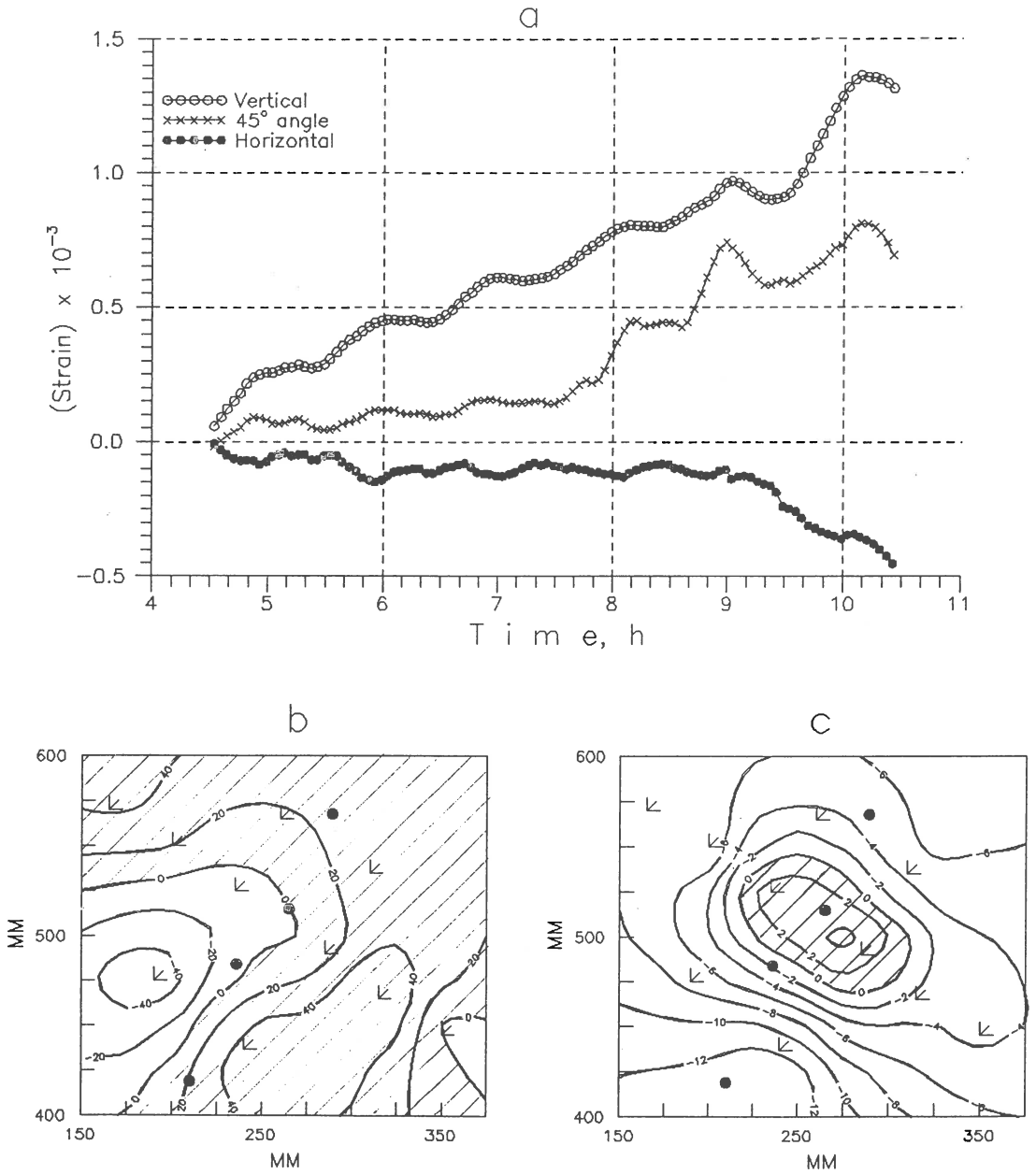
Fig.4. An example of variations of local strain in the region of socket No 2 on side I of the marble block (a), first invariant of the tensor of planar strain S on side I accumulated by cycle 9 (b), and S - anomaly in cycles 9-10 (c). Isolines at figures are given to scale $Sx10e^{-3}$. The regions of relative contraction of the surface are shaded.

The former model considers pore fluid as playing a key part in earthquake preparation; partial drying of the rocks during the dilatancy development increases their strength, while subsequent percolation of fluid from the surrounding massif diminishes it again. When the stresses increase, this results in an earthquake. The bay-like shape of a number of precursors and, first of all, of the ratio of Pand S-wave velocities is controlled by the phases of relative drying and delay in filling the pores and cracks with fluid. The duration and amplitude of the precursors depend on the relation between the rate of dilatancy development and fluid filtration.

The AUF model proceeds from more general ideas of the mechanics of failure, namely, that earthquake preparation progresses by gradual transition from volumetric dispersed failure to localized failure, irrespective of whether pore fluid is present. It is the division of material into regions of accelerated deformation in the zone of future macrorupture and slower deformation outside it which determines in this model the spatial-temporal variations of different fields observed as earthquake precursors. Localization of deformation along the rupture surface is caused by an interaction of the stress fields of cracks which increases with increasing crack size.

In the experiment with the large marble block, water injection began three days before the first cycle of loading. By comparing the measurements of travel times and amplitudes of elastic waves along the upper and lower paths of ultrasound surveying, we came to the conclusion that the water front reached the middle of the block where the holes were drilled by the beginning of the first cycle, i.e., the filtration rate amounted to about 10 cm/day.

Variations in the velocities of compressional and shear elastic waves and in their ratio may serve as parameters supplying information for understanding the process of macrorupture preparation [Hadly K.,1975]. Based on these data, the course of the experiment with the marble block may in our opinion be divided into 4 stages. During the first 5 cycles, the Vp, Vs and Vp/Vs were increasing. (Fig.3a). This may be interpreted as compaction of the material with increasing vertical load and a simultaneous relative increase in water saturation of the remaining pores and fractures, because the intrapore space contracts and the quantity of moisture inside the block is nearly the same.

During cycles 6-9 the Vp/Vs ratio decreased as a result of the beginning decrease in the velocities of compressional waves Vp, while Vs continued to increase. We suppose that at this stage of the experiment progressive dilatancy resulted in a partial drying of the block material which had a stronger effect on the Vp behavior. It was during cycle 6 that the load on the block reached 50% of the critical value at which, judging by the data of numerous laboratory experiments, microfractures begin to form at an increasing rate. The increase in Vs is related to the fact that the closure of earlier fractures still prevailed over the formation of new ones, while relative drying little affects the velocities of these waves, because the strain was transmitted by the rock frame.

The short interval of cycles 9-10 is characterized by a more rapid decrease in Vp/Vs and coincides (from the location of acoustic signals) with the formation of larger fractures in the central region of the block where the future macrorupture will occur. That interval was replaced by an interval of rapid recovery of Vp/Vs with progressive decrease in the velocities of both wave types. This stage terminated with the appearance of a shear macrorupture in the center of the block, which is confirmed both by visual observation and acoustic location (Figure 2).

The bay-like variation of Vp/Vs during cycles 9-10 is a classical precursor of dynamic instability, the interpretation of such anomalies being the basis of the development of the DD and AUF models. In our experiment the decrease of Vp/Vs during cycles 6-9 may be explained as a result of relative drying with progressive dilatancy, which does not contradict the DD model. However, the recovery of Vp/Vs in cycles 10-11 does not fit in this model. The latter assumes that the recovery of Vp/Vs occurs owing to increasing velocities of compressional elastic waves during the migration of the fluid into the dilated region and a repeated filling of the pore space by moisture. As for the experiment under discussion, the increase in Vp/Vs was simultaneous with a sharper decrease in shear wave velocity (Figure 3a). Taking into account the concentration of cracking in the region of future macrorupture during this period, we come to the conclusion that the recovery of the velocity ratio is a consequence of localization of unstable deformation in the region of incipient macrorupture, which is consistent with the AUF model.

At present, the theory of variation of wave amplitudes during the deformation of water-containing rocks is not sufficiently mature. For this reason we cannot reliably interpret the variations of Ap, As and Ap/As (Figure 4b) observed at different stages of the experiment. Of the greatest interest is the interval in cycles 9-10 where a distinct bay-like Ap/As anomaly appeared, a precursor of macrorupture. It was a result of sharp increase in shear wave amplitude As with a simultaneous decrease in Ap.

Detailed study of Figure 2 shows that as macrofailure is approached, the maximum of acoustic activity shifts to the end of the respective cycle of experiment. At the same time it is found that in the first cycles the maximas were recorded even before the end of a subcycle of loading. This effect seems to be due to the fact that a large block of rock contains a great number of weak places that dynamically fail even at small levels of loading. On the whole, the shifting of maxima of acoustic activity to the end of a loading-pause cycle (relative unloading) my be interpreted as a precursor of instability that is more general compared to the DD and AUE models. In the terrestrial conditions tectonic stresses fluctuate as a result of the action of cosmic and meteorologic factors, and because of previous earthquakes. Therefore, though a gradual increase in seismic activity is a general indicator of approaching instability, individual stages of its

local growth may only reflect a response to the change in the state of stress and be no indicator of an impending earthquake.

CONCLUSION

1. Deformation of large marble block which revealed precursors of macrofailure in local strain, the rate of acoustic emission, travel times and amplitudes of elastic • waves passing through the block.

2. The first phase of bay-like Vp/Vs anomalies (decrease) may be explained in the framework of the dilatant-diffusive model of earthquake preparation and the second one (recovery) by the model of avalanche-unstable fracturing.

3. The strain anomaly at the location of a future macrorupture had a complex form, a zone of relative reduction of the surface within a larger region of dilatancy, which is not considered in the DD and AUF models.

4. A regular shift of the maximum of acoustic emission in successive loading cycles manifested itself as a universal predictive indicator of dynamic instability.

ACKNOWLEDGMENTS

REFERENCES

Hadly K.,1975. Vp/Vs anomalies in dilatant rock samples. PAGEOPH, Vol.113,(1/2), 1-33.

Lockner D.A.,J.B.Walsh,J.D.Byerlee, 1977. Changes in seismic velocity and attenuation during deformation of granite. J.Geophys. Res.,Vol. 82, No.33, 5374-5378.

Myachkin V.I., W.F.Brace, G.A.Sobolev and J.H.Dieterich, 1975. Two models for earthquake forerunners. PAGEOPH, 113, 169-181.

Ponyatovskaya V.I., V.A.Terentiev, O.G.Shamina, 1989. Peculiarities of P and S elastic waves in stresed medium as possible failure precursors. Physics of the Earth, No.7, 28-37 (in russian).

Sobolev G.A. and A.V.Koltsov,1988. Large scale modeling of earthquake preparation and precursors. M., Nauka, 203.

CHAOTIC ANALYSIS OF A TIME SERIES COMPOSED OF SEISMIC EVENTS RECORDED IN GREECE.

G. Pavlos[1], D. Dialetis[2], J. Latoussakis[2] and M. Athanassiou[1].

(1) Demokritos University of Thrace.
(2) National Observatory of Athens.

Abstract
A chaotic analysis approach was applied to different earthquake time series recorded in Greek area in order to test the assumption that the earthquake process could be the manifestation of a chaotic low dimensional process. For the study of the seismicity we have used a peculiar time series consisting of time differences between two consecutive seismic events with magnitudes greater than 3.2. The time series was composed by the mainshocks and the aftershocks. The result of our study show that the underlying mechanism, as expressed by a time series of this kind can be described by low dimensional chaotic dynamics.

Introduction
For the study of the seismicity we can use different types of time series. In this study we used a peculiar "time series" composed by the time differences between two consecutive seismic events with magnitudes greater than 3.2, recorded in Greek area. In such a time series the ordinate represents consecutive events and the abscissa the time difference in hours between these events (Figure 1a).

We have found strong evidence for low dimensional chaotic dynamics. The chaotic character of the process underlying this time series, is supported by some noticeable tests against the low dimensional pseudo chaotic profile of pure stochastic processes of linear or non-linear coloured noises.

Chaotic analysis of experimental time series.
In the following we suppose that earthquake dynamics belongs to the category of dissipative conservative system dynamics **(Marek and Schreiber, 1991)**, which can reveal dynamics with strange attractor structure **(Pavlos et al., 1994)**.

In the following we use the reconstructed phase space vector

$$\vec{R}(t_i) = \{x(t_i), x(t_i + \tau), \ldots, x(t_i + (m-1)\tau\} \tag{1}$$

where τ is a delay time. In principle, τ is arbitrary as long as the values $x(t_i)$ and $x(t_i+\tau)$ are not highly correlated. If τ is too small the coordinates

become singular so that $x(t_i) \approx x(t_i+1)$. If τ is too big chaos makes $x(t_i)$ and $x(t_i+(m-1)\tau)$ causally disconnected by amplification of noise. In practice τ is chosen by trial and error searching for optimal results. This reconstructed phase space is used in order to test the existence of the strange attractor as well as its correlation dimension and the largest Lyapunov exponent of the dynamical flow **(Grasberger and Procaccia, 1983, Whitney, 1936, Wolf et al., 1985)**.

The correlation integral $C(r;m)$ is given by the relation

$$C(r;m) = \lim_{M \to \infty} \frac{1}{M^2} \sum_{i,j=1}^{M} \Theta[r - \|R(t_i) - R(t_j)\|] \qquad (2)$$

where $\Theta(a)$ Heaviside function and $\|R(t_i)-R(t_j)\|$ denotes the distance between the states $R(t_i)$, $R(t_j)$ in the m-dimensional reconstructed phase space. The correlation dimension D of the reconstructed m-dimensional orbit is given by **Grassberger and Procaccia [1983]**

$$D = \lim_{r \to \infty, m \to \infty} \frac{d \ln C(r;m)}{d \ln(r)} \qquad (3)$$

When the orbit evolves on a strange attractor manifold then the slope in a log-log plot of the correlation integral $C(r;m)$ in its scaling region, where $C(t;m) \approx r^{d(m)}$, must saturate at a final fractal value D as the embedding dimension m increases. According to an embedding theorem by **Whitney [1936]** the minimum dimension m_0 of an Euclidean space R_m in which we can found a smooth embedding of the attractor is $m_0=2D+1$.

As is well-known, the dynamical evolution of the system state on a strange attractor is very sensitive to the choice of initial conditions. This means that the dynamical flow in phase space must possess at least one positive Lyapunov exponent (L_{max}). In order to estimate experimentally the largest Lyapunov exponent we use the relation

$$L_{max} = \frac{1}{t_m - t_0} \sum_{i=1}^{m} \log_2 [d(t_i) / d(t_{i-1})] \qquad (4)$$

where $d(t)$ is the displacement vector of two nearby trajectories in (2D+1)-dimensional reconstructed phase space **[Wolf *et al.*, 1985]**. The evolution time step $\Delta t=t_i-t_{i-1}$ must be small enough in order to be revealed the deviation between neighbouring trajectories during this time step. A positive Lyapunov exponent λ_i means that there exists a direction in phase space along which the distance $d(t)$ of two neighbouring trajectories grows exponentially according to the relation

$$d(t) = d(t_0)e^{\lambda_i(t-t_0)} \qquad\qquad (5)$$

Low dimensional chaos and stochasticity versus chaoticity in earthquake process.

Fig. 1a shows the time series corresponding to time differences between consecutive events of earthquakes. The random character of the time series is revealed by the broadband form of the power spectrum (Fig. 1b) and the abruptly decaying autocorrelation function (Fig. 1c). The power spectrum shows approximately a two branches power law profile $P(\omega) \approx \omega^{-\alpha}$. The autocorrelation function reveals a first abrupt decay at the value 0.05 during the first ≈ 100 units of lag time.

Fig. 2 shows the probability density function of the seismic time series for the entire series and the first half of it. The form of these density function show the stationary and non-gaussian characteristics of this time series.

Fig. 3a shows the slopes $d(m)=d\ln C(r;m)/d\ln(r)$ with apparent plateau ($d(m)$=constant) at the scaling region where $C(r;m) \approx r^{d(m)}$ for low values of r. The slope $d(m)$ at the scaling region saturates as m increases at the value D=2-3. This result was found to be invariable for delay time $\tau<100$ units. According to **Provenzale et al.** [1991] in the case of stochastic processes the saturation of the scaling exponent seems to be forced by the shape of the power spectrum. This is consistent with the fact that both the power spectrum and the correlation integral are related to the second moments of the distribution. According to embedding theory the saturation value ($D \approx 3.2$) of the slope at the scaling region, as m increases supports the existence of a low dimensional attractor with fractal dimension $D \approx 3.2$. Moreover according to **Theiler (1991)** the concept of fractal dimension can be applied to time series in two distinct ways. The first is to indicate the number of degrees of freedom in the underlying dynamical system and the second to quantify the self-affinity or "crinkliness" of the trajectory through the phase space. The application of the test of Theiler can help to discriminate between them **(Pavlos et al., 1994)**.

Fig. 3b shows the slopes for values of Theiler parameter w=200 (higher than the decorrelation time of the time series). It is clear that in this case the values of the slopes at the scaling region are higher without clear saturation profile. This result indicates that some kind of self-affine noise may be present in the time series.

In order to reduce the possible noise of the dynamical system we have applied the SVD analysis of **Broomhead and King [1986]** and we have used the singular vectors obtained by SVD analysis for the reconstruction of the trajectory in phase space. In Fig. 3c we show the

slopes of the correlation integrals for delay time t=20 and Theiler parameter w=2000. There is a clear saturation of the slopes at the value 2.5-3. This result strongly support the fractal nature of the trajectory which is due to "close returns" in phase space.

According to embedding theory the saturation value of the slope in the scaling region, as m increases supports the existence of a low dimensional attractor.

Moreover in order to test the obtained results we have applied the "null" hypothesis of Theiler for linearly autocorrelated gaussian noise and for static nonlinear transform of linear gaussian noise. In Fig 4a we present the slopes corresponding to the earthquakes time series after phase randomisation and in Fig 4b the slopes for surrogate data sets which conserve the initial amplitude distribution function **(Theiler et al. 1992)**. In these figures is clear that we can not observe low saturation values of the slopes. This excludes the possibility of stochasticity in the earthquake process.

The chaotic (sensitive to initial conditions) character of the dynamical flow on the attractor is demonstrated by fig. 5 which shows the estimation of the largest Lyapunov exponent Lmax (see Eq. 4).The positive value of the largest Lyapunov exponent reveals strong sensitivity to the initial conditions of the supposed earthquake low dimensional dynamics.

Discussion

In this work we have presented strong evidences for the presence of low dimensional chaotic dynamics in a time series obtained from an earthquake process. From this point of view the chaotic character of seismic processes reveals some similarity with the chaotic dynamics of dripping faucet system **(Shaw, 1981, 1984)**. We could push further this similarity by supposing that the physical mechanism of earthquakes must be some kind of chaotic dripping of previously accumulated energy. The random or nonperiodical character of earthquakes must reflect the dynamical evolution on a low dimensional chaotic attracting set with fractal dimension $D \approx 3$ or a little higher according to SVD analysis. In such a case the corresponding phase space must have m>2D+1 degrees of freedom. This result is similar with the results obtained from our previous study of a time series composed of seismic events recorded in Japan **(Pavlos et al., 1994)**. The reconstruction of this phase space by using the seismic time series can be employed for the construction of a predictor function F_T which approximates the state flow function f_T.(Farmer and Sidorowich, 1987).

After this we believe that the low dimensional chaos for earthquakes supported by the present study in relation with the results

obtained by our previous study, could be helpful for the construction of new prediction algorithms of seismic events.
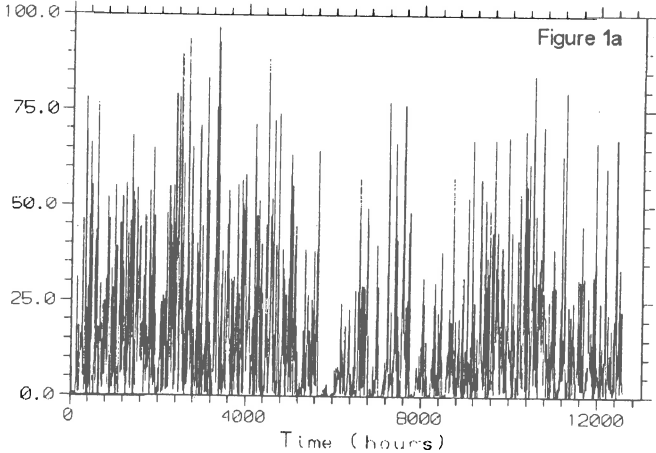

Fig. 1a. A seismic time series corresponding to time differences between consecutive events of earthquakes with magnitudes ⟩3.2, recorded in Greece.
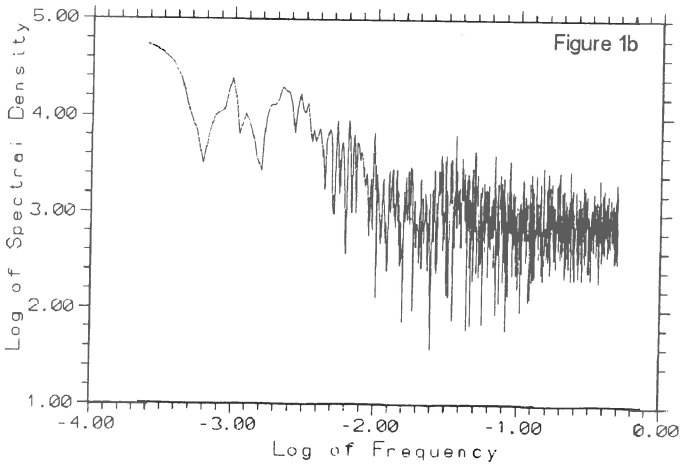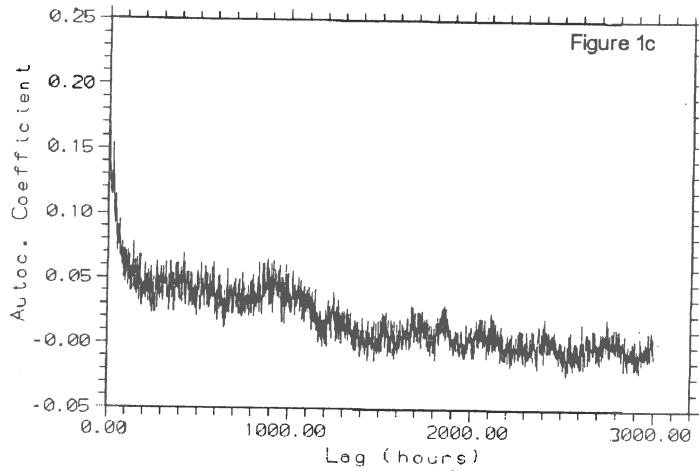

Fig. 1b. Spectral density for the seismic time series.

Fig. 1c. Autocorrelation function for the seismic time series. We can observe the decorrelation of signal (time differences) after ≈100 lag time units (seismic events).
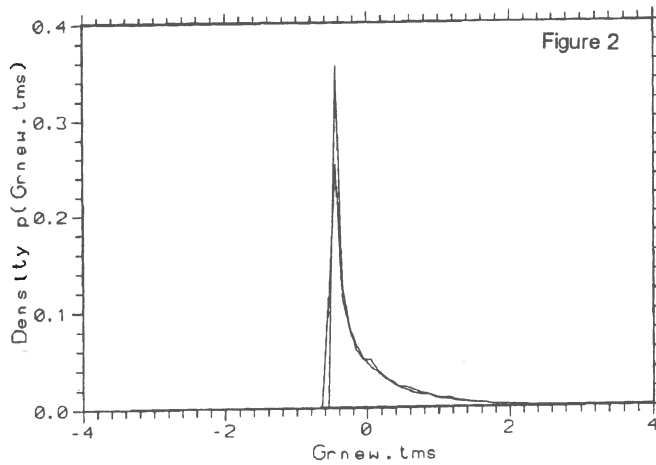

Fig. 2. Probability density function of the seismic time series for the entire and the first half.
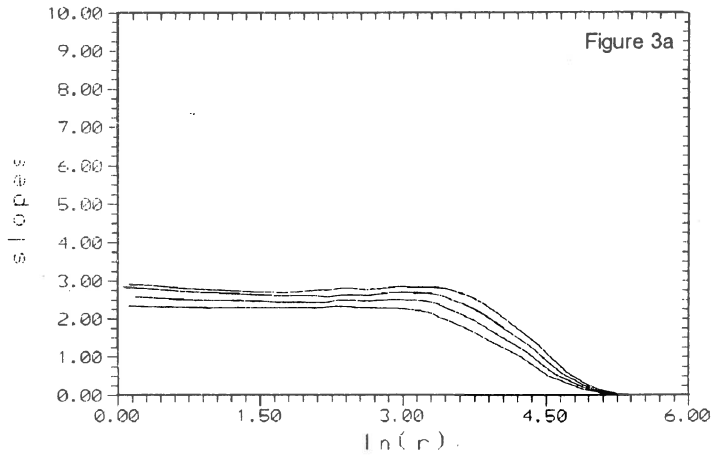
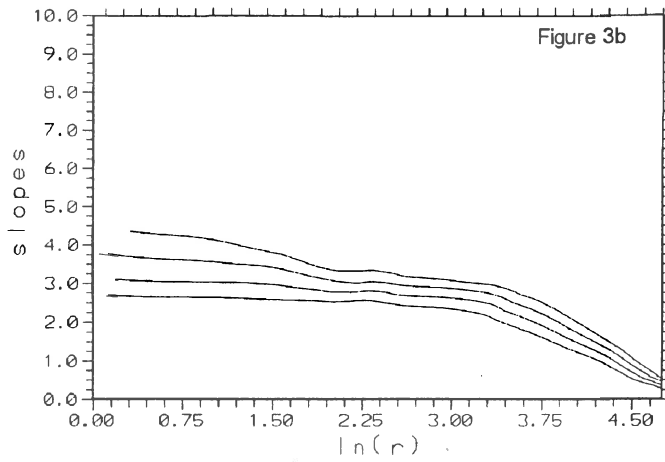Fig. 3a. Slopes dlnC(r;m)/dln(r) which reveal a tendency for saturation at the scaling region at the value D=3.

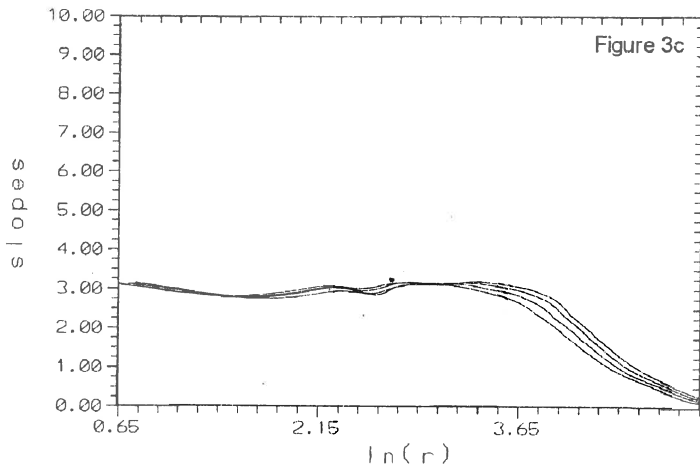Fig. 3b. Slopes dlnC(r;m)/dln(r) estimated for Theiler parameter w=200.

Fig. 3c. Slopes dlnC(r;m)/dln(r) of the correlation integrals for delay time t=20 and Theiler parameter w=2000 (reconstructed trajectory in phase space by SVD analysis).
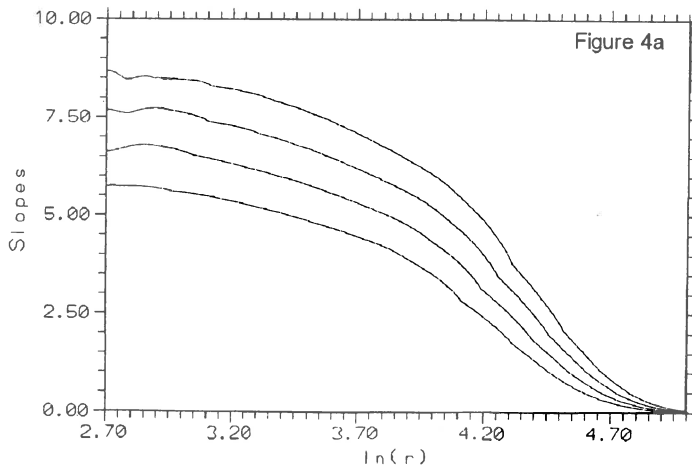

Fig. 4a. Slopes dlnC(r;m)/dln(r) estimated for the seismic time series after randomization of its Fourier phases.

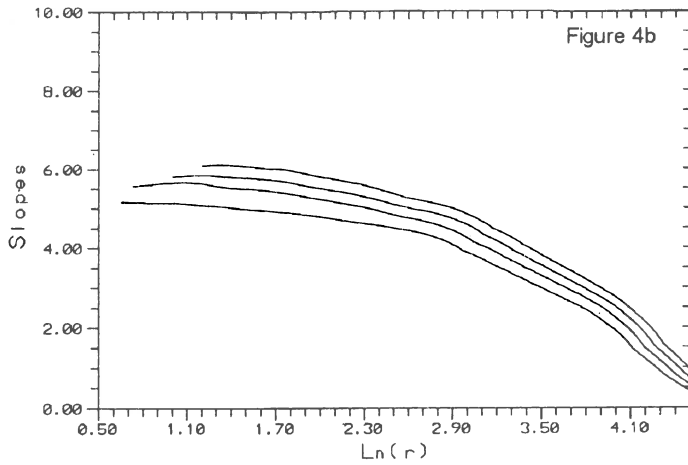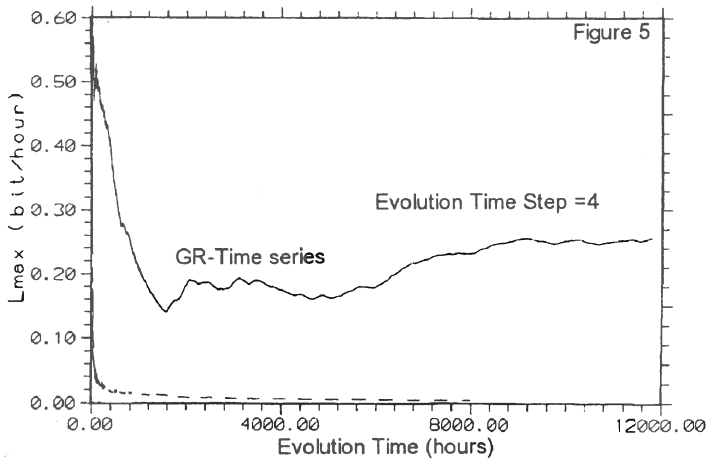Fig. 4b. Slopes dlnC(r;m)/dln(r) estimated for surrogate data sets.

Fig. 5. Estimation of the Largest Lyapunov exponent L_{max} as function of the evolution time on the attracting set. The L_{max} saturates at positive value ≈ 0.28.

REFERENCES

Broomhead, D. S. and King, G. P. [1986] "Extracting Qualitative Dynamics from Exprerimental Data", Physica D, **20**, 217-236.

Farmer, J. D. and Sidorowich, J. J. [1987] "Predicting Chaotic Time Series", Phys. Rev. Let., **59**, pp. 845-848.

Grassberger, P. and Procaccia, I. [1983] "Measuring the Strangeness of Strange Attractors", Physica D, **9**, 189-208.

Marek, M. and Schreiber, I. [1991] *Chaotic Behaviour of Deterministic Dissipative Systems*, Cambridge University Press.

Pavlos G.P., Karakatsanis L., Latoussakis J.B., Dialetis D., Papaioannou G. [1994] "Chaotic Analysis of a Time Series Composed of Seismic Events Recorded in Japan", International Journal of Bifurcation and Chaos, Vol. **4**, No. 1, 87-98.

Provenzale, A., Smith, L. A., Vio, R., Murante, G. [1991] "Distinguishing Low-Dimensional Dynamics and Randomness in Measured Time Series", submitted to Physica D.

Shaw, R. [1981] "Strange Attractors, Chaotic Behaviour and Information Flow", Z. Naturforsh., **36a**, 80-122.

Shaw, R. [1984] "The Dripping Faucet as a Model Chaotic System", The science frontier express series, Santa Crouz, CA.

Theiler, G. [1991] "Some Comments on the Correlation Dimension of 1/f^a Noise", Physics Letters A, **155**, 8,9, p.480.

Theiler G., Eubank S., Longtin A., Galdrikian B. and Farmer J.B. [1992] "Testing for nonlinearity in time series : the method of surrogate data", Physica D, **58**, 77-94.

Whitney, H. [1936] "Differentiable Manifolds", Ann. Math., 37.

Wolf, A., Swift J.B., Swinney H.L. and Vastano J. [1985] "Determining Lyapunov Exponents from a Time Series", Physica D., **16**, 285-317.

Seismic monitoring of a mine collapse

Wolfgang A. Lenhardt and Christiane Pascher

Central Institute for Meteorology and Geodynamics/Department of Geophysics, Vienna, Austria

ABSTRACT

On May 2, 1993 more than 200 seismic events from an underground mine in Tyrol/Austria were recorded with short-period seismometers of a local seismic network which was introduced in the late 1980s to monitor the natural seismicity in Tyrol in greater detail. The cause of this series of mining-associated events has become the subject of intensive investigations. The process of subsidence took two hours and affected a surface area of approximately 10.000 m². Underground observations revealed a number of discontinuities along which the rock mass was able to move. Seismic recordings of the close-by seismic stations revealed two types of mechanisms: One mechanism seems to be associated with pure block-sliding along several discontinuities - while other signals indicate additional collapse.

INTRODUCTION

On Sunday, May 2, 1993 a sequence of seismic events was recorded with short-period seismometers from the area of Schwaz, a town in Tyrol/Austria.

The Department of Geophysics of the Central Institute for Meteorology and Geodynamics in Vienna (Austria) maintaines four seismic stations in Tyrol equipped with Geotech S13 short-period seismometers which can be directly accessed from Vienna. Two of them (station Wattenberg 'WTTA' and Walderalm 'WATA') are situated 12 km from Schwaz. As it turned out, the observed seismic signals were related to a partial collapse of dolomite-mine workings near this town.

Mining has a long tradition in Schwaz - reaching its peak in production during the 16th century when silver was recovered from numerous galleries in the mining district of 'Falkenstein' near Schwaz. Today's production concentrates on underground dolomite mining. In places, mine workings extend over 140 m in vertical direction and reach diameters of approximately 80 m.

SEISMIC OBSERVATIONS

The main shock registered a magnitude of M1,9, which was even observed in Vienna as well as by foreign seismological stations. It constituted the last event of a sequence of events which was associated with a massive subsidence - up to 8,5 m in places - 340 m above the mine workings. The whole process took two hours and affected a surface area of 80 m x 150 m, thus roughly delineating one of the underground caverns. Underground observations revealed a number of discontinuities along which the rock mass was able to move. The total mass of the rock mass which filled one of the caverns amounted to approximately half a million cubic metres.

Seismic recordings of close-by seismic stations revealed two types of mechanisms during the collapse: One mechanism seems to be associated with pure block-sliding along several discontinuities - while other signals indicate collapse events which exhibit a long-period wavelet in the seismograms (Figure).
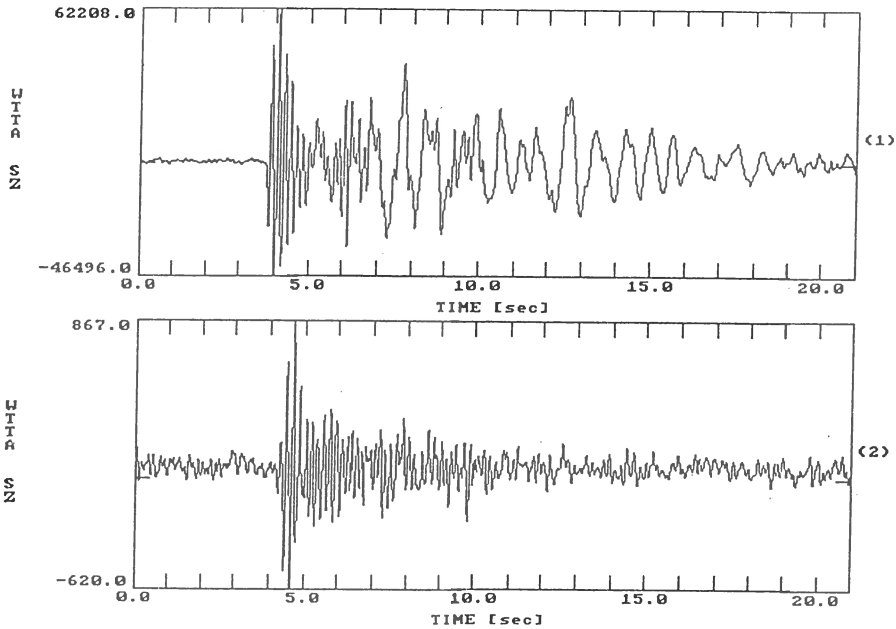
Seismic recordings with (1) and without (2) long-period wavelet

CONCLUSIONS

Three phases of the collapse can be recognized from seismic observations. The first phase seems to be a result of slip movement along one of the adjacent discontinuities and collapse of the roof. During the second phase the lower part of the roof block collapses, fills the mine workings and the higher part of the block starts to move. The third phase constitutes the final part of the process during which the subsidence on surface took place.

Not only the untypical history of seismic events - numerous foreshocks, culminating in the main shock at the end of the collapse - attracts attention, but also the fact that minor seismic activity is still carrying on.

A detailed paper will be published in a special issue of PAGEOPH.